April 1966

Submitted to

GEORGE C. MARSHALL SPACE FLIGHT CENTER

NATIONAL AERONAUTICS AND SPACE ADMINISTRATION

HUNTSVILLE, ALABAMA

BUREAU OF ENGINEERING RESEARCH

FINAL REPORT

for

NASA Contract NAS8-11155

A STUDY OF THE STABILITY OF REINFORCED CYLINDRICAL AND CONICAL SHELLS SUBJECTED TO VARIOUS TYPES AND COMBINATIONS OF LOADS

Project Director: William K. Rey

BER

COLLEGE OF ENGINEERING

THE UNIVERSITY OF ALABAMA 1831

UNIVERSITY OF ALABAMA

UNIVERSITY ALABAMA

FINAL REPORT

for

NASA Contract NAS8-11155

A STUDY OF THE STABILITY OF REINFORCED CYLINDRICAL AND CONICAL SHELLS SUBJECTED TO VARIOUS TYPES AND COMBINATIONS OF LOADS

Project Director: William K. Rey

Submitted to

GEORGE C. MARSHALL SPACE FLIGHT CENTER

NATIONAL AERONAUTICS AND SPACE ADMINISTRATION

BUREAU OF ENGINEERING RESEARCH

UNIVERSITY OF ALABAMA

UNIVERSITY, ALABAMA

APRIL 1966

CONTENTS

A STUDY OF THE STABILITY OF REINFORCED CYLINDRICAL AND CONICAL SHELLS SUBJECTED TO VARIOUS TYPES AND COMBINATIONS OF LOADS

SUMMARY

The investigation consisted of studies in the following three areas: analytical studies of the stress distribution in conical shells of both linearly varying thickness and constant thickness subjected to various types of loads; a study of the feasibility of using small plastic cylinders in investigations of the stability of circular cylindrical shells subjected simultaneously to axial compressive loads and internal pressure; and, an experimental and analytical study of the stress distribution in integrally stiffened panels subjected to axial loads.

INTRODUCTION

Theoretical and experimental investigations of cylindrical and conical shells began at the University of Alabama under the terms of Contract Number DA-01-009-ORD-334 with the Redstone Arsenal and Contract Number DA-01-009-ORD-866 with the U.S. Army Ordnance District, Birmingham, Alabama. Following these two studies, discussions were held with personnel of the Propulsion and Vehicle Engineering Division at the George C. Marshall Space Flight Center of the National Aeronautics and Space Administration to formulate a long range research program that would provide analytical procedures, design data and digital computer programs for the analysis and design of cylindrical and conical shells.

The first phase of the planned program was conducted under the terms of NASA Contract NAS8-5012 and the results were published by the University of Alabama Bureau of Engineering Research as a Summary Report in four sections as follows: Section 1 - "General Instability of an Orthotropic Circular Cylindrical Shell Subjected to a Pressure Combined with an Axial Load Considering Both Clamped and Simply Supported Edge Conditions" by Carl C. Steyer and Thomas A. Carlton, Jr.; Section 2 - "Stress in a Segment of a Conical Shell Subjected to Lateral Normal Load" by Chin Hao Chang; Section 3 - "General Instability of an Orthotropic Circular Conical Shell Subjected to Hydrostatic Pressure and a Compressive Axial Force" by Carl C. Steyer

and Shih-Cheng Zien; and Section 4 - "Matrix Shear Lag Analysis Utilizing a High-Speed Digital Computer" by William K. Rey.

The second phase of the research program was conducted under the terms of NASA Contract NAS8-5168 with the results presented in five technical reports as follows: Technical Report A - "Fortran II Computer Program for the Evaluation of a Donnell Type of Differential Equation for a Simply-Supported Cylindrical Shell" by Thomas D. Easter; Technical Report B - "Fortran II Computer Program for the Evaluation of a Donnell Type of Differential Equation for an Orthotropic Circular Conical Shell" by Thomas D. Easter, Colonel M. Pearson and Melvin K. Richardson; Technical Report C - "An Asympototic Solution for Conical Shells of Linearly Varying Thickness" by Chin Hao Chang; Technical Report D - "Literature Survey with Abstracts" by Raymond C. Montgomery; and Technical Report E - "Theoretical Analysis of the Static General Instability of an Orthotropic Circular Cylinder Subjected to an Axial Load, End Moment and Uniform Radial Pressure" by William S. Viall and Carl C. Steyer. The final report for contract NAS8-5168 included these five technical reports as appendices.

SCOPE OF WORK

Investigations were simultaneously conducted in the following three areas: analytical studies of conical shells; a study of the feasibility of using inexpensive plastic cylinders for experimental investigations of shell stability; and an analytical and experimental study of the stress distribution in integrally stiffened flat panels. The studies of conical shells were supervised by Dr. Chin Hao Chang of the Department of Engineering Mechanics while Dr. Thomas A. Carlton, Jr. of the Department of Civil Engineering supervised the feasibility study utilizing small plastic cylinders and Professor William K. Rey of the Department of Aerospace Engineering supervised the investigation of the stress distribution in integrally stiffened panels.

Conical Shells

Analyses of conical shells and conical shell segments subjected to lateral normal loads were presented as Section 2 of the Summary Report for NASA Contract NAS8-5012 and as Technical Report C for NASA Contract

NAS8-5168. In Appendix A, the analysis of conical shells of linearly varying thickness subjected to lateral normal loads is presented. This analysis includes corrections to a similar analysis which was previously presented in Technical Report C for NASA Contract NAS8-5168. In a numerical example, the corrected analysis was applied to a truncated semicircular conical segment that had simply supported generators with the small end fixed and the other end free. The lateral normal load applied to this conical segment was assumed to be constant in the meridional direction and to vary sinusoidally in the circumferential direction. The computer program used in the numerical example is presented as Computer Program 1 in Appendix D.

The analysis of conical shells of linearly varying thickness was extended to include thermal loads in Appendix B. In a numerical example, the truncated semicircular conical segment considered in Appendix A was analyzed for symmetrical and asymmetrical thermal loads. The computer program used in this analysis is included in Appendix D as Computer Program 2.

In Appendix C an analysis is presented for truncated conical shells of constant thickness. Two numerical examples are included. In the first example, a truncated semicircular conical segment supported and loaded in the same manner as the segment considered in Appendix A was analyzed for constant shell thickness. The computer program used for this analysis is identified as Computer Program 3 in Appendix D. In the second example, a conical frustum fixed at the small end and free at the large end was analyzed for a moment applied at the free end. Computer Program 4 in Appendix D was used in this analysis.

A paper titled "The Asymptotic Solutions of Conical Shells Subjected to Lateral Loads" by Chin Hao Chang containing the results presented in Appendices A and C has been accepted for presentation at the Fifth United States National Congress of Applied Mechanics to be held in Minneapolis, Minnesota during June 1966. An abstract of this paper will be published in the proceedings of the Congress.

Plastic Cylinders

The study of the feasibility of using small plastic cylinders in investigations of cylindrical shell stability was undertaken to determine

the nature of the problems encountered in fabricating and testing plastic cylinders. Since one of the objectives of the study was to evaluate the suitability of inexpensive cylinders for stability studies, a minimum of special equipment was used in the fabrication process. However, the fabrication procedure was designed to produce cylinders of uniform quality within the limitations imposed by the expense criteria. The results obtained in this investigation were not expected to be comprehensive enough to establish the validity of existing theories or provide useful design data. Since the progress report pertaining to this phase of the contract was deemed unsatisfactory by the Contracting Officer's Technical Representative, a number of revisions and additions were made in preparing the final report based upon the general and specific comments of the Contracting Officer's Technical Representative. These changes are incorporated in Appendix E.

Integrally Stiffened Panels

A series of tests were conducted to determine the stress distribution in three integrally stiffened panels instrumented with uniaxial strain gages and rectangular strain rosettes. All of the experimental data and a comparison of all of the experimental data with one theoretical analysis are contained in Appendix F. In Appendix G, a portion of the experimental data is analyzed in greater detail and compared with five different theoretical analyses.

The study of the stress distribution in integrally stiffened panels is being continued under the terms of NASA Contract NAS8-20164.

Literature Survey

During the contract period, lists of published articles pertaining to the contract subject matter and abstracts of certain articles were submitted with monthly reports. This information is included in this report as Appendix H.

CONCLUDING REMARKS

Each appendix of this report is itself a complete report. Therefore,

where appropriate, lists of symbols, discussions of results, lists of references and conclusions are included in the individual appendices. In order to reduce confusion, the tables, figures and references in each appendix have been numbered to indicate the appendix in which they appear rather than being numbered consecutively throughout the report.

APPENDIX A

ON CONICAL SHELLS OF LINEARLY VARYING THICKNESS SUBJECTED TO LATERAL NORMAL LOADS

By Chin Hao Chang

The contents of this appendix were previously submitted as Progress Report No. 1 for NASA Contract NAS8-11155.

APPENDIX A

ON CONICAL SHELLS OF LINEARLY VARYING THICKNESS SUBJECTED TO LATERAL NORMAL LOADS

By Chin Hao Chang*

INTRODUCTION

The theory of conical shells of linearly varying thickness in the framework of generalized plane stresses of linear theory of elasticity along with a general approach for solving the basic equations has been given in Reference [A1][1]. The three homogeneous equilibrium equations in terms of three displacement components were solved by the classic method of separation of variables. In turn, these solutions depend upon an eighth degree characteristic equation.

The basic equations may be regarded as the result of series expansions of the stresses and displacements in a parameter k which depends on the ratio of the thickness to length. Only the terms of zero and first order of k are retained in the expansions. In this paper, the characteristic equation is presented in a different form than previously used and is solved by an approximate method that is consistent with the theory.

Of the eight roots of the characteristic equation, four are real and the other four are complex. When the parameter k approaches zero asymptotically, it is found that the solution of the real roots corresponds to membrane theory while that of the complex roots corresponds to the bending effect. A general asymptotical solution is given including eight undetermined constants.

Generally there would be no difficulties in obtaining the particular solutions of the system due to lateral normal loads. However, when the load is uniformly distributed along meridians, the solution is near a

---

*Associate Professor of Engineering Mechanics, University of Alabama University, Alabama and Staff Associate for NASA Contract NAS8-11155.

[1]Numbers in brackets designate references at the end of this appendix.

singularity of the system. It is at a singularity for the asymptotical solution. The particular solution for this case is given.

For illustration, the analysis is applied to a semicircular truncated cone which has two generators simply supported, the smaller circular end fixed and the other end free. It is shown that the bending effects are confined to the neighborhood of the clamped edge as would be expected.

BASIC EQUATIONS

Let θ and s be the circumferential and meridional coordinates of the middle surface of an isotropic conical cone and u, v, w, be the circumferential, meridional and normal displacement components, respectively. Outward w is positive. When the thickness of the shell h is proportional to s and independent of θ, one has

$$h = \delta s \tag{A1}$$

where δ is a constant which for thin shells is very small. The elastic law assumes the following relationships between the stress resultants and displacement components:[2]

$$\begin{aligned}
N_s &= \mathcal{D}[sv' + \nu(u' \sec\alpha + v + w\tan\alpha) - k s^2 w''\tan\alpha] \\
N_\theta &= \mathcal{D}[u' \sec\alpha + v + w\tan\alpha + \nu s v' \\
&\quad + k(v\tan\alpha + w\tan^2\alpha + w''\sec^2\alpha + sw')\tan\alpha] \\
N_{s\theta} &= \mathcal{D}\frac{1-\nu}{2}[su' - u + v'\sec\alpha \\
&\quad + k\left(su' - u - \frac{sw''}{\sin\alpha} + \frac{w'}{\sin\alpha}\right)\tan^2\alpha] \\
N_{\theta s} &= \mathcal{D}\frac{1-\nu}{2}[su' - u + v'\sec\alpha \\
&\quad + k\left(v'\sec\alpha + \frac{sw''}{\sin\alpha} - \frac{w'}{\sin\alpha}\right)\tan^2\alpha]
\end{aligned} \tag{A2}$$

---

[2]Further details are given in Reference [A1].

$$
\begin{aligned}
M_s &= \mathcal{Q}ks[s^2w'' - sv' \tan\alpha + \nu (w'' \sec^2\alpha + sw' - u' \sec\alpha \tan\alpha)] \\
M_\theta &= \mathcal{Q}ks[w'' \sec^2\alpha + sw' + w \tan^2\alpha + v \tan\alpha + \nu s^2w'']
\end{aligned} \tag{A2}
$$

$$
M_{s\theta} = \mathcal{Q}k(1 - \nu)\, s[(sw'' - w') \sec\alpha - (su' - u) \tan\alpha]
$$

$$
M_{\theta s} = \mathcal{Q}k(1 - \nu)\, s[(sw'' - w' + \tfrac{1}{2} v' \tan\alpha) \sec\alpha - \tfrac{1}{2} (su' - u) \tan\alpha]
$$

in which N_s ..., $M_{\theta s}$ are stress resultants and stress moments per unit length. The dots indicate partial differentiation with respect to s; and the primes indicate partial differentiation with respect to θ; α is the complement of the half central angle of the cone;

$$
\mathcal{Q} = \frac{E\delta}{1 - \nu^2} \quad \text{and} \quad k = \frac{\delta^2}{12} \tag{A3}
$$

where E is Young's modulus of elasticity and ν is Poisson's ratio.

The six equations of equilibrium may be given in the following form:

$$
\begin{aligned}
(sN_s)' + N'_{\theta s} \sec\alpha - N_\theta &= - P_s s \\
(sN_{s\theta})' + N'_\theta \sec\alpha + N_{\theta s} - Q_\theta \tan\alpha &= - P_\theta s \\
N_\theta \tan\alpha + Q'_\theta \sec\alpha + (sQ_s)' &= P_r s \\
(sM_s)' + M'_{\theta s} \sec\alpha - M_\theta &= sQ_s \\
(sM_{s\theta})' + M'_\theta \sec\alpha + M_{\theta s} &= sQ_\theta \\
s(N_{\theta s} - N_{s\theta}) &= M_{\theta s} \tan\alpha
\end{aligned} \tag{A4}
$$

where Q_s and Q_θ are the transverse shear forces per unit length acting on sections perpendicular to the s and θ directions; P_r, P_s, and P_θ are surface loads per unit area in the normal, meridional and circumferential directions respectively.

Dropping the last equation of (A4), which is an identity, and making use of the fourth and fifth equations of (A4) to eliminate the transverse shearing forces Q_s and Q_θ in the other three equations, the

resulting three equations of equilibrium are:

$$
\begin{aligned}
&s(sN_{s\theta})^{\cdot} + sN_{\theta}' \sec\alpha + s\,N_{\theta s} - (sM_{s\theta})^{\cdot} \tan\alpha \\
&\qquad - M_{\theta s} \tan\alpha - M'_{\theta} \tan\alpha \sec\alpha = - P_{\theta} s^2 \\
&(sN_s)^{\cdot} + N_{\theta s}' \sec\alpha - N_{\theta} = - P_s\, s \\
&sN_{\theta} \tan\alpha + s(sM_s)^{\cdot\cdot} + (sM'_{s\theta})^{\cdot} \sec\alpha + (sM'_{\theta s})^{\cdot} \sec\alpha \\
&\qquad + M_{\theta}'' \sec^2\alpha - sM_{\theta}^{\cdot} = P_r s^2
\end{aligned}
\tag{A5}
$$

Substitution of the elastic law equations (A2) into equations (A5) results in the following equations of equilibrium in terms of the displacements:

$$
\begin{aligned}
&\frac{1-\nu}{2}s^2u^{\cdot\cdot} + u''\sec^2\alpha + (1-\nu)su^{\cdot} - (1-\nu)u + \frac{1+\nu}{2}sv^{\cdot\cdot}\sec\alpha \\
&\quad + (2-\nu)v'\sec\alpha + w'\tan\alpha\sec\alpha + k[\frac{3}{2}(1-\nu)s^2u^{\cdot\cdot}\tan\alpha \\
&\quad + 3(1-\nu)su^{\cdot}\tan\alpha - 3(1-\nu)u\tan\alpha - \frac{3-\nu}{2}s^2w'^{\cdot\cdot}\sec\alpha \\
&\quad - 3(1-\nu)sw^{\cdot\cdot}\sec\alpha + 3(1-\nu)w'\sec\alpha]\tan\alpha = -\frac{P_{\theta}s}{\mathcal{Q}} \\
&\frac{1+\nu}{2}su^{\cdot\cdot}\sec\alpha - \frac{3}{2}(1-\nu)u'\sec\alpha + s^2v^{\cdot\cdot} + \frac{1-\nu}{2}v''\sec^2\alpha \\
&\quad + 2sv^{\cdot} - (1-\nu)v + \nu sw^{\cdot}\tan\alpha - (1-\nu)w\tan\alpha \\
&\quad + k[\frac{1-\nu}{2}v''\tan\alpha\sec^2\alpha - v\tan\alpha - s^3w^{\cdot\cdot\cdot} + \frac{1-\nu}{2}sw'''\sec^2\alpha \\
&\quad - 3s^2w^{\cdot\cdot} - \frac{3-\nu}{2}w''\sec^2\alpha - sw^{\cdot} - w\tan^2\alpha]\tan\alpha = -\frac{P_s s}{\mathcal{Q}} \\
&[u'\sec\alpha + \nu sv^{\cdot} + v + w\tan\alpha]\tan\alpha + k[-\frac{3-\nu}{2}s^2u'^{\cdot\cdot}\sec\alpha \\
&\quad - (3+\nu)su^{\cdot\cdot}\sec\alpha + (3-5\nu)u'\sec\alpha - s^3v^{\cdot\cdot\cdot} + \frac{1-\nu}{2}sv'^{\cdot\cdot}\sec^2\alpha \\
&\quad - 6s^2v^{\cdot\cdot} + (2-\nu)v''\sec^2\alpha - 7sv^{\cdot} - v(1-\tan^2\alpha)]\tan\alpha \\
&\quad + k[s^4w^{\cdot\cdot\cdot\cdot} + 2s^2w'^{\cdot\cdot}\sec^2\alpha + w^{IV}\sec^4\alpha + 8s^3w^{\cdot\cdot\cdot} + 4sw'^{\cdot\cdot}\sec^2\alpha \\
&\quad + (11+3\nu)s^2w^{\cdot\cdot} + 2w''\tan^2\alpha\sec^2\alpha - (5-6\nu)w''\sec^2\alpha \\
&\quad - 2(1-3\nu)sw^{\cdot} - w(1-\tan^2\alpha)\tan^2\alpha] = \frac{P_r s}{\mathcal{Q}}
\end{aligned}
\tag{A6}
$$

Consider a segment of cone bounded by $\theta = 0$ and θ_1 and $s = L_1$ and L, $L_1 < L$. For convenience, a nondimensional variable y is introduced such that

$$y = \sqrt{\frac{s}{L}} \tag{A7}$$

Observations of equations (A6), shows that the displacement functions may be assumed in the form:

$$\begin{aligned} u &= A_n y^{\lambda_n - 1} \begin{matrix} \sin \\ \cos \end{matrix} \frac{n\pi\theta}{\theta_1} \\ v &= B_n y^{\lambda_n - 1} \begin{matrix} \cos \\ \sin \end{matrix} \frac{n\pi\theta}{\theta_1} \\ w &= C_n y^{\lambda_n - 1} \begin{matrix} \cos \\ \sin \end{matrix} \frac{n\pi\theta}{\theta_1} \end{aligned} \tag{A8}$$

in which A_n, B_n, C_n and λ_n are constants to be determined.

The upper set of the sinusoidal functions in (A8) is for a complete cone ($\theta_1 = 2\pi$). The lower set is for a segment of cone with two simply supported generator edges so that, along $\theta = 0$ and θ_1 ($< 2\pi$),

$$w = 0, \quad v = 0, \quad N_\theta = 0, \text{ and } M_\theta = 0 \tag{A9}$$

The reactions along the two generator edges are given by

$$S_\theta = Q_\theta + M'_{\theta s} \qquad \text{at } \theta = 0 \text{ and } \theta_1 \tag{A10}$$

S_θ is the transverse shearing force at a section perpendicular to the θ direction. The shearing force Q_θ may be obtained from equations (A4). In what follows the case in which only the lateral normal load appears is considered.[3] Thus

$$P_\theta = P_s = 0$$

and

$$P_r = P_{rn}(y) \begin{matrix} \cos \\ \sin \end{matrix} \frac{n\pi\theta}{\theta_1} \tag{A11}$$

---

[3] When the other loads exist, one may follow a similar procedure and by superposition obtain the appropriate solution.

Substitution of the assumed displacements and loading functions into equations (A6) yields

$$d_{11}A_n + d_{12}B_n + d_{13}C_n = 0$$

$$d_{21}A_n + d_{22}B_n + d_{23}C_n = 0$$

$$d_{31}A_n + d_{32}B_n + d_{33}C_n = \frac{L_P}{\mathcal{Q}} r_n(y)y^3 - \lambda_n \qquad \text{(A12)}$$

where

$$d_{11} = \frac{1 - \nu}{8}(1 + 3k\tan^2\alpha)(9 - \lambda_n^2) + m^2$$

$$d_{12} = \pm\frac{1}{4}[(7 - 5\nu) + (1 + \nu)\lambda_n]m$$

$$d_{13} = \pm[1 + \frac{k}{8}(3(9 - 11\nu) + 8\nu\lambda - (3 - \nu)\lambda_n^2)]m\tan\alpha$$

$$d_{22} = \frac{1}{4}(1 - \lambda_n^2) + (1 - \nu)(1 + \frac{1}{2}m^2) + k\tan^2\alpha(1 + \frac{1 - \nu}{2}m^2)$$

$$d_{23} = \frac{1}{2}\tan\alpha[(2 - \nu) - \nu\lambda_n] \qquad \text{(A13)}$$

$$- \frac{1}{8}k\tan\alpha[(1 - 8\tan^2\alpha + 2(7 - 3\nu)m^2)$$

$$- (3 + 2(1 - \nu)m^2)\lambda_n + 3\lambda_n^2 - \lambda_n^3]$$

$$d_{33} = \tan^2\alpha + \frac{1}{16}k[(13 - 12\nu) - 16(1 - \tan^2\alpha)\tan^2\alpha$$

$$+ 8(11 - 12\nu - 4\tan^2\alpha)m^2 + 16m^4$$

$$- 2(7 - 6\nu + 4m^2)\lambda_n^2 + \lambda_n^4]$$

and

$$m = \frac{n\pi}{\theta_1}\sec\alpha \qquad \text{(A14)}$$

The expressions for d_{21}, d_{31}, d_{32} are obtained by replacing λ_n with $-\lambda_n$ in d_{12}, d_{13}, d_{23}, respectively. The plus and minus signs which appear in front of one term correspond to the upper and lower set of sinusoidal functions henceforth.

In order to have non-trivial homogeneous solutions of the system of equations (A12), the determinant of the coefficients must vanish. This

results in an eighth degree characteristic equation for λ_n. Neglecting the terms of second and higher power of k, as was done in the derivation of the elastic law (A2) yields the characteristic equation in the following form:

$$G[\lambda_n^4 - 10\lambda_n^2 + 9] + k\,[\lambda_n^8 - g_6\lambda_n^6 + g_4\lambda_n^4 - g_2\lambda_n^2 + g_0] = 0 \tag{A15}$$

in which

$$G = 16(1 - \nu^2)\tan^2\alpha$$

$$g_6 = 4(7 - 4\nu) - 8\nu\tan^2\alpha + 16m^2$$

$$\begin{aligned} g_4 = {} & 2[127 - 136\nu + 24\nu^2 \\ & - 4(8 + 3\nu)\tan^2\alpha + 8(4 - 3\nu^2)\tan^4\alpha] \\ & + 16[(17 - 12\nu) - 6\tan^2\alpha]\, m^2 - 96m^4 \end{aligned}$$

$$\begin{aligned} g_2 = {} & 4[203 - 316\nu + 120\nu^2 \\ & - 2(80 - 61\nu)\tan^2\alpha + 40(4 - 3\nu^2)\tan^4\alpha] \\ & + 16[(71 - 72\nu) - 4(13 - 10\nu)\tan^2\alpha \\ & + 8(2 - \nu)\tan^4\alpha]\, m^2 \\ & + 64[(13 - 12\nu) - 2(4 - \nu)\tan^2\alpha]\, m^4 + 256m^6 \end{aligned} \tag{A16}$$

$$\begin{aligned} g_0 = {} & 9[(13 - 12\nu)(5 - 4\nu) - 8(8 - 7\nu)\tan^2\alpha + 16(4 - 3\nu^2)\tan^4\alpha] \\ & + 16[(215 - 412\nu + 192\nu^2) + 2(89 - 172\nu + 96\nu^2)\tan^2\alpha \\ & + 40(2 - \nu)\tan^4\alpha]\, m^2 \\ & - 32[(81 - 184\nu + 96\nu^2) + 4(16 - 13\nu)\tan^2\alpha - 8\tan^4\alpha]\, m^4 \\ & + 256[(3 - 4\nu) - 2\tan^2\alpha]\, m^6 + 256m^8 \end{aligned}$$

In view of the approximation made in the derivation of equation (A15) the following approximate method is suggested for solving this equation. Introducing

$$\lambda_n^2 = X_{no} + kX_{n1} \tag{A17}$$

into equation (A15) results in a sequence of equations associated with the various powers of k. The equations associated with the two lowest

powers of k are

$$X_{no}^2 - 10X_{no} + 9 = 0$$

and

$$X_{no}^4 - g_6X_{no}^3 + g_4X_{no}^2 - g_2X_{no} + g_0 + 2G(X_{no} - 5)X_{n1} = 0$$

from which

$$X_{no} = 1 \text{ and } 9 \tag{A18}$$

$$X_{n1} = -\frac{X_{no}^4 - g_6X_{no}^3 + g_4X_{no}^2 - g_2X_{no} + g_0}{2G(X_{no} - 5)} \tag{A19}$$

Thus, one has two roots of λ_n^2 which are denoted by λ_{n1}^2 and λ_{n2}^2

$$\lambda_{n1}^2 = 1 + k\frac{1 - g_6 + g_4 - g_2 + g_0}{8G}$$

$$\lambda_{n2}^2 = 9 - k\frac{9^4 - 9^3g_6 + 9^2g_4 - 9g_2 + g_0}{8G} \tag{A20}$$

Substituting these roots into equation (A15) yields a quadratic equation in λ_n^2 which gives

$$\lambda_{n3,4}^2 = \frac{1}{2}(g_6 - \lambda_{n2}^2 - \lambda_{n1}^2) \pm i\sqrt{\frac{1}{\lambda_{n1}^2\lambda_{n2}^2}(g_0 + \frac{9G}{k}) - \frac{1}{4}(g_6 - \lambda_{n2}^2 - \lambda_{n1}^2)^2} \tag{A21}$$

Hence the eight roots of λ_n are in two groups of four. One group of four consists of real numbers while the other group of four consists of complex numbers.

The next step is to solve for A_n and B_n in terms of C_n for each root of λ_n from any two of the homogeneous equations (A12). The eight constants C_n shall be determined by eight conditions at $y = \sqrt{\frac{L_1}{L}}$ and 1. The boundary conditions along the generator edges are satisfied by the choice of sinusoidal functions of the angle θ. At the two circular edges one has the following four boundary conditions at each edge.

For a built-in edge:

$$u = 0,\ v = 0,\ w = 0 \text{ and } w^{\cdot} = 0 \tag{A22}$$

For a free edge:

$$N_s = 0,\ M_s = 0,\ S_s = 0 \text{ and } T_s = 0 \tag{A23}$$

where

$$S_s = Q_s + \frac{1}{s} M'_{s\theta} \sec\alpha$$

$$T_s = N_{s\theta} - \frac{M_{s\theta}}{s} \tan\alpha \tag{A24}$$

are the transverse and tangential shearing forces, respectively, acting perpendicular to the s-direction. The shearing force Q_s can be obtained from equations (A4). For a simply supported edge:

$$w = 0, \quad M_s = 0 \quad N_s = 0 \quad \text{or} \quad v = 0$$

and

$$T_s = 0 \quad \text{or} \quad u = 0$$

ASYMPTOTIC SOLUTIONS

As the parameter k approaches zero, the two groups of roots λ_n approach the following asymptotic values:

$$\lambda_{1\ 2} = \pm 1, \qquad \lambda_{3\ 4} = \pm 3 \tag{A26}$$

$$\lambda_{5\ 6} = \rho(1 \pm i), \qquad \lambda_{7\ 8} = -\rho(1 \pm i) \tag{A27}$$

where

$$\rho \equiv \left| \frac{\sqrt{2}}{2} \left(\frac{G}{k}\right)^{\frac{1}{4}} \right| \tag{A28}$$

The subscript n has been and henceforth will be dropped for simplicity.

When the first group of λ, λ_i, (i = 1, 2, 3, and 4) is substituted into the first two equations of (A12) to eliminate A_i and B_i, and only the leading terms are retained, the solutions (A8) assume the following form:

$$u^I = \mp m\tan\alpha \left\{ \frac{C_1}{m^2 - 1} + \frac{C_2}{m^2 - 2(1-\nu)} \frac{1}{y^2} + \frac{C_3}{m^2} y^2 + \frac{4 + 4\nu - m^2}{m^2(7 - 2\nu - m^2)} \frac{C_4}{y^4} \right\} \begin{matrix} \sin \\ \cos \end{matrix} \frac{n\pi\theta}{\theta_1}$$

$$v^I = \tan\alpha \left\{ \frac{C_1}{m^2 - 1} + \frac{2C_2}{m^2 - 2(1-\nu)} \frac{1}{y^2} + \frac{3C_4}{m^2 - 7 + 2\nu} \frac{1}{y^4} \right\} \begin{matrix} \cos \\ \sin \end{matrix} \frac{n\pi\theta}{\theta_1} \qquad \text{(A29)}$$

$$w^I = \left\{ C_1 + C_2 y^{-2} + C_3 y^2 + C_4 y^{-4} \right\} \begin{matrix} \cos \\ \sin \end{matrix} \frac{n\pi\theta}{\theta_1}$$

When the second group of λ, λ_j, (j = 5, 6, 7, and 8) is used, following a similar procedure, and using some identities to convert the complex expressions into real expressions, the solutions are as follows:

$$u^{II} = \mp 2(2 + \nu) m\tan\alpha \frac{1}{\rho^2} y^{-1} \left\{ y^{\rho}[C_6 \cos(\rho \ell n y) - C_5 \sin(\rho \ell n y)] - y^{-\rho}[C_8 \cos(\rho \ell n y) - C_7 \sin(\rho \ell n y)] \right\} \begin{matrix} \sin \\ \cos \end{matrix} \frac{n\pi\theta}{\theta_1}$$

$$v^{II} = -\nu \tan\alpha \frac{1}{\rho} y^{-1} \left\{ y^{\rho}[(C_5 - C_6)\cos(\rho \ell n y) + (C_5 + C_6)\sin(\rho \ell n y)] - y^{-\rho}[(C_7 + C_8)\cos(\rho \ell n y) - (C_7 - C_8)\sin(\rho \ell n y)] \right\} \begin{matrix} \cos \\ \sin \end{matrix} \frac{n\pi\theta}{\theta_1} \qquad \text{(A30)}$$

$$w^{II} = y^{-1} \left\{ y^{\rho}[C_5 \cos(\rho \ell n y) + C_6 \sin(\rho \ell n y)] + y^{-\rho}[C_7 \cos(\rho \ell n y) + C_8 \sin(\rho \ell n y)] \right\} \begin{matrix} \cos \\ \sin \end{matrix} \frac{n\pi\theta}{\theta_1}$$

It is noted that the solutions of the first group correspond to those of membrane theory.

Based on the solutions (A29) and (A30), one may establish the orders of magnitude of the displacement components[4] as:

---

[4] It is assumed that the parameter m defined by (A14) is limited to small values such that differentiation with respect to θ does not affect the order of magnitude.

$$u^I,\ v^I,\ w^I,\ w^{II} = 0\ (\tfrac{1}{\rho 0})$$

$$v^{II} = 0\ (\tfrac{1}{\rho}) \quad \text{and} \quad u^{II} = 0\ (\tfrac{1}{\rho^2}) \tag{A31}$$

Due to u^I, v^I and w^I, the magnitudes of the corresponding stresses N_s^I, N_θ^I and $N_{\theta s}^I$ obtained by use of relations (A2) are also of the order of $(\frac{1}{\rho 0})$ and the moments are of the order of $(\frac{1}{\rho 3})$ and higher. The order properties of the stresses due to u^{II}, v^{II} and w^{II} are not as obvious and will be examined further in the discussion that follows.

Changing the variable s to y according to (A7) and then to η such that

$$y = \eta^{1/\rho} \tag{A32}$$

and neglecting the terms which are of the order of $\frac{1}{\rho 3}$ and higher, the stress-displacement relations (A2) assume the following form:

$$N_s = \mathcal{Q}[\tfrac{1}{2}\rho\eta v_{,\eta} + \nu(u_{,\theta}\sec\alpha + v + w\tan\alpha)]$$

$$N_\theta = \mathcal{Q}[(u_{,\theta}\sec\alpha + v + w\tan\alpha) + \tfrac{1}{2}\nu\rho\eta v_{,\eta}]$$

$$N_{\theta s} = N_{s\theta} = \mathcal{Q}\tfrac{1-\nu}{2}[\tfrac{1}{2}\rho\eta u_{,\eta} - u + v_{,\theta}\sec\alpha]$$

$$M_s = \mathcal{Q}kL\left\{\tfrac{1}{4}\rho^2[\eta^2 w_{,\eta\eta} + (1 - \tfrac{1}{\rho})\eta w_{,\eta}] - \tfrac{1}{4}\rho\eta w_{,\eta} - \tfrac{1}{2}\rho\eta v_{,\eta}\tan\alpha\right.$$
$$\left. + \nu(w_{,\theta\theta}\sec^2\alpha + \tfrac{1}{2}\rho\eta w_{,\eta} - u_{,\theta}\sec\alpha\tan\alpha)\right\} \tag{A33}$$

$$M_\theta = \mathcal{Q}kL[w_{,\theta\theta}\sec^2\alpha + \tfrac{1}{2}\rho\eta w_{,\eta} + w\tan^2\alpha + v\tan\alpha$$
$$+ \tfrac{\nu}{4}\left\{\rho^2[\eta^2 w_{,\eta\eta} + (1 - \tfrac{1}{\rho})\eta w_{,\eta}] - \rho\eta w_{,\eta}\right\}]$$

$$M_{s\theta} = \mathcal{Q}k(1-\nu)L[\tfrac{1}{2}\rho\eta w_{,\eta\theta}\sec\alpha - w_{,\theta}\sec\alpha - \tfrac{1}{2}\rho\eta u_{,\eta}\tan\alpha$$
$$+ u\tan\alpha]$$

$$M_{\theta s} = \mathcal{Q}kL(1-\nu)[\tfrac{1}{2}\rho\eta w_{,\eta\theta}\sec\alpha - w_{,\theta}\sec\alpha - \tfrac{1}{4}\rho\eta u_{,\eta}\tan\alpha$$
$$+ \tfrac{1}{2}u\tan\alpha + \tfrac{1}{2}v_{,\theta}\tan\alpha\sec\alpha]$$

where a subscript preceded by a comma represents the appropriate derivative.

When the displacements

$$u = u^{II} = \frac{1}{\rho^2} U$$
$$v = v^{II} = \frac{1}{\rho} V \qquad (A34)$$
$$w = w^{II} = W$$

are substituted into relationships (A33) and only the terms with the lowest order of $(\frac{1}{\rho})$ are retained, the following relationships are obtained:

$$N_s^{II} = \mathcal{Q}[\frac{1}{2}\eta V_{,\eta} + \nu W \tan\alpha]$$
$$N_\theta^{II} = \mathcal{Q}[W \tan\alpha + \frac{1}{2}\nu\eta V_{,\eta}]$$
$$N_{s\theta}^{II} = N_{\theta s}^{II} = \mathcal{Q}\frac{1-\nu}{2}\frac{1}{\rho}[\frac{1}{2}\eta U_{,\eta} + V_{,\theta}\sec\alpha]$$
$$M_s^{II} = \mathcal{Q}L(1-\nu^2)\tan^2\alpha\frac{1}{\rho^2}[\eta^2 W_{,\eta\eta} + \eta W_{,\eta}] \qquad (A35)$$
$$M_\theta^{II} = \nu M_s^{II}$$
$$M_{s\theta}^{II} = \mathcal{Q}2L(1-\nu)\tan^2\alpha\frac{1}{\rho^3}\eta W_{,\theta\eta}\sec\alpha$$

in which the relation

$$k = \frac{4}{\rho^4}(1-\nu^2)\tan^2\alpha \qquad (A36)$$

obtained from expression (A28) has been used.

Note that the normal stresses, N_s^{II} and N_θ^{II}, are of the same order as that of N_s^{I} and N_θ^{I}. It can be shown, however, that N_θ^{I} and N_s^{II} vanish identically. When only the terms of the lowest order of $(\frac{1}{\rho})$ are retained, one has

$$u = u^{I}, \qquad v = v^{I}, \qquad w = w^{I} + w^{II}$$

$$N_s = N_s^{I}, \quad N_\theta = N_\theta^{II}, \quad N_{s\theta} = N_{\theta s} = N_{s\theta}^{I} \tag{A37}$$

$$M_s = M_s^{II}, \quad M_\theta = M_\theta^{II}, \quad M_{s\theta} = M_{\theta s} = M_{s\theta}^{II}$$

By a similar comparison of order properties, one can show that the transverse and tangential shearing forces defined by equations (A10) and (A24) are

$$S_\theta = S_\theta^{II}, \qquad S_s = S_s^{II}, \qquad T_s = T_s^{I} = N_{s\theta}^{I} \tag{A38}$$

Thus, in the two sets of solutions, the membrane and bending effects are coupled by the lateral deflection w and are not separable.

Using equations (A37), (A38) and (A34) with the solutions (A29) and (A30), the stresses and moments may be given in the following final explicit form:

$$N_s = -2E\delta \tan\alpha \left[\frac{C_2}{m^2 - 2(1-\nu)} y^{-2} + \frac{3C_4}{m^2 - 7 + 2\nu} y^{-4}\right] \begin{matrix}\cos \\ \sin\end{matrix} \frac{n\pi\theta}{\theta_1}$$

$$N_\theta = E\delta y^{-1} \tan\alpha \Big\{ y^{\rho}[C_5 \cos(\rho \ell n y) + C_6 \sin(\rho \ell n y)]$$

$$+ y^{-\rho}[C_7 \cos(\rho \ell n y) + C_8 \sin(\rho \ell n y)] \Big\} \begin{matrix}\cos \\ \sin\end{matrix} \frac{n\pi\theta}{\theta_1}$$

$$N_{s\theta} = T_s = \mp E\delta \left\{ \frac{6\tan\alpha}{m(m^2 - 7 + 2\nu)} C_4 y^{-4} \right\} \begin{matrix}\sin \\ \cos\end{matrix} \frac{n\pi\theta}{\theta_1}$$

$$M_s = \frac{2E\delta}{\rho^2} \tan^2\alpha \, Ly \Big\{ y^{\rho}[C_6 \cos(\rho \ell n y) - C_5 \sin(\rho \ell n y)]$$

$$+ y^{-\rho}[-C_8 \cos(\rho \ell n y) + C_7 \sin(\rho \ell n y)] \Big\} \begin{matrix}\cos \\ \sin\end{matrix} \frac{n\pi\theta}{\theta_1}$$

$$M_\theta = \nu M_s$$

$$S_\theta = \mp \frac{2E\delta}{\rho^2} m(2 - \nu) \tan^2\alpha \, y^{-1} \Big\{ y^{\rho}[C_6 \cos(\rho \ell n y) - C_5 \sin(\rho \ell n y)]$$

$$+ y^{-\rho}[-C_8 \cos(\rho \ell n y) + C_7 \sin(\rho \ell n y)] \Big\} \begin{matrix}\sin \\ \cos\end{matrix} \frac{n\pi\theta}{\theta_1} \tag{A39}$$

$$S_s = \frac{E\delta}{\rho} \tan^2\alpha y^{-1} \left\{ y^{\rho}[(-C_5 + C_6)\cos(\rho\ell ny) - (C_5 + C_6)\sin(\rho\ell ny)] \right.$$

$$\left. + y^{-\rho}[(C_7 + C_8)\cos(\rho\ell ny) - (C_7 - C_8)\sin(\rho\ell ny)] \right\} \begin{matrix}\cos \\ \sin\end{matrix} \frac{n\pi\theta}{\theta_1}$$

and

$$\frac{\partial w}{\partial s} = \frac{\partial w^{II}}{\partial s}$$

$$= \frac{1}{2L}\rho y^{-3} \left\{ y^{\rho}[(C_5 + C_6)\cos(\rho\ell ny) - (C_5 - C_6)\sin(\rho\ell ny)] \right.$$

$$\left. -y^{-\rho}[(C_7 - C_8)\cos(\rho\ell ny) + (C_7 + C_8)\sin(\rho\ell ny)] \right\} \begin{matrix}\cos \\ \sin\end{matrix} \frac{n\pi\theta}{\theta_1}$$

PARTICULAR SOLUTIONS DUE TO LATERAL NORMAL LOADS

Let the lateral normal load given by (A11) be expressed in the form

$$P_{rn}(y) = a_n L^{\beta} y^{2\beta} \tag{A40}$$

i.e.

$$P_{rn}(s) = a_n s^{\beta}$$

where a_n and β are prescribed.

One may assume a set of particular solutions in a form similar to expressions (A8) except that in this case λ_n shall be replaced by

$$\lambda^* = 2\beta + 3 \tag{A41}$$

a known number. The particular solutions are readily obtained by solving simultaneously the three algebraic equations (A12) provided that λ^* is not one of the roots of the determinant. However, in one of the most common loadings, the load is uniformly distributed along meridians so that $\beta = 0$. Hence $\lambda^* = 3$ which is one of the roots for the asymptotic case. In this case, the approach must be modified. In what follows the particular solution due to this type of uniform load is given.

Since in this case λ^* is a finite constant when the parameter k approaches zero, the corresponding particular solution may be obtained

from the equations of membrane theory for the system.

Setting $k = 0$ and transforming the independent variable s to y, equations (A6) reduce to the following equations of equilibrium from membrane theory for a lateral load P_r:

$$\begin{aligned}
&\frac{1-\nu}{8}[y^2u_{,yy} + 3yu_{,y} - 8u] + \frac{1+\nu}{4}yu_{,\theta y}\sec\alpha + u_{,\theta\theta}\sec^2\alpha \\
&\quad + (2-\nu)v_{,\theta}\sec\alpha + w_{,\theta}\sec\alpha\tan\alpha = 0 \\
&\frac{1+\nu}{8}yu_{,\theta y}\sec\alpha - \frac{3}{2}(1-\nu)u_{,\theta}\sec\alpha + \frac{1}{4}y^2v_{,yy} + \frac{3}{4}yv_{,y} \\
&\quad + \frac{1-\nu}{2}v_{,\theta\theta}\sec^2\alpha - (1-\nu)v + \frac{1}{2}\nu yw_{,y}\tan\alpha - (1-\nu)w\tan\alpha = 0 \\
&u_{,\theta}\sec\alpha + \frac{1}{2}\nu yv_{,y} + v + w\tan\alpha = \frac{L}{\ell\tan\alpha}P_r y^2
\end{aligned} \tag{A42}$$

where

$$P_r = a_n \begin{matrix}\cos\\ \sin\end{matrix} \frac{n\pi\theta}{\theta_1} \tag{A43}$$

Let the particular solutions of equations (A42) be assumed as follows:

$$\begin{aligned}
u^P &= \bar{+}(d_1 + d_2\ell ny)y^2 \begin{matrix}\sin\\ \cos\end{matrix} \frac{n\pi\theta}{\theta_1} \\
v^P &= (b_1 + b_2\ell ny)y^2 \begin{matrix}\cos\\ \sin\end{matrix} \frac{n\pi\theta}{\theta_1} \\
w^P &= e_1(1 + \ell ny)y^2 \begin{matrix}\cos\\ \sin\end{matrix} \frac{n\pi\theta}{\theta_1}
\end{aligned} \tag{A44}$$

in which d_1, d_2, b_1, b_2 and e_1 are constants to be determined. When these assumed solutions are substituted into equations (A42) and the sinusoidal functions and y^2 are cancelled, the three equations are in the following form:

$$f_\phi \ell ny + h_\phi = \frac{a_n}{\tan\alpha}\frac{L}{\ell}\delta_{\phi 3} \tag{A45}$$

where the subscript φ ($\varphi = 1, 2, 3$) indicates the three equations of (A42) respectively, f_φ and h_φ are expressions of the physical constants that are to be determined, and $\delta_{\phi 3}$ is the Kronecker delta.

By equating the coefficients of both sides of equations (A45), two sets of algebraic equations are obtained. Each set contains three equations of the form

$$f_\phi = 0 \tag{A46}$$

$$h_\phi = \frac{a_n}{\tan\alpha}\frac{L}{\ell}\delta_{\phi 3} \tag{A47}$$

There are, however, only two of equations (A46) that are independent because $\lambda^* = 3$ is one of the roots of the determinant. Thus the five constants may be determined by the five independent equations of (A46) and (A47). The results are:

$$\begin{aligned}
u^P &= \mp \frac{a_n}{\tan\alpha}\frac{L}{E\delta}\frac{m}{3}\left\{\frac{1}{2m^2}\left[2m^4 - 3(5-\nu)m^2 - 3(1+\nu)\right]\right. \\
&\qquad \left. + (m^2 - 7 + 2\nu)\ell ny\right\} y^2 \begin{matrix}\sin \\ \cos\end{matrix} \frac{n\pi\theta}{\theta_1} \\
v^P &= \frac{a_n}{\tan\alpha}\frac{L}{E\delta}\frac{1}{6}\left[3(1-2\nu) - m^2\right] y^2 \begin{matrix}\cos \\ \sin\end{matrix} \frac{n\pi\theta}{\theta_1} \\
w^P &= \frac{a_n}{\tan^2\alpha}\frac{L}{E\delta}\frac{1}{3} m^2[m^2 - 7 + 2\nu](1 + \ell ny) \begin{matrix}\cos \\ \sin\end{matrix} y^2 \frac{n\pi\theta}{\theta_1}
\end{aligned} \tag{A48}$$

When these displacements are substituted into the expressions (A2) with $k = 0$ the corresponding stresses are

$$\begin{aligned}
N_s^P &= \frac{a_n L}{\tan\alpha}\left\{\frac{1}{6}(3 - m^2)y^2\right\} \begin{matrix}\cos \\ \sin\end{matrix} \frac{n\pi\theta}{\theta_1} \\
N_\theta^P &= \frac{a_n L}{\tan\alpha}\left[y^2\right] \begin{matrix}\cos \\ \sin\end{matrix} \frac{n\pi\theta}{\theta_1} \\
N_{s\theta}^P &= \mp \frac{a_n L}{\tan\alpha}\left[\frac{m}{3} y^2\right] \begin{matrix}\sin \\ \cos\end{matrix} \frac{n\pi\theta}{\theta_1}
\end{aligned} \tag{A49}$$

These particular solutions combined with those given by solutions (A29), (A30) and (A39) constitute the complete solutions.

NUMERICAL EXAMPLE

For the purpose of illustration, consider a truncated semicircular cone with the two generators simply supported. The lower set of solutions (A29), (A30), (A39), (A48) and (A49) apply in this case. Let the cone be clamped at the smaller end where $s = L_1$ and free at the other end where $s = L$ so that

$$\begin{aligned} u = v = w = \frac{\partial w}{\partial s} = 0 \qquad & \text{at} \quad y = \sqrt{\frac{L_1}{L}} \\ N_s = T_s = M_s = S_s = 0 \qquad & \text{at } y = 1 \end{aligned} \tag{A50}$$

By making use of the first two in each of the preceding two sets of boundary conditions, the constants C_1, C_2, C_3 and C_4 can be determined. The other four constants can then be determined by the remaining four boundary conditions.

The lateral normal loads are also known as wind loads. Usually there are two types of such loads: symmetrical and non-symmetrical. Since the asymptotic solutions are valid only for small values of n, only the two cases of $n = 1$ and $n = 2$ are considered.

Let

$$\begin{aligned} a_n &= p \qquad && \text{for} \quad n = 1 \\ &= 0 \qquad && \text{for} \quad n > 1 \end{aligned} \tag{A51}$$

so that

$$P_r = p \sin\theta$$

represents a symmetrical load. For

$$\begin{aligned} a_n &= \frac{4}{9}\sqrt{3}\, p \qquad && \text{for } n = 1 \\ &= \frac{2}{9}\sqrt{3}\, p \qquad && \text{for } n = 2 \\ &= 0 \qquad && \text{for } n > 2 \end{aligned}$$

so that

$$P_r = \frac{4}{9}\sqrt{3}\, p(\sin\theta + \frac{1}{2}\sin 2\theta) \tag{A52}$$

represents a non-symmetrical load. These two types of loads are shown in Figure A1.

For the numerical computations, the following values were assumed:

$$\alpha = 75^{o}, \qquad \nu = \frac{1}{3}, \qquad \sqrt{\frac{L_1}{L}} = 0.90 \tag{A53}$$

Considering $\frac{t}{R}$ as a parameter where R is the principal radius at a section of thickness t, $\delta = \frac{t}{R}\cos\alpha$. The eight roots of λ computed from expressions (A20), (A21) (A26), and (A27) are listed in Table A1. Comparison of the values of the roots for $n = 1$ and $n = 2$ with the asymptotic values shows that, for this case, the asymptotic results are satisfactory for practical use.

The asymptotic solutions for displacements, stresses and moments computed from expressions (A29), (A30) and (A39) combined with (A48) and (A49) may be given in the form:

$$F_n(y,\theta) = f_n(y) \begin{matrix}\sin \\ \cos\end{matrix} \frac{n\pi\theta}{\theta_1} \quad \text{for} \quad n = 1 \text{ and } 2 \tag{A54}$$

The function $f_n(y)$ is plotted in Figures A2 through A11.

CLOSING REMARKS

There are a number of approaches available for obtaining solutions for shells of revolution. Kalnins [A2] obtained a solution by treating the system of equations as a series of initial-value problems and included a comprehensive bibliography. Conical shells subjected to edge loads were studied by Clark and Garibotti [A3] by using the edge effect approach.

The solutions presented in this appendix are in explicit form and are readily used for practical purposes. The asymptotic solutions are

exact and applicable to conical shells if

$$\left[\frac{1}{12}\left(\frac{t}{R}\cos\alpha\right)^2\right]^{\frac{1}{4}} \ll 1.$$

When the above parameter is very small the symptotic solutions may be useful for conical shells of both linearly varying thickness and constant thickness.

In the numerical example, the bending effects diminish rapidly as the distance from the clamped edge increases. This is known as the edge effect or boundary layer phenomenon. The moments and shearing forces due to the bending effect are of higher order than the membrane stresses. However, the membrane stress N_θ induced by the bending effect is of the same order as the other membrane stresses. Therefore, solutions obtained by the membrane theory alone not only are incompatiable but also contain some errors that are not negligible for the membrane stress N_θ.

The deflection, particularly the normal component at the free end, in the given example is large compared to the thickness. For such a large displacement, the theory is applicable provided that the shell is not overstrained [4] . Thus the strain at the fixed end controls the validity of the results.

ACKNOWLEDGEMENT

The author wishes to thank M. H. Y. Chu for his assistance in programing the numerical computations.

REFERENCES

A1. Flugge, W.: Stresses in Shells. Second printing, Springer-Verlag, (Berlin), 1962.

A2. Kalnins, A.: Analysis of Shells of Revolution Subjected to Symmetrical and Nonsymmetrical Loads. Journal of Applied Mechanics, vol. 31, Trans. ASME, vol. 86. Series E, 1964, pp. 467-476.

A3. Clark, R. A. and Garibotti, J. F.: Longitudinal Bending of a Conical Shell. Presented at the 9th Midwestern Mechanics Conference, Cleveland, Ohio, April 1963.

A4. Love, A. E. H.: Mathematical Theory of Elasticity. Fourth Ed., Cambridge University Press, Cambridge, 1927, p. 553.

λ	$\frac{t}{R}$	n = 1	n = 2	Asymptotic Values
$\lambda_{1\,2}$	0.004	$\pm$0.999999	$\pm$1.0523	$\pm$1
	0.006	$\pm$0.999997	$\pm$1.1142	$\pm$1
	0.008	$\pm$0.999995	$\pm$1.1955	$\pm$1
$\lambda_{3\,4}$	0.004	$\pm$3.00003	$\pm$2.9851	$\pm$3
	0.006	$\pm$3.00007	$\pm$2.9663	$\pm$3
	0.008	$\pm$3.00013	$\pm$2.9397	$\pm$3
λ_{57} λ_{68}	0.004	$\pm$153.27(1.0027$\pm$i)	$\pm$152.75(1.0099$\pm$i)	$\pm$153.48(1$\pm$i)
	0.006	$\pm$125.09(1.0035$\pm$i)	$\pm$124.51(1.0149$\pm$i)	$\pm$125.32(1$\pm$i)
	0.008	$\pm$108.28(1.0045$\pm$i)	$\pm$107.77(1.0198$\pm$i)	$\pm$108.53(1$\pm$i)

TABLE A1. - VALUES OF λ

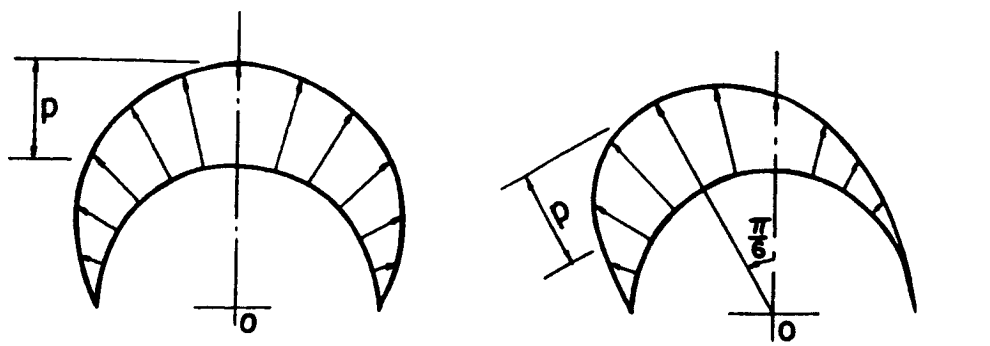

FIGURE A1. - LOAD CONFIGURATIONS.

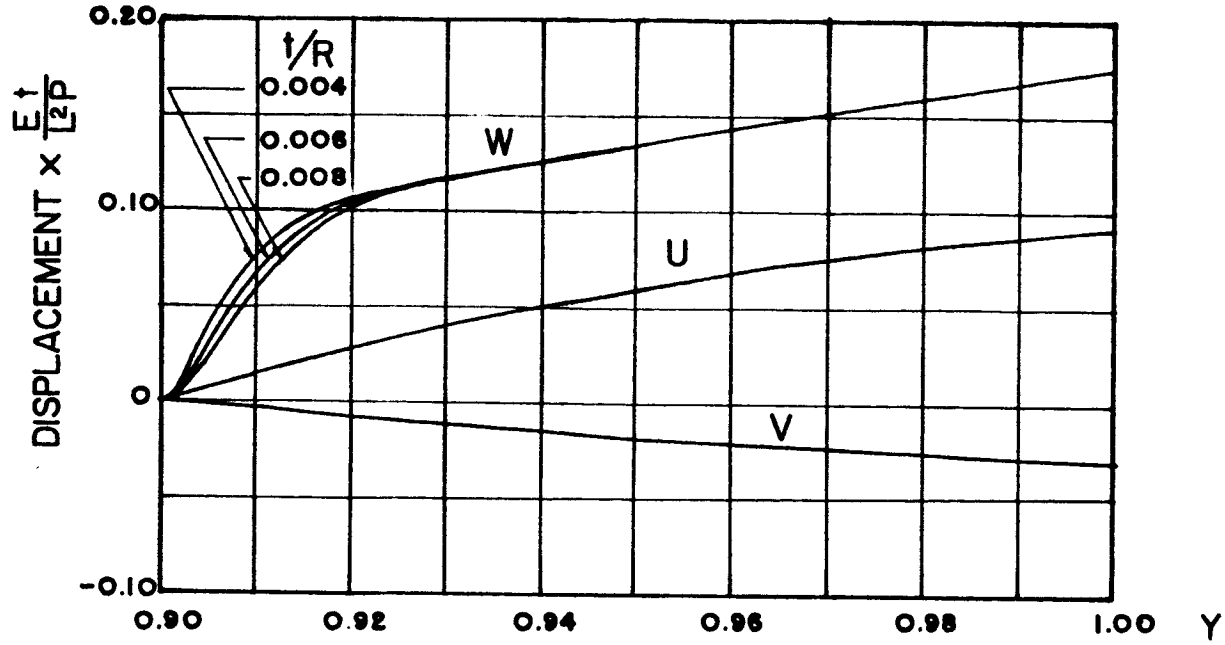

FIGURE A2. - DISPLACEMENTS U, V AND W FOR N = 1.

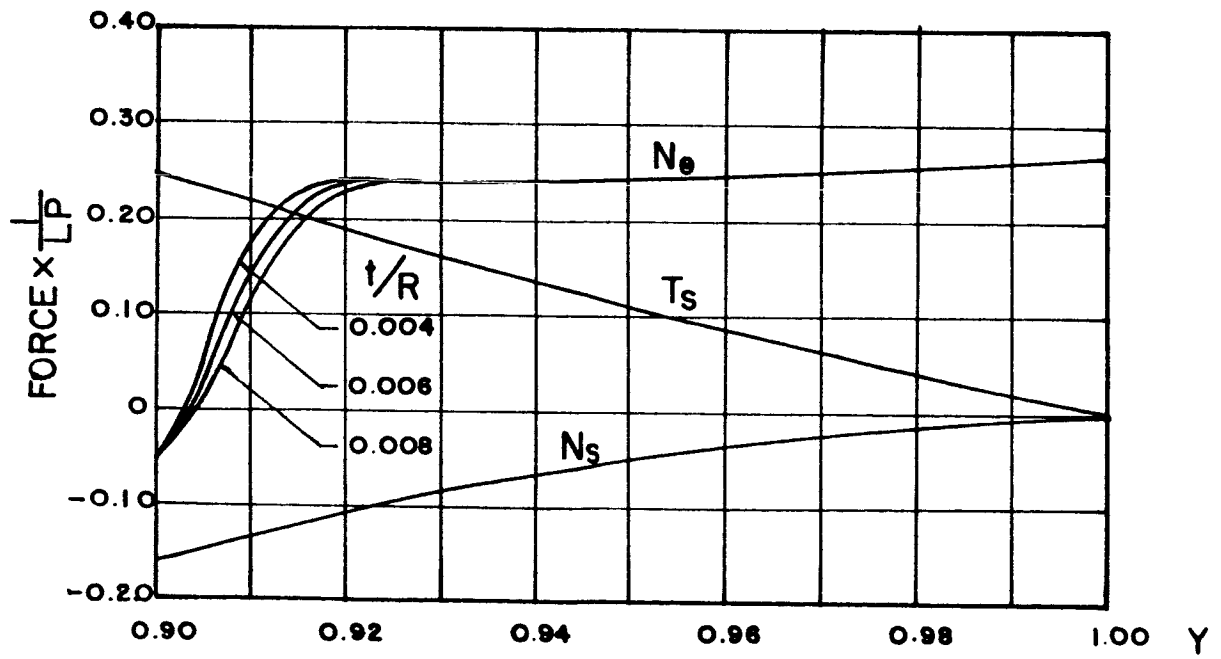

FIGURE A3. - MEMBRANE FORCES N_θ, T_s AND N_s FOR N = 1.

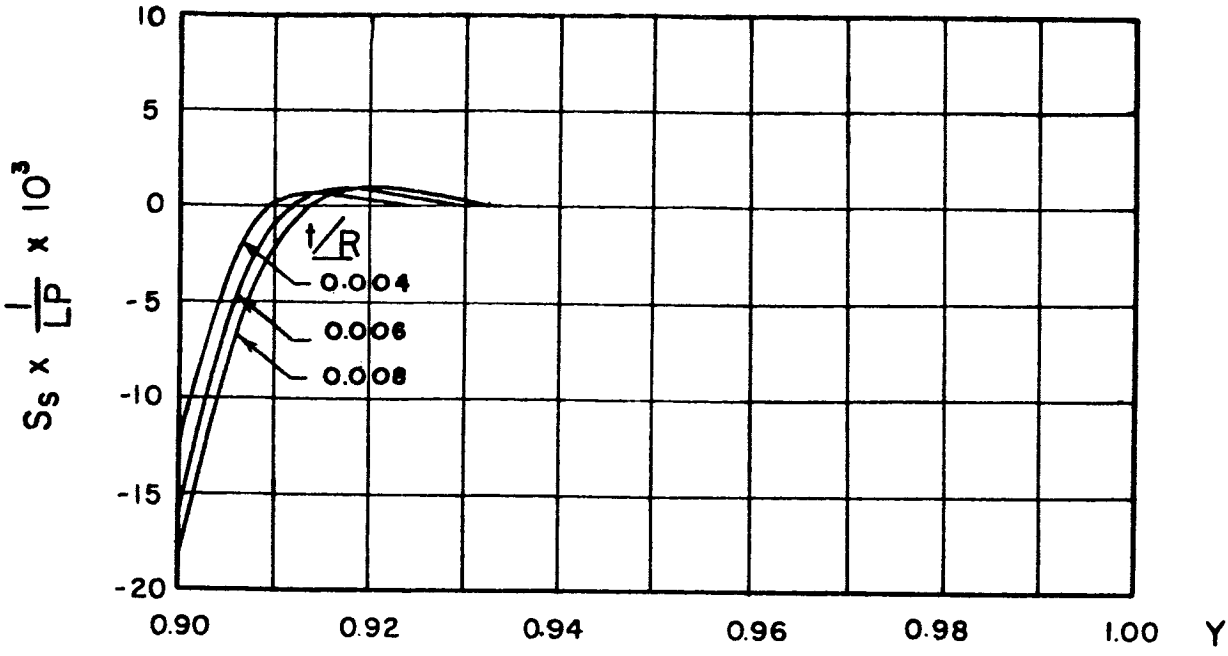

FIGURE A4. - TRANSVERSE SHEARING FORCE S_s FOR N = 1.

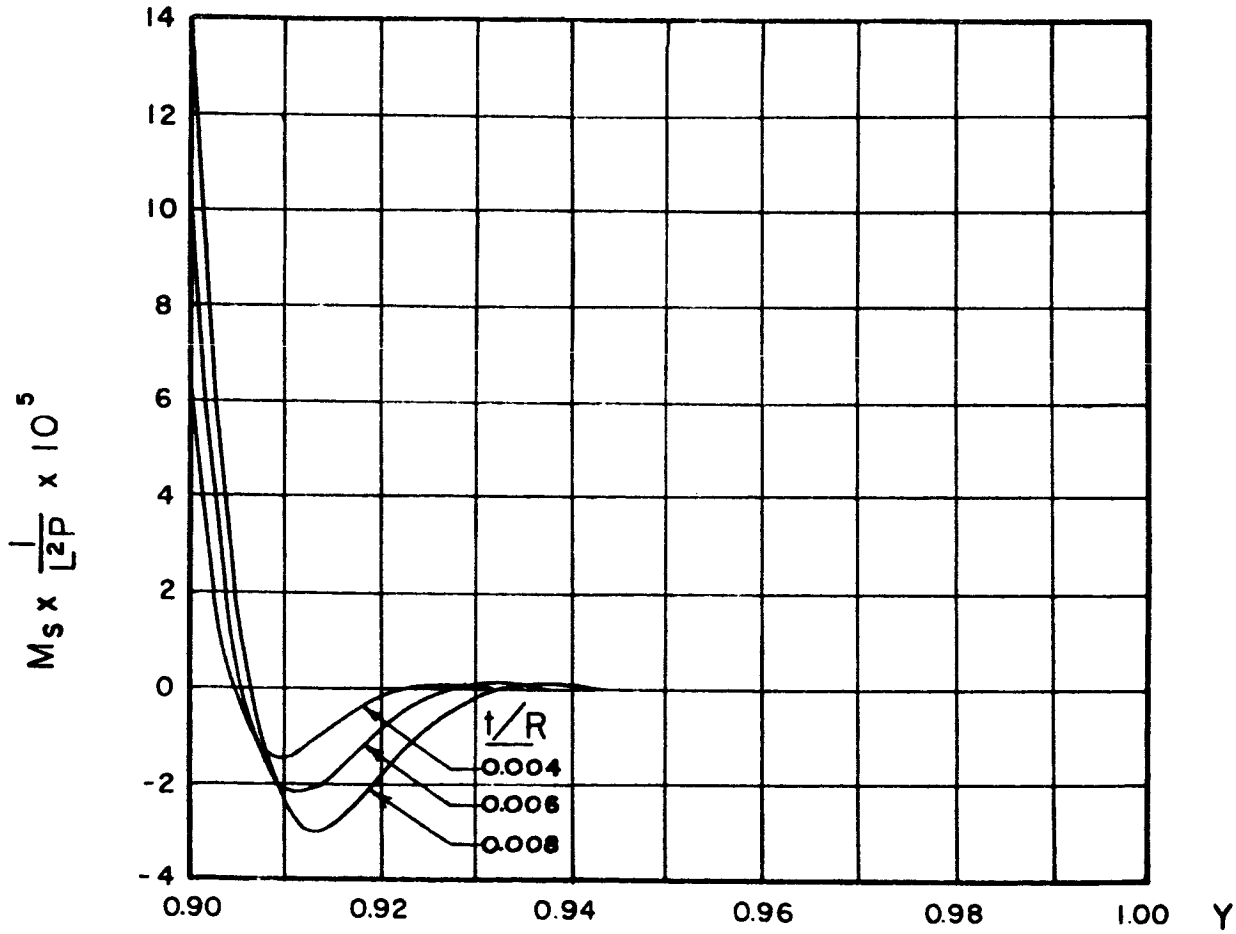

FIGURE A5. - NORMAL MOMENT M_s FOR N = 1.

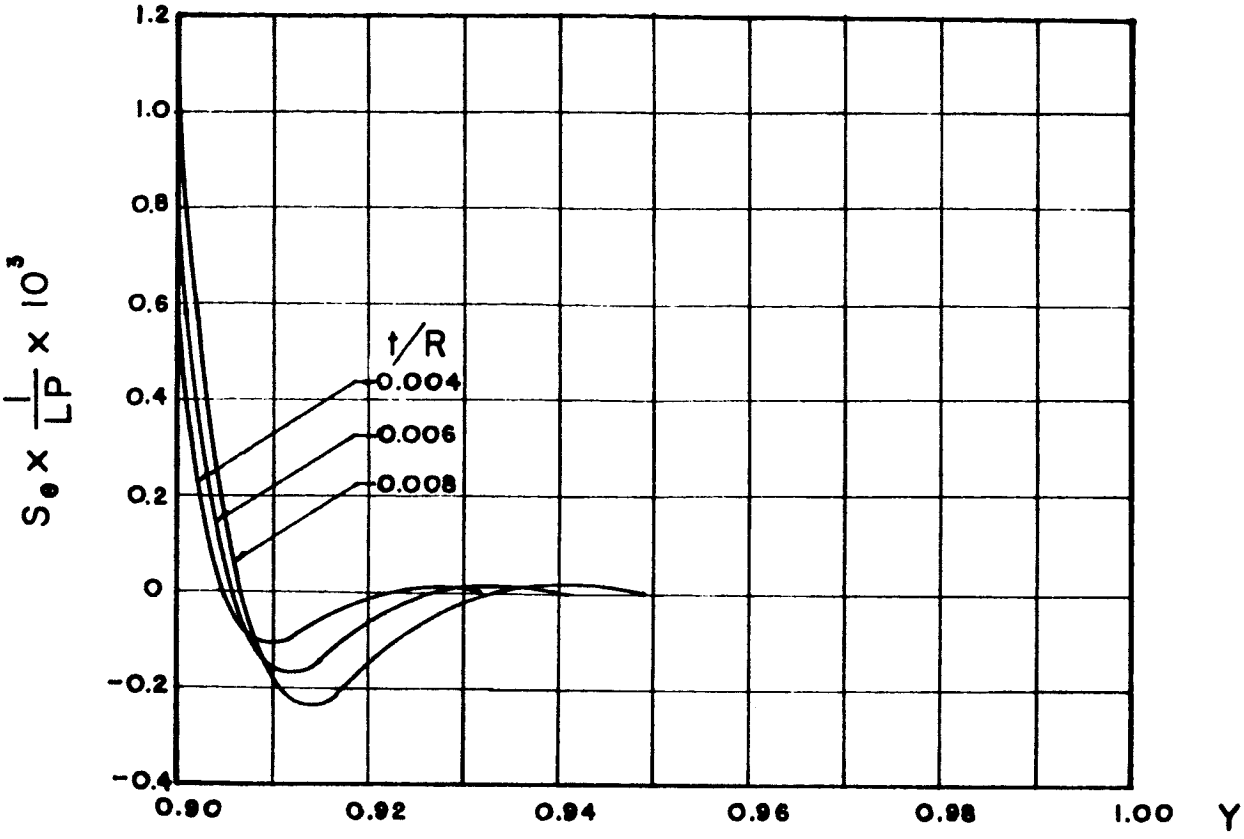

FIGURE A6. - TRANSVERSE SHEARING FORCE S_θ FOR N = 1.

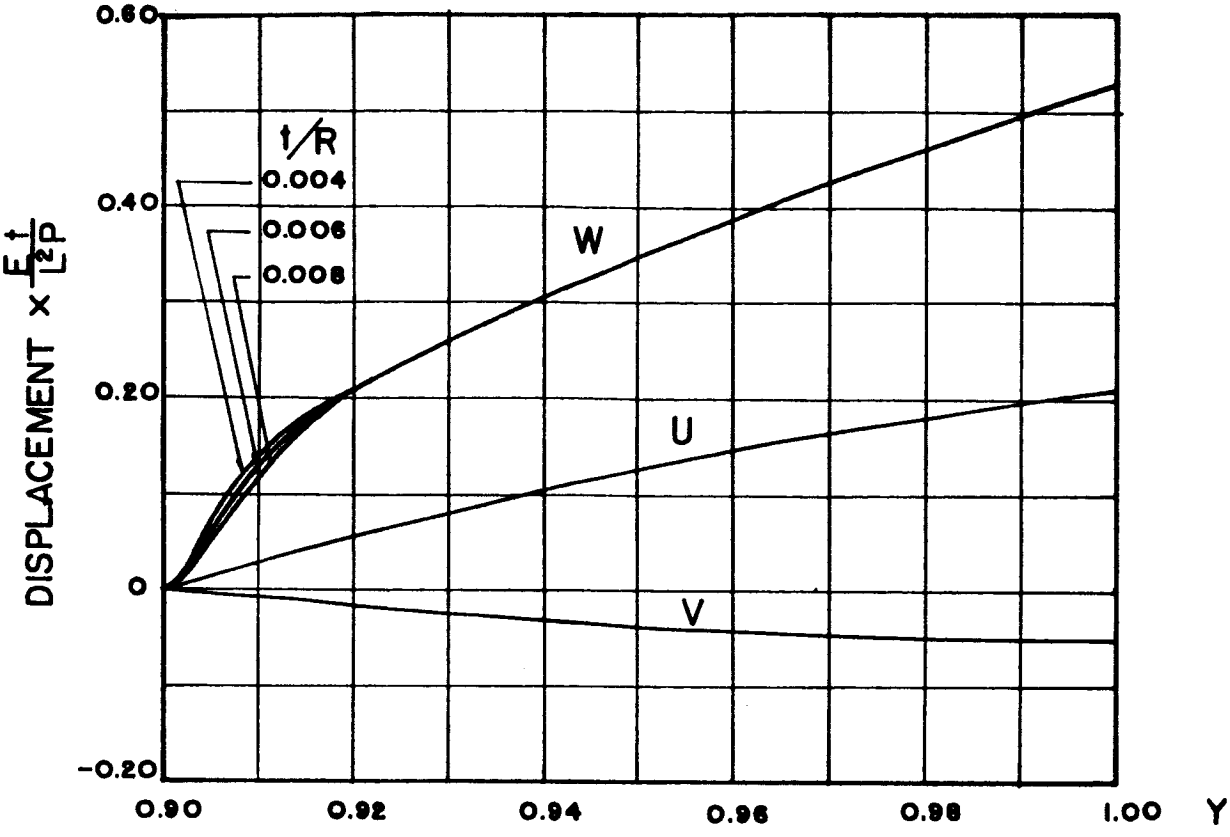

FIGURE A7. - DISPLACEMENTS U, V, AND W FOR N = 2.

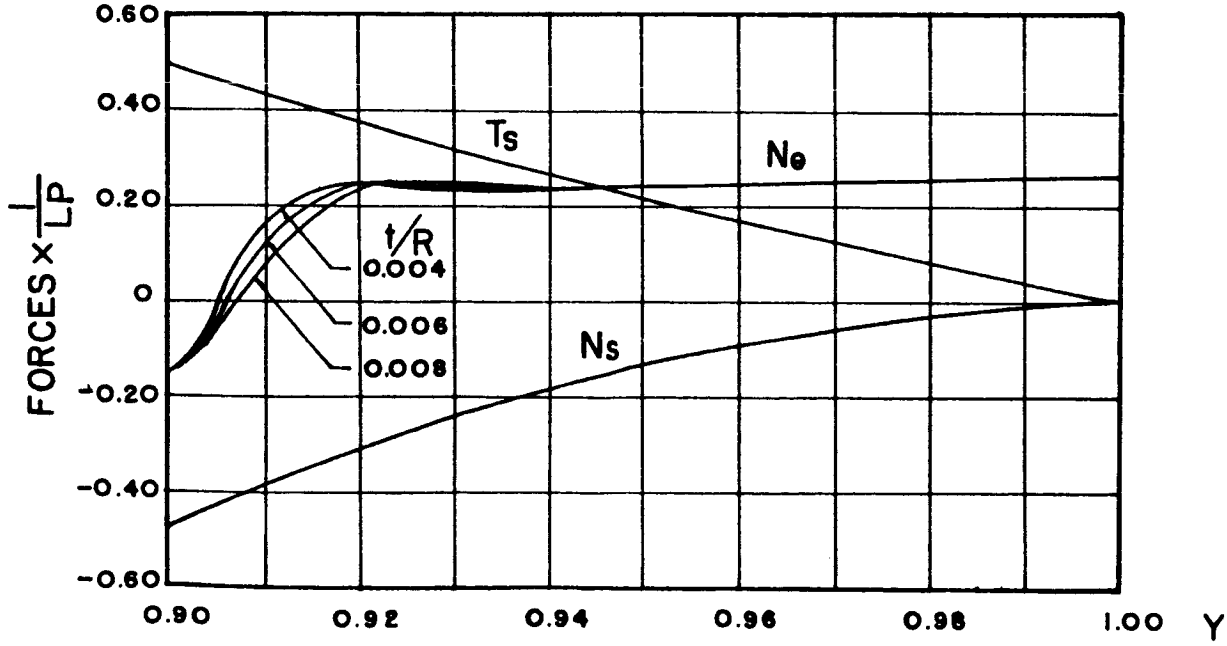

FIGURE A8. - MEMBRANE FORCES N_θ, T_s AND N_s FOR N = 2.

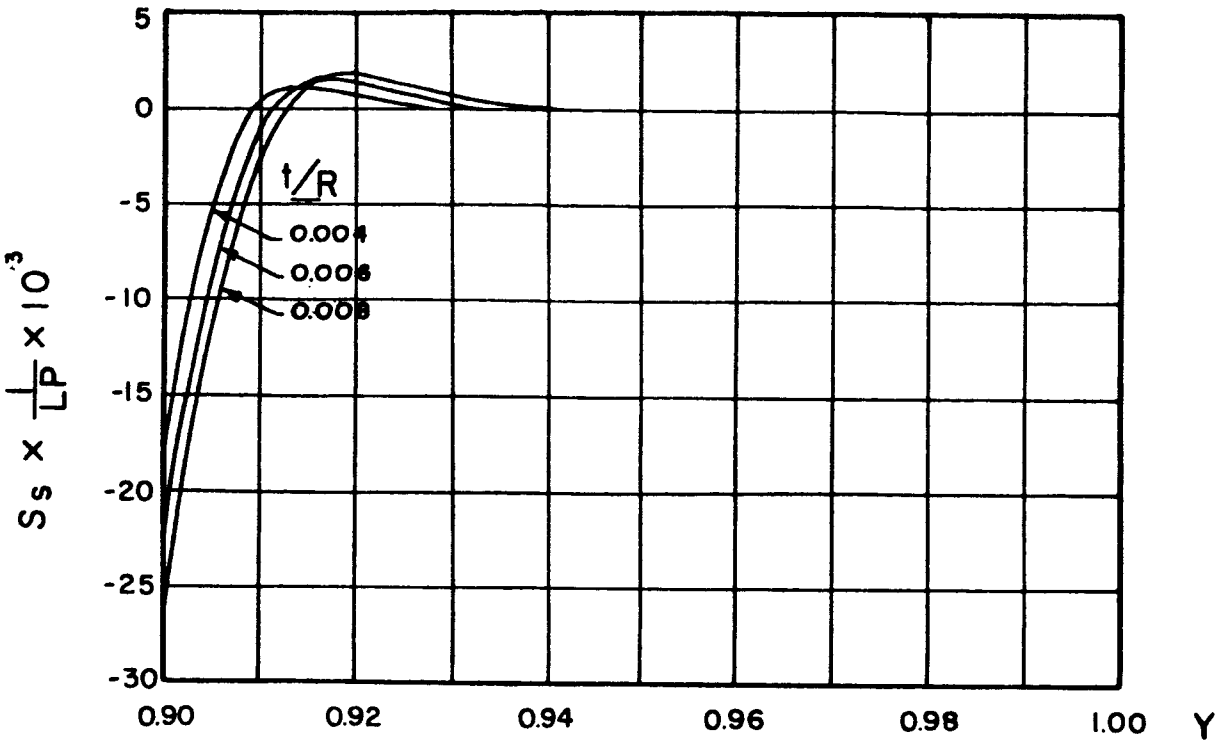

FIGURE A9. - TRANSVERSE SHEARING FORCE S_s FOR N = 2.

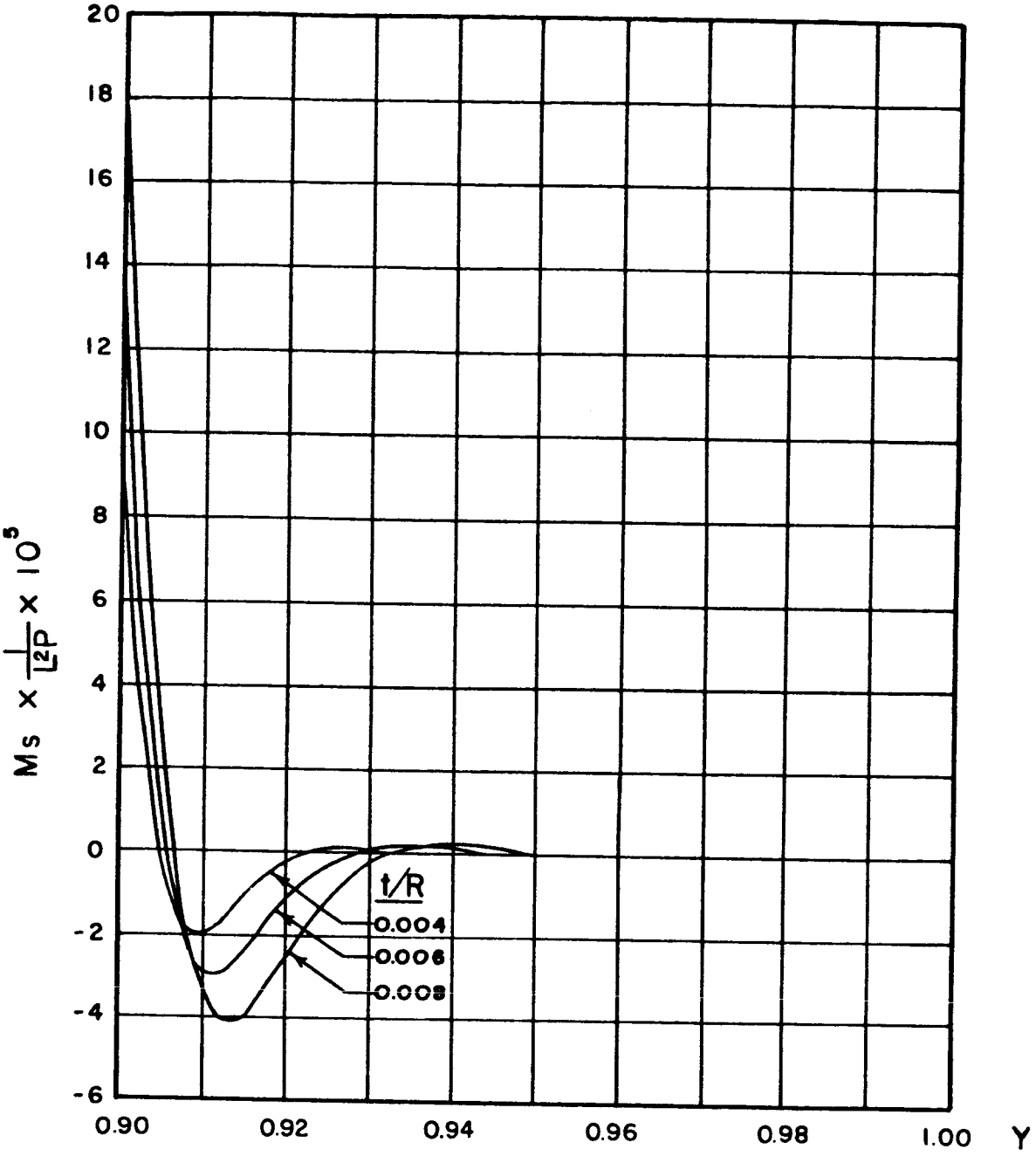

FIGURE A10. - NORMAL MOMENT M_S FOR N = 2.

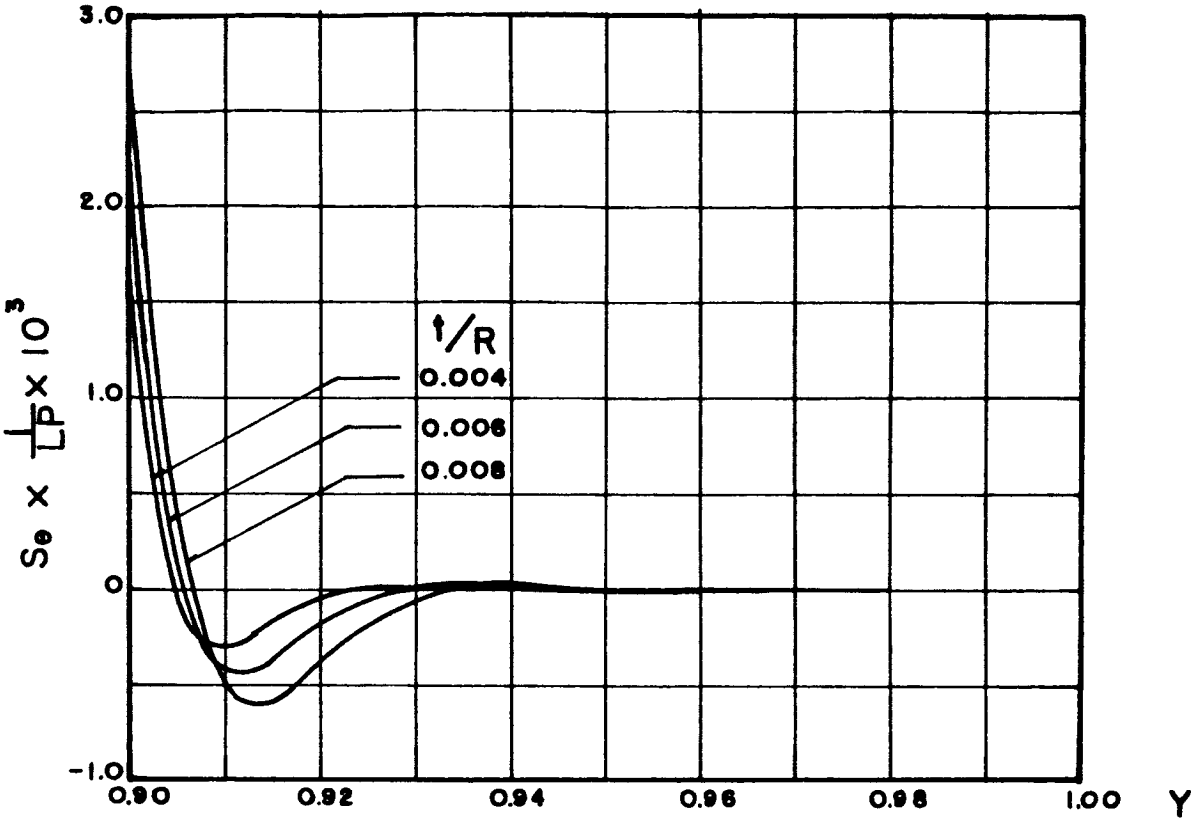

FIGURE All. - TRANSVERSE SHEARING FORCE S_θ FOR N = 2.

APPENDIX B

THE THERMAL EFFECT ON CONICAL SHELLS OF LINEARLY VARYING THICKNESS

By Chin Hao Chang

The contents of this appendix were previously submitted as Progress Report No. 2 for NASA Contract NAS8-11155.

APPENDIX B

THE THERMAL EFFECT ON CONICAL SHELLS OF LINEARLY VARYING THICKNESS

By Chin Hao Chang*

SUMMARY

A study of an isotropic conical shell of linearly varying thickness under a surface temperature was made in which the thermal effect on the shell was represented by an equivalent load. Asymptotic particular solutions due to the thermal load were obtained. These solutions may be combined with the complementary solutions of the shell obtained in Appendix A to constitute a set of complete solutions. A numerical example of a semicircular cone frustum subjected to temperature functions that are constant along the meridians and have a sinusoidal distribution in the circumferential direction is given.

INTRODUCTION

Analytical solutions of conical shells including thermal effect are not generally available. In this appendix an asymptotic solution of an isotropic conical shell with linearly varying thickness that includes the thermal effect was obtained by following the method developed in Appendix A in which the basic equations and the complementary solutions of these equations are given. These solutions are applied here without any alteration and the particular solution of the system of equations due to a thermal effect is obtained.

The thermal effect may be represented by an equivalent load which will be referred to as a thermal load. The thermal load is derived in the next section. The derivation considers a shell of revolution that, in general, has two principal curvatures in two respective membrane directions. Letting one of the two curvatures vanish and specifying the

*Associate Professor of Engineering Mechanics, University of Alabama, University, Alabama and Staff Associate for NASA Contract NAS8-11155.

other, the thermal load for a conical shell is obtained. This thermal load has components in all three directions of the reference coordinates used.

The temperature distribution considered is assumed to be a linear function of the normal coordinate and an arbitrary function of the two membrane coordinates. This type of temperature distribution is commonly used in shell theory as was the case for cylindrical shells in [B1] [1].

It is shown in this appendix that, for asymptotic solutions, the temperature variation in the normal direction is negligible. The asymptotic solutions are discussed. The solutions for the particular case of a constant temperature distribution along the meridians of the conical shell and a sinusoidal distribution in the circumferential direction are presented. Combining these solutions with the complementary solutions of the shell obtained in Appendix A, a numerical example of a semicircular cone frustum is given. The displacements, stress resultants and stress couples of the cone frustum are presented graphically. It was found that the effect of this type of thermal load is similar to the effect due to a lateral normal load.

THERMAL LOADS

Let Φ and θ be a set of orthogonal curvilinear coordinates describing the middle surface of a shell of revolution with a set of principal radii r_Φ and r_θ. When the classical Duhamel-Newmann law of thermoelasticity [B2] is used, the stresses, strains and temperature are related as follows:

$$\sigma_\Phi = \frac{E}{1-\nu^2}\left[\varepsilon_\Phi + \nu\varepsilon_\theta - (1+\nu)\beta T\right]$$

$$\sigma_\theta = \frac{E}{1-\nu^2}\left[\varepsilon_\theta + \nu\varepsilon_\Phi - (1+\nu)\beta T\right] \qquad \text{(B1)}$$

$$\sigma_{\theta\Phi} = \frac{E}{2(1+\nu)}\varepsilon_{\theta\Phi}$$

---

[1]Numbers in brackets designate references at the end of this appendix.

where σ_Φ and σ_θ are normal stresses, ε_Φ and ε_θ are normal strains in the Φ and θ directions, $\sigma_{\theta\Phi}$ and $\varepsilon_{\theta\Phi}$ are shearing stress and strain respectively, T is a temperature function and β is the coefficient of linear expansion.[2]

In what follows the relations for that portion of the stresses associated with the temperature function T only will be considered because those for the other loads are assumed to be known. The additional stresses due to T may be expressed in the form:

$$\sigma_\Phi^T = -\frac{E\beta}{1-\nu} T(\Phi, \theta, z)$$
$$\sigma_\theta^T = -\frac{E\beta}{1-\nu} T(\Phi, \theta, z) \qquad \text{(B2)}$$

in which

$$T(\Phi, \theta, z) = T_o(\Phi, \theta) + z\, T_1(\Phi, \theta) \qquad \text{(B3)}$$

where the coordinate z is in the normal direction of the middle surface, positive outward. The corresponding membrane stress resultants per unit length N_Φ^T, N_θ^T and stress couples per unit length M_Φ^T, M_θ^T due to the stresses (B2) are defined by

$$N_\Phi^T = \int_{-t/2}^{t/2} \sigma_\Phi^T (1+\frac{z}{r_\theta})dz, \qquad N_\theta^T = \int_{-t/2}^{t/2} \sigma_\theta^T (1+\frac{z}{r_\Phi})dz$$
$$M_\Phi^T = -\int_{-t/2}^{t/2} \sigma_\Phi^T (1+\frac{z}{r_\theta})z\,dz, \qquad M_\theta^T = -\int_{-t/2}^{t/2} \sigma_\theta^T (1+\frac{z}{r_\Phi})dz \qquad \text{(B4)}$$

and may be expressed in the following form:

$$N_\Phi^T = -\frac{Et}{1-\nu}\beta \left[T_o + \frac{T_1}{r_\theta}\frac{t^2}{12}\right]$$

---

[2]Symbols other than those defined in this appendix are the same as those used in Appendix A.

$$N_\theta^T = -\frac{Et}{1-\nu}\beta\left[T_o + \frac{T_1}{r_\Phi}\frac{t^2}{12}\right]$$

$$M_\Phi^T = \frac{E\beta}{1-\nu}\left[T_1 + \frac{T_o}{r_\Phi}\right]\frac{t^2}{12} \qquad \text{(B5)}$$

$$M_\Phi^T = \frac{E\beta}{1-\nu}\left[T_1 + \frac{T_o}{r_\theta}\right]\frac{t^2}{12}$$

The foregoing expressions may be converted into those for conical shells by letting

$$r_\theta = \infty, \quad \theta = \alpha, \quad r_\theta = s\cot\alpha \qquad \text{(B6)}$$

and the results are

$$N_s^T = -\frac{Et}{1-\nu}\beta\left[T_o + \frac{t^2}{12}\frac{T_1}{s}\tan\alpha\right]$$

$$N_\theta^T = -\frac{Et}{1-\nu}\beta\left[T_o\right] \qquad \text{(B7)}$$

$$M_s^T = \frac{E\beta}{1-\nu}\frac{t^3}{12}\left[\frac{T_o}{s}\tan\alpha + T_1\right]$$

$$M_\theta^T = \frac{E\beta}{1-\nu}\frac{t^3}{12}\left[T_1\right]$$

For conical shells with linearly varying thickness, $t = \delta s$, and expressions (B7) become

$$N_s^T = -\frac{E\beta\delta}{1-\nu}\left[T_o s + kT_1 s^2\tan\alpha\right]$$

$$N_\theta^T = -\frac{E\beta\delta}{1-\nu}\left[T_o s\right]$$

$$M_s^T = \frac{E\beta\delta}{1-\nu} k\left[T_o s^2 \tan\alpha + T_1 s^3\right] \qquad \text{(B8)}$$

$$M_\theta^T = \frac{E\beta\delta}{1-\nu} k\left[T_1 s^3\right]$$

where $k = \frac{\delta^2}{12}$. When these stress resultants and couples are substituted into equilibrium equations (A4) of Appendix A and the additional terms are denoted by P_s^T, P_r^T and P_θ^T, one has

$$P_s^T = (sN_s^T)' - N_\theta^T$$

$$= -\frac{E\beta\delta}{1-\nu}\left[T_o' s^2 + T_o s + 3kT_1 s^2 \tan\alpha + kT_1' s^3 \tan\alpha\right]$$

$$P_r^T = sN_\theta^T \tan\alpha + 2s(M_s^T)' + s^2(M_s^T)''$$

$$= -\frac{E\beta\delta}{1-\nu}\left\{T_o s^2 \tan\alpha - k\left[(s^5 \ddot{T}_1 + 8s^4 \dot{T}_1 + 12s^3 T_1)\right.\right.$$

$$\left.\left.+(s^4 \ddot{T}_o + 6s^3 \dot{T}_o + 6s^2 T_o)\tan\alpha\right]\right\} \qquad \text{(B9)}$$

$$P_\theta^T = s(N_\theta^T)' \sec\alpha - (M_\theta^T)' \tan\alpha \sec\alpha$$

$$= -\frac{E\beta\delta}{1-\nu}\left[(s^2 T_o') + kT_1' s^3 \tan\alpha\right]\sec\alpha$$

The above three expressions may be considered as the three components of the thermal load in the respective directions.

ASYMPTOTIC SOLUTIONS

It was shown in Appendix A that, for thin shells, the asymptotic solutions are pertinent for practical purposes. In what follows, asymptotic particular solutions of the shell due to the thermal load will be obtained.

Retaining the terms of the lowest order of k, the thermal loads (B9) are simplified to the following form:

$$P_s^T = -\frac{E\beta\delta}{1-\nu}\left[\dot{T}_o s^2 + T_o s\right]$$

$$P_r^T = -\frac{E\beta\delta}{1-\nu}\left[T_o s^2 \tan\alpha\right] \qquad \text{(B10)}$$

$$P_\theta^T = -\frac{E\beta\delta}{1-\nu}\left[s^2 T_o' \sec\alpha\right]$$

Note that the temperature function T_1 is not involved in these expressions.

For asymptotic solutions, the set of membrane equations may be used. Using the dimensionless variable y as the independent variable to replace s, the three equilibrium equations of membrane theory including the thermal loads (B10) were obtained from equations (A42) of Appendix A as:

$$\frac{1-\nu}{8}\left[y^2 u_{,yy} + 3yu_{,y} - 8u\right] + \frac{1+\nu}{4} yu_{,\theta y}\sec\alpha + u_{,\theta\theta}\sec^2\alpha$$

$$+ (2-\nu)v_{,\theta}\sec\alpha + w_{,\theta}\sec\alpha\tan\alpha = (1+\nu)\beta L\, y^2 T_{o,\theta}\sec\alpha \qquad \text{(B11)}$$

$$\frac{1+\nu}{8} yu_{,\theta y}\sec\alpha - \frac{3}{2}(1-\nu)u_{,\theta}\sec\alpha + \frac{1}{4} y^2 v_{,yy} + \frac{3}{4} yv_{,y}$$

$$+ \frac{1-\nu}{2} v_{,\theta\theta} \sec^2\alpha - (1-\nu)v + \frac{1}{2} \nu y w_{,y} \tan\alpha - (1-\nu) w \tan\alpha$$

$$= (1+\nu)\beta L y^2 \left[\frac{1}{2} y T_{o,y} + T_o\right]$$

$$u_{,\theta} \sec\alpha + \frac{1}{2} \nu y v_{,y} + v + w \tan\alpha = (1+\nu)\beta L y^2 T_o \tan\alpha$$

Let

$$T_o = Q_n y^{\omega_n} \begin{matrix} \cos \\ \sin \end{matrix} \frac{n\pi\theta}{\theta_1} \tag{B12}$$

where Q_n and ω_n are prescribed constants presumably real and finite. The particular solutions of equations (B11) may be assumed in the following form:

$$U^T = A_n y^{\lambda_n^* - 1} \begin{matrix} \sin \\ \cos \end{matrix} \frac{n\pi\theta}{\theta_1}$$

$$V^T = B_n y^{\lambda_n^* - 1} \begin{matrix} \cos \\ \sin \end{matrix} \frac{n\pi\theta}{\theta_1} \tag{B13}$$

$$W^T = C_n y^{\lambda_n^* - 1} \begin{matrix} \cos \\ \sin \end{matrix} \frac{n\pi\theta}{\theta_1}$$

in which coefficients A_n, B_n and C_n are to be determined. On substituting expressions (B12) and (B13) for equations (B11), factoring out the sinusoidal functions and setting

$$\lambda_n^* = \omega_n + 3 \tag{B14}$$

three linear algebraic equations are obtained for the three unknowns A_n, B_n and C_n. These equations can be solved by Cramer's rule provided

that λ_n^* does not make the determinant of the equations vanish. When $\omega_n = 0$, $\lambda_n^* = 3$ is one of the roots which will make the determinant vanish as has been shown in Appendix A. Physically this represents the case in which the temperature is constant along meridians. In this case the solutions are obtained by the same method as was used for the lateral normal uniform load in Appendix A.

Let

$$U^T = \left[d_1 + d_2 \ln y\right] y^2 \begin{matrix}\sin \\ \cos\end{matrix} \frac{n\pi\theta}{\theta_1}$$

$$V^T = b\, y^2 \begin{matrix}\cos \\ \sin\end{matrix} \frac{n\pi\theta}{\theta_1} \qquad \text{(B15)}$$

$$W^T = c(1 + \ln y)\, y^2 \begin{matrix}\cos \\ \sin\end{matrix} \frac{n\pi\theta}{\theta_1}$$

in which d_1, d_2, b and c are constants to be determined. When the assumed solutions (B15) combined with (B12) are substituted into equations (B11), the constants are:

$$d_1 = \mp \frac{1}{2} \frac{m\beta LQ_n}{1-V} \left\{(1+3\nu) - (5-\nu)\tan\alpha - \left[\frac{2}{3} m^2 - \frac{1}{m^2}(1+\nu)\right](1-\tan\alpha)\right\}$$

$$d_2 = \frac{1}{3} \frac{m\beta LQ_n}{1-V} \left\{(1 + 4\nu - m^2) - \tan\alpha(7 - 2\nu - m^2)\right\} \qquad \text{(B16)}$$

$$b = \frac{1}{6} \frac{m^2\beta LQ_n}{1-V} \left\{1 - \tan\alpha + \frac{3}{m^2}\left[\tan\alpha\,(1 - 2\nu) + 1\right]\right\}$$

$$c = \frac{m}{\tan\alpha}\, d_2$$

The corresponding stress resultants due to the thermal loads are readily obtained by use of the elastic law. The results are:

$$N_s^T = \frac{E\delta}{1-\nu^2}\left[(1-\nu)b - mV(d_1 - d_2)\right] y^2 \begin{matrix}\cos \\ \sin\end{matrix} \frac{n\pi\theta}{\theta_1}$$

$$N_\theta^T = \frac{E\delta}{1-\nu^2}\left[\nu(1+\nu)b - m(d_1 - d_2)\right] y^2 \begin{matrix}\cos \\ \sin\end{matrix} \frac{n\pi\theta}{\theta_1} \qquad \text{(B17)}$$

$$T_s^T = \frac{E\delta}{4(1+\nu)}\left[d_2 + 2mb\right] y^2 \begin{matrix}\sin \\ \cos\end{matrix} \frac{n\pi\theta}{\theta_1}$$

The stress couples induced by such thermal loads are of higher order and may be neglected. Combining the solutions (B14) and (B17) with the complementary solutions obtained in Appendix A the complete solutions are obtained for this case.

NUMERICAL EXAMPLE

Consider the semicircular truncated cone with two generators simply supported, the smaller circular end fixed and the other end free that was discussed in Appendix A. As in Appendix A, the following parameters are assumed:

$$\alpha = 75^\circ, \quad \nu = \frac{1}{3} \text{ and } \sqrt{\frac{L_1}{L}} = 0.90 \qquad \text{(B18)}$$

Numerical results for $n = 1$ and 2 were computed that can be used for symmetrical and asymmetrical distributions of temperature similar to the distribution of wind loads discussed in Appendix A. The results are given in the form

$$F_n(y,\theta) = f_n(y) \begin{matrix}\sin \\ \cos\end{matrix} \frac{n\pi\theta}{\theta_1} \qquad n = 1 \text{ and } 2 \qquad \text{(B19)}$$

in which the function $f_n(y)$ are presented in Figures B1 through B10 for $\frac{t}{R} = 0.004$, 0.006 and 0.008.

ACKNOWLEDGEMENT

The author wishes to thank Mr. H. Y. Chu for his assistance in programing the numerical computations.

REFERENCES

B1. Flügge, W. and Conrad, D. A.: Thermal Singularities for Cylindrical Shells. Proc. Third U.S. Nat. Congr. Appl. Mech., ASME, 1958, pp. 321-328.

B2. Sokolnikoff, Z. S.: Mathematical Theory of Elasticity. Second Ed., McGraw-Hill Book Co., New York, 1956, P. 359.

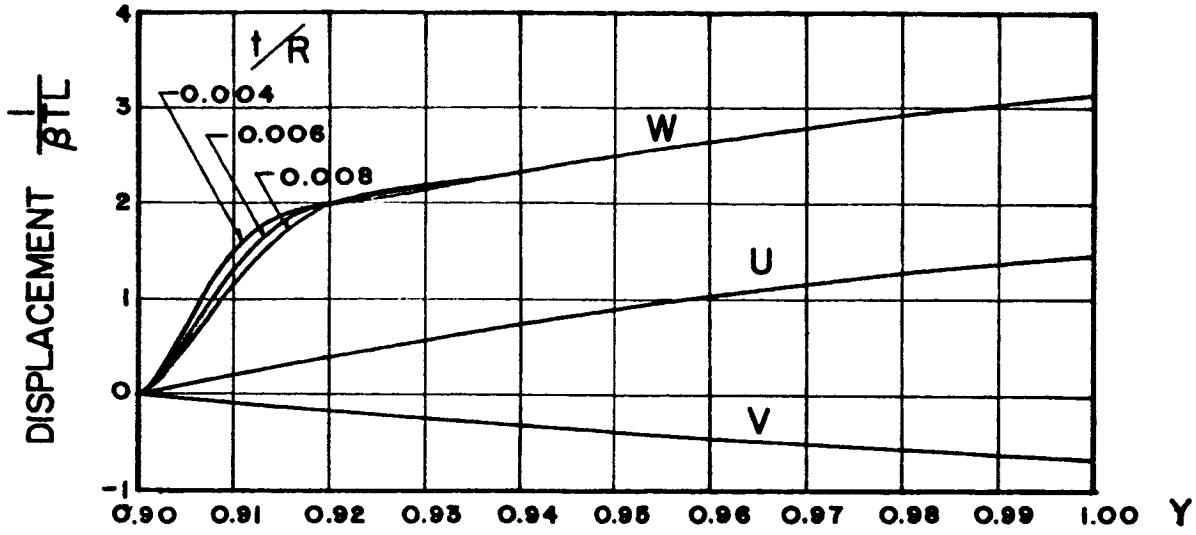

FIGURE B1. - DISPLACEMENTS U, V AND W FOR N = 1.

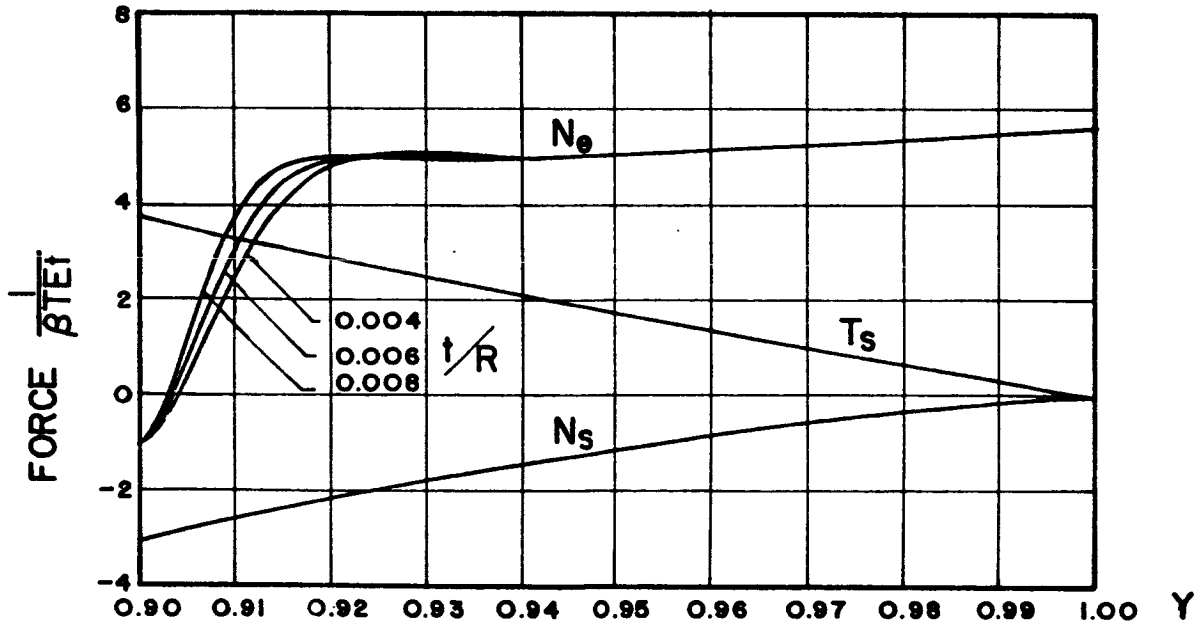

FIGURE B2. - MEMBRANE FORCES N_θ, T_s AND N_s FOR N = 1.

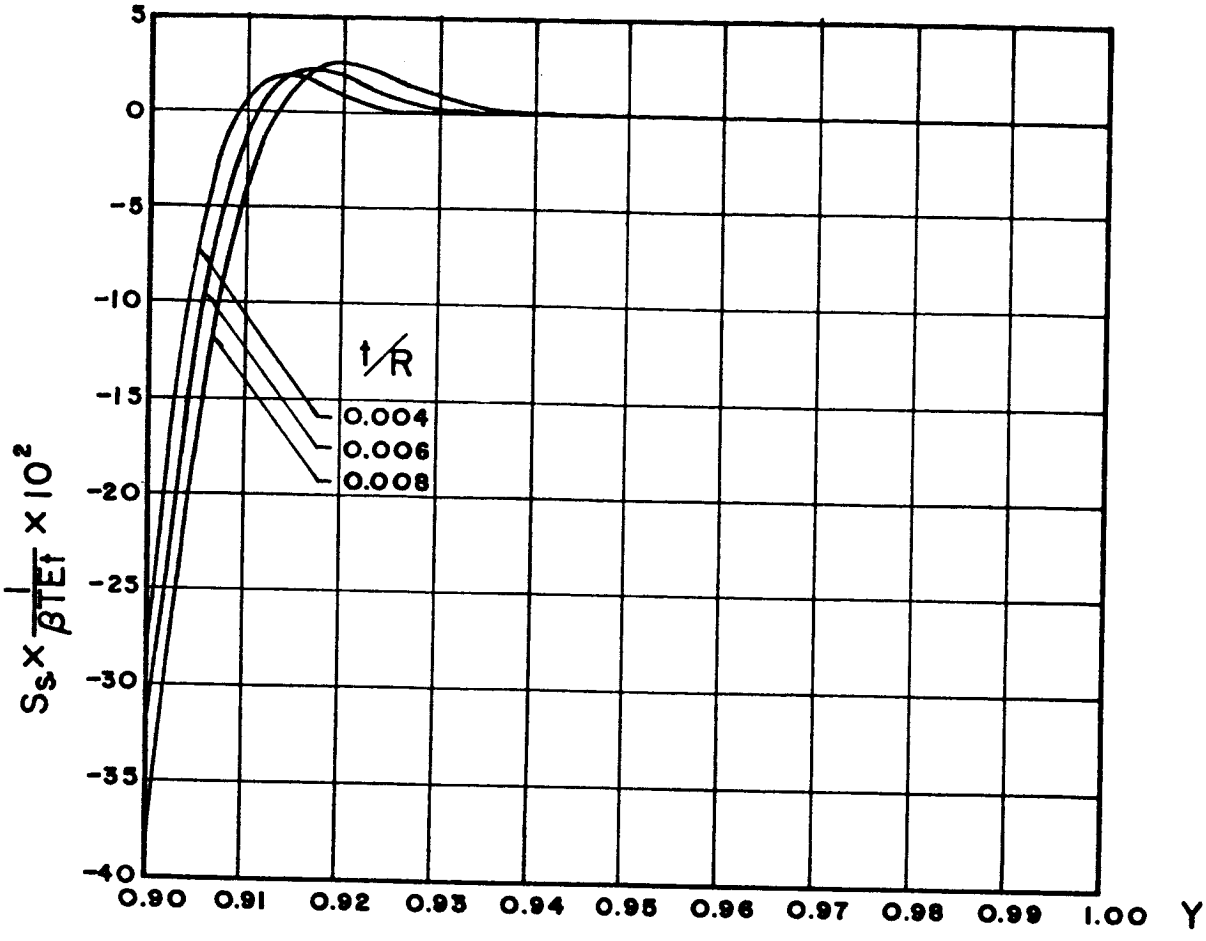

FIGURE B3. - TRANSVERSE SHEARING FORCE S_s FOR N = 1.

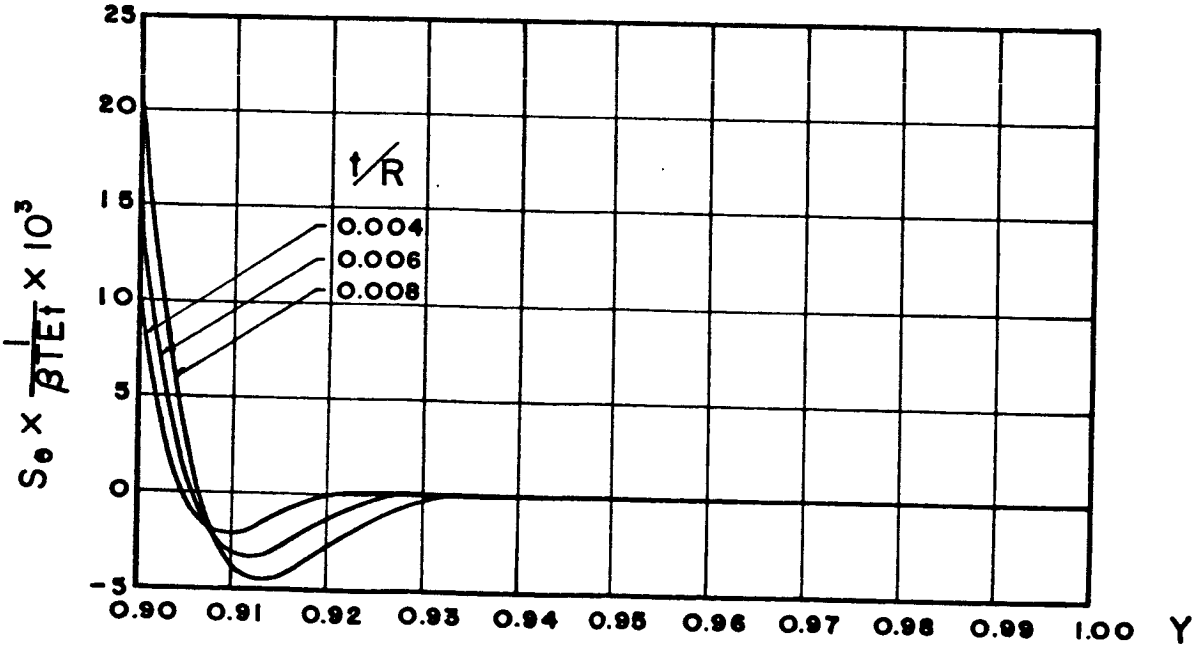

FIGURE B4. - TRANSVERSE SHEARING FORCE S_θ FOR N = 1.

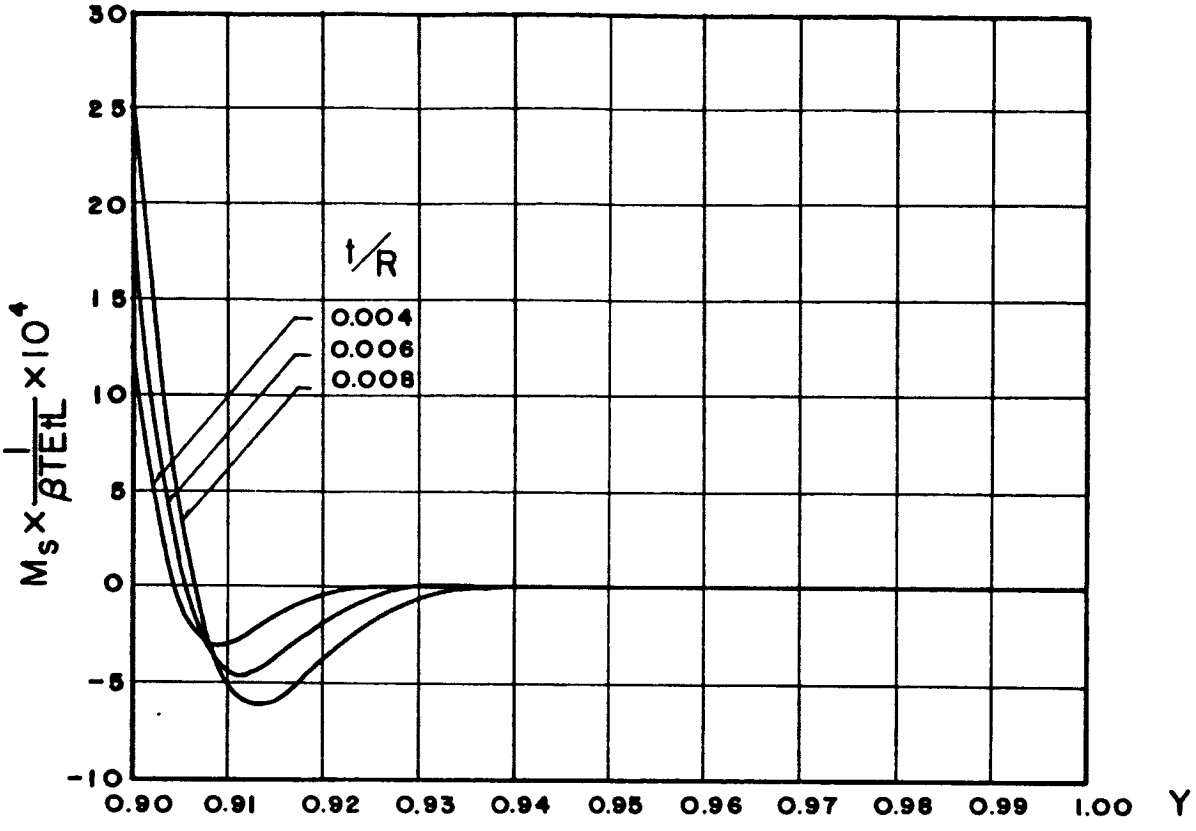

FIGURE B5. - NORMAL MOMENT M_s FOR N = 1.

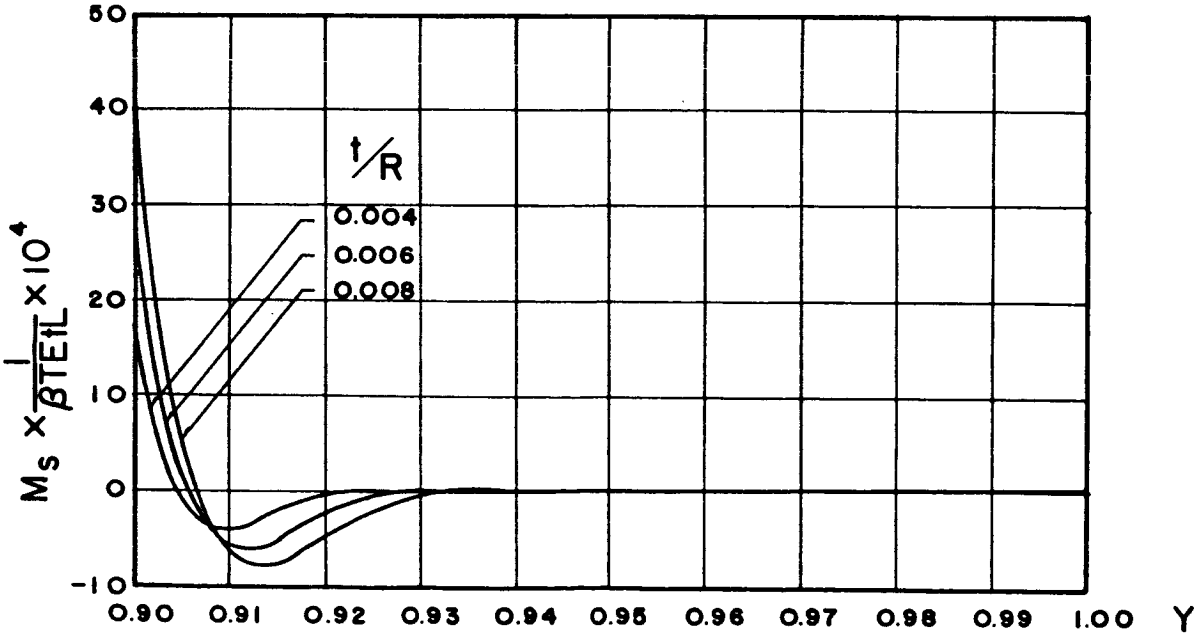

FIGURE B6. - NORMAL MOMENT M_s FOR N = 2.

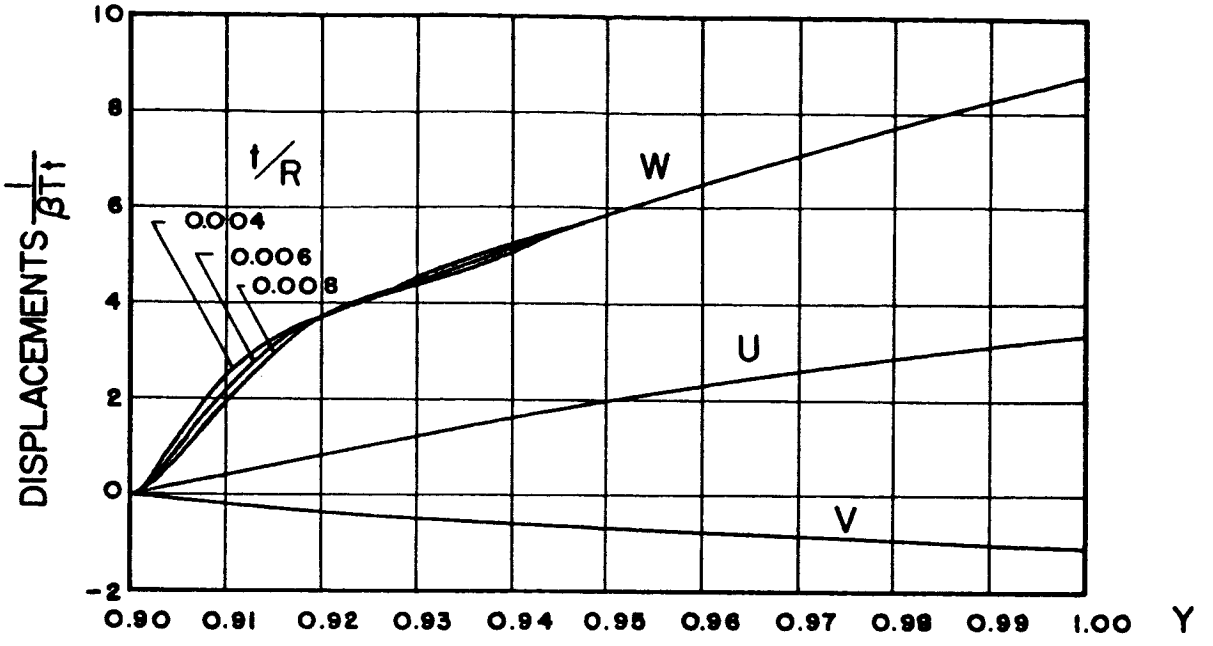

FIGURE B7. - DISPLACEMENTS U, V AND W FOR N = 2.

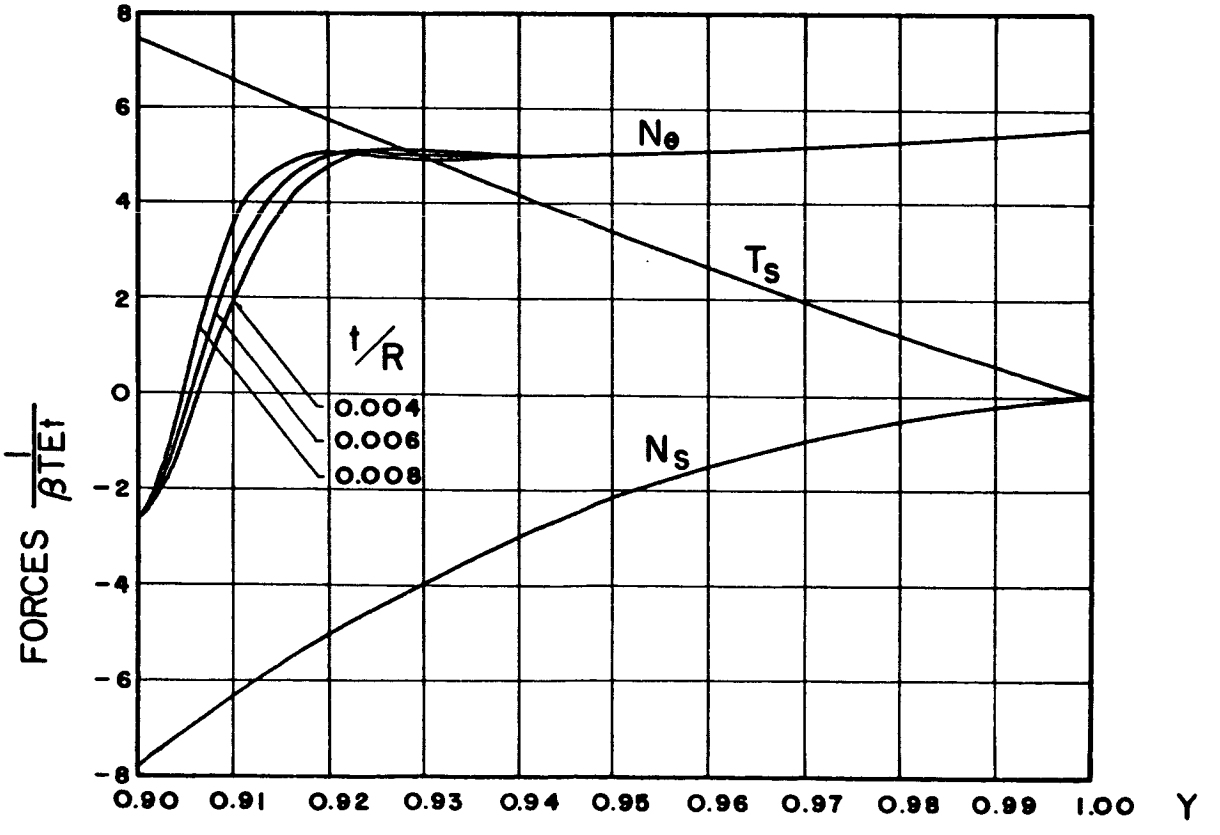

FIGURE B8. - MEMBRANE FORCES N_θ, T_s AND N_s FOR N = 2.

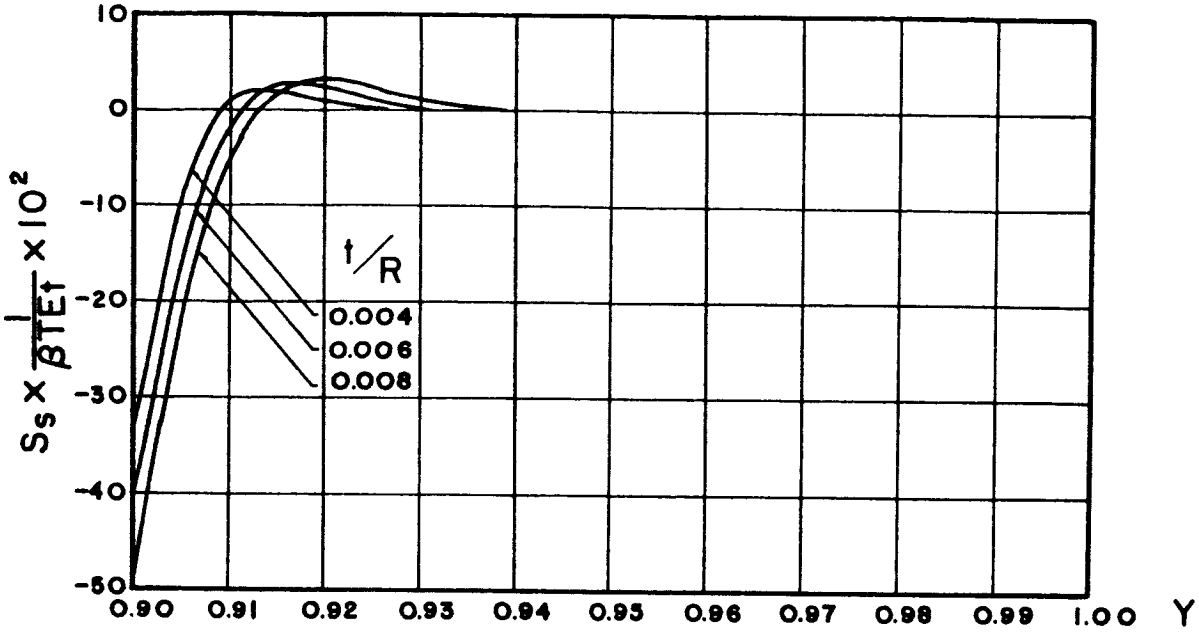

FIGURE B9. - TRANSVERSE SHEARING FORCE S_s FOR N = 2.

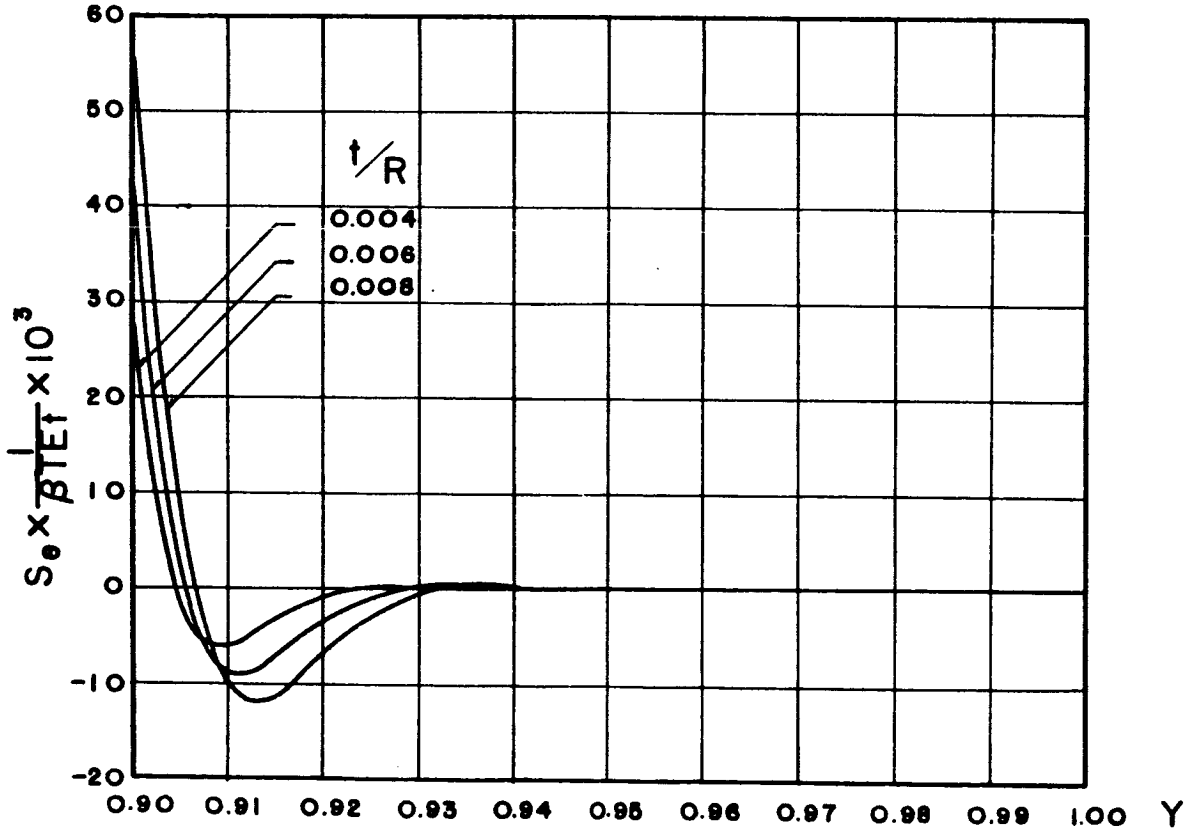

FIGURE B10. - TRANSVERSE SHEARING FORCE S_θ FOR N = 2.

APPENDIX C

AN ASYMPTOTIC SOLUTION OF CONICAL SHELLS OF CONSTANT THICKNESS

By Chin Hao Chang

The contents of this appendix were previously submitted as a part of Progress Report No. 6 for NASA Contract NAS8-11155.

APPENDIX C

AN ASYMPTOTIC SOLUTION OF CONICAL SHELLS OF CONSTANT THICKNESS

By Chin Hao Chang*

SUMMARY

A solution of truncated conical shells of constant thickness is obtained as the ratio of the thickness to the radius at the larger end goes to zero asymptotically by separating the solution into two parts: membrane and bending. These two parts are coupled by the lateral displacement. A particular solution due to lateral normal loads is also given and two numerical examples are presented. One numerical example considers a semicircular shell segment with the smaller end fixed, the other end free and the two generator edges simply supported. The shell is subjected to a lateral normal load which is constant in the meridional direction and varies sinusoidally in the circumferential direction. The other numerical example considers a cantilevered complete cone with the larger end free. A rigid plate is attached to the free end and a moment is applied. Comparisons with other available results are given in both examples.

INTRODUCTION

Concial shells of constant thickness have been studied by a number of investigators. The axial symmetrical solutions of such a shell have been well established [C1, C2] [1]; while for asymmetrical cases the solutions have been approached two different ways. One approach uses the method of power series [C2, C3 and C4], while the other treats the membrane and bending solutions separately. It has been found that, by

---

*Associate Professor of Engineering Mechanics, University of Alabama, University, Alabama and Staff Associate for NASA Contract NAS8-11155.

[1]Numbers in brackets designate references at the end of this appendix.

keeping the first order terms only, the bending solutions are in the form of Bessel functions [C5]. In reference [C5], by recognizing the rapid decay of the bending solutions near edges, an edge-zone solution was also presented to replace the solutions of Bessel functions. The power series approach was not recommended by several researchers [C6], [C7] because of slow convergence.

It was found in Appendix A that, for conical shells of linearly varying thickness, the solution consists of two parts: membrane and bending effect. Both parts are expressed as polynomial functions of y^{λ} as far as the y-function is concerned, where y is a dimensionless variable of length measured in the meridional direction and the λ's are real constants for the membrane solutions and complex numbers for the solutions of bending effect. Furthermore, the λ's of the membrane solutions will approach finite values while those of the bending solutions will become infinite as the ratio of the thickness of shell to the radius at a section approaches zero. These different characteristics of the two parts of the solutions enables them to be treated separately.

Since conical shells of linearly varying thickness and those of constant thickness will behave alike when the ratio of thickness to radius is very small, in this report an asymptotic solution of conical shells of constant thickness is obtained by assuming that the solution possesses characteristics similar to the solution for conical shells of linearly varying thickness. The asymptotic solution obtained includes the particular solution due to a lateral normal load. Two numerical examples are also given. One is for a semi-circular cone frustum similar to the one given in Appendix A. This example is designed to compare the results for the same shell with different types of thickness. The other is a complete cone frustum with the smaller circular end fixed and the other end free. At the free end a rigid plate is attached and a moment is applied. A solution for the latter example is available in [C5] so that a comparison can be made between the two solutions.

BASIC EQUATIONS

A set of exact equations for shells of revolution of isotropic and elastic material within the framework of generalized plane stresses of linear theory of elasticity is given in explicit form in Reference [C1].

For thin shells, using the approximations $r_1 + z \approx r_1$ and $r_2 + z \approx r_2$ where r_1 and r_2 are two principal radii of the middle surface of the shells and z is the normal distance measured from the middle surface to a generic point, the elastic relations between stress resultants, couples and displacements are simplified considerably. For a conical shell these relations are:

$$N_s = \frac{D}{L}\frac{1}{y^2}\left[\frac{1}{2}yv^{\cdot} + \upsilon(u'\sec\alpha + v + w\tan\alpha)\right]$$

$$N_\theta = \frac{D}{L}\frac{1}{y^2}\left[u'\sec\alpha + v + w\tan\alpha + \frac{\upsilon}{2}yv^{\cdot}\right]$$

$$N_{s\theta} = N_{\theta s} = \frac{D}{L}\frac{1-\upsilon}{2}\frac{1}{y^2}\left[\frac{1}{2}yu^{\cdot} - u + v'\sec\alpha\right]$$

$$M_s = D\,k\,\frac{1}{y^4}\left[\frac{1}{4}(y^2w^{\cdot\cdot} - yw^{\cdot}) + \upsilon\,(w''\sec^2\alpha + \frac{1}{2}y\,w^{\cdot})\right] \qquad (C1)$$

$$M_\theta = D\,k\,\frac{1}{y^4}\left[w''\sec^2\alpha + \frac{1}{2}y\,w^{\cdot} + \frac{\upsilon}{4}(y^2\,w^{\cdot\cdot} - y\,w^{\cdot})\right]$$

$$M_{s\theta} = M_{\theta s} = D\,k\,(1-\upsilon)\,\frac{1}{y^4}\left[\frac{1}{2}y\,w'^{\cdot}\sec\alpha - w'\sec\alpha\right]$$

in which $N_s, \ldots, M_{s\theta}$ are the normal and shearing stress resultants and couples in the directions indicated by the subscripts and $y = \sqrt{\frac{s}{L}}$. The s and θ are meridional and circumferential coordinates of the middle surface of the shell; u, v, and w are the circumferential, meridional and normal displacements, respectively. Outward w is positive. D and k are defined as follows:

$$D = \frac{Et}{1-\upsilon^2} \quad \text{and} \quad k = \frac{1}{12}\left(\frac{t}{L}\right)^2 = \frac{1}{12}\left(\frac{t}{R}\right)^2\cos^2\alpha \qquad (C2)$$

where E is Young's modulus of elasticity, ν is Poisson's ratio, t is thickness, L is the length from the apex to the larger end of the shell, $R = L \cos \alpha$ is the radius of the shell at $y = 1$, and the α is the base angle of the shell. The dots indicate partial differentiation with respect to y and the primes indicate partial differentiation with respect to θ.

When the equation of equilibrium of moments about the normal of a surface element is overlooked, the other five equations are:

$$\frac{1}{2} y N_s^{\cdot} + N_s + N'_{\theta s} \sec \alpha - N_\theta = - P_s L y^2$$

$$\frac{1}{2} y N_{s\theta}^{\cdot} + 2N_{s\theta} + N'_\theta \sec \alpha - Q_\theta \tan \alpha = - P_\theta L y^2$$

$$\frac{1}{2} y Q_s^{\cdot} + Q_s + Q'_\theta \sec \alpha + N_\theta \tan \alpha = P_r L y^2 \qquad \text{(C3)}$$

$$\frac{1}{2} y M_s^{\cdot} + M_s + M'_{\theta s} \sec \alpha - M_\theta = L y^2 Q_s$$

$$\frac{1}{2} y M_{s\theta}^{\cdot} + 2M_{s\theta} + M'_\theta \sec \alpha = L y^2 Q_\theta$$

where Q_s and Q_θ are the transverse shear forces per unit length acting on sections perpendicular to the s- and θ- directions; P_r, P_s, and P_θ are surface loads per unit area in normal, meridional, and circumferential directions, respectively.

The eleven equations in (C1) and (C3) govern the eleven unknowns involved. When the last two moment equations of (C3) are used to eliminate the transverse shearing forces Q_s and Q_θ in the second and third equations of (C3), the first three equations of (C3) become

$$\frac{1}{2} yN_s^{\cdot} + N_s + N_{\theta s}' \sec \alpha - N_\theta = - P_s Ly^2$$

$$\frac{1}{2} yN_{s\theta}^{\cdot} + 2N_{s\theta} + N_\theta' \sec \alpha - \frac{1}{Ly^2}\left[\frac{1}{2} y M_{s\theta}^{\cdot} + M_{s\theta} + M_{\theta s} \tan \alpha \right.$$

$$\left. + M_\theta' \tan \alpha \sec \alpha \right] = - P_\theta Ly^2 \qquad (C4)$$

$$N_\theta \tan \alpha + \frac{1}{Ly^2}\left[\frac{1}{4} y^2 M_s^{\cdot\cdot} + \frac{3}{4} yM_s^{\cdot} + (yM_{s\theta}^{\cdot} + 2 M_{s\theta}') \sec \alpha \right.$$

$$\left. + M_\theta'' \sec^2 \alpha - \frac{1}{2} y M_\theta^{\cdot}\right] = P_r Ly^2$$

Substituting equations (C1) into (C4), three equations for three unknown displacements are obtained. In what follows, instead of dealing with these three displacements, each displacement will be divided into three parts: the first part is due to membrane action, the second part is due to the bending effects and the third, the last part, is for the particular solutions due to lateral normal loads. Denoting these three parts by superscripts I, II, and P, respectively, the displacements may be expressed as

$$u = u^I + u^{II} + u^P$$

$$v = v^I + v^{II} + v^P \qquad (C5)$$

$$w = w^I + w^{II} + w^P$$

These three parts of solution will be discussed in the following sections.

MEMBRANE SOLUTIONS

The membrane solutions of conical shells of constant thickness are well known. However, available solutions are presented in forms of stress only. In what follows, the displacements will be obtained.

When equations (C1) with $k = 0$ are substituted into equations (C4), the three equations become

$$\frac{1-\upsilon}{8} y^2 u'' + \frac{1-\upsilon}{8} yu' - \frac{1-\upsilon}{2} u + u'' \sec^2 \alpha + \frac{1+\upsilon}{4} yv'' \sec \alpha$$

$$+ \frac{3-\upsilon}{2} v' \sec \alpha + w' \tan \alpha \sec \alpha = -\frac{1}{D} L^2 y^4 P_\theta$$

$$\frac{1+\upsilon}{4} yu'' \sec \alpha - \frac{3-\upsilon}{2} u' \sec \alpha + \frac{1}{4}[y^2 v'' + yv'] + \frac{1-\upsilon}{2} v'' \sec^2 \alpha \qquad (C6)$$

$$- v + \frac{\upsilon}{2} w' \tan \alpha - w \tan \alpha = -\frac{1}{D} L^2 y^4 P_s$$

$$u' \sec \alpha + v + w \tan \alpha + \frac{\upsilon}{2} yv' = \frac{1}{D} L^2 y^4 P_r$$

Assume

$$u = A y^\lambda \begin{matrix} \sin \\ \cos \end{matrix} \frac{n\pi\theta}{\theta_1}$$

$$v = B y^\lambda \begin{matrix} \cos \\ \sin \end{matrix} \frac{n\pi\theta}{\theta_1} \qquad (C7)$$

$$w = C y^\lambda \begin{matrix} \cos \\ \sin \end{matrix} \frac{n\pi\theta}{\theta_1}$$

where λ is an unknown constant; θ_1 is the central angle between two generators. Substitution of equations (C7) into the homogeneous part of equations (C6) and cancelling out the y and sinusoidal functions, one has three homogeneous algebraic equations for three unknown constants A, B, and C. Letting the determinant of the equations vanish in order to have nontrival solutions, results in the following characteristic equation for λ

$$\lambda^2(\lambda^2 - 4) = 0 \tag{C8}$$

When the values of λ are determined and substituted back into the algebraic equations one may express the constants A and B in terms of C. This gives the first part of the solutions of the displacements as follows:

$$u^I = \mp \frac{1}{m}\left\{\frac{m^2}{m^2-1}\left[C_1 - \left(\frac{1-\upsilon}{2(m^2-1)} - \ell ny\right) C_2\right] + C_3 y^2 + \frac{m^2-2(1+\upsilon)}{m^2-4} C_4 y^{-2}\right\} \begin{matrix}\sin \frac{n\pi\theta}{\theta_1} \\ \cos\end{matrix}$$

$$v^I = \left\{\frac{1}{m^2-1}\left[C_1 - \left(\frac{m^2-\upsilon}{2(m^2-1)} - \ell ny\right)C_2\right] + \frac{2}{m^2-4} C_4 y^{-2}\right\} \begin{matrix}\cos \frac{n\pi\theta}{\theta_1} \\ \sin\end{matrix} \tag{C9}$$

$$w^I = \frac{1}{\tan \alpha}\left\{C_1 + C_2 \ell ny + C_3 y^2 + C_4 y^{-2}\right\} \begin{matrix}\cos \frac{n\pi\theta}{\theta_1} \\ \sin\end{matrix}$$

where

$$m = \frac{n\pi}{\theta_1} \sec \alpha$$

The corresponding stresses may be obtained from (C1) as

$$N_s^I = \frac{Et}{L}\left\{\frac{1}{2(m^2-1)} C_2 y^{-2} - \frac{2}{m^2-4} C_4 y^{-4}\right\} \begin{matrix}\cos \frac{n\pi\theta}{\theta_1} \\ \sin\end{matrix} \tag{C10}$$

$$N_{s\theta}^I = \mp \frac{Et}{L} \frac{2}{m(m^2-4)} C_4 y^{-4} \begin{matrix}\sin \frac{n\pi\theta}{\theta_1} \\ \cos\end{matrix}$$

N_θ^I vanishes identically.

BENDING EFFECT SOLUTION

It was shown in Appendix A that the displacement functions due to bending may be assumed in the following form:

$$u^{II} = \frac{1}{\gamma^2} U$$

$$v^{II} = \frac{1}{\gamma} V \qquad \text{(C11)}$$

and

$$w^{II} = W$$

where

$$\gamma^4 = \frac{16}{k} \qquad \text{(C12)}$$

Thus $\gamma \to \infty$ as $t/R \to 0$. Furthermore, the y-function of U, V, and W may be expressed in forms of $y^{c\gamma}$ where c is a finite constant. Thus the differentiations with respect to y will change the orders of magnitude of the functions concerned. In order to avoid this, a new variable η is introduced such that

$$\eta = y^{\gamma} \qquad \text{(C13)}$$

When expressions (C11) and (C13) are substituted into the elastic relations (C1), retaining only the terms of the lowest order of $\frac{1}{\gamma}$, yields

$$N_s = \frac{D}{L}\left[\frac{1}{2}\,\eta\, V_{,\eta} + \upsilon\, W \tan\alpha\right]\eta^{-\frac{2}{\gamma}}$$

$$N_\theta = \frac{D}{L}\left[W \tan\alpha + \frac{1}{2}\,\upsilon\eta\, V_{,\eta}\right]\eta^{-\frac{2}{\gamma}}$$

$$N_{s\theta} = N_{\theta s} = \frac{D}{L}\frac{1-\upsilon}{2}\frac{1}{\gamma}\left[\frac{1}{2}\eta\, U,_{\eta} + V,_{\theta}\right]\sec\alpha\cdot\eta^{-\frac{2}{\gamma}}$$

$$M_s = D\frac{4}{\gamma^2}\left[\eta^2 W,_{\eta\eta} + \eta\, W,_{\eta}\right]\eta^{-\frac{4}{\gamma}} \qquad (C14)$$

$$M_\theta = \upsilon M_s$$

$$M_{s\theta} = M_{\theta s} = D\frac{8}{\gamma^3}(1-\upsilon)W,_{\theta\eta}\sec\alpha\cdot\eta^{-\frac{4}{\gamma}}$$

Transforming the variable y to η and making use of the asymptotic expressions (C14), the homogeneous part of equations (C4), when only the terms of the lowest order of $\frac{1}{\gamma}$ are retained, the following three equations are obtained:

$$\eta^2 V,_{\eta\eta} + \eta\, V,_{\eta} + 2\upsilon\,\eta\, W,_{\eta}\tan\alpha = 0 \qquad (C15a)$$

$$\frac{1}{4}\frac{1-\upsilon}{2}\left[\eta^2 U,_{\eta\eta} + \eta\, U,_{\eta} + 2\eta\, V,_{\theta\eta}\sec\alpha\right] + \left[W,_{\theta}\tan\alpha + \frac{1}{2}\upsilon\,\eta\, V,_{\theta\eta}\right]\sec\alpha = 0 \qquad (C15b)$$

and

$$\eta^4 W,_{\eta\eta\eta\eta} + 6\eta^3 W,_{\eta\eta\eta} + 7\eta^2 W,_{\eta\eta} + \eta\, W,_{\eta} + \eta^{\frac{4}{\gamma}}\left[W\tan^2\alpha + \frac{1}{2}\upsilon\,\eta\, V,_{\eta}\tan\alpha\right] = 0$$

Since

$$\eta^{\frac{4}{\gamma}} \to 1 \qquad \text{as} \qquad \gamma \to \infty$$

the last equation becomes

$$\eta^4 W,_{\eta\eta\eta\eta} + 6y^3 W,_{\eta\eta\eta} + 7\,\eta^2 W,_{\eta\eta} + \eta\, W,_{\eta} + W \tan^2 \alpha$$

$$+ \frac{1}{2}\, \upsilon\, \eta\, V,_{\eta} \tan \alpha = 0 \qquad \text{(C15c)}$$

The integration of equation (C15a) with respect to η results in

$$\eta\, V,_{\eta} = -2\, \upsilon\, W \tan \alpha \qquad \text{(C16)}$$

in which, without loss of generality, an integration constant has been dropped. Substitution of (C16) into equation (C15c) yields

$$\eta^4 W,_{\eta\eta\eta\eta} + 6\,\eta^3 W,_{\eta\eta\eta} + 7\,\eta^2 W,_{\eta\eta} + \eta\, W,_{\eta}$$

$$+ W \tan^2 \alpha\, (1-\upsilon^2) = 0 \qquad \text{(C17)}$$

Assuming

$$W = \frac{1}{\tan \alpha}\, \overline{C}\, \eta^{\lambda}\, \frac{\cos n\pi\theta}{\sin \theta_1} \qquad \text{(C18)}$$

equation (C17) results in a characteristic equation

$$\lambda^4 + (1-\upsilon^2) \tan^2 \alpha = 0 \qquad \text{(C19)}$$

which gives

$$\lambda = \pm q\,(1 \pm i) \qquad \text{(C20)}$$

where

$$q = \left| [(1-\upsilon^2) \tan^2 \alpha]^{\frac{1}{4}}\, \frac{\sqrt{2}}{2} \right| \qquad \text{(C21)}$$

Letting

$$V = \overline{B}\,\eta^{\lambda} \begin{matrix}\cos \\ \sin\end{matrix} \frac{n\pi\theta}{\theta_1}$$

$$U = \overline{A}\,\eta^{\lambda} \begin{matrix}\sin \\ \cos\end{matrix} \frac{n\pi\theta}{\theta_1} \qquad (C22)$$

and making use of equations (C16) and (C15b)

$$\overline{B} = -\frac{2\upsilon}{\lambda}\overline{C}$$

$$\overline{A} = \pm\frac{4}{\lambda^2}(2+\upsilon)\,m\,\overline{C} \qquad (C23)$$

where $\overline{A}$, $\overline{B}$, and $\overline{C}$ are complex numbers. When the identity

$$\eta^{i} = \cos(\ell n\,\eta) + i\sin(\ell n\eta)$$

is used and the complex numbers are transformed to real numbers, one has

$$W = \frac{1}{\tan\alpha}\Big\{\eta^{q}[C_5\cos(q\,\ell n\eta) + C_6\sin(q\,\ell n\eta)] + \eta^{-q}[C_7\cos(q\,\ell n\eta) + C_8\sin(q\,\ell n\eta)]\Big\} \begin{matrix}\cos \\ \sin\end{matrix} \frac{n\pi\theta}{\theta_1}$$

$$V = -\frac{\upsilon}{q}\Big\{\eta^{q}[(C_5-C_6)\cos(q\ell n\eta) + (C_5+C_6)\sin(q\ell n\eta)] - \eta^{-q}[(C_7+C_8)\cos(q\ell n\eta) + (C_8-C_7)\sin(q\ell n\eta)]\Big\} \begin{matrix}\cos \\ \sin\end{matrix} \frac{n\pi\theta}{\theta_1} \qquad (C24)$$

$$U = \mp\frac{2(2+\upsilon)m}{q^2}\Big\{\eta^{q}[C_6\cos(q\ell n\eta) - C_5\sin(q\ell n\eta)] - \eta^{-q}[C_8\cos(q\ell n\eta) - C_7\sin(\ell n\eta)]\Big\} \begin{matrix}\sin \\ \cos\end{matrix} \frac{n\pi\theta}{\theta_1}$$

Expressing in terms of the variable y and denoting

$$\gamma q = \rho \tag{C25}$$

the solutions given in (C11) and the induced stress forces and couples obtained from (C14) assume the following final forms:

$$W^{II} = \frac{1}{\tan \alpha}\left\{y^{\rho}[C_5 \cos(\rho \ell n y) + C_6 \sin(\rho \ell n y)] + y^{-\rho}[C_7 \cos(\rho \ell n y) + C_8 \sin(\rho \ell n y)]\right\} \begin{matrix}\cos \\ \sin\end{matrix} \frac{n\pi\theta}{\theta_1}$$

$$v^{II} = \frac{\upsilon}{\rho} Y_1$$

$$u^{II} = \mp \frac{2(2+\upsilon)m}{\rho^2} Y_2$$

$$N_s^{II} = 0$$

$$N_\theta^{II} = \frac{Et}{L} \tan \alpha \, w^{II} \frac{1}{y^2} \tag{C26}$$

$$M_s^{II} = \frac{2Et}{\rho^2} \tan \alpha \frac{1}{y^4} Y_2$$

$$M_\theta^{II} = \upsilon M_s^{II}$$

$$M_{s\theta}^{II} = \mp \frac{2(1-\upsilon)}{\rho^3} m \tan \alpha \frac{1}{y^4}\left\{y^{\rho}[(C_5+C_6)\cos(\rho \ell n y) + (C_6-C_5)\sin(\rho \ell n y)] - y^{-\rho}[(C_7-C_8)\cos(\rho \ell n y) + (C_8+C_7)\sin(\rho \ell n y)]\right\} \begin{matrix}\cos \\ \sin\end{matrix} \frac{n\pi\theta}{\theta_1}$$

$$S_s^{II} = \frac{Et}{L} \tan\alpha \frac{1}{\rho} \frac{1}{y^4} Y_1$$

$$S_\theta^{II} = \mp \frac{Et}{L} 2(2-\upsilon) \frac{1}{\rho^2} m \tan\alpha \frac{1}{y^4} Y_2$$

where

$$Y_1 = y^{\rho}[(C_6-C_5)\cos(\rho \ell ny) - (C_5+C_6)\sin(\rho \ell ny)] + y^{-\rho}[(C_8+C_7)\cos(\rho \ell ny) + (C_8-C_7)\sin(\rho \ell ny)]$$

$$Y_2 = y^{\rho}[C_6 \cos(\rho \ell ny) - C_5 \sin(\rho \ell ny)] - y^{-\rho}[C_8 \cos(\rho \ell ny) - C_7 \sin(\rho \ell ny)]$$

A PARTICULAR SOLUTION

Consider a conical shell subjected to a lateral normal load which is constant along the meridians and has a sinusoidal distribution in the circumferential direction. This was the case treated in Appendix A. The set of equations (C6) of membrane theory may be used for the particular solution.

Let

$$P_\theta = P_s = 0$$

$$P_r = p_n \begin{matrix}\cos \\ \sin\end{matrix} \frac{n\pi\theta}{\theta_1} \qquad (C27)$$

and assume

$$u^p = d_1 y^4 \begin{matrix}\sin \\ \cos\end{matrix} \frac{n\pi\theta}{\theta_1}$$

$$v^p = d_2 y^4 \begin{matrix} \cos \\ \sin \end{matrix} \frac{n\pi\theta}{\theta_1} \tag{C28}$$

$$w^p = d_3 y^4 \begin{matrix} \cos \\ \sin \end{matrix} \frac{n\pi\theta}{\theta_1}$$

where d_1, d_2, and d_3 are coefficients to be determined by the substitution of expressions (C27) and (C28) into equations (C6). When this is done the results are

$$\begin{aligned} u^p &= \pm \frac{p_n L^2}{Eh} \frac{1}{12} \frac{m}{\tan \alpha} [11 + 2\upsilon - m^2] y^4 \begin{matrix} \sin \\ \cos \end{matrix} \frac{n\pi\theta}{\theta_1} \\ v^p &= \frac{p_n L^2}{Eh} \frac{1}{12 \tan \alpha} [3(1-2\upsilon) - m^2] y^4 \begin{matrix} \cos \\ \sin \end{matrix} \frac{n\pi\theta}{\theta_1} \\ w^p &= \frac{p_n L^2}{Eh} \frac{1}{12 \tan \alpha} (m^2-1)(m^2-9) y^4 \begin{matrix} \cos \\ \sin \end{matrix} \frac{n\pi\theta}{\theta_1} \end{aligned} \tag{C29}$$

The corresponding stresses obtained from (C1) with $k = 0$ are:

$$\begin{aligned} N_s^p &= \frac{p_n L}{6 \tan \alpha} (3-m^2) y^2 \begin{matrix} \cos \\ \sin \end{matrix} \frac{n\pi\theta}{\theta_1} \\ N_\theta^p &= \frac{p_n L}{\tan \alpha} y^2 \begin{matrix} \cos \\ \sin \end{matrix} \frac{n\pi\theta}{\theta_1} \\ N_{\theta s}^p &= \pm \frac{p_n L}{3 \tan \alpha} m y^2 \begin{matrix} \sin \\ \cos \end{matrix} \frac{n\pi\theta}{\theta_1} \end{aligned} \tag{C30}$$

By retaining the solutions of the lowest order of $\frac{1}{\rho}$, one finally has the complete solutions for a shell subjected to the lateral load (C7)

$$
\begin{aligned}
&u = u^I + u^p, \quad v = v^I + v^p, \\
&w = w^I + w^{II} + w^p; \\
&N_s = N_s^I + N_s^p, \quad N_\theta = N_\theta^{II} + N_s^p, \\
&N_{s\theta} = N_{\theta s} = T_s = N_{s\theta}^I + N_{s\theta}^p \\
&M_s = M_s^{II} \qquad M_\theta = M_\theta^{II} \\
&M_{\theta s} = M_{s\theta} = M_{s\theta}^{II}, \quad S_\theta = S_\theta^{II} \\
&S_s = S_s^{II}
\end{aligned}
\tag{C31}
$$

NUMERICAL EXAMPLES

In what follows, two numerical examples are given. One is the engine shroud discussed in Appendix A. The other is a cantilevered complete cone frustum for which the numerical solutions are available in [C4] and [C5]. Comparisons of the present solution with those given in [C5] will be made.

Example 1

The engine shroud considered is a semicircular truncated conical shell segment which has two generators simply supported with the small end fixed and the other end free. Thus the lower set of sinusoidal functions of the solutions is used with the following boundary conditions for the solution:

$$
\begin{aligned}
&u = v = w = \frac{\partial w}{\partial s} = 0 \qquad \text{at } y = \sqrt{\frac{L_1}{L}} \\
&N_s = T_s = M_s = S_s = 0 \quad \text{at } y = 1
\end{aligned}
\tag{C32}
$$

The same material and geometrical constants as used in Appendix A are used here, i.e.,

$$\upsilon = \frac{1}{3},\ \alpha = 75^{o} \text{ and } \frac{L_1}{L} = 0.90 \tag{C33}$$

Numerical results for $\frac{t}{R} = 0.006$ and $n = 1, 2$ are computed. The results are given in the form

$$F_n(y, \theta) = f_n(y) \begin{matrix} \sin \\ \cos \end{matrix} \frac{n\pi\theta}{\theta_1} \qquad n = 1 \text{ and } 2 \tag{C34}$$

The functions $f_n(y)$ are shown as the solid lines in Figures C1 through C7. The respective functions obtained in Appendix A are also shown in these figures by dotted lines if there are some differences.

Example 2

In this example, a cantilevered complete cone frustum fixed at the smaller end is considered. At the larger free end, a rigid plate is attached and a moment, M, is applied about a horizontal axis. Thus the solutions are symmetrical about the vertical axis through the center of the cone. For such a complete cone, the upper set of sinusoidal functions of the solutions is used with the angle θ measured from the vertical line taking $n = 1$ and $\theta_1 = \Pi$.

The boundary conditions at the free end, referring to [C4], can be given as follows:

$$\begin{aligned}
&\pi R_1 [\bar{T}_s + \bar{S}_s \sin\alpha - \bar{N}_s \cos\alpha] = 0 \\
&\pi R_1 [\bar{M}_s - R_1 (\bar{N}_s \sin\alpha + \bar{S}_s \cos\alpha)] = -M \\
&\bar{u} \sec\alpha + \bar{v} + \bar{w} \tan\alpha = 0 \\
&\frac{\partial \bar{w}}{\partial s} + \frac{1}{R_1} [\bar{v} \sin\alpha - \bar{w} \cos\alpha] = 0
\end{aligned} \tag{C35}$$

where $R_1 = \frac{R}{\sin \alpha}$ and a function with a bar indicates that the function is of function of y only. When the asymptotic solutions are used and the terms of the lowest order of $\frac{1}{\rho}$ are retained, the conditions (C35) become

$$\bar{N}_{s\theta}^{I} - \bar{N}_{s}^{I} \cos \alpha = 0$$

$$\bar{N}_{s}^{I} = \frac{M}{\pi R_1^2} \frac{1}{\sin \alpha}$$

$$\bar{u}^{I} \sec \alpha + \bar{v}^{I} + (\bar{w}^{I} + \bar{w}^{II}) \tan \alpha = 0 \qquad \text{at } y = 1 \tag{C36}$$

$$\frac{\partial \bar{w}^{II}}{\partial s} = 0$$

The other four boundary conditions at the fixed end are:

$$u^{I} = v^{I} = w^{I} + w^{II} = \frac{\partial w^{II}}{\partial s} = 0 \qquad \text{at } y = \sqrt{\frac{L_1}{L}} \tag{C37}$$

The following material and geometrical constants are used:

$$\upsilon = 0.3, \quad \frac{t}{R} = \frac{1}{40}, \quad \tan \alpha = \frac{4}{3}, \text{ and } \frac{L_1}{L} = \frac{5}{8} \tag{C38}$$

Two sets of stress ratios, σ_2/σ_{1Mmax} and σ_m/σ_{1Mmax}, were computed, and are given in Figure C8, where

$$\sigma_2 = \frac{N_\theta}{t}$$

$$\sigma_{1Mmax} = \frac{N_s}{t}\Big]_{max} \tag{C39}$$

$$\sigma_m = \frac{6M_s}{h^2}$$

CLOSING REMARKS

The asymptotic solutions obtained are relatively simple when compared to other available solutions for conical shells of constant thickness. The results of the first example show that the difference between the solutions for linearly varying thickness and constant thickness is relatively small. This indicates that the assumption that these two types of shell will behave alike when the ratio of thickness to radius is very small is acceptable.

The difference between the present and other available solutions shown in the second example may be attributed to the relatively large ratio of t/R which is $\frac{1}{40}$. Such a shell is relatively thick for the application of the asymptotic solutions. Nevertheless, the results may still be valuable for preliminary design purposes assuming that the other solutions are better than the present solutions. This assumption, however, needs further verification which can probably be obtained by an experimental study.

REFERENCES

C1. Flugge, W.: Stresses in Shells. Second printing, Springer-Verlag, (Berlin), 1960, pp. 590-593.

C2. Love, A. E. H. : A Treatise of the Mathematical Theory of Elasticity. Dover Publication, New York, N. Y., 4th ed., 1944.

C3. Wilson, B.: Asymmetrical Bending of Conical Shells. Proc. ASCE 86, EM 3 (Jour. Eng. Mech. Div.), June 1960, pp. 119-139.

C4. Thruston, G. A.: A Numerical Solution for Thin Conical Shells Under Asymmetrical Loads. Proceedings of the 4th Midwestern Conference on Solid Mechanics, Austin, Texas, The University of Texas, 1959, pp. 171-194.

C5. Clark, R. A., and Garibotti, J. F.: Longitudinal Bending of a Conical Shell. Proceedings of the 8th Midwestern Mechanics Conference, 1963.

C6. Hoff, N. J.: Thin Circular Conical Shell under Arbitrary Loads. Jour. Appl. Mech., Trans. ASME, Vol. 22, No. 4, Dec. 1955, pp. 557-562. Discussion by F. W. Pohle, Jour. Appl. Mech. Trans. ASME, Vol. 23, No. 2, June 1956, pp. 322-323.

C7. Seide, Paul: A Donnell Type Theory for Asymmetrical Bending and Buckling of Thin Conical Shells. Jour. Appl. Mech. ASME, Vol. 24, No. 4, Dec. 1957, pp. 517-552.

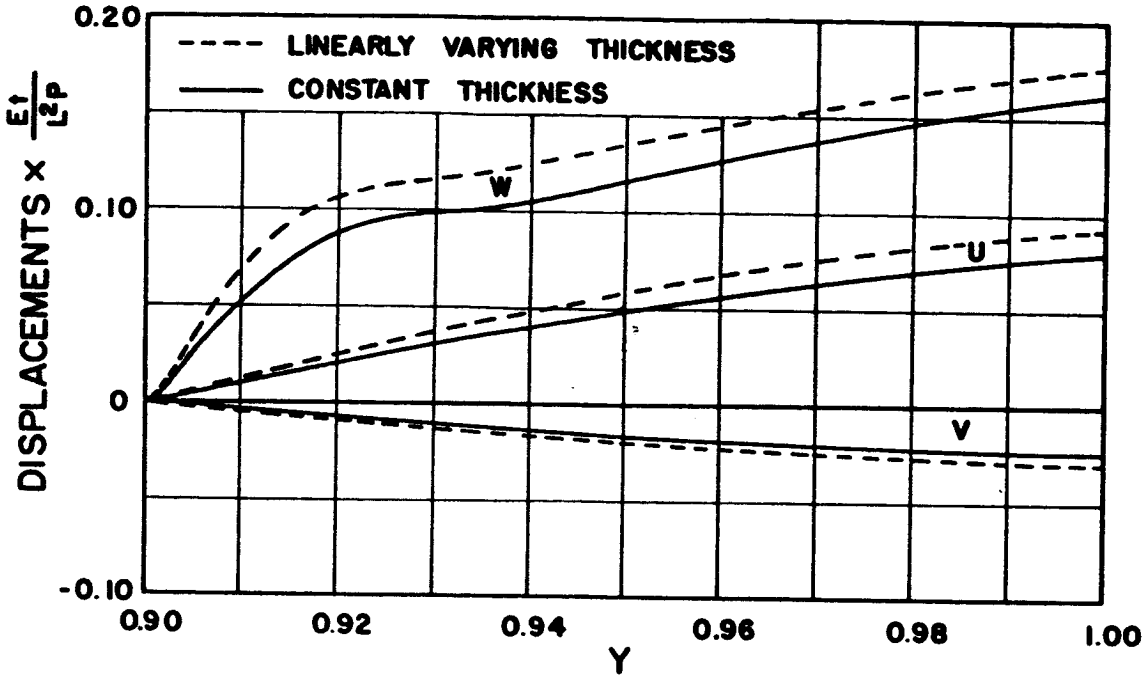

FIGURE C1. - DISPLACEMENTS U, V AND W FOR N= 1.

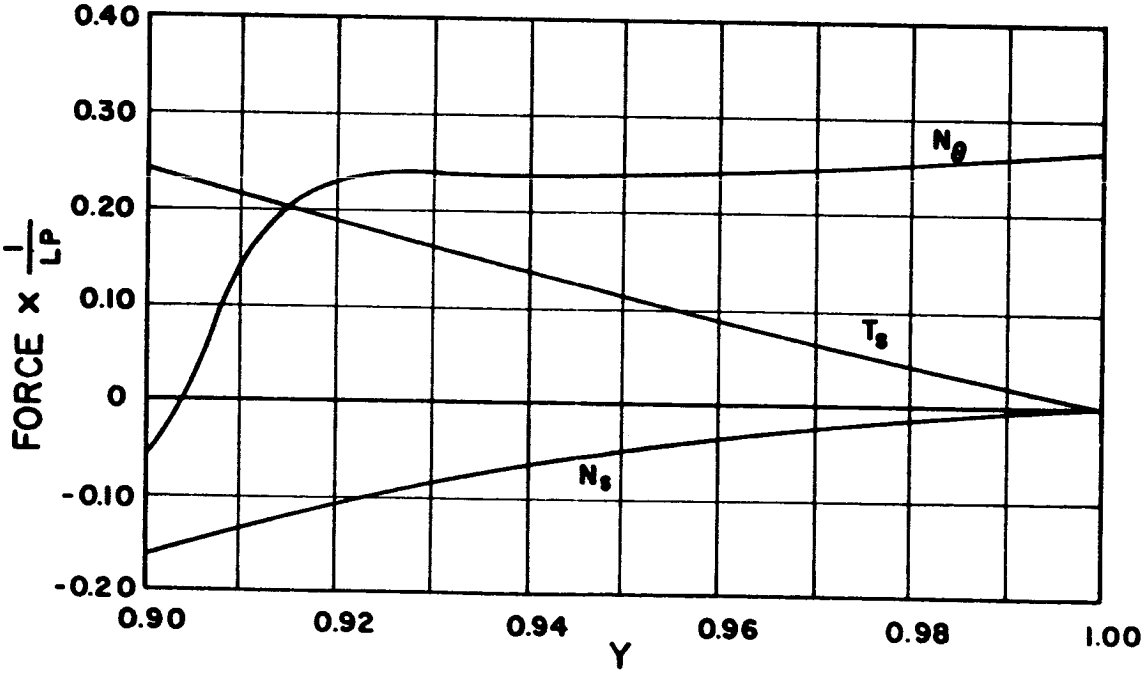

FIGURE C2. - MEMBRANE FORCES N_θ, T_s AND N_s FOR N = 1.

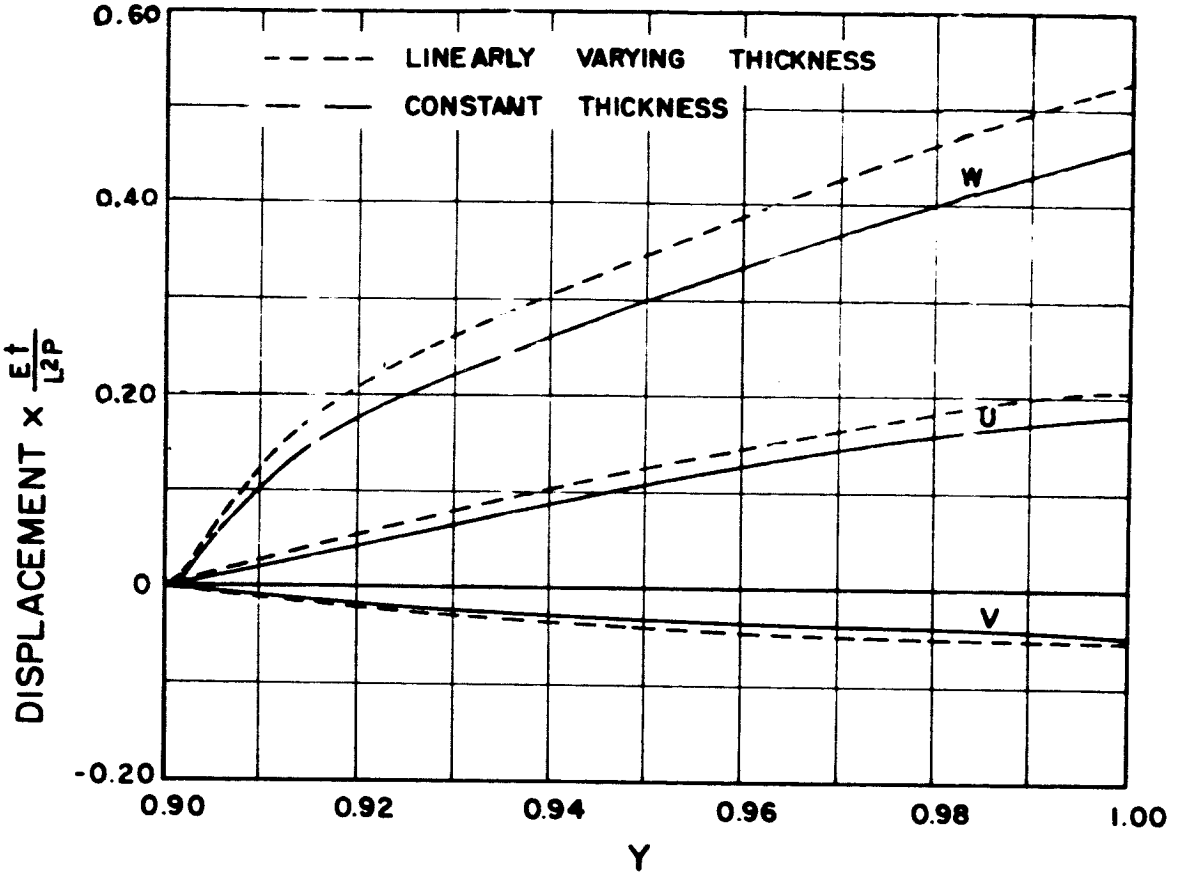

FIGURE C3. - DISPLACEMENTS U, V AND W FOR N = 2.

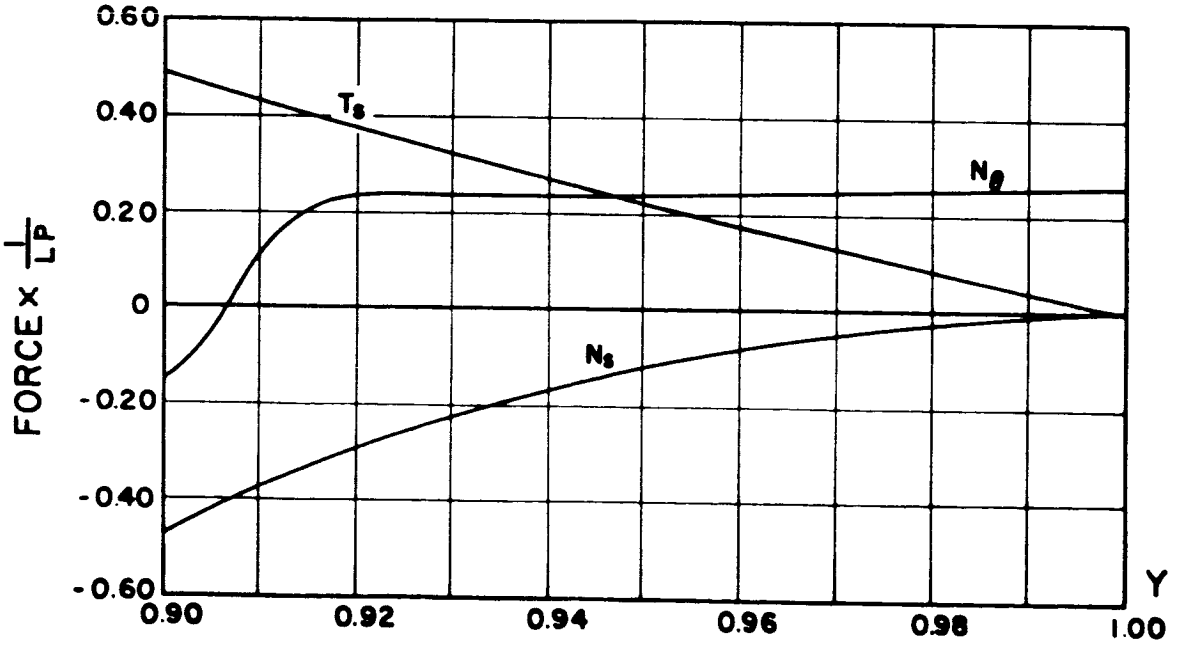

FIGURE C4. - MEMBRANE FORCES N_θ, T_s AND N_s FOR N = 2.

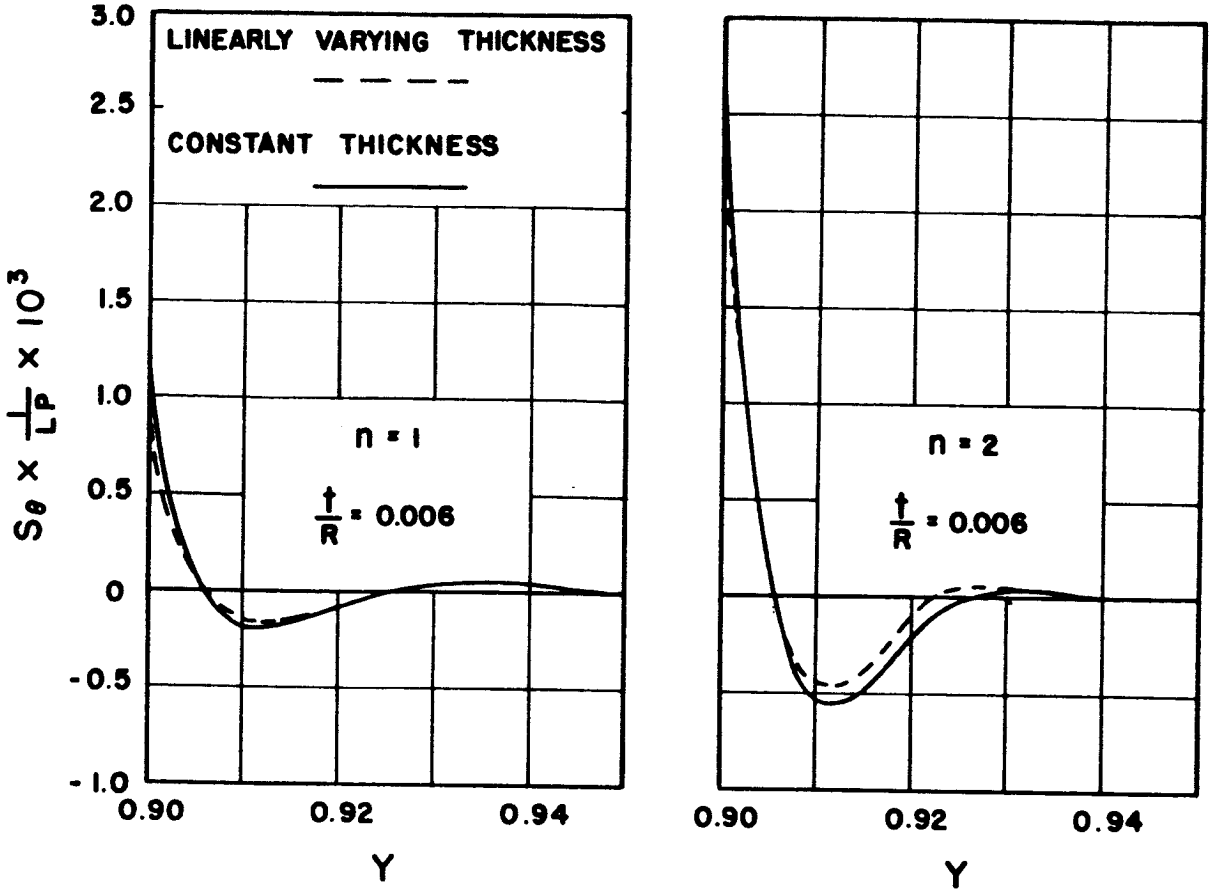

FIGURE C5. - TRANSVERSE SHEARING FORCE S_θ.

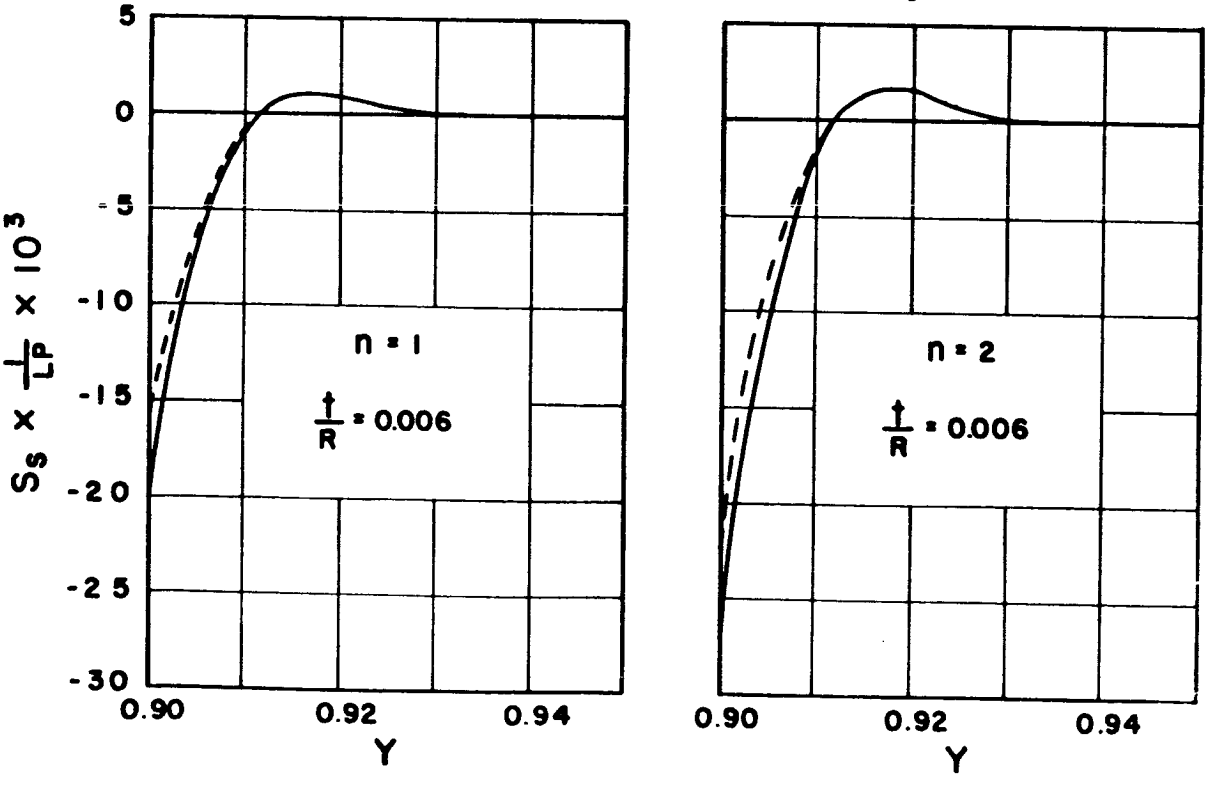

FIGURE C6. - TRANSVERSE SHEARING FORCE S_s.

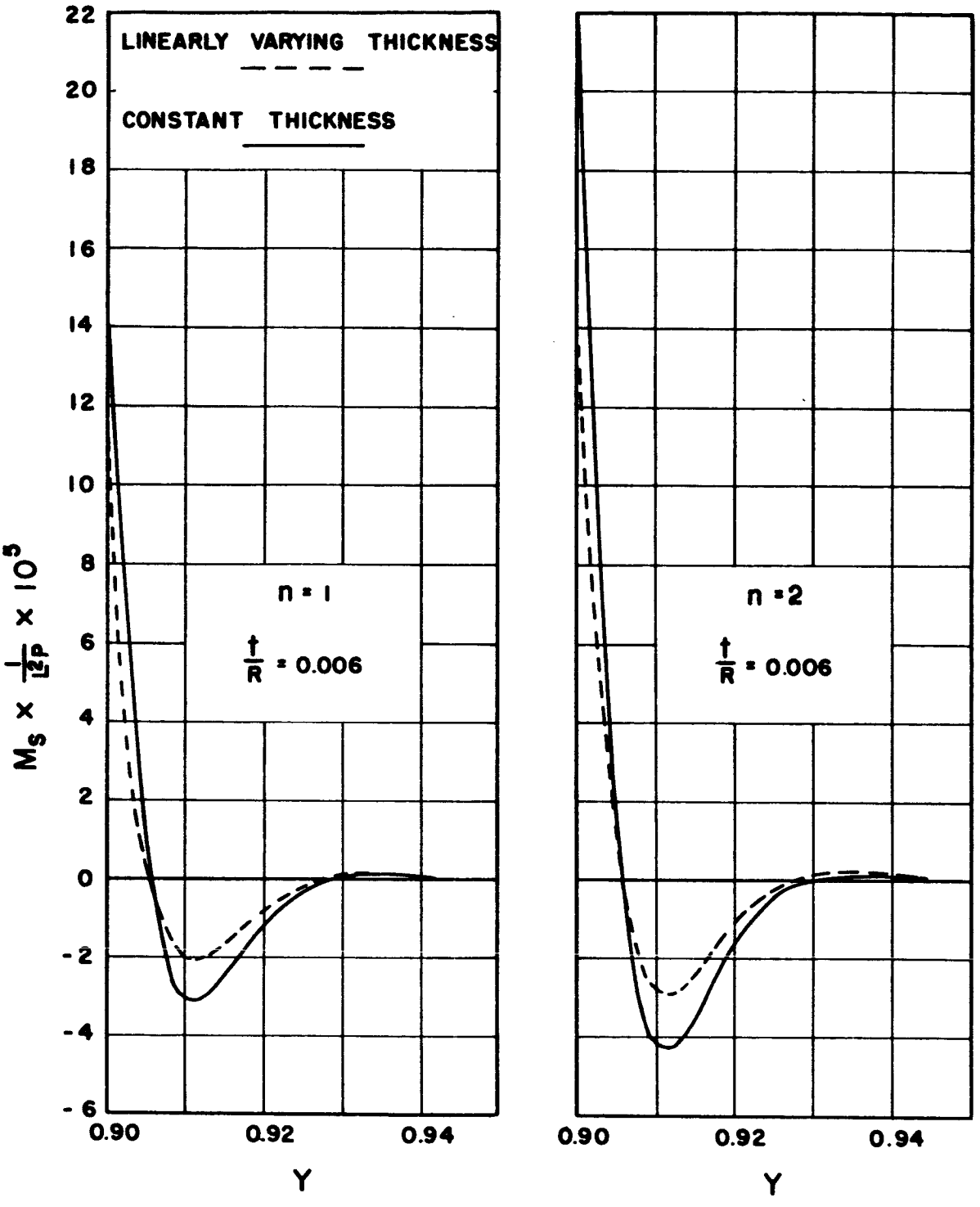

FIGURE C7. - NORMAL MOMENT M_s.

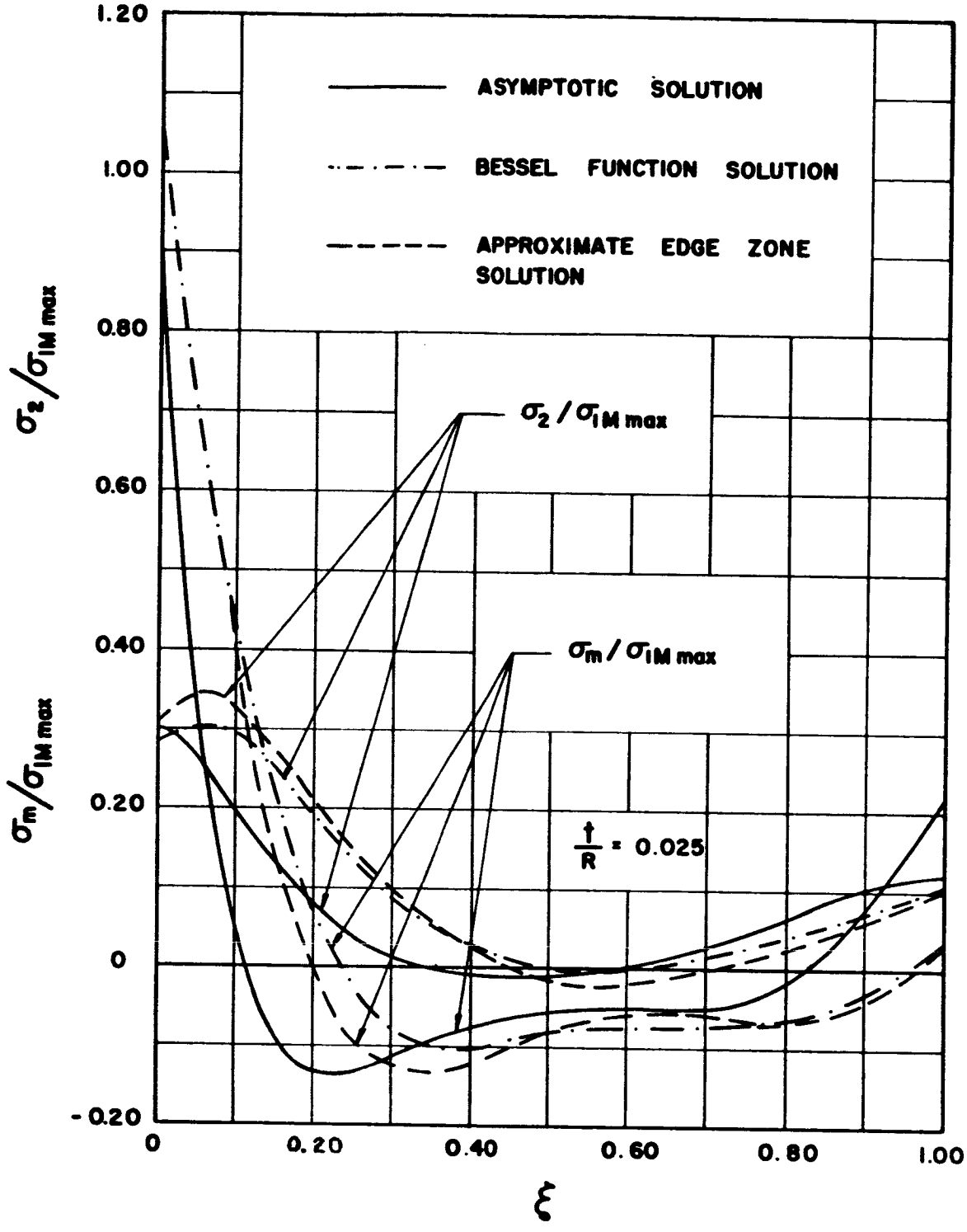

FIGURE C8. - STRESSES FOR EXAMPLE 2.

APPENDIX D

COMPUTER PROGRAMS FOR CONICAL SHELLS

By Han Yun Chu

The contents of this appendix were previously submitted as a part of Progress Report No. 6 for NASA Contract NAS8-11155.

COMPUTER PROGRAMS FOR CONICAL SHELLS

By Han Yun Chu*

The Univac Solid-State Fortran II language is used for the computer programs included.

The following table shows the relationship between the symbols used in the computer programs and those in the equations:

In equations	$\frac{Et}{pL^2}d_1$	$\frac{Et}{pL^2}d_2$	$\frac{Et}{pL^2}b_1$	$\frac{Et}{pL^2}C_i$	$\frac{Et}{pL^2}w$	$\frac{1}{pL^2}M_s$
In programs	D(1)	D(2)	D(3)	C(i)	W	Y

$\frac{1}{pL}S_s$	$\frac{Et}{pL^2}u$	$\frac{Et}{pL^2}v$	$\frac{Et}{pL}\frac{\partial w}{\partial s}$	$\frac{1}{pL}N_s$	$\frac{1}{pL}N_\theta$	$\frac{1}{pL}T_s$	$\frac{1}{pL}S_\theta$
Z	E	F	G	H	A	B	X

τ	α	ν	L	δ	k	ρ	y	ξ	m	β	$\sigma_{2m}/\sigma_{1m_{max}}$	$\sigma_m/\sigma_{1m_{max}}$
TS	S	P	FLI	DB	FKS	Q	T	R	U	CT	RN	RM

COMPUTER PROGRAMS

Computer Program 1

Computer program 1 is for the numerical example given in Appendix A.

---

*Graduate student in Engineering Mechanics, University of Alabama, University, Alabama and Graduate Research Associate for NASA Contract NAS8-11155.

```
      DIMENSION D(3), C(8)
2     READ 1, TS, S, P, R, U
1     FORMAT (5E15.7)
      FL1=373.312/0.96593
      DB=TS/FL1
      FKS=DB**2/12.0
      Q=(SQRT(2.0)/2.0)*((16.0*(1.0-P**2)*(TAN(S))**2)/FKS)**(1.0/4.0)
      Q=ABS(Q)
      PRINT 4, S, P, R, FL1, DB, FKS, Q
4     FORMAT (6HS    = ,E15.7,/,6HP    = ,E15.7,/,6HR    = ,E15.7,/,
     1          6HFL1 = ,E15.7,/,6HDB  = ,E15.7,/,6HFKS = ,E15.7,/,
     2          6HQ    = ,E15.7,/)
      V=Q*LN(R)
      D(1)=U/(TAN(S)*3.0)*(U**2-3.0*(5.0-P)/2.0-3.0*(1.0+P)/(2.0*U**2))
      D(2)=U/TAN(S)/3.0*(U**2-7.0+2.0*P)
      D(3)=1.0/(6.0*TAN(S))*(3.0*(1.0-2.0*P)-U**2)
      C(1)=(U**2-1.0)/TAN(S)*(-D(3)*R**2-((1.0+P)*D(3)-U*P*(D(1)-D(2))+
     1(1.0-P)/4.0*U*(D(2)+2.0*U*D(3)))/((1.0-P**2)*R**2)+U*(D(2)+2.0*U*
     2D(3))/(8.0*(1.0+P)*R**4))
      C(2)=(U**2-2.0*(1.0-P))/(2.0*(1.0-P**2)*TAN(S))*((1.0+P)*D(3)-U*P
     1*(D(1)-D(2))+(1.0-P)*U*(D(2)+2.0*U*D(3))/4.0)
      C(3)=U/TAN(S)*((U*D(3)-D(1)-D(2)*LN(R))+U/(2.0*(1.0-P**2)*R**4)
     1*((1.0+P)*D(3)-U*P*(D(1)-D(2))+(1.0-P)/4.0*U*(D(2)+2.0*U*D(3)))
     2-(D(2)+2.0*U*D(3))/(12.0*(1.0+P)*R**6)*(U**2+2.0*(1.0+P)))
      C(4)=-(U*(D(2)+2.0*U*D(3))*(U**2-7.0+2.0*P))/(24.0*(1.0+P)*TAN(S))
      CT=(R**Q*(3.0*COS(V)-SIN(V))+R**(-Q)*(COS(V)-SIN(V)))/(R**Q*(-COS(
     1V)+SIN(V))+R**(-Q)*(COS(V)+SIN(V)))
      C(6)=-(C(1)*R+C(2)/R+C(3)*R**3+C(4)/R**3+U/TAN(S)*D(2)*(1.0+LN(R))
     1*R**3)/(R**Q*((2.0+CT)*COS(V)+SIN(V))+R**(-Q)*(CT*COS(V)+SIN(V)))
      C(5)=(2.0+CT)*C(6)
      C(7)=CT*C(6)
      C(8)=C(6)

      PRINT 7, (J, C(J), J=1, 8)
7     FORMAT (2HC(, I2, 4H) = , E15.7, /)
5     READ 6, T
6     FORMAT (E15.7)
      W=(C(1)+C(2)/T**2+C(3)*T**2+C(4)/T**4+U/TAN(S)*D(2)*(1.0+LN(T))*T*
     1*2+T**(-1)*(T**Q*(C(5)*COS(Q*LN(T))+C(6)*SIN(Q*LN(T)))+T**(-Q)*(C(
     27)*COS(Q*LN(T))+C(8)*SIN(Q*LN(T)))))
      Y=(2.0/Q**2*T*(T**Q*(C(6)*COS(Q*LN(T))-C(5)*SIN(Q*LN(T)))+T**(-Q)
     1*(-C(8)*COS(Q*LN(T))+C(7)*SIN(Q*LN(T)))))*(TAN(S))**2
      Z=(1.0/(Q*T)*(T**Q*((-C(5)+C(6))*COS(Q*LN(T))+(-C(5)-C(6))
```

```
     1*SIN(Q*LN(T)))+T**(-Q)*((C(7)+C(8))*COS(Q*LN(T))+(-C(7)+C(8))
     2*SIN(Q*LN(T)))))*(TAN(S))**2
      E=U*TAN(S)*(C(1)/(U**2-1.0)+C(2)/((U**2-2.0*(1.0-P))*T**2)+C(3)
     1*T**2/U**2+((U**2-4.0*(1.0+P))*C(4))/(U**2*(U**2-7.0+2.0*P)*T**4))
     2+(D(1)+D(2)*LN(T))*T**2
      F=TAN(S)*(C(1)/(U**2-1.0)+(2.0*C(2))/(U**2-2.0*(1.0=P))
     1*T**(-2)+3.0*C(4)/((U**2-7.0+2.0*P)*T**4))+D(3)*T**2
      G=Q/(2.0*T**3)*(T**Q*((C(5)+C(6))*COS(Q*LN(T))+(-C(5)+C(6))
     1*SIN(Q*LN(T)))+T**(-Q)*((-C(7)+C(8))*COS(Q*LN(T))
     2+(-C(7)-C(8))*SIN(Q*LN(T))))
      H=-2.0*TAN(S)*(C(2)/((U**2-2.0*(1.0-P))*T**2)+3.0*C(4)/((U**2-7.0+
     12.0*P)*T**4))+T**2/(1.0-P**2)*((1.0+P)*D(3)-U*P*(D(1)-D(2)))
      A=1.0/(1.0-P**2)*(D(3)*(1.0+P)-U*(D(1)-D(2)))*T**2
     1+T**(-1)*(T**Q*(C(5)*COS(Q*LN(T))+C(6)*SIN(Q*LN(T)))
     2+T**(-Q)*(C(7)*COS(Q*LN(T))+C(8)*SIN(Q*LN(T))))*TAN(S)
      B=((6.0*TAN(S)*C(4))/(U*(U**2-7.0+2.0*P)*T**4)
     1+((D(2)+2.0*U*D(3))*T**2)/(4.0*(1.0+P)))
      X=2.0*U*(2.0-P)/(Q**2*T)*(T**Q*(C(6)*COS(Q*LN(T))-C(5)*SIN(Q*
     1LN(T)))+T**(-Q)*(-C(8)*COS(Q*LN(T))+C(7)*SIN(Q*LN(T))))
     2*(TAN(S))**2
      PRINT 8, W, TS, Y, Z, E, F, U, G, H, A, B, T, X
8     FORMAT (4HW = , E19.7, 15X, 4HTS= , E15.7, /, 4HY = , E19.7, /,
     1          4HZ = , E19.7, /,    4HE = , E19.7, /, 4HF = , E19.7, 15X,
     2          4HU = , E15.7, /,    4HG = , E19.7, /, 4HH = , E19.7, /,
     3          4HA = , E19.7, /,    4HB = , E19.7, 15x, 4HT = , E15.7, /,
     4          4HX = , E19.7, 3/)
      GO TO 5
      END
DATA CARDS:
0.40          1.309          0.33          0.90          3.86
0.40          1.309          0.33          0.90          7.72
0.60          1.309          0.33          0.90          3.86
0.60          1.309          0.33          0.90          7.72
0.80          1.309          0.33          0.90          3.86
0.80          1.309          0.33          0.90          7.72

0.900
0.902
 ---
      PRINT 7, (J, C(J), J=1, 8)
7     FORMAT (2HC(, I2, 4H) = , E15.7, /)
5     READ 6, T
6     FORMAT (E15.7)
      W=(C(1)+C(2)/T**2+C(3)*T**2+C(4)/T**4+U/TAN(S)*D(2)*(1.0+LN(T))*T*
     1*2+T**(-1)*(T**Q*(C(5)*COS(Q*LN(T))+C(6)*SIN(Q*LN(T)))+T**(-Q)*(C(
     27)*COS(Q*LN(T))+C(8)*SIN(Q*LN(T)))))
      Y=(2.0/Q**2*T*(T**Q*(C(6)*COS(Q*LN(T))-C(5)*SIN(Q*LN(T)))+T**(-Q)
```

```
     1*(-C(8)*COS(Q*LN(T))+C(7)*SIN(Q*LN(T)))))*(TAN(S))**2
      Z=(1.0/(Q*T)*(T**Q*((-C(5)+C(6))*COS(Q*LN(T))+(-C(5)-C(6))
     1*SIN(Q*LN(T)))+T**(-Q)*((C(7)+C(8))*COS(Q*LN(T))+(-C(7)+C(8))
     2*SIN(Q*LN(T)))))*(TAN(S))**2
      E=U*TAN(S)*(C(1)/(U**2-1.0)+C(2)/((U**2-2.0*(1.0-P))*T**2)+C(3)
     1*T**2/U**2+((U**2-4.0*(1.0+P))*C(4))/(U**2*(U**2-7.0+2.0*P)*T**4))
     2+(D(1)+D(2)*LN(T))*T**2
      F=TAN(S)*(C(1)/(U**2-1.0)+(2.0*C(2))/(U**2-2.0*(1.0=P))
     1*T**(-2)+3.0*C(4)/((U**2-7.0+2.0*P)*T**4))+D(3)*T**2
      G=Q/(2.0*T**3)*(T**Q*((C(5)+C(6))*COS(Q*LN(T))+(-C(5)+C(6))
     1*SIN(Q*LN(T)))+T**(-Q)*((-C(7)+C(8))*COS(Q*LN(T))
     2+(-C(7)-C(8))*SIN(Q*LN(T))))
      H=-2.0*TAN(S)*(C(2)/((U**2-2.0*(1.0-P))*T**2)+3.0*C(4)/((U**2-7.0+
     12.0*P)*T**4))+T**2/(1.0-P**2)*((1.0+P)*D(3)-U*P*(D(1)-D(2)))
      A=1.0/(1.0-P**2)*(D(3)*(1.0+P)-U*(D(1)-D(2)))*T**2
     1+T**(-1)*(T**Q*(C(5)*COS(Q*LN(T))+C(6)*SIN(Q*LN(T)))
     2+T**(-Q)*(C(7)*COS(Q*LN(T))+C(8)*SIN(Q*LN(T))))*TAN(S)
      B=((6.0*TAN(S)*C(4))/(U*(U**2-7.0+2.0*P)*T**4)
     1+((D(2)+2.0*U*D(3))*T**2)/(4.0*(1.0+P)))
      X=2.0*U*(2.0-P)/(Q**2*T)*(T**Q*(C(6)*COS(Q*LN(T))-C(5)*SIN(Q*
     1LN(T)))+T**(-Q)*(-C(8)*COS(Q*LN(T))+C(7)*SIN(Q*LN(T))))
     2*(TAN(S))**2
      PRINT 8, W, TS, Y, Z, E, F, U, G, H, A, B, T, X
 8    FORMAT (4HW = , E19.7, 15X, 4HTS= , E15.7, /, 4HY = , E19.7, /,
     1          4HZ = , E19.7, /,    4HE = , E19.7, /, 4HF = , E19.7, 15X,
     2          4HU = , E15.7, /,    4HG = , E19.7, /, 4HH = , E19.7, /,
     3          4HA = , E19.7, /,    4HB = , E19.7, 15x, 4HT = , E15.7, /,
     4          4HX = , E19.7, 3/)
      GO TO 5
      END
DATA CARDS:
0.40          1.309          0.33          0.90          3.86
0.40          1.309          0.33          0.90          7.72
0.60          1.309          0.33          0.90          3.86
0.60          1.309          0.33          0.90          7.72
0.80          1.309          0.33          0.90          3.86
0.80          1.309          0.33          0.90          7.72

0.900
0.902
 ---
0.912
0.916
 ---
0.940
0.950
 ---
1.000
```

Computer Program 2

Computer program 2 is for the numerical example given in Appendix B.

The same program as Computer Program 1 is used except cards D(1), D(2) and D(3) are replaced by the following cards respectively.

```
      D(1)=U/(6.0*(1.0-P))*(3.0*(1.0+3.0*P)-3.0*(5.0-P)*TAN(S)
     1-(2.0*U**2-3.0*(1.0+P)/U**2)*(1.0-TAN(S)))
      D(2)=U/(3.0*(1.0-P))*((1.0+4.0*P-U**2)-TAN(S)*(7.0-2.0*P-U**2))
      D(3)=U**2/(6.0*(1.0-P))*(1.0-TAN(S)+3.0/U**2*((1.0-2.0*P)
     1*TAN(S)+1.0))
```

Computer Program 3

Computer Program 3 is for the first numerical example given in Appendix C.

```
      DIMENSION D(3), C(8)
      READ 1, TS, S, P, R
1     FORMAT (4E15.7)
      FL1=373.312/0.96593
      Q=(48.0*(1.0-P**2))**(0.25)*(FL1*TAN(S)/TS)**(0.5)
      Q=ABS(Q)
      PRINT 2, TS, S, P, R, FL1, Q
2     FORMAT (6HTS =, E15.7, /, 6HS =, E15.7, /, 6HP =, E15.7,
     1/, 6HR  =, E15.7, /, 6HFL1 =, E15.7, /, 6HQ  =, E15.7, 3/)
      V=Q*LN(R)
      BT=12.0*TAN(S)
3     READ 4, T
4     FORMAT (E15.7)
      DO 5, UR=1.0, 2.0, 1.0
      U=3.86*UR
      D(1)=-U*(11.0+2.0*P-U**2)/BT
      D(2)=(3.0*(1.0-2.0*P)-U**2)/BT
      D(3)=(U**2-1.0)*(U**2-9.0)/BT
      C(4)=2.0*U**2*(U**2-4.0)/BT
      C(2)=12.0*((U**2-1.0)**2)/BT
      C(1)=((U**2-P)/(2.0*(U**2-1.0))-LN(R))*C(2)-(U**2-1.0)
     1*(2.0*C(4)/(R**2*(U**2-4.0))+D(2)*R**4)
      C(3)=-U*D(1)*R**2-(U**2-2.0-2.0*P)*C(4)/(R**4*(U**2-4.0))
     1-U**2/(R**2*(U**2-1.0))*(C(1)-((1.0-P)/(2.0*(U**2-1.0))
     2-LN(R))*C(2))
      CK=(R**Q*(3.0*COS(V)-SIN(V))+R**(-Q)*(COS(V)-SIN(V)))
```

```
     1/(R**Q*(-COS(V)+SIN(V))+R**(-Q)*(CK*COS(V)+SIN(V)))
      C(6)=-(C(1)+C(2)*LN(R)+C(3)*R**2+C(4)*R**(-2)+D(3)*R**4)
     1/(R**Q*((CK+2.0)*COS(V)+SIN(V))+R**(-Q)*(CK*COS(V)+SIN(V)))
      C(7)=CK*C(6)
      C(5)=C(7)+2.0*C(6)
      C(8)=C(6)
      VT=Q*LN(T)
      W=1.0/TAN(S)*(C(1)+C(2)*LN(T)+C(3)*T**2+C(4)*T**(-2)+D(3)*T**4
     1+T**Q*(C(5)*COS(VT)+C(6)*SIN(VT))+T**(-Q)*
     2(C(7)*COS(VT)+C(8)*SIN(VT)))
      Y=2.0*TAN(S)/(Q**2*T**4)*(T**Q*(C(6)*COS(VT)-C(5)*SIN(VT))
     1+T**(-Q)*(-C(8)*COS(VT)+C(7)*SIN(VT)))
      Z=TAN(S)/(Q*T**4)*(T**Q*((C(6)-C(5))*COS(VT)-(C(5)+C(6))*SIN(VT))
     1+T**(-Q)*((C(8)+C(7))*COS(VT)-(C(7)-C(8))*SIN(VT)))
      E=1.0/U*(U**2/(U**2-1.0)*(C(1)-((1.0-P)/(2.0*(U**2-1.0))
     1-LN(T))*C(2))+C(3)*T**2+(U**2-2.0-2.0*P)*C(4)
     2/(T**2*(U**2-4.0)))+D(1)*T**4
      F=1.0/(U**2-1.0)*(C(1)-((U**2-P)/(2.0*(U**2-1.0))-LN(T))*C(2))
     1+2.0*C(4)/(T**2*(U**2-4.0))+D(2)*T**4
      G=Q/(2.0*TAN(S)*T**2)*(T**Q*((C(5)+C(6))*COS(VT)
     1+(C(6)-C(5))*SIN(VT))-T**(-Q)*((C(7)-C(8))*COS(VT)
     2+(C(8)+C(7))*SIN(VT)))
      H=C(2)/(2.0*(U**2-1.0)*T**2)-2.0*C(4)/((U**2-4.0)*T**4)
     1+T**2/(1.0-P**2)*((2.0+P)*D(2)-P*U*D(1)+P*D(3))
      A=T**2/(1.0-P**2)*((2.0*P+1.0)*D(2)-U*D(1)+D(3))+1.0/T**2
     1*(T**Q*(C(5)*COS(VT)+C(6)*SIN(VT))+T**(-Q)*
     2(C(7)*COS(VT)+C(8)*SIN(VT)))
      B=2.0*C(4)/(U*(U**2-4.0)*T**4)+T**2/(2.0*(1.0+P))
     1*(D(1)+U*D(2))
      X=2.0*TAN(S)*(2.0-P)*U/(Q**2*T**4)*(T**Q*(C(6)*COS(VT)
     1-C(5)*SIN(VT))+T**(-Q)*(-C(8)*COS(VT)+C(7)*SIN(VT)))
      PRINT 6, W, T, Y, Z, E, F, U, G, H, A, B, X
6     FORMAT (5H W = ,E19.7, 15X, 4HT = ,E15.7, /, 5H Y = ,E19.7, /,
     15H Z = ,E19.7, /, 5H E = ,E19.7, /, 5H F = ,E19.7, 15X,
     24HU = ,E15.7, /, 5H G = ,E19.7, /, 5H H = ,E19.7, /,
     35H A = ,E19.7, /, 5H B = ,E19.7, /, 5H X = ,E19.7, 3/)
5     CONTINUE
      GO TO 3
      END
DATA CARDS:
0.6                1.309              0.333              0.90
0.900
0.902
 ---
0.912
0.916
 ---
```

```
0.940
0.950
---
1.000
```

Computer Program 4

Computer Program 4 is for the second numerical example in Appendix C.

```
      DIMENSION C(8)
      READ 1, TS, S, P, R
1     FORMAT (4E15.7)
      FL1=13.333
      PI=3.1416
      BJ=1.0/(PI*(COS(S))**2*SIN(S))
      Q=ABS((48.0*(1.0-P**2))**(0.25)*(FL1*TAN(S)/TS)**(0.5))
      U=1.0/COS(S)
      PRINT 4, TS, S, P, Q, R, U
4     FORMAT (6H TS = ,E15.7,/,6H S  = ,E15.7,/,6H P  = ,E15.7,/,
     16H Q  = ,E15.7,/,6H R  = ,E15.7,/,6H U  = ,E15.7,3/)
      V=Q*LN(R)
      C(1)=(U**2-1.0)*BJ/ R**2
      C(2)=0
      C(3)=-BJ*(1.0+P+U**2/2.0)/R**4
      C(4)=-(U**2-4.0)*BJ/2.0
      DET=(R**Q-R**(-Q))**2-4.0*(SIN(V))**2
      BET=C(1)+C(2)*LN(R)+C(3)*R**2+C(4)/R**2
      C(5)=-1.0/DET*(BET*(R**Q*(COS(V)+SIN(V))-R**(-Q)*(COS(V)-SIN(V)))
     1+P*BJ*(1.0-R**(-2.0*Q)+2.0*(SIN(V))**2+SIN(2.0*V)))
      C(6)=1.0/DET*(BET*((R**Q-R**(-Q))*COS(V)-(R**Q-3.0*R**(-Q))*
     1SIN(V))+P*BJ*(SIN(2.0*V)+COS(2.0*V)-R**(-2.0*Q)))
      C(7)=P*BJ-C(5)
      C(8)=P*BJ-2.0*C(5)-C(6)
      PRINT 7, (J, C(J), J=1, 8)
7     FORMAT (2HC(, I2, 4H) = , E15.7, /)
5     READ 6,  XC
6     FORMAT (E15.7)
      T=SQRT((5.0*XC+8.333)/13.333)
      VT=Q*LN(T)
      HM=-2.0*C(4)/(R**4*(U**2-4.0))
      A=1.0/T**2*(T**Q*(C(5)*COS(VT)+C(6)*SIN(VT))
     1+T**(-Q)*(C(7)*COS(VT)+C(8)*SIN(VT)))
      Y=2.0*TAN(S)/(Q**2*T**4)*(T**Q*(C(6)*COS(VT)-C(5)*SIN(VT))
     1-T**(-Q)*(C(8)*COS(VT)-C(7)*SIN(VT)))
      RM=6.0*Y*FL1/(TS*HM)
```

```
      RN=A/HM
      PRINT 9, HM, T, Y, A, RM, XC, RN
9     FORMAT (4HHM = , E15.7, 15X, 4HT  =, E15.7, /, 4HY  = , E15.7, /,
     14HA = , E15.7, /, 4HRM =, E15.7, 15X, 4HXC =, E15.7, /, 4HRN =, E15.7, 3/)
      GO TO 5
      END
```

DATA CARDS

```
0.2             0.927           0.3             0.7900
0.00
0.02
- --
0.20
0.25
1.00
```

APPENDIX E

STABILITY OF SMALL PLASTIC CYLINDERS SUBJECTED TO INTERNAL PRESSURE AND AXIAL COMPRESSION

By Thomas A. Carlton, Jr. and Gustavo A. Aramayo

The contents of this appendix were previously submitted as Progress Report No. 3 for NASA Contract NAS8-11155.

APPENDIX E

STABILITY OF SMALL PLASTIC CYLINDERS SUBJECTED TO INTERNAL PRESSURE AND AXIAL COMPRESSION

By Thomas A. Carlton, Jr.* and Custavo A. Aramayo**

INTRODUCTION

The development of theoretical criteria for the buckling of monocoque and stiffened thin shell flight structures has taken place at a rapid pace under the impetus of the space program. The experimental verification of these criteria has made only limited progress. The reasons for the gap which has developed between theory and experimental verification are numerous. The use of high speed computers has made possible the rapid solution of complex shell stability equations. Thus, it has been possible to generate theoretical design data at a much faster rate than it can be experimentally verified.

Unfortunately, the idealized conditions assumed in the theoretical solutions are not realized in either model or prototype shell. In order to determine if the lack of ideal conditions in a physical model imposes a severe limitation on the use of totally theoretical design methods, an extensive experimental investigation must be undertaken.

In those cases where a particular structural configuration has been dictated by space and service requirements, both model and prototype have been constructed and tested so as to establish the practical limitations of that structure. The information gained is usually limited to the particular structure being studied and is not readily extrapolated to the general analysis of such structures.

It would be desirable to undertake a comprehensive experimental program to provide the necessary confidence in theoretical design criteria so that, at most, only limited non-destructive prototype testing

---

*Professor of Civil Engineering, University of Alabama, University, Alabama and Staff Associate for NASA Contract NAS8-11155.

**Graduate Student in Engineering Mechanics, University of Alabama, University, Alabama and Graduate Research Associate for NASA Contract NAS8-11155.

would be indicated. The practicability of such a program is dependent on being able to provide a large number of suitable models at a reasonable cost. Therein lies the primary objective of this study: to determine if suitable models for experimental shell stability studies can be inexpensively fabracated from commercially available sheets of cellulose acetate.

Under the terms of Contract NAS8-11155, an experimental study was conducted to determine the suitability of cylindrical shells fabricated from flat sheets of cellulose acetate for verifying theories of shell stability. The unstiffened plastic cylinders were subjected to various combinations of axial compressive load and internal pressure. A total of thirty-two cylinders were fabricated. However, data were collected for only twenty-three cylinders. The remaining cylinders were either destroyed during installation in the testing machine or had initial imperfections that made them unsuitable for testing.

It was initially proposed to conduct tests using cylinders of various L/D and r/t ratios. However, the actual test program was limited to one value of L/D and three values of r/t. Limitations on the r/t ratio were due mainly to the difficulties encountered in the installation of the cylinders into the loading device.

TEST SPECIMENS

The cylindrical shell models were prepared from flat cellulose acetate sheets measuring 20 inches by 50 inches. Thicknesses used were 0.0075, 0.010, and 0.015 inches. These sheets were cut to form the projection of the external wall of the cylinders and a longitudinal seam was formed by making a lap joint and gluing with Fibestos cement. Depending upon the wall thickness of the cylinder, two different overlaps were used for the longitudinal seam. A 1/8 inch overlap was used for the cylinders of the 0.010 and 0.015 inch wall thickness and a 1/4 inch overlap was used for the cylinders having a wall thickness of 0.0075 inches. An attempt was made to fabricate cylinders with a wall thickness of 0.005 inches, but inability to fabricate suitable models precluded the continuation of this effort.

The basic dimensions of the cylinders were: Length 20 inches,

average diameter 15 inches, and wall thicknesses of 0.0075, 0.010, and 0.015 inches resulting in radius-to-thickness ratios of 1000, 750, and 500 respectively. Wall thickness had a variation of ± 0.0002 inches as determined with a dial indicator reading to the nearest 0.0001 inches as shown in Figure E1. The diameter of the cylinders was within 0.05 per cent of the nominal mid-wall dimension of 15 inches. The diameter of each cylinder was determined by measuring the circumferential length and seam overlap prior to fabrication.

Coupons from each test cylinder were obtained in an attempt to determine the material properties of the individual specimen. At least two flat coupons 1 inch wide and having various gage lengths were cut from each flat sheet and tested in tension. Due to slippage of the coupons in the grips and, perhaps, other factors, the results of the tension tests of coupons from the same sheet exhibited large variations and were of little value in determining the tensile modulus of elasticity and Poisson's ratio. No attempt was made to determine the compressive modulus of elasticity of the flat coupons since compressive tests of the coupons would have required lamination of several coupons or some other device to prevent buckling that would have introduced additional unknowns.

In a further attempt to determine the material properties, data collected in the testing of the individual cylinders were analyzed. From the test of a cylinder at zero internal pressure, the modulus of elasticity in compression can be computed from the load-deformation curve and the dimensions of the cylinder. Then, if the vertical deformation of the unstrained cylinder is totally restrained when the internal pressure is applied, i.e., $\varepsilon_y = 0$, it is possible to compute Poisson's ratio. When the cylinder is clamped to the loading head, the difference between the internal pressure force on the loading head and the load required to prevent vertical deformation in the cylinder is used to compute the longitudinal tensile stress, σ_y, in the cylinder wall. The hoop stress, σ_x, is equal to $p(r/t)$. Thus, Poisson's ratio, ν, is σ_y/σ_x. However, measured forces indicated that slipping occurred between the cylinder and the loading head in every test, thus, partially relieving the induced σ_y stress. For this reason, it was necessary to disregard experimentally determined values of Poisson's ratio and use an assumed value of 0.3.

Furthermore, analysis of the test cylinder data showed that slippage occurred between the cylinders and supports. Since the displacement measurements made during the tests were obtained by measuring the relative displacement of the heads of the testing machine and the amount of slippage was indeterminate, this data could not be used to determine the compressive modulus of elasticity.

The experimentally determined values of the modulus of elasticity were all considerably less than the manufacturers specified value of 400,000 psi. However, because of the scatter in the test results and the unknown uncertainities in the tests conducted to determine the modulus of elasticity, the manufacturers nominal value of 400,000 psi was used in the analysis of the stability tests. Although it seems reasonable to assume that there are only small variations in the modulus of elasticity from sheet to sheet, it is possible that some of the scatter observed in the tests of the cylinders was due to variations in the compressive modulus of elasticity.

EQUIPMENT AND PRECEDURES

An Instron universal testing machine was used for applying the load and measuring the load and displacement as shown in Figures E2 and E3. The displacement measured was the total movement of the machine platen and therefore included any slipping between the loading head and the test cylinder. The load was transferred to the cylinders by means of end loading plates. The plates were designed to fit into the test cylinder a distance of one inch. The lower plate was fastened to the movable head of the machine and the upper plate was fastened to a load cell. The cylinders were installed in the loading rig by sliding the ends of the specimen over the loading plates and then clamping to the loading plates with a metal strap one-half inch wide. Thus, the load was transferred through the clamps into the cylinder. The clamps also helped seal any pressure leaks resulting from a lack of fit between the cylinder and the loading plates.

Internal pressure was provided from an air supply at 150 p.s.i. The air passed through a pressure regulator and a relief valve before going into the cylinder. A constant pressure was maintained during each test

by allowing a regulated amount of air to escape from the cylinder. Internal pressure was measured by means of a manometer reading in inches of mercury. Load versus displacement was obtained from an X - Y recorder with an electric strain gage load cell providing the load input and a resistance potentiometer providing machine crosshead movement as the displacement input.

The cylinder specimens were deformed at a constant rate. In order to determine the effect of rate of loading on the critical buckling load, two different rates were investigated. These rates were 0.005 and 0.05 inches/minute displacement of the crosshead of the loading machine. At low values of internal pressure, the buckling load resulting from the high rate of deformation was about 3 per cent higher than the buckling load obtained using the lower rate. However, at values of internal pressure of 1.5 p.s.i. and higher, no difference in the buckling loads was found at the two different rates of deformation. The data collected represent values of buckling corresponding to the slow rate of loading.

The load-deformation curve for the test cylinders was essentially linear over most of the range. However, near the maximum load, a sharp but smooth transition into a horizontal plateau of constant load and increasing deformation occurred. Critical buckling load was determined from this horizontal plateau of the load-deformation curve.

In some cases, the formation of isolated diamond-shaped buckles occurred prior to any indication of buckling in the load-deformation curve. The load at which this occurred was not recorded since the critical buckling load was found to be only slightly higher. The formation of buckles in the unpressurized cylinders was predominant around the seam in regions that showed some initial imperfections. At higher loads, the buckles showed a more uniform distribution and they were always more numerous in areas having such initial imperfections as dents and ripples.

In the pressurized cylinder tests, the internal pressure eliminated most of the visible evidence of imperfections in the cylinders. In the pressurized tests, the formation of the diamond-shaped buckles was preceded by the formation of a uniform circumferential ripple at top and bottom of the specimen. At the critical buckling load established by the load-deformation curve, some diamond shape buckles appeared in the same regions and progressed in the circumferential direction. These

buckles, in contrast with the ones formed in unpressurized tests, had their maximum dimension in the circumferential direction. Circumferential tension in cylinders subjected to axial compression tends to suppress the formation of diamond shaped buckles. Furthermore, the introduction of internal pressure into a cylinder increases the circumferential tension and, if the external pressure exceeds a certain limit, diamond shaped buckles are suppressed and the axisymmetric mode prevails. However, the presence of initial imperfections tends to suppress the axisymmetric buckle. In the tests conducted, the initial imperfections coupled with the low values of internal pressure produced diamond shaped buckles rather than axisymmetric buckles.

The tests were conducted by first applying the internal pressure to the cylinder while preventing any movement of the testing machine platen. The restraining force was recorded. The axial compressive load was then applied to the cylinder while the internal pressure remained constant. Each cylinder was subjected to a series of tests in which the internal pressure was varied from test to test and in which the cylinder was ultimately destroyed. After a cylinder was buckled at one value of internal pressure, the load and pressure were relieved, the pressure was increased by 1/2 psi and the cylinder was again loaded to the critical buckling load at the increased internal pressure. This procedure was established after one cylinder was first buckled several times with zero internal pressure and then loaded until buckling with internal pressures of 1, 2, 3 and 4 psi. Finally, this same cylinder was again buckled at zero internal pressure and no significant change in the buckling strength determined in the first test was observed. This procedure was repeated with other cylinders and the uniformity of test results indicated no effect on the mechanical properties due to repeated testing. These tests showed that the same cylinder could be used several times provided that the deformation was stopped as soon as the critical buckling load was reached.

The wave length of the buckles were not measured because this was not considered important in achieving the study objectives. Since the criterion of failure of the cylinders was a plateau in the load-displacement curve, the load was released as soon as a plateau was observed in the load displacement curve. This procedure permitted an individual

cylinder to be tested many times. However, in many of the tests only an incomplete system of buckles had formed when this criterion was observed. Therefore, the test procedure used would have required modification to permit measurement of the wave lengths of the buckles.

THEORETICAL BUCKLING CRITERION

A summary of the theoretical buckling criteria for pressurized and unpressurized monocoque thin shells is presented by Harris, Suer, Skene, and Benjamin [E1] *. Critical buckling stress for the unpressurized cylinder based on Donnell's [E2] equations is given in terms of a buckling coefficient, K_c. For the case of unpressurized long cylinders, this theoretical buckling coefficient becomes

$$K_c = \frac{4\sqrt{3}}{\pi^2}\left(\frac{L^2}{rt}\right)\sqrt{1-\nu^2} \qquad \text{(E1)}$$

The equation for critical stress is

$$\frac{\sigma_{cr}}{\eta} = K_c \pi^2 D\left(\frac{t}{L}\right)^2 \qquad \text{(E2)}$$

Substitution of the buckling coefficient into the critical stress equation results in the following equation for critical stress

$$\frac{\sigma_{cr}}{\eta} = \left(\frac{E}{\sqrt{3(1-\nu^2)}}\right)\left(\frac{t}{r}\right) \qquad \text{(E3)}$$

where $\eta = 1$ for the case of elastic buckling.

For a cylinder subjected to a combination of axial load and internal pressure, the critical stress and internal pressure are expressed in terms of the following non-dimensional parameters:

$$\bar{\sigma}_{cr} = \frac{\sigma_{cr}}{E}\left(\frac{r}{t}\right) \qquad \text{(E4)}$$

---

*Numbers in brackets designate references at the end of this appendix.

$$\bar{p} = \frac{p}{E}\left(\frac{r}{t}\right)^2 \qquad \text{(E5)}$$

where σ_{cr} is the stress in the cylinder at buckling.

Lo, Crate, and Schwartz [E3] indicate that this stress is equal to the stress in the cylinder corresponding to the load in the cylinder at the time of local buckling in any particular region of the shell. Thus, from these parameters and in accordance with Lo's analysis, the value of $\bar{\sigma}_{cr}$ increases from 0.376 for $\bar{p} = 0$ to a maximum of 0.605 for $\bar{p} = 0.169$. The Flugge theory [E4] indicates that the value of $\bar{\sigma}_{cr}$ is equal to 0.605 for all values of $\bar{p}$.

Following Lo's analysis, another non-dimensional parameter,

$$\Delta\bar{\sigma}_{cr} = \bar{\sigma}_{cr} - \bar{\sigma}_{cro} \qquad \text{(E6)}$$

can be determined. The only new term is $\bar{\sigma}_{cro}$, the non-dimensional stress corresponding to a condition of zero internal pressure. The definition of the stress term is the same as the one indicated for the non-dimensional buckling stress. Test results can be interpreted as a per cent of the theoretical buckling stress computed by equation (E3). Both the theoretical and experimental buckling stress and the internal pressures are substituted into equations (E4) and (E5) for comparison purposes.

In the analysis of the unpressurized cylinders, equation (E1) is rewritten in the following form

$$K_c = \frac{4\sqrt{3}}{\pi^2}(Z) \qquad \text{(E7)}$$

where the value of Z is as follows:

$$Z = \frac{L^2}{rt}\sqrt{1 - \nu^2} \qquad \text{(E8)}$$

also, equation (E4) is rewritten in the following form:

$$\sigma_{cr} = E\,\bar{\sigma}_{cr}\left(\frac{t}{r}\right) \qquad \text{(E9)}$$

EXPERIMENTAL DATA

The results of the experimental study are presented in Tables EI, EII, EIII, and EIV. For ease in analysis, these data are further summarized in graphical form. The experimental data have been substituted into equations E4 and E5 and the results plotted in Figures E4, E5, and E6. Each of these figures presents the data for a particular value of r/t. The variation in sheet thickness was not accounted for in these figures since it was a random variation over each sheet rather than a variation of thickness between cylinders. The critical buckling stress, σ_{cr}, was computed as the net buckling load divided by the cross-sectional area of the cylinder wall. The net buckling load is the total load on the cylinder at buckling minus the internal pressure reaction load, $p(\pi r^2)$. Each of the above figures contains all of the satisfactory experimental values of $\bar{\sigma}_{cr}$ vs $\bar{p}$ for a particular r/t ratio. In addition, the values of $\bar{\sigma}_{cr}$ have been averaged for each value of $\bar{p}$ and a curve sketched for these average values of $\bar{\sigma}_{cr}$. The theoretical relationship according to Lo [E3] is also shown on each of these figures. It should be noted that the experimental data more closely approximates the theory for the highest r/t ratio of 1000. The average values, taken from Figures E4, E5, and E6, have been summarized in Figure E7 for comparison purposes.

The data of Tables EI, EII, and EIII have also been substituted into equation E6 and the results plotted in Figures E8, E9, and E10. Average values from these graphs are summarized in Figure E11. These figures emphasize the stabilizing influence of internal pressure. Lo, Crate, and Schwartz [E3] have suggested that better correlation between theory and experiment can be obtained if the increment in buckling parameter, $\Delta\bar{\sigma}_{cr}$, is plotted against the pressure parameter, $\bar{p}$.

The experimental data for the unpressurized cylinders are presented in Figure E12 as a plot of the stress parameter, $\bar{\sigma}_{cr}$, versus the r/t ratio. A best fit curve for these data was determined by the method of least squares. The equation for this curve is as follows:

$$\bar{\sigma}_{cr} = 0.209 - 0.00003 \frac{r}{t} \qquad \text{(E10)}$$

Using equation E10, for r/t ratios of 500, 750, and 1000, values of $\bar{\sigma}_{cr}$ were computed respectively as 0.194, 0.186, and 0.179. It follows then, from equation E9, that, for the unpressurized cylinders, the best fit experimental values of the critical buckling stress, σ_{cr}, are respectively 155.00, 99.20, and 71.60 p.s.i. Equation E2 was solved for the buckling coefficient, K_c, for the case of elastic buckling and the materials and geometry used in this study. The values of the buckling coefficient, K_c, are respectively $(4.438)(\sigma_{cr})$, $(9.9855)(\sigma_{cr})$, and $(17.752)(\sigma_{cr})$ for r/t ratios of 500, 750, and 1000. Using the values of critical buckling stress, σ_{cr}, computed above, the experimental buckling coefficients, K_c, become respectively 687.89, 990.56, and 1271.04. The values of Z computed from equation E8 are 3060, 4591, and 6120 for wall thicknesses of 0.015, 0.010, and 0.0075, respectively.

The values of experimental K_c and Z computed above have been plotted on log-log paper in Figure E13 after the manner of Harris, Suer, Skene, and Benjamin [E1]. Superimposed on this plot are the theoretical and the 90 per cent probability curves taken from the same reference.

ANALYSIS OF RESULTS

The fabrication of the test cylinders from flat sheets of plastic was performed in a relatively unsophistocated manner. The sheets were hand trimmed and the longitudinal joint was formed on a flat table so that, at this point, the specimen looked more like a flat envelope than a cylinder. Although several different adhesives and techniques were investigated, the material tended to wrinkle along the seam resulting in a joint in which small local imperfections were readily noticeable. Unfortunately, it is not possible to represent the quality of the specimen in terms of initial local imprefections. However, it must be assumed that all had some local imperfections.

In view of the above observations on local imperfections, several interesting observations can be made from Figures E4, E5, and E6. It can

be observed that, for all three r/t ratios represented in these figures, the curve for the average values tends to flatten out and become parallel to the theoretical curve of Lo as $\bar{p}$ increases. Since the same cylinders were used in most cases for the full range of $\bar{p}$, it appears that the effect of local imperfections is less at high pressures. This is slightly misleading since many of the highly imperfect cylinders were actually destroyed before the higher values of internal pressure could be reached.

Assuming that the scatter in the experimental data is directly related to the quality of the cylinder, it is obvious that a large number of tests must be conducted when relatively imperfect cylinders are used. Although the behavior of the individual models is erratic, the curves representing the averages of the several tests behave very much according to theory. An error in the modulus of elasticity would shift all data points for the tests conducted on an individual cylinder an equal relative amount, but the scatter between tests of different cylinders is strictly a function of the local imperfections in the models and of the testing procedure. The trend of the averages is a measure of the ability of cellulose acetate to serve as a material from which to construct the models.

Another interesting observation can be made concerning the effect of initial imperfections as a function of r/t ratio. In figure E4, for an r/t of 500, the scatter is large and the trend of the averages is irregular. In Figure E5 for an r/t of 750, the trend of the averages is smoother and more closely approaches the theoretical curve. In Figure E6, for an r/t of 1000, the trend of the averages is quite smooth and indicates that the behavior of the cylinders can be approximated by the theory of Lo. Thus, it appears that, when pressurized, test data for the cylinders having the higher r/t ratios, or at least made from the thinner materials, are less effected by the initial imperfections. This assumes that models of all thicknesses had the same relative initial imperfections.

According to Lo, Crate, and Schwartz [E3], a better correlation between theory and experiment can be obtained if the increment in buckling parameter, $\Delta\bar{\sigma}_{cr}$, as computed by equation E6, is plotted against the pressure parameter, $\bar{p}$. This appears to be verified by the results shown in Figure E8 for the cylinders having an r/t of 500. However, Figures E9 and E10 for the higher r/t ratios show the data points to fall well

above the theory line of Lo. In attempting to verify the theory, Lo assumed that the unpressurized buckling parameter, $\bar{\sigma}_{cro}$, was always equal to 0.36, and subtracted this value from the experimental pressurized buckling parameter, $\bar{\sigma}_{cr}$, to obtain the incremental buckling parameter, $\Delta\bar{\sigma}_{cr}$. However, from Figures E4, E5, and E6 it is seen that the unpressurized buckling parameter, $\bar{\sigma}_{cro}$, determined in the experimental program at the University of Alabama is of the order of 0.2. Had the theoretical unpressurized buckling parameter, 0.36, been used to compute the points shown in Figures E9 and E10, the results would have very closely approximated the theory of Lo. To a lesser extent, the same would have been true for the higher values of $\bar{p}$ shown in Figure E8. Thus, it is clearly seen that the effects of pressurization quickly minimize the influence of model imperfections on the buckling strength of cylinders made with thinner materials. Also, at higher pressures, the thicker materials are less influenced by the initial imperfections. The theory of Lo appears to be satisfactory for determining the critical buckling strength of high r/t, pressurized cylinders and for lower r/t cylinders having high internal pressures. The references cited contain the results of twelve independent experimental investigations. Since the results obatined in this study compare satisfactorily with the experimental results in the cited references, no attempt was made to obtain comparisons with the large number of other investigations that are available in the literature.

The critical buckling parameter, $\bar{\sigma}_{cr}$, of the unpressurized cylinders has been plotted against r/t in Figure E12, and a best fit curve determined by least squares. The values of $\bar{\sigma}_{cr}$ determined from this curve together with the respective r/t ratios was used to compute values of K_c and Z from equations E2 and E8 respectively. These values have been plotted in Figure E13 against the theoretical curve of these quantities and the 90 per cent probability curve. It is noted that, in each case, the results determined from the best fit line fall above the 90 per cent probability line. Furthermore, in only two cases do the individual test results fall below the 90 per cent probability line.

CONCLUSIONS

The limited nature of the experimental work performed in this investigation does not permit reaching a large number of broad conclusions. However, within the scope of the work performed, several limited but important conclusions can be drawn.

1. The large amount of scatter in the test results indicates that more care should be taken in fabricating the test specimens and in conducting the individual tests. Several nearly identical specimens should be tested and the average of the results used for analysis purposes.

2. The manner in which the data obtained using cylinders fabricated from cellulose acetate tend to verify the theory of Lo, Crate, and Schwartz [E3], indicates that the use of this material for providing low cost test cylinders should be encouraged. However, a satisfactory method of determining the modulus of elasticity must be used.

3. For cylinders having high r/t ratios, the effect of initial local imperfections on buckling strength is quickly minimized by internal pressure. The more rigid the walls of the cylinder, the higher must be the internal pressure to satisfactorily minimize the imperfections.

4. In studying unpressurized cylinders, the test specimens should be as nearly free of initial imperfections as possible. The presence of such imperfections critically influences the buckling strength of such cylinders.

5. The theory of Lo, Crate, and Schwartz [E3] is satisfactory for determining the critical buckling strength of pressurized unstiffened cylinders provided that the walls behave as a membrane.

6. Test cylinders of cellulose acetate can be buckled elastically several times without materially effecting the critical buckling load. This is true for both the pressurized and the unpressurized conditions.

REFERENCES

E1. Harris, A. L.; Herbert, S. S.; Skene, W. T.; and Benjamin, R.J.: The Stability of Thin-Walled Unstiffened Cylinders Under Axial Compression Including Effects of Internal Pressure. Journal of the Aeronautical Sciences, Vol. 24, No. 8, August 1957, p. 587.

E2. Batdorf, S. B.: A Simplified Method of Elastic-Stability Analysis for Thin Cylindrical Shells. NACA Rept. 874, 1947.

E3. Lo, H.; Crate, H.; and Schwartz, E. B.: Buckling of Thin Walled Cylinders Under Axial Compression and Internal Pressure. NACA Report 1027, 1951

E4. Flugge, W.: Die Stabilitat Der Krieszylinderschale. Ing-Archiv, Bd. II, Heft 5, December, 1932, pp. 463-506.

TABLE EI. - TEST RESULTS FOR CYLINDERS WITH r/t of 500.

Specimen Number	p	$\bar{p}$	P_{cr}	σ_{cr}	$\bar{\sigma}_{cr}$	$\Delta\bar{\sigma}_{cr}$
15	0	0	120.0	169.76	0.211	0
24	0	0	99.0	140.05	0.175	0
28	0	0	108.0	152.78	0.191	0
29	0	0	130.0	183.91	0.230	0
30	0	0	133.0	188.15	0.235	0
15	1	0.625	223.3	315.90	0.395	0.184
24	1	0.625	171.3	242.34	0.303	0.128
28	1	0.625	233.3	330.05	0.413	0.222
29	1	0.625	250.3	354.10	0.443	0.213
30	1	0.625	253.3	358.34	0.448	0.213
15	2	1.250	186.6	263.98	0.330	0.119
24	2	1.250	166.6	235.67	0.294	0.119
28	2	1.250	256.6	363.01	0.454	0.263
29	2	1.250	256.6	363.01	0.454	0.224
30	2	1.250	259.6	367.26	0.459	0.224
15	3	1.875	172.9	244.60	0.305	0.094
24	3	1.875	144.9	204.99	0.256	0.081
28	3	1.875	314.9	445.49	0.557	0.366
29	3	1.875	270.9	383.24	0.479	0.249
30	3	1.875	264.9	374.75	0.468	0.233
24	4	2.500	133.2	188.44	0.236	0.061
28	4	2.500	293.2	414.79	0.518	0.327
29	4	2.500	271.2	383.67	0.479	0.249
30	4	2.500	263.2	372.35	0.465	0.230
28	5	3.125	271.5	384.09	0.480	0.289
29	5	3.125	321.5	454.83	0.568	0.338
28	6	3.750	249.8	353.39	0.442	0.251
29	6	3.750	299.8	424.13	0.530	0.300

TABLE EII. - TEST RESULTS FOR CYLINDERS WITH r/t of 750.

Specimen Number	p	$\bar{p}$	P_{cr}	σ_{cr}	$\bar{\sigma}_{cr}$	$\Delta\bar{\sigma}_{cr}$
6	0	0	51	108.24	0.202	0
7	0	0				
8	0	0	52	110.36	0.207	0
9	0	0	30	63.67	0.119	0
14	0	0	41	87.02	0.163	0
16	0	0	25	53.06	0.099	0
21	0	0	43	91.26	0.171	0
22	0	0				
6	1	1.406	95.3	202.27	0.379	0.177
7	1	1.406	113.3	240.47	0.451	
8	1	1.406	113.3	240.47	0.451	0.244
9	1	1.406	131.3	278.67	0.521	0.402
14	1	1.406	118.3	251.08	0.471	0.308
16	1	1.406	104.3	221.37	0.415	0.316
21	1	1.406	136.3	289.28	0.289	0.118
22	1	1.406	114.3	242.59	0.455	
7	2	2.812	107.6	228.37	0.428	
9	2	2.812	146.6	311.15	0.583	0.464
14	2	2.812	141.6	300.53	0.563	0.400
16	2	2.812	126.6	268.70	0.504	0.405
21	2	2.812	139.6	296.29	0.555	0.384
22	2	2.812	113.6	241.11	0.452	
7	3	4.218	111.9	237.50	0.445	
9	3	4.218	162.9	345.74	0.648	0.529
14	3	4.218	126.9	269.34	0.505	0.342
16	3	4.218	124.9	265.09	0.497	0.398
21	3	4.218	129.9	275.70	0.517	0.346
22	3	4.218	116.9	248.11	0.465	

TABLE EII. - TEST RESULTS FOR CYLINDERS WITH r/t of 750-CONCLUDED.

Specimen Number	p	$\bar{p}$	P_{cr}	σ_{cr}	$\bar{\sigma}_{cr}$	$\Delta\bar{\sigma}_{cr}$
7	4	5.625	153.2	325.15	0.609	
9	4	5.625	133.2	287.70	0.530	0.411
14	4	5.625	133.2	282.70	0.530	0.367
21	4	5.625	148.2	314.54	0.589	0.418
22	4	5.625	138.2	293.32	0.550	
7	5	7.031	126.5	268.48	0.503	
21	5	7.031	141.5	300.32	0.563	0.392
22	5	7.031	141.5	300.32	0.563	

Note: Values of $\Delta\bar{\sigma}_{cr}$ are not given for cylinders 7 and 22 since tests were not conducted on these cylinders in the unpressurized condition.

TABLE EIII.- TEST RESULTS FOR CYLINDERS WITH r/t of 1000.

Specimen Number	p	$\bar{p}$	P_{cr}	σ_{cr}	$\bar{\sigma}_{cr}$	$\Delta\bar{\sigma}_{cr}$
11	0	0				
17	0	0				
18	0	0				
26	0	0	21	59.42	0.148	0
31	0	0	31	87.72	0.219	0
32	0	0	31	87.72	0.219	0
11	1	2.50	88.3	249.8	0.624	
17	1	2.50	68.3	193.26	0.483	
18	1	2.50	48.3	136.67	0.342	
26	1	2.50	83.3	235.71	0.589	0.441
31	1	2.50	83.3	235.71	0.589	0.370
32	1	2.50	97.3	275.32	0.688	0.469
11	2	5.00	66.6	188.45	0.471	
17	2	5.00	73.6	208.25	0.521	
18	2	5.00	74.6	211.09	0.528	
26	2	5.00	91.6	259.19	0.649	0.501
31	2	5.00	91.6	259.19	0.647	0.428
32	2	5.00	94.6	267.68	0.669	0.450
17	3	7.50	79.9	226.08	0.565	
18	3	7.50	79.9	226.08	0.565	
26	3	7.50	87.9	248.72	0.622	0.474
31	3	7.50	74.9	211.94	0.530	0.311
32	3	7.50	97.9	277.02	0.693	0.474
17	4	10.0	83.2	235.42	0.588	
32	4	10.0	78.2	211.27	0.553	0.334

Notes: 1. In Tables EI, EII and EIII, P_{cr} is expressed in pounds; σ_{cr} and p are expressed in psi; $\bar{p}$, $\bar{\sigma}_{cr}$ and $\Delta\bar{\sigma}_{cr}$ are dimensionless.

2. Unpressurized tests were not conducted on cylinders 11, 17, 18.

TABLE EIV. - TEST RESULT AVERAGES

p	$\bar{p}$	r/t	$\bar{\sigma}_{cr}$	$\Delta\bar{\sigma}_{cr}$
0	0	500	0.208	0
1	0.625	500	0.400	0.192
2	1.250	500	0.398	0.190
3	1.875	500	0.413	0.205
4	2.500	500	0.425	0.217
5	3.125	500	0.524	0.316
6	3.750	500	0.486	0.276
0	0	750	0.160	0
1	1.406	750	0.429	0.261
2	2.812	750	0.514	0.413
3	4.218	750	0.513	0.404
4	5.625	750	0.562	0.399
5	7.031	750	0.543	0.392
0	0	1000	0.195	0
1	2.50	1000	0.553	0.427
2	5.00	1000	0.581	0.460
3	7.50	1000	0.595	0.420
4	10.00	1000	0.571	0.334

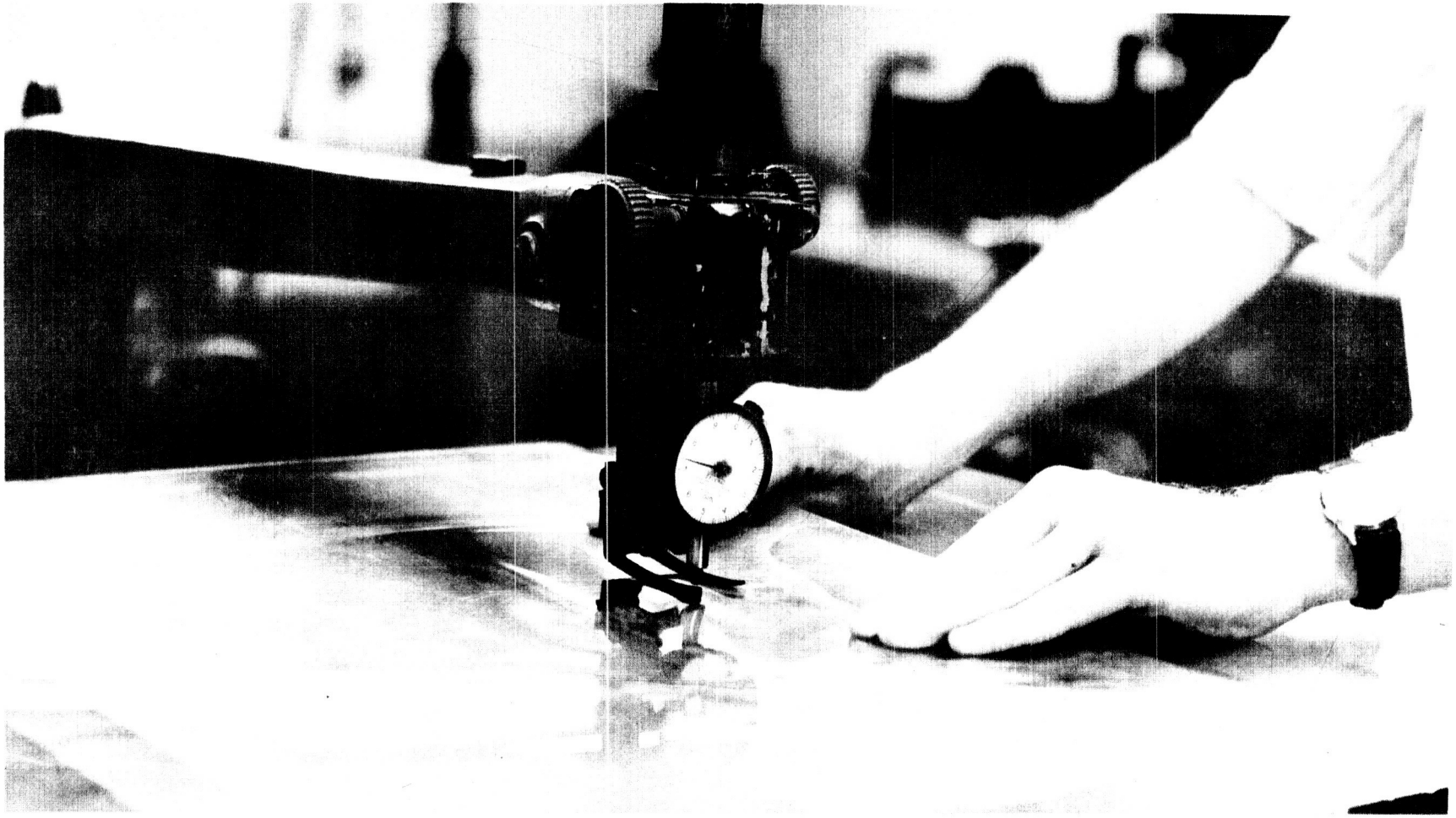

FIGURE E1. - THICKNESS MEASUREMENT.

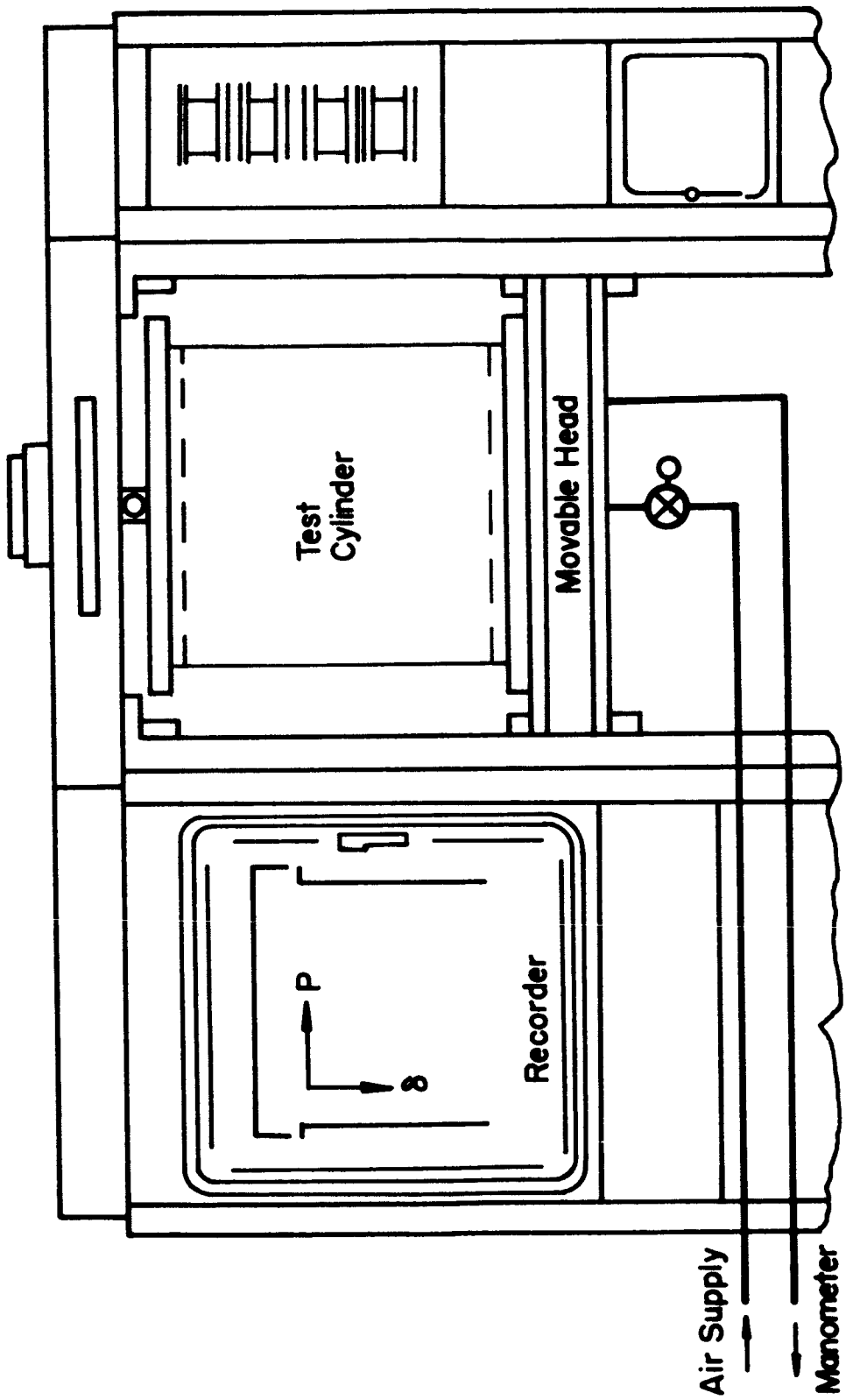

FIGURE E2. - TESTING MACHINE.

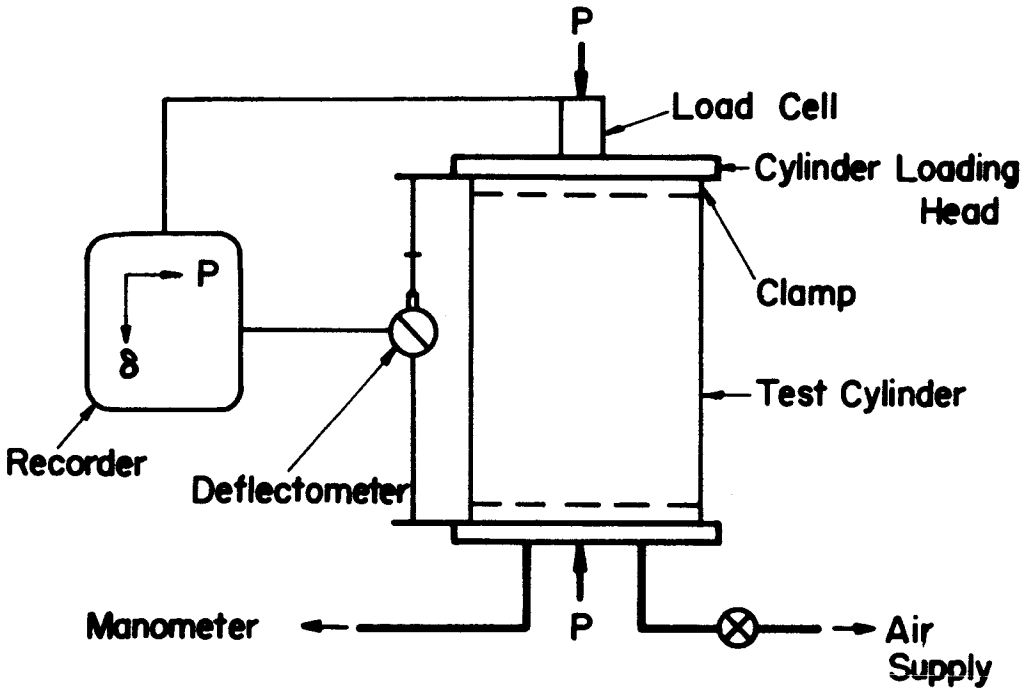

FIGURE E3. - SCHEMATIC OF TEST ARRANGEMENT.

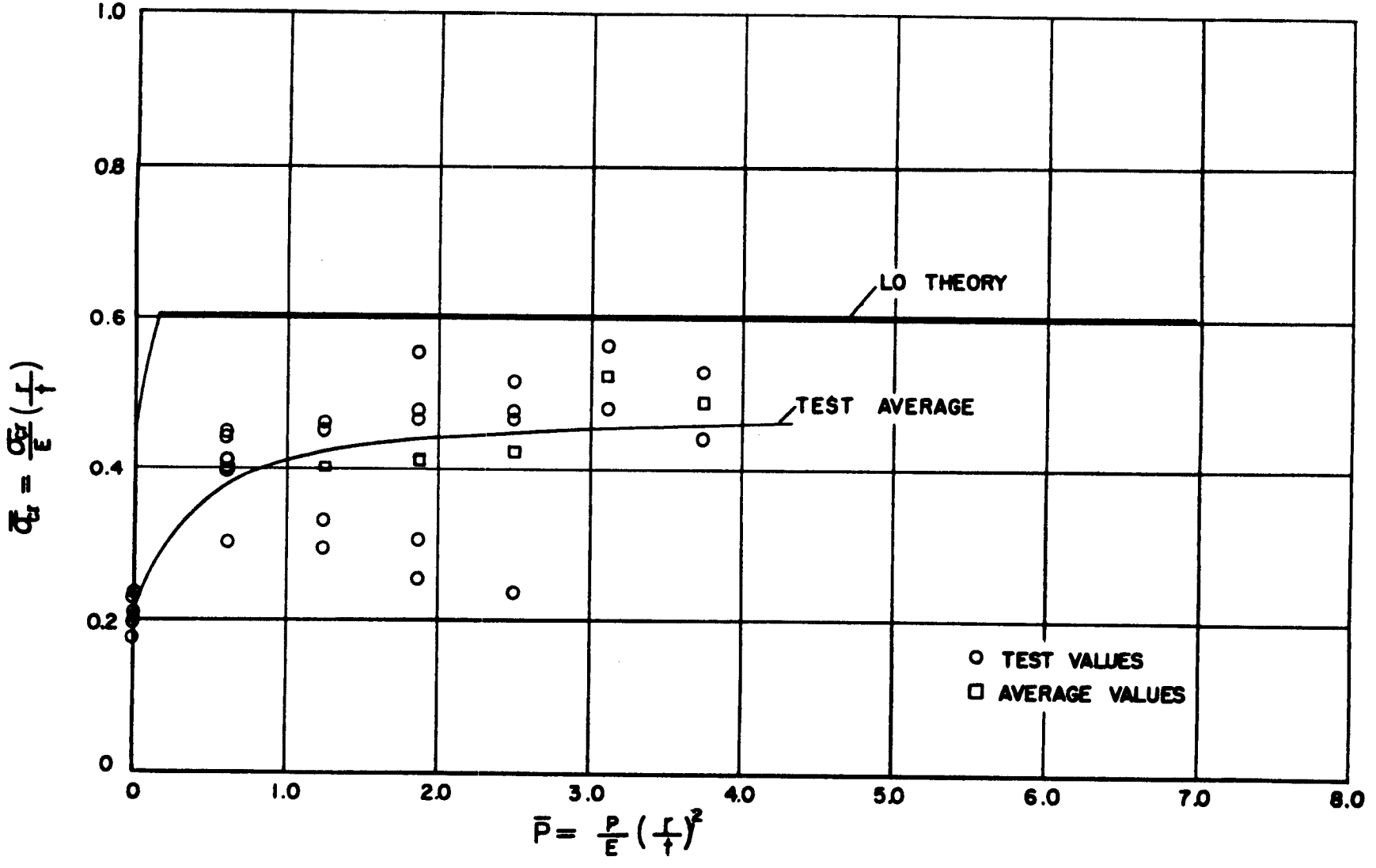

FIGURE E4. - TEST RESULTS FOR CYLINDERS WITH r/t of 500.

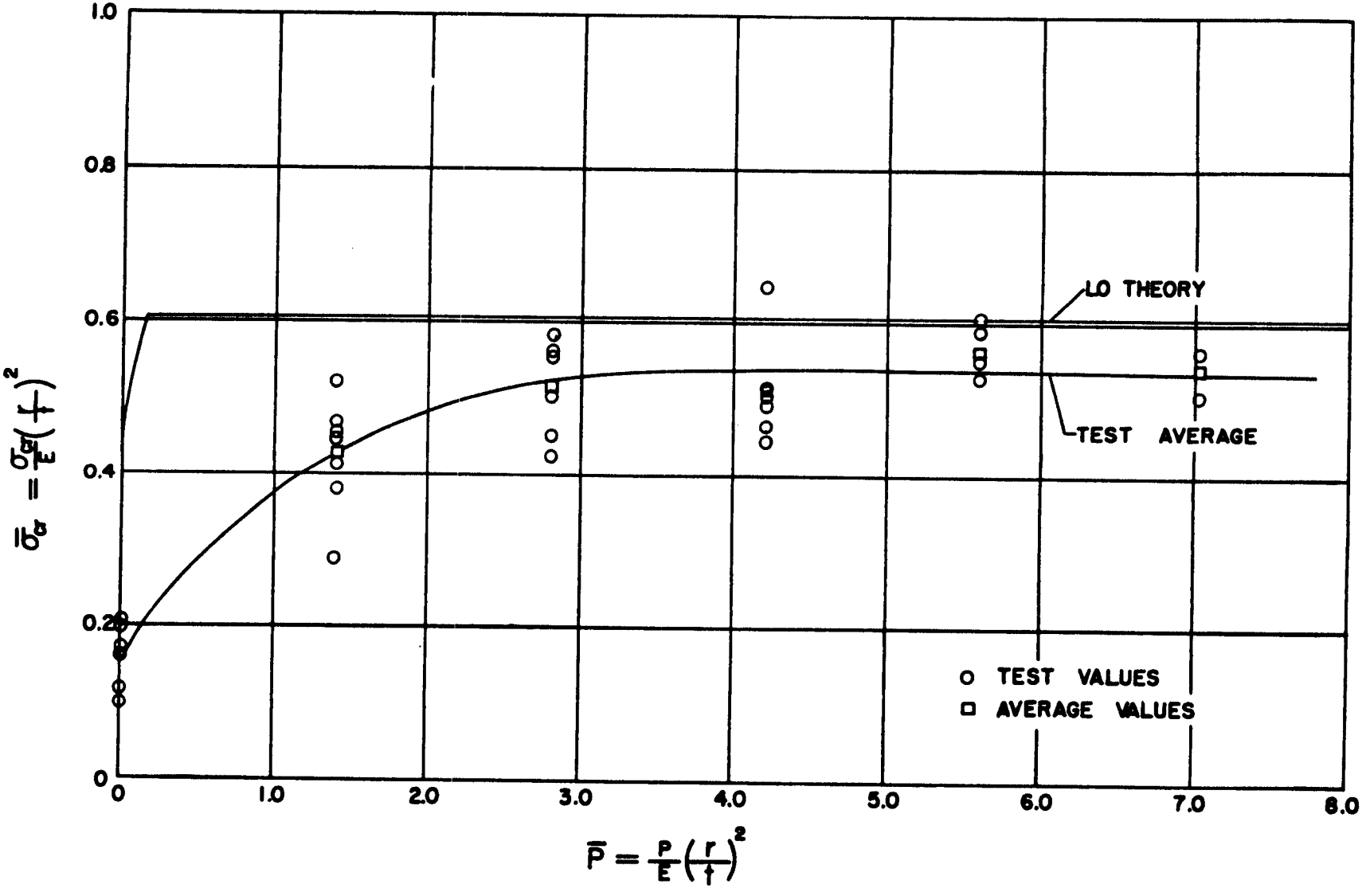

FIGURE E5. - TEST RESULTS FOR CYLINDERS WITH r/t of 750.

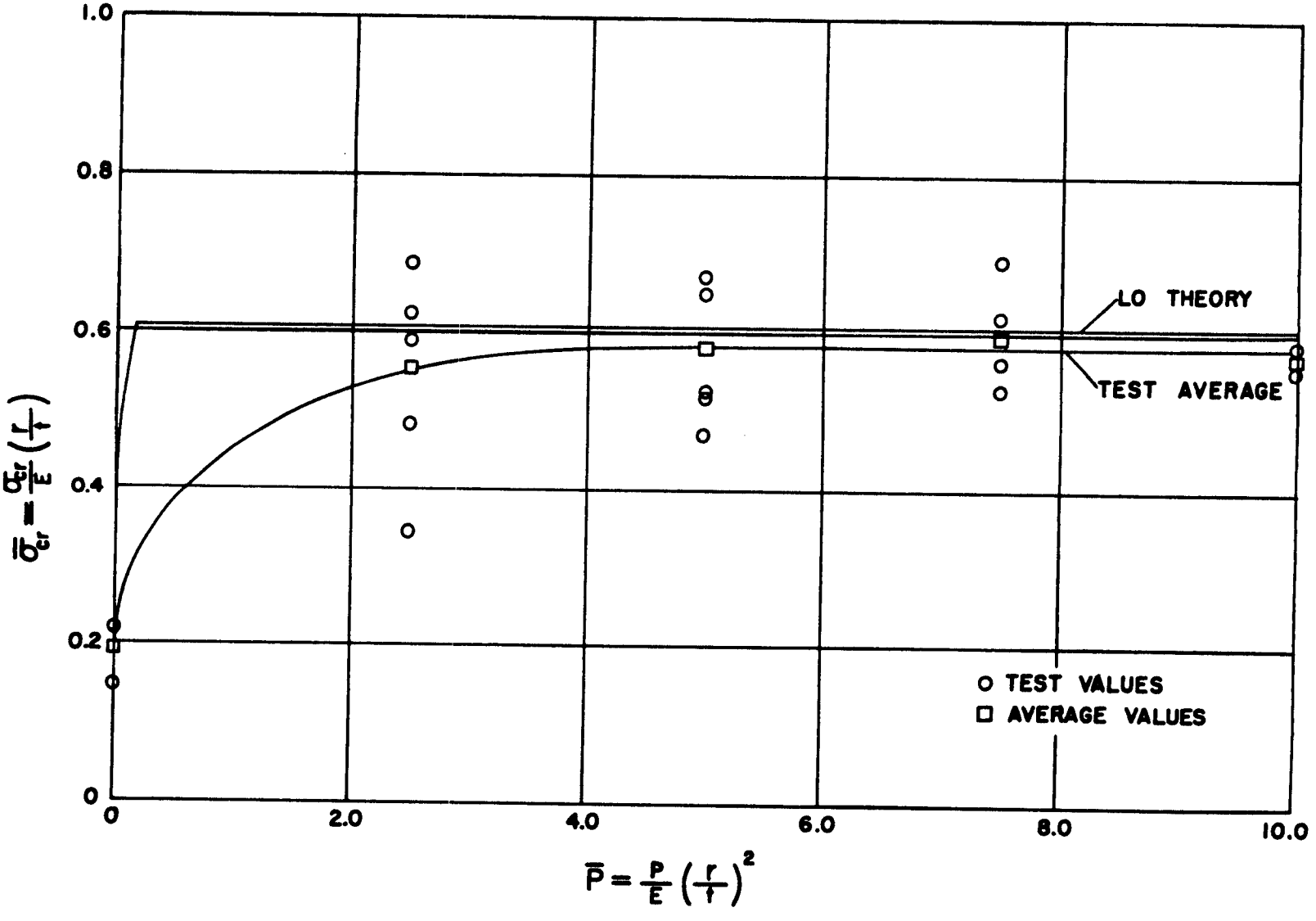

FIGURE E6. - TEST RESULTS FOR CYLINDERS WITH r/t of 1000.

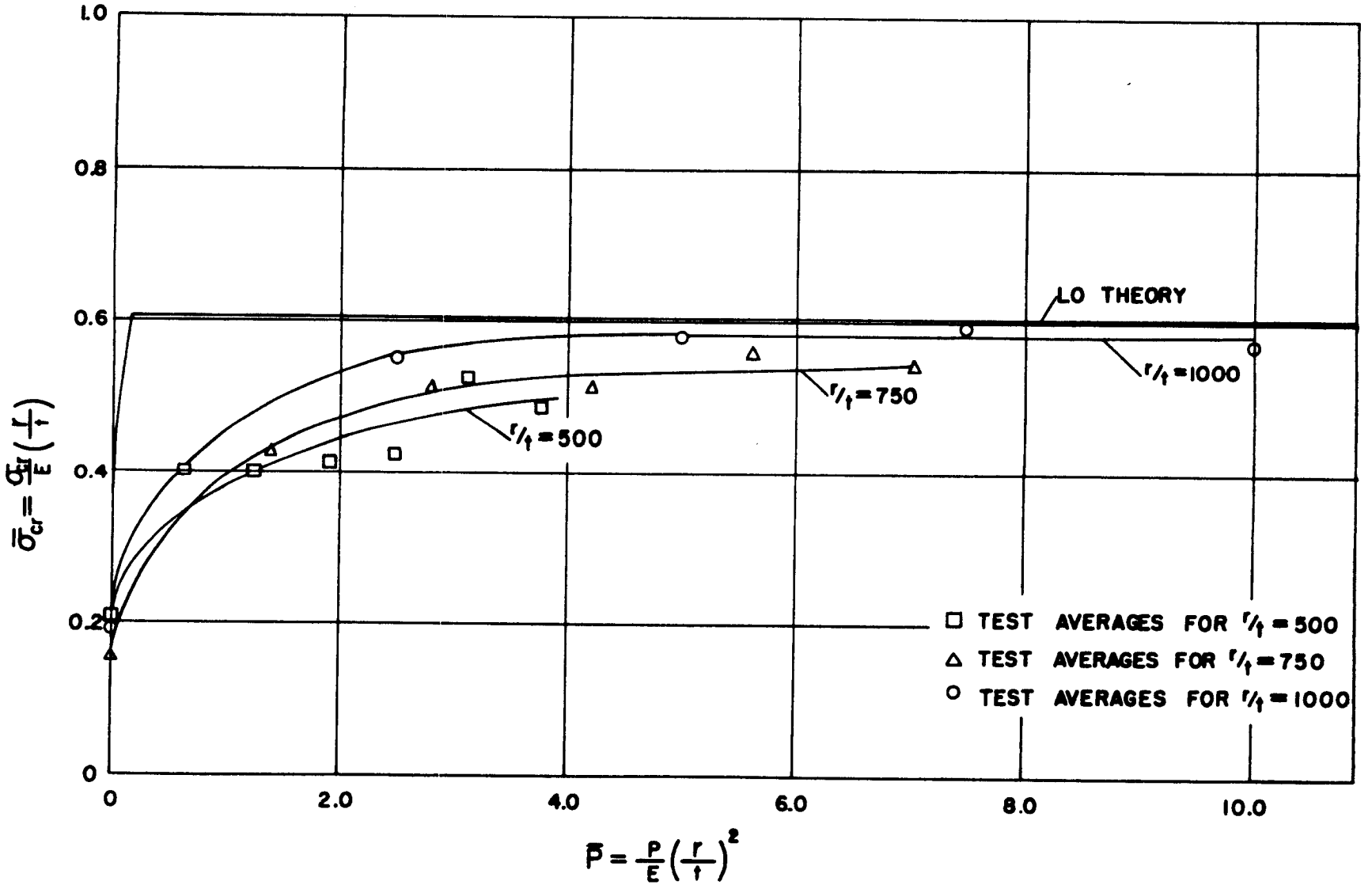

FIGURE E7. - SUMMARY OF AVERAGE TEST VALUES.

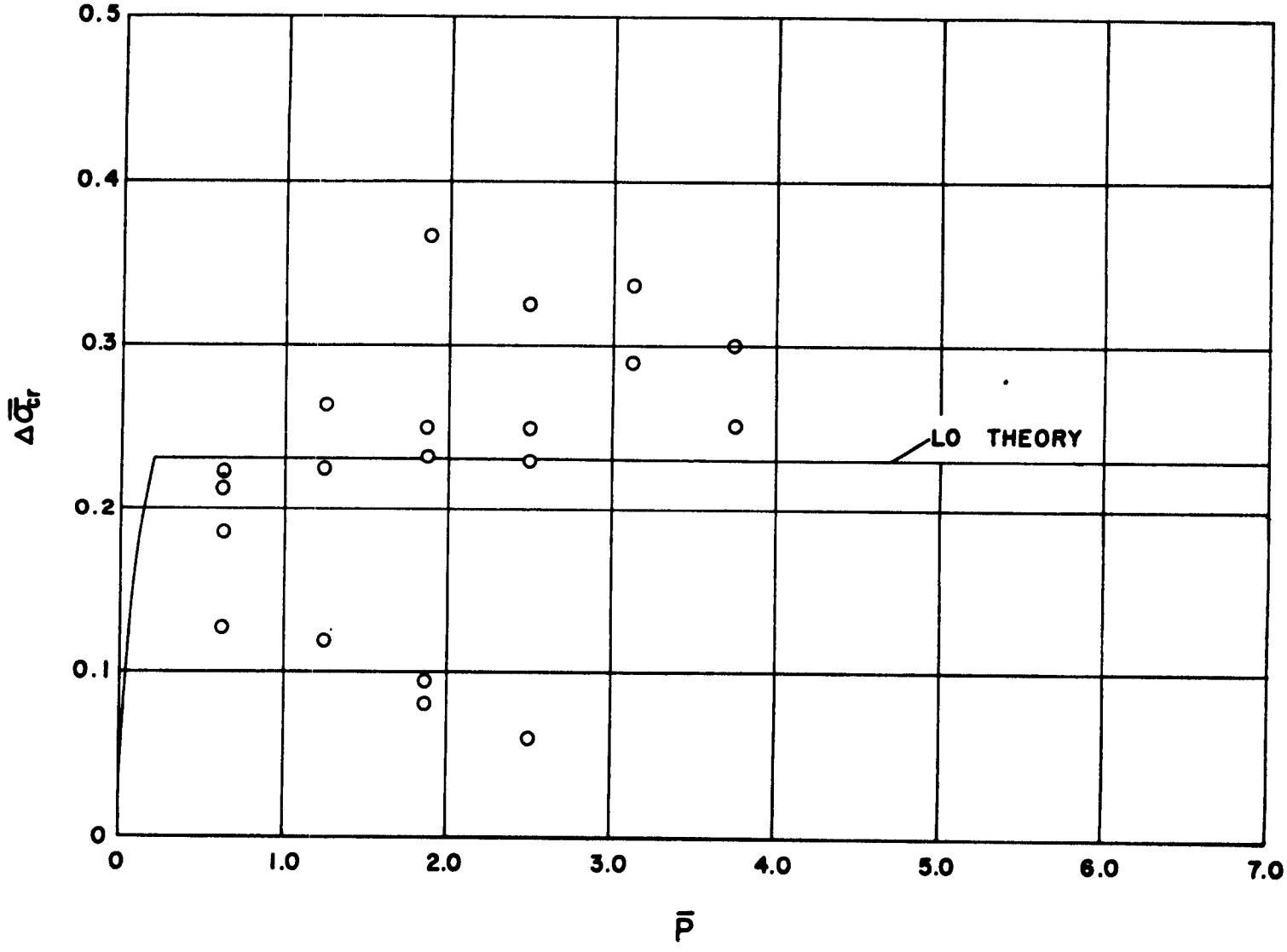

FIGURE E8. - TEST VALUES OF $\Delta\bar{\sigma}_{cr}$ for r/t of 500.

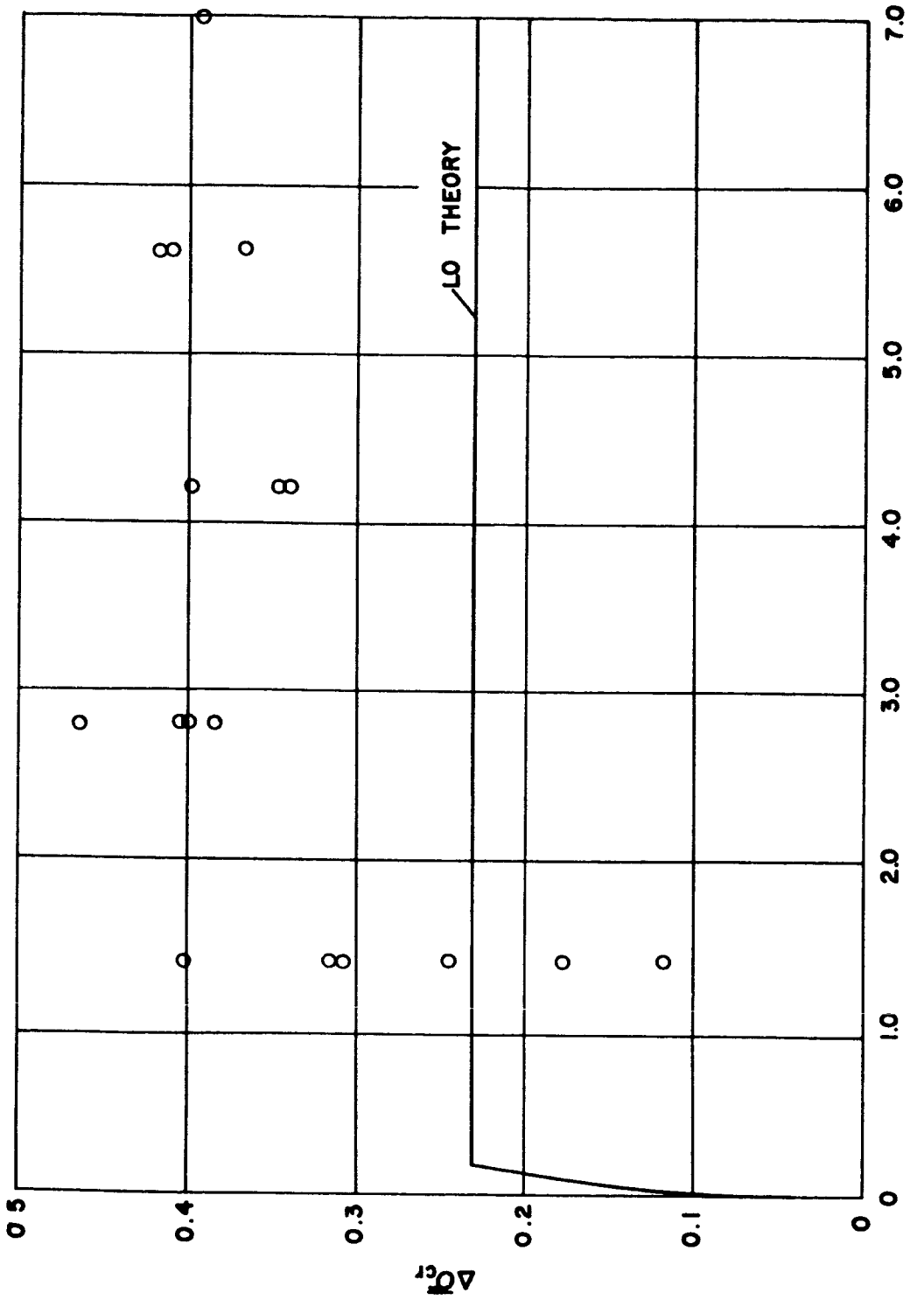

FIGURE E9. - TEST VALUES OF $\Delta\bar{\sigma}_{cr}$ FOR r/t OF 750.

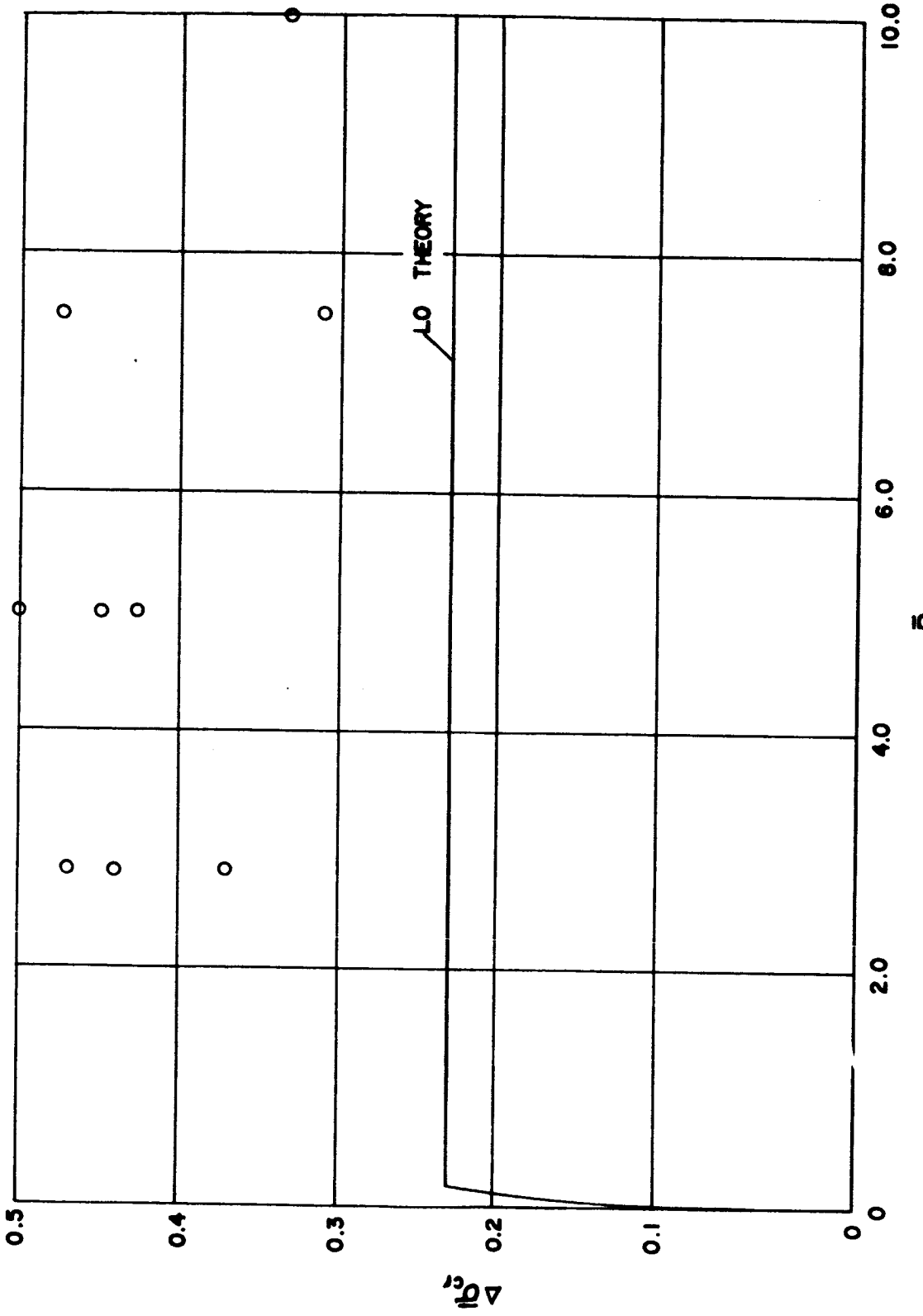

FIGURE E10. - TEST VALUES OF $\Delta\bar{\sigma}_{cr}$ FOR r/t OF 1000.

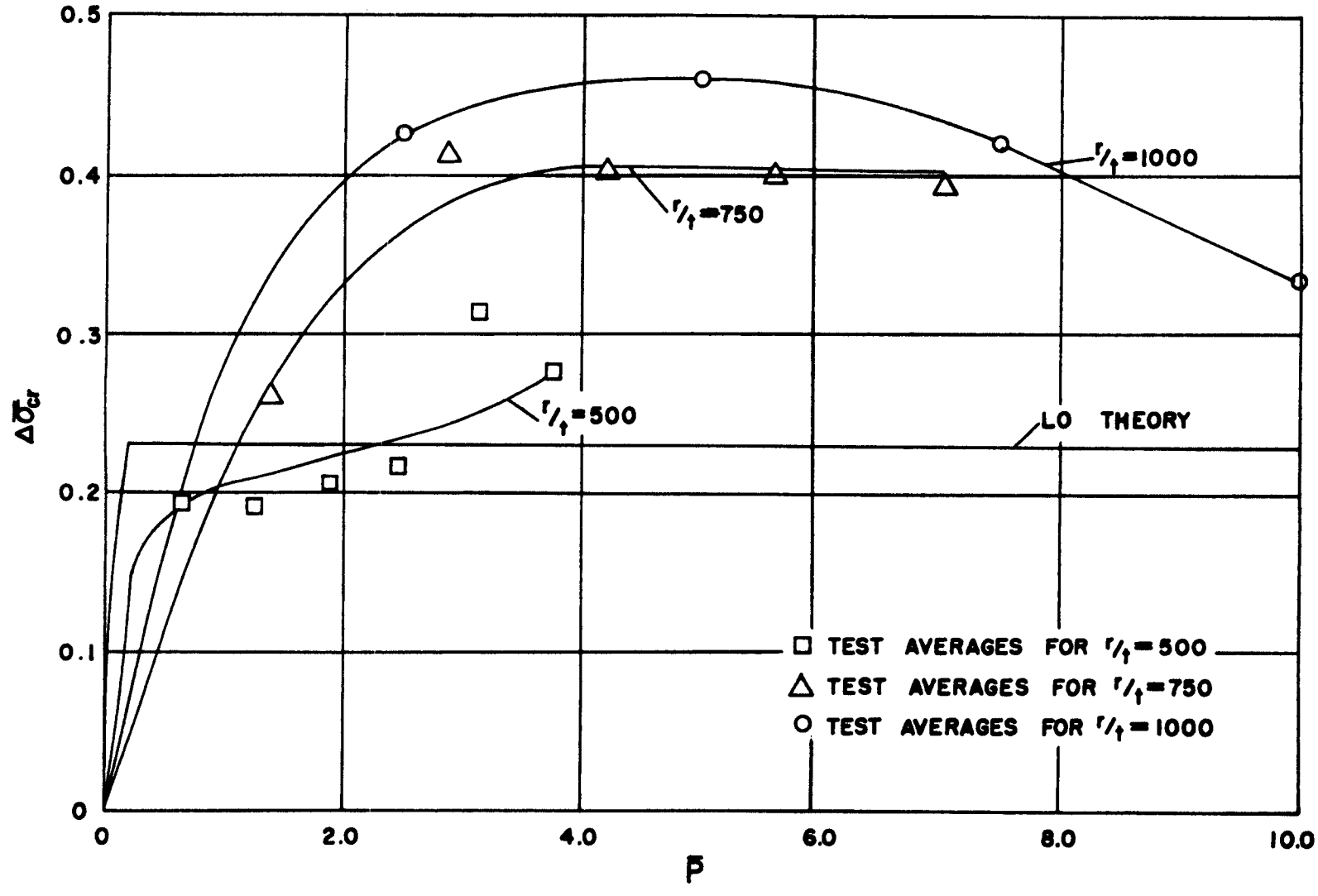

FIGURE E11. - AVERAGE VALUES OF $\Delta\bar{\sigma}_{cr}$.

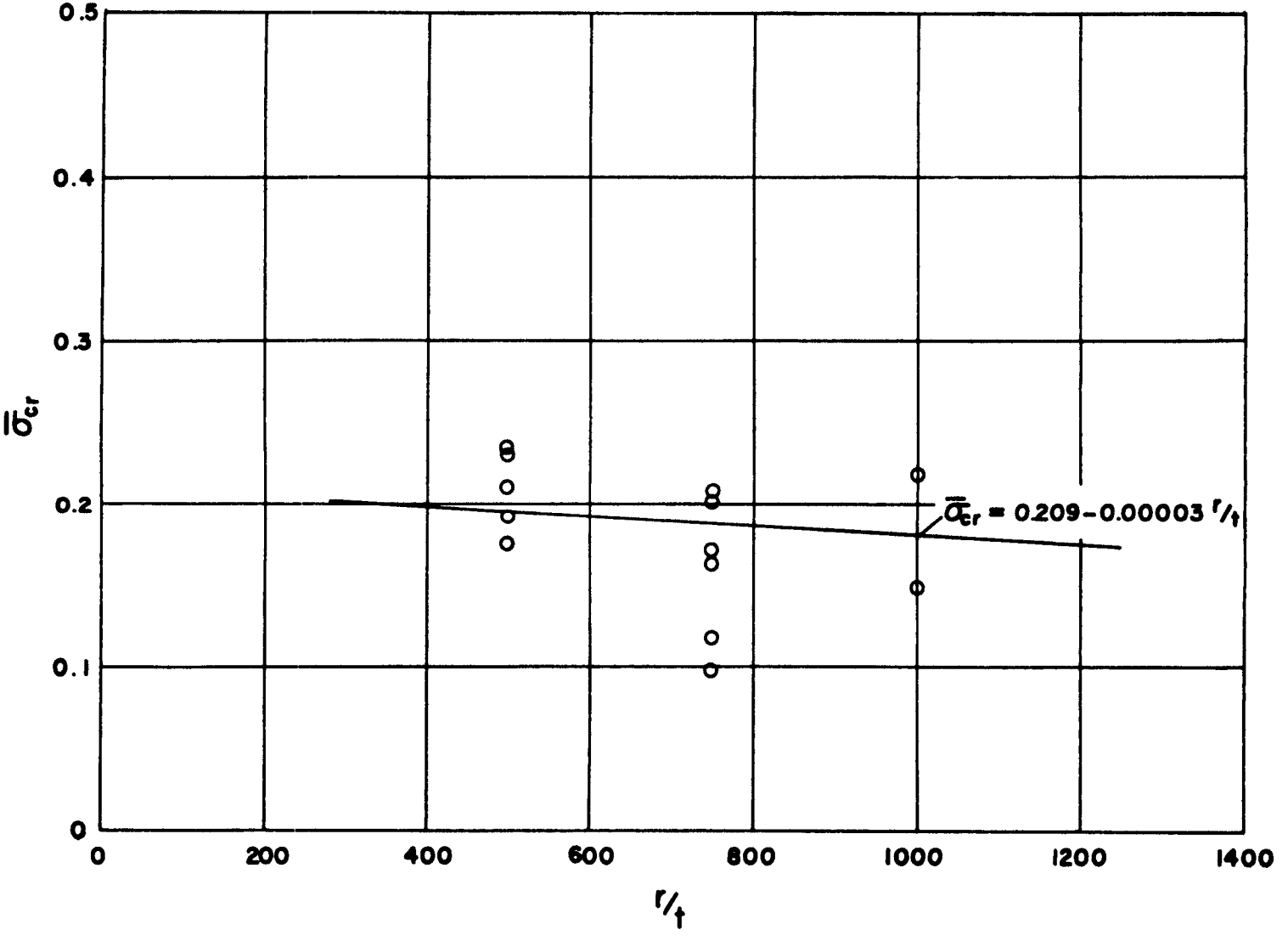

FIGURE E12. - BEST FIT CURVE FOR UNPRESSURIZED CYLINDERS.

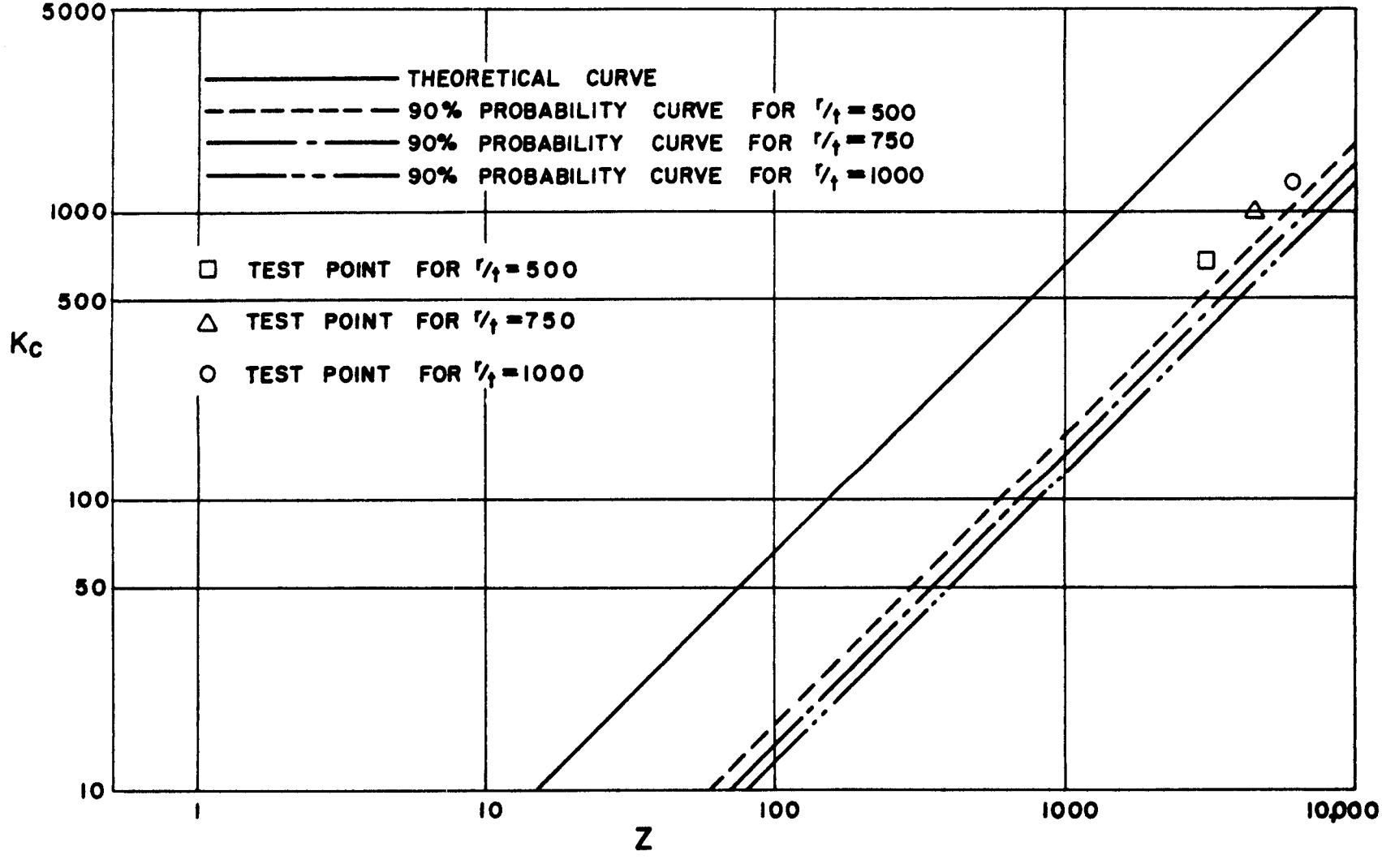

FIGURE E13. - BUCKLING COEFFICIENT, K_c, FOR UNPRESSURED CYLINDERS.

APPENDIX F

SHEAR LAG STUDY OF THREE INTEGRALLY STIFFENED PANELS

By William K. Rey

The contents of this appendix were previously submitted as Progress Report No. 4 for NASA Contract NAS8-11155.

SHEAR LAG STUDY OF THREE INTEGRALLY STIFFENED PANELS

By William K. Rey*

SUMMARY

An experimental study was conducted to determine the effect upon the stress distribution in integrally stiffened panels of varying the ratio of the stiffener area to the sheet area. Three aluminum alloy panels with rectangular integral stiffeners were instrumented with foil strain gages to determine the strain distribution in the stiffeners and the webs under axial compressive loads. The ratio of the stiffener area to the sheet area was approximately one-half, one and two in the three panels tested. Each of the panels was tested under four different loading conditions.

The experimental results were compared with a theoretical analysis. Relatively good agreement was obtained between the experimental results and the theoretical analysis except for the section adjacent to the end at which the load was applied.

INTRODUCTION

Integrally stiffened panels are being utilized in many structures such as the thrust structure of the Saturn C-5 launch vehicle since this type of construction provides the necessary strength with a minimum of weight for certain types of loads. When a concentrated load is applied to one of the stiffeners, the manner in which the load is distributed through the panel is influenced by shearing deformations in the thin webs that connect the stiffeners. This influence is commonly referred to as shear lag. The precise stress distribution throughout a stiffened panel must be known to permit the application of minimum weight design principles.

In a previous study (ref. F1), a survey of the literature indicated a number of theoretical analyses were available for predicting the stress distribution in stiffened panels but no experimental data were available

*Professor of Aerospace Engineering, University of Alabama, University, Alabama and Project Director of NASA Contract NAS8-11155.

for evaluating the different analyses when applied to integrally stiffened panels. Data that are available for panels with stiffeners attached by welding or riveting are of doubtful value when integrally stiffened panels are considered. Furthermore, the data that are available for panels with attached stiffeners were obtained by testing panels in which the total stiffener area was greater than the sheet area whereas some of the integrally stiffened panels of interest have a total stiffener area less than the sheet area.

The test results in this report were obtained in the first phase of an experimental program designed to provide stress distribution data for integrally stiffened panels of various configurations. This phase of the experimental study was undertaken to determine the effect on the stress distribution of varying the ratio of the stiffener area to the sheet area in integrally stiffened flat panels with constant cross-section stiffeners of the same size. Additional tests are planned to investigate the effects of varying the number of stiffeners, using stiffeners of different sizes on the same panel and varying the stiffener area over the panel length.

In order to provide some measure of the effectiveness of the test program, a matrix analysis of each panel based upon the Maxwell-Mohr method of analyzing statically indeterminate structures was accomplished. When additional data become available from later phases of the test program, all of the experimental data will be compared with other theoretical analyses.

EXPERIMENTAL INVESTIGATION

Specimens

Three integrally stiffened panels were prepared from a one inch thick 7075-T651 aluminum alloy plate. As indicated in Figure F1, each panel consisted of seven uniformly spaced rectangular stiffeners of constant cross-section. Each panel was twenty-four inches long in the direction of loading by approximately seventeen and five-eights inches wide. The cross-sections of the panels, identified as Panels B, C, and D, are shown in Figures F2, F3, and F4 respectively.

Bonded resistance type foil strain gages with a gage length of one-eighth of an inch were applied to each panel with a contact cement. As

shown in Figure F5, ninety-four uniaxial gages and twenty-four rectangular rosette gages were used on Panels B and C to provide a total of one hundred and sixty-six strain gage channels. On Panel D, as shown in Figure F6, one hundred and ten uniaxial gages and twenty-four rectangular rosette gages were used to supply one hundred and eighty-two strain gage channels.

Machining of the three panels was accomplished in a shaper as shown in Figure F7. Because of the limitations imposed by this machining operation, it was impossible to maintain tolerances as close as desired. The actual cross-sectional dimensions shown in Figures F2, F3, and F4 indicate the variations in web thickness and stiffener cross-sections. The dimensions were very nearly constant over the twenty-four inch length. The aluminum alloy used is stress-relieved by stretching after solution heat-treatment. However, machining evidentally relieves additional stresses which results in some warpage of the panels.

Equipment

Loading of the panels was accomplished by a hydraulic 60,000 pound universal testing machine equipped with a load maintainer. Considerable effort was expended in attempts to insure that loads were applied in the desired manner. As shown in Figure F8, loads were applied so as to minimize the introduction of any bending moment into the panels. Each of the panels was tested under four different loading conditions which are identified in Figure F9 as loading conditions I, II, III, IV.

Each of the strain gage channels on the panels served as one of the arms in a Wheatstone bridge circuit. In order to provide temperature compensation, three foil gages mounted in small aluminum blocks (dummy gage blocks) served as the other three arms of the Wheatstone bridge. Each strain gage channel was equipped with an individual dummy gage block in order to permit switching outside of the bridge and minimize the effect of changes in contact resistance. The dummy blocks were mounted in a frame adjacent to the testing machine as shown in Figure F10.

Current was applied to the Wheatstone bridges by a size 8D, 12-volt, lead-acid storage battery. A variable resistor in series with each of the bridge circuits permitted the voltage impressed on each bridge to be reduced to approximately ten volts and provided the means for calibrating

each bridge. The output of the bridge circuits was routed through a two hundred channel cross-bar type switching unit to an amplifier. The output of the amplifier was in turn supplied to a four digit digital voltmeter and a digital printer. An overall view of the testing machine and associated instrumentation is shown in Figure F10. The control console is shown in Figure F11 with the digital voltmeter at top, channel selector and indicator below the voltmeter, amplifier and amplifier power supply below the selector, digital printer below the amplifier and the power supply for the printer at the bottom of the console.

Figures F12 and F13 are photographs of the two sides of a panel positioned in the testing machine.

Test Procedure

Prior to each test, current was applied to all the strain gage channels for a period of approximately one hour during which the temperature of the panel increased due to heating by the gage current. Temperature equilibrium in the panel was achieved prior to testing.

After achieving temperature equilibrium, a pre-load was applied to the panel and all strain gage bridges were balanced and calibrated. Calibration was accomplished by shunting a known resistor across one arm of the bridge to simulate a pre-determined strain was indicated by the digital voltmeter. Periodically, during each test, the calibration was verified to compensate for any decay in the battery voltage.

For the loading conditions identified at I, II, and III in Figure F9, a preliminary test was conducted to determine if the same load was being applied to each of the loaded stiffeners and if the load was being symmetrically supported by the base. This was accomplished by monitoring all the strain gages on the loaded stiffeners and the strain gages on all stiffeners at the section adjacent to the supporting base. This preliminary test was also used to detect bending introduced by misalignment of the panel or loading fixtures. Adjustments were made on the basis of the preliminary tests until satisfactory loading was achieved. Improvements in the supporting base and loading fixtures were made during the test program to simplify the load balancing procedure. Therefore, not all of the tests were conducted with exactly the same loading and supportint fixtures.

For loading conditions I, II, and III, loads were applied in 1000

pound increments up to a maximum load of 5000 pounds on Panels B and C and in 500 pound increments up to a maximum load of 2500 pounds on Panel D. For loading condition IV, loads were applied in 500 pound increments up to a maximum load of 2500 pounds on Panels B and C and in 250 pound increments up to a maximum load of 1250 pounds on Panel D. At each increment of load the strain was recorded by the digital printer for each of the strain gage channels.

The data recorded by the digital printer was plotted as load versus net strain for each of the strain gage channels. This preliminary plot of the data was used to correct for any zero shift during testing and also to detect inoperative gage channels or other apparent errors in the data. From the corrected curves, the strain corresponding to a load of 1000 pounds was determined for each channel. This corrected strain was used in a computer program to determine the stress at each of the gage locations. For each rosette location, the computer program determined the magnitude and direction of the principal stresses, the magnitude and direction of the maximum shearing stress, the normal stresses parallel and normal to the stiffeners and the shearing stress parallel to the stiffeners. The computer program is given in Appendix F1 in Fortran II.

MATRIX ANALYSIS

In order to provide a comparison between the experimental results and one of the available theoretical analyses, an analysis based upon the Maxwell-Mohr method was performed for each panel using matrix notation. This type of analysis is the same as the analysis referred to as Method I in reference F1. The generalized force system employed in the analysis is identified in Figure F14 in which the generalized forces q_1 through q_{36} represent the axial forces in the stiffeners at the indicated locations and q_{37} through q_{60} represent the shear flow in the indicated web. The generalized force system is shown in greater detail in Figure F15 for that portion of the panel between stiffeners 2 and 3 and between 2.7 and 5.7 inches from the loaded end. The forces in the stiffeners, q_1 through q_{36}, are assumed to be positive when compressive and the shear flows, q_{37} through q_{60}, are assumed posi-

tive when the shear flow acts upward on the left-hand edge of a web element as shown in Figure F15. The generalized force system was selected to provide a direct comparison between the theoretical analysis and the experimental results by providing a generalized force at each of the strain gage locations in the stiffeners. The notation used in the matrix analysis corresponds to the notation used in reference F2.

Matrix of Flexibility Coefficients

The matrix of flexibility coefficients, $\left[a_{ij}\right]$, is a 60 x 60 symmetrical matrix, given by

$$\left[a_{ij}\right] = \begin{bmatrix} a_{1,1} & a_{1,2} & a_{1,3} & \cdots & a_{1,60} \\ a_{2,1} & a_{2,2} & a_{2,3} & \cdots & a_{2,60} \\ \vdots & & & & \\ a_{60,1} & a_{60,2} & a_{60,3} & & a_{60,60} \end{bmatrix}$$

Referring to Figures F1 and F14 for the necessary dimensions and denoting the equivalent stiffener areas of stiffeners 1, 2, 3, and 4 as A_1, A_2, A_3, A_4, respectively, the 124 non-zero flexibility coefficients are:

$$a_{1,1} = a_{9,9} = \frac{L_1}{3A_1E}$$

$$a_{1,2} = a_{2,1} = a_{8,9} = a_{9,8} = \frac{L_1}{6A_1E}$$

$$a_{2,2} = a_{8,8} = \frac{L_1 + L_2}{3A_1E}$$

$$a_{3,3} = a_{4,4} = a_{5,5} = a_{6,6} = a_{7,7} = \frac{2L_2}{3A_1E}$$

$$a_{2,3} = a_{3,2} = a_{3,4} = a_{4,3} = a_{4,5} = a_{5,4} = a_{5,6} = a_{6,5} = a_{6,7} = a_{7,6}$$
$$= a_{7,8} = a_{8,7} = \frac{L_2}{6A_1E}$$

$$a_{10,10} = a_{18,18} = \frac{L_1}{3A_2E}$$

$$a_{10,11} = a_{11,10} = a_{17,18} = a_{18,17} = \frac{L_1}{6A_2E}$$

$$a_{11,11} = a_{17,17} = \frac{L_1 + L_2}{3A_2E}$$

$$a_{12,12} = a_{13,13} = a_{14,14} = a_{15,15} = a_{16,16} = \frac{2L_2}{3A_2E}$$

$$a_{11,12} = a_{12,11} = a_{12,13} = a_{13,12} = a_{13,14} = a_{14,13} = a_{14,15} = a_{15,14}$$
$$= a_{15,16} = a_{16,15} = a_{16,17} = a_{17,16} = \frac{L_2}{6A_2E}$$

$$a_{19,19} = a_{27,27} = \frac{L_1}{3A_3E}$$

$$a_{19,20} = a_{20,19} = a_{26,27} = a_{27,26} = \frac{L_1}{6A_3E}$$

$$a_{20,20} = a_{26,26} = \frac{L_1 + L_2}{3A_3E}$$

$$a_{21,21} = a_{22,22} = a_{23,23} = a_{24,24} = a_{25,25} = \frac{2L_2}{3A_3E}$$

$$a_{20,21} = a_{21,20} = a_{21,22} = a_{22,21} = a_{22,23} = a_{23,22} = a_{23,24} = a_{24,23}$$
$$= a_{24,25} = a_{25,24} = a_{25,26} = a_{26,25} = \frac{L_2}{6A_3E}$$

$$a_{28,28} = a_{36,36} = \frac{L_1}{3A_4E}$$

$$a_{28,29} = a_{29,28} = a_{35,36} = a_{36,35} = \frac{L_1}{6A_4E}$$

$$a_{29,29} = a_{35,35} = \frac{L_1 + L_2}{3A_4E}$$

$$a_{30,30} = a_{31,31} = a_{32,32} = a_{33,33} = a_{34,34} = \frac{2L_2}{3A_4E}$$

$$a_{29,30} = a_{30,29} = a_{30,31} = a_{31,30} = a_{31,32} = a_{32,31} = a_{32,33} = a_{33,32}$$
$$= a_{33,34} = a_{34,33} = a_{34,35} = a_{35,34} = \frac{L_2}{6A_4E}$$

$$a_{37,37} = a_{44,44} = \frac{L_1 b_1}{Gt_1}$$

$$a_{38,38} = a_{39,39} = a_{40,40} = a_{41,41} = a_{42,42} = a_{43,43} = \frac{L_2 b_1}{Gt_1}$$

$$a_{45,45} = a_{52,52} = \frac{L_1 b_2}{Gt_2}$$

$$a_{46,46} = a_{47,47} = a_{48,48} = a_{49,49} = a_{50,50} = a_{51,51} = \frac{L_2 b_2}{Gt_2}$$

$$a_{53,53} = a_{60,60} = \frac{L_1 b_3}{Gt_3}$$

$$a_{54,54} = a_{55,55} = a_{56,56} = a_{57,57} = a_{58,58} = a_{59,59} = \frac{L_2 b_3}{Gt_3}$$

The remaining 3476 elements of $\left[a_{ij}\right]$ are zero.

Unit External Load Matrix

The twenty-four generalized forces q_{11} through q_{18}, q_{20} through q_{27} and q_{28} through q_{36} were selected as the redundants. The unit external load matrix, $\left[g_{im}\right] = \left[g_{jn}\right]$, is a 60 x 4 matrix obtained by replacing the external loads by unit loads.

The elements of the first column of $\left[g_{im}\right]$ represent the values of the generalized forces in the determinate structure when $P_1 = 1$ and $P_2 = P_3 = P_4 = 0$. They are:

$$g_{1,1} = g_{2,1} = g_{3,1} = \cdots = g_{9,1} = 1$$

$$g_{10,1} = g_{11,1} = g_{12,1} = \cdots = g_{60,1} = 0$$

The elements of the second column of $\left[g_{im}\right]$, obtained by setting $P_2 = 1$ and $P_1 = P_3 = P_4 = 0$, are:

$$g_{1,2} = 0$$

$$g_{2,2} = g_{3,2} = g_{4,2} = \cdots = g_{10,2} = 1$$

$$g_{11,2} = g_{12,2} = g_{13,2} = \cdots = g_{36,2} = 0$$

$$g_{37,2} = \frac{1}{L_1}$$

$$g_{38,2} = g_{39,2} = g_{40,2} = \cdots = g_{60,2} = 0$$

The elements of the third column of $\left[g_{im}\right]$, obtained by setting $P_3 = 1$ and $P_1 = P_2 = P_4 = 0$, are:

$$g_{1,3} = 0$$

$$g_{2,3} = g_{3,3} = g_{4,3} = \cdots = g_{9,3} = 1$$

$$g_{10,3} = g_{11,3} = g_{12,3} = \cdots = g_{18,3} = 0$$

$$g_{19,3} = 1$$

$$g_{20,3} = g_{21,3} = g_{22,3} = \cdots = g_{36,3} = 0$$

$$g_{37,3} = \frac{1}{L_1}$$

$$g_{38,3} = g_{39,3} = g_{40,3} = \cdots = g_{44,3} = 0$$

$$g_{45,3} = \frac{1}{L_1}$$

$$g_{46,3} = g_{47,3} = g_{48,3} = \cdots = g_{60,3} = 0$$

The elements of the fourth column of $\left[g_{im}\right]$, obtained by setting $P_4 = 1$ and $P_1 = P_2 = P_3 = 0$, are:

$$g_{1,4} = 0$$

$$g_{2,4} = g_{3,4} = g_{4,4} = \cdots = g_{9,4} = 1$$

$$g_{10,4} = g_{11,4} = g_{12,4} = \cdots = g_{27,4} = 0$$

$$g_{28,4} = 1$$

$$g_{29,4} = g_{30,4} = g_{31,4} = \cdots = g_{36,4} = 0$$

$$g_{37,4} = \frac{1}{L_1}$$

$$g_{38,4} = g_{39,4} = g_{40,4} = \cdots = g_{44,4} = 0$$

$$g_{45,4} = \frac{1}{L_1}$$

$$g_{46,4} = g_{47,4} = g_{48,4} = \cdots = g_{52,4} = 0$$

$$g_{53,4} = \frac{1}{L_1}$$

$$g_{54,4} = g_{55,4} = g_{56,4} = \cdots = g_{60,4} = 0$$

Unit Redundant Force Matrix

The unit redundant force matrix, $\left[g_{ir}\right] = \left[g_{js}\right]$, is a 60 x 24 matrix. The elements of this matrix are the values of the generalized forces when the redundant forces are replaced by unit loads. The twenty-four redundants, q_{11} through q_{18}, q_{20} through q_{27} and q_{29} through q_{36}, were identified as redundants one through twenty-four, respectively (q_{11} as redundant number one, q_{12} as redundant number two, etc., with q_{36} as redundant number twenty-four). For example, the elements in the first column of $\left[g_{ir}\right]$ are the values of the generalized forces when q_{11} is replaced by a unit force while the other twenty-three redundants are zero. The 138 non-zero elements of $\left[g_{ir}\right]$ are:

$$\left.\begin{aligned} g_{11+n+8m,\,1+n+m} &= 1 \\ g_{2+n,\,1+n+8m} &= -1 \end{aligned}\right\} \quad \begin{aligned} &\text{where } n = 0, 1, 2, \ldots, 7 \\ &\text{and } m = 0, 1, 2 \end{aligned}$$

$$g_{37+8n,1+8m} = -\frac{1}{L_1}$$

$$g_{38+8n,1+8m} = \frac{1}{L_2}$$

$$g_{38+8n,2+8m} = -\frac{1}{L_2}$$

$$g_{39+8n,2+8m} = \frac{1}{L_2}$$

$$g_{39+8n,3+8m} = -\frac{1}{L_2}$$

$$g_{40+8n,3+8m} = -\frac{1}{L_2}$$

$$g_{40+8n,4+8m} = -\frac{1}{L_2}$$

$$g_{41+8n,4+8m} = \frac{1}{L_2}$$

$$g_{41+8n,5+8m} = -\frac{1}{L_2}$$

$$g_{42+8n,5+8m} = \frac{1}{L_2}$$

$$g_{42+8n,6+8m} = -\frac{1}{L_2}$$

$$g_{43+8n,6+8m} = \frac{1}{L_2}$$

$$g_{43+8n,7+8m} = -\frac{1}{L_2}$$

$$g_{44+8n,7+8m} = \frac{1}{L_1}$$

$$g_{44+8n,8+8m} = -\frac{1}{L_1}$$

where $m = 0, 1, 2$ and $n = 0, 1, \ldots, m$

External Load Matrix

For the four loading conditions considered, the external load matrix, $\left[P_{mn}\right]$, is a diagonal matrix. To simplify computations, the external loads were considered as unit loads. Therefore,

$$\left[P_{mn}\right] = \begin{bmatrix} 1 & 0 & 0 & 0 \\ 0 & 1 & 0 & 0 \\ 0 & 0 & 1 & 0 \\ 0 & 0 & 0 & 1 \end{bmatrix}$$

Matrix Computation

After forming the $\left[a_{ij}\right]$, $\left[g_{im}\right]$, $\left[g_{ir}\right]$, and $\left[P_{mn}\right]$ matrices, the following matrix operations were performed:

1. Evaluate $\left[a_{rn}\right] = \left[g_{ri}\right]\left[a_{ij}\right]\left[g_{jn}\right]$ where $\left[g_{ri}\right]$ is the transpose of $\left[g_{ir}\right]$.
2. Evaluate $\left[a_{rs}\right] = \left[g_{ri}\right]\left[a_{ij}\right]\left[g_{js}\right]$.
3. Evaluate $\left[a_{rs}^{-1}\right]$, the inverse of $\left[a_{rs}\right]$.
4. Evaluate $\left[G_{rm}\right] = -\left[a_{rs}^{-1}\right]\left[a_{rn}\right]$.
5. Evaluate $\left[G_{im}\right] = \left[g_{im}\right] + \left[g_{ir}\right]\left[G_{rm}\right]$.
6. Evaluate $\left[q_{in}\right] = \left[G_{im}\right]\left[P_{mn}\right]$.

The matrix, $\left[q_{in}\right]$, is a 60 x 4 matrix the elements of which represent the magnitudes of the generalized forces for the four loading conditions considered. In this case, since $\left[P_{mn}\right]$ is a unit matrix, $\left[q_{in}\right] = \left[G_{im}\right]$.

The computer program used for the above matrix computations is given in Appendix F2.

The numerical values used in the matrix analysis were as follows:

For all panels: $L_1 = 2.700"$, $L_2 = 3.000"$, $E = 10.5 \times 10^6$ psi,
$G = 3.9 \times 10^6$ psi.

For Panel B: $b_1 = 2.6154"$, $b_2 = 2.6095"$, $b_3 = 2.6085"$
$t_1 = 0.0985"$, $t_2 = 0.0935"$, $t_3 = 0.0995"$

$A_1 = 0.4114$ in^2, $A_2 = 0.5300$ in^2, $A_3 = 0.5286$ in^2,

$A_4 = 0.2698$ in^2.

For Panel C: $b_1 = 2.840"$, $b_2 = 2.846"$, $b_3 = 2.6085"$

$t_1 = 0.099"$, $t_2 = 0.1015"$, $t_3 = 0.09925"$

$A_1 = 0.6684$ in^2, $A_2 = 0.7917$ in^2, $A_3 = 0.7908$ in^2 ,

$A_4 = 0.3938$ in^2.

For Panel D: $b_1 = 2.7675"$, $b_2 = 2.77675"$, $b_3 = 2.770"$

$t_1 = 0.096"$, $t_2 = 0.1005"$, $t_3 = 0.1005"$

$A_1 = 0.2743$ in^2, $A_2 = 0.4139$ in^2, $A_3 = 0.4203$ in^2,

$A_4 = 0.2122$ in^2.

The results of the matrix analysis are given in Tables F1 through F4 for Panel B, Tables F5 through F8 for Panel C and Tables F9 through F12 for Panel D. In each of these tables, the stress in each stiffener is given at nine locations corresponding to the locations of the generalized forces in the stiffeners and the shearing stress in each web is given at eight locations.

DATA

The experimental data are given in Tables F13 through F44. The data from two tests of Panel B for each of the four loading conditions are given in Tables F13 through F20. The data from two tests of Panel C for each of the four loading conditions are given in Tables F21 through F28. The data from three tests of Panel D for each of the four loading condi-

tions are given in Tables F29 through F40. The averages of the three tests of Panel D for each of the four loading conditions are given in Tables F41 through F44. In each of these tables, the stress in each stiffener is given at nine locations corresponding to the uniaxial strain gage locations shown in Figures F5 and F6. The state of stress at each of the strain rosette locations shown in Figures F5 and F6 is expressed in terms of the normal stress perpendicular to the stiffeners (σ_x), the normal stress parallel to the stiffeners (σ_y), and the shearing stress (τ_{xy}). Positive normal stresses are compressive stresses.

The results of the matrix analysis are plotted along with the experimental results in Figures F16 through F75. For each of the four loading conditions on a panel, the theoretical analysis and the experimental results are shown in a series of five curves as follows:

a) the normal stress, σ_y, in each of the stiffeners versus the distance from the loaded end of the panel (Figures F16, F21, F26, F31, F36, F41, F46, F51, F56, F61, F66, F71);
b) the shearing stress, τ_{xy}, in each web versus the distance from the loaded end of the panel (Figures F17, F22, F27, F32, F37, F42, F47, F52, F57, F62, F67, F72);
c) the normal stress, σ_y, parallel to the stiffeners in each web versus the distance from the loaded end of the panel (Figures F18, F23, F28, F33, F38, F43, F48, F53, F58, F63, F68, F73);
d) the normal stress, σ_x, perpendicular to the stiffeners in each web versus the distance from the loaded end of the panel (Figures F19, F24, F29, F34, F39, F44, F49, F54, F59, F64, F69, F74);
e) the chordwise distribution of the normal stress, σ_y, in the stiffeners across eight panel sections (Figures F20, F25, F30, F35, F40, F45, F50, F55, F60, F65, F70, F75).

ANALYSIS OF RESULTS

The theoretically predicted distribution of the normal stress in the stiffeners was in good agreement with the experimentally determined values

for all panels although the agreement was not uniform throughout the panels. In general, the largest difference between the theoretically predicted stresses in the stiffeners and the experimentally determined stresses occurred at the loaded end of the panel and the difference decreased as the distance from the loaded end increased. In all panels for all loading conditions, the theoretical and experimental stresses were very nearly equal to each other at the supported end of the panel. In Panels B and C the experimental stress was less than the theoretical stress in the loaded stiffener at the section adjacent to the applied load whereas in Panel D the experimental stress exceeded the theoretical stress at that section. This difference in behavior of the three panels may be attributed to the relative size of the stiffeners. The experimental results indicate that in Panels B and C the applied load was not uniformly distributed across the cross-section of the larger and thicker stiffeners of these panels at the gage section 0.3 inch below the applied load resulting in experimental stresses on the surface of the stiffeners less than the theoretical stresses which were based upon an assumed uniform distribution across a stiffener corss-section. In Panel D, with relatively small stiffeners, the test results indicate that the load had not diffused from the stiffener into the web at the section adjacent to the applied load resulting in experimental stresses that were larger than the theoretical stresses. As explained in reference 1, the analysis used assumed that the effective stiffener area consisted of the actual stiffener area plus one-half of the web area on each side of the stiffener. The theoretical analysis and the experimental results indicate that the panels were long enough to achieve an essentially uniform stress distribution across the cross-section at the supported end of the panel.

The experimentally determined shearing stresses in the webs agreed very closely with the theoretical stresses at certain sections but were in poor agreement at other sections. In general, the agreement was somewhat closer in Panels C and D than in Panel B. In all tests, the theoretical and experimental shearing stresses in the webs were nearly equal in the webs adjacent to the loaded stiffener. The largest differences between the theoretical and experimental shearing stresses in the webs occurred in the webs farthest from the loaded stiffener and at sections near the top (loaded end) of the panel. These differences may be due in

part to the failure to achieve boundary conditions at the loaded end in tests that correspond to the boundary conditions assumed in the theoretical analysis.

The theoretical analysis assumed that the normal stress in the webs acting perpendicular to the stiffeners was zero. The test results indicate that at certain sections this normal stress was relatively large for some of the loading conditions. However, the variation in this normal stress over the panel length was frequently erratic. This normal stress may have been introduced into the panel by the test boundary conditions at both the loaded end and the supported end of the panel since strains normal to the stiffeners were restrained. This restraint would produce stresses in the web normal to the stiffeners.

As previously noted, the theoretical analysis was based upon an effective stiffener area that included the area of adjacent webs. Therefore, the theoretical analysis assumed that the normal stress in the webs acting parallel to the stiffeners was equal to the normal stress in the stiffeners to which the webs were attached. Since the strain gauge rosettes were placed on the webs midway between the stiffeners, a direct comparison of theoretical and experimental stress was not made. However, the experimental data indicates that, as the distance from the loaded end of the panel increased, the normal stress in the webs acting parallel to the stiffeners approached the normal stress in the stiffeners in agreement with the stress distribution assumed for the idealized panel.

CONCLUDING REMARKS

Since the three test panels were of the same general configuration and only one theoretical analysis was considered, it is not possible to make any broad generalizations concerning the validity of the theoretical analysis. However, the general trend of agreement between the experimental results and the theoretical analysis implies that a satisfactory experimental procedure was employed and also that the idealized structure and assumed stress distribution used in the theoretical analysis approaches the actual conditions. Since the realtive agreement between the theoretical and experimental results was the same for all three panels, the

accuracy of the theoretical analysis appears to be independent of the ratio of the stiffener area to the sheet area. The test results show that the ratio of stiffener area to sheet area does affect the stress distribution in a stiffened panel.

The effects of varying the number of stiffeners, using stiffeners of different sizes on the same panel and tapering the stiffener cross-section over the length of the panel are now being investigated under the terms of NASA Contract NAS8-20164.

APPENDIX F1

COMPUTER PROGRAM FOR REDUCTION OF TEST DATA

This program in Fortran II was used for test data obtained from 110 uniaxial gages and 24 rosette gages providing 182 strain gage channels. Modifications were necessary when a different number of gages were used.

```
C                          INPUT-OUTPUT FORMATS
C
1     FORMAT (40X,54HTHE FOLLOWING DATA ARE THE RESULT OF THE RESOLUTION
      1 of,2/,35X,65HSTRESSES FROM STRAINS OBTAINED DURING A TESTING PROG
      2RAM CONDUCTED,2/,35X,56HAT THE UNIVERSITY OF ALABAMA UNDER CONTRAC
      3T NAS 8-11155.,3/,40X,24HALL STRESSES ARE IN PSI.,2/,40X,48HALL AN
      4GLES ARE IN DEG. MEASURED FROM THE X AXIS.,4/)
2     FORMAT (/,6F10.2,/)
3     FORMAT (36X,58HTHE FOLLOWING MATERIAL PROPERTIES ARE USED IN CALCU
      1LATION,,2/,36X,23HMODULUS OF ELASTICITY -,F4.1,6X,21HMODULUS OF RI
      2GIDITY -,F4.1,2/,52X,16HPOISSONS RATIO -,F15.8,3/)
4     FORMAT (40X,2A5,/)
5     FORMAT (55X,8HTEST NO.,2A5,2/)
6     FORMAT (14(13F6.1,/))
7     FORMAT (31X,17HUNIAXIAL GAGE NO.,I3,6X,8HSTRAIN -,F7.1,6X,9HSIGMA
      1Y -,F12.6,2/)
8     FORMAT (55X,11HROSETTE NO.,I4,2/,40X,9HSIGMA X -,F12.6,9X,9HSIGMA
      1Y -,F12.6,2/,40X,9HSIGMA 1 -,F12.6,9X,9HTHETA 1 -,F12.6,2/,40X9HS
      2IGMA 2 -,F12.6,9X,9HTHETA 2 -,F12.6,2/,40X,9HSIGMA S -,F12.6,9X,9H
      3THETA S -,F12.6,2/,40X,8HTAU XY -,F12.6,10X,7HTAU S -,F12.6,2/)
C
C
C                              START PROGRAM
C
      DIMENSION GF(4), C(2), E(182), S(182), V(10)
      PRINT 1,
      READ 2, A, G, GF
      C(1)=(A/(2.0*G))-1.0    $    C(2)=A/(1.0-C(1)*C(1))
```

```
      PRINT 3, A, G, C(1)
10    READ 4, T, O
      PRINT 5, T, O
      READ 6, E
      DO 11 I=1, 110
11    S(I)=2.0*E(I)*A/GF(1)
      PRINT 7, (I, E(I), S(I), I=1,110)
      DO 13 I=111,180,3
      DO 12 J=1,3
12    E(I+J-1)=2.0*E(I+J-1)/GF(J+1)
      V(8)=E(I)-E(I+1)+E(I+2) $ V(4)=C(2)*(E(I)+C(1)*E(I+2))
      V(6)=C(2)*(E(I+2)+C(1)*E(I)) $ V(7)=(V(4)+V(6))/2.0
      V(9)=(V(6)-V(4))/2.0 $ V(1)=C(2)*(V(8)+C(1)*E(I+1))
      V(2)=C(2)*(E(I+1)+C(1)*V(8)) $ V(8)=(V(1)-V(2))/2.0
      V(10)=SQRT(V(9)*V(9)+V(8)*V(8)) $ V(3)=V(7)-V(10)
      V(5)=V(7)+V(10) $ V(4)=ARCTAN(V(9)/ABS(V(8)))
      IF (V(8)) 21,22,23
21    V(6)=90.0*(V(4)/3.14159265-1.0) $ GO TO 13
22    IF (V(9)) 32,31,31
31    V(6)=-45.0 $ GO TO 13
32    V(6)=45.0 $ GO TO 13
23    V(6)=-V(4)*90.0/3.14159265
13    V(4)=90.0+V(6) $ V(8)=45.0+V(6) $ PRINT 8, I,( (V(J), J=1,10)
      IF (E(182)) 10, 10, 40
40    STOP
      END
```

APPENDIX F2

COMPUTER PROGRAM FOR MATRIX ANALYSIS

The following program in Fortran IV was used to perform the necessary matrix computations.

```
C     MAIN ROUTINE
      REAL L1, L2
      DIMENSION GRI(24,60),ARS(24,24),UNIT(24,24),GRM(24,4),CARN(24,4),
     1    ARN(24,4),AIJ(60,60),TEMP2(60,4),GIR(60,24),GIM(60,4),
     2    GJN(60,4),QIN(60,4),TEMP1(34,60),PMN(4,4),A(4)
      EQUIVALENCE (ARS(1,1),GRI(1,1)),(UNIT(1,1),GRI(1,25)),(GRM(1,1),
     1    GRI(1,49)),(CARN(1,1),GRI(1,53)),(ARN(1,1),GRI(1,57)),
     2    (TEMP2(1,1),AIJ(1,1)),(GIR(1,1),AIJ(1,5)),(GIM(1,1),AIJ(1,29))
     3    ,(GJN(1,1),AIJ(1,33)),(GIN(1,1),AIJ(,37))
      DATA L1,L2,B1,B2,B3/2.7,3.0,2.7675,2.77675,2.77/
      DATA T1,T2,T3/0.096,0.1005,0.1005/,E,G/10.5E+6,3.9E+6/
      DATA (A(I),I=1,4)/0.2743,0.4139,0.4203,0.2122/
5     FORMAT(35H1THE UNIT REDUNDANT FORCE MATRIX IS///60(2(12F10.6,/),/)
     1)
13    FORMAT(89H1THE MATRIX OF FLEXIBILITY COEFFICIENTS IS (VALUES HAVE
     1BEEN SCALED BY A FACTOR OF 10**6)///60(5(6P12F10.6,/),/))
20    FORMAT(18H1THE MATRIX ARN IS//)
21    FORMAT(22X,4E20.9,/)
29    FORMAT(58H1THE MATRIX ARS IS SINGULAR. EXECUTION HAS BEEN TERMINAT
     1ED/1H1)
41    FORMAT(19H1THE MATRIX CARN IS//)
43    FORMAT(18H1THE MATRIX QIN IS//)
44    FORMAT(33H1THE UNIT EXTERNAL LOAD MATRIX IS///60(22X,4F10.6,/),/)
C     COMPUTE THE ELEMENTS OF THE MATRIX PMN
      DO 30 I=1,4
      DO 33 J=1,4
33    PMN(I,J)=0
30    PMN(I,I)=1
C     COMPUTE THE ELEMENTS OF THE MATRIX GRI WHICH IS THE TRANSPOSE OF
```

```
C       THE UNIT REDUNDANT FORCE MATRIX GIR.
      DO 1 I=1,24
      DO 1 J=1,60
1     GRI(I,J) = 0
      DO 2 K=1,8
      N = K-1
      DO 2 L=1,3
      M = L-1
      GRI(1+N+8*M,11+N+9*M) = 1
2     GRI(1+N+8*M,2+N) = -1
      DO 3 K=1,3
      M = K-1
      DO 3 L=1,K
      N = L-1
      GRI(1+8*M,37+8*N) = -1.0/L1
      DO 4 I=1,6
      GRI(I+8*M,37+I+8*N) = 1.0/L2
4     GRI(I+1+8*M,37+I+8*N) = -1.0/L2
      GRI(7+8*M,44+8*N) = 1.0/L1
3     GRI(8+8*M,44+8*N) = -1.0/L1
      PRINT 5, GRI
C     COMPUTE THE MATRIX OF FLEXIBILITY COEFFICIENTS AIJ
      DO 6 I=1,60
      DO 6 J=I,60
6     AIJ(I,J) = 0
      DO 7 I=1,4
      T = L1/(3.0*E*A(I))
      AIJ(9*I-8,9*I-8) = T
      AIJ(9*I,9*I) = T
      T = L1/(6.0*E*A(I))
      AIJ(9*I-8,9*I-7) = T
      AIJ(9*I-1,9*I) = T
      T = (L1+L2)/(3.0*E*A(I))
      AIJ(9*I-7,9*I-7) = T
      AIJ(9*I-1,9*I-1) = T
      T = (2.0*L2)/(3.0*E*A(I))
```

```
      DO 8 J=2,6
8     AIJ(9*I-J,9*I-J) = T
      T = L2/(6.0*E*A(I))
      DO 7 J=1,6
7     AIJ(9*I-J-1,9*I-J) = T
      T = (L1*B1)/(G*T1)
      AIJ(37,37) = T
      AIJ(44,44) = T
      T = (L2*B1)/(G*T1)
      DO 9 I=38,43
9     AIJ(I,I) = T
      T = (L1*B2)/(G*T2)
      AIJ(45,45) = T
      AIJ(52,52) = T
      T = (L2*B2)/(G*T2)
      DO 10 I=46,51
10    AIJ(I,I) = T
      T = (L1*B3)/(G*T3)
      AIJ(53,53) = T
      AIJ(60,60) = T
      T = (L2*B3)/(G*T3)
      DO 11 I=54,59
11    AIJ(I,I) = T
      DO 12 I=1,60
      DO 12 J=I,60
12    AIJ(J,I) = AIJ(I,J)
      PRINT 13,((AIJ(I,J),J=1,60),I=1,60)
C     PERFORM THE MATRIX MULTIPLICATION TEMP1 = GRI * AIJ.
      DO 14 I=1,24
      DO 14 J=1,60
      TEMP1(I,J) = 0
      DO 14 K=1,60
14    TEMP1(I,J) = GRI(I,K)*AIJ(K,J)+TEMP1(I,J)
C     SET GIR EQUAL TO THE TRANSPOSE OF GRI.
      DO 15 I=1,60
      DO 15 J=1,24
```

```
15    GIR(I,J) = GRI(J,I)
C     CLEAR ALL ELEMENTS OF MATRIX GJN TO ZERO.
      DO 16 I=1,60
      DO 16 J=1,4
16    GJN(I,J) = 0
C     COMPUTE NON-ZERO ELEMENTS OF MATRIX GJN FROM FORMULAE.
      DO 17 I=2,9
      DO 17 J=1,4
17    GJN(I,J) = 1
      GJN(1,1) = 1
      GJN(10,2) = 1
      GJN(19,3) = 1
      GJN(28,4) = 1
      DO 18 I=2,4
18    GJN(37,I) = 1.0/L1
      GJN(45,3) = 1.0/L1
      GJN(45,4) = 1.0/L1
      GJN(53,4) = 1.0/L1
      PRINT 44,((GJN(I,J),J=1,4),I=1,60)
C     PERFORM THE MATRIX MULTIPLICATION ARN = TEMP1 * GJN
      DO 19 I=1,24
      DO 19 J=1,4
      ARN(I,J) = 0
      DO 19 K=1,60
19    ARN(I,J) = TEMP1(I,K)*GJN(K,J)+ARN(I,J)
      PRINT 20
      PRINT 21,((ARN(I,J),J=1,4),I=1,24)
C     PERFORM THE MATRIX MULTIPLICATION ARS = TEMP1 * GIR
      DO 23 I=1,24
      DO 23 J=1,24
      ARS(I,J) = 0
      DO 23 K=1,60
23    ARS(I,J) = TEMP1(I,K)*GIR(K,J)+ARS(I,J)
C     SET UP IDENTITY MATRIX UNIT FOR INVERSION
      DO 25 I=1,24
      DO 24 J=1,24
```

```
24    UNIT(I,J) = 0
25    UNIT(I,I) = 1
C     INVERT THE MATRIX ARS AND LEAVE RESULT IN THE MATRIX UNIT.
      DO 32 M=1,24
28    T = ARS(M,M)
      IF(T.NE.0.0) GO TO 35
      DO 26 J=M,24
      IF(ARS(J,M).EQ.0.0) GO TO 26
      DO 27 L=M,24
      T = ARS(M,L)
      ARS(M,L) = ARS(J,L)
27    ARS(J,L) = T
      GO TO 28
26    CONTINUE
      PRINT 29
      STOP
35    K1 = M+1
      DO 34 L=K1,48
34    ARS(M,L) = ARS(M,L)/T
      DO 32 K=1,24
      IF(K.EQ.M) GO TO 32
      S = ARS(K,M)
      K1 = M+1
      DO 31 L=K1,48
31    ARS(K,L) = ARS(K,L)-S*ARS(M,L)
32    CONTINUE
C     PERFORM THE MATRIX MULTIPLICATION GRM = -UNIT * ARN
      DO 36 I=1,24
      DO 36 J=1,4
      GRM(I,J) = 0
      DO 36 K=1,24
36    GRM(I,J) = -UNIT(I,K)*ARN(K,J)+GRM(I,J)
C     PERFORM THE MATRIX MULTIPLICATION TEMP2 = GIR * GRM
      DO 37 I=1,60
      DO 37 J=1,4
      TEMP2(I,J) = 0
```

```
      DO 37 K=1,24
37    TEMP2(I,J) = GIR(I,K)*GRM(K,J)+TEMP2(I,J)
C     PERFORM THE MATRIX ADDITION GIM = GJN + TEMP2
      DO 38 I=1,60
      DO 38 J=1,4
38    GIM(I,J) = GJN(I,J)+TEMP2(I,J)
C     PERFORM THE MATRIX MULTIPLICATION CARN = TEMP1 *GIM
      DO 39 I=1,24
      DO 39 J=1,4
      CARN(I,J) = 0
      DO 39 K=1,60
39    CARN(I,J) = TEMP1(I,K)*GIM(K,J)+CARN(I,J)
      PRINT 41
      PRINT 21,((CARN(I,J),J=1,4),I=1,24)
C     PERFORM THE MATRIX MULTIPLICATION QIN = GIM * PMN.
      DO 42 I=1,60
      DO 42 J=1,4
      QIN(I,J) = 0
      DO 42 K=1,4
42    QIN(I,J) = GIM(I,K)*PMN(K,J)+QIN(I,J)
      PRINT 43
      PRINT 21,((QIN(I,J),J=1,4),I=1,60)
      STOP
      END
```

REFERENCES

F1. Rey, William K.: Matrix Shear Lag Analysis Utilizing A High-Speed Digital Computer. Section IV of the Summary Report for NASA Contract NAS8-5012, November 1962.

F2. Bruhn, E. F.: Analysis and Design of Flight Vehicle Structures. Tri-State Offset Company, 1965.

TABLE F1. - MATRIX ANALYSIS OF PANEL B FOR LOADING CONDITION I

P = 1 kip

y	Stiff. No. 1	Web. No. 1	Stiff. No. 2	Web. No. 2	Stiff. No. 3	Web. No. 3	Stiff. No. 4
in.	σ_y	τ_{xy}	σ_y	τ_{xy}	σ_y	τ_{xy}	σ_y
0.3	2430.7		0		0		0
1.5		1195.6		456.3		121.8	
3.0	1657.8		382.6		156.1		121.3
4.5		650.6		377.2		108.5	
6.0	1190.5		545.7		294.9		241.3
7.5		352.9		275.1		86.9	
9.0	937.0		596.9		391.9		337.5
10.5		197.3		188.1		64.3	
12.0	795.3		607.3		455.4		408.6
13.5		111.9		122.5		44.4	
15.0	714.9		604.8		495.3		457.8
16.5		62.4		74.8		28.3	
18.0	670.1		600.0		519.0		489.0
19.5		31.0		39.3		15.2	
21.0	647.8		596.5		531.3		505.9
22.5		9.2		12.0		4.7	
23.7	641.9		595.4		534.6		510.6

TABLE F2. - MATRIX ANALYSIS OF PANEL B FOR LOADING CONDITION II

P = 1 kip

y	Stiff. No. 1	Web. No. 1	Stiff. No. 2	Web. No. 2	Stiff. No. 3	Web. No. 3	Stiff. No. 4
in.	σ_y	τ_{xy}	σ_y	τ_{xy}	σ_y	τ_{xy}	σ_y
0.3	0		1886.8		0		0
1.5		-591.8		807.7		175.8	
3.0	382.6		1205.1		296.4		175.0
4.5		-227.1		411.0		134.8	
6.0	545.7		860.9		438.4		324.2
7.5		-71.2		211.3		88.0	
9.0	596.9		709.4		500.8		421.5
10.5		-14.5		114.0		53.7	
12.0	607.3		641.0		531.0		480.9
13.5		3.4		63.4		31.5	
15.0	604.8		609.4		546.8		515.8
16.5		6.7		35.0		17.7	
18.0	600.0		594.6		555.4		535.4
19.5		4.9		17.3		8.8	
21.0	596.5		588.2		559.6		545.1
22.5		1.7		5.1		2.6	
23.7	595.4		586.5		560.7		547.7

TABLE F3. - MATRIX ANALYSIS OF PANEL B FOR LOADING CONDITION III
P = 1 kip

y	Stiff. No. 1	Web. No. 1	Stiff. No. 2	Web. No. 2	Stiff. No. 3	Web. No. 3	Stiff. No. 4
in.	σ_y	τ_{xy}	σ_y	τ_{xy}	σ_y	τ_{xy}	σ_y
0.3	0		0		1891.8		0
1.5		-241.4		-876.6		487.5	
3.0	156.1		296.4		1225.4		485.4
4.5		-193.4		-472.0		148.9	
6.0	294.9		438.4		890.8		650.1
7.5		-134.9		-260.1		23.1	
9.0	391.9		500.8		739.8		675.7
10.5		- 88.4		-150.2		- 12.7	
12.0	455.4		531.0		667.2		661.6
13.5		- 55.6		- 88.4		- 18.1	
15.0	495.3		546.8		630.5		641.7
16.5		- 33.0		- 50.9		- 14.3	
18.0	519.0		555.4		611.5		625.9
19.5		- 17.0		- 25.9		- 8.4	
21.0	531.3		559.6		602.5		616.6
22.5		- 5.1		- 7.8		- 2.7	
23.7	534.6		560.7		600.1		613.9

TABLE F4.- MATRIX ANALYSIS OF PANEL B FOR LOADING CONDITION IV
P = 1 kip

y	Stiff. No. 1	Web No. 1	Stiff. No. 2	Web No. 2	Stiff. No. 3	Web No. 3	Stiff. No. 4
in.	σ_y	τ_{xy}	σ_y	τ_{xy}	σ_y	τ_{xy}	σ_y
0.3	0		0		0		1853.2
1.5		-93.8		-282.5		-743.0	
3.0	60.7		87.5		242.7		1113.4
4.5		-83.6		-229.0		-361.0	
6.0	120.7		162.1		325.1		714.0
7.5		-66.9		-162.5		-175.3	
9.0	168.8		210.8		337.9		520.0
10.5		-49.5		-108.3		- 89.3	
12.0	204.3		240.5		330.8		421.2
13.5		-34.2		- 69.0		- 47.2	
15.0	228.9		257.9		320.9		369.0
16.5		-21.8		- 41.4		- 25.0	
18.0	244.5		268.7		313.0		341.4
19.5		-11.7		- 21.5		- 12.0	
21.0	253.0		272.6		308.3		328.1
22.5		- 3.6		- 6.5		- 3.5	
23.7	205.3		273.9		307.0		324.6

TABLE F5. - MATRIX ANALYSIS OF PANEL C FOR LOADING CONDITION I
P = 1 kip

y	Stiff. No. 1	Web No. 1	Stiff. No. 2	Web No. 2	Stiff. No. 3	Web No. 3	Stiff. No. 4
in.	σ_y	τ_{xy}	σ_y	τ_{xy}	σ_y	τ_{xy}	σ_y
0.3	1496.1		0		0		0
1.5		938.6		324.1		91.2	
3.0	1120.7		204.7		81.4		62.1
4.5		587.4		283.3		84.2	
6.0	859.8		316.1		158.8		125.7
7.5		363.6		224.6		71.9	
9.0	698.2		366.1		218.2		180.1
10.5		227.4		167.5		57.3	
12.0	597.2		387.0		261.1		223.4
13.5		141.6		118.2		42.6	
15.0	534.3		394.6		290.6		255.6
16.5		84.8		77.2		28.9	
18.0	496.6		396.7		309.4		277.4
19.5		44.3		42.5		16.4	
21.0	476.9		397.0		319.6		289.9
22.5		13.5		13.3		5.2	
23.7	471.5		396.9		322.5		293.4

TABLE F6. - MATRIX ANALYSIS OF PANEL C FOR LOADING CONDITION II
P = 1 kip

y	Stiff. No. 1	Web No. 1	Stiff. No. 2	Web No. 2	Stiff. No. 3	Web No. 3	Stiff. No. 4
in.	σ_y	τ_{xy}	σ_y	τ_{xy}	σ_y	τ_{xy}	σ_y
0.3	0		1263.1		0		0
1.5		-511.9		631.7		139.5	
3.0	204.7		871.6		171.6		95.0
4.5		-250.7		359.7		115.0	
6.0	316.1		639.2		266.9		181.9
7.5		-112.6		203.4		83.3	
9.0	366.1		518.8		313.8		244.9
10.5		- 47.0		118.0		56.4	
12.0	387.0		455.7		338.0		287.5
13.5		- 17.2		69.2		36.4	
15.0	394.6		422.7		350.9		315.1
16.5		- 4.8		39.7		22.1	
18.0	396.7		405.6		357.9		331.8
19.5		- 0.6		20.1		11.5	
21.0	397.0		397.7		361.3		340.5
22.5		0.1		6.1		3.5	
23.7	396.9		395.6		362.2		342.8

TABLE F7. - MATRIX ANALYSIS OF PANEL C FOR LOADING CONDITION III
P = 1 kip

y	Stiff. No. 1	Web No. 1	Stiff. No. 2	Web No. 2	Stiff. No. 3	Web No. 3	Stiff. No. 4
in.	σ_y	τ_{xy}	σ_y	τ_{xy}	σ_y	τ_{xy}	σ_y
0.3	0		0		1264.5		0
1.5		-203.6		-694.4		408.4	
3.0	81.4		171.6		885.5		277.9
4.5		-174.1		-417.4		166.5	
6.0	158.8		266.9		662.1		403.8
7.5		-133.7		-252.6		52.9	
9.0	218.2		313.8		544.9		443 8
10.5		- 96.6		-157.1		7.5	
12.0	261.1		338.0		481.6		449.5
13.5		- 66.3		- 98.3		- 7.6	
15.0	290.6		350.9		446.6		443.7
16.5		- 42.3		- 59.4		- 9.9	
18.0	309.4		357.9		427.5		436.2
19.5		- 23.0		- 31.3		- 7.0	
21.0	319.6		361.3		418.0		431.0
22.5		- 7.1		- 9.6		- 2.4	
23.7	322.5		362.2		415.5		429.3

TABLE F8. - MATRIX ANALYSIS OF PANEL C FOR LOADING CONDITION IV
P = 1 kip

y	Stiff. No. 1	Web No. 1	Stiff. No. 2	Web No. 2	Stiff. No. 3	Web No. 3	Stiff. No. 4
in.	σ_y	τ_{xy}	σ_y	τ_{xy}	σ_y	τ_{xy}	σ_y
0.3	0		0		0		1269.7
1.5		-77.6		-212.2		-627.7	
3.0	31.0		47.5		139.0		842.5
4.5		-71.7		-182.9		-354.3	
6.0	62.9		90.9		201.9		574.6
7.5		-61.1		-141.5		-197.8	
9.0	90.0		122.4		221.9		425.1
10.5		-48.7		-103.0		-112.9	
12.0	111.7		143.8		224.8		339.7
13.5		-36.3		- 71.2		- 65.1	
15.0	127.8		157.5		221.9		290.5
16.5		-24.6		- 45.7		- 36.8	
18.0	138.7		165.9		218.1		262.7
19.5		-13.9		- 24.9		- 18.5	
21.0	144.9		170.2		215.5		248.8
22.5		- 4.4		- 7.7		- 5.5	
23.7	146.7		171.4		214.7		245.0

TABLE F9. - MATRIX ANALYSIS OF PANEL D FOR LOADING CONDITION I
P = 1 kip

y	Stiff. No. 1	Web No. 1	Stiff. No. 2	Web No. 2	Stiff. No. 3	Web No. 3	Stiff. No. 4
in.	σ_y	τ_{xy}	σ_y	τ_{xy}	σ_y	τ_{xy}	σ_y
0.3	3645.6		0		0		0
1.5		1423.9		504.6		141.7	
3.0	2300.1		560.9		234.3		181.2
4.5		706.8		399.6		123.0	
6.0	1558.1		761.6		432.7		355.9
7.5		350.5		273.4		94.0	
9.0	1190.0		806.4		561.4		489.4
10.5		181.1		174.7		65.7	
12.0	999.9		805.1		639.6		582.9
13.5		96.0		106.8		42.9	
15.0	899.1		794.1		685.4		643.9
16.5		50.6		61.7		26.0	
18.0	846.0		784.4		711.0		680.7
19.5		24.2		31.1		13.5	
21.0	820.6		778.5		723.7		699.9
22.5		7.0		9.3		4.1	
23.7	814.0		776.8		727.0		705.1

TABLE F10. - MATRIX ANALYSIS OF PANEL D FOR LOADING CONDITION II
P = 1 kip

y	Stiff. No. 1	Web No. 1	Stiff. No. 2	Web No. 2	Stiff. No. 3	Web No. 3	Stiff. No. 4
in.	σ_y	τ_{xy}	σ_y	τ_{xy}	σ_y	τ_{xy}	σ_y
0.3	0		2416.0		0		0
1.5		-593.6		849.1		197.9	
3.0	560.9		1487.7		420.4		253.0
4.5		-191.1		401.8		145.5	
6.0	761.6		1062.0		604.2		459.8
7.5		- 42.7		193.7		89.3	
9.0	806.4		891.2		679.1		586.7
10.5		12.4		99.3		51.3	
12.0	805.1		819.7		713.6		659.5
13.5		10.5		52.9		28.5	
15.0	794.1		788.5		731.1		700.0
16.5		9.3		28.1		15.3	
18.0	784.4		774.5		740.3		721.6
19.5		5.6		13.5		7.3	
21.0	778.5		768.5		744.8		732.0
22.5		1.8		4.0		2.1	
23.7	776.8		767.0		746.0		734.7

TABLE F11.- MATRIX ANALYSIS OF PANEL D FOR LOADING CONDITION III
P = 1 kip

y	Stiff. No. 1	Web No. 1	Stiff. No. 2	Web No. 2	Stiff. No. 3	Web No. 3	Stiff. No. 4
in.	σ_y	τ_{xy}	σ_y	τ_{xy}	σ_y	τ_{xy}	σ_y
0.3	0		0		2379.3		0
1.5		-248.0		-878.1		507.7	
3.0	234.3		420.4		1484.5		602.1
4.5		-189.0		-432.9		135.6	
6.0	432.7		604.2		1076.8		841.8
7.5		-122.5		-219.9		13.3	
9.0	561.4		679.1		909.6		860.6
10.5		- 74.5		-118.4		- 15.4	
12.0	639.6		713.6		835.7		838.7
13.5		- 43.6		- 65.7		- 17.0	
15.0	685.4		731.1		800.7		814.6
16.5		- 24.4		- 36.0		- 12.1	
18.0	711.0		740.3		783.6		797.3
19.5		- 12.1		- 17.7		- 6.7	
21.0	723.7		744.8		775.8		787.8
22.5		- 3.6		- 5.2		- 2.1	
23.7	727.0		746.0		773.8		785.1

TABLE F12. - MATRIX ANALYSIS OF PANEL D FOR LOADING CONDITION IV
P = 1 kip

y	Stiff. No. 1	Web No. 1	Stiff. No. 2	Web No. 2	Stiff. No. 3	Web No. 3	Stiff. No. 4
in.	σ_y	τ_{xy}	σ_y	τ_{xy}	σ_y	τ_{xy}	σ_y
0.3	0		0		0		2356.3
1.5		-95.9		-284.5		-787.3	
3.0	90.6		126.5		324.6		1349.5
4.5		-83.2		-221.4		-355.6	
6.0	178.0		229.9		420.9		844.2
7.5		-63.6		-147.9		-161.0	
9.0	244.7		293.4		430.3		615.4
10.5		-44.5		- 92.5		- 77.2	
12.0	291.4		329.8		419.4		505.7
13.5		-29.0		- 55.5		- 38.7	
15.0	321.9		350.0		407.3		450.8
16.5		-17.6		- 31.7		- 19.6	
18.0	340.4		360.8		398.7		422.9
19.5		- 9.1		- 15.8		- 9.2	
21.0	350.0		366.0		393.9		409.8
22.5		- 2.8		- 4.7		- 2.6	
23.7	352.6		367.4		392.5		406.5

TABLE F13. - TEST RESULTS FOR PANEL B

(Loading Condition I, Test No. 7)
P = 1 kip

y	Stiff No. 1	Web. No. 1			Stiff. No. 2	Web. No. 2			Stiff No. 3	Web. No. 3			Stiff No. 4
in.	σ_y	σ_x	σ_y	τ_{xy}	σ_y	σ_x	σ_y	τ_{xy}	σ_y	σ_x	σ_y	τ_{xy}	σ_y
0.3	1962.8				0				0				0
1.5		11.4	602.8	782.3		-579.8	-46.8	39.6		-698.8	-34.1	1.5	
3.0	2133.3				205.9				79.0				56.2
4.5		261.0	1080.1	697.1		54.9	202.0	357.7		60.5	20.9	108.1	
6.0	1538.7				442.9				164.3				70.7
7.5		138.3	983.5	573.8		61.6	333.2	394.2		279.8	234.1	152.2	
9.0	1035.4				582.1				261.9				176.8
10.5		96.0	856.6	301.4		125.6	451.0	353.1		320.6	368.8	143.1	
12.0	867.1				632.1				363.9				305.7
13.5		77.0	737.7	197.9		--	--	--		186.1	471.9	108.1	
15.0	731.9				602.9				432.5				405.5
16.5		36.4	653.0	112.6		116.6	560.2	164.4		150.6	513.7	79.1	
18.0	669.5				615.5				490.7				474.1
19.5		6.8	613.6	74.6		50.2	620.3	111.1		130.6	565.0	59.4	
21.0	517.7				553.1				513.6				513.6
22.5		59.3	573.6	7.6		177.2	606.1	50.2		169.5	595.1	39.6	
23.7	567.7				546.9				513.6				496.9

TABLE F14. - TEST RESULTS FOR PANEL B

(Loading Condition I, Test No. 8)

P = 1 kip

y	Stiff. No. 1	Web. No. 1			Stiff. No. 2	Web. No. 2			Stiff. No. 3	Web. No. 3			Stiff. No. 4
in.	σ_y	σ_x	σ_y	τ_{xy}	σ_y	σ_x	σ_y	τ_{xy}	σ_y	σ_x	σ_y	τ_{xy}	σ_y
0.3	2054.3				0				0				0
1.5		-21.1	604.0	759.5		-550.4	-45.0	53.3		-665.2	-68.1	4.6	
3.0	2070.9				266.2				72.8				45.8
4.5		182.0	1007.6	722.9		121.5	195.3	377.4		46.6	16.1	100.4	
6.0	1509.5				453.3				135.2				64.5
7.5		215.7	968.7	528.1		207.6	412.8	424.6		348.1	253.6	127.8	
9.0	1095.8				531.8				268.3				180.9
10.5		111.5	866.1	298.3		144.3	494.9	340.9		288.0	357.5	129.4	
12.0	864.9				613.4				386.8				297.3
13.5		35.1	748.2	190.2		--	--	--		190.6	403.7	97.4	
15.0	723.6				607.1				459.5				403.4
16.5		22.5	673.1	95.9		62.4	558.0	162.8		147.4	504.3	70.0	
18.0	636.3				594.7				505.3				482.4
19.5		26.9	612.3	60.9		78.0	605.0	102.0		125.9	550.9	48.7	
21.0	567.7				578.1				540.6				511.5
22.5		67.2	609.6	-9.1		124.5	596.2	59.4		93.4	564.6	50.2	
23.7	548.9				536.5				567.7				565.6

TABLE F15.- TEST RESULTS FOR PANEL B

(Loading Condition II, Test No. 6)
P = 1 kip

y	Stiff. No. 1	Web. No. 1			Stiff. No. 2	Web. No. 2			Stiff. No. 3	Web. No. 3			Stiff. No. 4
in.	σ_y	σ_x	σ_y	τ_{xy}	σ_y	σ_x	σ_y	τ_{xy}	σ_y	σ_x	σ_y	τ_{xy}	σ_y
0.3	0				1530.3				0				0
1.5		133.3	462.0	-464.2		-5.8	563.5	811.2		-252.7	-29.3	102.0	
3.0	203.8				1507.4				247.4				99.8
4.5		-115.1	766.9	-310.5		-62.8	664.4	499.2		55.0	227.0	214.6	
6.0	484.5				914.8				434.6				262.0
7.5		-56.5	683.2	-63.9		-100.1	639.0	270.9		79.0	447.4	127.8	
9.0	582.2				719.4				503.2				395.0
10.5		-34.9	649.1	-15.2		6.8	626.1	153.7		122.6	479.1	94.4	
12.0	580.1				640.4				534.4				480.3
13.5		17.6	609.1	27.4		--	--	--		56.1	539.2	62.4	
15.0	565.6				611.3				551.0				530.2
16.5		--	--	--		-4.0	618.2	76.1		105.9	602.2	35.0	
18.0	532.3				571.8				565.5				561.4
19.5		39.3	599.9	15.2		44.0	614.0	53.3		98.2	616.2	27.4	
21.0	515.6				553.1				582.2				569.7
22.5		101.2	563.1	-15.2		110.6	616.3	24.3		65.8	642.4	44.1	
23.7	501.1				503.2				542.7				534.4

TABLE F16. - TEST RESULTS FOR PANEL B

(Loading Condition II, Test No. 7)
P = 1 kip

y	Stiff. No. 1	Web. No. 1			Stiff. No. 2	Web. No. 2			Stiff. No. 3	Web. No. 3			Stiff. No. 4
in.	σ_y	σ_x	σ_y	τ_{xy}	σ_y	σ_x	σ_y	τ_{xy}	σ_y	σ_x	σ_y	τ_{xy}	σ_y
0.3	0				1526.2				0				0
1.5		55.8	451.8	-491.6		-64.8	534.8	792.9		-229.4	-8.7	112.6	
3.0	216.2				1522.0				255.8				95.6
4.5		-124.5	751.2	-307.4		-116.8	724.7	497.7		56.6	231.7	200.9	
6.0	499.0				908.6				403.1				262.0
7.5		-72.0	698.6	-67.0		-42.7	638.1	260.2		86.8	445.9	129.4	
9.0	576.0				740.2				515.6				401.3
10.5		41.0	654.6	-10.6		-30.4	613.2	156.8		79.2	484.8	91.3	
12.0	584.3				652.9				544.8				484.5
13.5		-10.3	611.9	24.3		--	--	--		46.8	548.5	59.4	
15.0	573.9				607.1				592.6				553.8
16.5		13.0	619.9	10.6		50.0	570.4	74.6		85.7	566.1	45.6	
18.0	536.4				569.7				567.6				588.4
19.5		12.8	570.0	25.9		93.6	614.6	53.3		88.8	588.0	27.4	
21.0	511.5				551.2				553.1				476.0
22.5		62.4	570.5	-22.8		102.8	605.3	28.9		90.4	592.7	44.1	
23.7	507.3				526.0				553.1				584.3

TABLE F17. - TEST RESULTS FOR PANEL B

(Loading Condition III, Test No. 6)
P = 1 kip

y	Stiff. No. 1	Web. No. 1			Stiff. No. 2	Web. No. 2			Stiff. No. 3	Web. No. 3			Stiff. No. 4
in.	σ_y	σ_x	σ_y	τ_{xy}	σ_y	σ_x	σ_y	τ_{xy}	σ_y	σ_x	σ_y	τ_{xy}	σ_y
0.3	0				0				1580.2				0
1.5		51.2	17.7	16.7		403.2	505.5	-722.9		372.6	623.8	735.1	
3.0	8.3				253.7				1844.2				401.3
4.5		36.3	195.5	-181.1		47.7	785.8	-476.4		111.9	966.0	261 8	
6.0	99.8				430.4				1064.6				767.2
7.5		-34.5	329.0	-184.2		-82.7	728.2	-296.8		-153.5	861.7	32.0	
9.0	274.5				515.6				873.3				798.4
10.5		-9.4	404.2	-153.7		-102.6	645.2	-185.7		-158.5	772.7	27.4	
12.0	345.2				544.8				738.1				781.8
13.5		-48.0	449.1	-82.2		--	--	--		-64.1	722.2	-7.6	
15.0	399.2				544.8				669.5				729.8
16.5		-6.1	463.6	-47.2		-11.8	619.7	-50.2		-42.6	688.4	16.7	
18.0	422.1				542.7				684.1				682.0
19.5		21.8	473.3	-32.0		20.8	643.4	-21.3		30.4	709.1	21.3	
21.0	451.2				528.1				640.4				657.0
22.5		97.9	528.7	-67.0		116.8	610.1	0		124.8	683.6	62.4	
23.7	455.4				467.8				559.3				603.0

TABLE F18. - TEST RESULTS FOR PANEL B

(Loading Condition III, Test No. 7)
P = 1 kip

y	Stiff. No. 1	Web. No. 1			Stiff. No. 2	Web. No. 2			Stiff. No. 3	Web. No. 3			Stiff. No. 4
in.	σ_y	σ_x	σ_y	τ_{xy}	σ_y	σ_x	σ_y	τ_{xy}	σ_y	σ_x	σ_y	τ_{xy}	σ_y
0.3	0				0				2060.5				0
1.5		37.2	12.9	12.2		341.3	542.3	-695.5		349.0	515.8	660.5	
3.0	0				249.5				1653.0				393.0
4.5		19.2	181.3	-176.5		-34.4	811.5	-456.6		129.0	980.3	238.9	
6.0	135.2				430.4				1091.6				719.4
7.5		-54.6	330.4	-182.6		-124.7	701.2	-295.3		-113.3	846.5	41.1	
9.0	280.7				507.3				867.0				773.5
10.5		-49.8	382.0	-162.8		-117.1	637.3	-187.2		-77.9	767.3	21.3	
12.0	353.5				534.4				765.2				756.8
13.5		-29.4	468.0	-76.1		--	--	--		-98.3	693.7	16.7	
15.0	432.5				551.0				702.8				731.9
16.5		12.6	495.0	-35.0		-92.5	600.1	-47.2		-56.5	683.2	12.2	
18.0	442.9				553.1				663.3				696.5
19.5		-24.5	519.6	-13.7		26.9	612.3	-3 0		48.8	665.6	15.2	
21.0	445.0				536.4				619.6				640.4
22.5		74.7	533.2	-44.1		87.5	645.7	-4.6		115.5	667.9	35.0	
23.7	492.8				490.7				586.3				619.6

TABLE F19.- TEST RESULTS FOR PANEL B

(Loading Condition IV, Test No. 6)

P = 1 kip

y	Stiff. No. 1	Web. No. 1			Stiff. No. 2	Web. No. 2			Stiff. No. 3	Web. No. 3			Stiff. No. 4
in.	σ_y	σ_x	σ_y	τ_{xy}	σ_y	σ_x	σ_y	τ_{xy}	σ_y	σ_x	σ_y	τ_{xy}	σ_y
0.3	0				0				0				1707.0
1.5		-51.2	-17.7	44.1		94.5	-0.5	-44.1		372.0	461.5	-592.0	
3.0	2.1				41.6				187.1				1418.0
4.5		29.6	39.4	-44.1		102.9	160.4	-225.2		-36.4	681.9	-379.0	
6.0	12.5				114.4				363.9				860.8
7.5		26.7	92.4	-89.8		8.7	273.3	-202.4		-144.0	494.9	-222.2	
9.0	66.6				180.9				401.3				627.9
10.5		0.5	149.9	-82.2		-42.4	293.0	-140.0		-137.9	451.3	-91.3	
12.0	116.9				218.3				363.9				488.6
13.5		-7.1	176.3	-53.3		--	--	--		-85.5	386.3	-48.7	
15.0	156.0				249.5				361.8				422.1
16.5		13.0	175.0	-36.5		-0.6	282.6	-53.3		-59.2	366.2	-19.8	
18.0	187.1				247.4				334.8				384.6
19.5		-16.3	210.6	-16.7		4.2	309.2	-39.6		-9.6	354.3	-1.5	
21.0	187.1				249.5				318.1				338.9
22.5		16.4	246.8	-30.4		55.3	301.9	-16.7		19.3	356.2	15.2	
23.7	207.9				226.6				291.1				326.4

TABLE F20. - TEST RESULTS FOR PANEL B

(Loading Condition IV, Test No. 7)
P = 1 kip

y	Stiff. No. 1	Web. No. 1			Stiff. No. 2	Web. No. 2			Stiff. No. 3	Web. No. 3			Stiff. No. 4
in.	σ_y	σ_x	σ_y	τ_{xy}	σ_y	σ_x	σ_y	τ_{xy}	σ_y	σ_x	σ_y	τ_{xy}	σ_y
0.3	0				0				0				1696.6
1.5		4.7	1.6	19.8		75.9	-7.0	-62.4		361.2	478.5	-657.5	
3.0	10.4				41.6				180.9				1403.5
4.5		7.8	23.5	-38.0		120.0	174.6	-223.7		25.8	732.5	-406.4	
6.0	21.2				112.3				349.3				865.0
7.5		-9.0	96.7	-85.2		1.0	274.8	-216.1		-53.8	567.7	-210.0	
9.0	60.3				158.0				386.7				625.8
10.5		2.1	154.6	-83.7		-23.8	299.5	-146.1		-96.1	440.8	-89.8	
12.0	118.5				189.2				372.2				486.6
13.5		-8.7	184.1	-51.7		--	--	--		-71.5	391.1	-44.1	
15.0	155.9				245.4				355.6				417.9
16.5		-25.6	207.4	-32.0		-64.1	289.7	-54.8		-43.7	363.3	-13.7	
18.0	193.4				232.9				330.6				370.1
19.5		-0.7	212.3	-18.3		-13.0	270.0	-32.0		4.4	359.1	-3.0	
21.0	185.0				228.7				309.8				341.0
22.5		5.4	213.9	-35.0		18.1	289.0	-10.7		13.6	349.9	15.2	
23.7	214.2				195.4				301.5				311.9

TABLE F21. - TEST RESULTS FOR PANEL C

(Loading Condition I, Test No. 9)
P = 1 kip

y	Stiff. No. 1	Web. No. 1			Stiff. No. 2	Web. No. 2			Stiff. No. 3	Web. No. 3			Stiff. No. 4
in.	σ_y	σ_x	σ_y	τ_{xy}	σ_y	σ_x	σ_y	τ_{xy}	σ_y	σ_x	σ_y	τ_{xy}	σ_y
0.3	1312.0				0				0				0
1.5		-50.9	514.7	718.4		-350.4	-38.1	67.0		-511.7	-52.4	15.2	
3.0	1253.8				180.9				37.4				20.8
4.5		106.5	697.4	581.4		102.8	147.5	289.2		9.3	3.2	67.0	
6.0	941.9				311.9				81.1				35.3
7.5		85.9	628.5	447.5		219.5	288.1	321.1		160.2	146.9	74.6	
9.0	729.8				355.5				176.7				101.9
10.5		98.2	603.7	313.5		137.6	338.7	258.7		160.4	203.9	92.8	
12.0	575.9				395.0				230.8				197.5
13.5		20.4	518.5	200.9		71.0	373.9	202.4		113.8	180.8	32.0	
15.0	499.0				407.5				309.8				268.2
16.5		41.9	471.9	139.9		159.7	454.5	307.1		140.7	348.1	60.9	
18.0	451.2				413.8				336.8				316.0
19.5		34.1	448.4	86.8		44.9	431.4	94.4		111.3	373.0	35.0	
21.0	422.1				397.1				345.1				328.5
22.5		116.3	460.3	45.7		49.6	433.0	71.5		102.2	430.4	22.8	
23.7	386.7				378.4				356.6				336.8

TABLE F22. - TEST RESULTS FOR PANEL C

(Loading Condition I, Test No. 10)
P = 1 kip

y	Stiff. No. 1	Web. No. 1			Stiff. No. 2	Web. No. 2			Stiff. No. 3	Web. No. 3			Stiff. No. 4
in.	σ_y	σ_x	σ_y	τ_{xy}	σ_y	σ_x	σ_y	τ_{xy}	σ_y	σ_x	σ_y	τ_{xy}	σ_y
0.3	1345.2				0				0				0
1.5		-54.0	517.7	733.6		-372.1	-41.5	-206.9		-538.1	-69.8	-1.5	
3.0	1264.2				185.0				49.9				37.4
4.5		30.3	684.1	605.7		70.1	111.6	290.7		-14.0	-4.8	71.5	
6.0	925.2				286.9				72.8				66.5
7.5		103.0	655.3	455.1		169.9	275.0	318.1		110.5	121.4	95.9	
9.0	731.9				355.5				166.3				110.2
10.5		31.5	601.4	305.9		122.1	341.7	264.9		186.8	226.8	100.4	
12.0	588.4				413.8				230.8				199.6
13.5		9.5	510.6	187.2		99.0	383.6	193.3		132.7	287.1	62.4	
15.0	499.0				411.7				314.0				362.0
16.5		75.8	450.5	127.8		92.8	377.3	138.5		108.1	336.8	47.2	
18.0	449.1				415.8				338.9				316.0
19.5		46.5	436.1	95.9		58.7	398.7	89.8		105.2	377.4	35.0	
21.0	395.0				390.9				357.6				330.6
22.5		80.5	427.1	44.1		-80.1	587.7	77.6		91.3	397.5	33.5	
23.7	393.0				380.5				365.9				334.8

TABLE F23. - TEST RESULTS FOR PANEL C

(Loading Condition II, Test No. 8)
P = 1 kip

y	Stiff. No. 1	Web. No. 1			Stiff. No. 2	Web. No. 2			Stiff. No. 3	Web. No. 3			Stiff. No. 4
in.	σ_y	σ_x	σ_y	τ_{xy}	σ_y	σ_x	σ_y	τ_{xy}	σ_y	σ_x	σ_y	τ_{xy}	σ_y
0.3	0				1226.7				0				0
1.5		123.3	404.1	-523.6		57.3	431.5	678.8		-226.4	-36.8	63.9	
3.0	141.4				981.4				143.5				52.0
4.5		-47.8	511.6	-313.6		-36.9	532.0	433.8		-13.5	120.1	141.5	
6.0	282.8				659.1				253.7				164.3
7.5		-3.0	460.5	-111.1		-20.1	458.8	228.3		36.5	258.0	89.8	
9.0	336.8				507.3				330.6				253.7
10.5		-23.3	424.4	-27.4		-4.7	418.4	112.6		22.7	290.6	76.1	
12.0	370.1				430.4				347.2				301.5
13.5		-34.4	416.5	7.6		-3.2	410.6	74.6		19.8	356.2	36.5	
15.0	370.1				411.7				361.8				349.3
16.5		18.4	388.9	25.9		6.0	401.3	56.3		54.1	397.1	18.3	
18.0	361.8				388.8				403.4				380.5
19.5		52.6	417.4	41.1		24.7	407.7	44.1		20.1	418.6	15.2	
21.0	353.2				388.8				401.2				382.6
22.5		94.2	357.0	6.1		85.2	441.2	30.4		20.1	418.6	-15.2	
23.7	353.2				374.3				388.8				370.1

TABLE F24. - TEST RESULTS FOR PANEL C

(Loading Condition II, Test No. 9)
P = 1 kip

y	Stiff. No. 1	Web. No. 1			Stiff. No. 2	Web. No. 2			Stiff. No. 3	Web. No. 3			Stiff. No. 4
in.	σ_y	σ_x	σ_y	τ_{xy}	σ_y	σ_x	σ_y	τ_{xy}	σ_y	σ_x	σ_y	τ_{xy}	σ_y
0.3	0				1241.3				0				0
1.5		97.4	366.4	-520.5		88.3	438.1	703.1		-228.1	-79.0	62.4	
3.0	133.1				991.8				151.8				56.1
4.5		-18.3	525.9	-312.0		26.7	549.8	444.4		-16.7	98.2	153.7	
6.0	274.5				671.6				289.0				160.1
7.5		-24.7	469.7	-108.1		-40.3	435.1	220.7		17.8	226.6	92.8	
9.0	345.1				515.6				351.4				247.4
10.5		1.6	449.7	-21.3		4.6	421.6	121.8		-14.6	265.3	70.1	
12.0	353.5				438.7				357.6				303.6
13.5		40.2	429.8	10.7		-15.6	410.4	80.7		-23.7	312.0	36.5	
15.0	363.9				413.8				376.3				347.2
16.5		49.4	395.5	41.1		38.6	412.6	57.8		-19.0	338.6	32.0	
18.0	372.2				405.4				382.6				380.5
19.5		33.9	386.0	35.0		26.3	424.9	42.6		-21.9	379.1	10.7	
21.0	355.5				388.8				399.2				380.5
22.5		58.6	373.8	13.7		86.8	445.9	47.2		26.1	387.5	3.0	
23.7	343.1				368.0				386.7				368.0

TABLE F25. - TEST RESULTS FOR PANEL C

(Loading Condition III, Test No. 8)
P = 1 kip

y	Stiff. No. 1	Web. No. 1			Stiff. No. 2	Web. No. 2			Stiff. No. 3	Web. No. 3			Stiff. No. 4
in.	σ_y	σ_x	σ_y	τ_{xy}	σ_y	σ_x	σ_y	τ_{xy}	σ_y	σ_x	σ_y	τ_{xy}	σ_y
0.3	0				0				1137.3				0
1.5		37.2	12.9	-12.2		252.6	436.7	-630.1		306.6	376.4	537.2	
3.0	0				145.5				998.0				249.5
4.5		50.1	137.9	-170.5		-25.9	564.9	-426.1		25.4	632.6	196.3	
6.0	41.6				264.0				706.9				440.8
7.5		-36.5	199.4	-194.8		-66.6	467.6	-273.9		-15.1	572.8	35.0	
9.0	131.0				314.0				571.8				507.3
10.5		-23.9	249.5	-137.0		-40.3	447.6	-196.3		-102.2	484.4	-4.6	
12.0	203.8				359.7				492.8				503.2
13.5		-16.1	285.5	-86.8		-14.1	415.1	-109.6		-69.6	483.2	-27.4	
15.0	247.4				370.1				465.7				490.7
16.5		-8.2	309.0	-42.6		-51.3	402.2	-57.8		-32.4	483.6	-12.2	
18.0	278.6				365.9				457.4				472.0
19.5		21.2	310.9	-19.8		-6.3	413.7	-28.9		-9.2	479.2	-10.7	
21.0	286.9				363.9				434.6				449.1
22.5		109.6	316.6	-36.5		63.5	437.8	-3.0		35.8	490.6	-9.1	
23.7	303.6				338.9				413.8				422.1

TABLE F26. - TEST RESULTS FOR PANEL C

(Loading Condition III, Test No. 9)
P = 1 kip

y	Stiff. No. 1	Web. No. 1			Stiff. No. 2	Web. No. 2			Stiff. No. 3	Web. No. 3			Stiff. No. 4
in.	σ_y	σ_x	σ_y	τ_{xy}	σ_y	σ_x	σ_y	τ_{xy}	σ_y	σ_x	σ_y	τ_{xy}	σ_y
0.3	0				0				1133.2				0
1.5		23.3	8.1	-7.6		247.9	422.6	-619.4		325.3	382 9	534.2	
3.0	0				153.9				998.0				262.0
4.5		405.5	265.1	-41.1		14.4	574.7	-414.0		71.9	636.2	205.5	
6.0	70.7				282.8				721.5				440.8
7.5		335.4	116.1	42.7		-49.4	494.4	-266.3		-15.1	585.3	25.9	
9.0	141.4				326.4				582.2				544.8
10.5		-273.7	179.7	-62.4		-31.0	450.9	-193.3		-99.0	493.8	-7.6	
12.0	197.5				338.9				524.0				517.7
13.5		-8.3	284.1	-85.2		-54.3	417.8	-118.7		-78.9	480.0	-27.4	
15.0	249.5				361.8				478.2				480.3
16.5		-9.8	304.3	-41.1		-46.6	403.9	-62.4		-27.7	497.7	-35.0	
18.0	262.0				376.3				453.3				478.2
19.5		-2.0	327.8	18.3		-15.6	410.4	-28.9		-16.9	493.2	0	
21.0	272.4				372.2				453.3				463.7
22.5		92.6	339.8	-35.0		52.7	454.9	7.6		71.5	498.8	-13.7	
23.7	305.6				343.1				424.2				440.8

TABLE F27. - TEST RESULTS FOR PANEL C

(Loading Condition IV, Test No. 7)
P = 1 kip

y	Stiff. No. 1	Web. No. 1			Stiff. No. 2	Web. No. 2			Stiff. No. 3	Web. No. 3			Stiff. No. 4
in.	σ_y	σ_x	σ_y	τ_{xy}	σ_y	σ_x	σ_y	τ_{xy}	σ_y	σ_x	σ_y	τ_{xy}	σ_y
0.3	0				0				0				1218.4
1.5		-46.5	-16.1	15.2		68.1	-30.5	-66.9		233.9	405.3	-611.8	
3.0	0				0				139.3				948.1
4.5		46.7	16.2	15.3		77.9	135.1	-194.8		-38.5	514.8	-377.4	
6.0	10.4				72.8				207.9				594.7
7.5		102.6	35.5	30.5		3.6	134.3	-185.7		-40.4	422.7	-193.3	
9.0	27.0				135.1				266.1				467.8
10.5		-142.5	29.7	-30.4		-33.4	208.8	-143.1		-107.5	295.5	-106.5	
12.0	68.6				143.5				259.9				353.5
13.5		-24.4	124.6	-54.8		-42.7	193.1	-100.4		-110.4	348.5	-63.9	
15.0	81.1				170.5				230.8				299.4
16.5		-7.3	138.9	-31.9		-87.7	181.7	-22.8		-36.3	261.9	-45.7	
18.0	83.2				189.2				228.7				274.5
19.5		-19.6	151.2	-28.9		-24.1	199.6	-21.3		-53.4	247.7	-16.7	
21.0	89.4				170.5				214.2				245.3
22.5		2.1	154.6	-22.8		17.8	214.8	-4.6		22.6	265.7	-9.1	
23.7	116.4				145.5				207.9				235.0

TABLE F28. - TEST RESULTS FOR PANEL C

(Loading Condition IV, Test No. 8)
P = 1 kip

y	Stiff. No. 1	Web. No. 1			Stiff. No. 2	Web. No. 2			Stiff. No. 3	Web. No. 3			Stiff. No. 4
in.	σ_y	σ_x	σ_y	τ_{xy}	σ_y	σ_x	σ_y	τ_{xy}	σ_y	σ_x	σ_y	τ_{xy}	σ_y
0.3	0				0				0				1224.7
1.5		37.2	12.9	12.2		89.9	10.3	-60.9		260.2	397.8	-613.3	
3.0	0				0				120.6				931.5
4.5		55.9	19.3	-42.6		59.3	128.7	-197.9		0.3	519.9	-400.3	
6.0	0				58.2				239.1				630.0
7.5		11.1	70.4	-80.7		-7.2	163.9	-190.2		-48.2	399.2	-182.6	
9.0	27.0				104.0				245.3				459.5
10.5		-1.3	82.7	-74.6		-38.1	194.7	-138.5		-104.3	304.9	-100.4	
12.0	58.2				139.3				249.5				361.8
13.5		17.4	114.2	-62.4		-16.4	185.6	-92.8		-31.5	288.5	-77.6	
15.0	83.2				153.9				257.8				316.0
16.5		2.0	142.1	-35.0		-19.4	201.2	-56.3		-53.3	260.1	-50.2	
18.0	104.0				158.0				237.0				268.2
19.5		2.1	154.6	-16.7		-8.6	209.1	-33.5		-20.8	258.9	-24.4	
21.0	108.1				137.2				228.7				255.7
22.5		51.7	155.1	-25.9		31.8	218.9	-9.1		59.7	241.1	-12.2	
23.7	126.8				137.2				210.0				218.3

TABLE F29. - TEST RESULTS FOR PANEL D

(Loading Condition I, Test No. 1)
P = 1 kip

y	Stiff No. 1	Web. No. 1			Stiff. No. 2	Web. No. 2			Stiff No. 3	Web. No. 3			Stiff No. 4
in.	σ_y	σ_x	σ_y	τ_{xy}	σ_y	σ_x	σ_y	τ_{xy}	σ_y	σ_x	σ_y	τ_{xy}	σ_y
0.3	5015.0				0				0				0
1.5		-186.6	700.5	764.0		-778.4	- 86.5	- 51.7		-930.2	- 72.5	- 24.4	
3.0	3376.6				370.1				137.2				62.4
4.5		324.6	1542.9	831.0		196.2	267.5	356.1		- 93.1	- 32 2	60.9	
6.0	2083.4				657.0				162.2				74.9
7.5		153.3	1300.6	493.1		277.8	561.9	429.2		283.0	256.0	130.9	
9.0	1438.8				773.5				349.3				232.9
10.5		174.3	1091.6	307.4		272.1	693.0	331.8		262.0	465.0	121.8	
12.0	1068.7				794.3				515.6				
13.5		74.6	940.7	161.3		133.0	794.5	200.9		79.4	559.8	106.5	
15.0	856.6				777.6				615.4				540.6
16.5		71.2	856.3	103.5		86.4	778.4	118.7		- 7.1	646.3	63.9	
18.0	785.9				752.7				706.9				657.0
19.5		21.3	780.8	42.6		- 37.7	752.1	76.1		67.8	772.0	9.1	
21.0	673.6				756.8				736.0				706.9
22.5		105.1	809.8	- 51.7		222.2	842.3	15.2		210.4	779.8	-21.3	
23.7	765.1				677.8				711.1				677.8

TABLE F30. - TEST RESULTS FOR PANEL D

(Loading Condition I, Test No. 2)
P = 1 kip

y	Stiff. No. 1	Web No. 1			Stiff. No. 2	Web No. 2			Stiff. No. 3	Web No. 3			Stiff. No. 4
in.	σ_y	σ_x	σ_y	τ_{xy}	σ_y	σ_x	σ_y	τ_{xy}	σ_y	σ_x	σ_y	τ_{xy}	σ_y
0.3	4882.0				0				0				128.9
1.5		-174.2	713.2	782.3		-756.6	-70.6	-36.5		-1006.2	-1.8	-36.5	
3.0	3318.4				353.5				54.1				41.6
4.5		301.2	1570.8	827.9		168.3	257.9	371.4		-46.6	-16.1	88.3	
6.0	2079.2				673.7				170.5				83.2
7.5		171.9	1307.0	493.1		274.7	552.5	432.2		236.4	239.9	146.1	
9.0	1418.0				765.1				345.1				232.9
10.5		75.0	1065.6	277.0		262.8	689.8	334.8		178.2	435.9	118.7	
12.0	1052.1				785.9				499.0				415.8
13.5		83.9	943.9	146.1		151.3	726.0	200.9		185.0	604.6	76.1	
15.0	831.7				748.5				586.3				544.8
16.5		33.9	843.4	85.2		80.0	734.6	106.5		114.0	688.2	48.7	
18.0	748.5				752.7				677.8				657.0
19.5		49.2	765.5	45.7		43.1	796.7	21.3		139.0	763.4	0	
21.0	698.6				752.7				731.9				702.8
22.5		95.7	781.6	-36.5		136.2	828.9	-9.1		142.3	797.8	-9.1	
23.7	736.0				665.3				711.1				752.7

TABLE F31. - TEST RESULTS FOR PANEL D

(Loading Condition I, Test No. 3)
P = 1 kip

y	Stiff. No. 1	Web No. 1			Stiff. No. 2	Web No. 2			Stiff. No. 3	Web No. 3			Stiff. No. 4
in.	σ_y	σ_x	σ_y	τ_{xy}	σ_y	σ_x	σ_y	τ_{xy}	σ_y	σ_x	σ_y	τ_{xy}	σ_y
0.3	4998.4				0				0				128.9
1.5		-152.5	704.0	791.4		-734.9	-79.8	-45.7		-945.6	-44.6	-27.4	
3.0	3310.1				382.6				79.0				49.9
4.5		306.2	1586.4	849.2		103.1	235.3	386.6		-55.9	-19.3	85.2	
6.0	2091.7				682.0				178.8				70.7
7.5		196.7	1307.3	493.1		268.5	558.7	426.1		230.2	246.0	140.0	
9.0	1447.1				794.3				357.6				220.4
10.5		96.8	1106.4	292.2		300.0	702.7	334.8		206.1	445.6	115.7	
12.0	1085.3				785.9				494.8				420.0
13.5		83.9	943.9	158.3		129.6	735.2	210.0		166.4	598.2	70.0	
15.0	914.8				765.1				627.9				548.9
16.5		52.6	849.9	91.3		123.6	766.3	118.7		135.7	704.0	51.7	
18.0	773.5				777.6				711.1				627.9
19.5		170.3	832.4	0		67.9	797.0	33.5		108.1	769.3	24.4	
21.0	773.5				790.1				711.1				690.3
22.5		80.2	784.6	-33.5		136.2	828.9	-3.0		170.2	807.4	-12.2	
23.7	785.9				682.0				702.8				636.2

TABLE F32. - TEST RESULTS FOR PANEL D

(Loading Condition II, Test No. 1)
P = 1 kip

y	Stiff. No. 1	Web No. 1			Stiff. No. 2	Web No. 2			Stiff. No. 3	Web No. 3			Stiff No 4
in.	σ_y	σ_x	σ_y	τ_{xy}	σ_y	σ_x	σ_y	τ_{xy}	σ_y	σ_x	σ_y	τ_{xy}	σ_y
0.3	0				4104.4				0				0
1.5		160.5	679.3	-557.0		39.2	587.4	803.6		-294.6	-18.8	76.1	
3.0	324.4				1921.2				349.3				162.2
4.5		-176.5	953.6	-219.2		-99.0	938.8	429.2		44.5	306.5	176.5	
6.0	711.1				1156.0				578.0				353.5
7.5		-65.1	892.3	-42.6		-15.8	817.9	194.8		72.8	441.1	124.8	
9.0	815.0				869.1				652.9				524.0
10.5		15.3	837.0	36.5		-56.2	770.6	124.8		45.7	656.2	54.8	
12.0	790.1				781.8				715.2				
13.5		-189.7	716.1	30.4		27.6	799.6	79.1		52.1	725.0	24.4	
15.0	756.8				752.7				731.9				657.0
16.5		-183.5	709.9	30.4		43.1	796.7	39.6		80.1	759.6	-3.0	
18.0	706.9				769.3				740.2				748.5
19.5		30.4	759.1	3.0		46.3	831.1	18.3		74.0	790.8	-9.1	
21.0	661.2				752.7				723.6				765.1
22.5		89.5	787.8	-60.9		136.2	828.9	-21.3		139.2	813.3	-18.3	
23.7	744.4				657.0				694.5				731.2

TABLE F33. - TEST RESULTS FOR PANEL D

(Loading Condition II, Test No. 2)
P = 1 kip

y	Stiff. No. 1	Web No. 1			Stiff No. 2	Web No. 2			Stiff. No. 3	Web No 3			Stiff No 4
in.	σ_y	σ_x	σ_y	τ_{xy}	σ_y	σ_x	σ_y	τ_{xy}	σ_y	σ_x	σ_y	τ_{xy}	σ_y
0.3	0				4154.3				0				0
1.5		80.0	709.7	-593.6		-1.0	615.1	800.5		-306.9	-6.4	76.1	
3.0	345.1				1937.8				345.1				133.1
4.5		-157.8	985.0	-200.9		-198.1	962.7	447.5		38.3	312.7	176.5	
6.0	719.4				1172.7				578.0				357.6
7.5		6.2	883.7	-57.8		6.0	833.8	203.9		73.2	541.0	118.7	
9.0	810.9				894.1				673.7				532.3
10.5		34.3	836.4	24.4		18.2	771.4	130.9		73.6	665.9	94.4	
12.0	810.9				790.1				731.9				619.6
13.5		-49.9	814.4	-15.2		43.1	796.7	76.1		45.9	731.2	24.4	
15.0	773.5				773.5				748.5				694.5
16.5		-12.6	827.3	39.6		43.1	796.7	63.9		2.6	749.4	30.4	
18.0	744.4				761.0				761.0				744.4
19.5		-51.7	769.8	0		108.1	769.3	18.3		83.4	819.0	-18.3	
21.0	744.4				756.8				748.5				744.4
22.5		92.6	772.2	-517.4		126.7	775.7	-24.4		167.2	848.0	-27.4	
23.7	773.5				669.5				748.5				698.6

TABLE F34. - TEST RESULTS FOR PANEL D

(Loading Condition II, Test No. 3)
P = 1 kip

y	Stiff. No. 1	Web No. 1			Stiff. No. 2	Web No. 2			Stiff. No. 3	Web No. 3			Stiff. No. 4
in.	σ_y	σ_x	σ_y	τ_{xy}	σ_y	σ_x	σ_y	τ_{xy}	σ_y	σ_x	σ_y	τ_{xy}	σ_y
0.3	0				4121.0				0				0
1.5		67.6	722.0	-672.7		169.2	532.6	901.0		-254.2	3.5	91.3	
3.0	320.3				1954.5				353.5				128.0
4.5		-30.4	1070.7	-210.0		-61.5	1026.6	471.8		60.0	328.5	197.9	
6.0	719.4				1168.5				603.0				369.9
7.5		9.4	918.1	-48.7		-6.3	871.1	210.0		60.8	553.3	118.7	
9.0	823.4				902.4				665.3				548.9
10.5		37.1	852.8	27.4		67.9	797.0	124.8		51.9	675.0	54.8	
12.0	802.6				794.3				694.5				636.2
13.5		30.7	809.0	39.6		55.4	784.3	63.9		42.8	721.8	21.3	
15.0	752.7				773.5				731.9				694.5
16.5		39.9	787.3	24.4		70.9	781.4	48.7		52.3	774.9	12.2	
18.0	715.2				740.2				748.5				736.0
19.5		67.8	772.0	9.1		74.0	790.8	15.2		74.0	790.8	-3 0	
21.0	686.1				736.0				756.8				752.7
22.5		198.1	817.1	-33.5		111.3	803.7	-21.3		145.4	807.2	-12.2	
23.7	769.3				640.4				740.2				702.8

TABLE F35. - TEST RESULTS FOR PANEL D

(Loading Condition III, Test No. 1)
P = 1 kip

y	Stiff. No. 1	Web No. 1			Stiff. No. 2	Web No. 2			Stiff. No. 3	Web No. 3			Stiff. No. 4
in.	σ_y	σ_x	σ_y	τ_{xy}	σ_y	σ_x	σ_y	τ_{xy}	σ_y	σ_x	σ_y	τ_{xy}	σ_y
0.3	0				0				4241.6				0
1.5		46.6	16.1	15.2		293.8	683.9	-797.5		395.9	644.4	733.6	
3.0	0				316.0				1962.8				548.9
4.5		-8.4	246.6	-185.7		6.6	1008.6	-447.5		97.0	1156.4	176.5	
6.0	141.4				590.5				1239.2				981.4
7.5		4.6	434.1	-203.9		-105.4	895.0	-277.0		-83.1	1060.7	-24.4	
9.0	386.7				682.0				973.1				985.5
10.5		-13.6	552.5	-130.9		-111.9	801.3	-155.2		-114.4	966.7	-60.9	
12.0	524.0				686.1				885.7				910.7
13.5		-25.7	629.8	-63.9		-34.4	811.5	-115.7		-86.8	876.5	-70.0	
15.0	623.8				702.8				860.8				852.5
16.5		-19.3	683.6	-45.7		-6.6	771.2	-57.8		6.1	858.7	-51.7	
18.0	640.4				727.7				785.9				835.8
19.5		-3.6	755.6	-30.4		49.2	790.5	-39.6		15.3	837.0	-36.5	
21.0	627.9				715.2				831.7				856.6
22.5		98.8	791.0	-94.4		133.0	819.5	-48.7		170.3	832.4	-30.4	
23.7	777.6				657.0				777.6				748.5

TABLE F36. - TEST RESULTS FOR PANEL D

(Loading Condition III, Test No. 2)
P = 1 kip

y	Stiff. No. 1	Web No. 1			Stiff. No. 2	Web No. 2			Stiff. No. 3	Web No. 3			Stiff. No. 4
in.	σ_y	σ_x	σ_y	τ_{xy}	σ_y	σ_x	σ_y	τ_{xy}	σ_y	σ_x	σ_y	τ_{xy}	σ_y
0.3	0				0				4195.8				0
1.5		37.2	12.9	12.2		1103.8	964.3	-526.6		405.2	647.6	730.5	
3.0	0				320.2				1966.9				528.1
4.5		17.8	243.4	-200.9		-33.7	1011.3	-450.5		75.4	1165.5	179.6	
6.0	141.4				578.0				1255.8				989.7
7.5		-60.5	436.5	-207.0		-86.8	876.5	-283.1		-67.6	1057.8	-27.4	
9.0	395.0				673.7				993.9				998.0
10.5		-29.2	530.5	-127.8		-90.2	817.1	-158.3		-98.9	963.8	-63.9	
12.0	511.5				686.1				885.7				935.6
13.5		5.3	633.9	-82.2		-12.8	777.4	-100.4		71.4	873.5	-67.0	
15.0	598.8				702.8				831.7				910.7
16.5		5.5	683.9	-39.6		12.0	777.6	-57.8		-9.5	836.7	-36.5	
18.0	611.3				748.5				802.6				825.7
19.5		33.5	718.5	-30.4		33.8	793.5	-42.6		27.8	849.6	-36.5	
21.0	648.7				723.6				781.8				790.1
22.5		111.1	753.7	-100.4		157.9	844.8	-60.9		120.7	831.9	-30.4	
23.7	731.9				640.4				736.0				706.9

TABLE F37. - TEST RESULTS FOR PANEL D

(Loading Condition III, Test No. 3)
P = 1 kip

y	Stiff. No. 1	Web No. 1			Stiff. No. 2	Web No. 2			Stiff. No. 3	Web No. 3			Stiff. No. 4
in.	σ_y	σ_x	σ_y	τ_{xy}	σ_y	σ_x	σ_y	τ_{xy}	σ_y	σ_x	σ_y	τ_{xy}	σ_y
0.3	0				0				4187.5				58.2
1.5		-83.8	-29.0	-3.0		262.6	639.8	-706.2		408.3	632.0	672.7	
3.0	0				303.6				2021.0				503.2
4.5		-27.0	265.1	-179.6		-92.7	982.6	-423.1		38.0	1127.6	173.5	
6.0	149.7				582.2				1251.7				952.3
7.5		-1.6	440.2	-197.9		-155.2	844.5	-289.2		-111.0	1051.1	-3.0	
9.0	378.4				669.5				989.7				1056.2
10.5		-38.4	552.3	-124.8		-143.0	782.2	-155.2		-173.4	938.0	33.5	
12.0	515.6				711.1				898.2				939.8
13.5		-28.8	630.4	-79.1		-68.7	758.0	-100.4		55.8	895.5	-51.7	
15.0	565.5				706.9				848.3				869.1
16.5		-10.0	686.8	-42.6		-34.6	761.5	-48.7		-52.8	855.0	-12.2	
18.0	648.7				719.4				810.9				819.2
19.5		21.1	730.9	-30.4		27.6	799.6	-42.6		52.6	849.9	-30.4	
21.0	669.5				715.4				790.1				785.9
22.5		129.7	760.2	-88.3		157.8	819.8	-36.5		188.9	838.9	-30.4	
23.7	748.5				648.7				711.1				723.6

TABLE F38. - TEST RESULTS FOR PANEL D

(Loading Condition IV, Test No. 1)
P = 1 kip

y	Stiff. No. 1	Web No. 1			Stiff. No. 2	Web No. 2			Stiff. No. 3	Web No. 3			Stiff. No. 4
in.	σ_y	σ_x	σ_y	τ_{xy}	σ_y	σ_x	σ_y	τ_{xy}	σ_y	σ_x	σ_y	τ_{xy}	σ_y
0.3	0				0				0				4220.8
1.5		0	0	0		27.9	9.7	-63.9		302.9	637.1	-733.6	
3.0	0				45.7				286.9				1904.6
4.5		87.1	88.4	-42.6		-5.4	231.0	-249.6		-145.7	897.7	-377.4	
6.0	0				170.5				453.3				1006.3
7.5		-5.7	156.1	-109.6		-51.4	364.8	-228.3		-103.2	629.6	-188.7	
9.0	104.0				303.6				469.9				723.6
10.5		-11.6	237.2	-97.4		-51.3	389.8	-143.1		-60.3	486.4	-103.5	
12.0	241.2				307.7				453.3				536.4
13.5		-42.4	293.1	-60.9		-7.7	446.4	-106.5		-153.3	479.2	-79.1	
15.0	278.6				378.4				449.1				465.7
16.5		-32.9	346.2	-45.7		-94.6	433.0	-82.2		-106.9	445.4	-51.7	
18.0	332.7				395.0				590.5				432.1
19.5		-11.0	412.0	-36.5		35.6	428.2	-57.8		-14.0	428.4	-51.7	
21.0	345.1				432.5				407.5				357.6
22.5		54.2	434.6	-76.1		76.0	475.4	-67.0		116.2	447.8	-57.8	
23.7	365.9				403.4				390.9				345.1

TABLE F39. - TEST RESULTS FOR PANEL D

(Loading Condition IV, Test No. 2)
P = 1 kip

y	Stiff. No. 1	Web No. 1			Stiff. No. 2	Web No. 2			Stiff. No. 3	Web No. 3			Stiff. No. 4
in.	σ_y	σ_x	σ_y	τ_{xy}	σ_y	σ_x	σ_y	τ_{xy}	σ_y	σ_x	σ_y	τ_{xy}	σ_y
0.3	0				0				0				4108.5
1.5		-27.9	-9.7	9.1		96.2	16.6	-82.2		346.7	743.8	-855.3	
3.0	-37.4				49.9				316.0				1892.1
4.5		-9.1	46.7	-57.8		56.6	244.2	-249.6		25.1	965.1	-441 4	
6.0	0				174.7				499.0				1014.7
7.5		208.5	230.2	-33.5		-29.8	355.6	-219.2		-50.2	714.5	-161.3	
9.0	79.0				274.5				440.8				702.8
10.5		87.7	263.2	-48.7		-85.5	361.3	-127.8		-122.1	548.2	-103.5	
12.0	187.1				316.0				474.1				507.3
13.5		-26.9	290.1	-63.9		-26.6	365.0	-88.3		-44.8	483.5	-63.9	
15.0	299.4				353.5				449.1				469.9
16.5		4.4	359.1	-33.5		-76.2	364.5	-70.0		4.6	434.1	-45.7	
18.0	307.7				370.1				436.6				428.3
19.5		-8.0	371.5	-33.5		38.5	387.6	-48.7		35.6	428.2	-39.6	
21.0	365.9				399.2				424.2				407.5
22.5		47.8	365.8	-63.9		-38.5	387.6	-48.7		78.9	409.9	-27.4	
23.7	399.2				378.4				390.9				353.5

TABLE F40. - TEST RESULTS FOR PANEL D

(Loading Condition IV, Test No. 3)
P = 1 kip

y	Stiff. No. 1	Web No. 1			Stiff. No. 2	Web No. 2			Stiff. No. 3	Web No. 3			Stiff. No. 4
in.	σ_y	σ_x	σ_y	τ_{xy}	σ_y	σ_x	σ_y	τ_{xy}	σ_y	σ_x	σ_y	τ_{xy}	σ_y
0.3	-29.1				-33.3				0				4125.1
1.5		-46.6	-16.1	15.2		83.6	-21.0	-70.0		374.4	703.5	-827.9	
3.0	-45.7				0				270.3				1875.4
4.5		-43.3	18.3	-36.5		31.8	218.9	-243.5		-21.6	924 0	-395.7	
6.0	0				158.0				478.2				1031.3
7.5		15.9	121.9	-88.3		-20.5	333.9	-203.9		-50.3	689.5	-155.2	
9.0	95.6				249.5				478.2				590.5
10.5		-5.6	181.0	-79.1		-8.1	346.5	-118.7		-122.2	523.3	-97.4	
12.0	174.7				299.4				457.4				532.3
13.5		-33.2	246.3	-51.7		16.8	371.8	-94.4		-100.7	464.2	-45.7	
15.0	262.0				324.4				440.8				445.0
16.5		-73.3	323.9	-60.9		-57.7	346.0	-70.0		-69.8	433.3	-33.5	
18.0	282.8				345.1				390.9				382.6
19.5		-1.9	340.3	-57.8		-26.7	340.1	-76.1		-29.7	380.6	-36.5	
21.0	382.6				353.5				357.6				316.0
22.5		26.1	375.0	-97.4		41.6	372.0	-100.4		44.7	381.4	-42.6	
23.7	399.2				349.3				303.6				274.5

TABLE F41. - AVERAGE OF TEST RESULTS FOR PANEL D

(Loading Condition I; Test Nos. 1, 2, 3; P = 1 kip)

y	Stiff. No. 1	Web. No. 1			Stiff. No. 2	Web. No. 2			Stiff. No. 3	Web. No. 3			Stiff. No. 4
in.	σ_y	σ_x	σ_y	τ_{xy}	σ_y	σ_x	σ_y	τ_{xy}	σ_y	σ_x	σ_y	τ_{xy}	σ_y
0.3	4965.1				0				0				85.9
1.5		-171.1	705.9	779.2		-756.6	-79.0	-44.6		-960.7	-39.6	-29.4	
3.0	3335.0				368.7				90.1				51.3
4.5		301.7	1566.7	836.0		155.9	253.6	371.4		-65.2	-22.5	78.1	
6.0	2084.8				670.9				170.5				76.3
7.5		173.9	1305.0	493.1		273.7	557.7	429.2		249.9	247.3	139.0	
9.0	1434.6				777.6				350.7				228.7
10.5		115.4	1087.9	292.2		278.3	695.2	333.8		215.4	448.8	118.7	
12.5	1068.7				788.6				503.1				418.1
13.5		80.8	942.8	155.2		138.0	751.9	203.9		143.6	587.5	84.2	
15.0	867.7				763.7				609.9				544.8
16.5		52.6	849.9	93.3		96.7	759.8	114.6		80.8	651.6	54.8	
18.0	769.3				761.0				698.6				647.3
19.5		80.2	792.9	29.4		24.4	781.9	43.6		185.8	768.2	11.2	
21.0	715.2				766.5				726.3				700.0
22.5		93.7	792.0	40.6		164.9	833.4	1.0		174.3	795.0	-14.2	
23.7	762.3				675.0				708.3				688.9

TABLE F42. - AVERAGE OF TEST RESULTS FOR PANEL D

(Loading Condition II; Test Nos. 1, 2, 3; P = 1 kip)

y	Stiff. No. 1	Web. No. 1			Stiff. No. 2	Web. No. 2			Stiff. No. 3	Web. No. 3			Stiff. No. 4
in.	σ_y	σ_x	σ_y	τ_{xy}	σ_y	σ_x	σ_y	τ_{xy}	σ_y	σ_x	σ_y	τ_{xy}	σ_y
0.3	0				4126.6				0				0
1.5		102.7	703.7	-607.8		69.1	578.4	835.0		-285.2	-7.2	81.2	
3.0	329.9				1937.8				349.3				141.4
4.5		121.6	1003.1	-210.0		-119.5	976.0	449.5		47.6	315.9	183.6	
6.0	716.6				1165.7				586.3				360.3
7.5		-16.5	898.0	-49.7		-5.1	840.9	202.9		68.9	511.8	120.7	
9.0	816.4				888.5				663.9				535.1
10.5		28.9	842.1	29.4		9.9	779.7	126.8		57.1	665.7	68.0	
12.0	801.2				788.7				713.9				627.9
13.5		-69.6	779.8	18.2		42.0	793.5	73.0		46.9	732.1	23.4	
15.0	761.0				766.6				737.4				682.0
16.5		-52.0	774.8	31.5		52.4	791.6	50.7		45.0	761.3	13.2	
18.0	722.2				756.8				749.9				742.9
19.5		85.3	767.0	4.0		76.1	797.1	17.3		77.1	800.2	-10.1	
21.0	697.2				748.5				742.9				754.1
22.5		126.7	792.4	-48.7		124.7	802.8	-22.3		150.6	822.8	-19.3	
23.7	762.4				655.6				727.7				710.9

TABLE F43. - AVERAGE OF TEST RESULTS FOR PANEL D

(Loading Condition III; Test Nos. 1, 2, 3; P = 1 kip)

y	Stiff. No. 1	Web. No. 1			Stiff. No. 2	Web. No. 2			Stiff. No. 3	Web. No. 3			Stiff. No. 4
in.	σ_y	σ_x	σ_y	τ_{xy}	σ_y	σ_x	σ_y	τ_{xy}	σ_y	σ_x	σ_y	τ_{xy}	σ_y
0.3	0				0				4208.3				19.4
1.5		0	0	8.0		553.4	762.7	-676.8		403.1	641.3	712.3	
3.0	0				313.3				1983.6				526.7
4.5		-5.9	251.7	-188.7		-39.9	1000.8	-440.4		70.1	1149.8	176.5	
6.0	144.2				583.6				1248.9				974.5
7.5		-19.2	436.9	-202.9		-115.8	872.0	-283.1		-87.2	1056.5	18.3	
9.0	386.7				675.1				985.6				1013.2
10.5		-27.1	545.1	-127.8		-115.0	800.2	-156.2		-128.9	956.2	-30.4	
12.0	517.0				694.4				889.9				928.7
13.5		-16.4	634.7	-75.1		-38.6	782.3	-105.5		13.5	881.8	-62.9	
15.0	596.0				704.2				846.9				877.4
16.5		-7.9	681.8	-42.6		-9.7	770.1	-54.8		-18.7	850.1	-33.5	
18.0	633.5				731.9				799.8				826.9
19.5		17.0	735.0	-30.4		36.9	794.5	-41.6		31.9	845.5	-34.5	
21.0	648.7				718.1				801.2				810.9
22.5		113.2	768.3	-94.4		149.6	828.0	-48.7		160.0	834.4	-30.4	
23.7	752.7				648.7				741.6				726.3

TABLE F44. - AVERAGE OF TEST RESULTS FOR PANEL D

(Loading Condition IV; Test Nos. 1, 2, 3; P = 1 kip)

y	Stiff. No. 1	Web. No. 1			Stiff. No. 2	Web. No. 2			Stiff. No. 3	Web. No. 3			Stiff. No. 4
in.	σ_y	σ_x	σ_y	τ_{xy}	σ_y	σ_x	σ_y	τ_{xy}	σ_y	σ_x	σ_y	τ_{xy}	σ_y
0.3	-9.7				-11.1				0				4151.5
1.5		-24.8	-8.6	8.1		69.2	1.8	-72.0		341.3	694.8	-805.6	
3.0	-27.7				31.9				291.1				1890.7
4.5		11.6	51.1	-45.6		27.7	231.4	-247.6		-47.4	928.9	-404.8	
6.0	0				167.7				476.8				1017.4
7.5		72.9	169.4	-77.1		-33.9	351.4	-217.1		-67.9	677.9	-168.4	
9.0	92.9				275.9				463.0				672.3
10.5		23.5	227.1	-75.1		-48.3	366.2	-129.9		-101.5	519.3	-101.5	
12.0	201.0				307.7				461.6				525.3
13.5		-34.2	276.5	-58.8		-5.8	394.4	-96.4		-99.6	475.6	-62.9	
15.0	280.0				352.1				446.3				460.5
16.5		-33.9	343.1	-46.7		-76.5	381.2	-74.1		-57.4	437.6	-43.6	
18.0	307.7				370.1				472.7				414.3
19.5		-7.0	374.6	-42.6		15.8	385.3	-60.9		-2.7	412.4	-42.6	
21.0	364.5				395.1				396.4				360.4
22.5		42.7	391.8	-79.1		26.4	411.7	-72.0		79.9	413.0	-42.6	
23.7	388.1				377.0				361.8				324.4

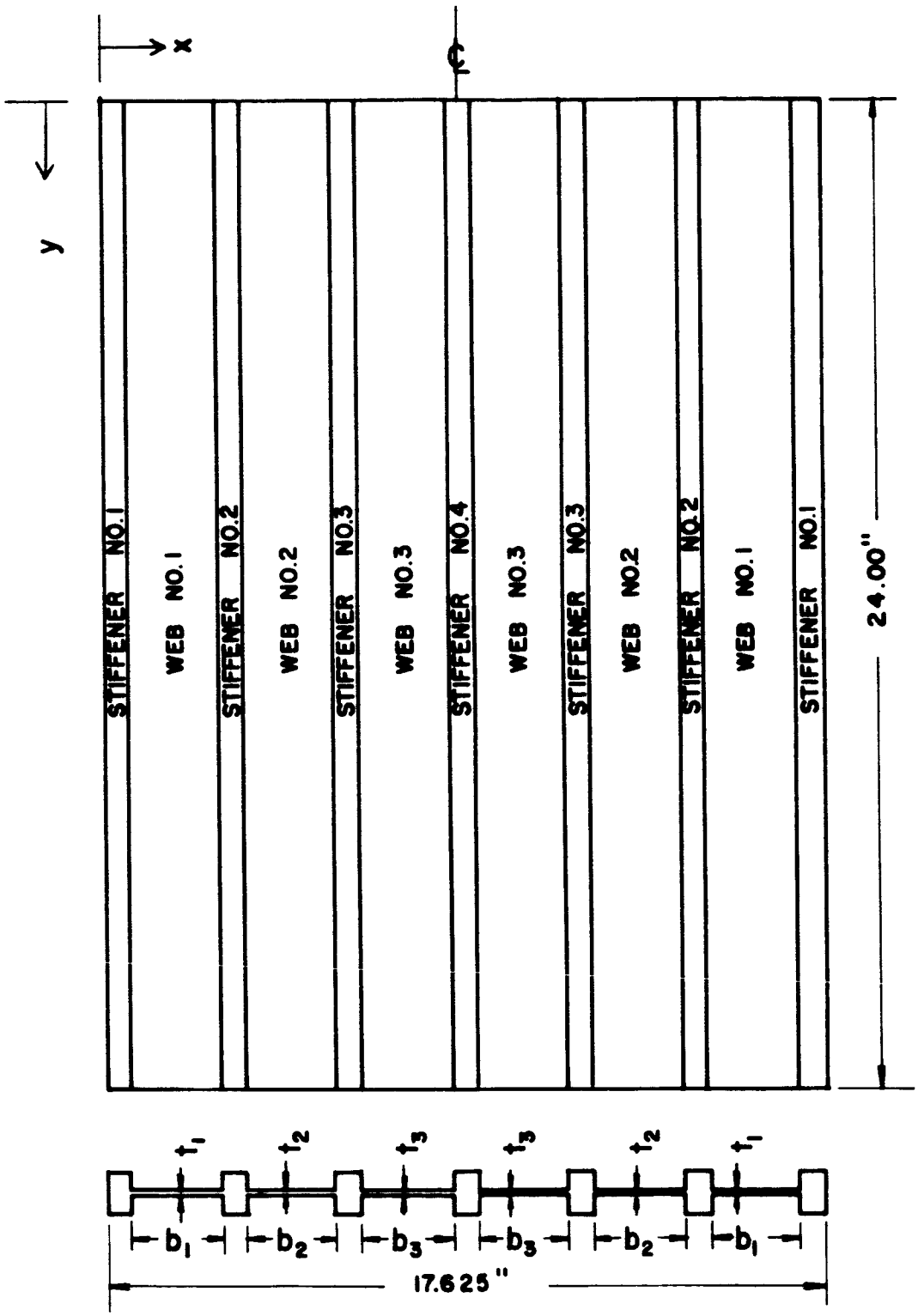

FIGURE F1. - TYPICAL PANEL CONFIGURATION.

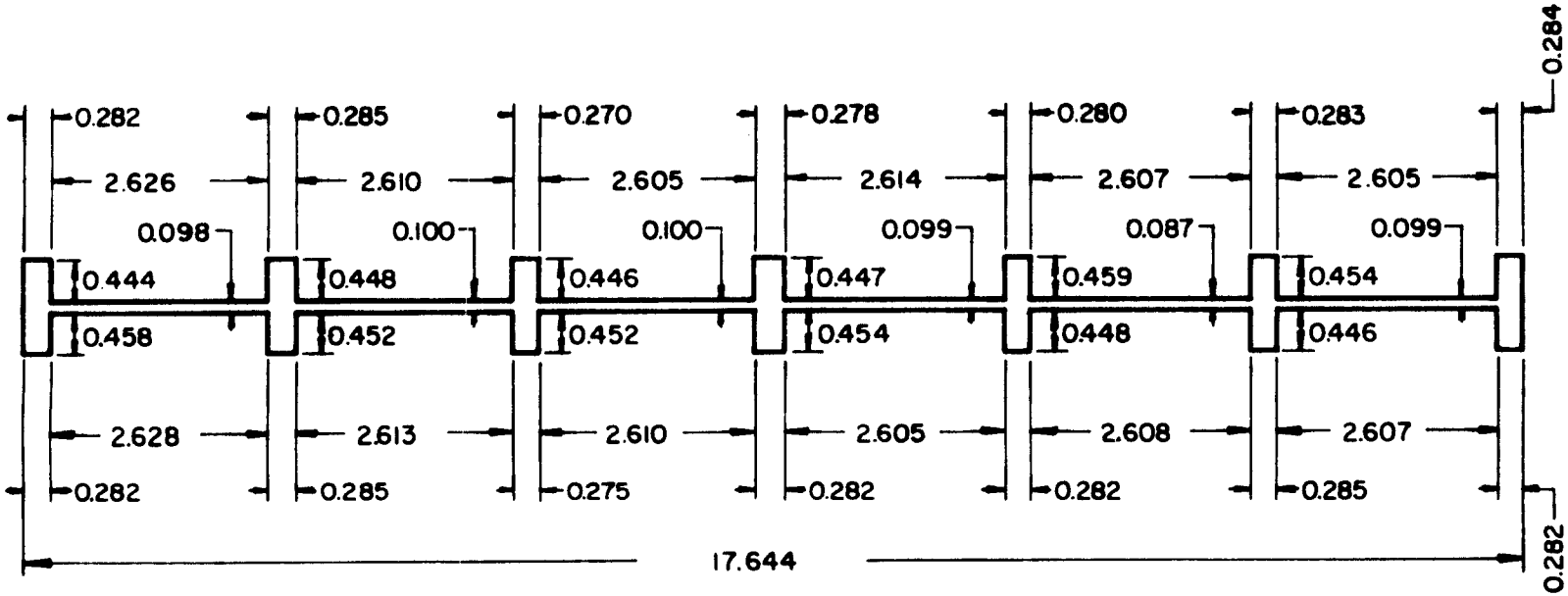

PANEL LENGTH 24.00

ALL DIMENSIONS IN INCHES

FIGURE F2. - CROSS-SECTION OF PANEL B.

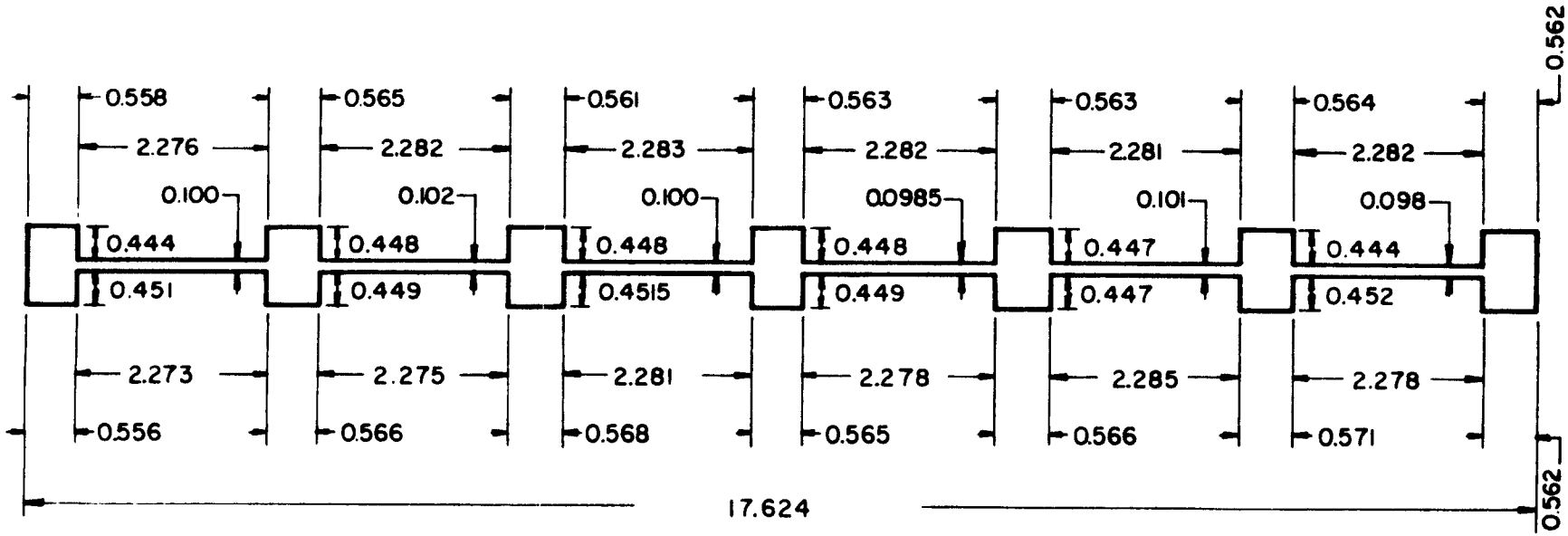

PANEL LENGTH 24.00

ALL DIMENSIONS IN INCHES

FIGURE F3. - CROSS-SECTION OF PANEL C.

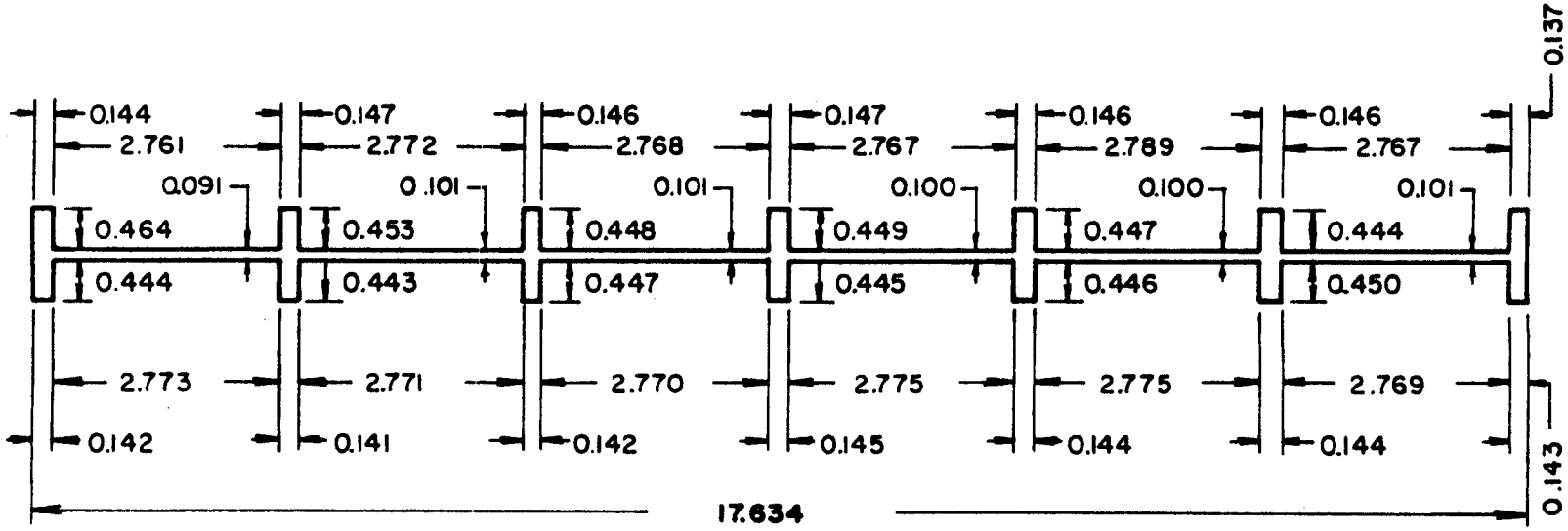

PANEL LENGTH 24.00

ALL DIMENSIONS IN INCHES

FIGURE F4. - CROSS-SECTION OF PANEL D.

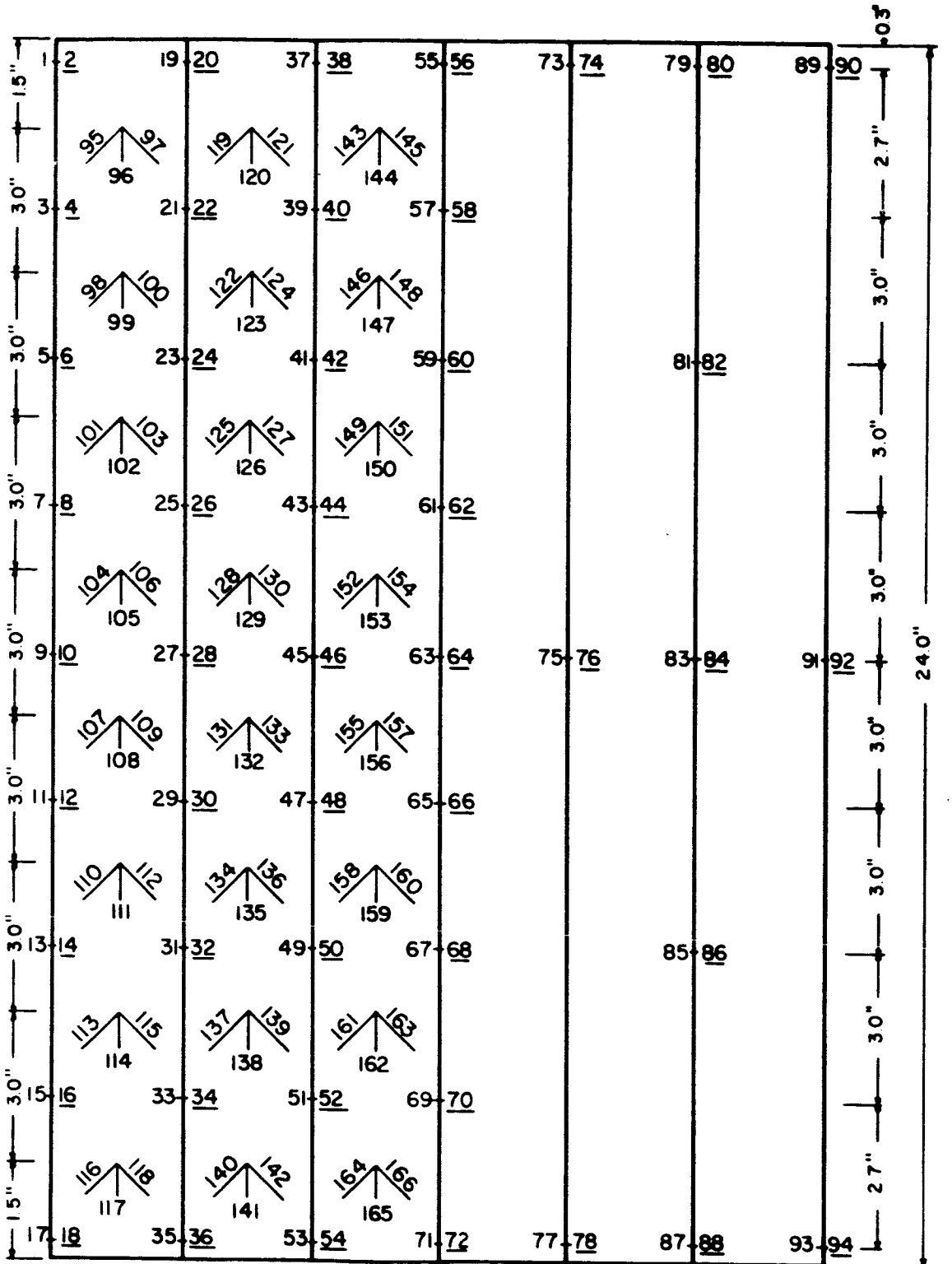

UNDERSCORED CHANNEL NUMBERS INDICATE GAGES ON REVERSE SIDE OF PANEL. GAGES 1 THRU 94 ARE UNIAXIAL GAGES. GAGES 95 THRU 166 ARE ROSETTES.

FIGURE F5. - STRAIN GAGE CHANNELS FOR PANELS B AND C.

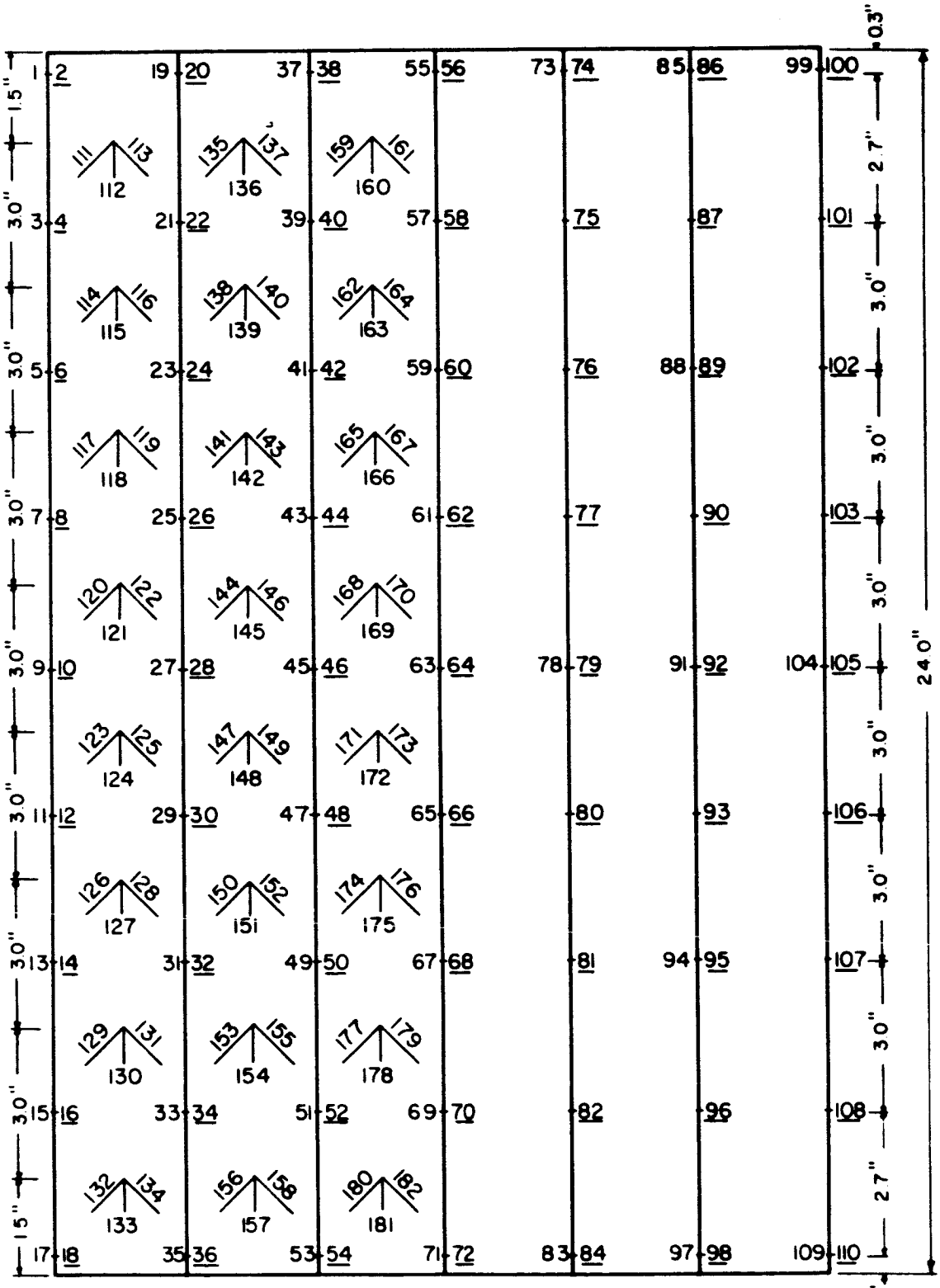

UNDERSCORED CHANNEL NUMBERS INDICATE GAGES ON REVERSE SIDE OF PANEL GAGES I THRU 110 ARE UNIAXIAL GAGES. GAGES 111 THRU 182 ARE ROSETTES.

FIGURE F6. - STRAIN GAGE CHANNELS FOR PANEL D.

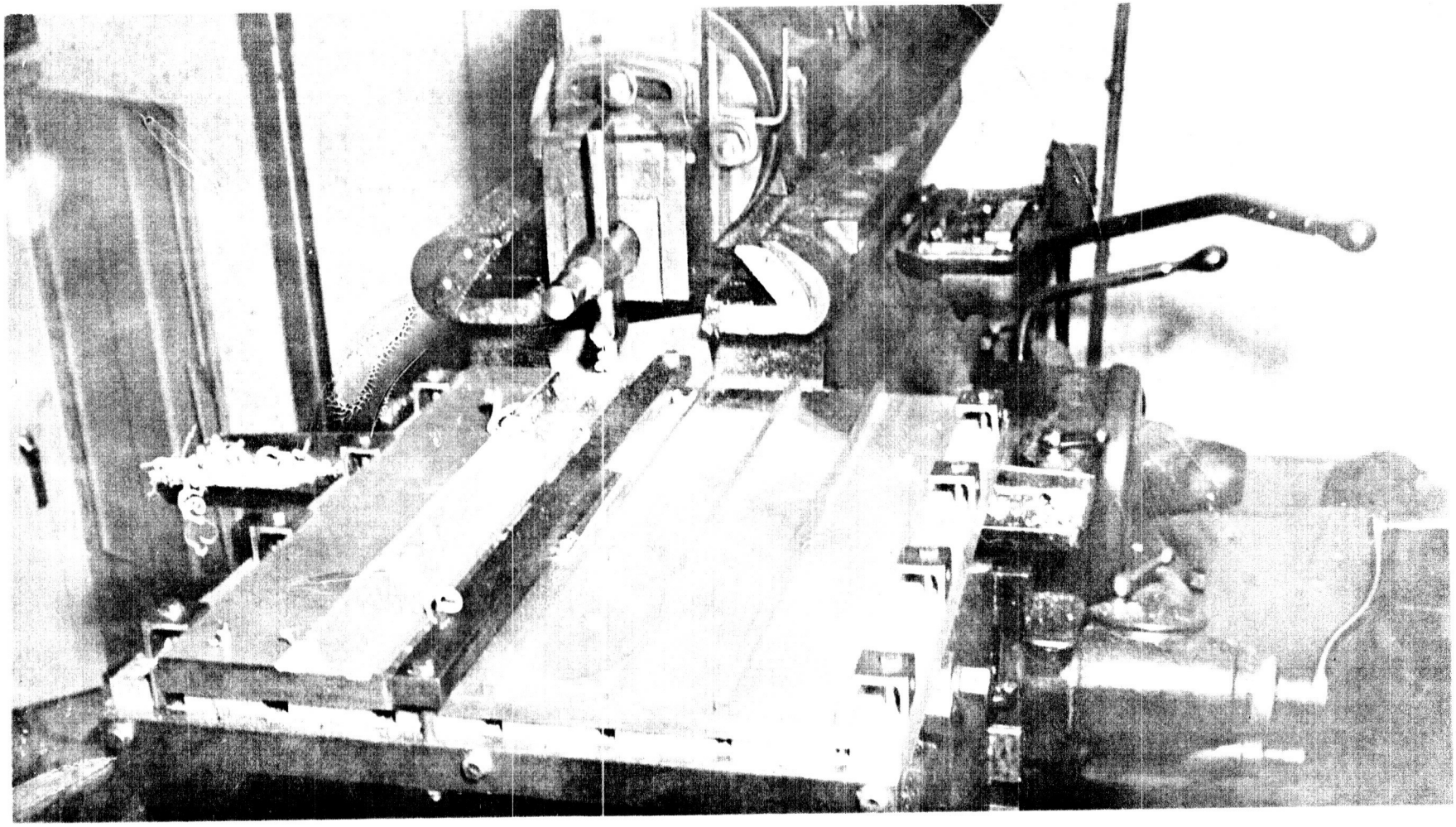

FIGURE F7. - MACHINING OF PANEL.

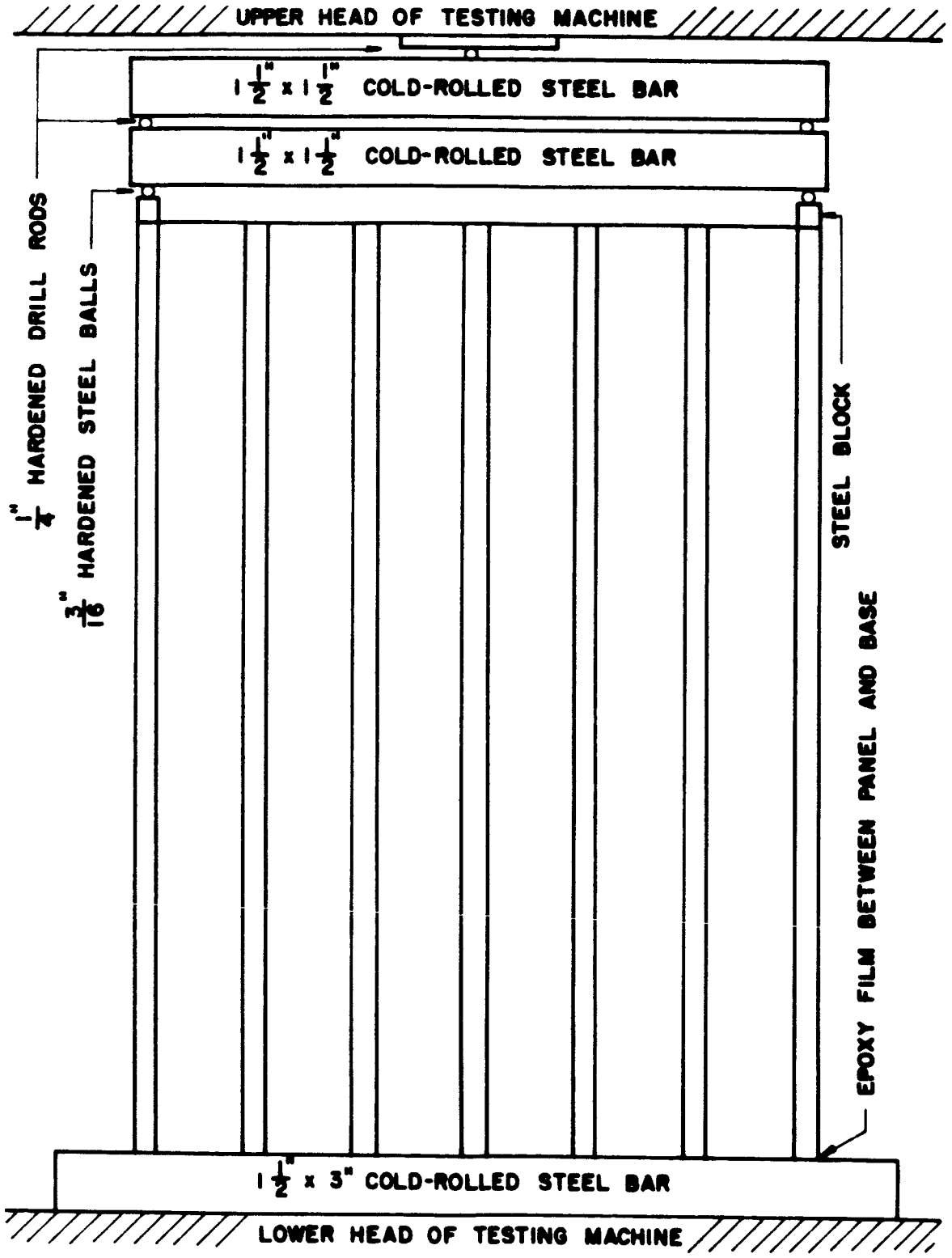

FIGURE F8. - TYPICAL LOADING ARRANGEMENT.

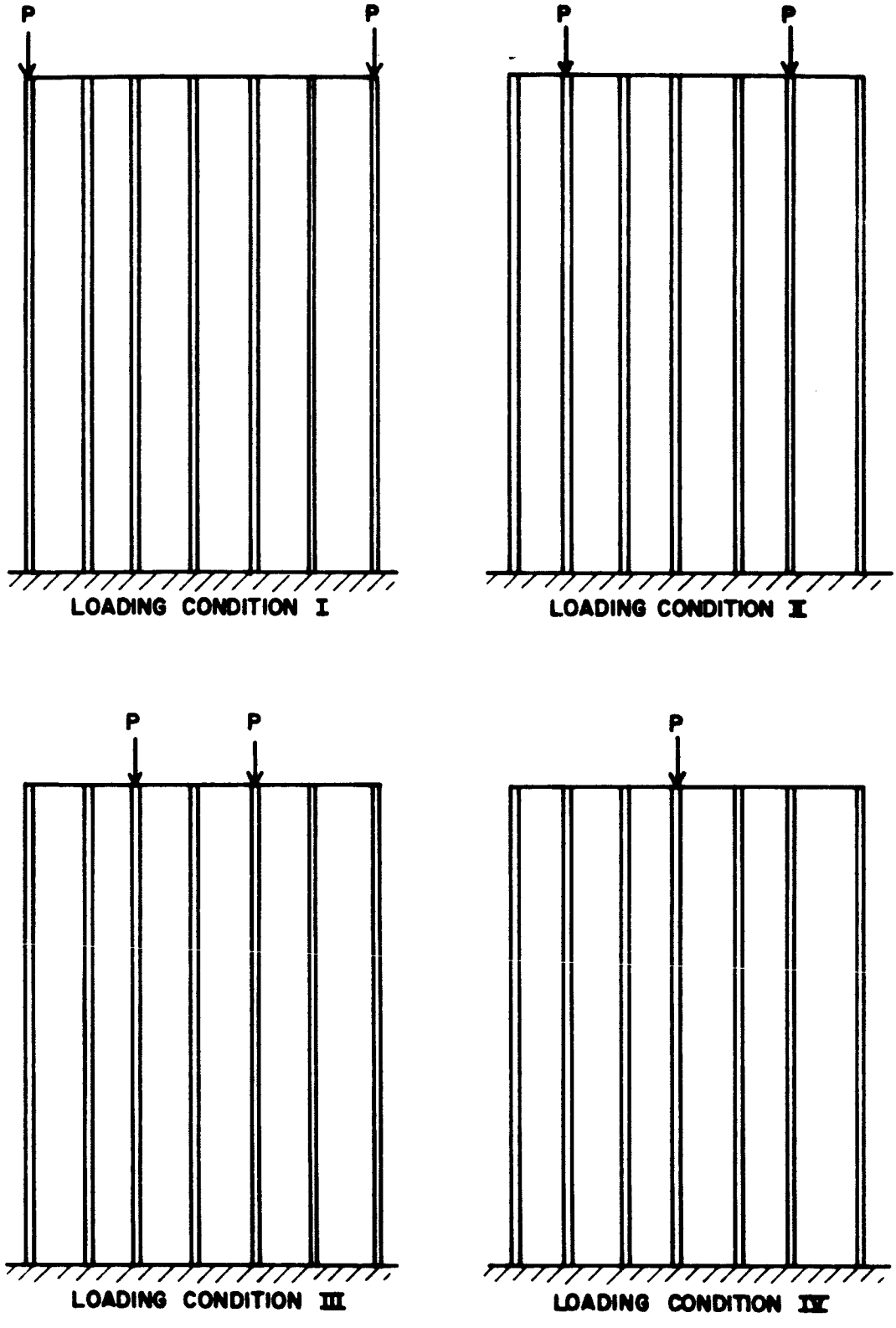

FIGURE F9. - FOUR LOADING CONDITIONS.

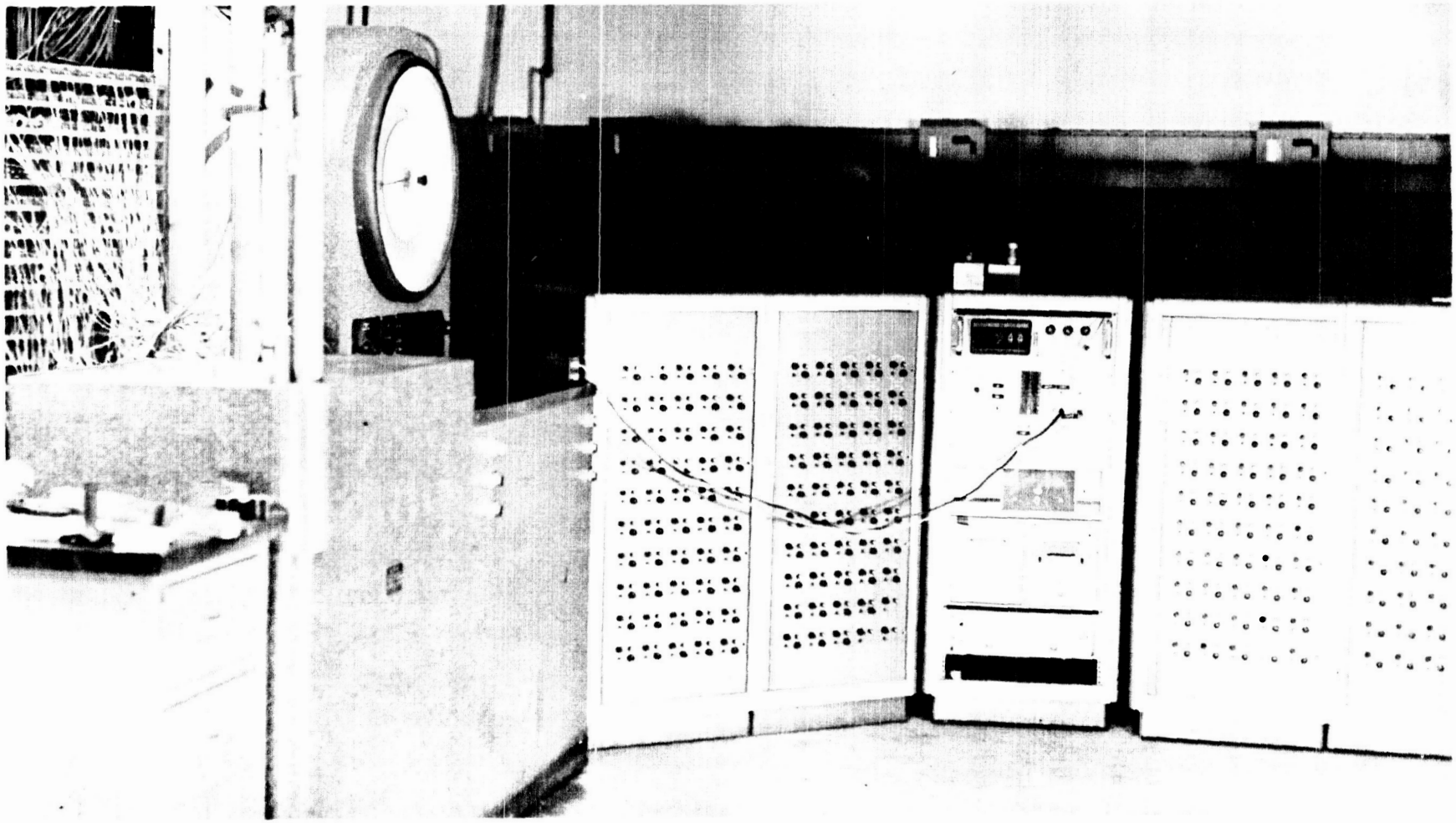

FIGURE F10. - OVERALL VIEW OF TEST EQUIPMENT.

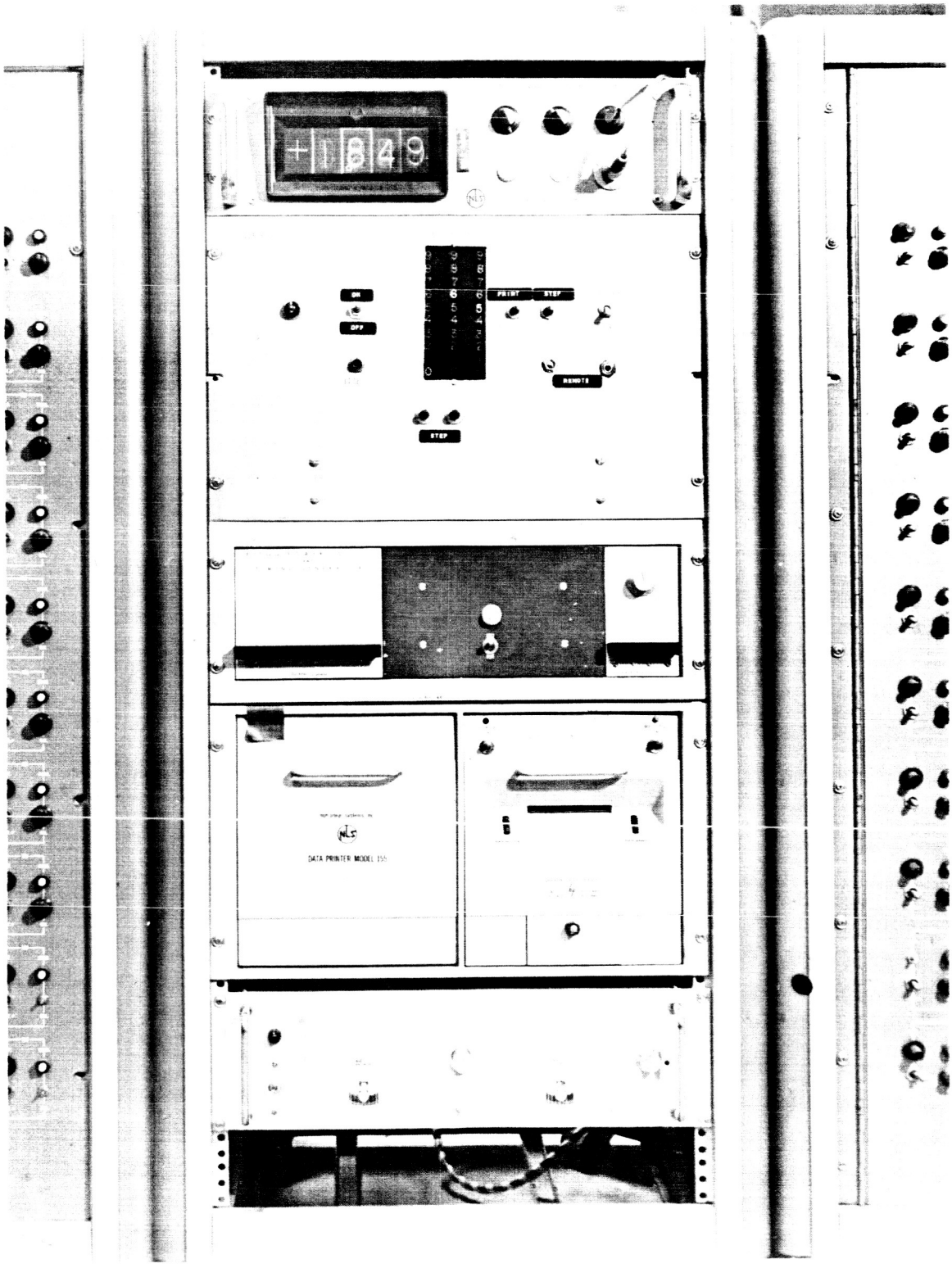

FIGURE F11. - CONTROL CONSOLE.

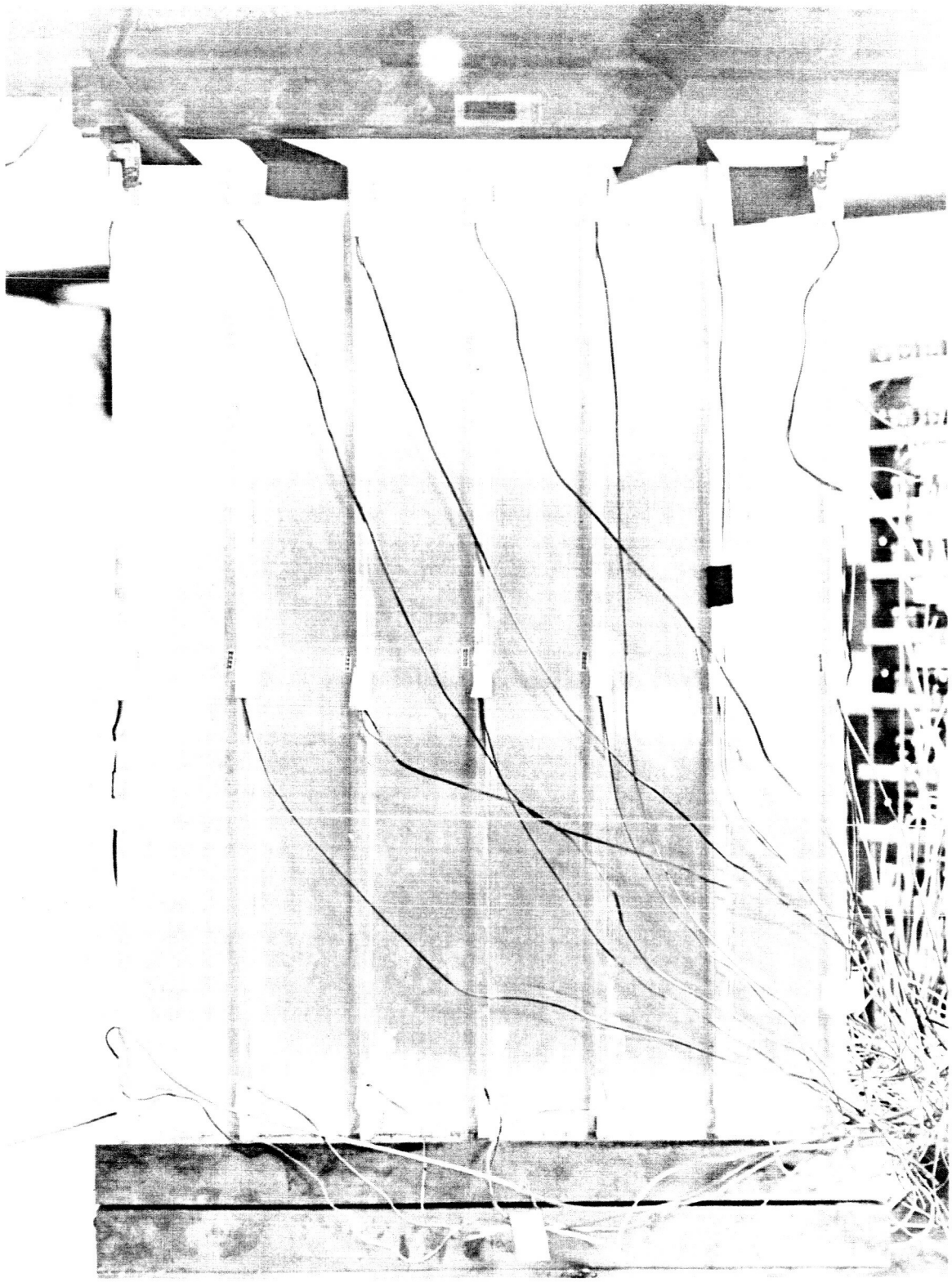

FIGURE F12. - FRONT VIEW OF PANEL.

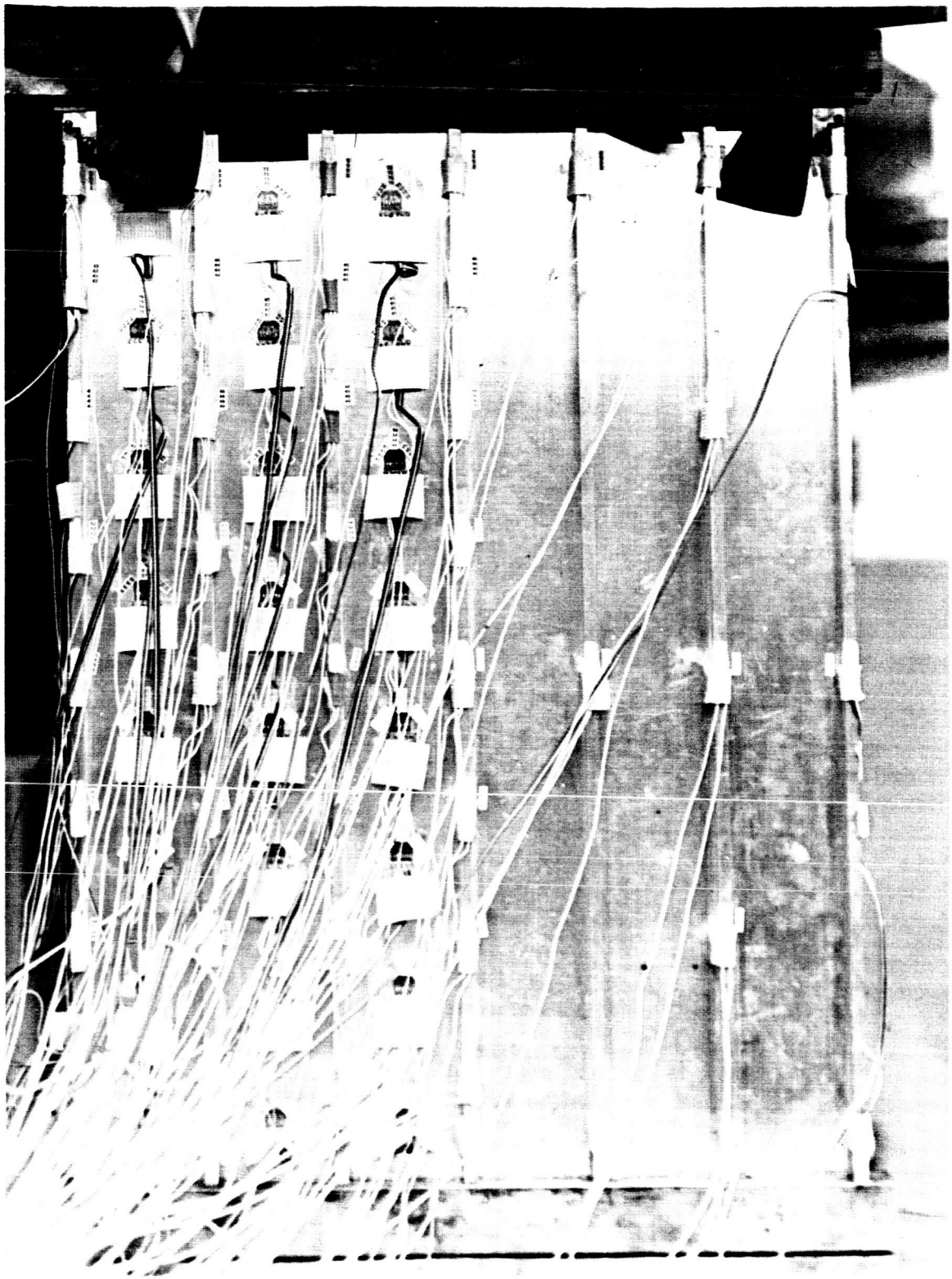

FIGURE F13. - REAR VIEW OF PANEL.

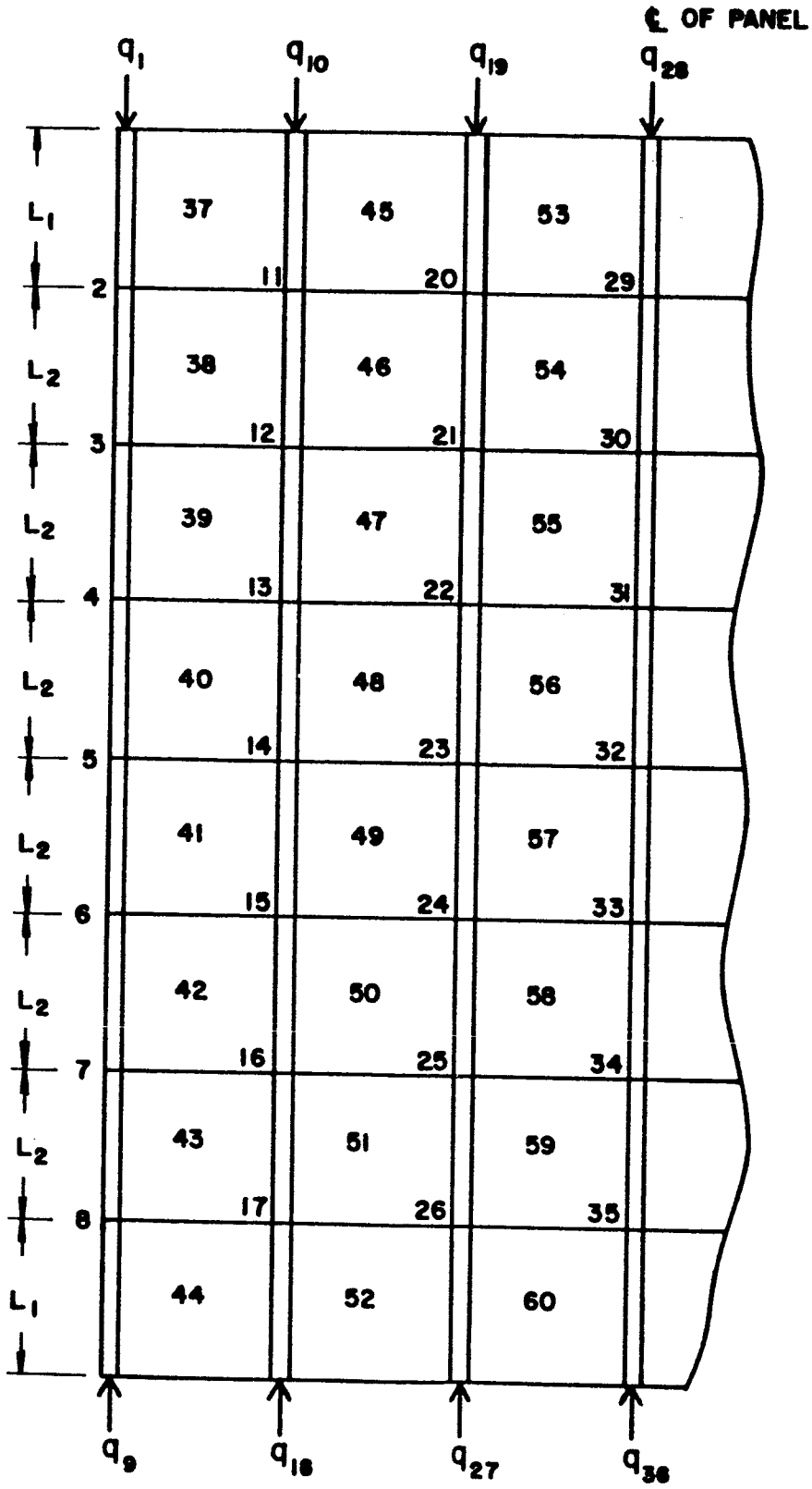

FIGURE F14. - GENERALIZED FORCE SYSTEM.

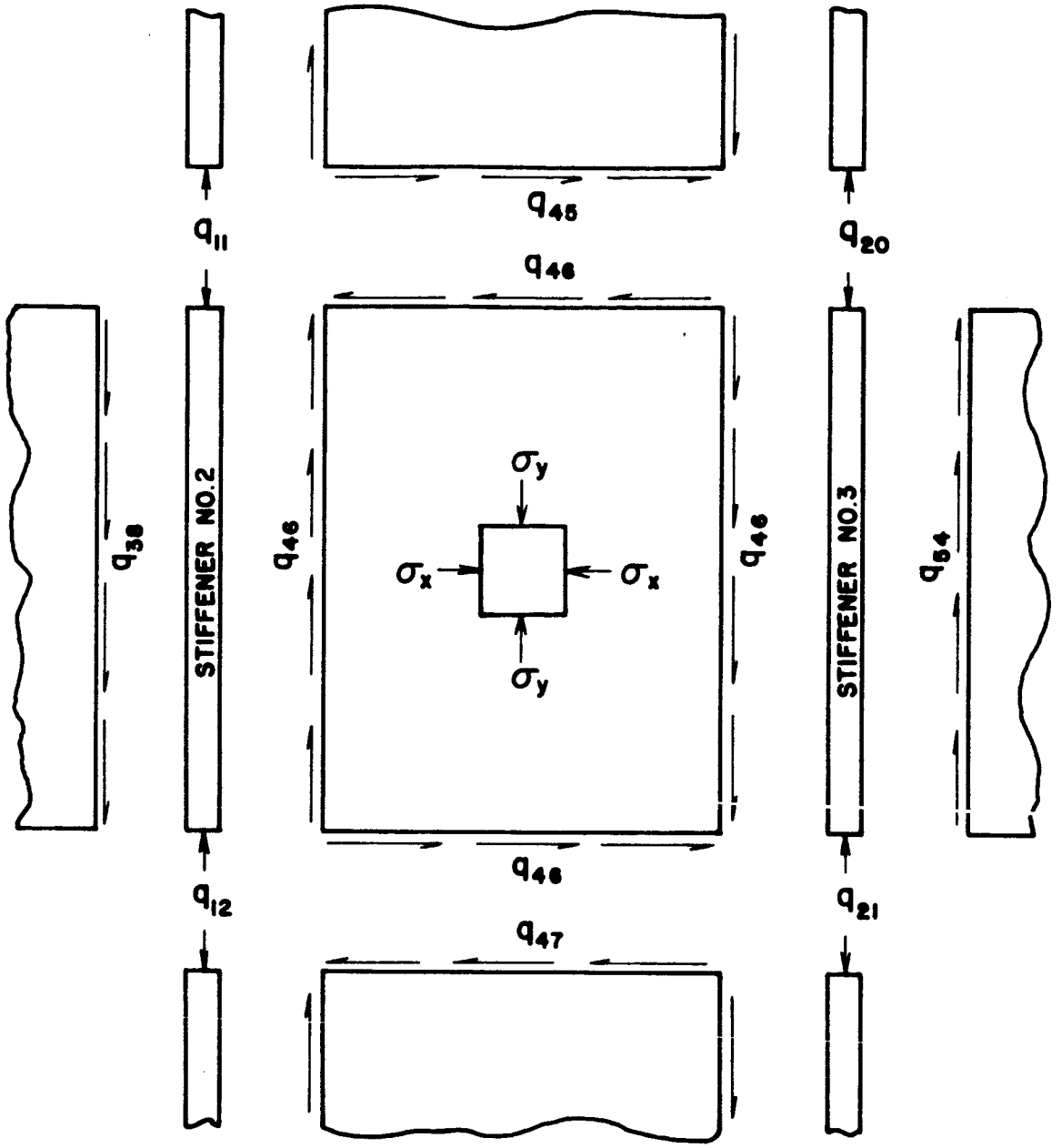

FIGURE F15. - GENERALIZED FORCE SYSTEM DETAILS.

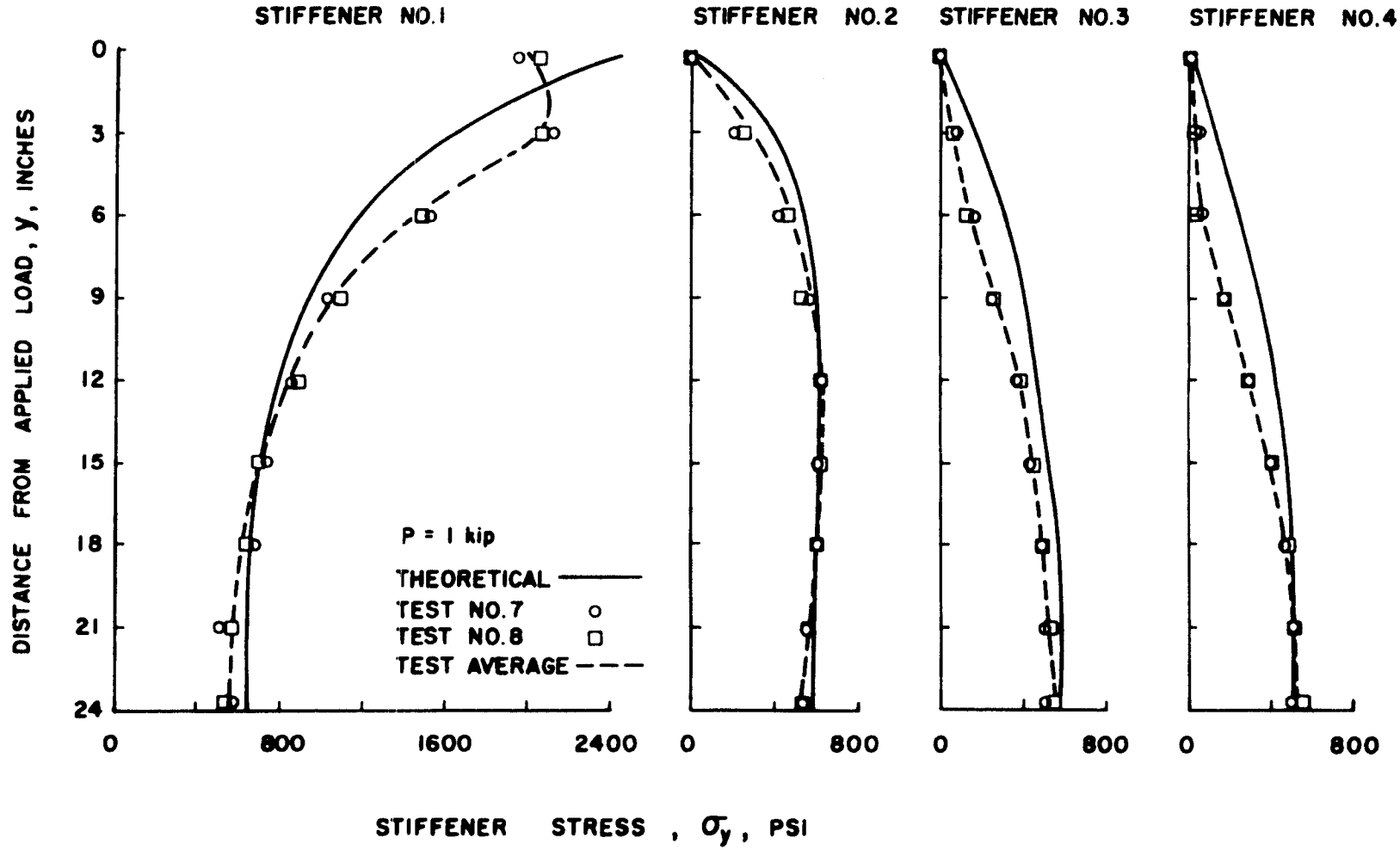

FIGURE F16. - NORMAL STRESS IN STIFFENERS OF PANEL B FOR LOADING CONDITION I.

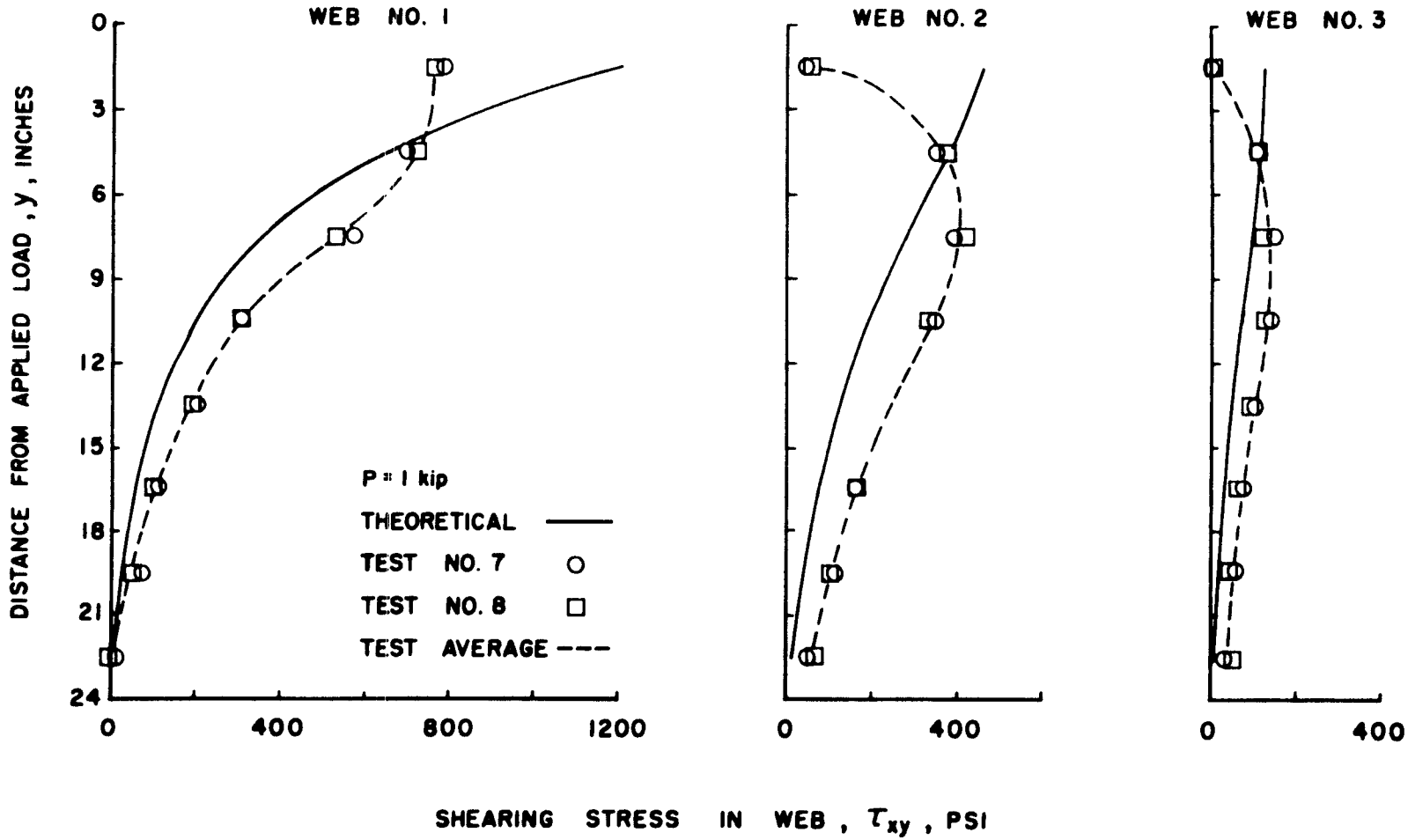

FIGURE F17. - SHEARING STRESS IN WEB OF PANEL B FOR LOADING CONDITION I.

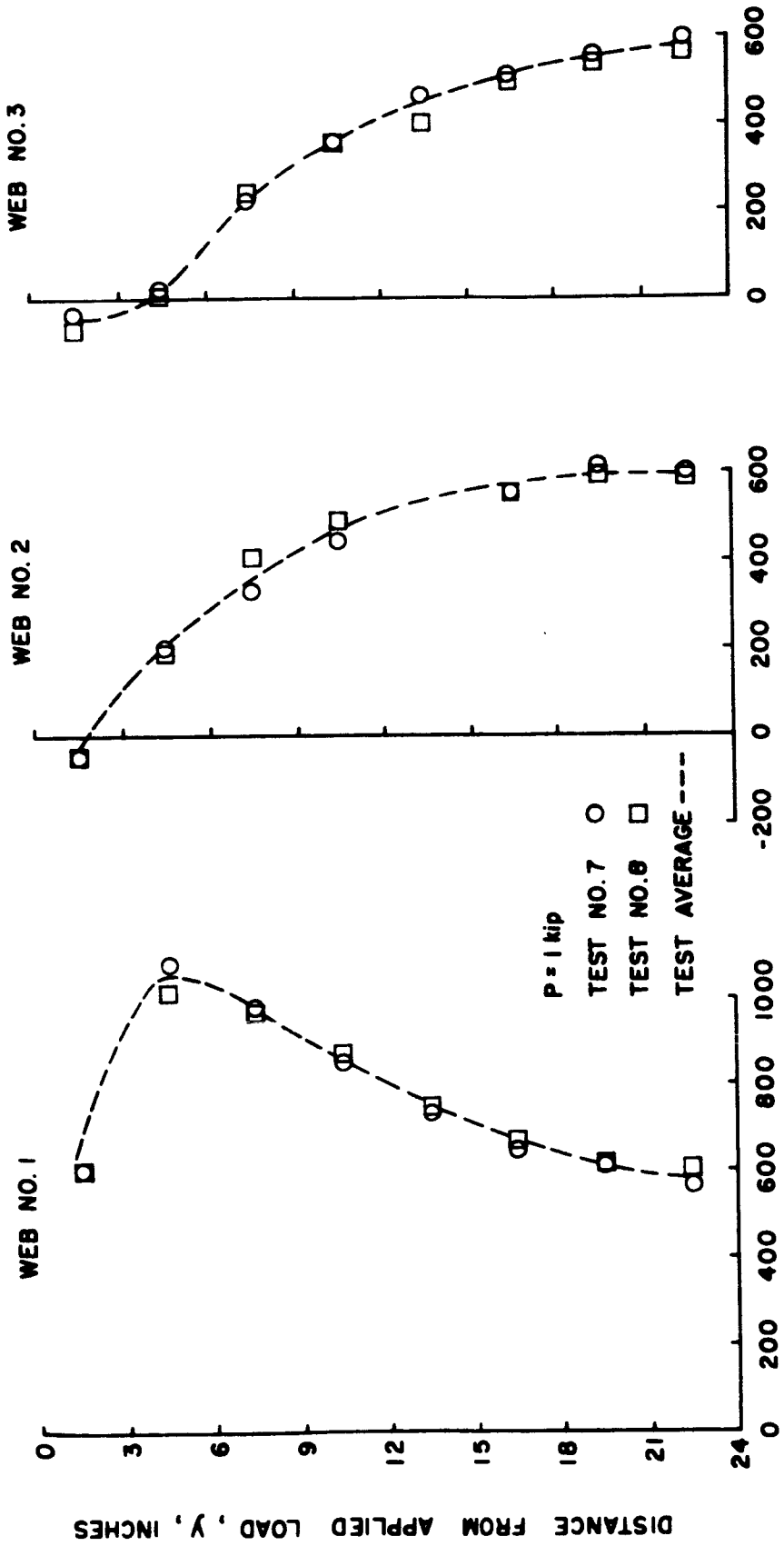

FIGURE F18. - NORMAL STRESS IN WEB OF PANEL B FOR LOADING CONDITION I.

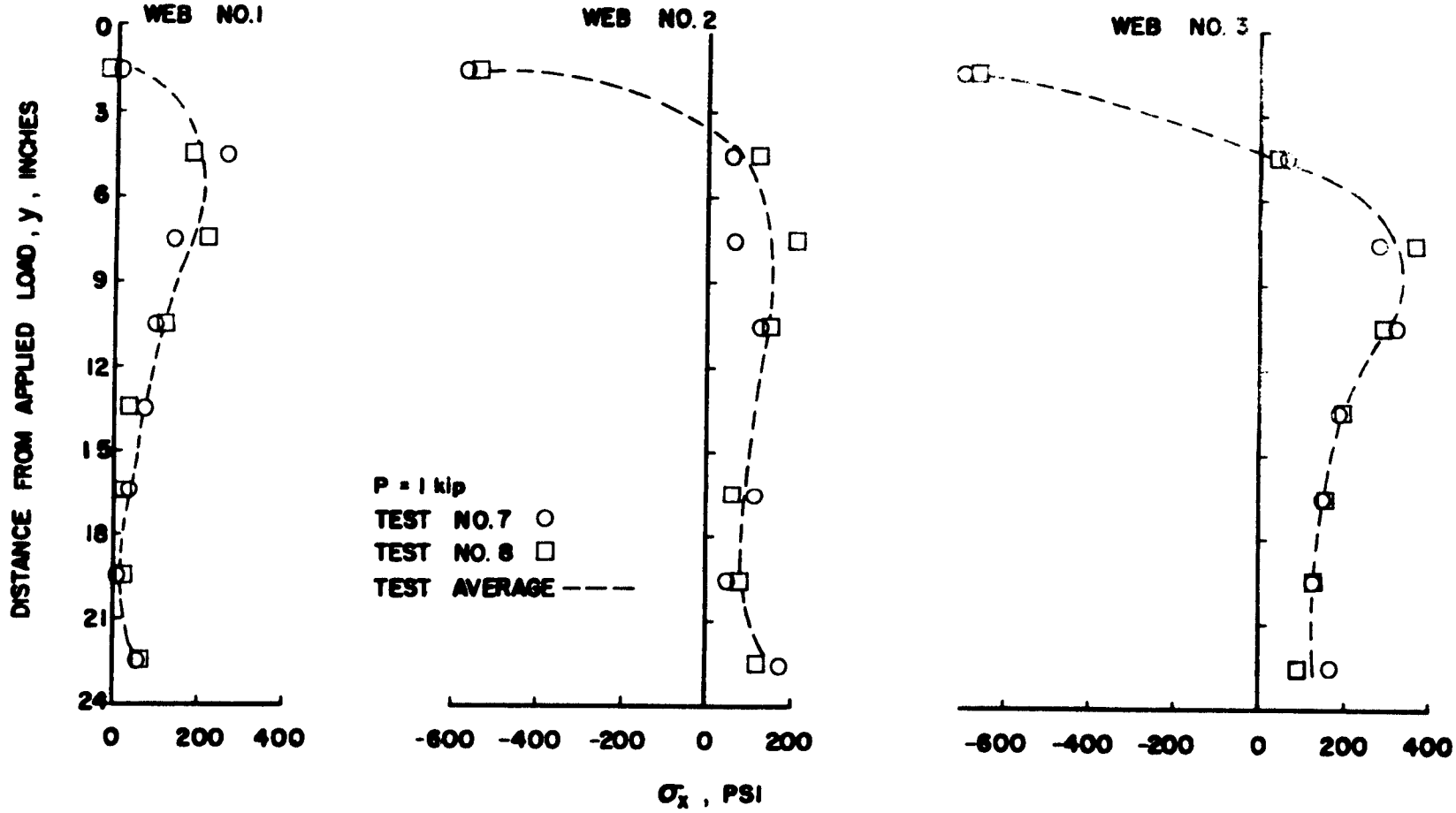

FIGURE F19. - NORMAL STRESS IN WEB OF PANEL B FOR LOADING CONDITION I.

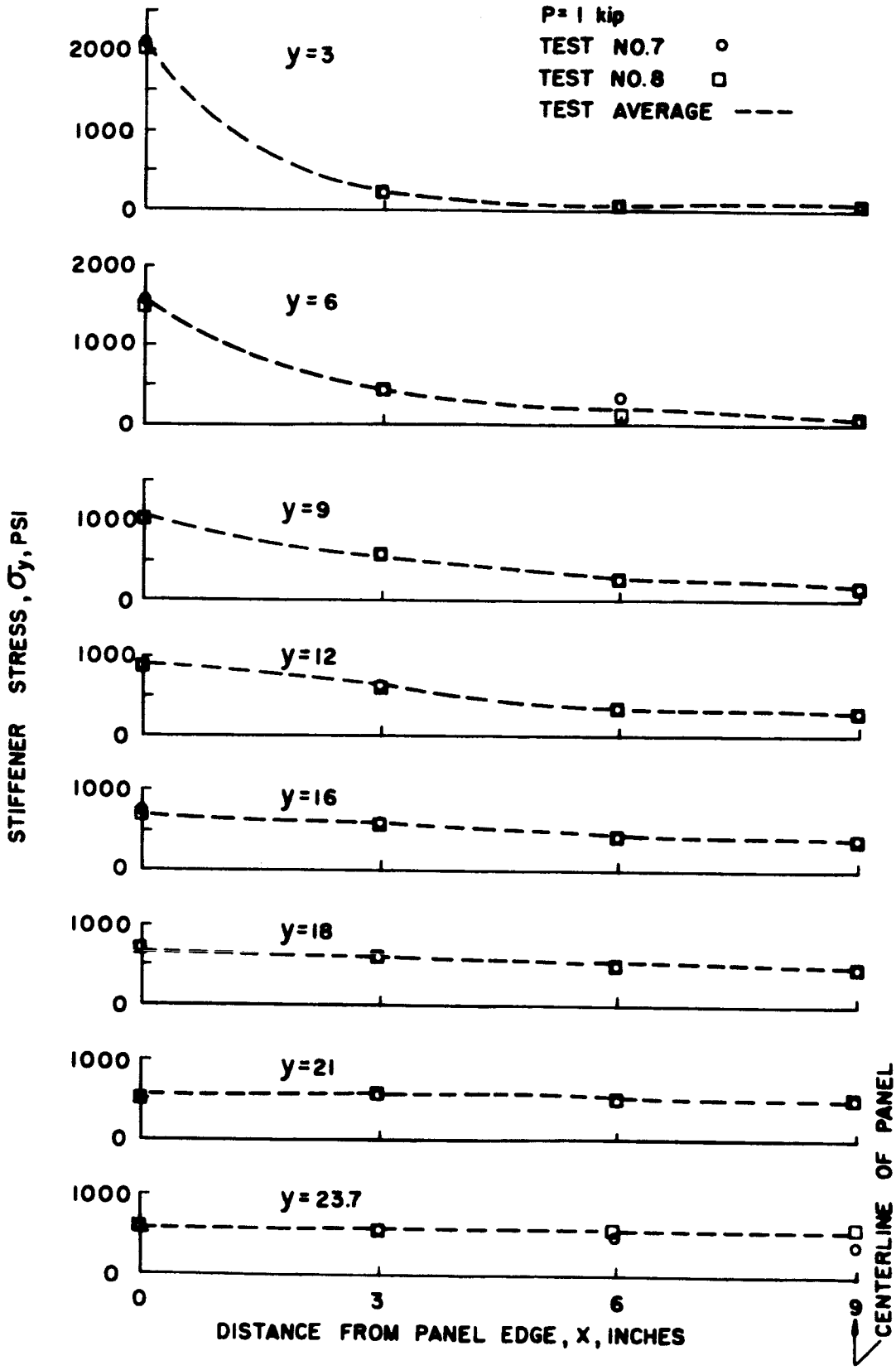

FIGURE F20. - CHORDWISE DISTRIBUTION OF STIFFENER NORMAL STRESS IN PANEL B FOR LOADING CONDITION I.

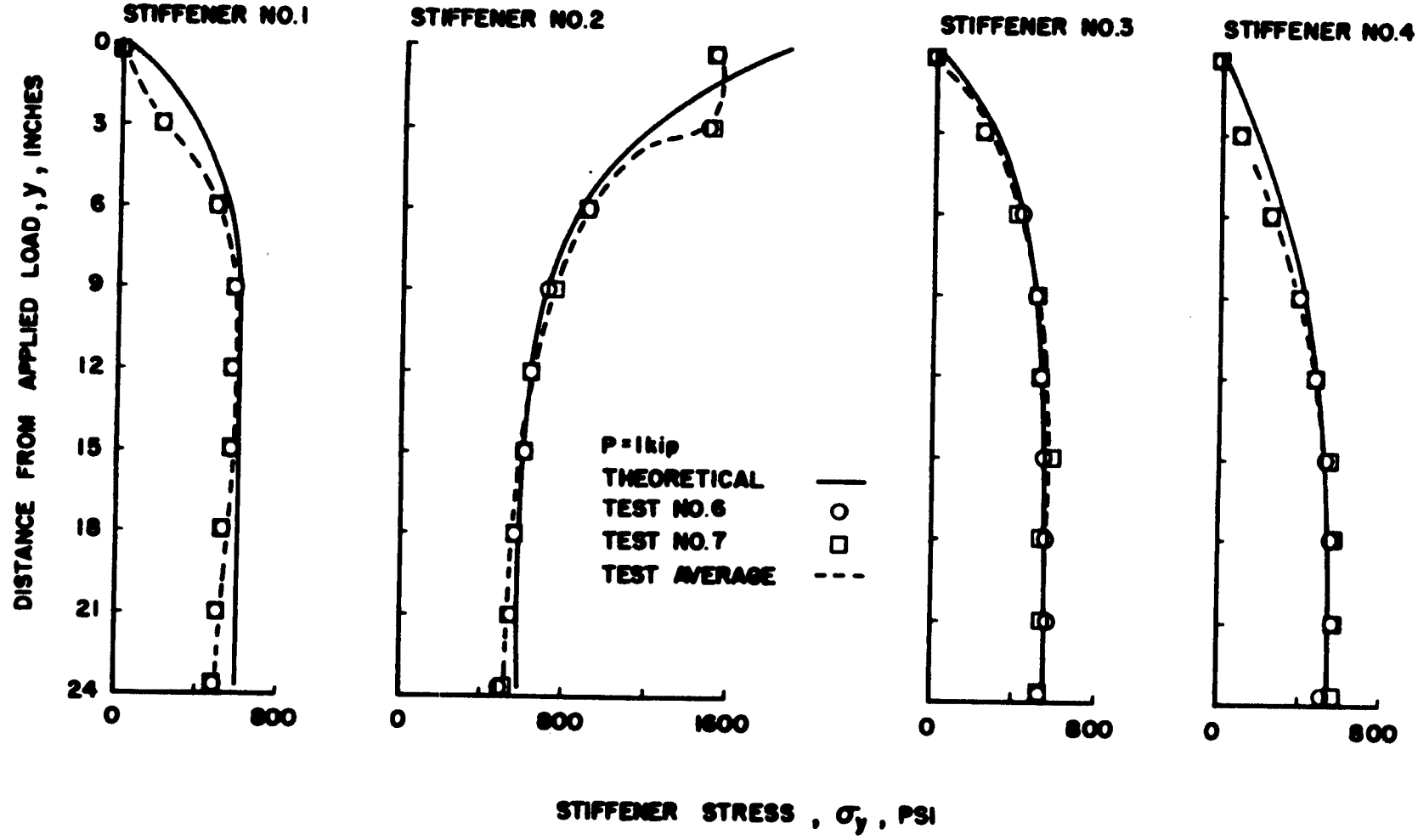

FIGURE F21. - NORMAL STRESS IN STIFFENERS OF PANEL B FOR LOADING CONDITION II.

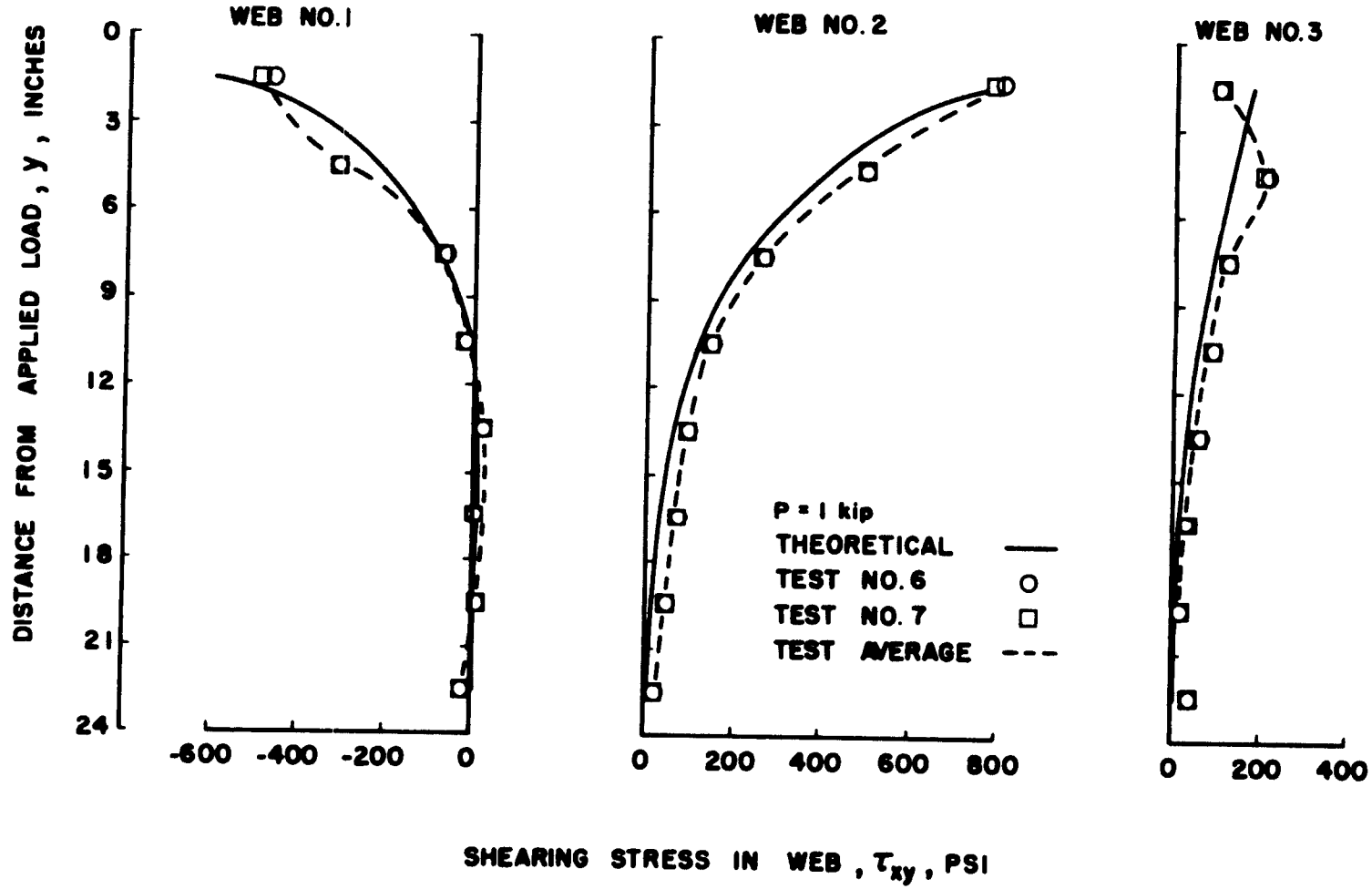

FIGURE F22. - SHEARING STRESS IN WEB OF PANEL B FOR LOADING CONDITION II.

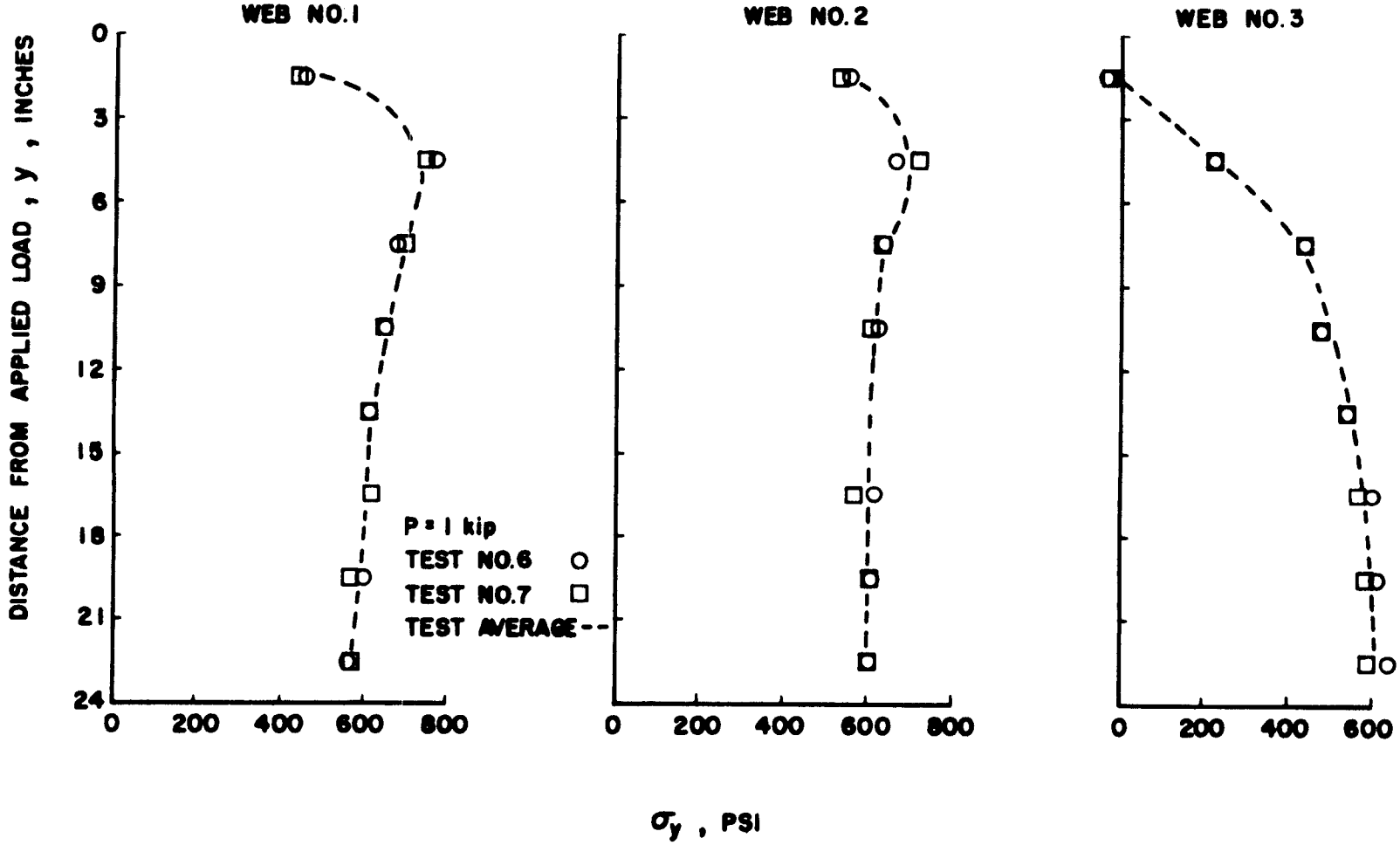

FIGURE F23. - NORMAL STRESS IN WEB OF PANEL B FOR LOADING CONDITION II.

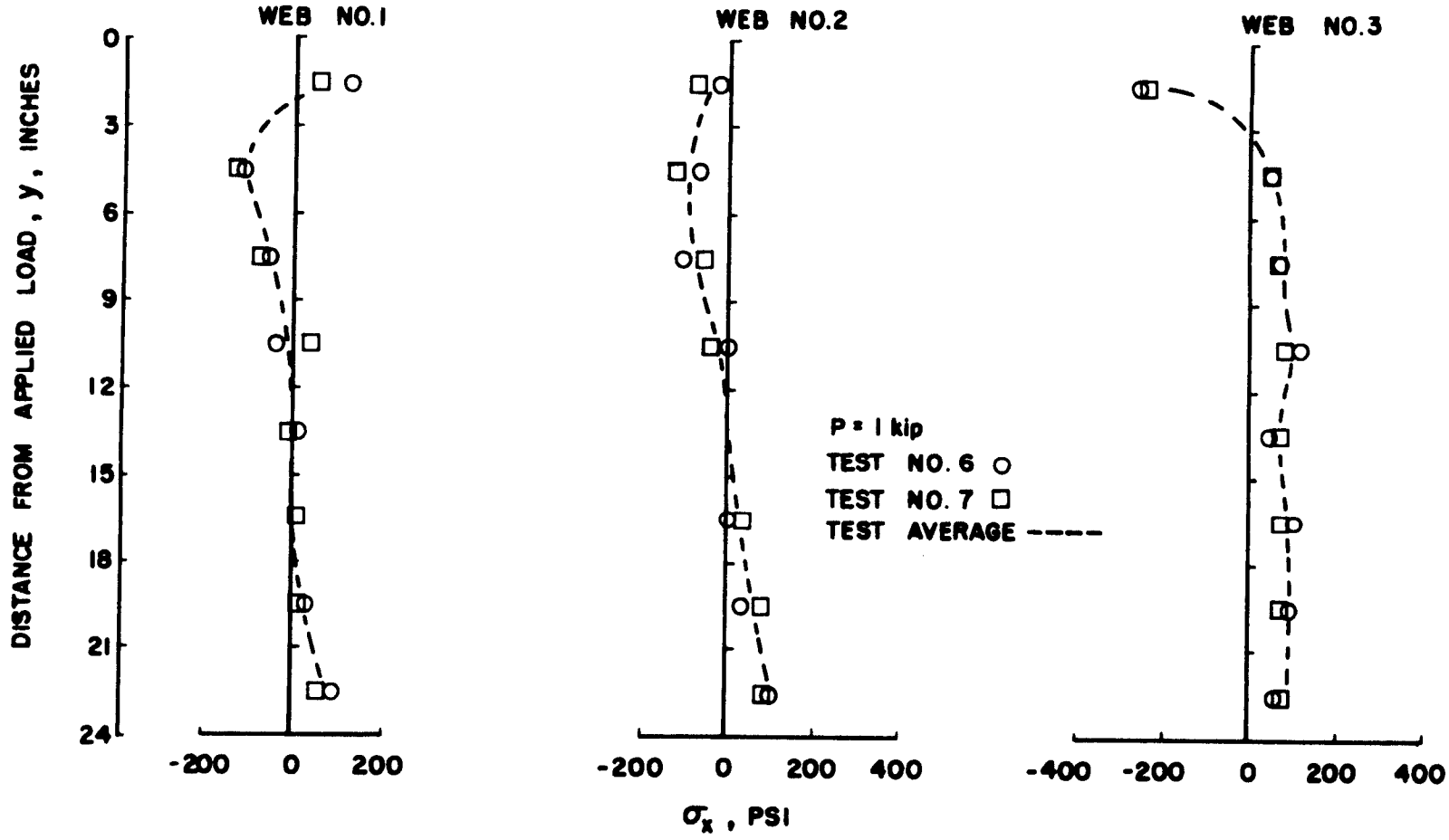

FIGURE F24. - NORMAL STRESS IN WEB OF PANEL B FOR LOADING CONDITION II.

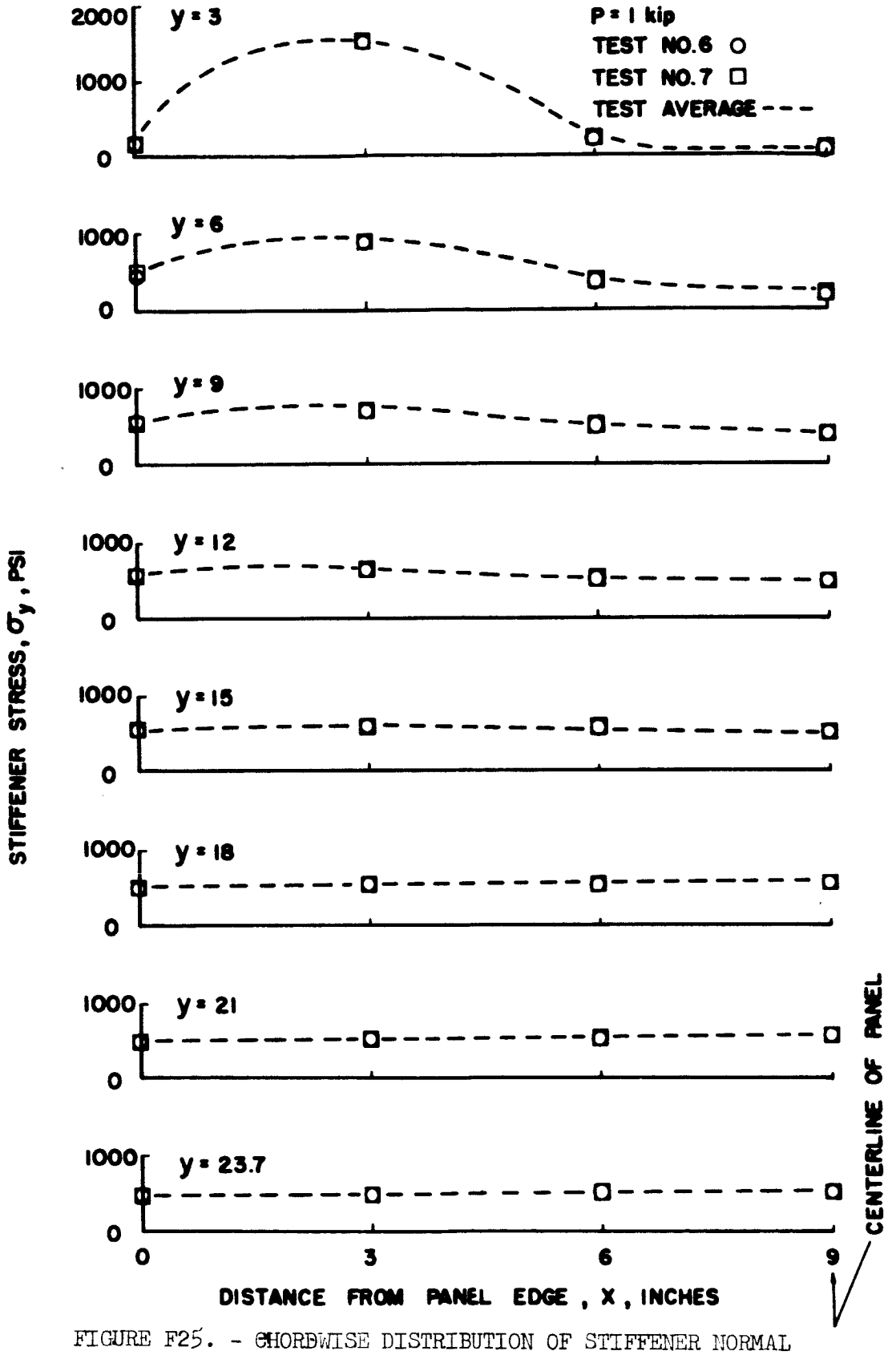

FIGURE F25. - CHORDWISE DISTRIBUTION OF STIFFENER NORMAL STRESS IN PANEL B FOR LOADING CONDITION II.

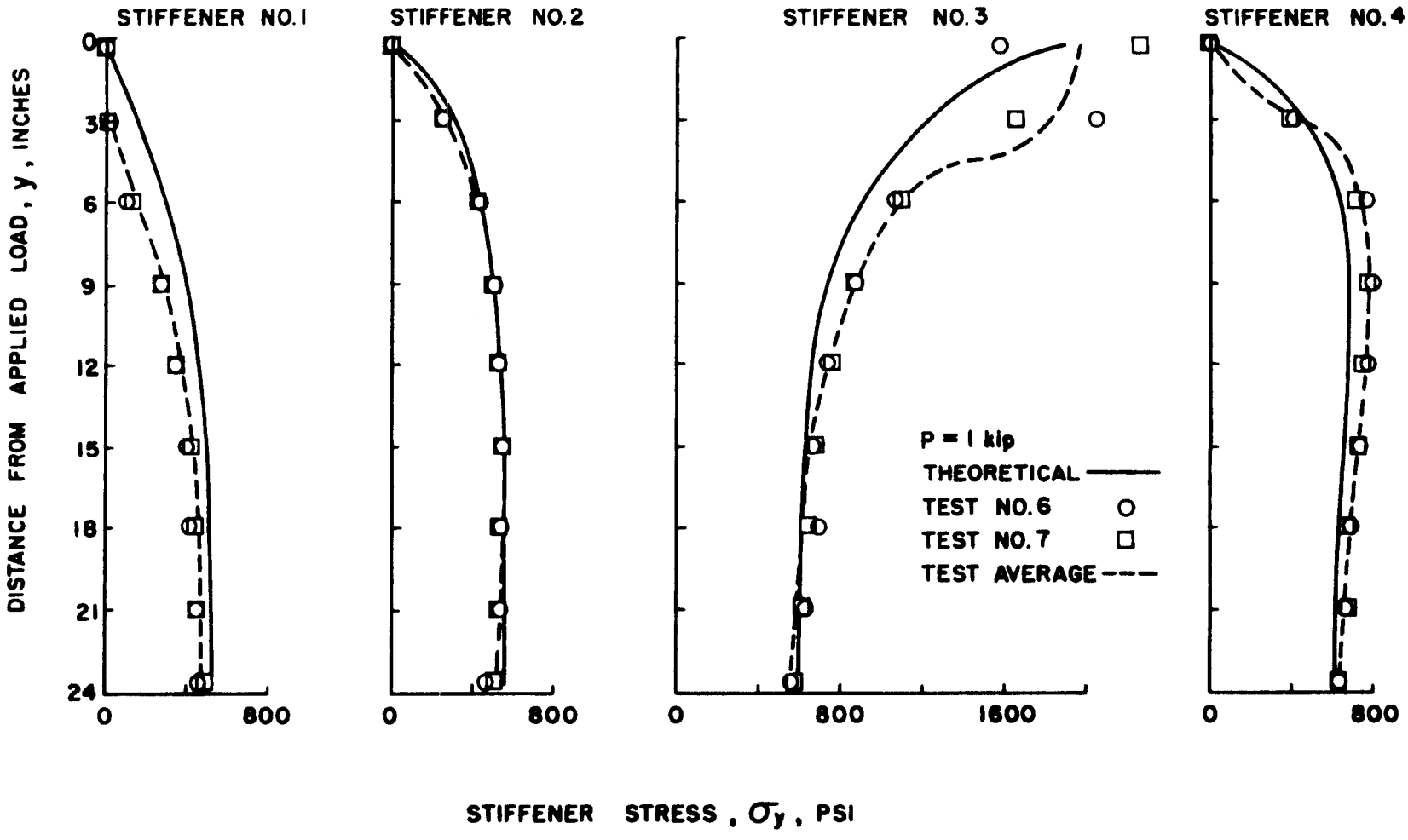

FIGURE F26. - NORMAL STRESS IN STIFFENER OF PANEL B FOR LOADING CONDITION III.

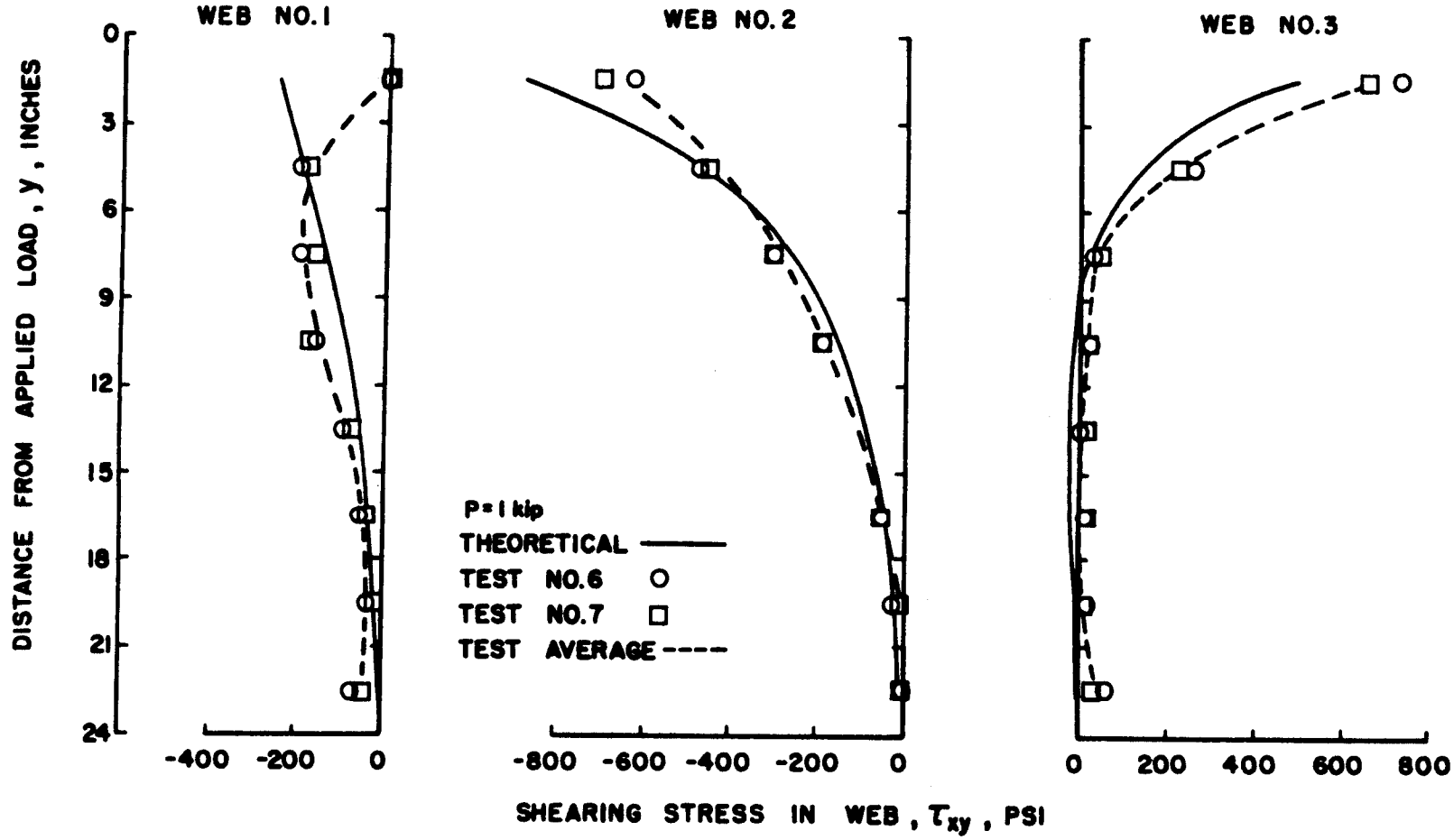

FIGURE F27. - SHEARING STRESS IN WEB OF PANEL B FOR LOADING CONDITION III.

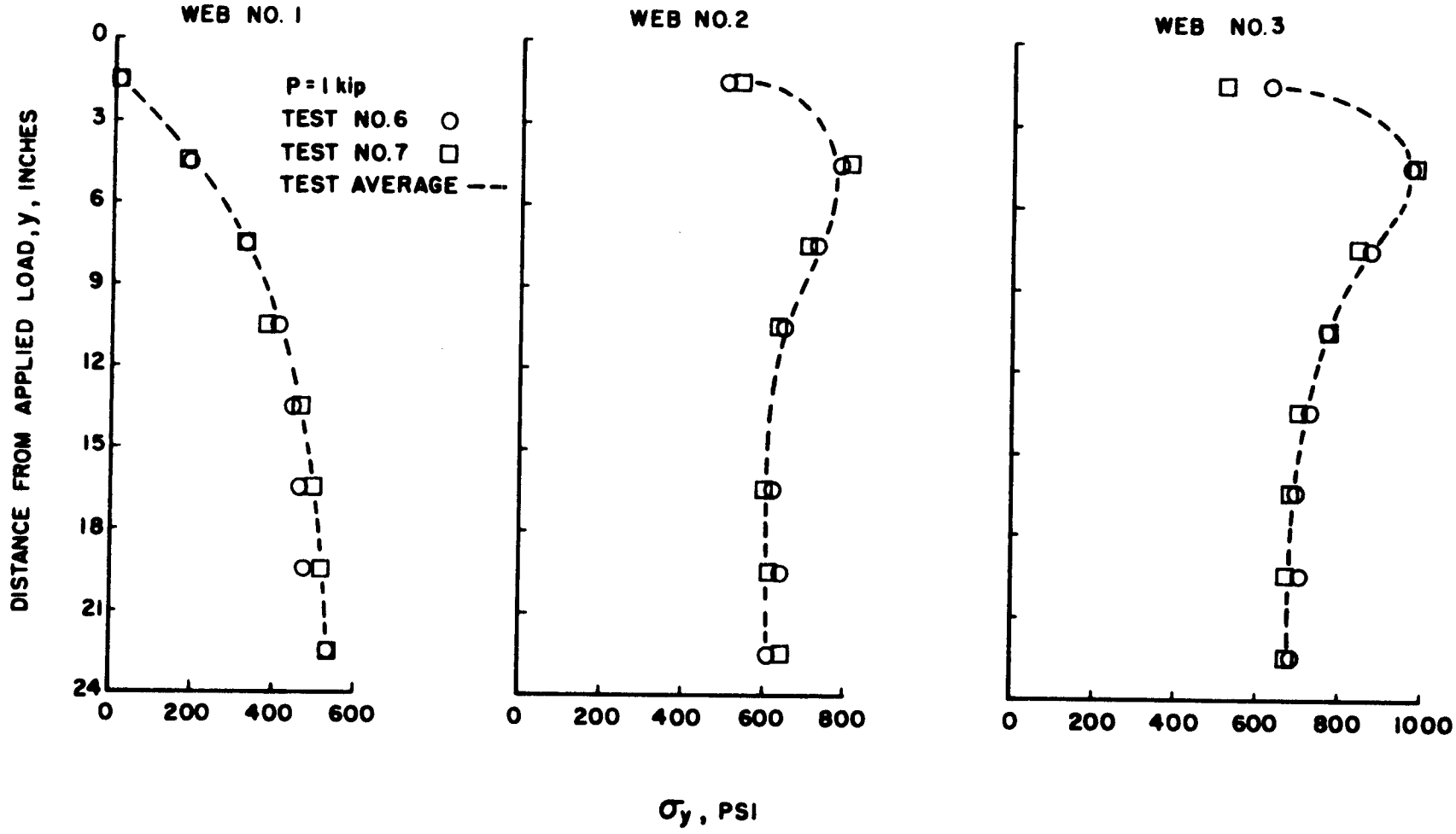

FIGURE F28. - NORMAL STRESS IN WEB OF PANEL B FOR LOADING CONDITION III.

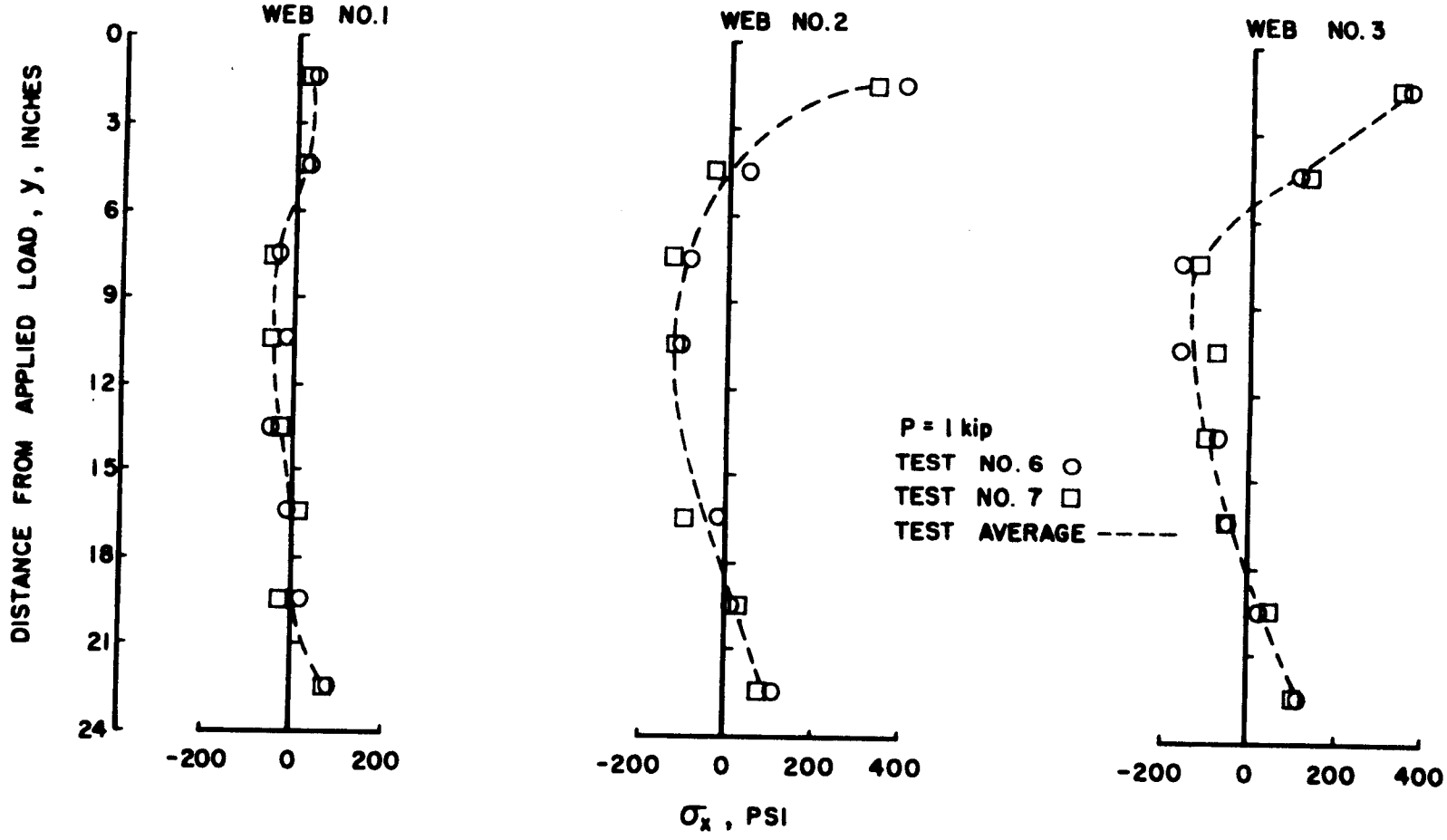

FIGURE F29. - NORMAL STRESS IN WEB OF PANEL B FOR LOADING CONDITION III.

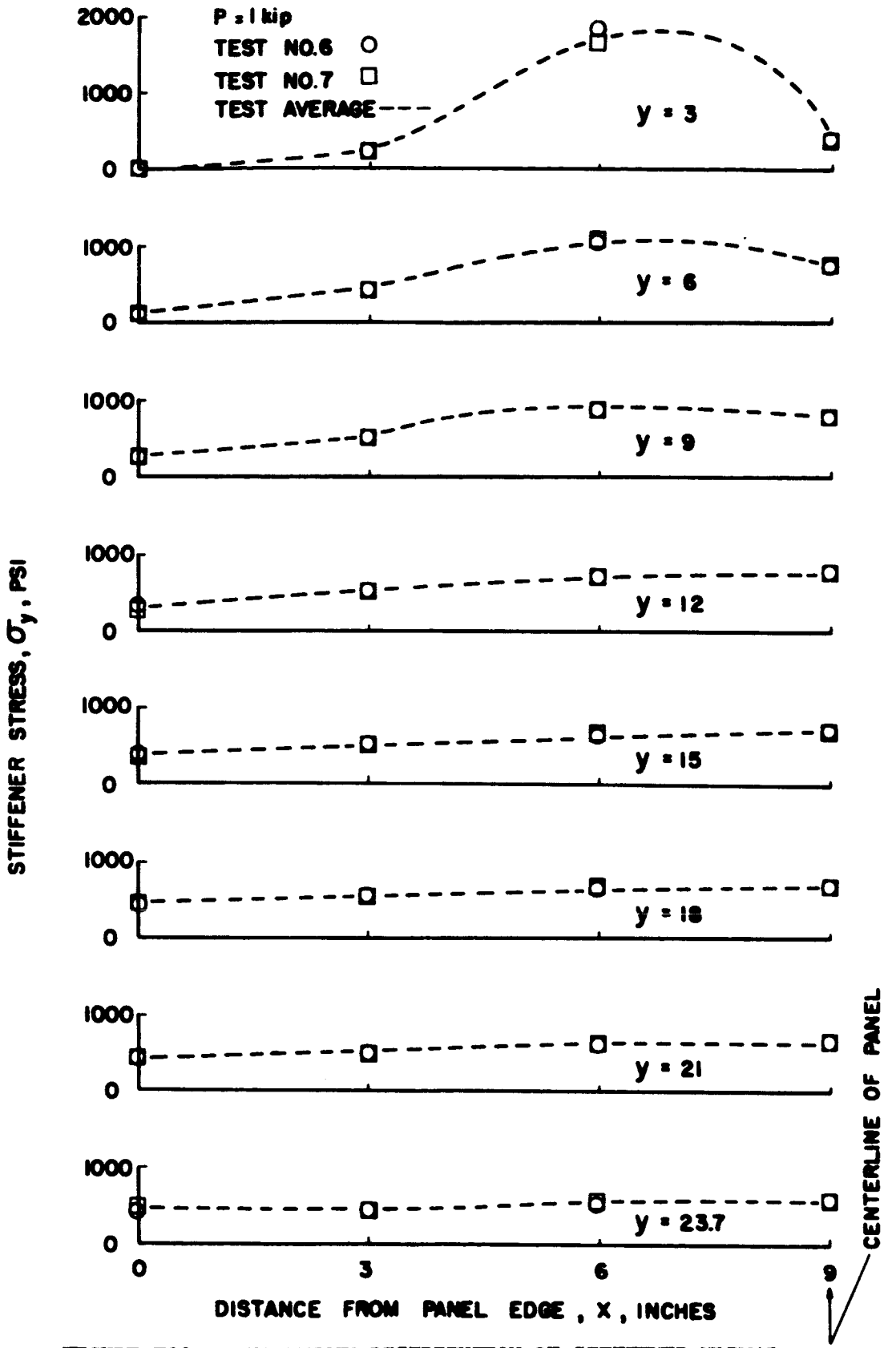

FIGURE F30. - CHORDWISE DISTRIBUTION OF STIFFENER NORMAL STRESS IN PANEL B FOR LOADING CONDITION III.

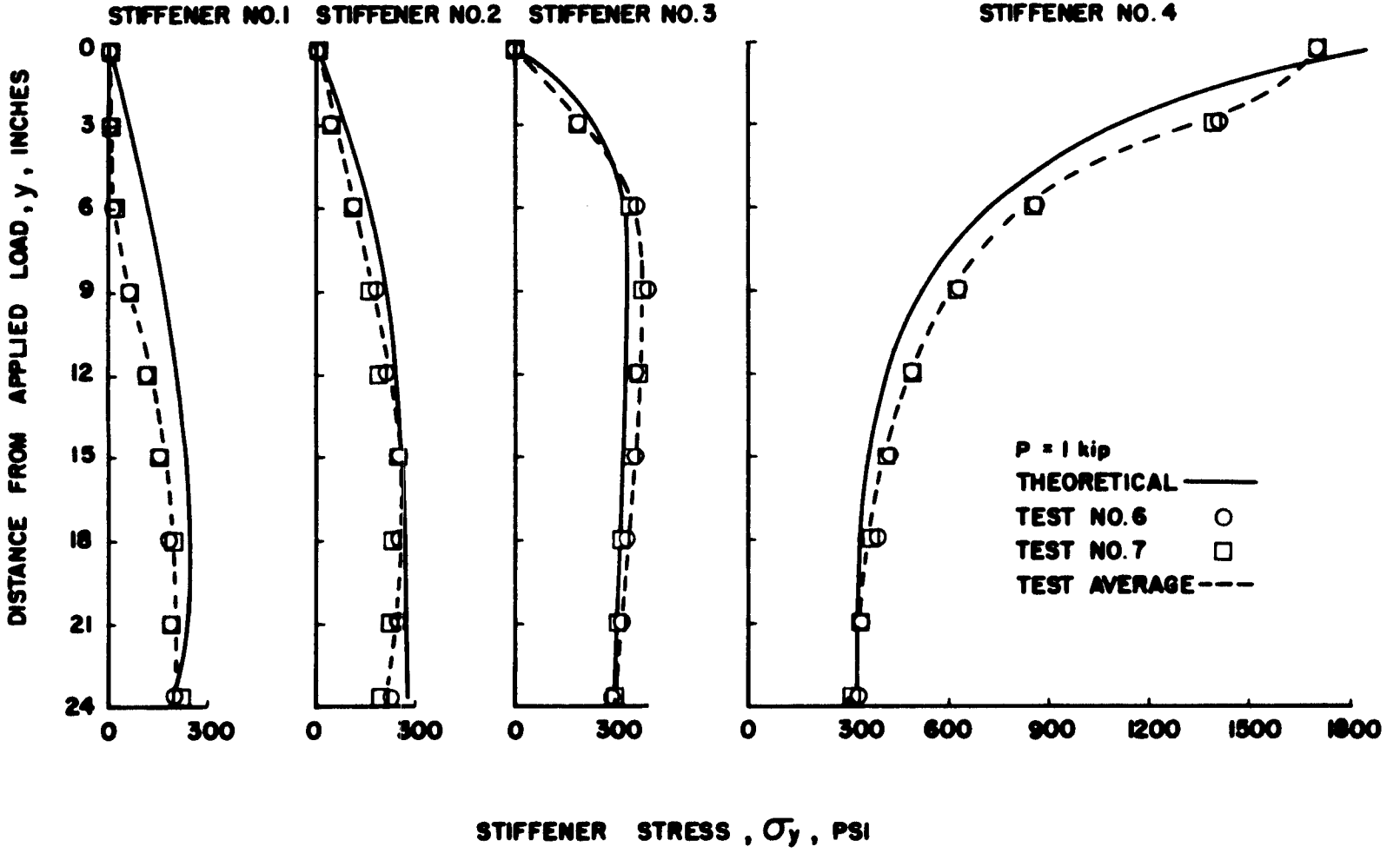

FIGURE F31. - NORMAL STRESS IN STIFFENERS OF PANEL B FOR LOADING CONDITION IV.

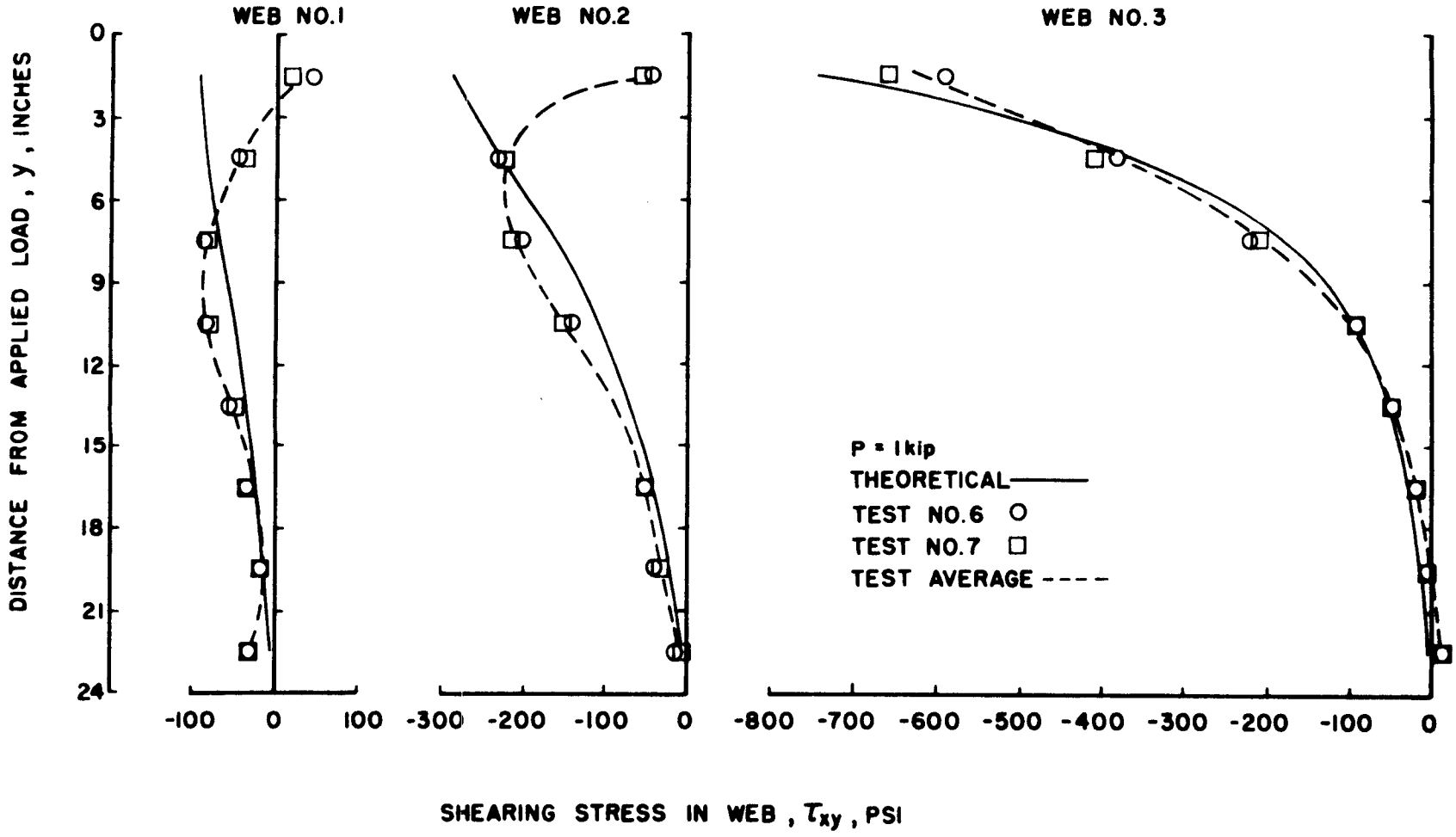

FIGURE F32. - SHEARING STRESS IN WEB OF PANEL B FOR LOADING CONDITION IV.

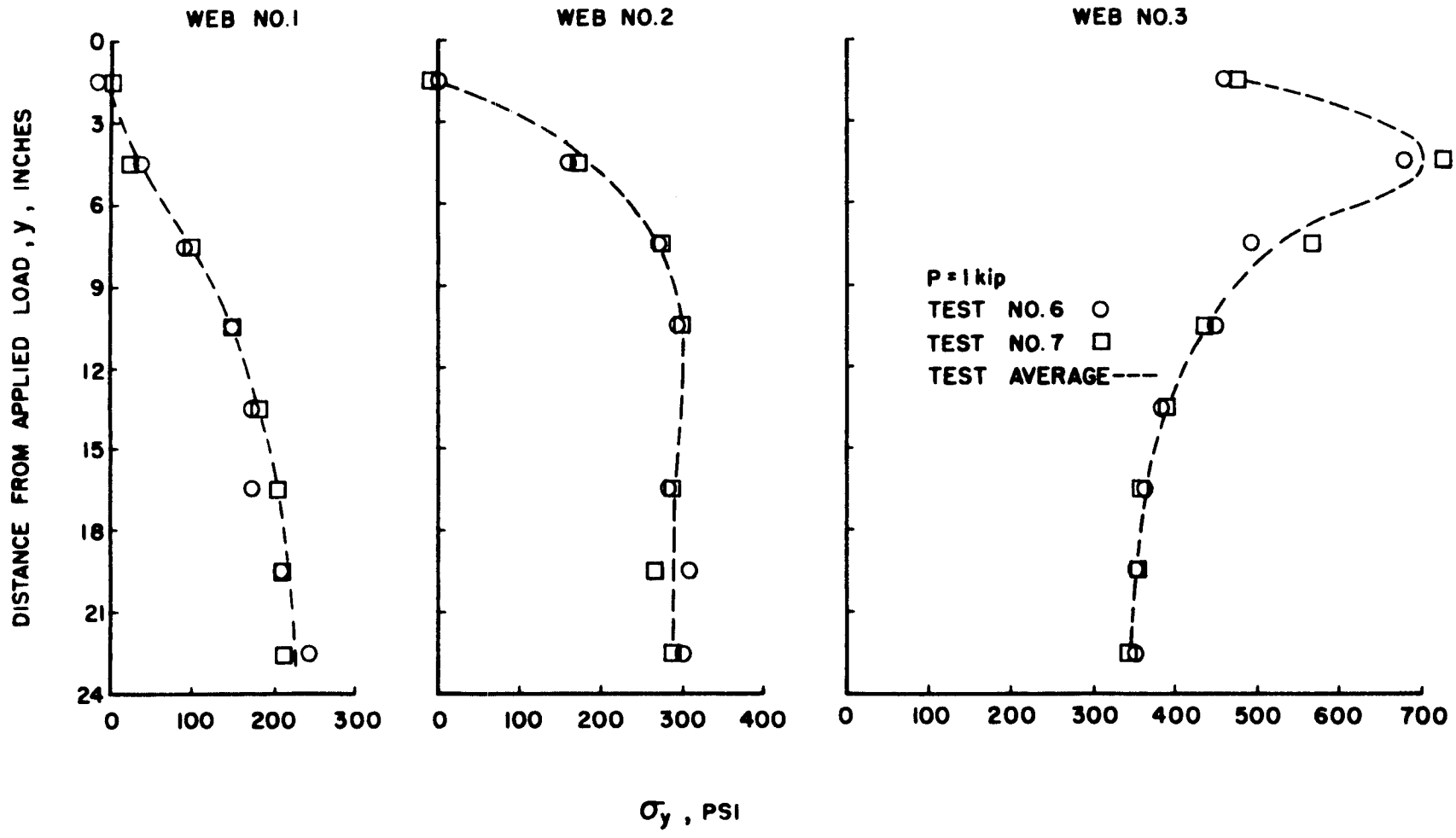

FIGURE F33. - NORMAL STRESS IN WEB OF PANEL B FOR LOADING CONDITION IV.

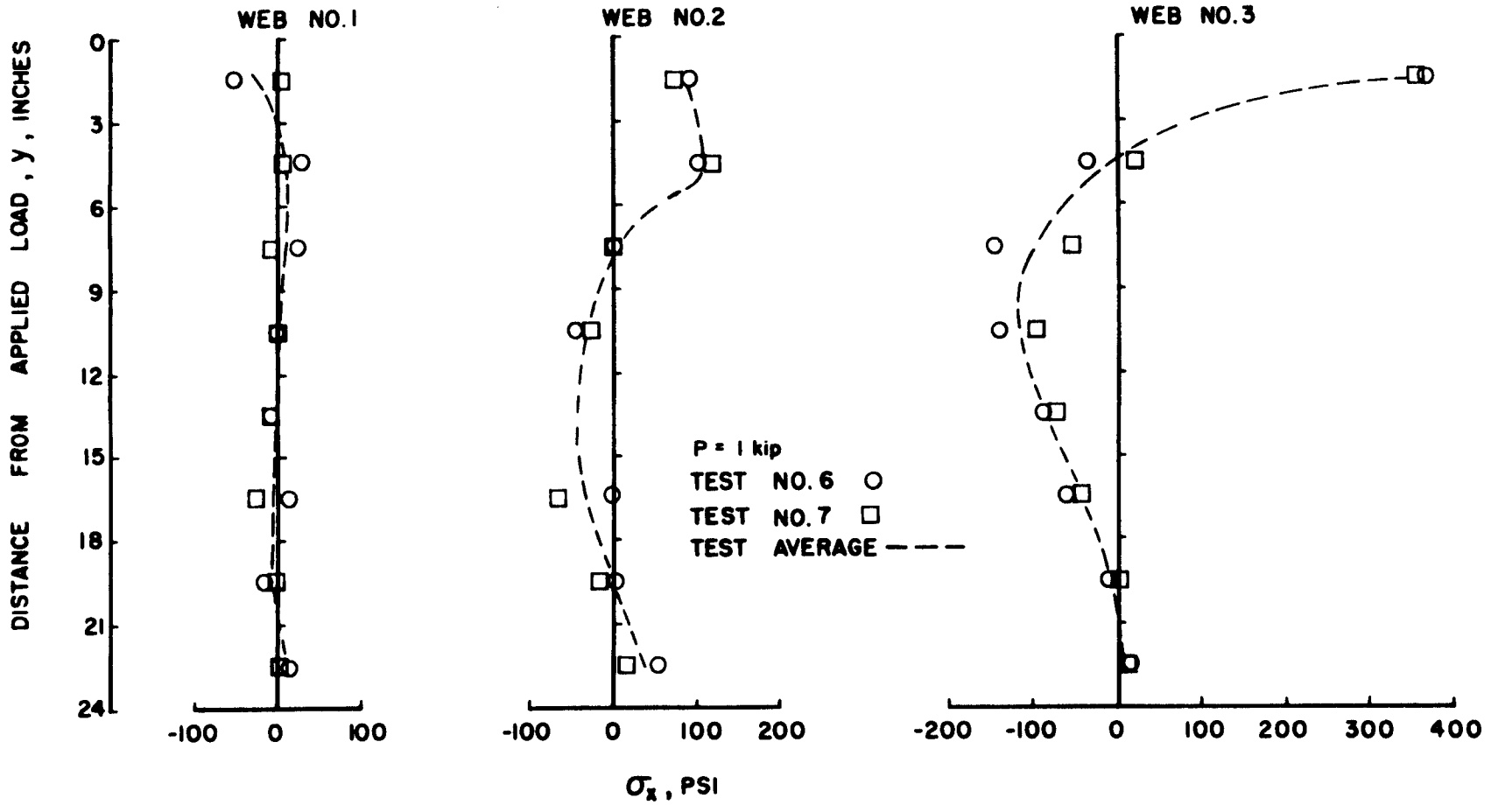

FIGURE F34. - NORMAL STRESS IN WEB OF PANEL B FOR LOADING CONDITION IV.

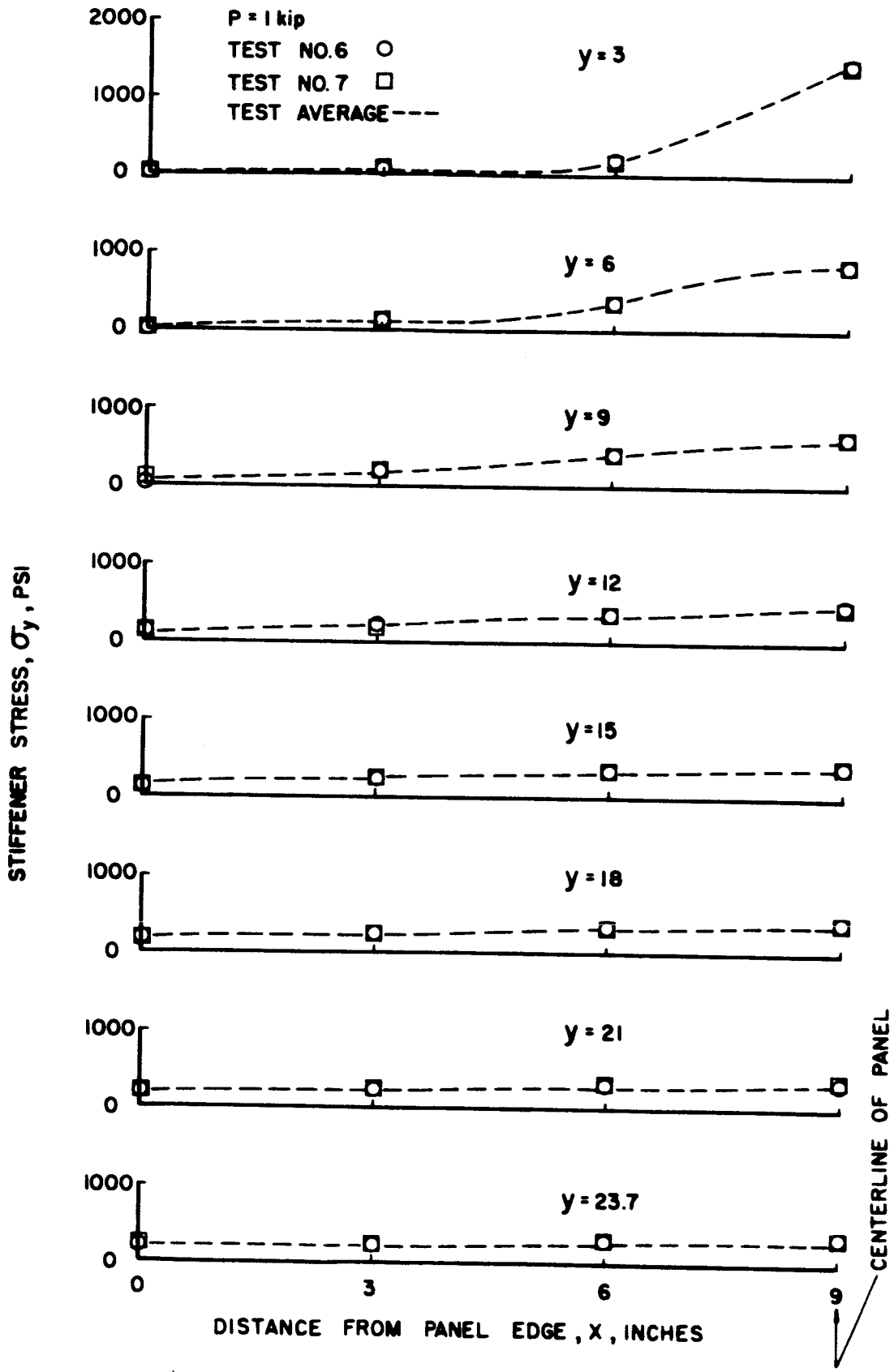

FIGURE F35. - CHORDWISE DISTRIBUTION OF STIFFENER NORMAL STRESS IN PANEL B FOR LOADING CONDITION IV.

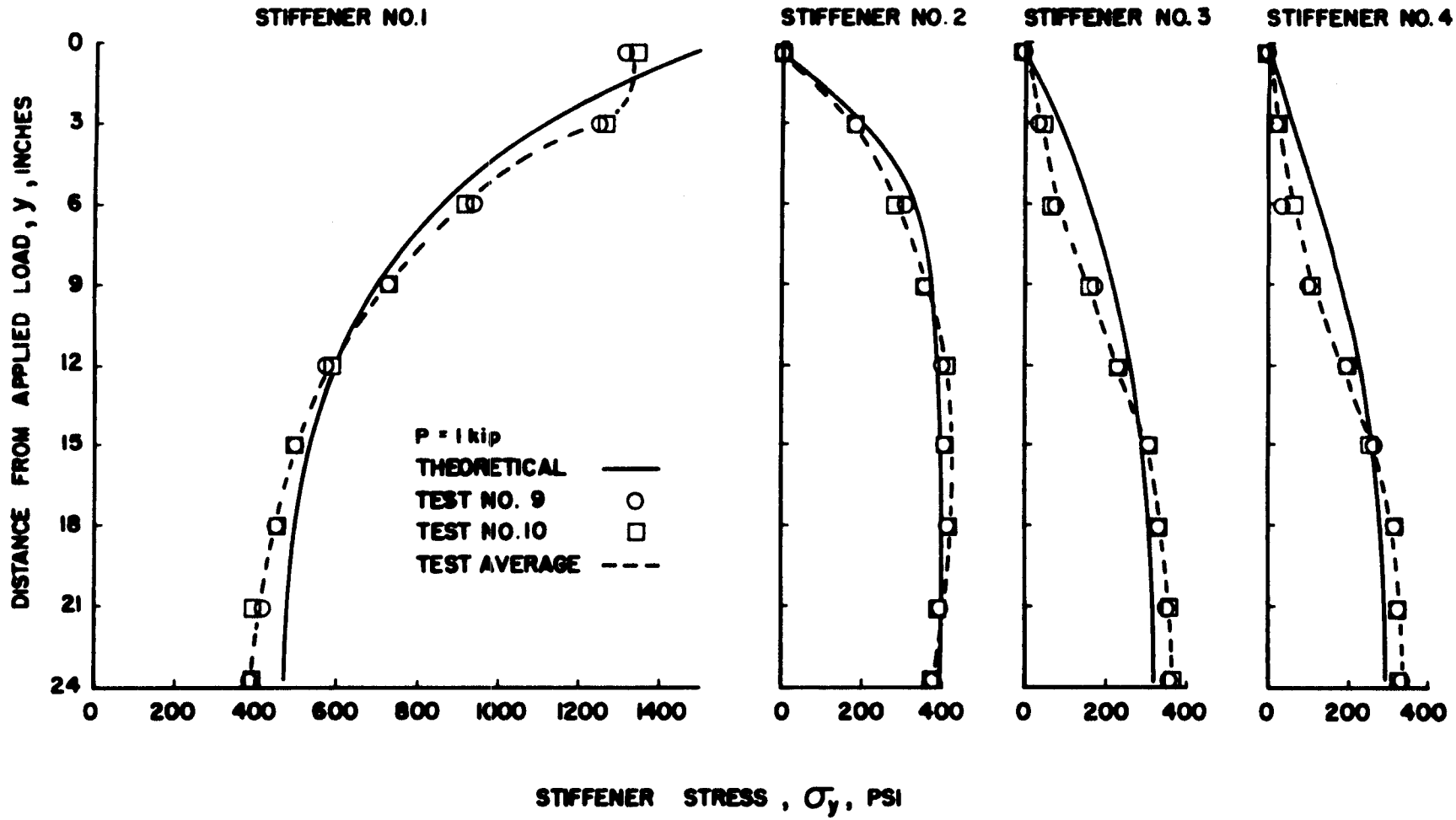

FIGURE F 36. - NORMAL STRESS IN STIFFENERS OF PANEL C FOR LOADING CONDITION I.

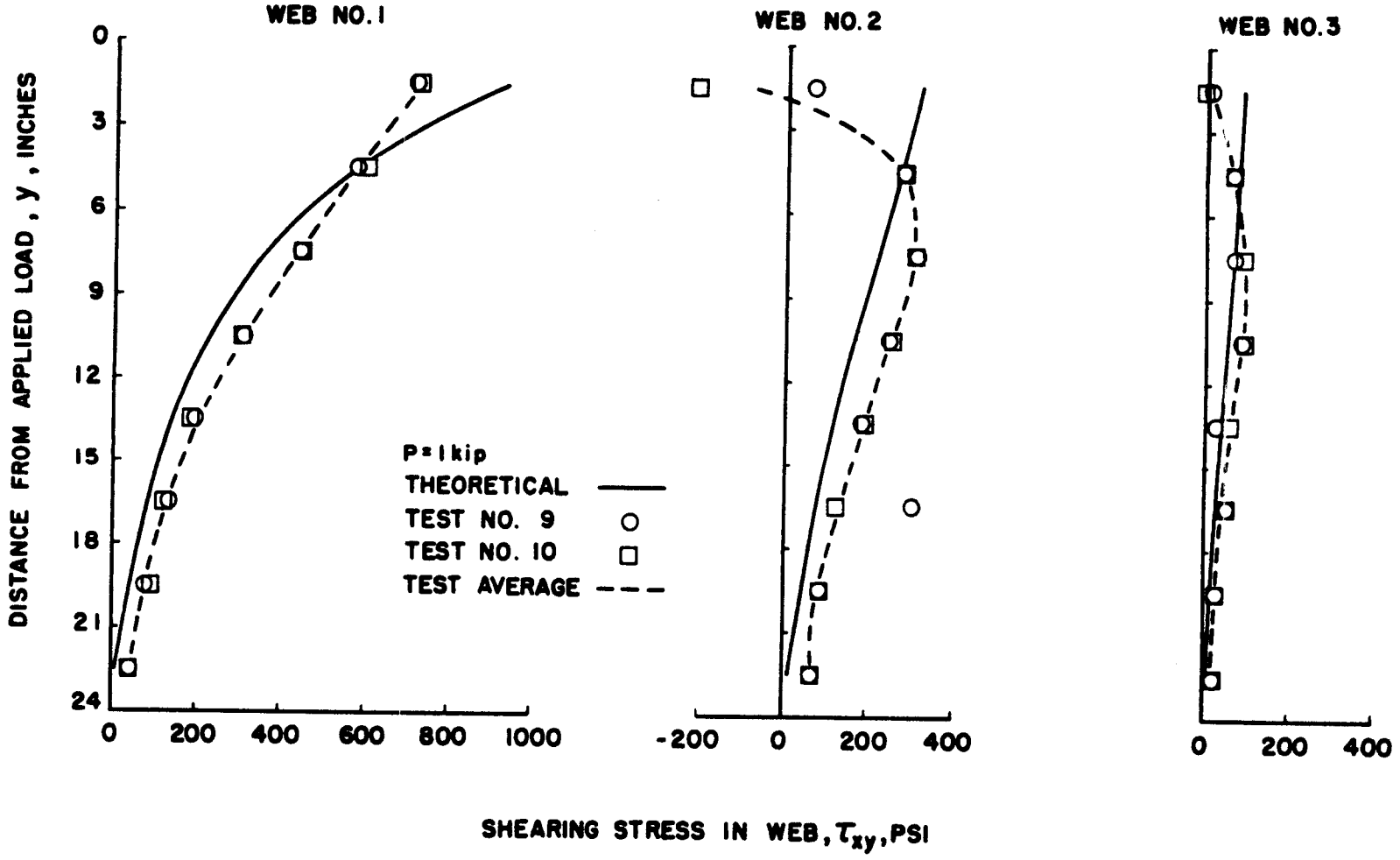

FIGURE F37. - SHEARING STRESS IN WEB OF PANEL C FOR LOADING CONDITION I.

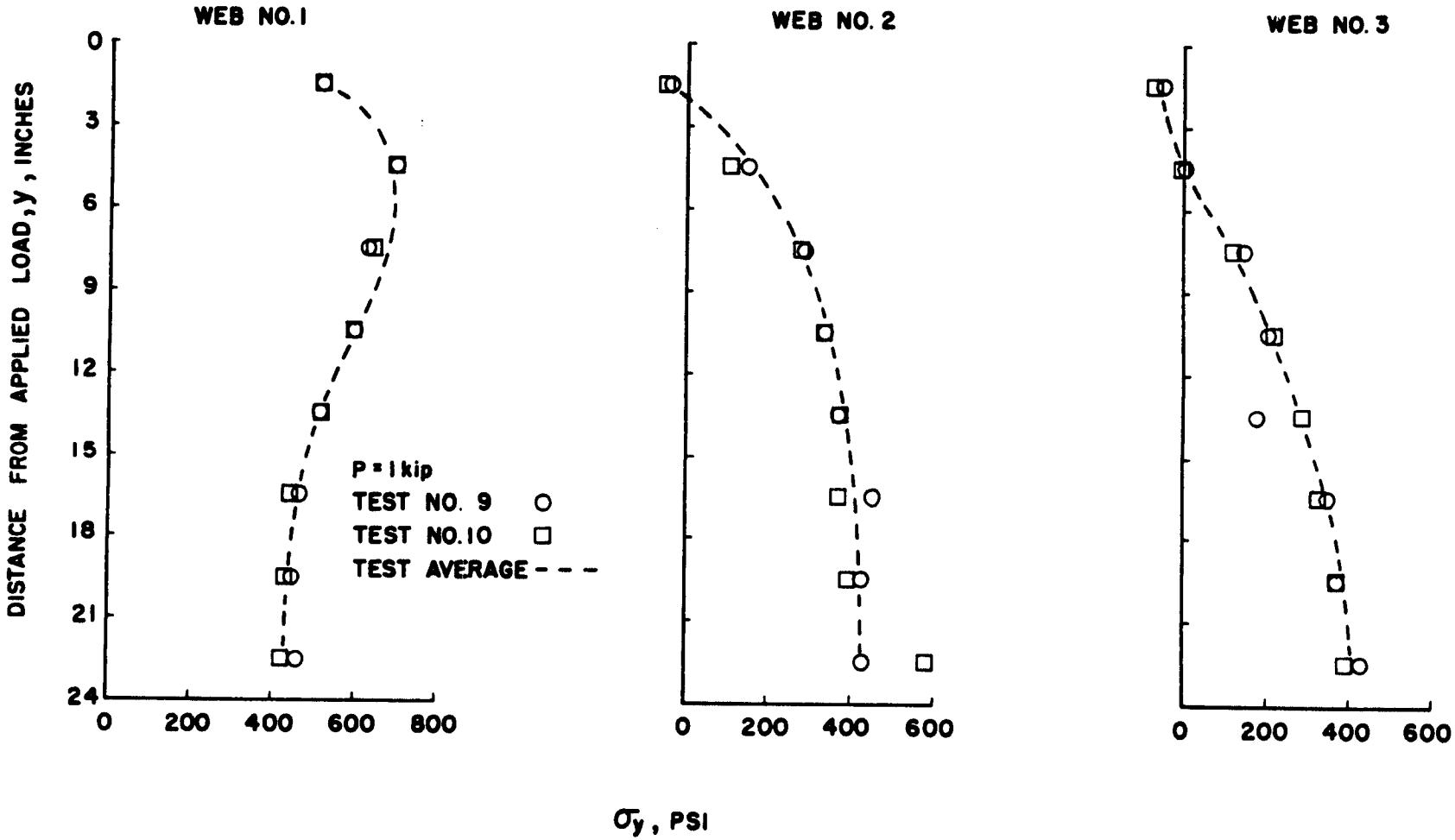

FIGURE F38. - NORMAL STRESS IN WEB OF PANEL C FOR LOADING CONDITION I.

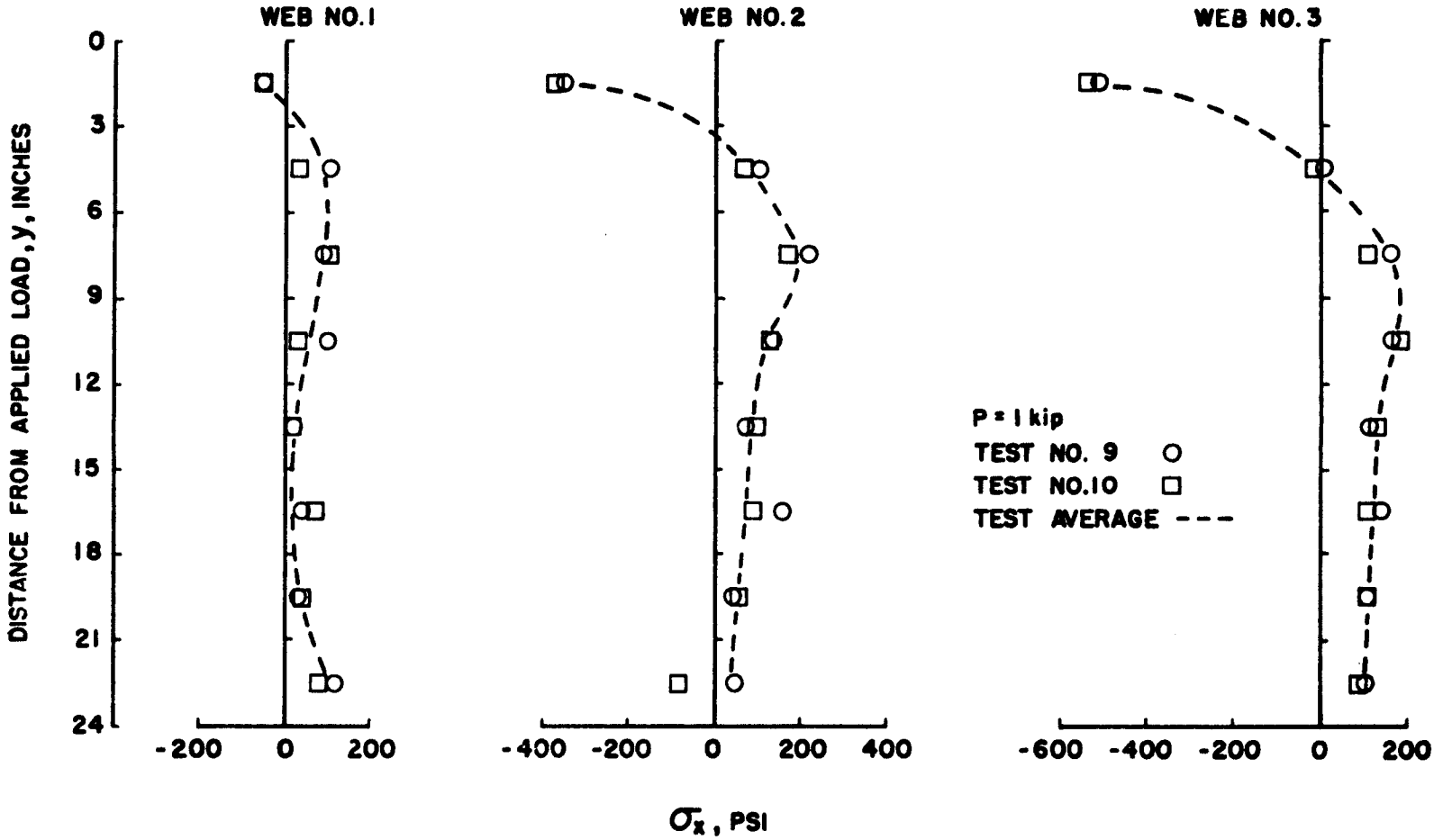

FIGURE F39. - NORMAL STRESS IN WEB OF PANEL C FOR LOADING CONDITION I.

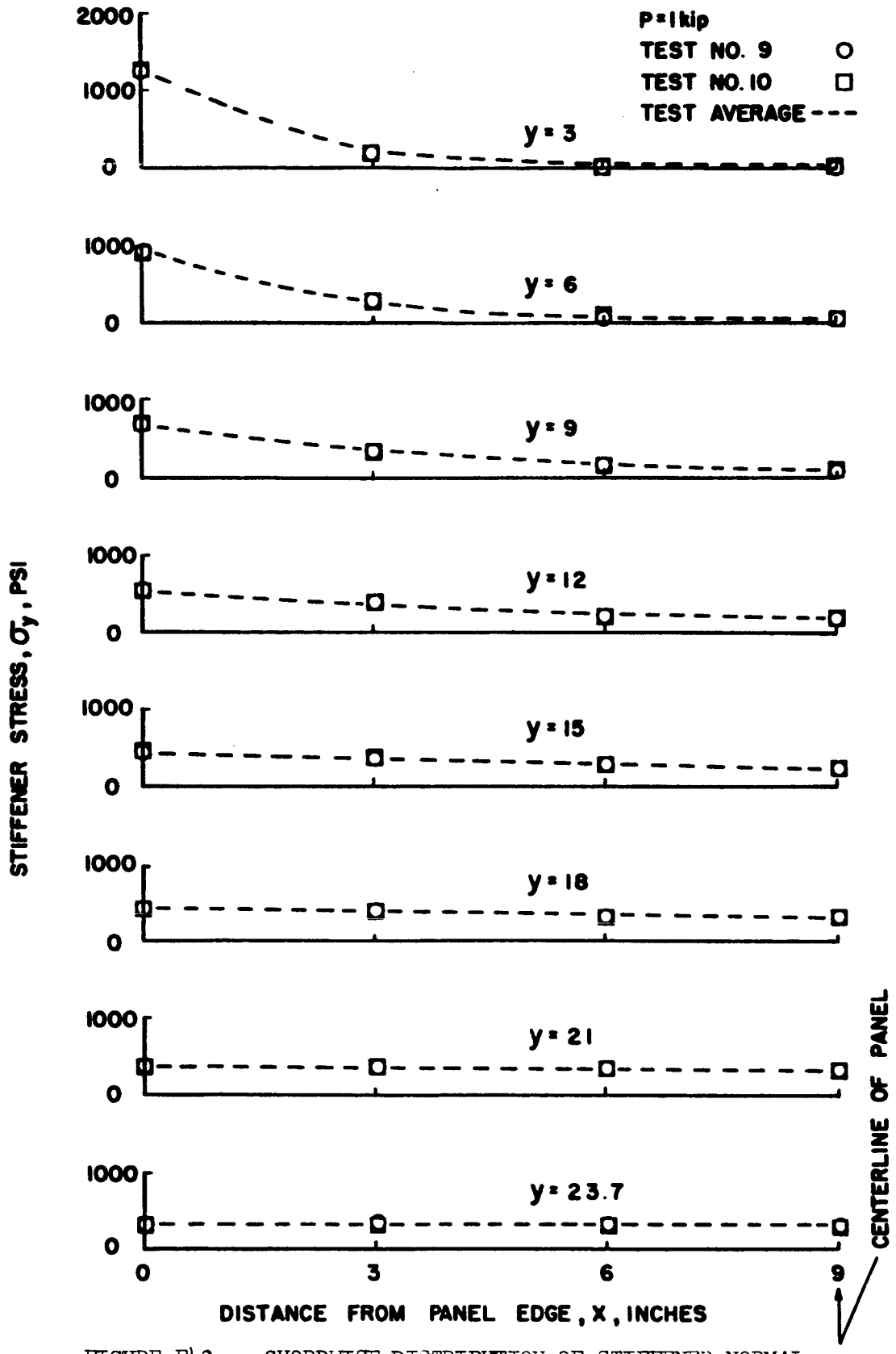

FIGURE F40. - CHORDWISE DISTRIBUTION OF STIFFENER NORMAL STRESS IN PANEL C FOR LOADING CONDITION I.

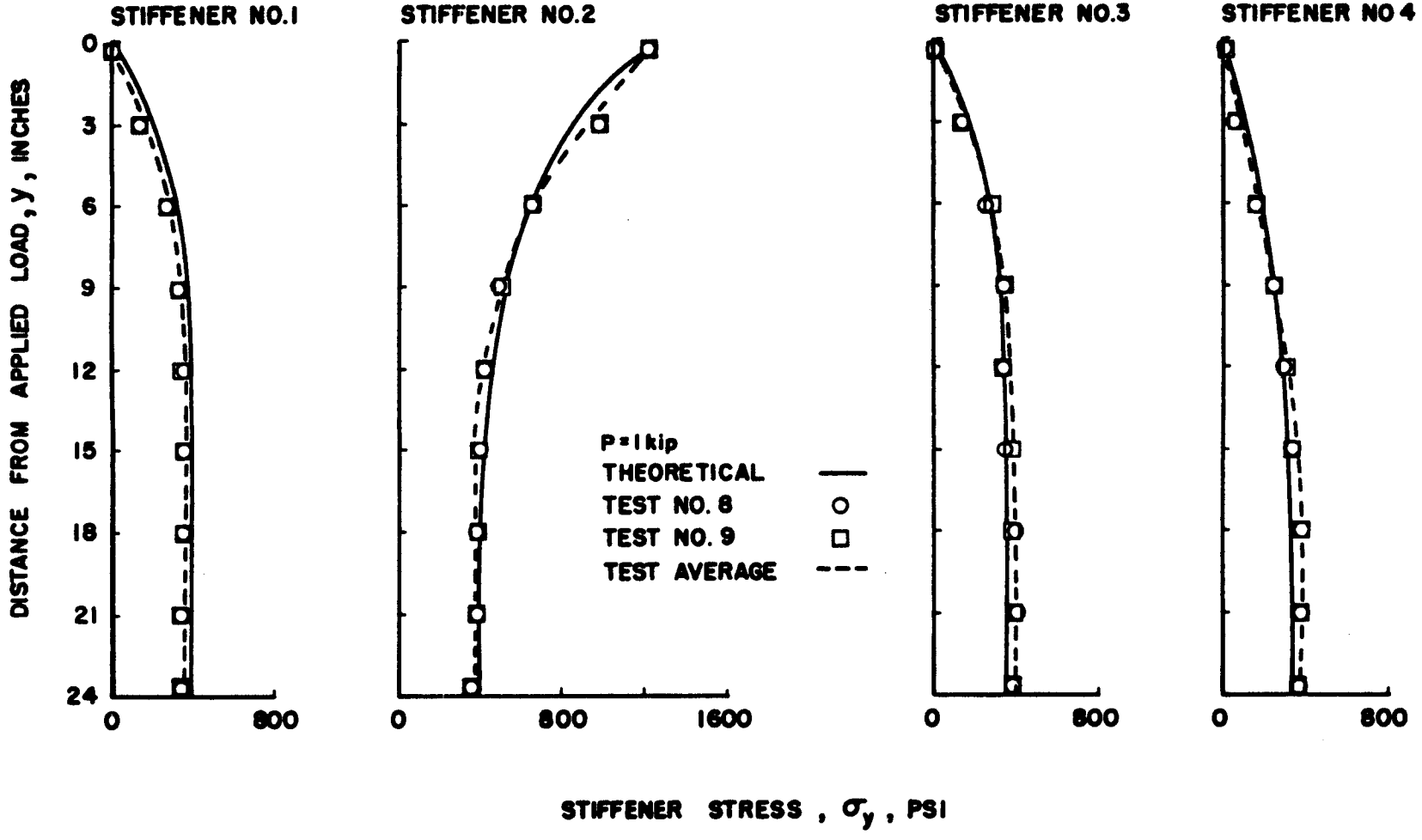

FIGURE F41. - NORMAL STRESS IN STIFFENERS OF PANEL C FOR LOADING CONDITION II.

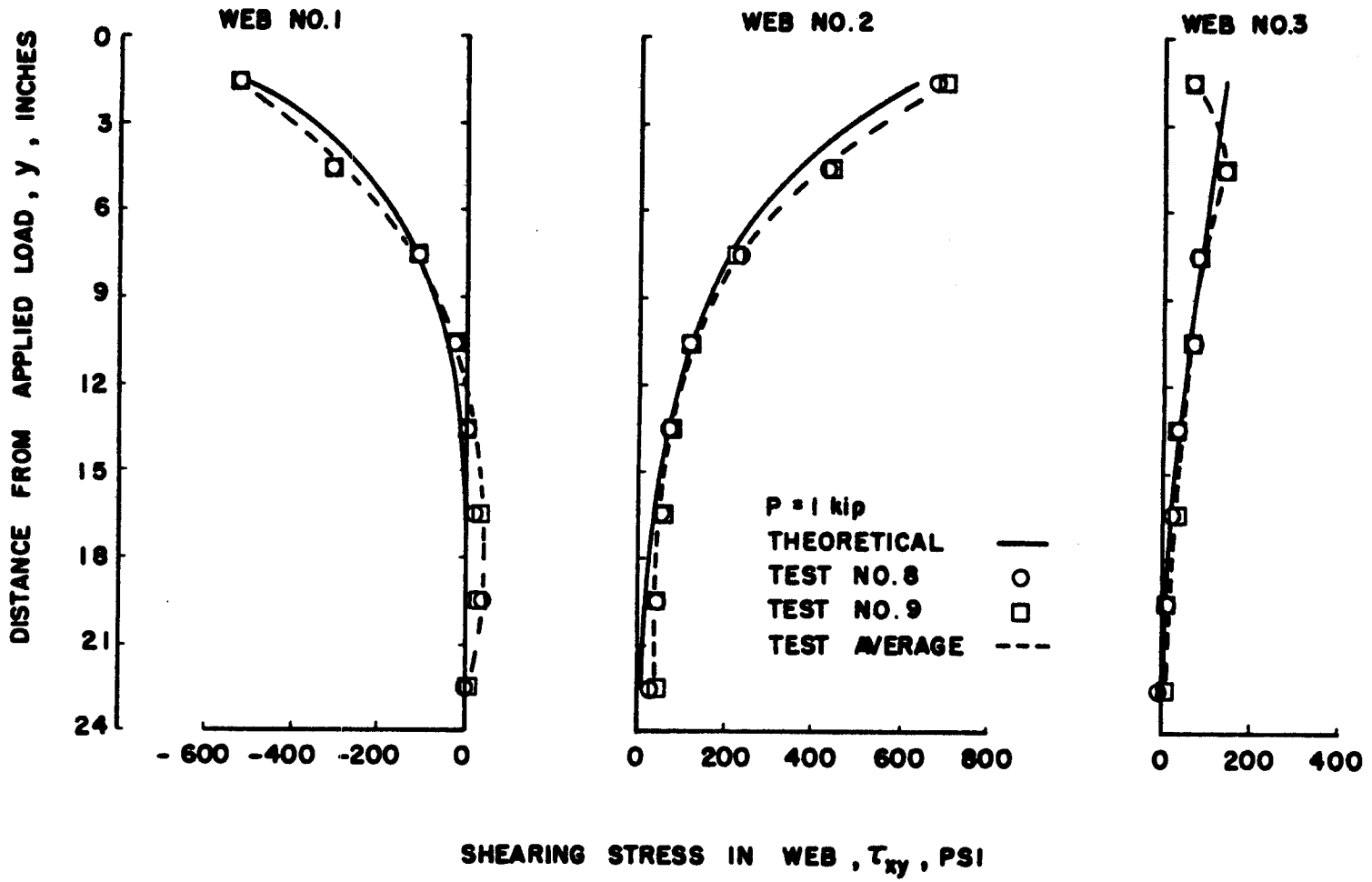

FIGURE F42. - SHEARING STRESS IN WEB OF PANEL C FOR LOADING CONDITION II.

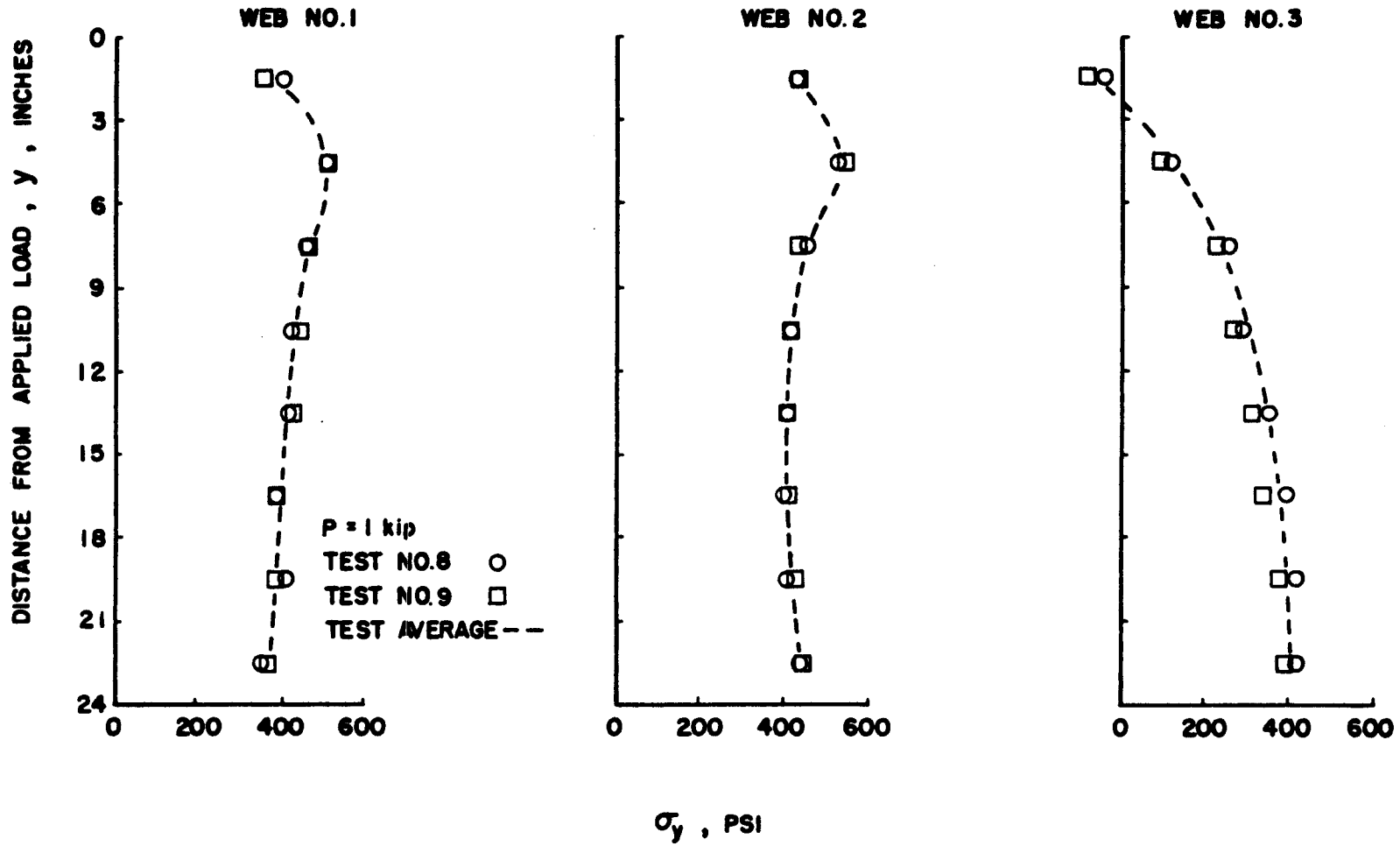

FIGURE F43. - NORMAL STRESS IN WEB OF PANEL C FOR LOADING CONDITION II.

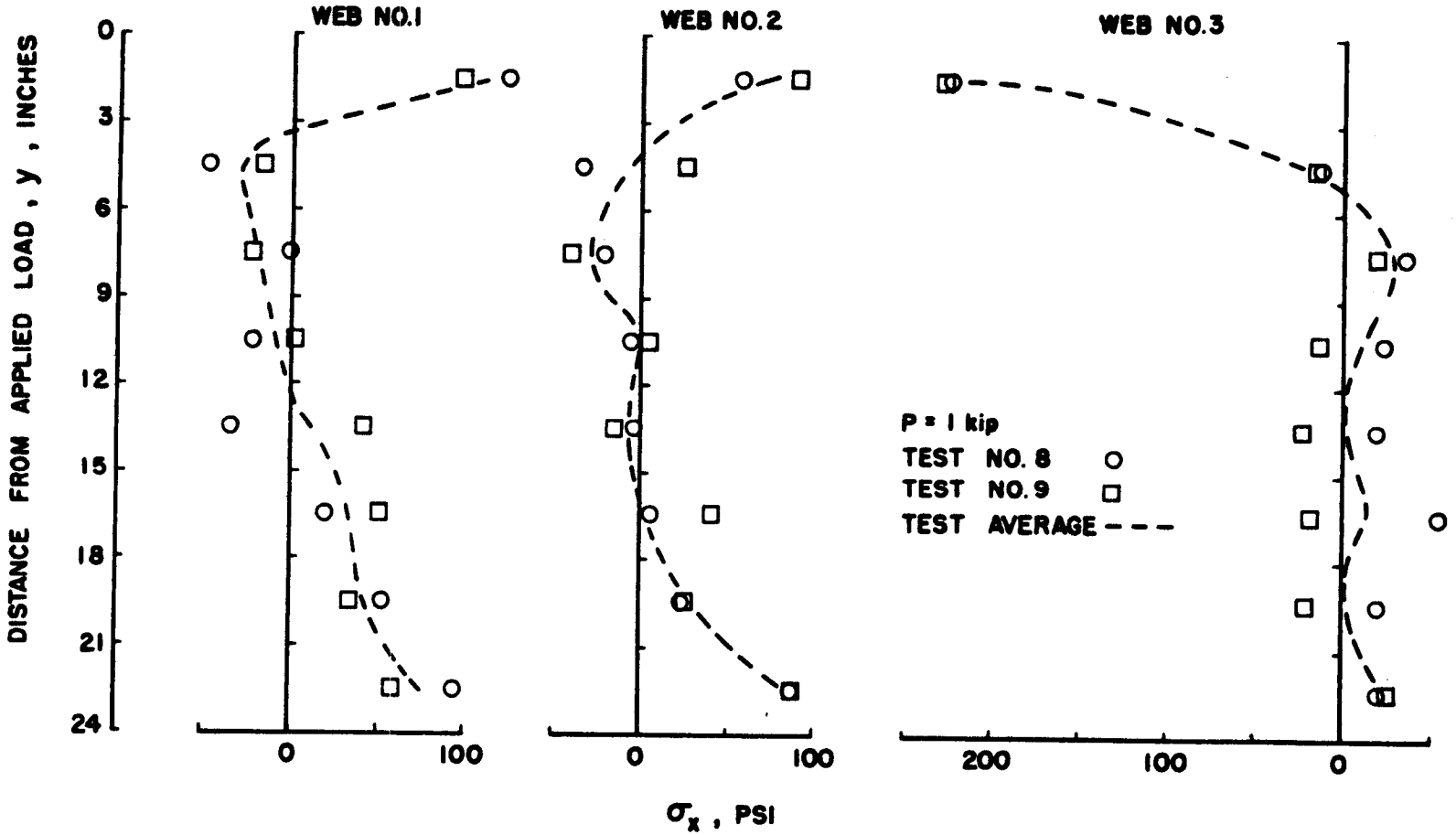

FIGURE F44. - NORMAL STRESS IN WEB OF PANEL C FOR LOADING CONDITION II.

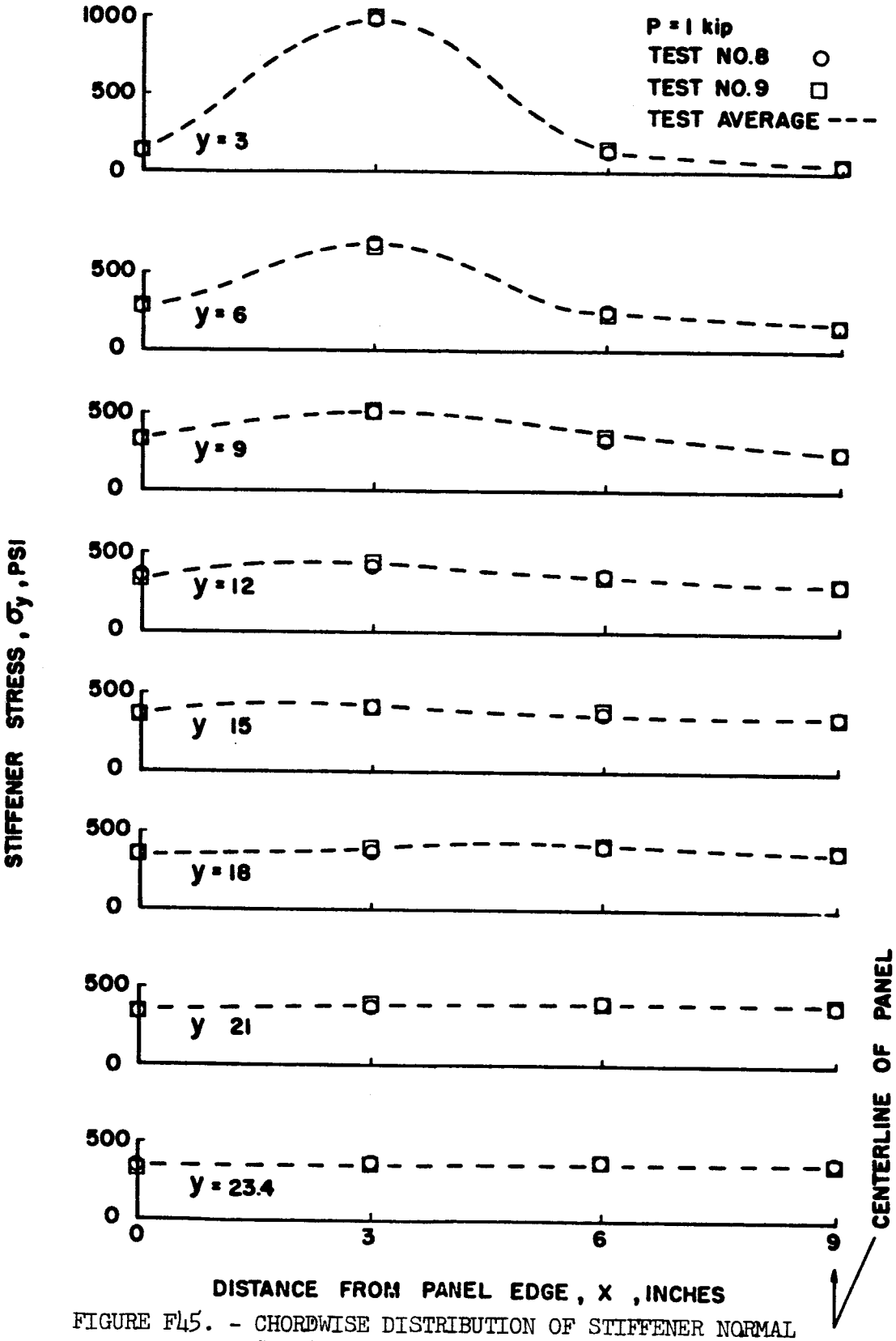

FIGURE F45. - CHORDWISE DISTRIBUTION OF STIFFENER NORMAL STRESS IN PANEL C FOR LOADING CONDITION II.

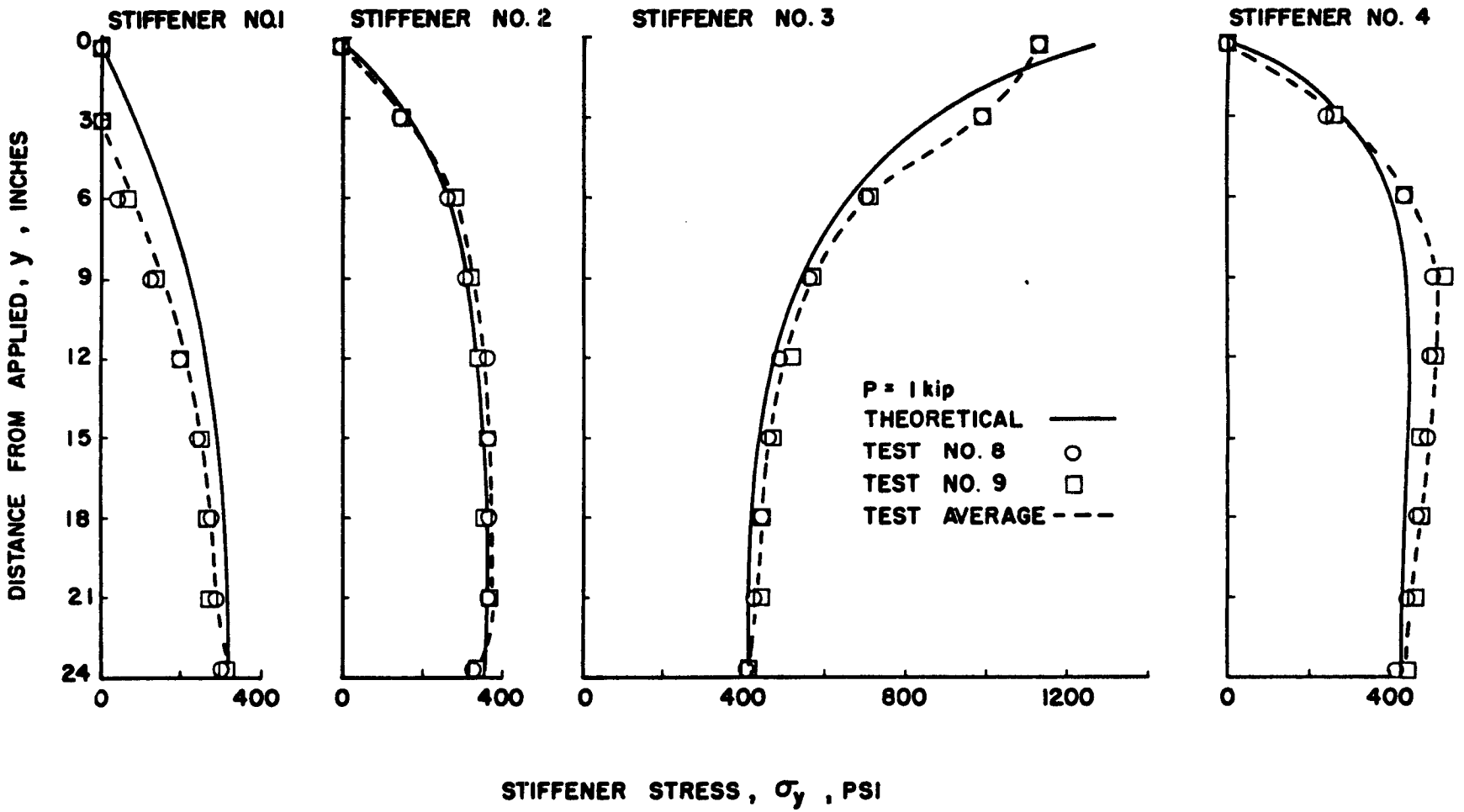

FIGURE F46. - NORMAL STRESS IN STIFFENERS OF PANEL C FOR LOADING CONDITION III.

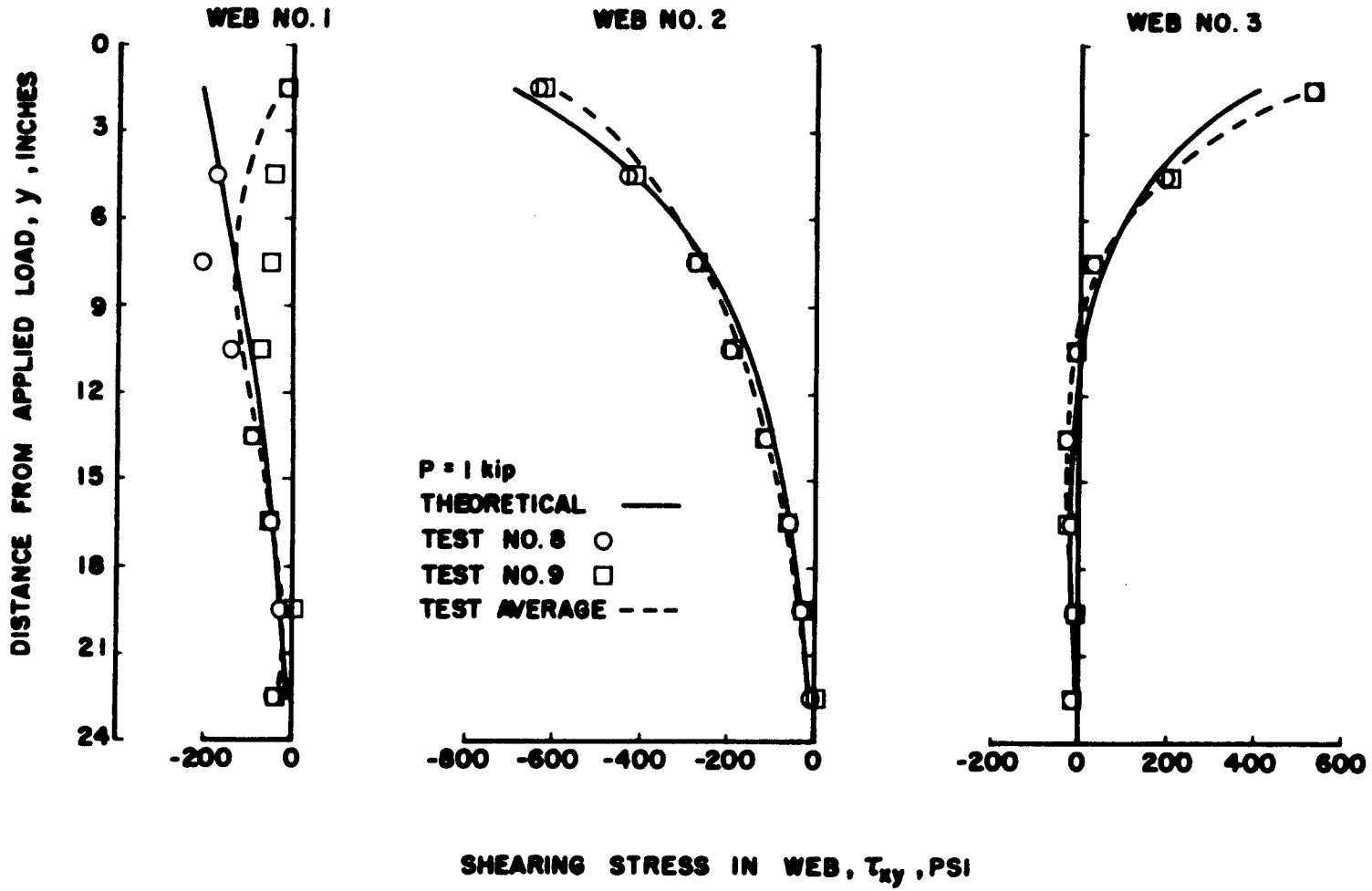

FIGURE F47. - SHEARING STRESS IN WEB OF PANEL C FOR LOADING CONDITION III.

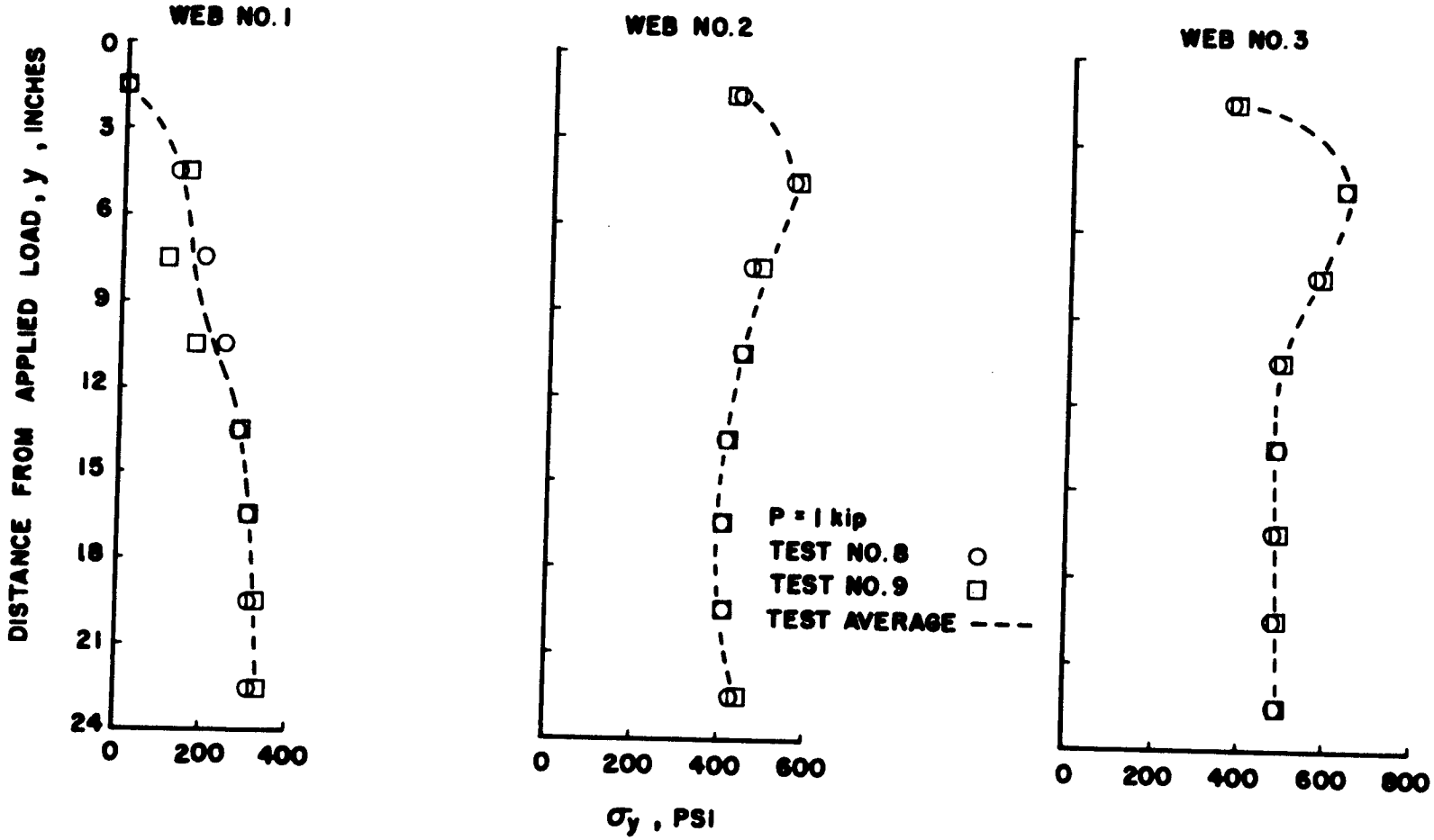

FIGURE F48. - NORMAL STRESS IN WEB OF PANEL C FOR LOADING CONDITION III.

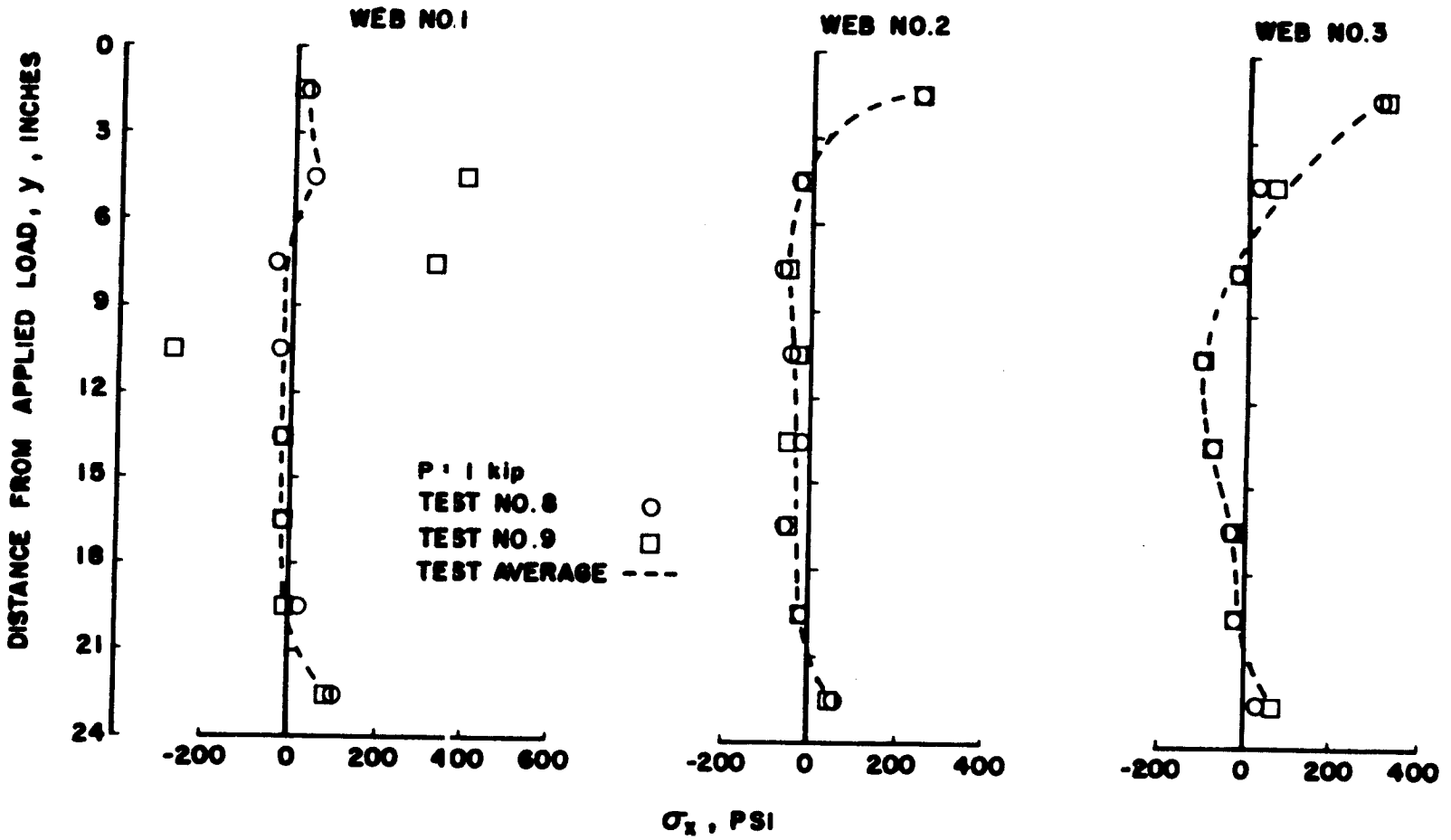

FIGURE F49. - NORMAL STRESS IN WEB OF PANEL C FOR LOADING CONDITION III.

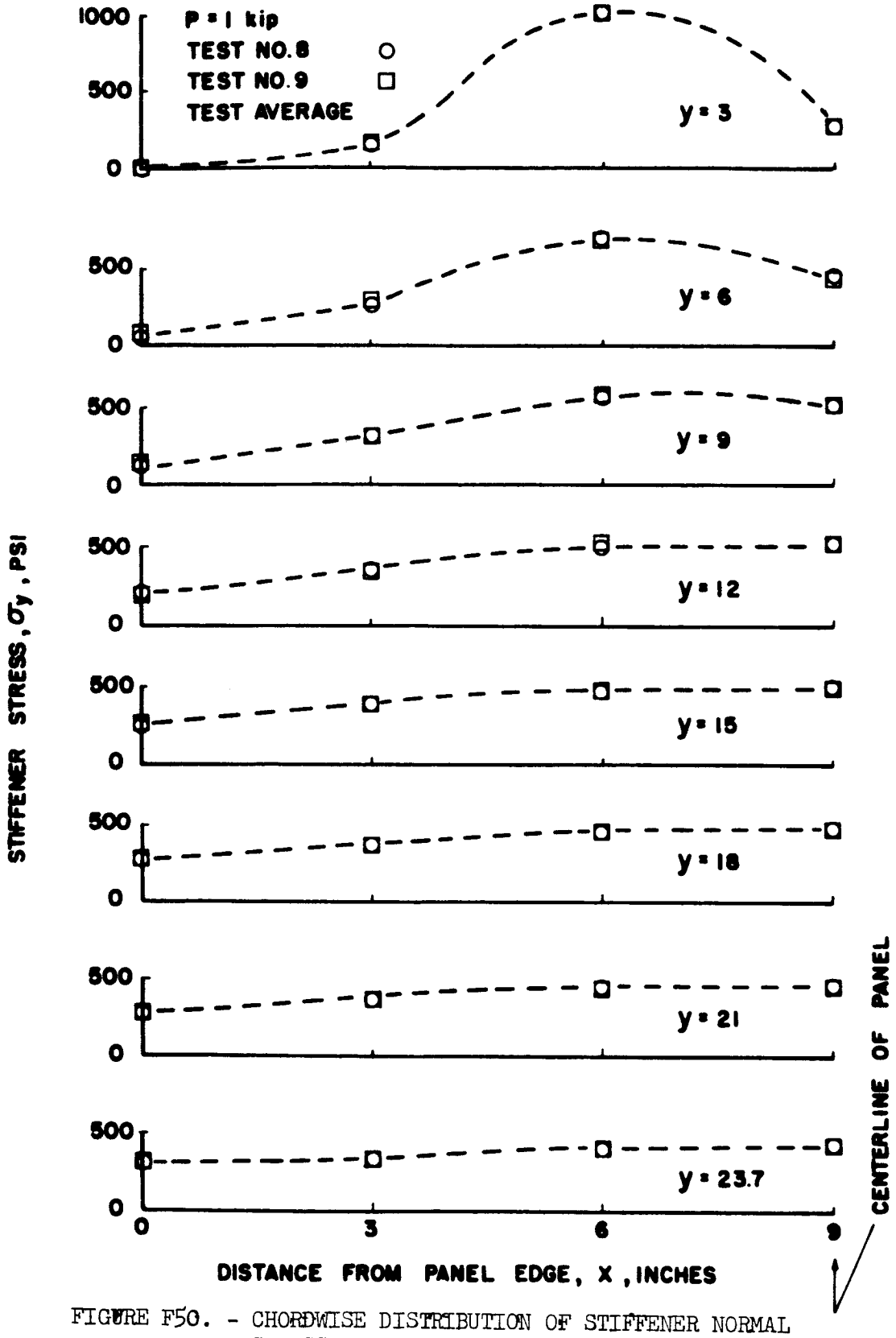

FIGURE F50. - CHORDWISE DISTRIBUTION OF STIFFENER NORMAL STRESS IN PANEL C FOR LOADING CONDITION III.

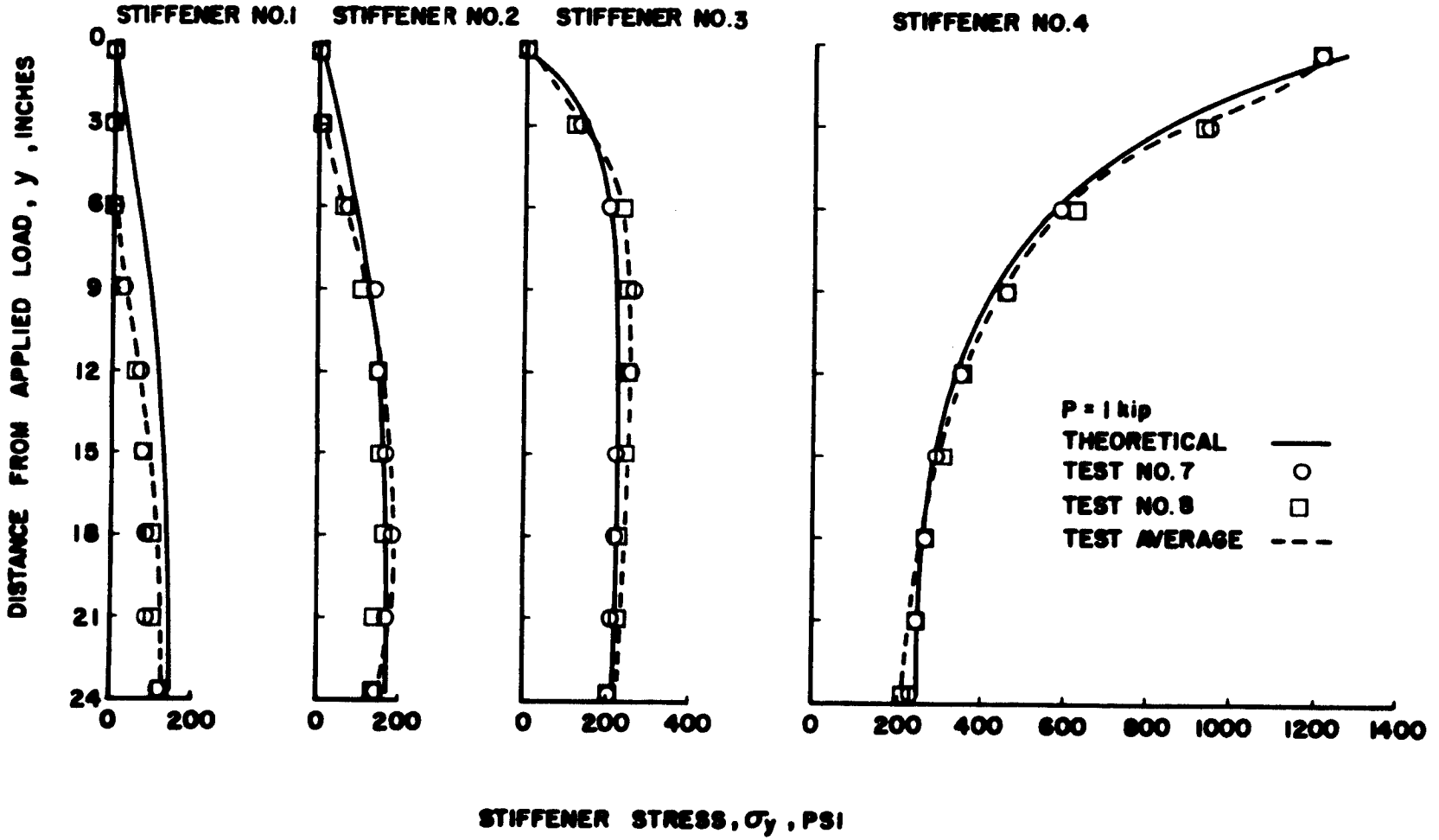

FIGURE F51. - NORMAL STRESS IN STIFFENERS OF PANEL C FOR LOADING CONDITION IV.

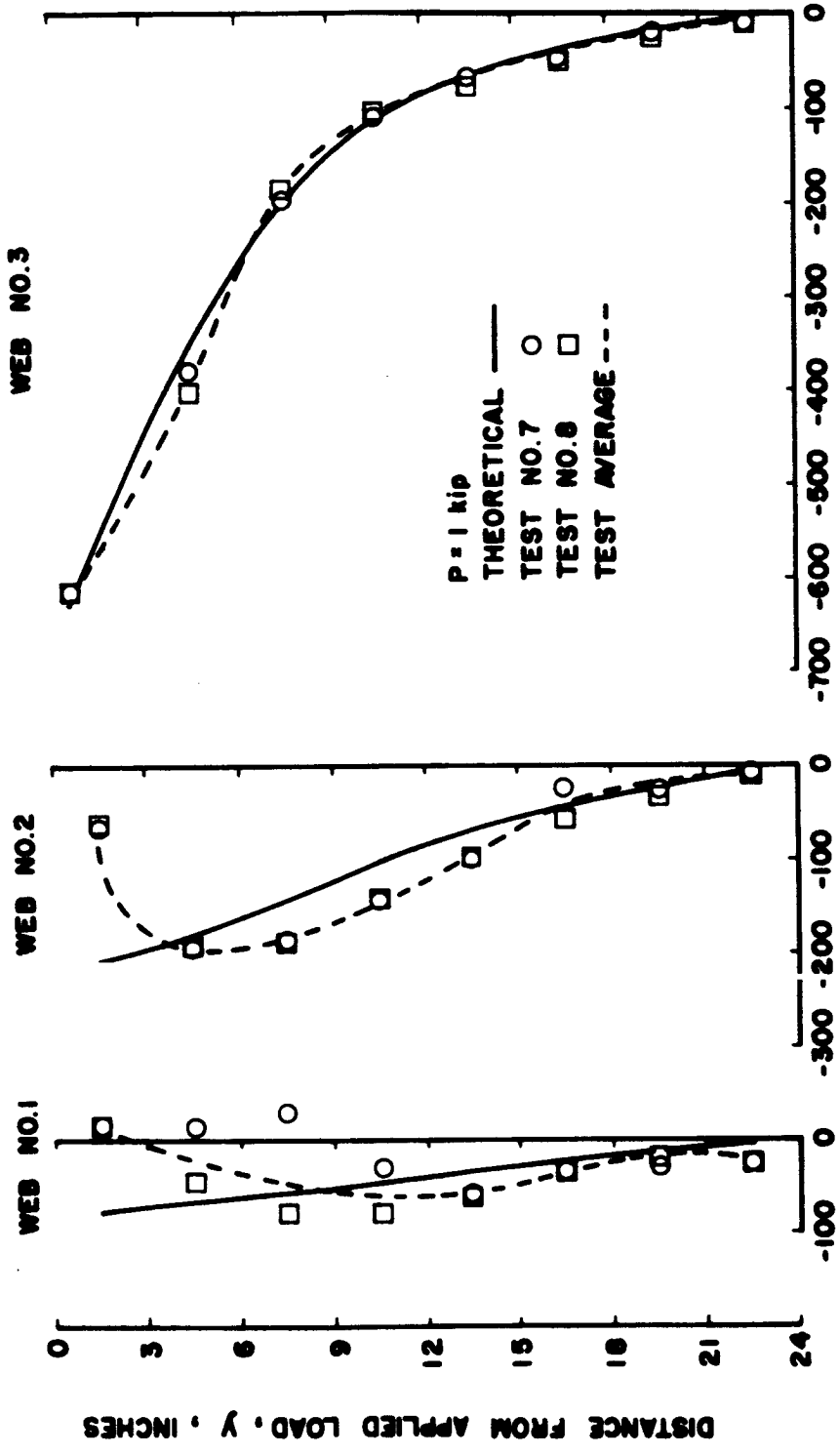

FIGURE F52. - SHEARING STRESS IN WEB OF PANEL C FOR LOADING CONDITION IV.

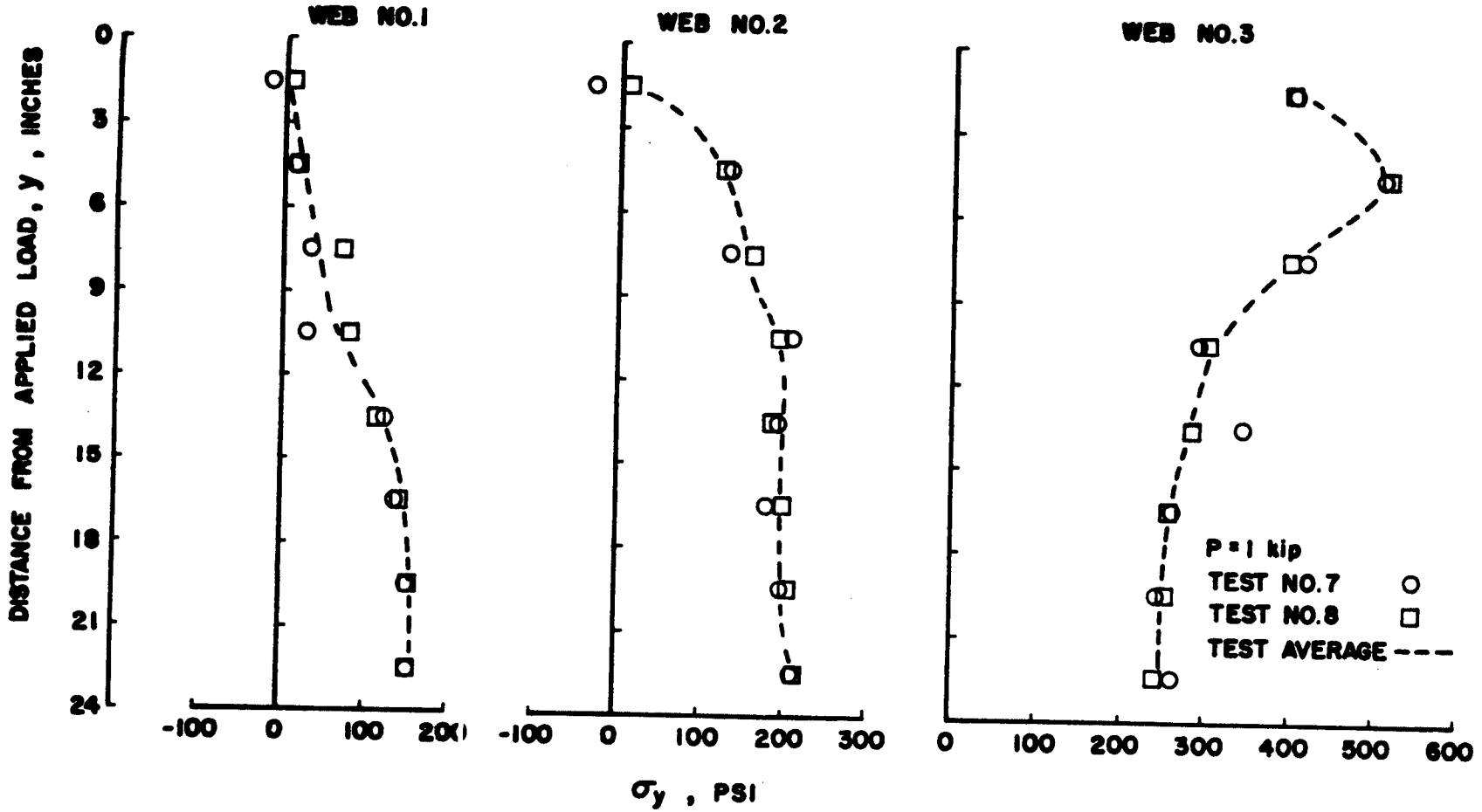

FIGURE F53. - NORMAL STRESS IN WEB OF PANEL C FOR LOADING CONDITION IV.

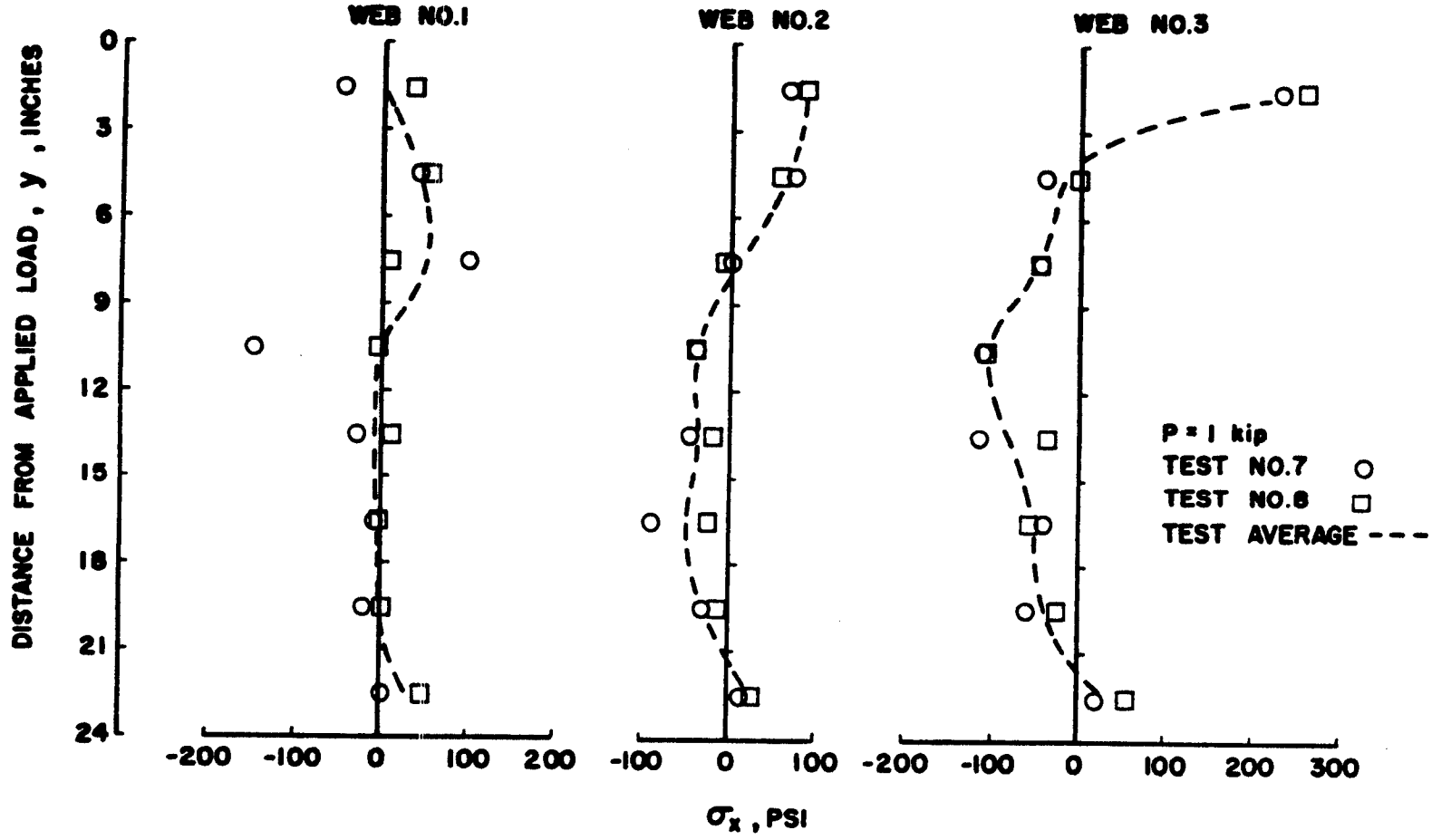

FIGURE F54. - NORMAL STRESS IN WEB OF PANEL C FOR LOADING CONDITION IV.

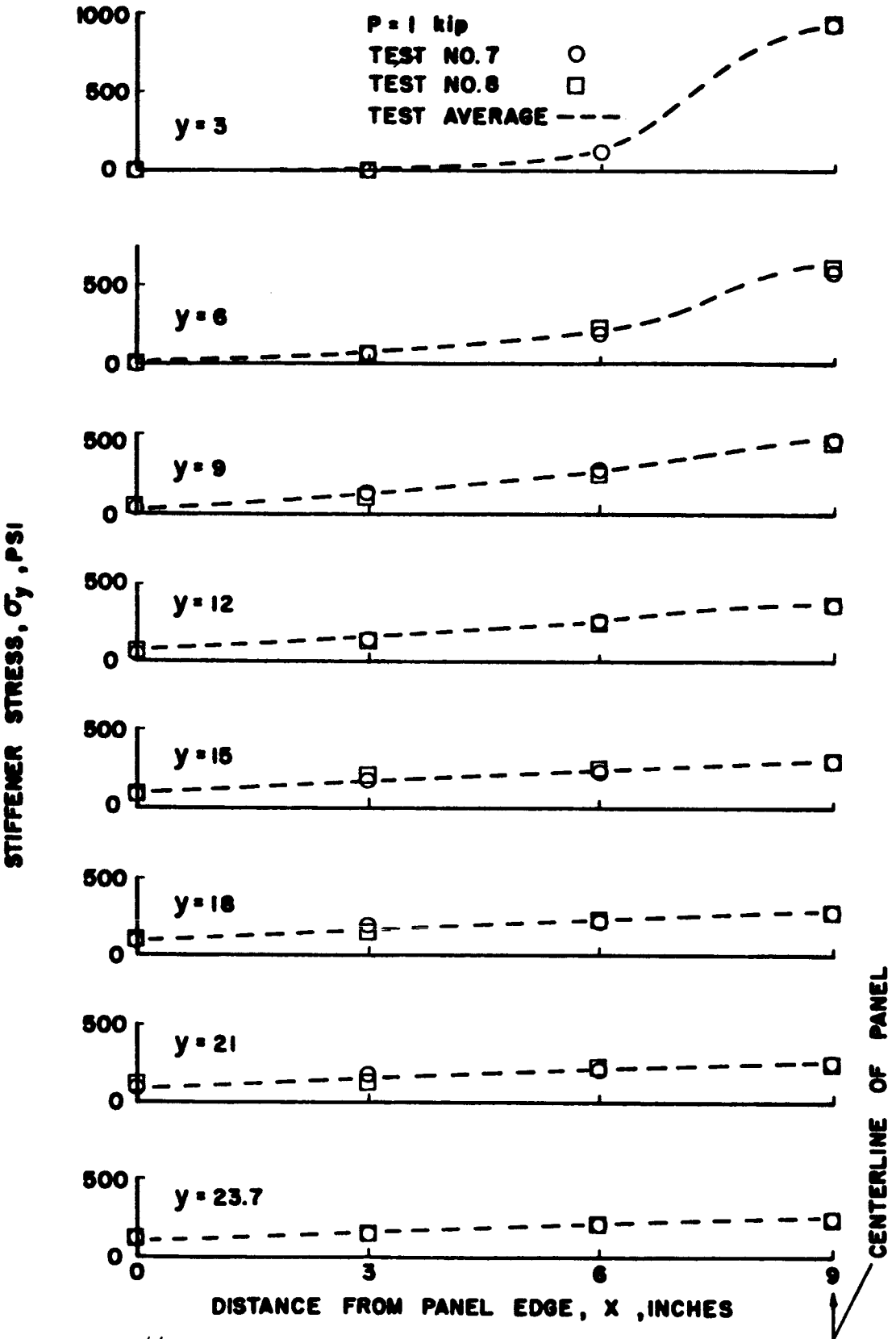

FIGURE F55. - CHORDWISE DISTRIBUTION OF STIFFENER NORMAL STRESS IN PANEL C FOR LOADING CONDITION IV.

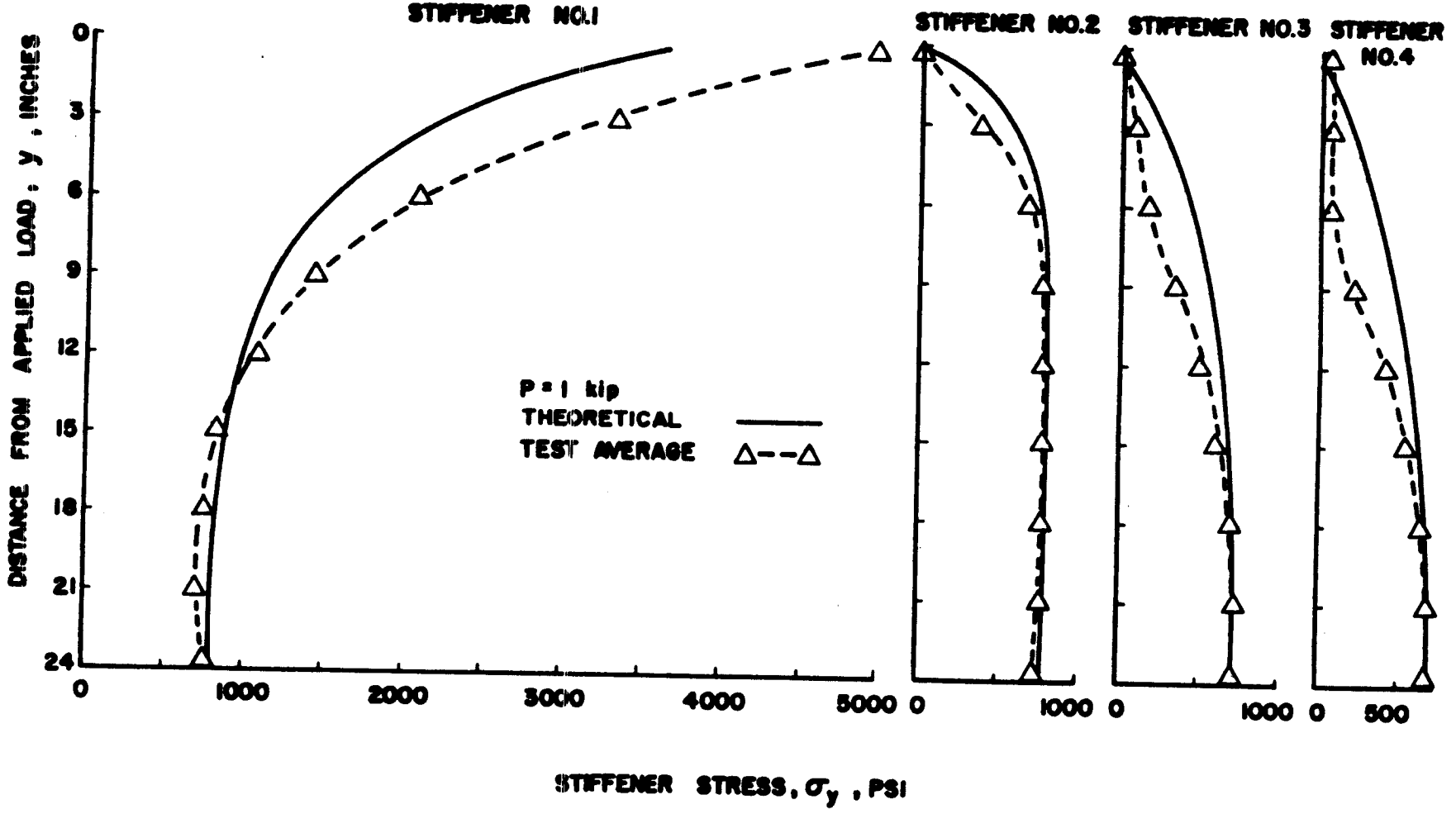

FIGURE F56. - NORMAL STRESS IN STIFFENERS OF PANEL D FOR LOADING CONDITION I.

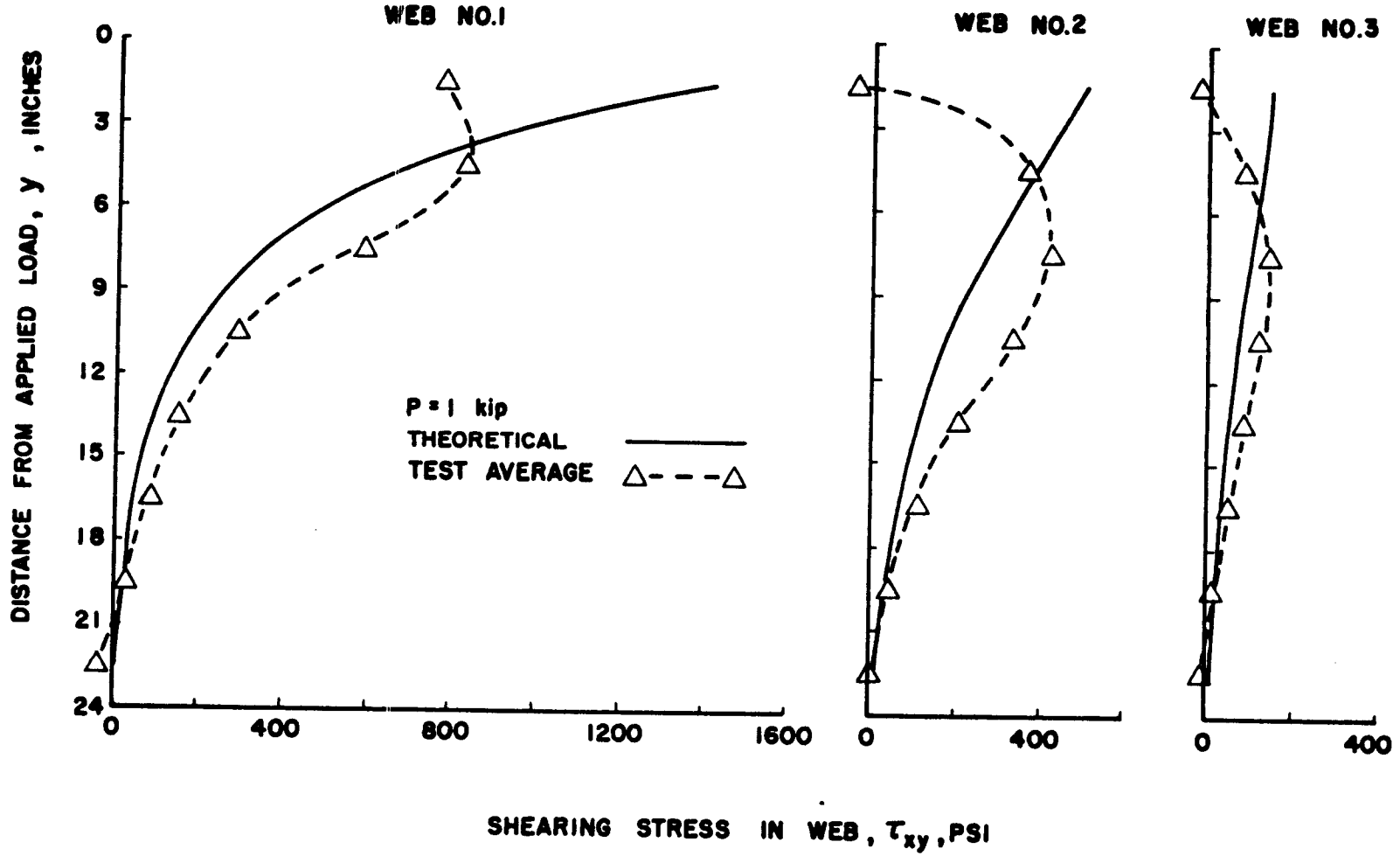

FIGURE F57. - SHEARING STRESS IN WEB OF PANEL D FOR LOADING CONDITION I.

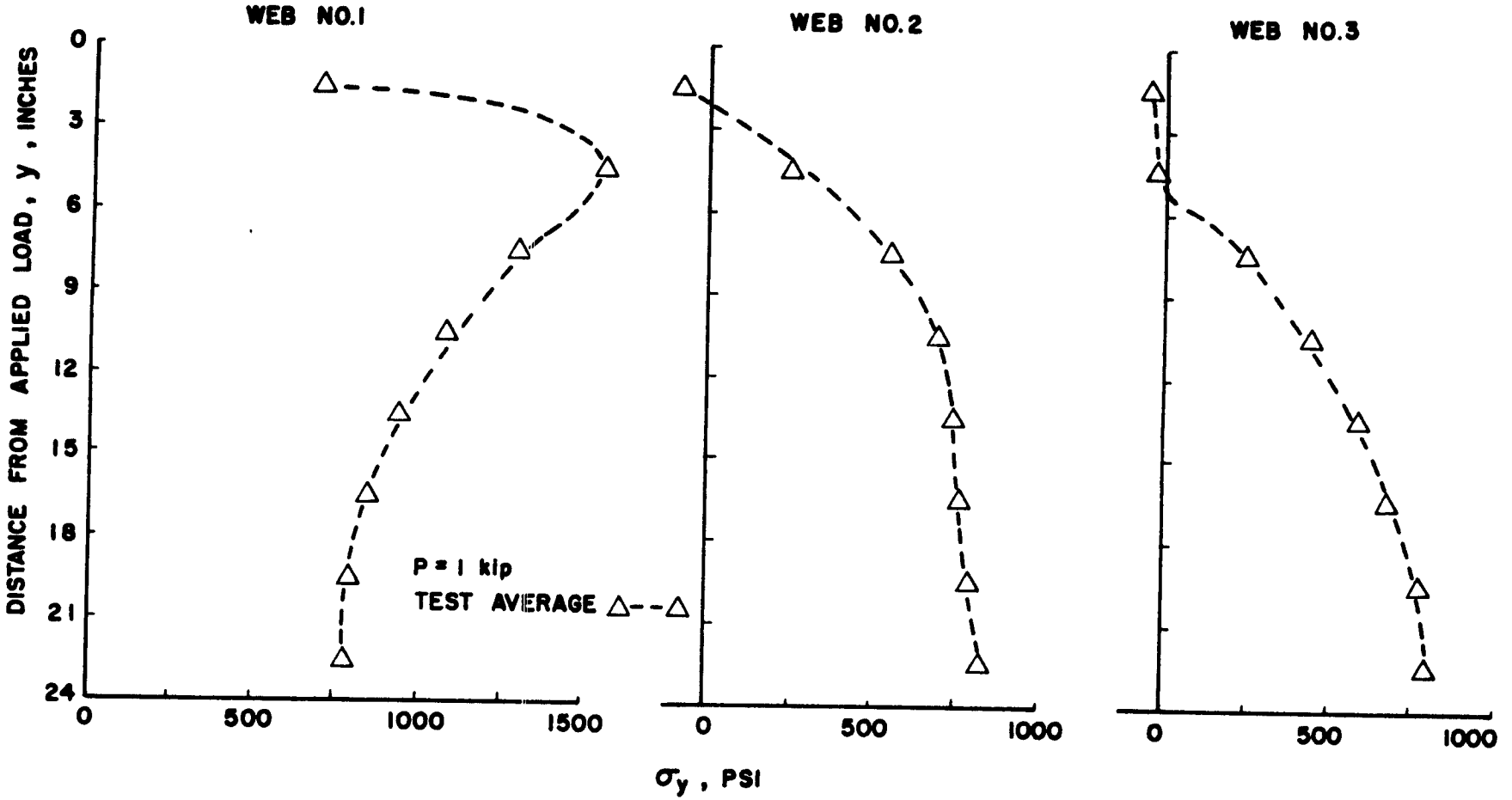

FIGURE F58. - NORMAL STRESS IN WEB OF PANEL D FOR LOADING CONDITION I.

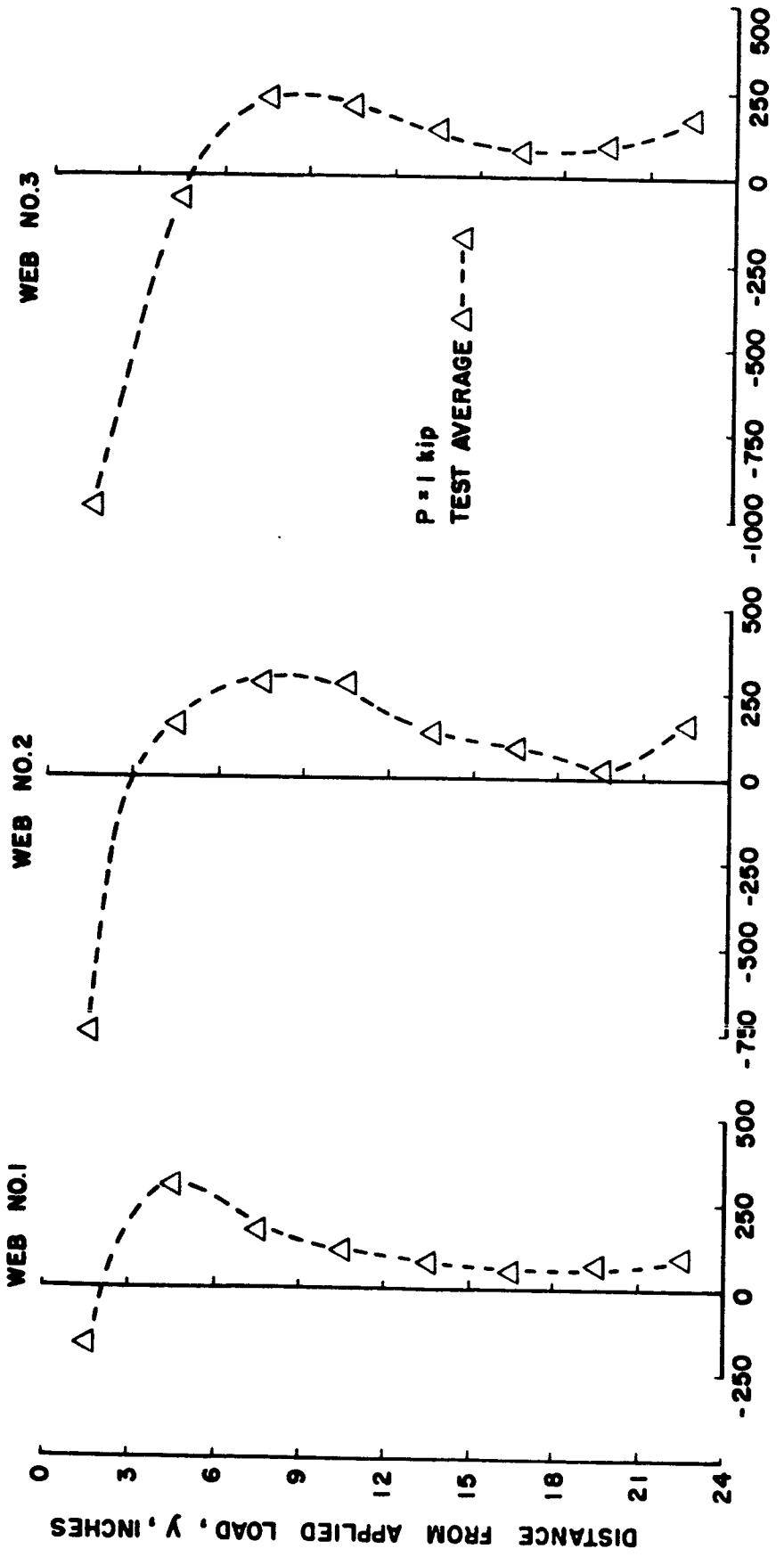

FIGURE F59. - NORMAL STRESS IN WEB OF PANEL D FOR LOADING CONDITION I.

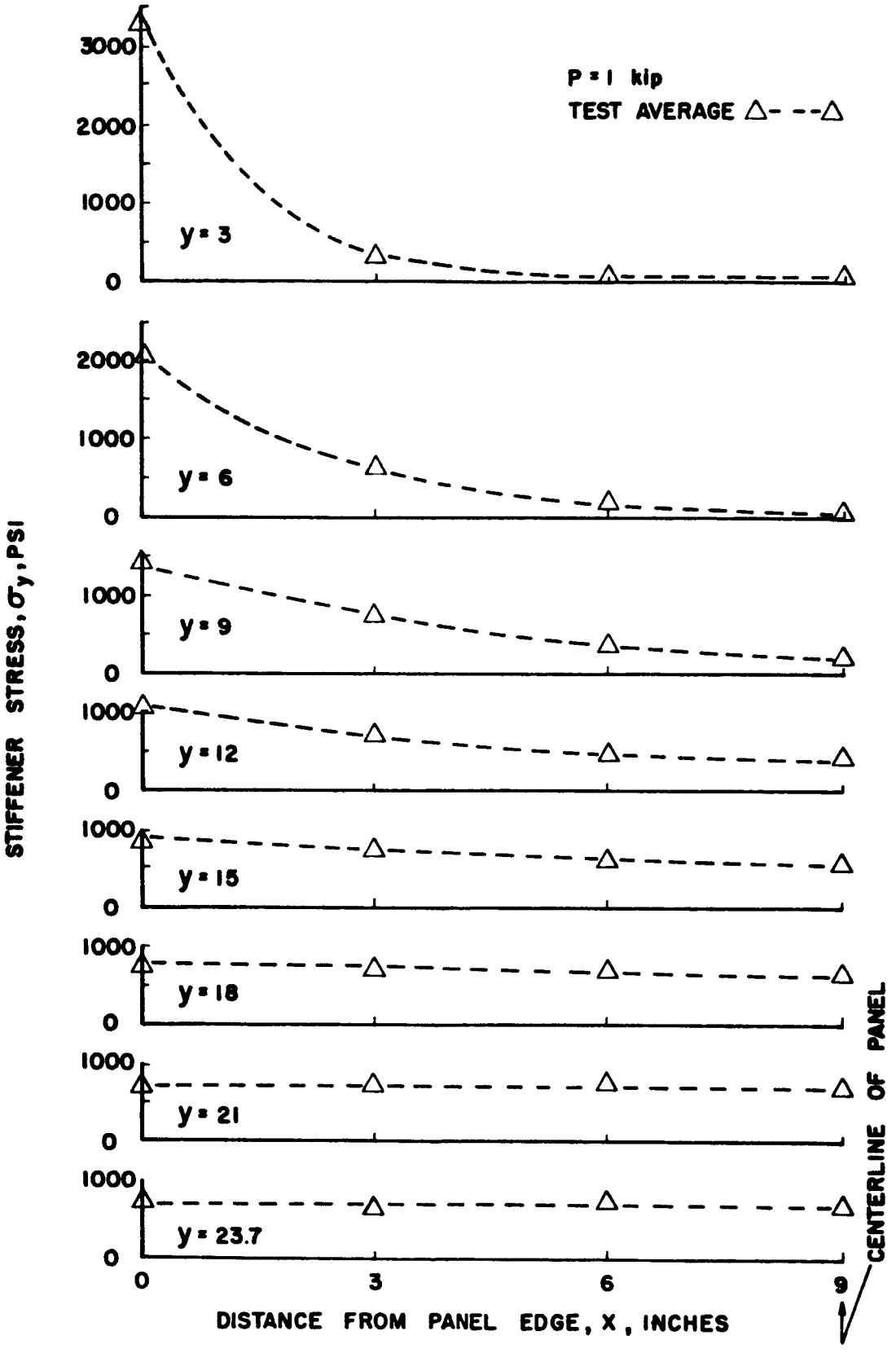

FIGURE F60. - CHORDWISE DISTRIBUTION OF STIFFENER NORMAL STRESS IN PANEL D FOR LOADING CONDITION I.

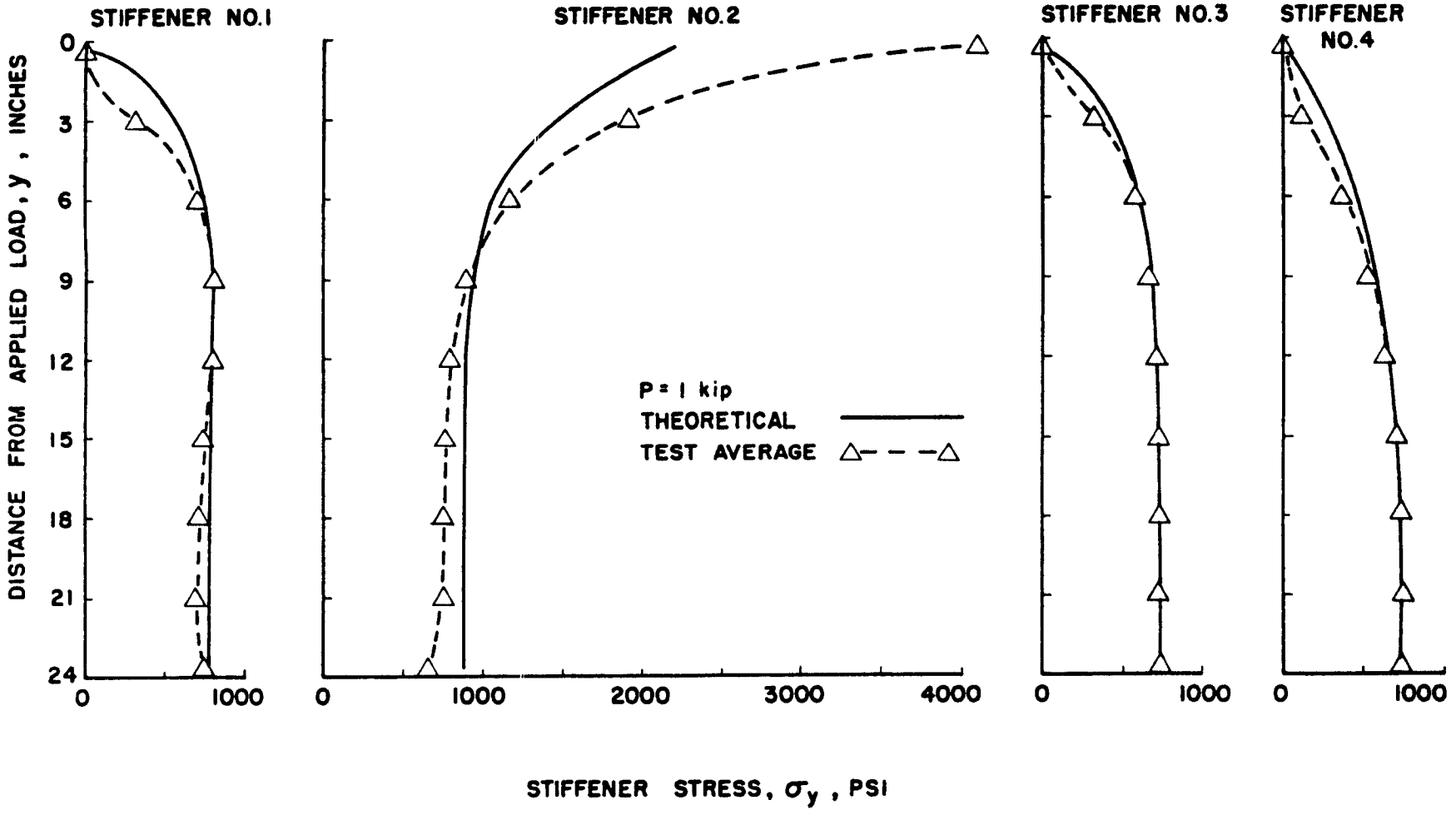

FIGURE F61. - NORMAL STRESS IN STIFFENERS OF PANEL D FOR LOADING CONDITION II.

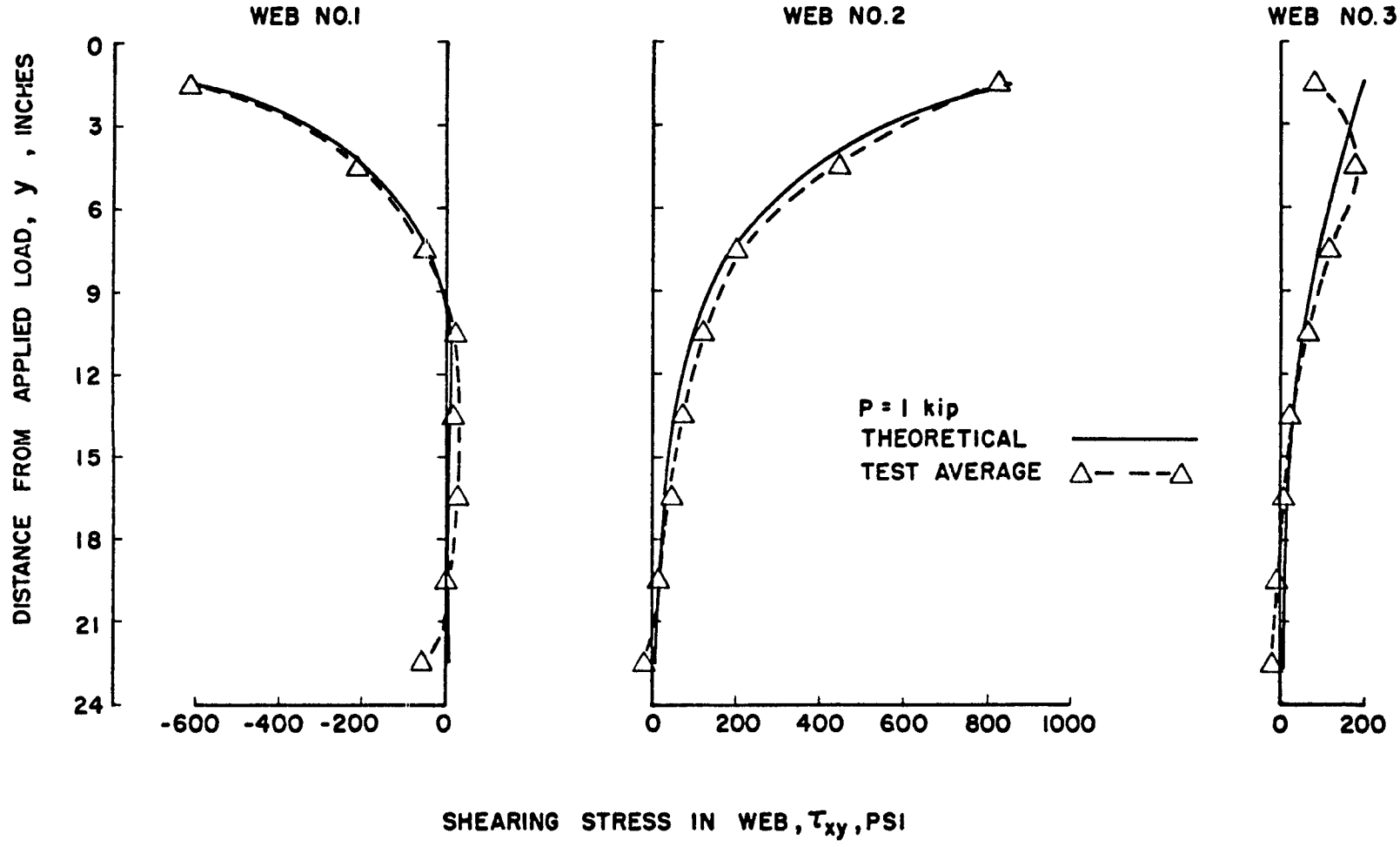

FIGURE F62. - SHEARING STRESS IN WEB OF PANEL D FOR LOADING CONDITION II.

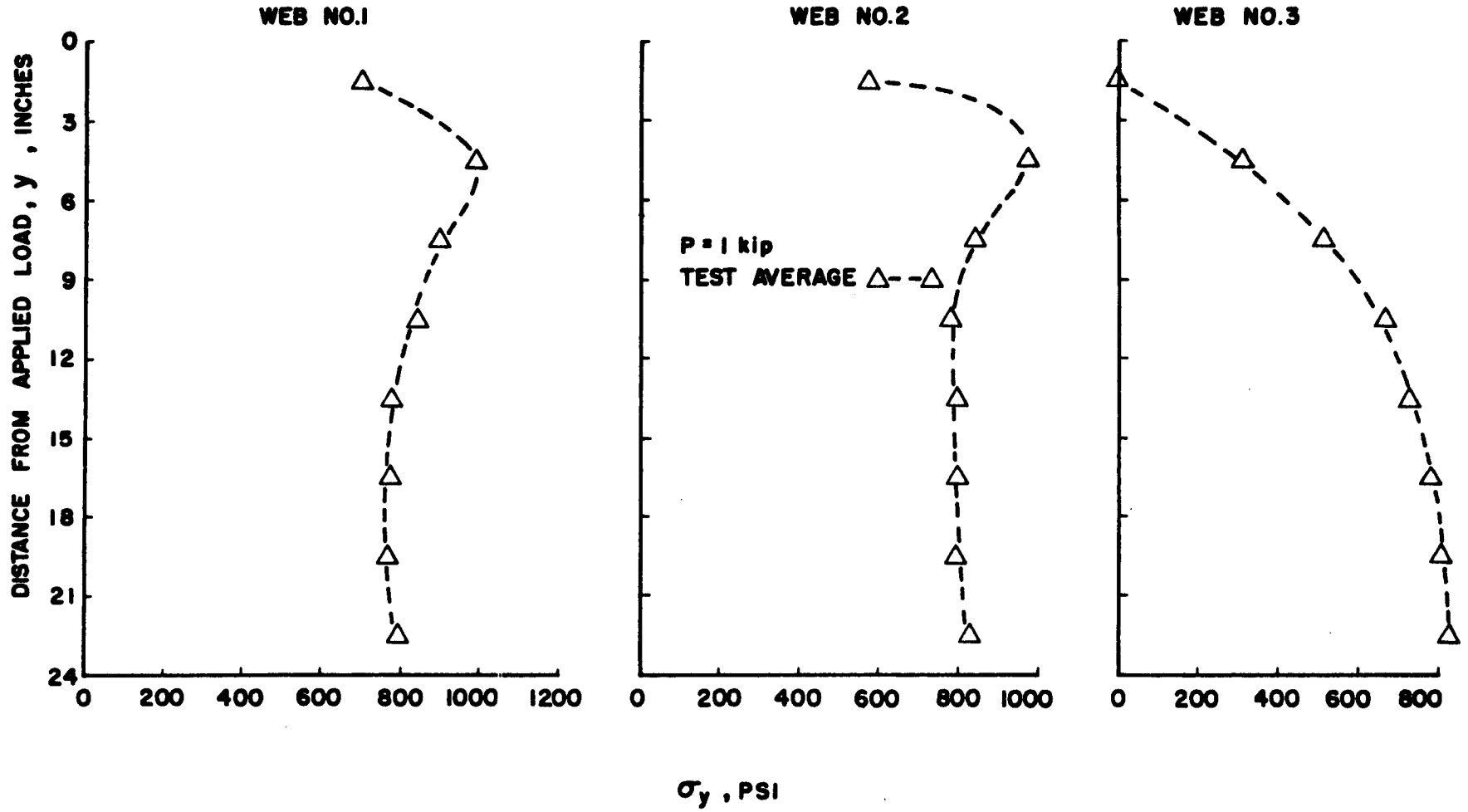

FIGURE F63. - NORMAL STRESS IN WEB OF PANEL D FOR LOAD CONDITION II.

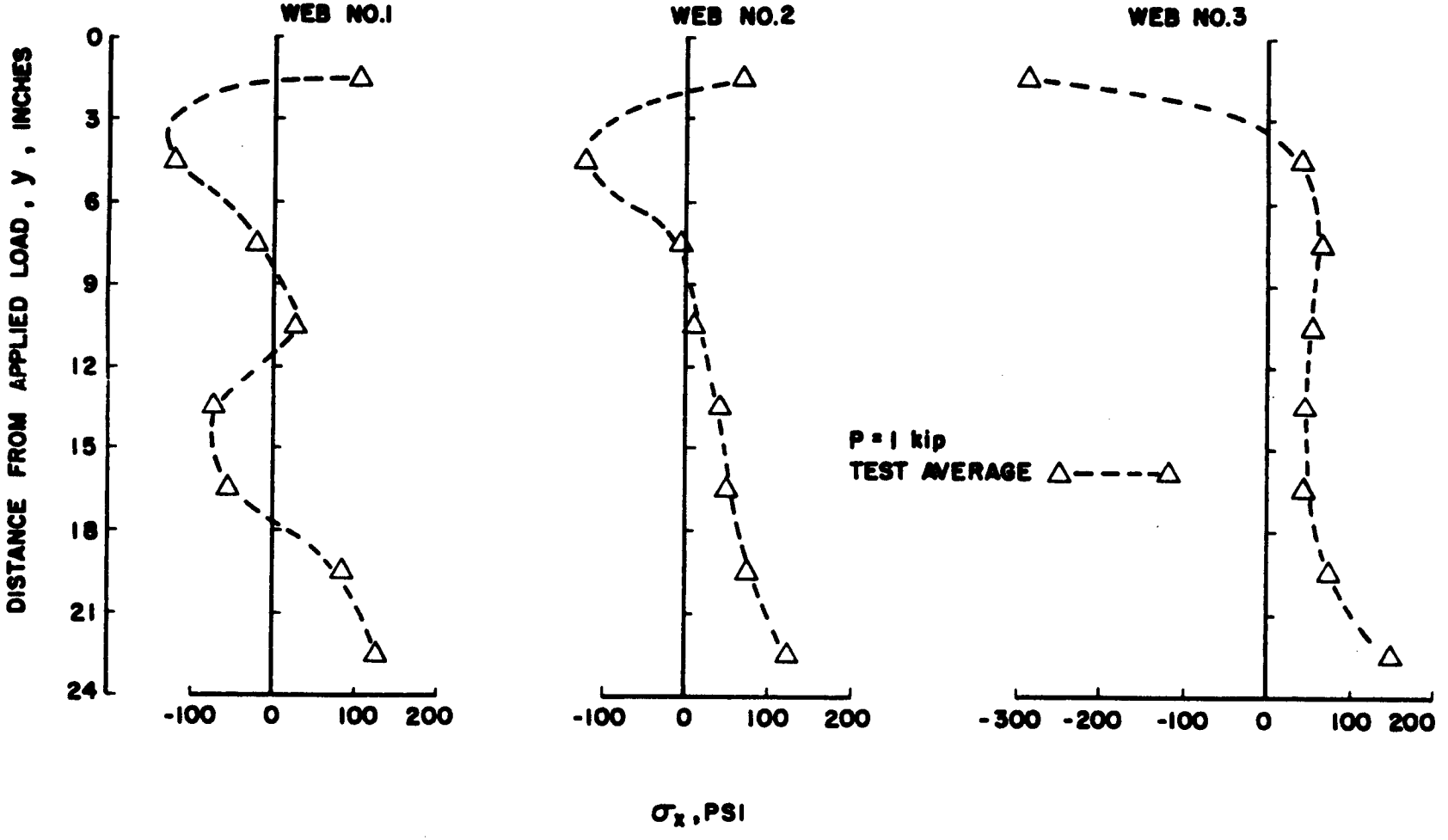

FIGURE F64. - NORMAL STRESS IN WEB OF PANEL D FOR LOADING CONDITION II.

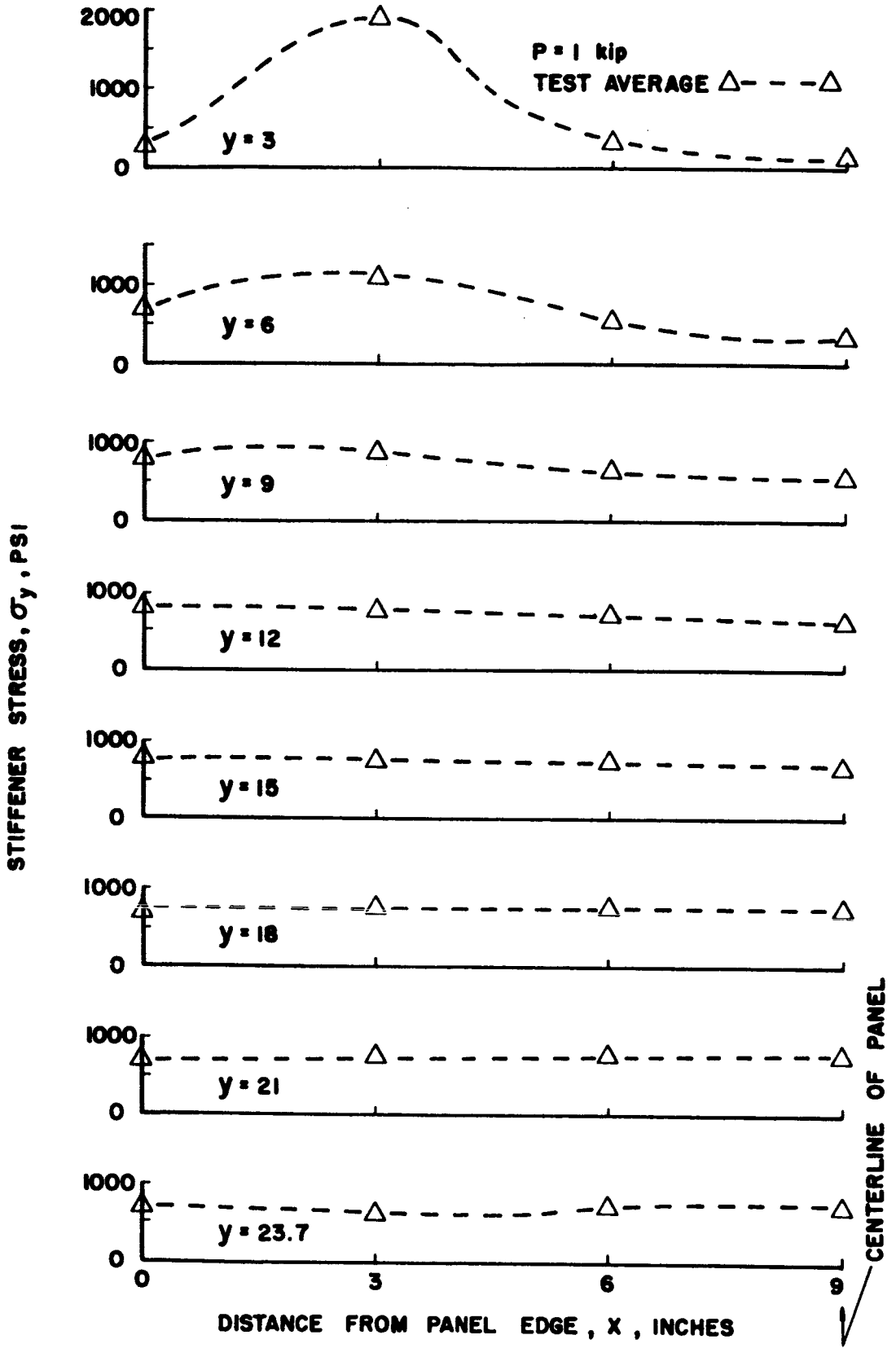

FIGURE F65. - CHORDWISE DISTRIBUTION OF STIFFENER NORMAL STRESS IN PANEL D FOR LOADING CONDITION II.

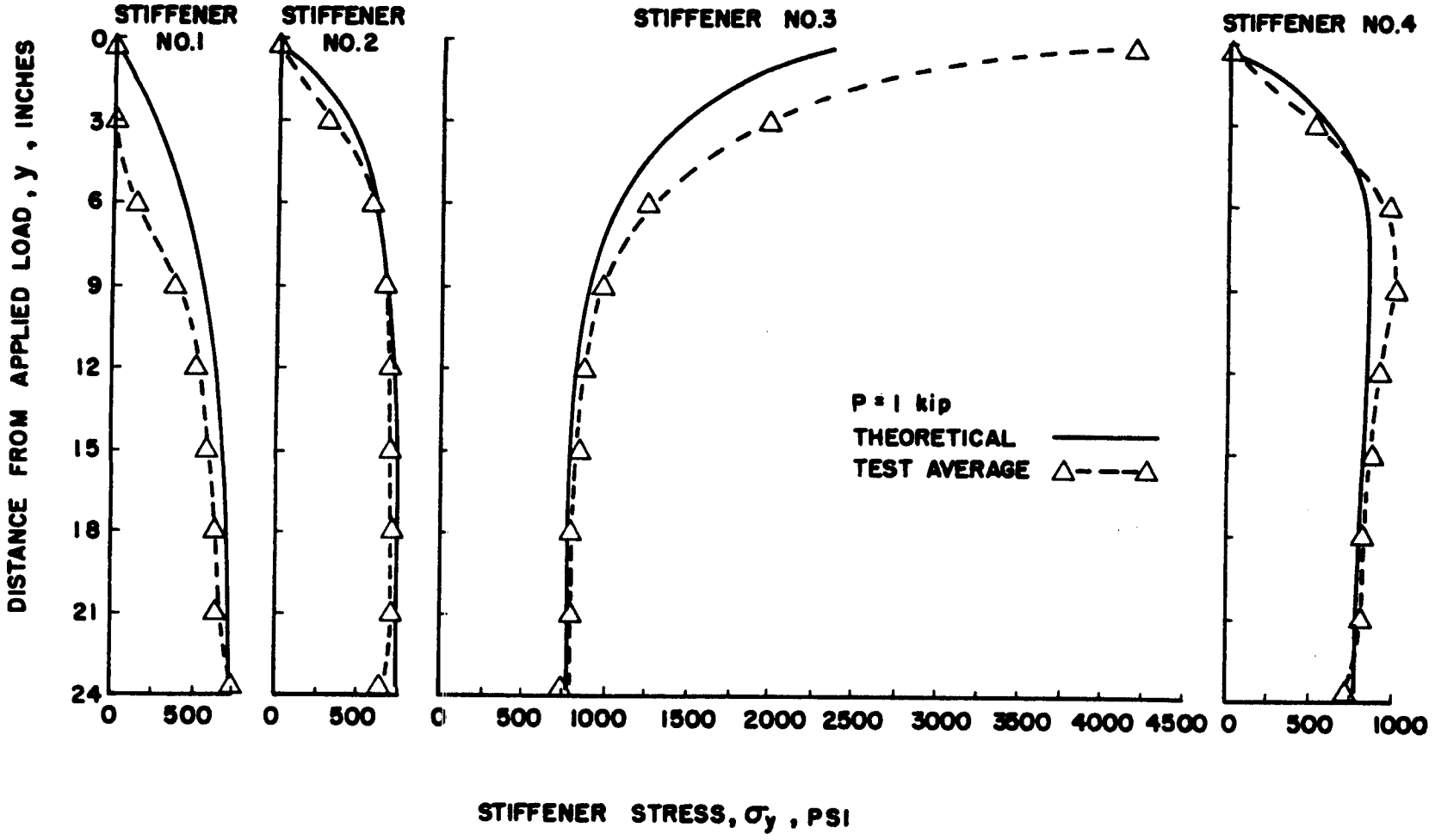

FIGURE F66. - NORMAL STRESS IN STIFFENERS OF PANEL D FOR LOADING CONDITION III.

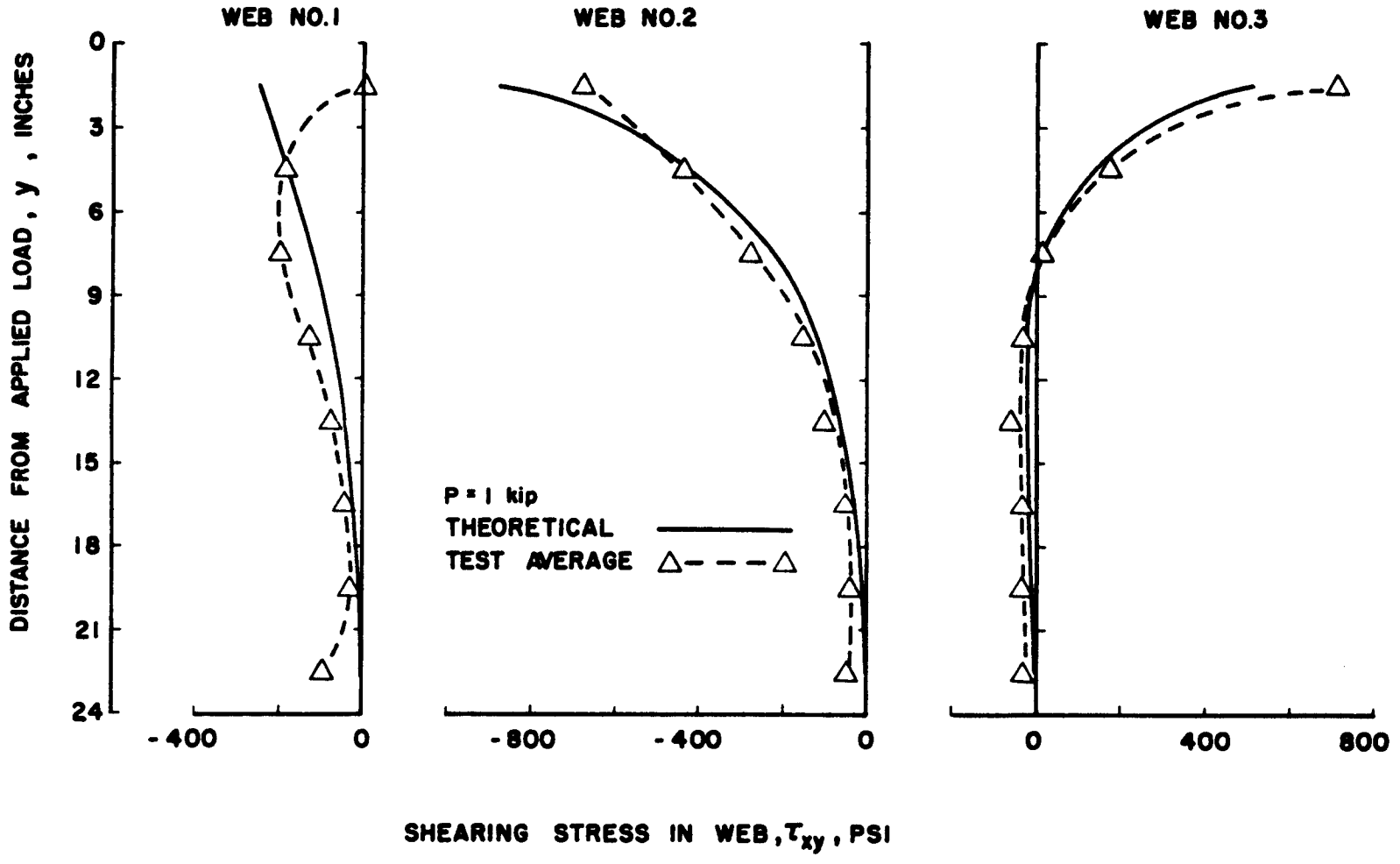

FIGURE F67. - SHEARING STRESS IN WEB OF PANEL D FOR LOADING CONDITION III.

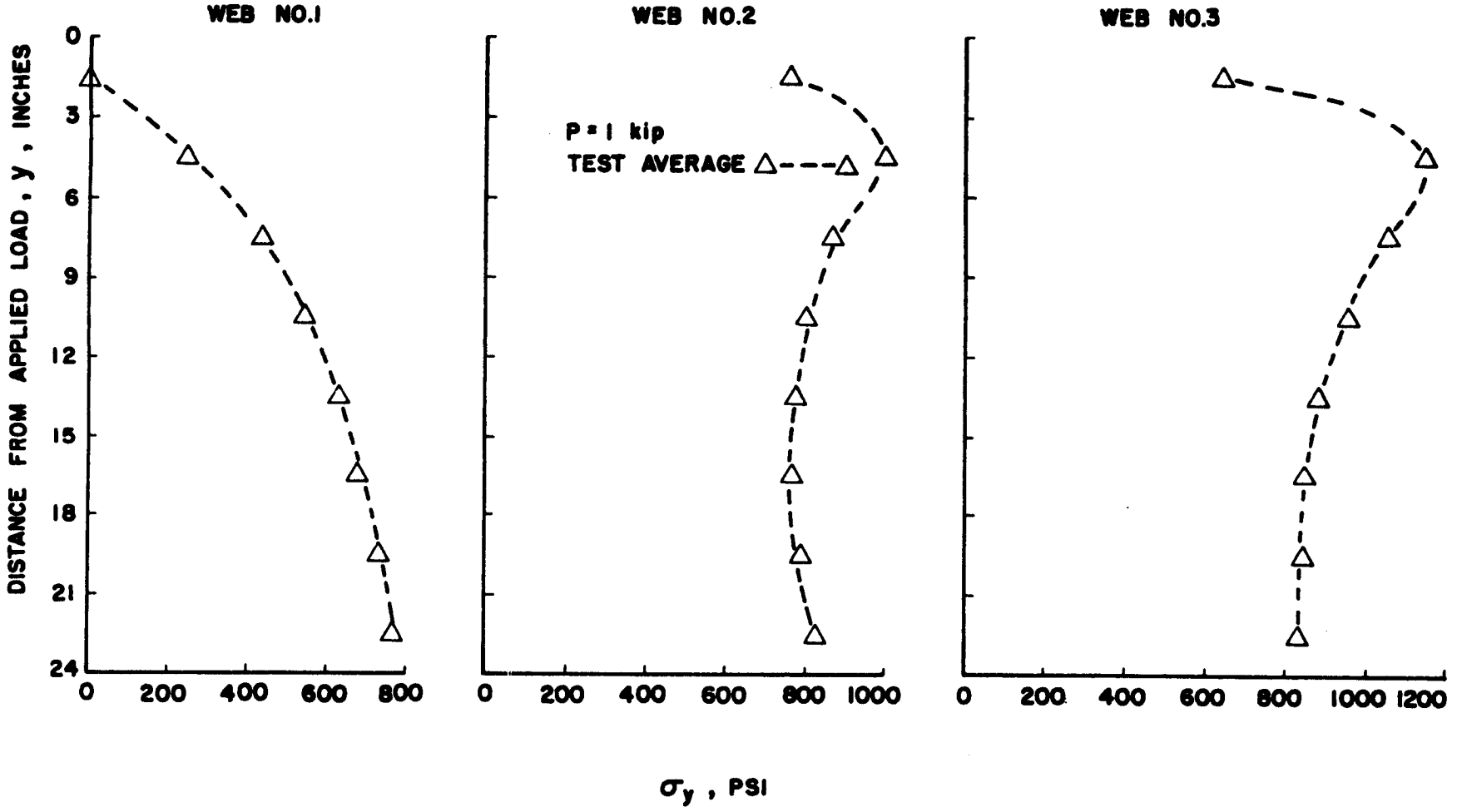

FIGURE F68. - NORMAL STRESS IN WEB OF PANEL D FOR LOADING CONDITION III.

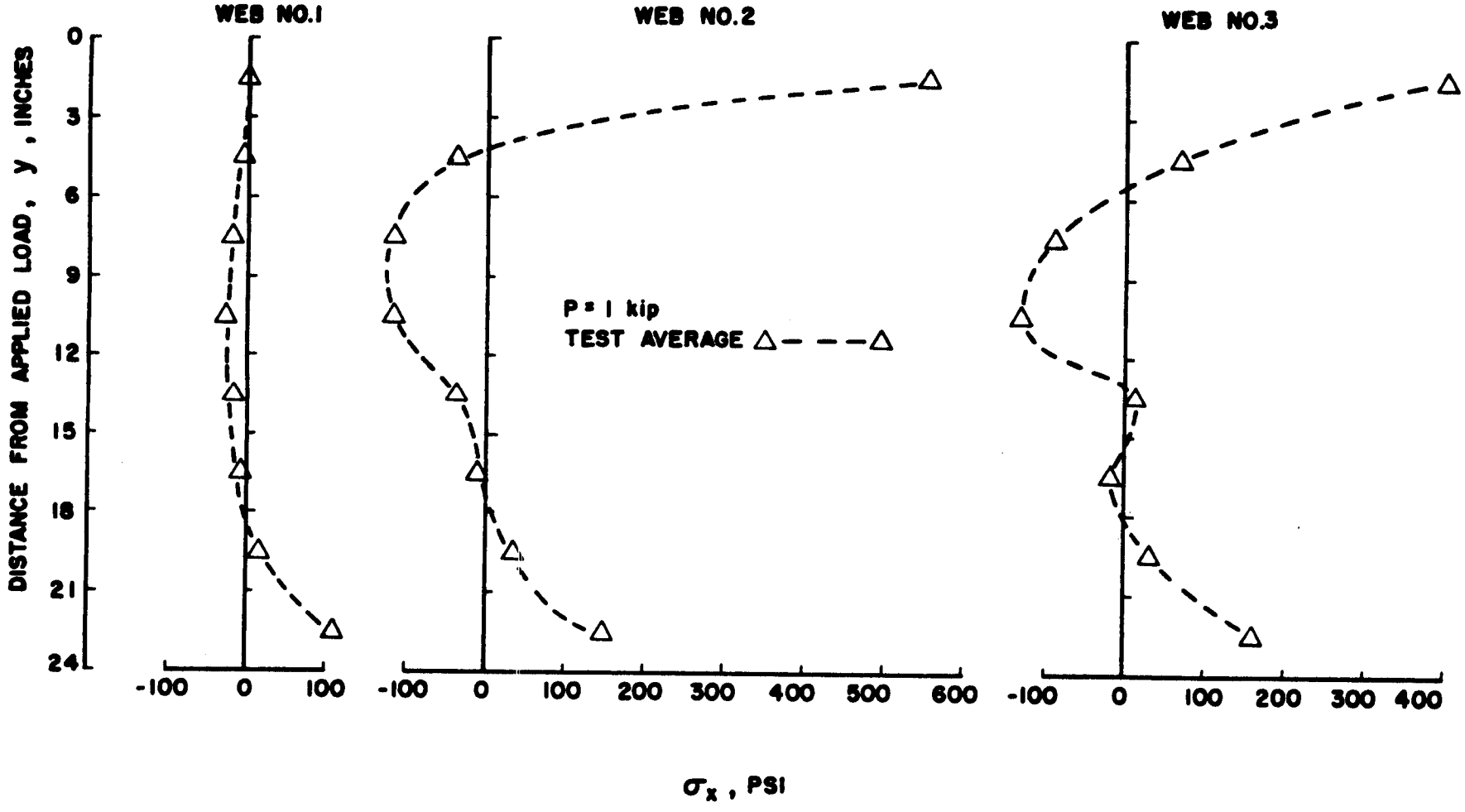

FIGURE F69. - NORMAL STRESS IN WEB OF PANEL D FOR LOADING CONDITION III.

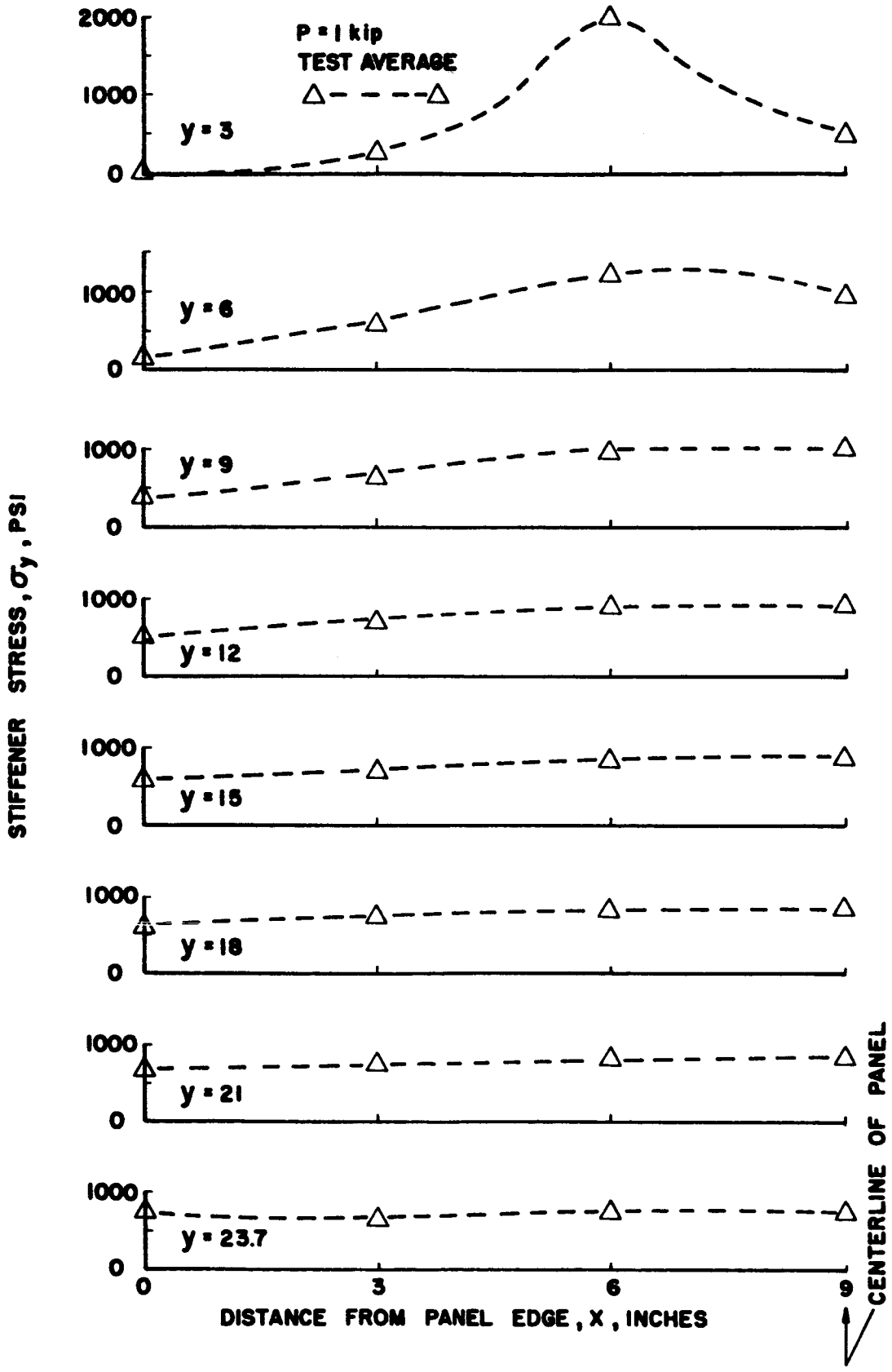

FIGURE F70. - CHORDWISE DISTRIBUTION OF STIFFENER NORMAL STRESS IN PANEL D FOR LOADING CONDITION III.

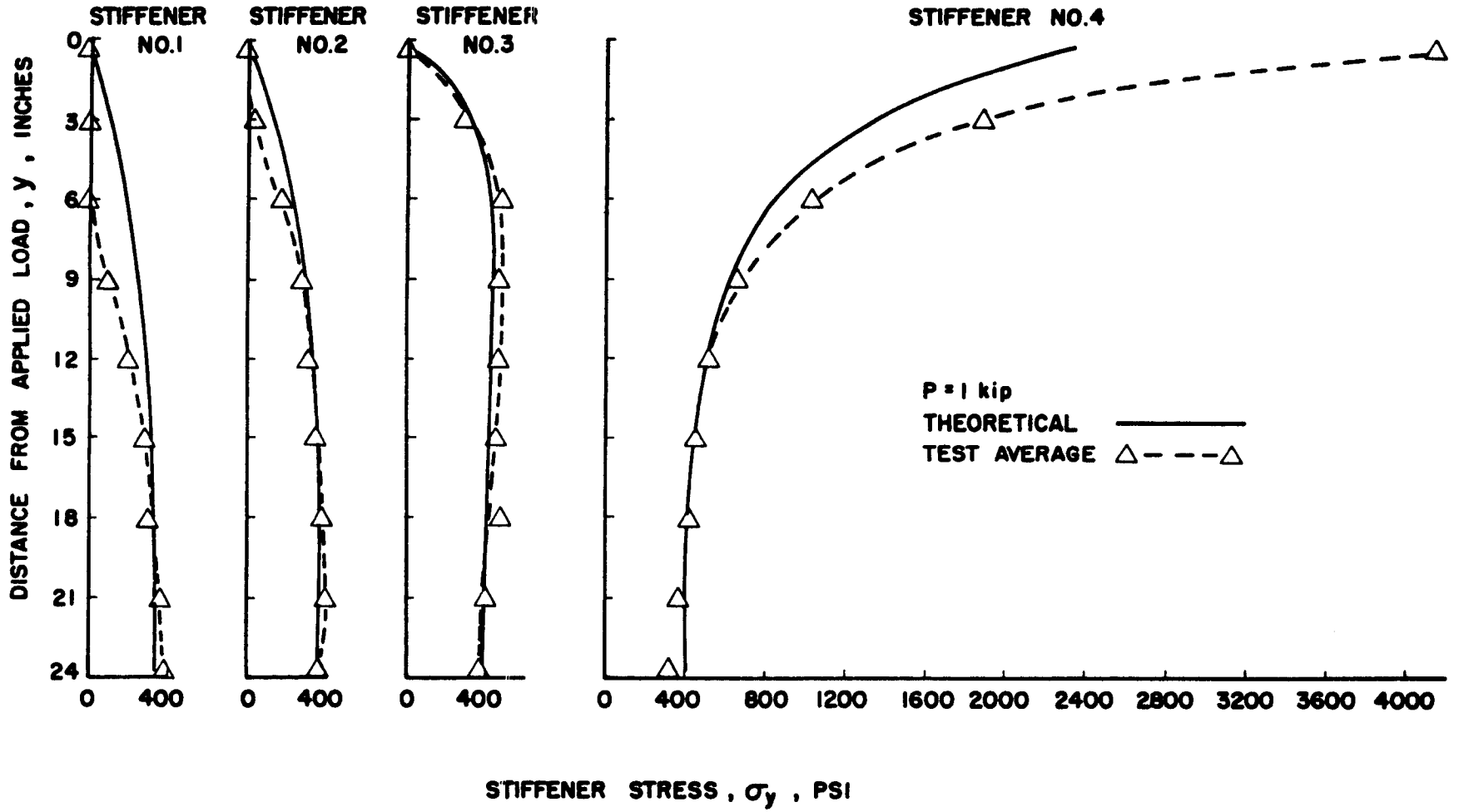

FIGURE F71. - NORMAL STRESS IN STIFFENERS OF PANEL D FOR LOADING CONDITION IV.

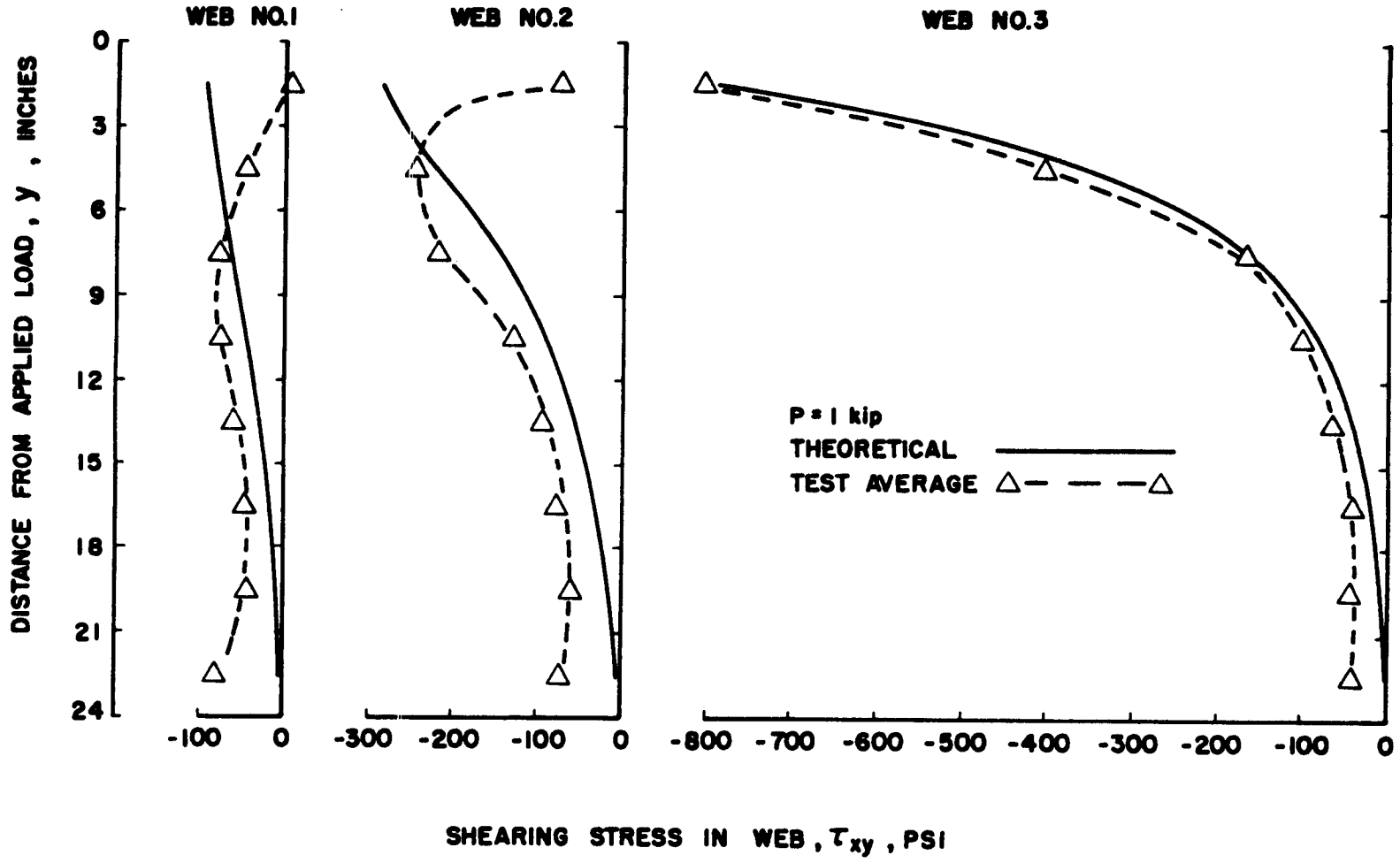

FIGURE F72. - SHEARING STRESS IN WEB OF PANEL D FOR CONDITION IV.

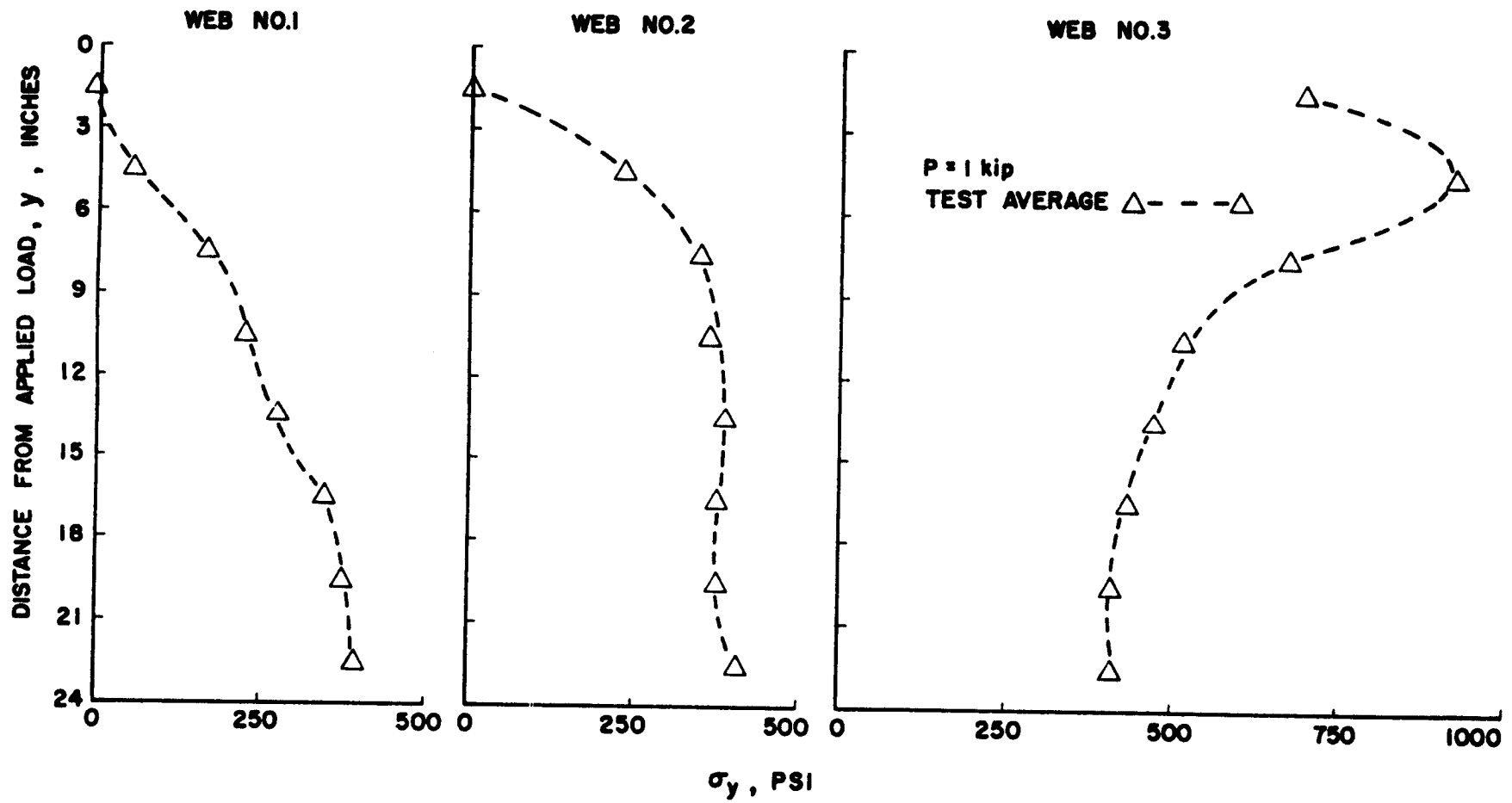

FIGURE F73. - NORMAL STRESS IN WEB OF PANEL D FOR LOADING CONDITION IV.

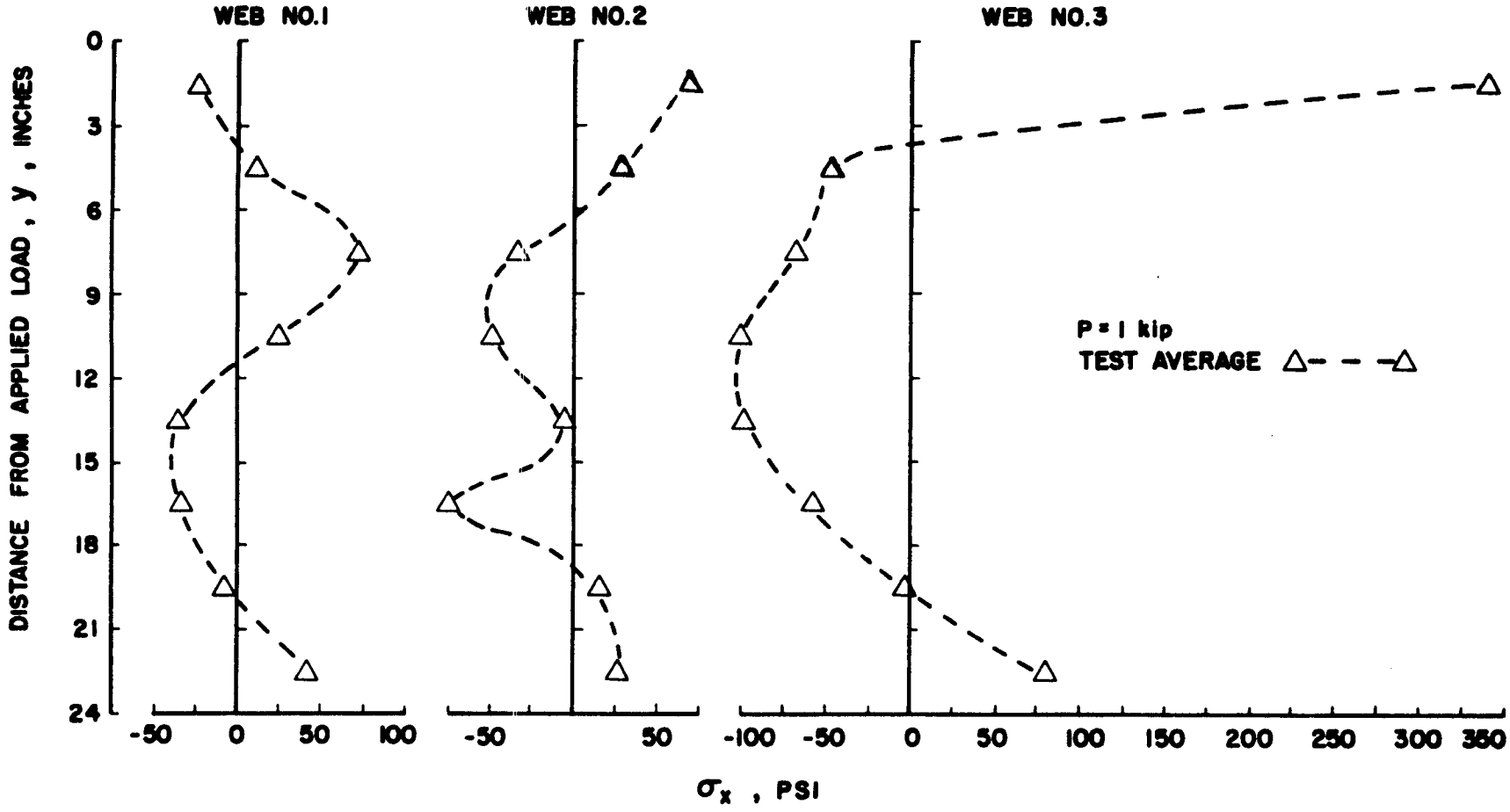

FIGURE F74. - NORMAL STRESS IN WEB OF PANEL D FOR LOADING CONDITION IV.

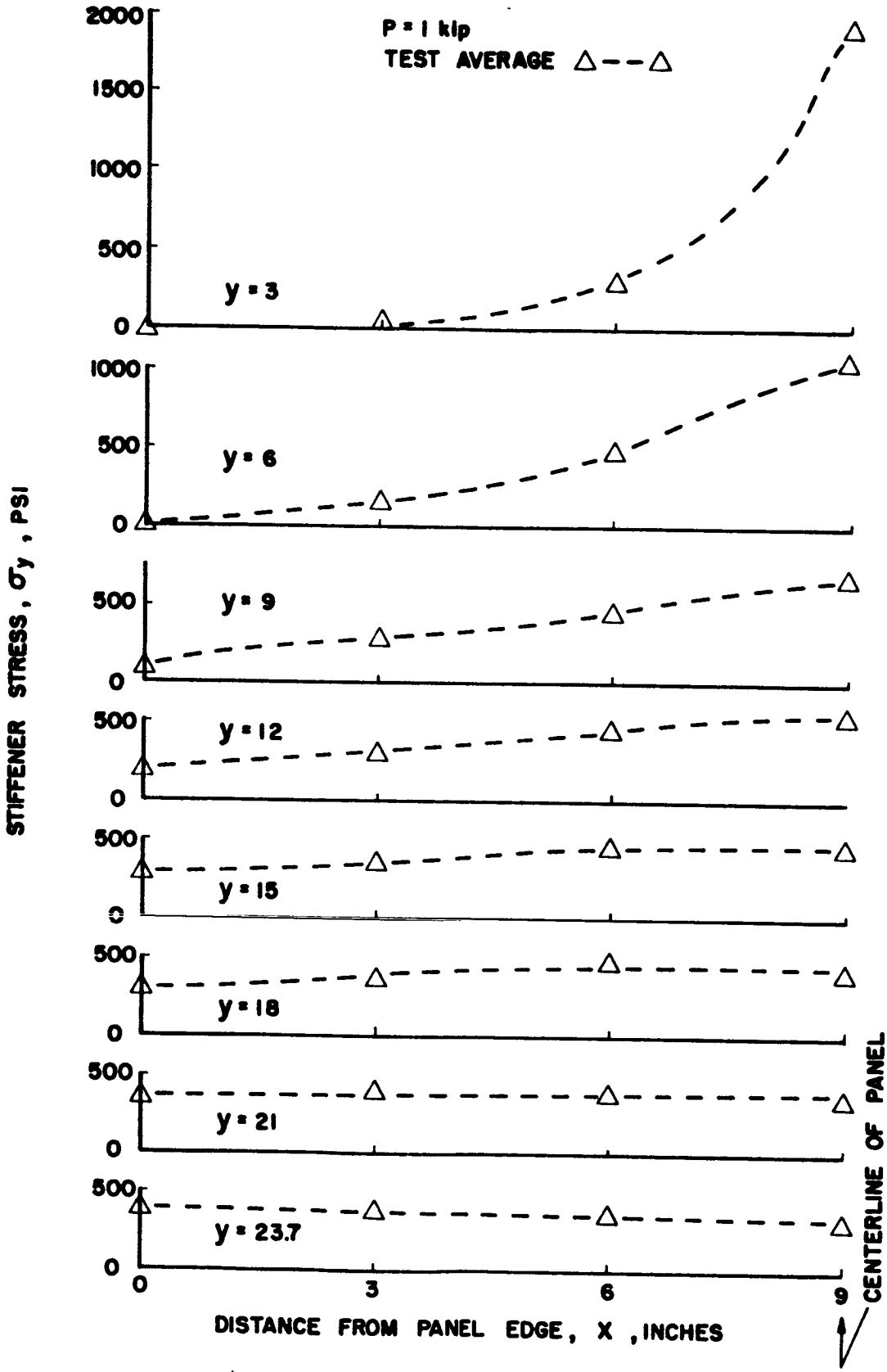

FIGURE F75. - CHORDWISE DISTRIBUTION OF STIFFENER NORMAL STRESS IN PANEL D FOR LOADING CONDITION IV.

APPENDIX G

COMPARISON OF SEVERAL ANALYTICAL SOLUTIONS TO THE SHEAR LAG PROBLEM WITH EXPERIMENTAL DATA

By Dennis M. Rigsby

The contents of this appendix were previously submitted as Progress Report No. 5 for NASA Contract NAS8-11155 and were also submitted as a Master's Thesis in the Department of Aerospace Engineering of the University of Alabama.

APPENDIX G

TABLE OF SYMBOLS

A cross sectional area of stiffener, in^2, when used with a subscript. Also used as an arbitrary constant in Appendix C.

A_F area of flange, in^2

A_L area of stiffener, in^2

a one half panel width, in

B arbitrary constant used in Appendix C

b distance between stiffeners, in

b_c distance from centroid of flange to centroid of areas of remaining stiffeners, in

b_s distance from centroid of flange to centroid of substitute-single stringer, in

c constant

D differential operator denoting $\frac{d}{dx}$

e base of natural logarithms

E Young's modulus

F end load used in Appendix B

G modulus of rigidity

I unit matrix

k_x dimensionless parameter used in stress function solution, $k_x = (1 + \frac{t_x}{t})$

k_y dimensionless parameter used in stress function solution, $k_y = (1 + \frac{t_y}{t})$

k parameter used in minimum potential energy equations, Appendix B: $k = \left(\frac{Gt}{bEA_s}\right)^{1/2}$

L length of panel

M coefficient matrix used in differential equation solution, Appendix A

m $\frac{A_F}{A_L}$ in minimum potential energy solution,

$\frac{A_F}{ak_x t}$ in stress function solution

n number of stringers in half panel or when used as a subscript it represents the number of the stiffener or panel under consideration

O origin of cartesian coordinate system

P applied axial load, pounds

P_o uniform stress at infinity, psi

P_x average normal stress in direction O_x, psi

P_y average normal stress in direction O_y, psi

q shear flow, lb/in

s circumferential distance

t thickness of sheet material

t_x area of reinforcing material added in direction O_x, per unit width of sheet

t_y area of reinforcing material added in direction O_y, per unit width of sheet

T_o end load, stress function solution, pounds

T_∞ load at infinity, pounds

U strain energy

α variable used in stress function solution

β angle of rotation, stringer-sheet solution

γ shearing strain

ε normal strain

ζ $\frac{\lambda}{0.04712}$

θ_n roots to transcendental equation, stress function solution and stringer sheet solution

λ parameter used in differential equation solution

μ Poisson's ratio

π ratio of circumference of circle to diameter, approximately 3.1416

σ normal stress

τ shearing stress

Φ stress function

φ variable used in minimum potential energy solution

COMPARISON OF SEVERAL ANALYTICAL SOLUTIONS TO THE SHEAR LAG PROBLEM WITH EXPERIMENTAL DATA

By Dennis M. Rigsby*

INTRODUCTION

Shear lag is the term commonly used to describe the influence that shearing deformations have on the stress distribution in sheet-stringer types of construction [G2][1]. Experimental evidence has shown that the stress distribution in sheet-stringer structures subjected to bending cannot be adequately predicted by the elementary flexure theory. The difference between the stress distribution predicted by elementary flexure theory and the experimentally determined distribution is due in part to the fact that the theoretical assumption that plane sections remain plane after bending is not satisfied in sheet-stringer structures. If plane sections remained palne after bending, the sheet between stringers would have to have infinite shearing rigidity, i. e., no shearing strains. Since the thin sheet between stiffeners actually has very little shear stiffness and the sheet suffers large shearing deformations under load, the assumption of infinite shearing rigidity is not satisfied in this type of structure. As a result of these shear deformations, the stresses in the stringers are less than the predicted stresses. Since the stringer stresses lag behind predicted values, the effect has been described as shear lag.

Thus, the problem of the stress analyst is the determination of the stress distribution in box beams taking into consideration shearing strains. In a hollow, rectangular box beam under pure bending, the surface under compression behaves as a flat, stiffened panel subjected to an axial compressive load. In this appendix a flat stiffened panel under axial load has been investigated.

---

*Graduate Student in Aerospace Engineering, University of Alabama, University, Alabama and Graduate Research Assistant for NASA Contract NAS8-11155.

[1]Numbers in brackets refer to references at the end of this appendix.

Although many investigators have obtained solutions to the shear lag problem, all of their solutions appear to have shortcomings. Because of the simplifying assumptions made, some of the less rigorous solutions are valid only for certain special cases, while some of the more mathematically rigorous solutions are quite cumbersome to apply.

One of the first investigators in the United States to give much attention to the problem was Younger in 1930 [G30]. He presented formulas for the efficiency of a box beam with walls of uniform thickness, which may be considered as the limiting case of a large number of very small stringers. His analysis was limited by the assumption of a constant cross section.

Many investigators attempted to solve the problem by first deriving the differential equations of equilibrium of either the stringers or the sheet material and then solving the equations for the stresses by one of several methods. Winny [G29], one of the early British investigators, obtained a Fourier series solution to the differential equations of equilibrium of the stresses in the skin between the spars of a stressed skin wing. Kuhn [G20] proposed a numerical integration type solution for the differential equations. Goodey [G13] solved the differential equations of equilibrium of the stringer forces using the minimum potential energy theory and the calculus of variations.

In 1946 Goodey [G13] published a comprehensive series of articles each concerned with some aspect of the problem of shear lag, or stress diffusion, as it is known to the British. His method of approach required the determination of a stress function for the particular system under consideration. The stress functions he obtained led to expressions for the stresses which are difficult to use; however, his expressions based on the minimum potential energy theory, mentioned earlier, are very easy to apply.

Borsari and Yu [G3] conducted theoretical and experimental investigations of the distribution of strains in a plywood sheet-stringer combination used as the chord member of a box beam acted upon by bending loads. The theoretical solution was obtained with the help of the principle of minimum potential energy and certain simplifying assumptions. Strain measurements were made on a built-up box beam by means of electrical resistance strain gages. A satisfactory agreement between the

theoretical and experimental strains was reported.

Fine [G10] developed a stress function for the spanwise stress in the flat surface of a box beam under uniformly distributed transverse load. He compared the stresses obtained from this solution with those predicted by the stringer-sheet solution. The two solutions were in good agreement.

Kuhn [G19] proposed a solution based upon the use of a substitute single stringer in place of the actual stringers. It was necessary to use a successive approximation method for locating the substitute single stringer. In view of the approximate nature of the solution, Kuhn considered the successive approximations an unwarranted complication. For this reason he developed an empirical one-step method to locate the substitute single stringer [G20] . For the empirical determination of the location of the substitute single stringer, shear strain measurements alongside the flanges of three panels of constant section and two panels of variable section were used. Two panels with tapered flanges and a small number of stringers were also investigated. An empirical factor was chosen based upon the comparison of these tests with theoretical strains predicted by the substitute stringer method. The resulting solution permitted the analysis of multistringer panels with very little computational effort. Results of this type of analysis were good and the method found wide acceptance in industry.

Akao [G1] proposed a stress analysis of a rib-stiffened plate based upon the use of groups of orthogonal statically indeterminate force functions. These eigenfunction groups are presented as finite difference equations.

Several investigators have made experimental studies of shear lag. White and Antz [G28] reported an investigation made of the stress distribution in thin reinforced panels. Test specimens were constructed of Alclad aluminum sheet reinforced with extruded bulb angles. Results were compared with strains predicted by theory based on the differential equations of equilibrium of the axial forces in the stiffeners. Agreement between experiment and theory indicated the method was well founded.

Lovett and Rodee [G21] conducted an experimental investigation of two beams composed of I-sections connected by a stiffened sheet subjected to a uniform bending moment. The result of the investigation was the

determination of an effective shear modulus for the sheet in the sheet-stringer combination. It was found that the modulus decreases rapidly under light loadings from the elastic value to some other value depending upon the sheet thickness. The thick sheet gave higher values of effective shear modulus than the thin sheet.

Chiarito [G5] reported the results of tests made on two aluminum alloy box beams with corrugated covers. Angles formed from sheet were used for corner flanges in one beam while extruded angles were used for the corner flanges in the other beam. Electric strain gages were used to measure strains in each beam. The experimental results compared favorably with theoretical results obtained by the substitute-single-stringer theory.

Chiarito [G6] also reported the results of an experimental investigation of two box beams loaded to destruction in an effort to verify the shear lag theory at stresses beyond the yield point. An open box beam made of 24S-T aluminum alloy and steel bulkheads was used for the tests. The theoretical and experimental stresses were in good agreement.

Peterson [G24] reported the results of tests which were made on a beam having more camber than is likely to be found in an actual wing in order to determine whether the substitute single stringer theory might be applied over the entire practical range of camber. Results indicated that the elementary theory overestimates the maximum stress and the substitute-single-stringer theory underestimates it.

In addition to the purely theoretical and experimental solutions already mentioned, some effort has been directed towards an analog type solution. Newton [G23] in 1945 and Ross [G27] in 1947 proposed a solution based upon the analogy between the distribution of stresses in flat stiffened panels and the distribution of electric current in a ladder type resistance network. The application of this method is limited because the panel must be divided into a finite number of bays having constant stresses. Results of this method were reported to have good agreement with experimental data.

Goland [G12] established an analogy between the stress flow in flat stringer-sheet panels and the plane potential flow in an incompressible fluid. The author did not give numerical examples or experimental verification of the method.

The use of a mechanical analogy was proposed by Kuhn [G16]. Here,

again, the division of the panel into a finite number of bays limits the method.

In the investigation of the bending vibrations of box beams, it is first necessary to determine the shape of the deformed beam due to a static loading. If the effect of shearing deformations are ignored and the elementary theory is used to predict the mode shapes, the predicted natural frequencies can be greatly in error from the actual frequencies. Davenport and Kruszewski [G8] found that by using the substitute-single-stringer method in calculating the static stresses and deformations of the beam, the resulting calculated natural frequencies and mode shapes were in much better agreement with experiment.

Purpose and Scope

The objectives of this study were: (1) to consider several of the existing analytical solutions to the shear lag problem, (2) to apply these solutions to a panel with particular properties and loading conditions, (3) to solve for the stress distribution in the panel, and (4) to compare the results of the various theories with experimental data for the same panel with the main objective being the determination of the best method of shear lag analysis.

The following theoretical solutions are treated:

Appendix G1 - Differential equation solution.

Appendix G2 - Minimum potential energy equations.

Appendix G3 - Stress function solution.

Appendix G4 - Substitute-single-stringer method.

Appendix G5 - Minimum energy solution using matrix methods.

COMPARISON OF ANALYTICAL SOLUTIONS WITH EXPERIMENTAL DATA.

Experimental Data

Panels B and C referred to in this appendix correspond to panels B and C in Appendix F. Details of the experimental procedure, data reduction, and construction of the test panels are given in Appendix F.

Differential Equation Solution

The differential equations of equilibrium of the normal stresses in the stringers of a stringer-sheet combination are derived in Appendix G1 and one method of solving these equations is presented as a numerical example. The solutions are presented as a linear combination of exponential functions. Results of this solution are compared with experimental data in Figures G3 and G4 for panels B and C, respectively. Examination of Figures G3 and G4 reveals the following information:

1. The theoretical curves and the experimental values for the normal stresses in the stringers indicate the same type stress distribution within the panel. For the loaded stringer, both methods indicate a stress equal to P/A at the loaded end with the value decreasing exponentially as the distance from the loaded end increases. For the stringer adjacent to the loaded stringer, theory and experiment both indicate normal stresses which increase from zero at the loaded end to a maximum stress then slowly decrease as the distance from the loaded end increases. For the remaining two stringers, theory predicts stresses which increase from zero at the loaded end to some higher value then decrease slowly as the distance from the loaded end increases. The experimental values increase from zero at the loaded end, but do not reach some maximum value then decrease as did the theoretically predicted stresses.
2. Agreement between theory and experiment is poor except at the loaded end. The theoretically predicted stresses for stringers 1, 2, and 3 are non-conservative. For stringer 4 of panel C the predicted stresses are conservative up to a point about 7 inches from the loaded end then they, too, become non-conservative. In panel B the predicted stresses in stringer 4 are conservative up to a point about 15 inches from the loaded end.
3. Overall agreement between theory and experiment is better for panel B than for panel C.

Minimum Potential Energy Equations.

Goodey's analysis [G11] of the diffusion of end load into a panel having (2N-1) stringers is presented in Appendix G2. His final equations have the form of a finite sume of terms involving trigonometric and exponential functions. As analysis of the diffusion of a 2000 pound end load

in panels B and C was made using these equations. Results of this analysis are presented in Figures G5 and G6 along with experimental data for comparison. Examination of Figures G5 and G6 reveal the following information:

1. Both experimental and theoretical results indicate that, at some distance from the loaded end, the end load is uniformly distributed among the stringers.
2. For the loaded stringer, the agreement between theory and experiment is good with the best agreement at the loaded end. For panel B, the agreement is poor except at the loaded end. Agreement between theory and experiment for the unloaded stringers in panel C is fair.
3. Theoretically predicted stresses are conservative.

Stress Function Solution

A stress function for a panel reinforced at the loaded end perpendicular to the stringer is presented in Appendix G3. Although panel C does not have a reinforced end, a comparison is made between the analytical solution and experimental data in Figure G7. Agreement between theory and experiment is not, and was not expected to be, good. The method is presented because it represents another approach to the problem, although for a slightly different configuration.

The stringer-sheet theory is also given in Appendix G3. This represents one of the easier theories to apply; however, it can only be applied to the loaded stringer as a quick investigation of the equation will reveal. This analysis was applied to the loaded stringers of panels B and C and the results plotted in Figures G8 and G9 with experimental data. Investigation of the two curves indicates good agreement between theory and experiment, the theoretical solution being slightly non-conservative in one region and slightly conservative in another.

The Substitute Single Stringer Method

The method for analyzing multistringer panels using a substitute stringer is presented in Appendix G4. Results of this method applied to panels B and C having a 2000 pound end load are presented in Figures G10 and G11 with experimental data. Due to the nature of the solution, stresses

in the unloaded stringers cannot be predicted; however, it can be seen from the curves that the stresses in the substitute stringer are quite close to the stresses in the stringer adjacent to the loaded stringer. Agreement between predicted stresses and experimental stresses in the loaded stringer is also good.

Minimum Energy Solution Using Matrix Methods

An outline of the analysis of panels B and C utilizing matrix methods based upon the Maxwell-Mohr method is presented in Appendix G5. A detailed analysis of this type would be practically impossible without the aid of a digital computer. The Univac 1107, located at the University of Alabama Research Institute, Huntsville, Alabama, was used. Results of these analyses are presented in Figures G12 and G13 with experimental data. This analysis was performed in the preparation of Appendix F.

For panel B, the agreement between theory and experiment is fair, better agreement existing in stringer 4 than in the others. The theory is conservative throughout most of the panel. Better overall agreement between theory and experiment exist in the case of panel C, but in this case stringer 4 does not exhibit as good agreement as in panel B. Also, theoretical stresses in stringer 4 were on the non-conservative side.

CONCLUSIONS

As was previously, stated, the main objective of this phase of the contract was the comparison of several existing theories of shear lag analysis with some of the experimental data. The conclusions reported in this appendix are based on the comparison of the theoretically predicted normal stresses in the stringers with the experimentally determined normal stresses. The conclusions would probably be different if normal and shearing stresses in the sheet had been included in the analyses and comparisons. The comparisons led to the conclusion that the best method of analysis consists of a combination of the methods studied rather than any one method by itself. Based on the comparisons reported, the following methods of analysis are suggested:

Based on Accuracy

1. If it is only desired to predict the stresses in the loaded

stringer, either the stringer-sheet theory or the substitute-single-stringer theory should be used. The agreement between theory and experiment is about the same for both methods.

2. If it is desired to predict the state of stress in the loaded stringer and approximate the stresses in the adjacent stringers, the substitute-single-stringer method is preferable.
3. If it is desired to predict the stresses in each stringer of the panel, the analysis based on the solution of the differential equations of equilibrium of the normal stresses using minimum potential energy considerations is preferable. The stringer-sheet theory or substitute-single-stringer theory could be used at the same time to predict the stresses in the loaded stringer.

Based on Time Required to Perform Analysis

1. If it is desired to perform a quick analysis, the substitute-single-stringer method is suggested.
2. If it is desired to obtain a more complete picture of the stress distribution in the panel than the substitute-single-stringer method allows, use of the minimum potential energy equations is suggested.
3. The other methods of analysis discussed in the preceeding chapter take much more time to perform than either of the two above and could not be used to perform a quick analysis.

Based on the Type of Structure to Which the Solution is Applicable

1. Since the experimental data used for purposes of comparison was obtained from simple structures, i.e., ones having constant skin thickness and equally spaced stiffeners having the same constant area, a great deal cannot be said about the applicability of the various methods to other structures. It would seem probable, based on the form of equations involved, that the matrix method solution presented in Appendix F would apply to more configurations than would any of the other methods.

Time did not permit a study of all of the available methods of solution. Among the methods which have been omitted might be a better method than any reported in this appendix. The research reported herein should be continued using the following analytical methods or analogies for comparison:

1. Akao's finite difference equations,
2. Fine's stress function solution,
3. Goland's hydrodynamic analogy,
4. Ross and Newton's electrical analogy,
5. Kuhn's mechanical analog.

The research should be further continued to include the analysis of panels having

1. unequally spaced stiffeners,
2. stiffeners with different areas,
3. variable skin thickness,
4. stiffeners which have areas varying along the length of the panel,
5. skin which varies along the length of the panel,
6. combinations of the above.

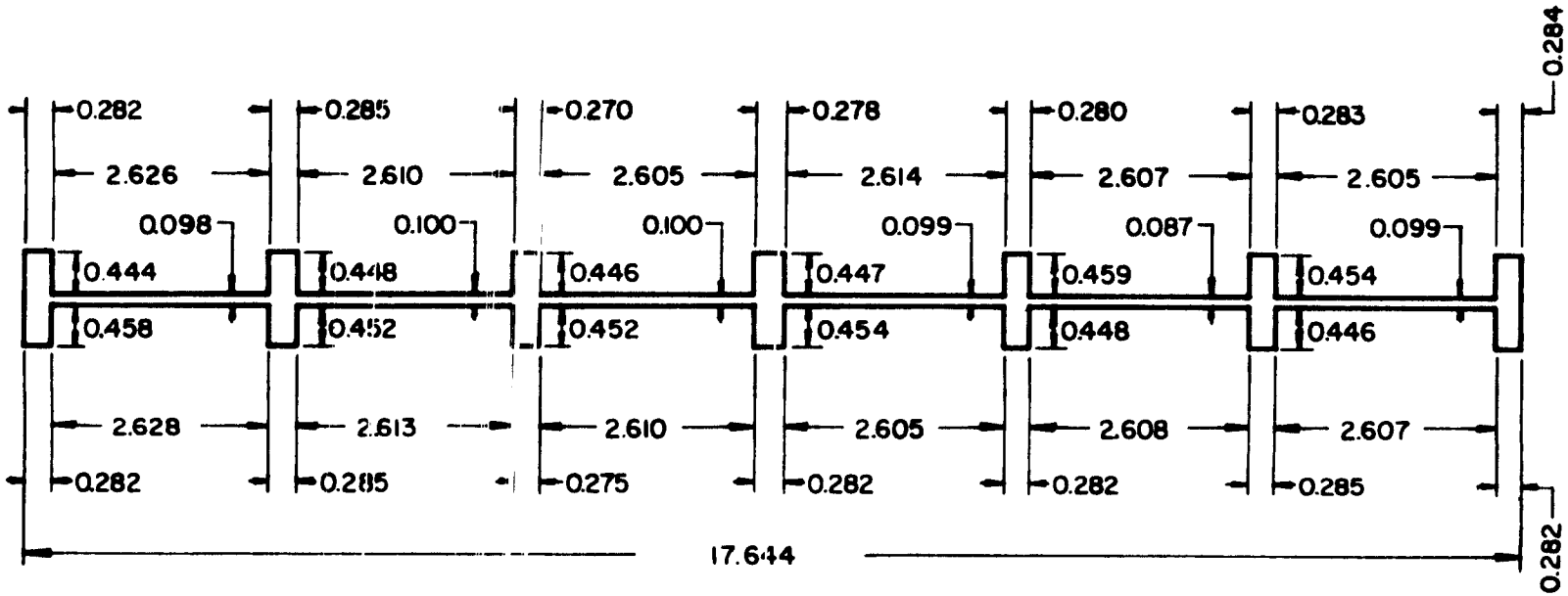

PANEL LENGTH 24.00

ALL DIMENSIONS IN INCHES

FIGURE G1. - CROSS-SECTION OF PANEL B

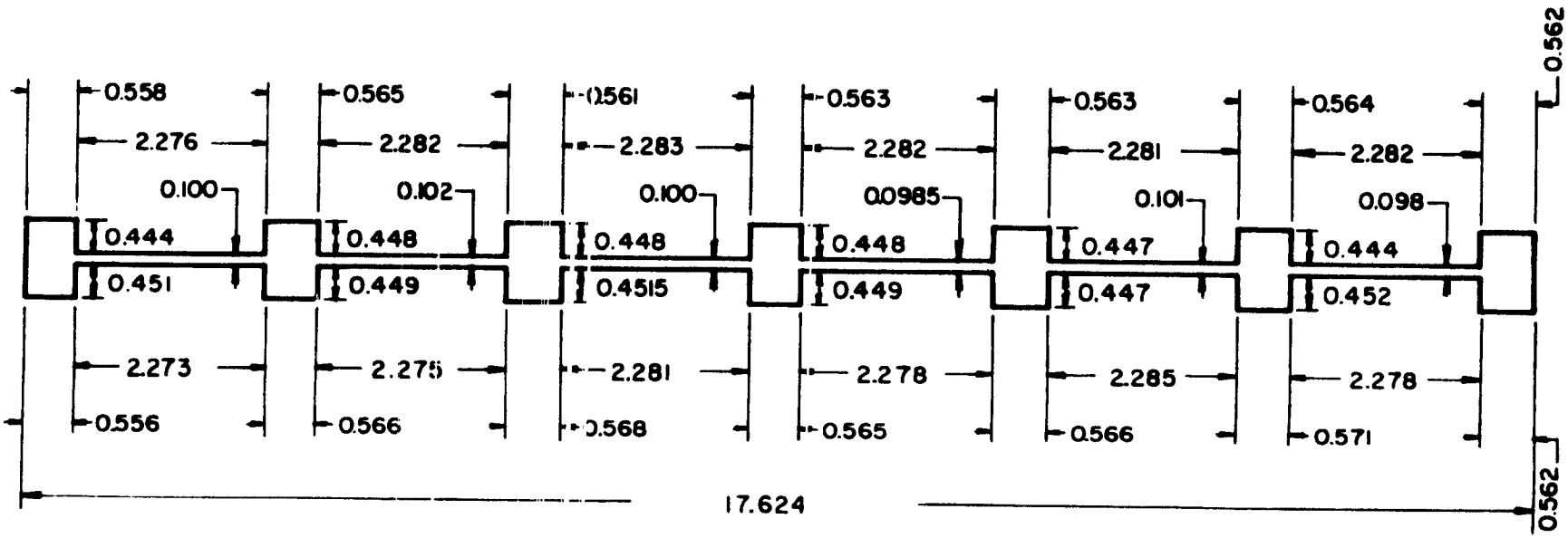

PANEL LENGTH 24.00

ALL DIMENSIONS IN INCHES

FIGURE G2. - CROSS-SECTION OF PANEL C

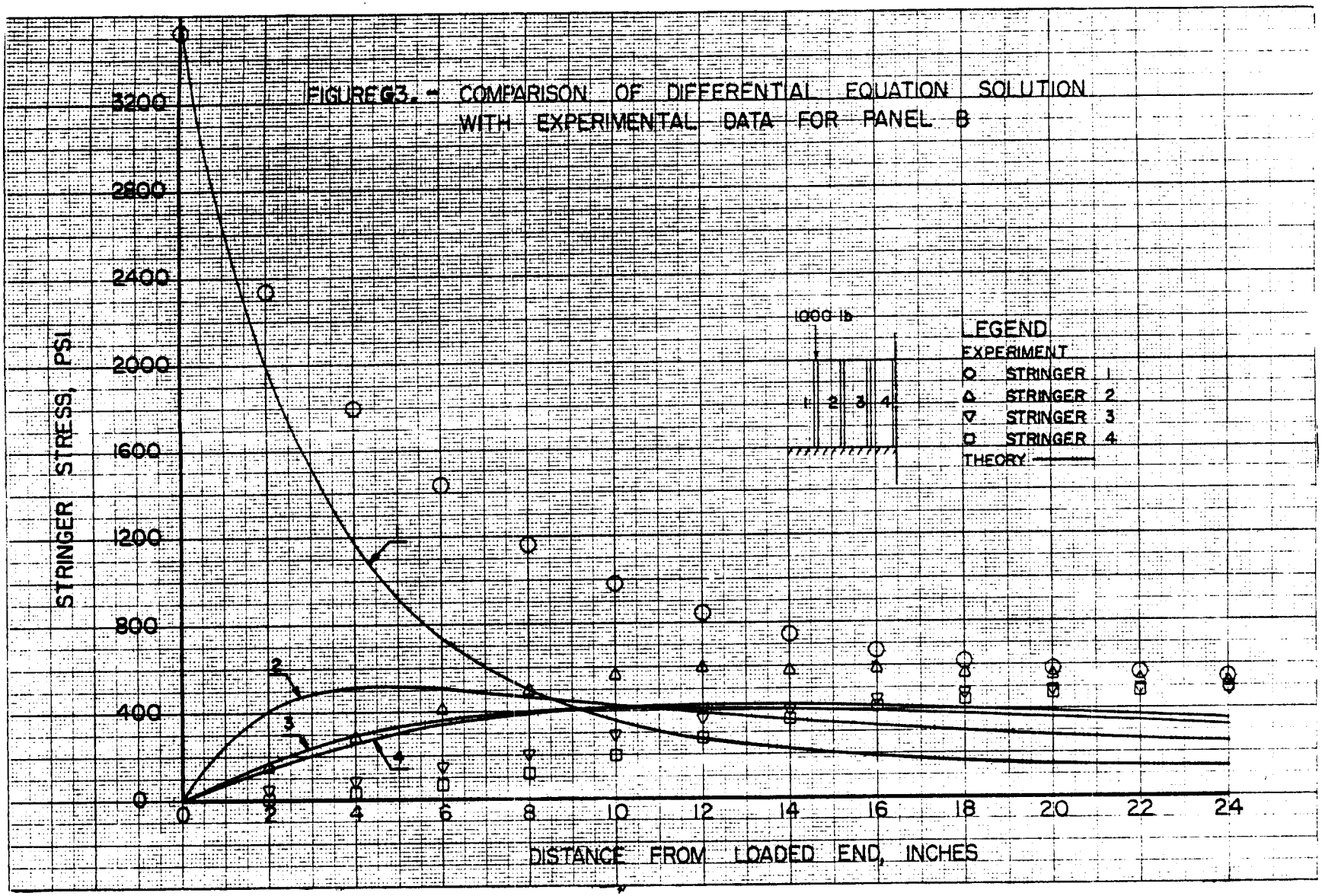

FIGURE 13. - COMPARISON OF DIFFERENTIAL EQUATION SOLUTION WITH EXPERIMENTAL DATA FOR PANEL B

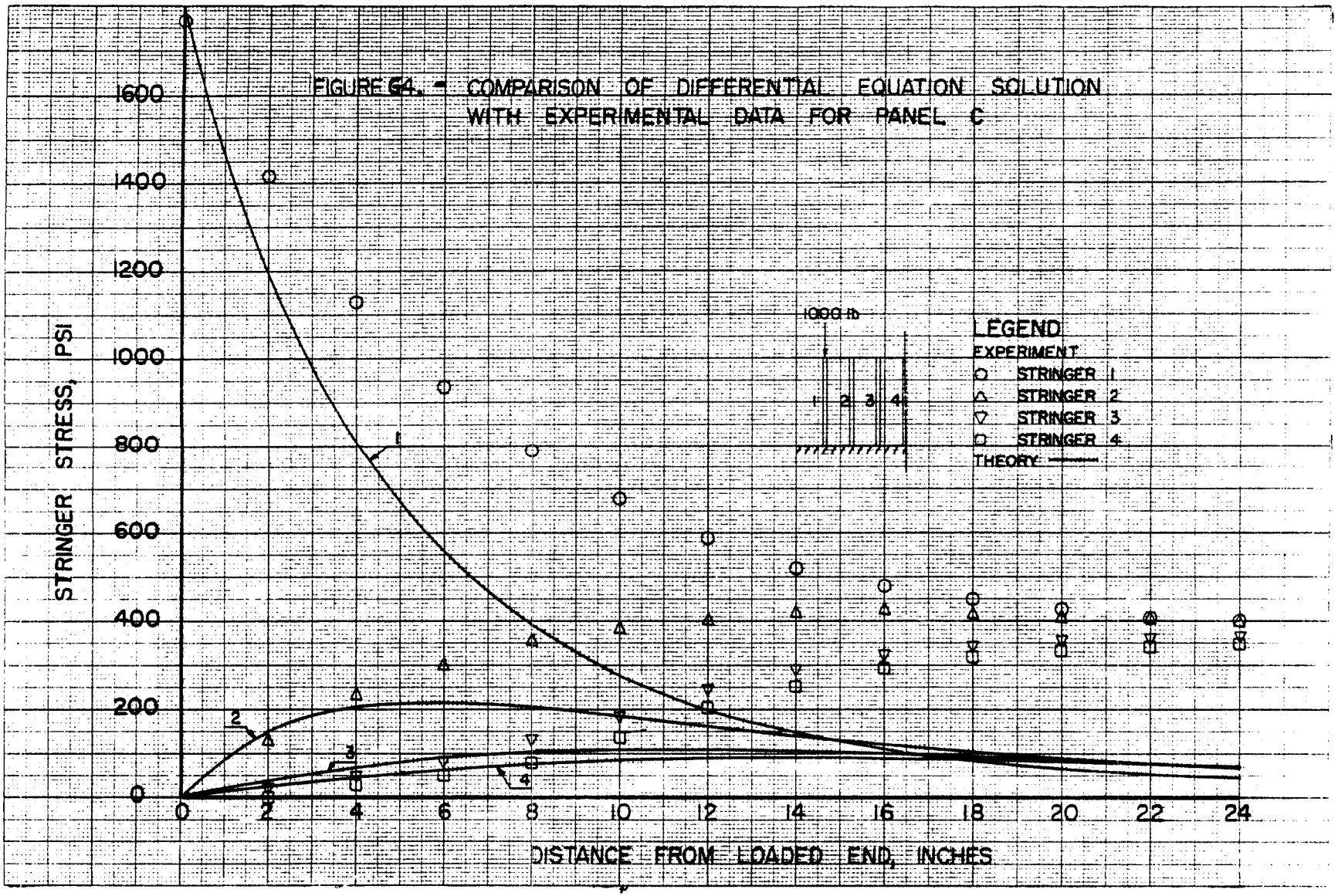

FIGURE 64. - COMPARISON OF DIFFERENTIAL EQUATION SOLUTION WITH EXPERIMENTAL DATA FOR PANEL C

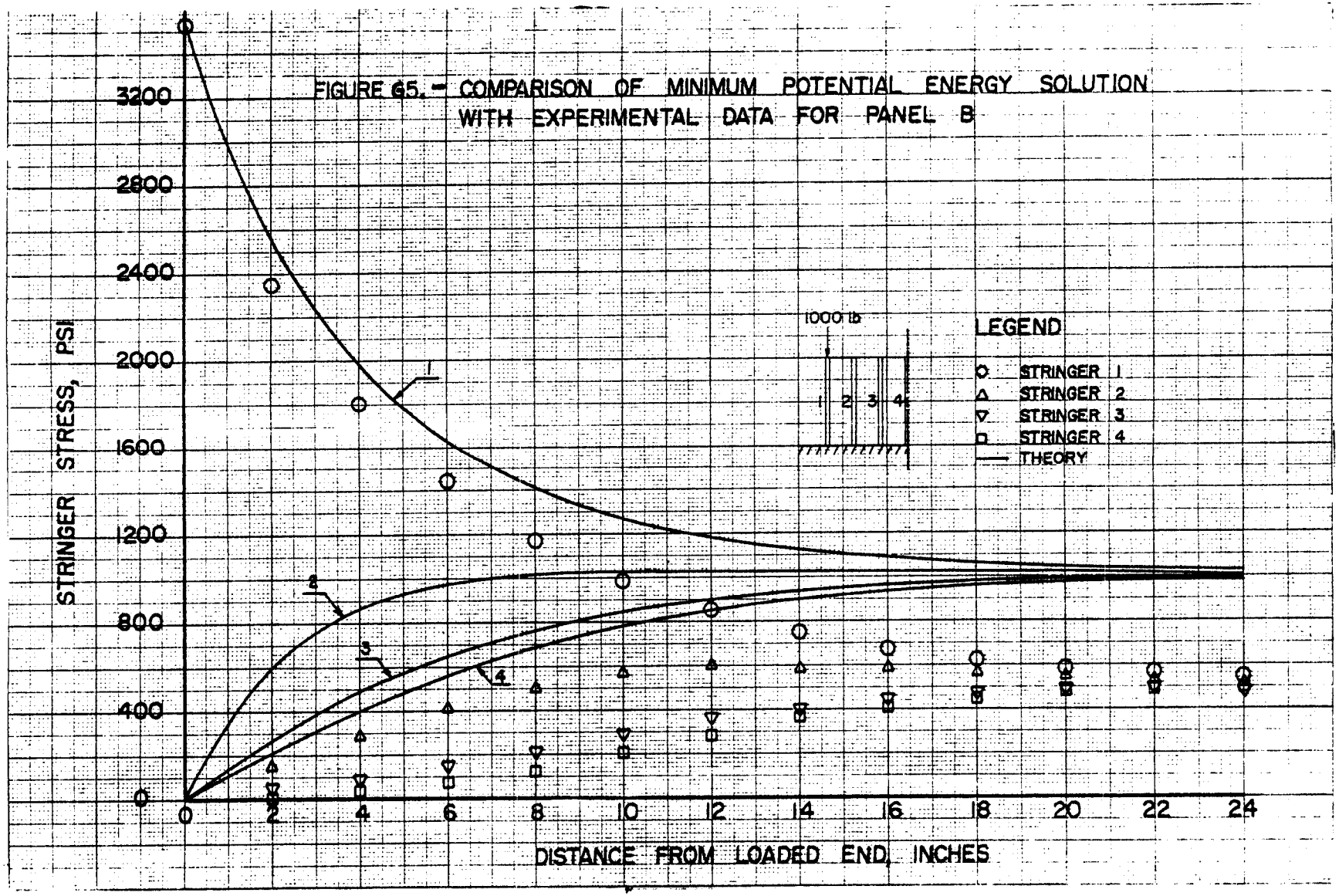

FIGURE 65. - COMPARISON OF MINIMUM POTENTIAL ENERGY SOLUTION WITH EXPERIMENTAL DATA FOR PANEL B

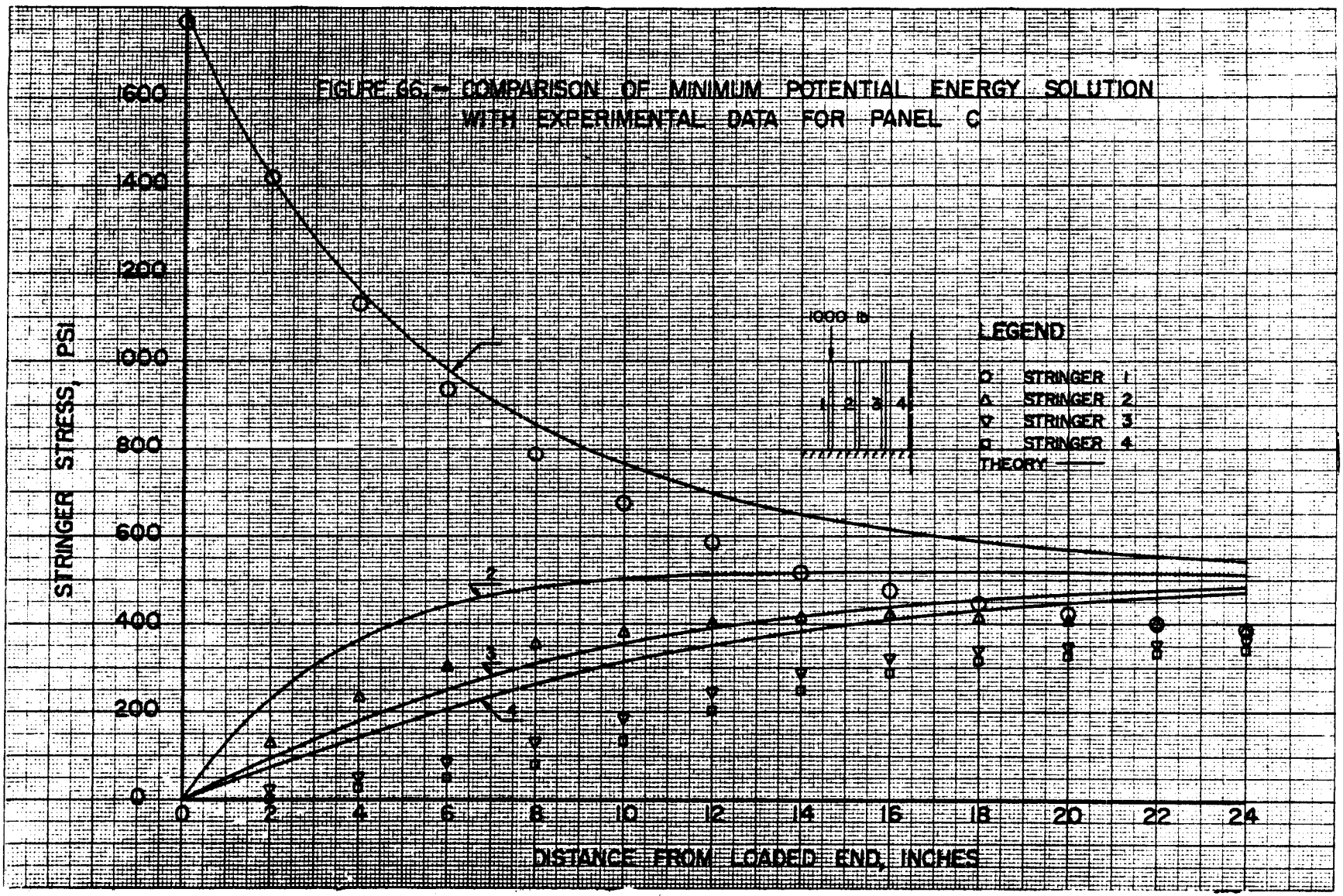

FIGURE 66.- COMPARISON OF MINIMUM POTENTIAL ENERGY SOLUTION WITH EXPERIMENTAL DATA FOR PANEL C

FIGURE 67 - COMPARISON OF STRESS FUNCTION SOLUTION WITH EXPERIMENTAL DATA FOR PANEL C
STRINGER STRESS, PSI
1600
1400
1200
1000
800
600
400
200
0
0
2
4
6
8
10
12
14
16
18
20
22
24
DISTANCE FROM LOADED END, INCHES
LEGEND
THEORY
EXPERIMENT
1000 lb.

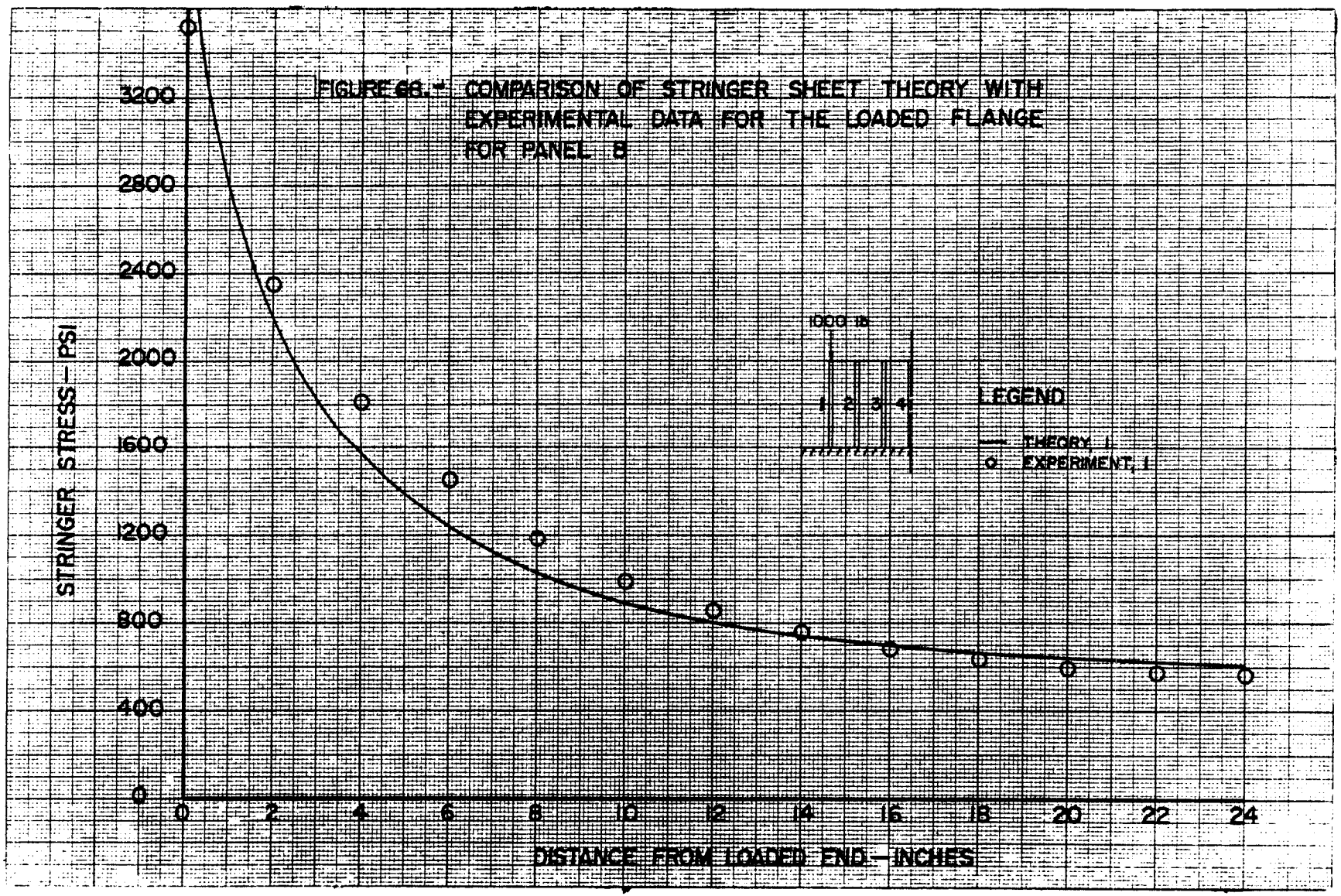

FIGURE 66.- COMPARISON OF STRINGER SHEET THEORY WITH EXPERIMENTAL DATA FOR THE LOADED FLANGE FOR PANEL B

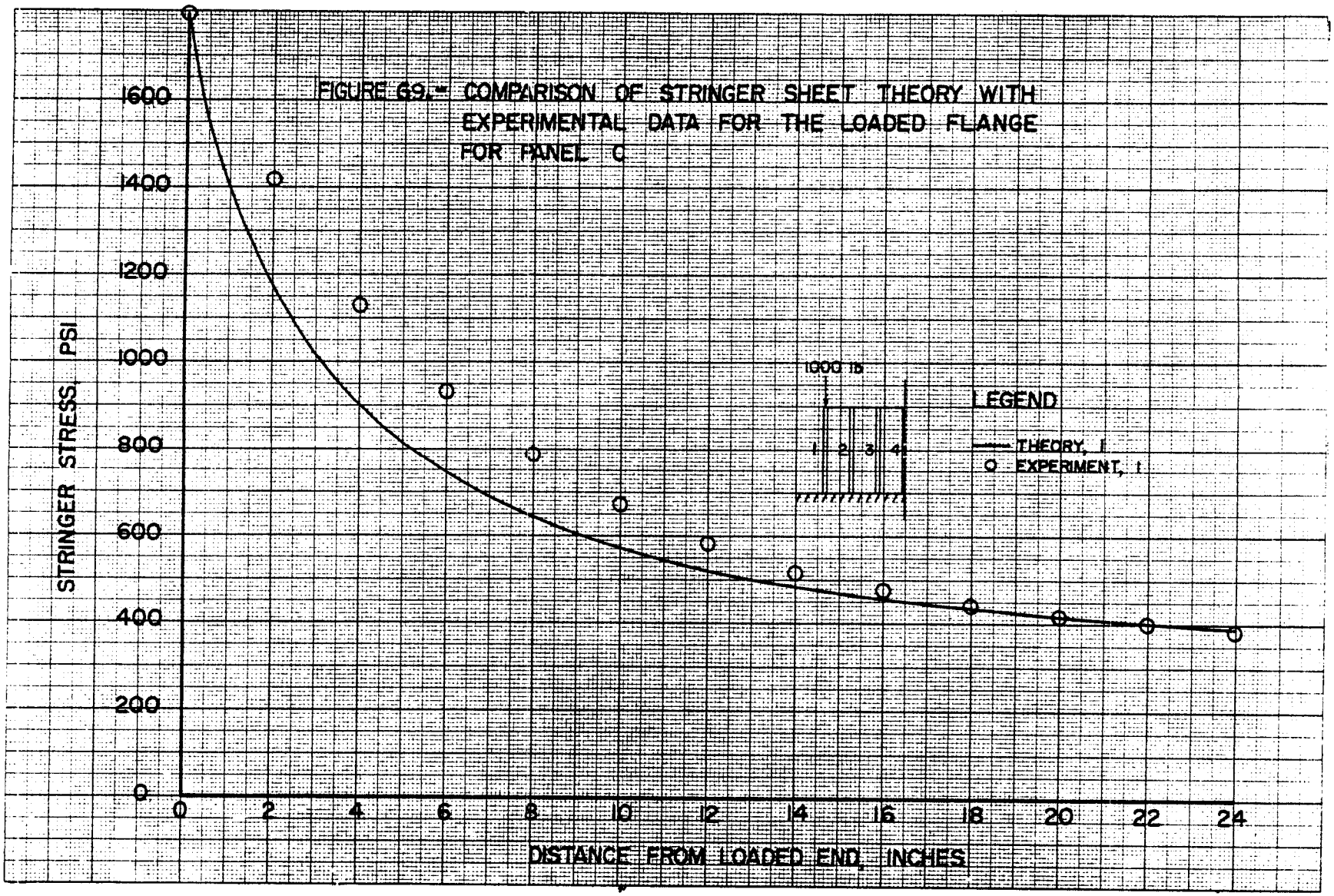

FIGURE 69.- COMPARISON OF STRINGER SHEET THEORY WITH EXPERIMENTAL DATA FOR THE LOADED FLANGE FOR PANEL C

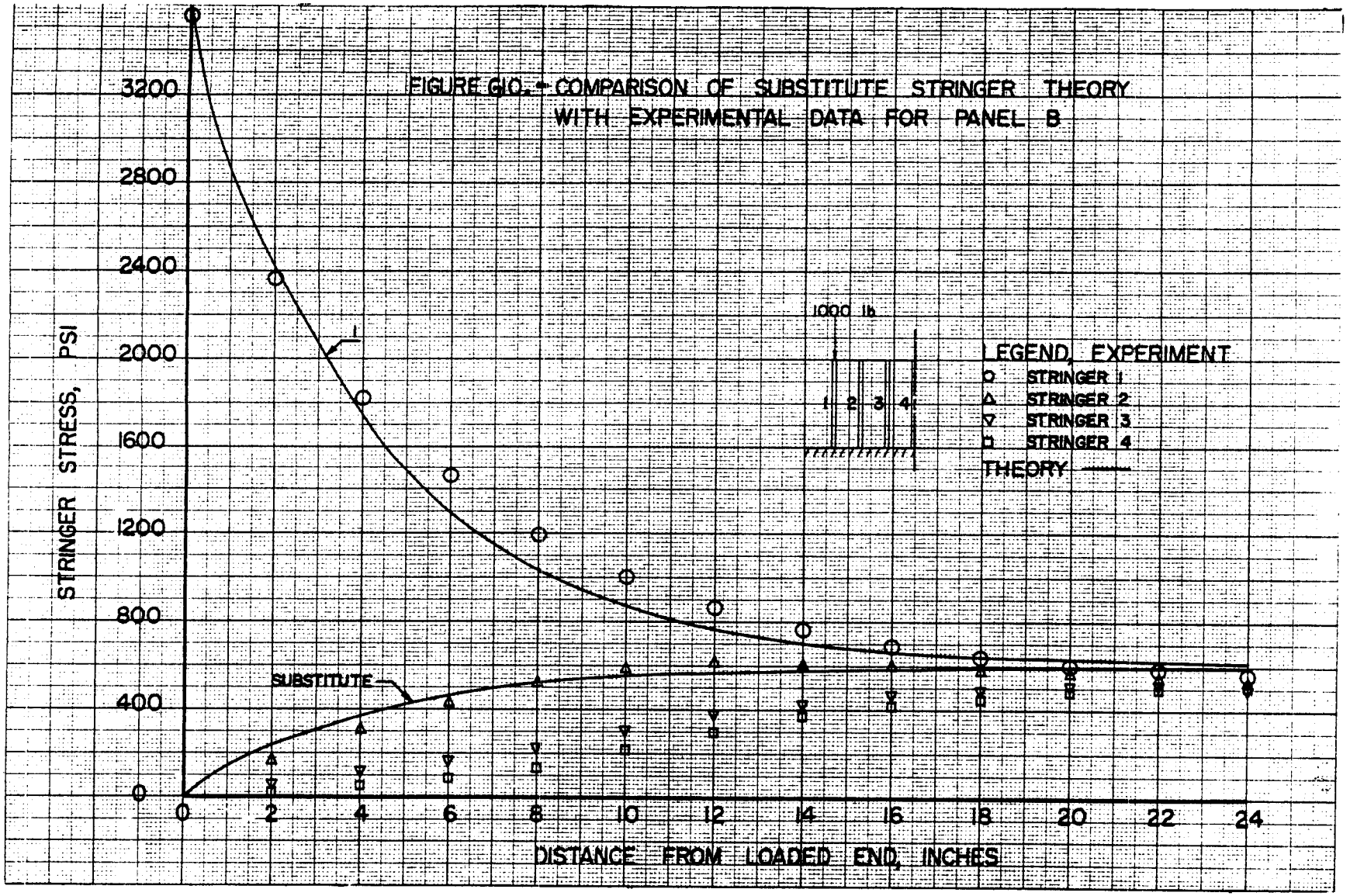

FIGURE G10. - COMPARISON OF SUBSTITUTE STRINGER THEORY WITH EXPERIMENTAL DATA FOR PANEL B

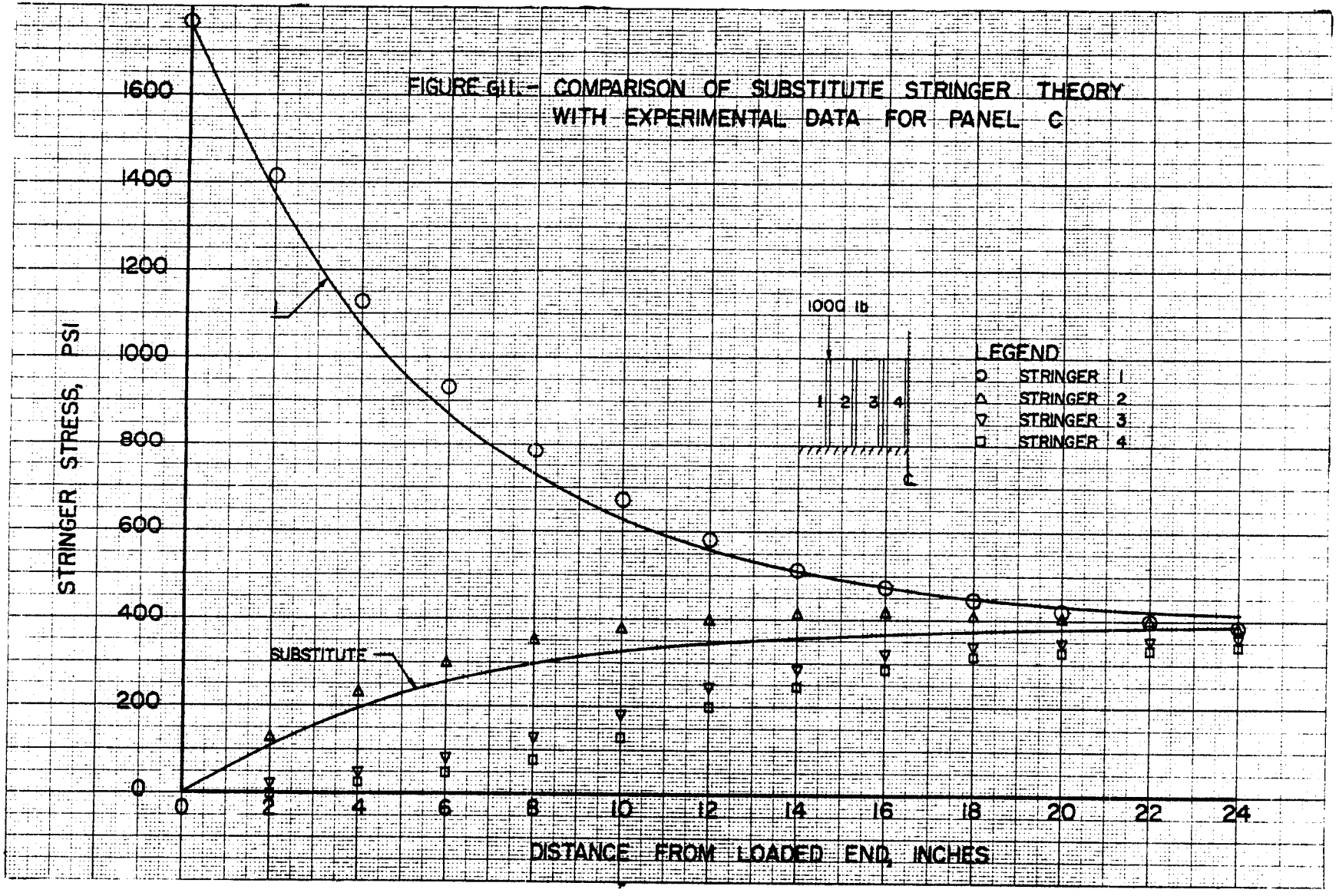
FIGURE 611 - COMPARISON OF SUBSTITUTE STRINGER THEORY WITH EXPERIMENTAL DATA FOR PANEL C
STRINGER STRESS, PSI
1600
1400
1200
1000
800
600
400
200
0
SUBSTITUTE
1000 lb
1 2 3 4
LEGEND
STRINGER 1
STRINGER 2
STRINGER 3
STRINGER 4
0 2 4 6 8 10 12 14 16 18 20 22 24
DISTANCE FROM LOADED END, INCHES

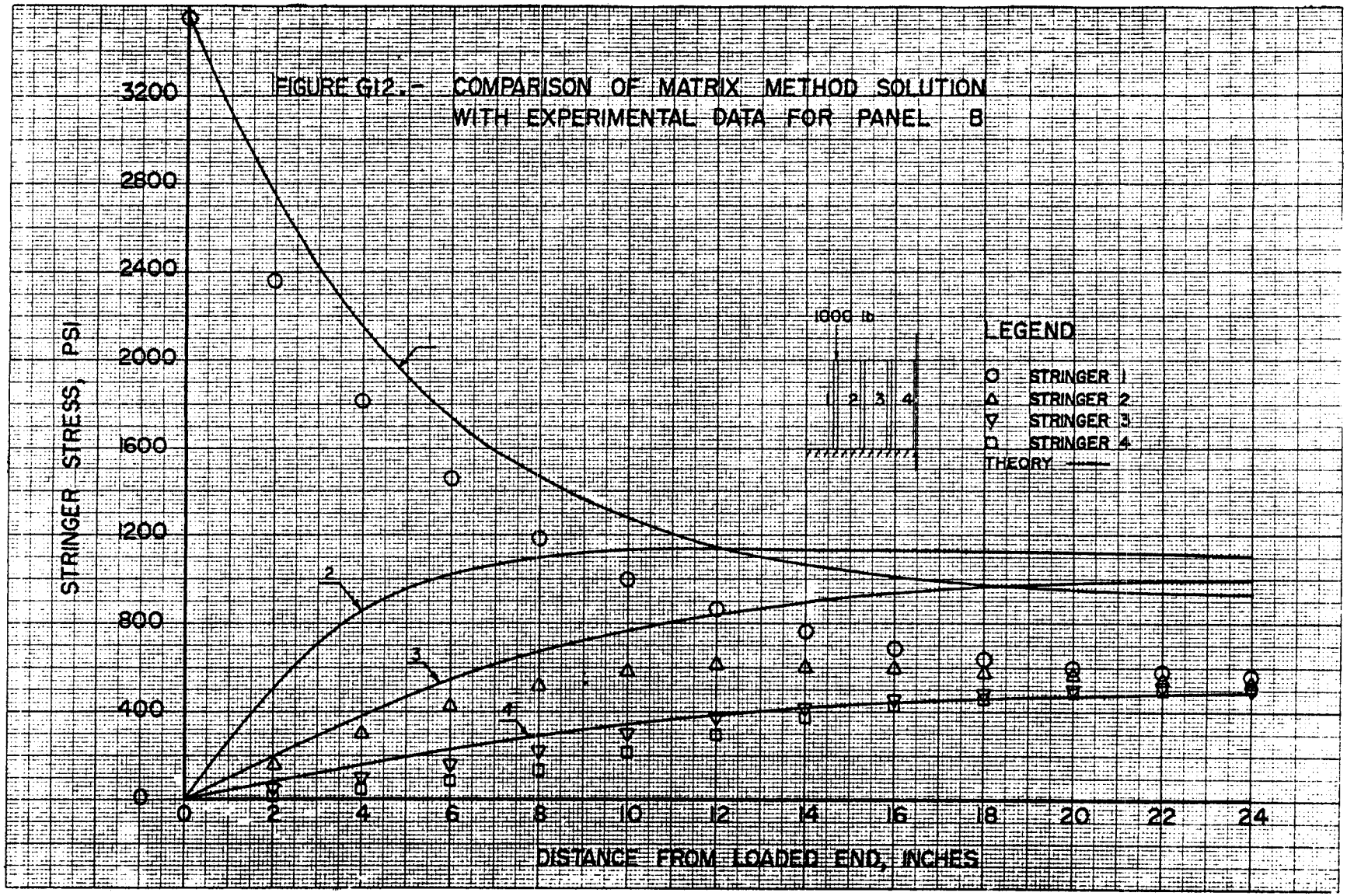

FIGURE G12.- COMPARISON OF MATRIX METHOD SOLUTION WITH EXPERIMENTAL DATA FOR PANEL B

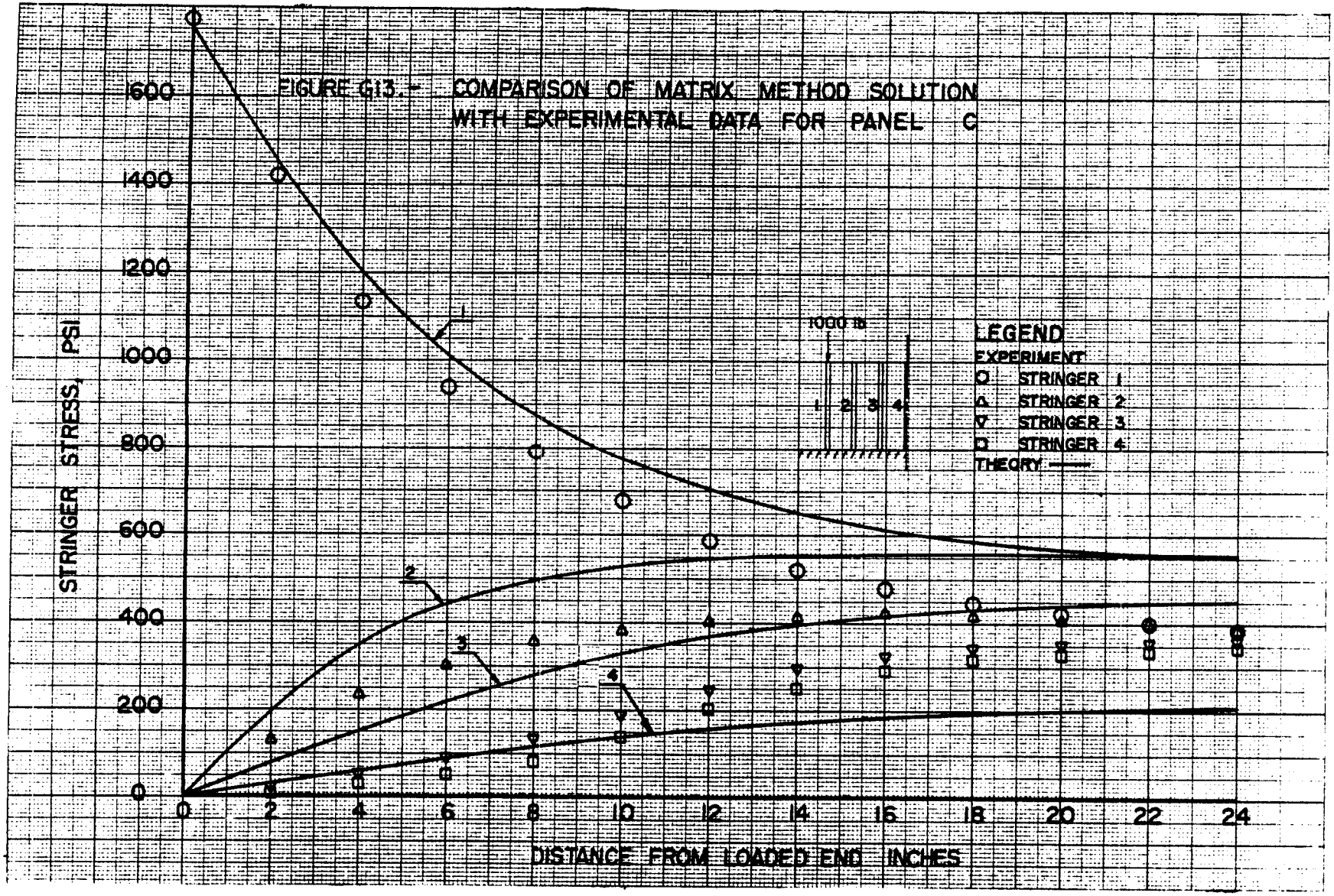

FIGURE G13.- COMPARISON OF MATRIX METHOD SOLUTION WITH EXPERIMENTAL DATA FOR PANEL C

APPENDIX G1

DIFFERENTIAL EQUATION SOLUTION

Figure G1-1 represents one-half of a longitudinally stiffened panel, symmetric about the center line, subjected to an axial compressive load on the outer stringer. From Figure G1-1b, a free-body diagram of the outer normal stresses and the sheet carries only shearing stresses, summing forces in the vertical direction,

$$(\sigma_1 + d\sigma_1)A_1 - \tau_1 t dx - \sigma_1 A = 0,$$

or

$$\frac{d\sigma_1}{dx} - \frac{t}{A_1}\tau_1 = 0. \qquad \text{(G1-1)}$$

From G1-1c, a free-body diagram of stringer 2,

$$\tau_1 t dx + (\sigma_2 + d\sigma_2)A_2 - \sigma_2 A_2 - \tau_2 t dx = 0,$$

or

$$\frac{d\sigma_2}{dx} - \frac{t}{A_2}(\tau_2 - \tau_1) = 0. \qquad \text{(G1-2)}$$

From G1-1d, a free-body diagram of stringer 3,

$$\tau_2 t dx + (\sigma_3 + d\sigma_3)A_3 - \sigma_3 A_3 - \tau_3 t dx = 0,$$

or

$$\frac{d\sigma_3}{dx} - \frac{t}{A_3}(\tau_3 - \tau_2) = 0. \qquad \text{(G1-3)}$$

In general,

$$\frac{d\sigma_n}{dx} - \frac{t}{A_n}(\tau_n - \tau_{n-1}) = 0,$$

or

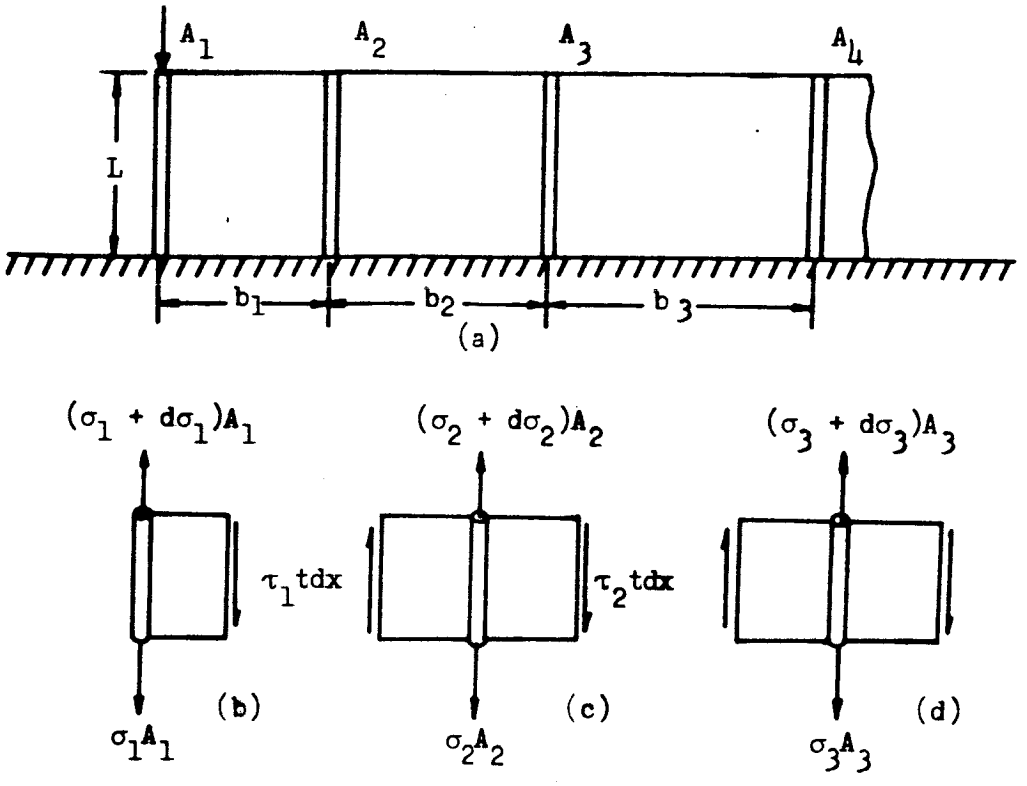

FIGURE G1-1. - LONGITUDINALLY STIFFENED PANEL SUBJECTED TO AXIAL LOAD.

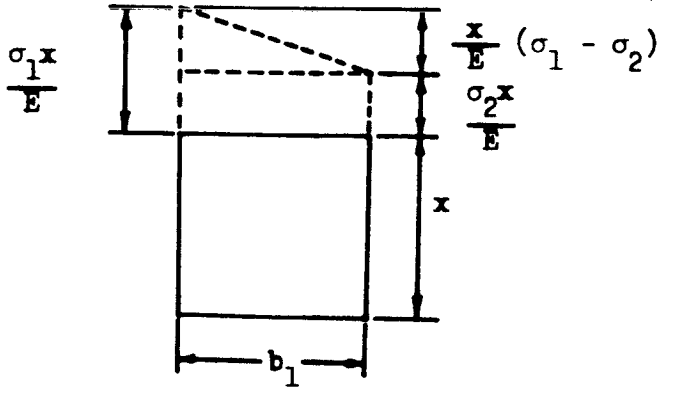

FIGURE G1-2. - SECTION OF SHEET USED IN DETERMINING SHEAR STRAIN.

$$\frac{d\sigma_n}{dx} = \frac{t}{A_n}(\tau_n - \tau_{n-1}) \ . \qquad \text{(G1-4)}$$

Differentiating Equation G1-4 with respect to x,

$$\frac{d^2\sigma_n}{dx^2} = \frac{t}{A_n}\left[\frac{d\tau_n}{dx} - \frac{d\tau_{n-1}}{dx}\right]. \qquad \text{(G1-5)}$$

If we assume tan $\gamma = \gamma$; then from Figure G1-2 the shear strain at station x is given by

$$\gamma_1 = \frac{x}{b_1 E}(\sigma_1 - \sigma_2) \ . \qquad \text{(G1-6)}$$

The incrememt of shear strain is

$$d\gamma = \frac{(\sigma_1 - \sigma_2)}{bE}\, dx. \qquad \text{(G1-7)}$$

The increment of shear stresses is

$$\frac{d\tau_1}{dx} = \frac{G}{b_1 E}(\sigma_1 - \sigma_2) \ , \qquad \text{(G1-8)}$$

or, in general,

$$\frac{d\tau_n}{dx} = \frac{G}{b_n E}(\sigma_n - \sigma_{n+1}) \ . \qquad \text{(G1-9)}$$

Substituting Equation G1-9 into Equation G1-5,

$$\frac{d^2\sigma_n}{dx^2} = \frac{t}{A_n}\left[\frac{G}{b_n E}(\sigma_n - \sigma_{n+1}) - \frac{G}{b_n E}(\sigma_{n-1} - \sigma_n)\right] .$$

Assuming b_n = constant = b,

$$\frac{d^2\sigma_n}{dx^2} = \frac{Gt}{bA_n E}\left[2\sigma_n - \sigma_{n+1} - \sigma_{n-1}\right] \ . \qquad \text{(G1-10)}$$

Numerical Example

The value of A_n is determined from the dimensions of the left hand stringer shown in Figure G2. Thus,

$A_n = (0.556)(1.0) = 0.556.$

This value is used throughout although the actual areas of the other stringers differ by a small amount. The value of b is given by the distance between the centroid of the left hand stringer and the adjacent stringer. Thus,

$$b = \frac{0.556}{2} + 2.273 + \frac{0.556}{2} = 2.829.$$

The mechanical properties of the material are

$$G = (3.9)(10^6) \text{ psi},$$

$$E = (10.5)(10^6) \text{ psi}.$$

Substituting properties of panel C into Equation G1-10 for stringer 1, 2, 3, and 4 yields

$$\frac{d^2\sigma_1}{dx^2} = \frac{(3.9)(10^6)(0.1)}{(2.829)(0.556)(10.5)(10^6)}\left[2\sigma_1 - \sigma_2 - \cancel{\sigma_0}^{0}\right]$$

$$\frac{d^2\sigma_1}{dx^2} = 0.04712\sigma_1 - 0.02356\sigma_2 \qquad \text{(G1-11)}$$

$$\frac{d^2\sigma_2}{dx^2} = 0.02356[2\sigma_2 - \sigma_3 - \sigma_1]$$

$$= 0.04712\sigma_2 - 0.02356\sigma_3 - 0.02356\sigma_1 \qquad \text{(G1-12)}$$

$$\frac{d^2\sigma_3}{dx^2} = 0.02356[2\sigma_3 - \sigma_4 - \sigma_2]$$

$$= 0.04712\sigma_3 - 0.02356\sigma_4 - 0.02356\sigma_2 \qquad \text{(G1-13)}$$

$$\frac{d^2\sigma_4}{dx^2} = 0.02356[2\sigma_4 - \sigma_5 - \sigma_3] .$$

Since the panel has 7 stringers and is symmetric about the center line,

$\sigma_5 = \sigma_3$ by symmetry.

$$\frac{d^2\sigma_4}{dx^2} = 0.04712\sigma_4 - 0.04712\sigma_3 \ . \qquad \text{(G1-14)}$$

Writing Equations G1-11, G1-12, G1-13, and G1-14 in matrix notation

$$D^2 \begin{bmatrix} \sigma_1 \\ \sigma_2 \\ \sigma_3 \\ \sigma_4 \end{bmatrix} = \begin{bmatrix} .04712 & -.02356 & 0 & 0 \\ -.02356 & .04712 & -.02356 & 0 \\ 0 & -.02356 & .04712 & -.02356 \\ 0 & 0 & -.04712 & .04712 \end{bmatrix} \begin{bmatrix} \sigma_1 \\ \sigma_2 \\ \sigma_3 \\ \sigma_4 \end{bmatrix} \qquad \text{(G1-15)}$$

where D^2 denotes $\frac{d^2}{dx^2}$:

The characteristic equation is obtained from the matrix

$$\begin{bmatrix} 0.04712 - \lambda & -0.02356 & 0 & 0 \\ -0.02356 & 0.04712 - \lambda & -0.02356 & 0 \\ 0 & -0.02356 & 0.04712 - \lambda & -0.02356 \\ 0 & 0 & -0.04712 & 0.04712 - \lambda \end{bmatrix}$$

setting its determinant equal to zero

$$\begin{vmatrix} 1 - \zeta & -1/2 & 0 & 0 \\ -1/2 & 1 - \zeta & -1/2 & 0 \\ 0 & -1/2 & 1 - \zeta & -1/2 \\ 0 & 0 & -1 & 1 - \zeta \end{vmatrix} = 0$$

where $\zeta = \frac{\lambda}{0.04712}$.

Expanding the determinant

$$\zeta^4 - 4\zeta^3 + 5\zeta^2 - 2\zeta + 0.125 = 0. \qquad \text{(G1-16)}$$

The roots to Equation A16 are

$$\zeta_1 = 0.6103445$$

$$\zeta_2 = 0.0761025$$

$$\zeta_3 = 1.9135555$$

$$\zeta_4 = 1.3999975$$

so that

$$\lambda_1 = 0.02875943$$

$$\lambda_2 = 0.00358594$$

$$\lambda_3 = 0.09016673$$

$$\lambda_4 = 0.06596788$$

The solution to Equation G1-15 is

$$\begin{bmatrix} \sigma_1 \\ \sigma_2 \\ \sigma_3 \\ \sigma_4 \end{bmatrix} = \left[e^{-\sqrt{M}x} \right] \begin{bmatrix} k_1 \\ k_2 \\ k_3 \\ k_4 \end{bmatrix} \qquad \text{(G1-17)}$$

where M is the coefficient matrix of Equation G1-15. The term $e^{-\sqrt{M}x}$ is most easily determined from the relation

$$e^{-\sqrt{M}x} = e^{-\sqrt{\lambda_1}x} z_1 + e^{-\sqrt{\lambda_2}x} z_2 + e^{-\sqrt{\lambda_3}x} z_3 + e^{-\sqrt{\lambda_4}x} z_4 \qquad \text{(G1-18)}$$

where the z's are given by

$$(\lambda_1 - \lambda_2)(\lambda_1 - \lambda_3)(\lambda_1 - \lambda_4)z_1 = (M - \lambda_2 I)(M - \lambda_3 I)(M - \lambda_4 I) \qquad \text{(G1-19)}$$

$$(\lambda_2 - \lambda_1)(\lambda_2 - \lambda_3)(\lambda_2 - \lambda_4)z_2 = (M - \lambda_1 I)(M - \lambda_3 I)(M - \lambda_4 I) \qquad \text{(G1-20)}$$

$$(\lambda_3 - \lambda_1)(\lambda_3 - \lambda_2)(\lambda_3 - \lambda_4)z_3 = (M - \lambda_1 I)(M - \lambda_2 I)(M - \lambda_4 I) \qquad \text{(G1-21)}$$

$$(\lambda_4 - \lambda_1)(\lambda_4 - \lambda_2)(\lambda_4 - \lambda_3)z_4 = (M - \lambda_1 I)(M - \lambda_2 I)(M - \lambda_3 I) \qquad \text{(G1-22)}$$

where I is the unit matrix.

Performing the calculations indicated:

$$z_1 = \begin{bmatrix} 0.43689435 & 0.31665946 & -0.17716203 & -0.22736339 \\ 0.31665946 & 0.25973232 & -0.13806731 & -0.17716203 \\ -0.17716203 & -0.13806731 & 0.08257029 & 0.08929606 \\ -0.45472678 & -0.35432402 & 0.17859217 & 0.25973235 \end{bmatrix} \quad \text{(G1-23)}$$

$$z_2 = \begin{bmatrix} 0.06816075 & 0.13602883 & 0.17771962 & 0.09618382 \\ 0.13602883 & 0.24588038 & 0.32839648 & 0.17771962 \\ 0.17771962 & 0.32839648 & 0.42360001 & 0.23221266 \\ 0.19236764 & 0.35543923 & 0.46442530 & 0.24588037 \end{bmatrix} \quad \text{(G1-24)}$$

$$z_3 = \begin{bmatrix} 0.06863274 & -0.13604887 & 0.18572910 & -0.10164644 \\ -0.13604887 & 0.25436184 & -0.33934175 & 0.18572910 \\ 0.18572910 & -0.33934175 & 0.44009096 & -0.23769531 \\ -0.20329288 & 0.37145820 & -0.47539065 & 0.25436184 \end{bmatrix} \quad \text{(G1-25)}$$

$$z_4 = \begin{bmatrix} 0.42631324 & -0.31663507 & -0.18628016 & 0.23282548 \\ -0.31663507 & 0.24003309 & 0.14901589 & -0.18628016 \\ -0.18628016 & 0.14901589 & 0.05375296 & -0.08380958 \\ 0.46565096 & -0.37256030 & -0.16761910 & 0.24003311 \end{bmatrix} \quad \text{(G1-26)}$$

At $x = 0$,

$$e^{-\sqrt{M}x} = I.$$

So that equation G1-17 becomes

$$\begin{bmatrix} \sigma_1 \\ \sigma_2 \\ \sigma_3 \\ \sigma_4 \end{bmatrix} = \begin{bmatrix} 1 & 0 & 0 & 0 \\ 0 & 1 & 0 & 0 \\ 0 & 0 & 1 & 0 \\ 0 & 0 & 0 & 1 \end{bmatrix} \begin{bmatrix} k_1 \\ k_2 \\ k_3 \\ k_4 \end{bmatrix} \quad \text{(G1-27)}$$

Also at $x = 0$,

$$\sigma_1 = \frac{P}{A} \approx 1800$$

$$\sigma_2 = \sigma_3 = \sigma_4 = 0.$$

Therefore, from Equation G1-27

$$k_1 = 1800$$

$$k_2 = 0$$

$$k_3 = 0$$

$$k_4 = 0.$$

The solution of Equation G1-15 is thus

$$\begin{bmatrix}\sigma_1\\ \sigma_2\\ \sigma_3\\ \sigma_4\end{bmatrix} = \left(e^{-0.16958605x} \begin{bmatrix} 0.43689435 & 0.31665946 & -0.17716203 & -0.22736339 \\ 0.31665946 & 0.25973232 & -0.13806731 & -0.17716203 \\ -0.17716203 & -0.13806731 & 0.08257029 & 0.08929606 \\ -0.45472678 & -0.35432402 & 0.17859217 & 0.25973235 \end{bmatrix} \right.$$

$$+ e^{-0.059882718x} \begin{bmatrix} 0.06816075 & 0.13602883 & 0.17771962 & 0.09618382 \\ 0.13602883 & 0.24588038 & 0.32839648 & 0.17771962 \\ 0.17771962 & 0.32839648 & 0.42360001 & 0.23221266 \\ 0.19236764 & 0.35543923 & 0.46442530 & 0.24588037 \end{bmatrix}$$

$$+ e^{-0.30027775x} \begin{bmatrix} 0.06863274 & -0.13604887 & 0.18572910 & -0.10164644 \\ -0.13604887 & 0.25436184 & -0.33934175 & 0.18572910 \\ 0.18572910 & -0.33934175 & 0.44009096 & -0.23769531 \\ -0.20329288 & -0.37145820 & -0.47539065 & 0.25436184 \end{bmatrix}$$

$$\left. + e^{-0.25684213x} \begin{bmatrix} 0.42631324 & -0.31663507 & -0.18628016 & 0.23282548 \\ -0.31663507 & 0.24003309 & 0.14901589 & -0.18628016 \\ -0.18628016 & 0.14901589 & 0.05375296 & -0.08380958 \\ 0.46565096 & -0.37256030 & -0.16761910 & 0.24003311 \end{bmatrix} \right) \begin{bmatrix} 1800 \\ 0 \\ 0 \\ 0 \end{bmatrix}$$

or

$$\sigma_1 = [0.43689435e^{-0.16958605x} + 0.06816075e^{-0.059882718x} + 0.06863274e^{-0.30027775x} + 0.42631324e^{-0.25684213x}] 1800$$

$$\sigma_2 = [0.31665946e^{-0.16958605x} + 0.13602883e^{-0.059882718x} + 0.13604887e^{-0.30027775x} + 0.31663507e^{-0.25684213x}] 1800$$

$$\sigma_3 = [-0.17716203e^{-0.16958605x} + 0.17771962e^{-0.059882718x} + 0.18572910e^{-0.30027775x} - 0.18628016e^{-0.25684213x}] 1800$$

$$\sigma_4 = [-0.45472678e^{-0.16958605x} + 0.19236764e^{-0.059882718x} - 0.20329288e^{-0.30027775x} + 0.46565096e^{-0.25684213x}] 1800$$

The stresses obtained from the above solution are plotted in Figure G4 along with the experimental data.

APPENDIX G2

MINIMUM POTENTIAL ENERGY EQUATIONS

Goodey [G13] presented an analysis of the diffusion of an end load into a panel with (2N-1) stringers. In this solution, the stringers are treated as discrete members separated by panels of skin which transmit only shear stresses.

The panel considered is shown in Figure G2-1 where the notation used is also given.

Following is an outline of the analysis:

1. Considering elements of the stringers and longerons, differential equations of equilibrium of the forces were obtained.
2. Equations from step 1 were integrated from x to ∞.
3. The differential equation for the total strain energy, U, for half the complete panel was derived.
4. Conditions of minimum strain energy were then obtained by applying the method of the calculus of variations to the integral for U, resulting in N independent equations. These equations were then substituted into the results of step 2 yielding a set of second order differential equations.
5. A solution was assumed for the equations in step 4.
6. Through the use of boundary conditions, various trigonometric identities, and algebraic manipulations, the constants of integration were evaluated.
7. The final solutions were presented as follows:

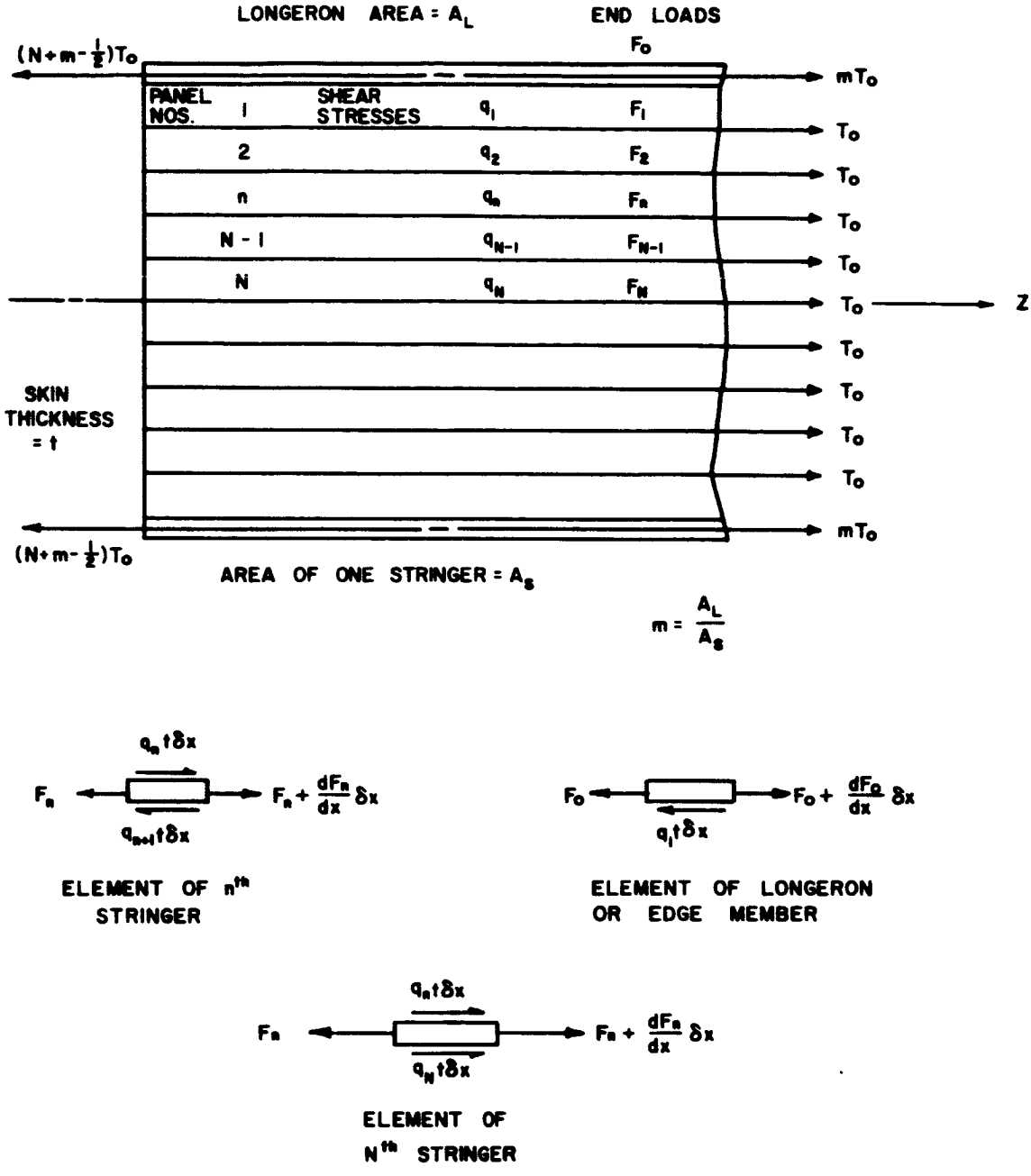

FIGURE G2-1. - NOTATION USED IN MINIMUM POTENTIAL ENERGY SOLUTION.

$$\frac{F_o}{T_\infty} = m - \left(N + m - \frac{1}{2}\right) \cdot$$

$$\sum_{r=1}^{r=N} \frac{[\cos(2N\varphi_r)\sin(2N-1)\varphi_r]\, e^{-2kx(\sin\varphi_r)}}{\sin\varphi_r \left[N + \dfrac{m - \frac{1}{2}}{1+4m(m-1)\sin^2\varphi_r}\right]} \qquad \text{(G2-2)}$$

$$\frac{F_n}{T_\infty} = 1 + (2N + 2M - 1) \cdot$$

$$\sum_{r=1}^{r=N} \frac{[\cos(2N\varphi_r)\cos 2(N-n)\varphi_r]\, e^{-2kx(\sin\varphi_r)}}{N + \dfrac{m - \frac{1}{2}}{1+4m(m-1)\sin^2\varphi_r}} \qquad \text{(G2-3)}$$

$n = 1, 2, 3, \ldots, N$

where $m = \dfrac{A_L}{A_S}$, $k = \left[\dfrac{Gt}{bEA_S}\right]^{1/2}$, $\varphi_r = \dfrac{r}{2N+1}$, r = 1 to N.

For the special case when m = 1 the above equations reduced to

$$\frac{F_o}{T_\infty} = 1 + 2\sum_{r=1}^{r=N} \cos^2\varphi_r\, e^{-2kx\sin\varphi_r} \qquad \text{(G2-4)}$$

$$\frac{F_n}{T_\infty} = 1 + 2\sum_{r=1}^{r=N} \cos\varphi_r \cos(2N+1)\varphi_r\, e^{-2kx\sin\varphi_r} \qquad \text{(G2-5)}$$

Numerical Example

Consider panel C as shown in Figure G2. It is assumed that all stiffener areas are the same and that b = 2.84 = constant, t = 0.1 = constant. This panel is, according to Goodey's nomenclature, a 5 stringer, 2 longeron panel. Thus

$$2N-1 = 5 ,$$

$$N = 3 .$$

Since the areas of the stiffeners are assumed to be equal, the ratio of longeron area to stringer area is

$$m = \frac{A_L}{A_S} = 1$$

so that equations G2-4 and G2-5 can be used. Remembering that

$$\varphi_r = \frac{r\pi}{2N+1} = \frac{r\pi}{7} \text{ radians},$$

then

$$\frac{F_o}{T_\infty} = 1 + 2\sum_{r=1}^{3} \cos^2\varphi_r e^{-2kx\sin\varphi_r}$$

$$= 1 + 2\left(\cos^2\varphi_1 e^{-2kx\sin\varphi_1} + \cos^2\varphi_2 e^{-kx\sin\varphi_2} + \cos^2\varphi_3 e^{-2kx\sin\varphi_3}\right). \quad \text{(G2-6)}$$

Substituting the value of φ_r into Equation G2-6,

$$\frac{F_o}{T_\infty} = 1 + 2\left(0.811945e^{-0.86836kx} + 0.388939e^{-1.5634kx} + 0.049461e^{-1.97489kx}\right). \quad \text{(G2-7)}$$

Using equation G2-5 for stringer 1,

$$\frac{F_1}{T_\infty} = 1 + 2\sum_{r=1}^{3} \cos\varphi_r \cos 3\varphi_r e^{-2xk\sin\varphi_r}.$$

Substituting the value of φ_r,

$$\frac{F_1}{T_\infty} = 1 + 2\left(0.199576e^{-0.86836kx} - 0.561796e^{-1.5634kx} - 0.138925e^{-1.94978kx}\right). \quad \text{(G2-8)}$$

Using equation G2-5 for stringer 2

$$\frac{F_2}{T_\infty} = 1 + 2\sum_{r=1}^{r=3} \cos\varphi_r \cos 5\varphi_r e^{-2kx\sin\varphi_r}.$$

Substituting the value of φ_r,

$$\frac{F_2}{T_\infty} = 1 + 2\left(-0.561589e^{-0.86836kx} - 0.138874e^{-1.5634kx} + 0.200652e^{-1.94478kx}\right). \qquad (G2\text{-}9)$$

Likewise for stringer 3

$$\frac{F_3}{T_\infty} = 1 + 2\left(-0.90082e^{-0.86836kx} + 0.62365e^{-1.5634kx} - 0.22268e^{-1.94978kx}\right). \qquad (G2\text{-}10)$$

Equations G2-7, G2-8, G2-9 and G2-10 apply to any 7 stringer panel with m = 1 and b and t constant. Thus they can be used for the analysis of panel B as well as C, the only difference being in the value of k.

Numerical evaluation of the above equations was performed at increments of x = 1 inch from x = 0 to x = 24. To expedite these calculations, a digital computer program was written for the Univac Solid State 80 which is on the University of Alabama's main campus. The machine language used was Bama-Bell II which is a floating point mathematical interpretative system for the USS 80.[2]

The program used follows:

```
200     I556901000
201     I506901000
202     0600000000
203     0800000005
204     I201100109
205     6400400000
206     3400109300
```

[2]Gray, William J.: Bama-Bell II, Floating Point Mathematical Interpretative System for USS 80 System. University of Alabama Computer Center.

```
207     3103300301
208     R601301301
209     3106301301
210     3104300302
211     R601302302
212     3107302302
213     3105300303
214     R601303303
215     3108303303
216     1301302302
217     1302303303
218     3102303401
219     1101401401
220     3401100401
221     I241400401
222     1101400400
223     7000023206
224     7000003202
225     I260000000
226     R403000000
zzz       200        Note: the z's must be a double punch nine over
                         eight.
```

Writing the equations to be evaluated in the general form

$$\frac{F_n}{T_\infty} = 1 + 2\left(C_1 e^{-0.86836kx} + C_2 e^{-1.5634kx} + C_3 e^{-1.97489kx}\right),$$

the following shows the necessary data locations for use of the above given program:

100 T_∞ (in floating point)

101	5010000000	
102	5020000000	
103	4986836000	(negative)
104	5015634000	(negative)
105	5019497800	(negative)
106	C_1	(in floating point)
107	C_2	(in floating point)
108	C_3	(in floating point)
109	k	(in floating point)

The print out, in floating point, is of the form:

x	f(x)
x_1	$f(x_1)$
x_2	$f(x_2)$
.	.
.	.
.	.
5124000000	f(24)

For panel C having a 1000 load on each longeron,

$$T_\infty = \frac{2000}{2(0.5557)+2(0.5632)+2(0.5618)+0.5612} = 509.86$$

$$k = \left[\frac{(3.9)(10^6)(0.1)}{(10.5)(10^6)(2.84)(0.555)}\right]^{1/2} = 0.15355.$$

Equations G2-7, G2-8, G2-9 and G2-10 are shown plotted in Figure G6 along with experimental data for comparison.

APPENDIX G3

STRESS FUNCTION SOLUTION

Goodey [G13] presented a stress function type solution for the analysis of a plane sheet reinforced in two directions at right angles. This analysis was as follows:

Referring to Figure G3-1, the following equations were obtained for the stiffeners.

$$\varepsilon_x = \frac{1}{E}(\sigma_x - \mu\sigma_y) \tag{G3-1}$$

$$\varepsilon_y = \frac{1}{E}(\sigma_y - \mu\sigma_x) \tag{G3-2}$$

$$G = \frac{E}{2(1+\mu)} = \frac{\tau_{xy}}{\varepsilon_{xy}} \quad . \tag{G3-3}$$

Defining the average normal stress as

$$\frac{P_{sheet} + P_{stiffener}}{A_{sheet} + A_{stiffener}} ,$$

the average stress in direction O_x is

$$\frac{t\sigma_x + t_x(\sigma_x - \mu\sigma_y)}{t + tx} = P_x \tag{G3-4}$$

and the average stress in direction O_y is

$$\frac{t\sigma_y + ty(\sigma_y - \mu\sigma_x)}{t + ty} = P_y \ . \tag{G3-5}$$

Defining

$$k_x = 1 + \frac{tx}{t}, \quad tk_x = t + tx \tag{G3-6}$$

and

$$k_y = 1 + \frac{t_y}{t} , \quad tk_y = t + ty. \tag{G3-7}$$

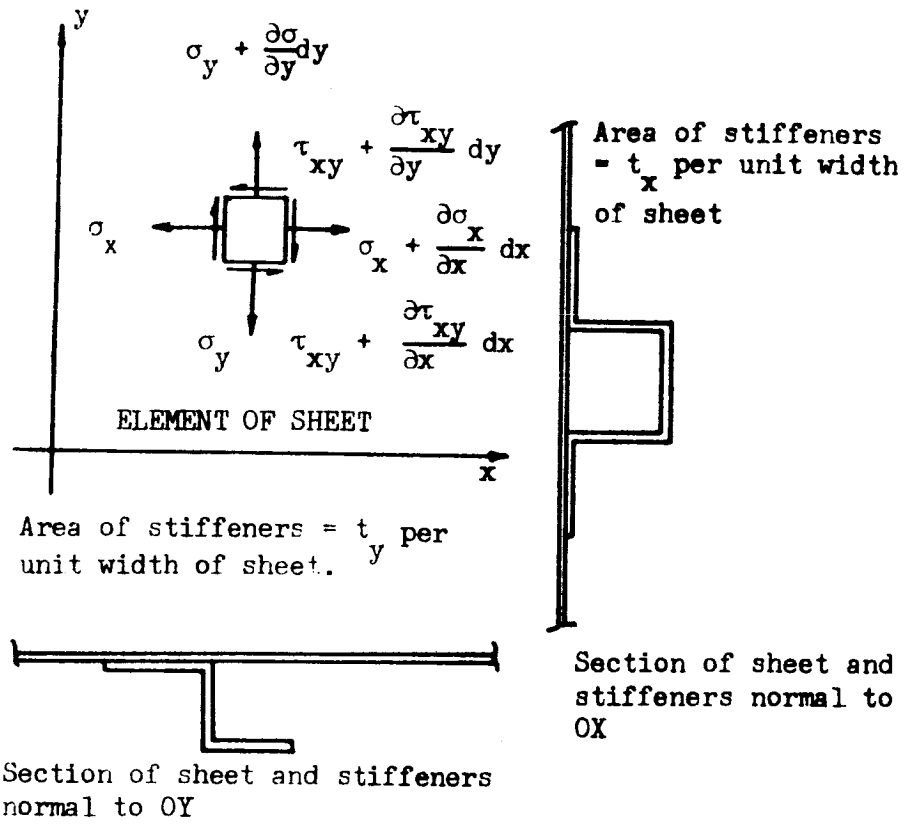

FIGURE G3-1. - DIAGRAM OF PLAIN SHEET REINFORCED IN TWO DIRECTIONS AT RIGHT ANGLES.

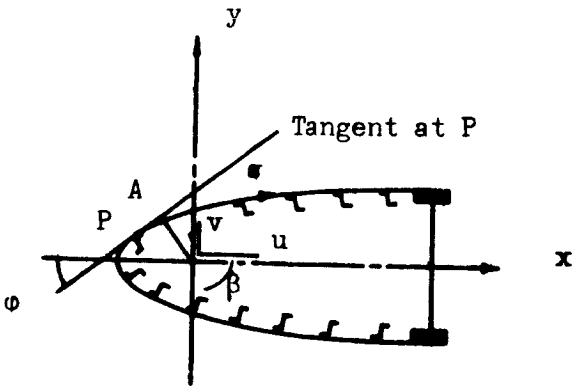

FIGURE G3-2. - VIEW OF CROSS-SECTION LOOKING ALONG OZ IN POSITIVE DIRECTION OF Z.

Substituting Equations G3-6 and G3-7 into Equations G3-4 and G3-5, yields, after some manipulation,

$$P_x = \sigma_x - \mu\sigma_y\left(1 - \frac{1}{k_x}\right) \tag{G3-8}$$

$$P_y = \sigma_y - \mu\sigma_x\left(1 - \frac{1}{k_y}\right). \tag{G3-9}$$

Distributing the area of the stiffeners in the x direction uniformly over the sheet results in the free-body diagrams of Figure G3-3.

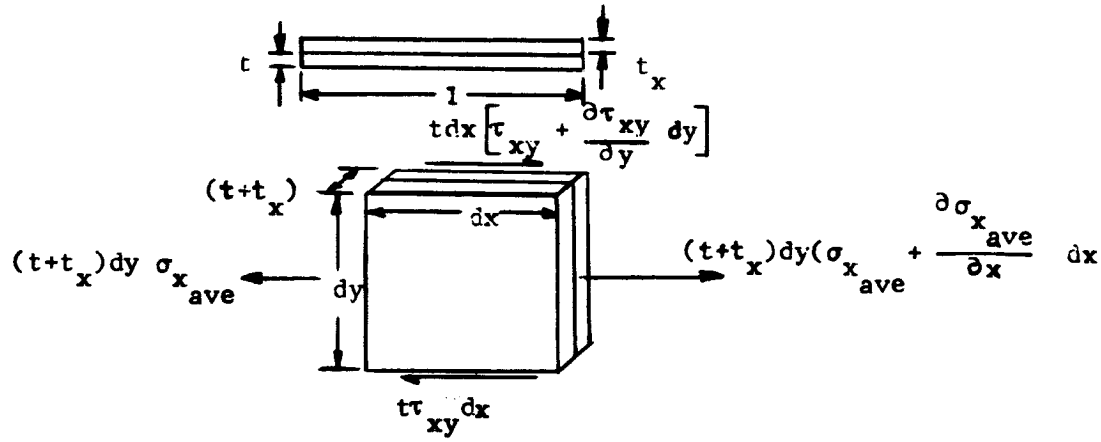

FIGURE G3-3. - FREE-BODY SHOWING FORCES IN x DIRECTION ACTING ON ELEMENT OF SHEET AND STRINGER

Summation of forces in the x direction yields

$$(t + t_x)\frac{\partial \sigma_{x_{ave}}}{\partial x} + t\frac{\partial \tau_{xy}}{\partial y} = 0. \tag{G3-10}$$

Substituting Equation G3-4 into Equation G3-10 for $\sigma_{x_{ave}}$ results in

$$\frac{\partial}{\partial x}\ \sigma_x t + (\sigma_x - \mu\sigma_y)t_x\ + t\frac{\partial \tau_{xy}}{\partial y} = 0. \tag{G3-11}$$

From Equation G3-4,

$$\frac{\partial}{\partial x}\ \partial_x t + (\partial_x - \mu\partial_y)t_x\ + t\frac{\partial \tau_{xy}}{\partial y} = \frac{\partial}{\partial x}\ P_x(t+t_x)\ + t\frac{\partial \tau_{xy}}{\partial y}$$

$$= t\frac{\partial \tau_{xy}}{\partial y} + \frac{\partial}{\partial x}(P_x k_x t) \tag{G3-12}$$

so that

$$t\frac{\partial \tau_{xy}}{\partial y} + \frac{\partial}{\partial x}\left(tP_x k_x\right) = 0$$

or

$$\frac{\partial \tau_{xy}}{\partial y} + k_x \frac{\partial P_x}{\partial x} = 0. \tag{G3-13}$$

Similarly, the area of the stiffeners in the y direction may be distributed and forces summed in the y direction. The following equation results

$$\frac{\partial \tau_{xy}}{\partial x} + k_y \frac{\partial P_y}{\partial y} = 0. \tag{G3-14}$$

Equations G3-13 and G3-14 are satisfied if we express the stresses in terms of a stress function Φ, where

$$\tau_{xy} = -\frac{\partial^2 \Phi}{\partial x \partial y} \tag{G3-15}$$

$$P_x = \frac{1}{k_x}\frac{\partial^2 \Phi}{\partial y^2} \tag{G3-16}$$

$$P_y = \frac{1}{k_y}\frac{\partial^2 \Phi}{\partial x^2}\,. \tag{G3-17}$$

Substituting Equations G3-8 and G3-9 into Equations G3-1 and G3-2 and rewriting Equation G3-3 yields

$$E\varepsilon_x = P_x - P_y\frac{\mu}{k_x} \tag{G3-18}$$

$$E\varepsilon_y = P_y - P_x\frac{\mu}{k_y} \tag{G3-19}$$

$$E\varepsilon_{xy} = 2(1+\mu)\tau_{xy}\,. \tag{G3-20}$$

Now, using the relations,

$$\varepsilon_x = \frac{\partial u}{\partial x}$$

$$\varepsilon_y = \frac{\partial v}{\partial y}$$

$$\varepsilon_{xy} = \frac{\partial v}{\partial x} + \frac{\partial u}{\partial y}$$

$$P_x = \frac{1}{k_x}\frac{\partial^2 \Phi}{\partial y^2}$$

$$P_y = \frac{1}{k_y}\frac{\partial^2 \Phi}{\partial x^2}$$

$$\tau_{xy} = -\frac{\partial^2 \Phi}{\partial x \partial y}$$

and substituting into Equations G3-18, G3-19, and G3-20

$$E\frac{\partial u}{\partial x} = \frac{1}{k_x}\frac{\partial^2 \Phi}{\partial y^2} - \frac{\mu}{k_x}\frac{1}{k_y}\frac{\partial^2 \Phi}{\partial x^2}, \qquad \text{(G3-21)}$$

$$E\frac{\partial v}{\partial y} = \frac{1}{k_y}\frac{\partial^2 \Phi}{\partial x^2} - \frac{\mu}{k_y}\frac{1}{k_x}\frac{\partial^2 \Phi}{\partial y^2}, \qquad \text{(G3-22)}$$

$$E\left(\frac{\partial v}{\partial x} + \frac{\partial u}{\partial y}\right) = 2(1 + \mu)\left(-\frac{\partial^2 \Phi}{\partial x \partial y}\right). \qquad \text{(G3-23)}$$

Differentiating Equation G3-21 twice with respect to y,

$$E\frac{\partial^3 u}{\partial x \partial y^2} = \frac{1}{k_x}\frac{\partial^4 \Phi}{\partial y^4} - \frac{\mu}{k_x k_y}\frac{\partial^4 \Phi}{\partial x^2 \partial y^2}. \qquad \text{(G3-24)}$$

Differentiating Equation G3-22 twice with respect to x,

$$E\frac{\partial^3 v}{\partial y \partial x^2} = \frac{1}{k_y}\frac{\partial^4 \Phi}{\partial x^4} - \frac{\mu}{k_x k_y}\frac{\partial^4 \Phi}{\partial y^2 \partial x^2}. \qquad \text{(G3-25)}$$

Adding Equations G3-24 and G3-25 then substituting Equation G3-23 yields

$$\frac{1}{k_y}\frac{\partial^4 \Phi}{\partial x^4} + 2\left[1 + \mu\left(1 - \frac{1}{k_x k_y}\right)\right]\frac{\partial^4 \Phi}{\partial x^2 \partial y^2} + \frac{1}{k_x}\frac{\partial^4 \Phi}{\partial y^4} = 0. \qquad \text{(G3-26)}$$

If $k_x = k_y = 1$, this equation reduces to the familiar equation $\nabla^4 \Phi = 0$ for a plane un-reinforced sheet.

Assume a solution of Equation G3-26 of the form

$$\Phi = (A\cosh\alpha_1\lambda y + B\cosh\alpha_2\lambda y)\sin\lambda x \qquad \text{(G3-27)}$$

where α_1 and α_2 satisfy the equation

$$\frac{\alpha^4}{k_x} - 2\left[1 + \mu(1 - \frac{1}{k_x k_y})\right]\alpha^2 + \frac{1}{k_y} = 0 \ , \qquad \text{(G3-28)}$$

or

$$\frac{\alpha_1^2}{k_x} \ , \ \frac{\alpha_2^2}{k_x} = 1 + \mu(1 - \frac{1}{k_x k_y}) \pm \sqrt{\left[1 + \mu(1 - \frac{1}{k_x k_y})\right]^2 - \frac{1}{k_x k_y}} \ ; \qquad \text{(G3-29)}$$

and A and B are constants.

The stresses are now given by the equations

$$-\tau_{xy} = \frac{\partial^2\Phi}{\partial x \partial y} = \lambda^2\cos\lambda x\left(A\alpha_1\sinh\alpha_1\lambda y + B\alpha_2\sinh\alpha_2\lambda y\right) \ , \qquad \text{(G3-30)}$$

$$k_x P_x = \frac{\partial^2\Phi}{\partial y^2} = \lambda^2\sin\lambda x\left(A\alpha_1^2\cosh\alpha_1\lambda y + B\alpha_2^2\cosh\alpha_2\lambda y\right) \ , \qquad \text{(G3-31)}$$

$$k_y P_y = \frac{\partial^2\Phi}{\partial x^2} = -\lambda^2\sin\lambda x\left(A\cosh\alpha_1\lambda y + B\cosh\alpha_2\lambda y\right) . \qquad \text{(G3-32)}$$

In order to satisfy the condition $P_y = 0$ when $y = \pm a$, it is necessary that

$$A\cosh\alpha_1\lambda a + B\cosh\alpha_2\lambda a = 0$$

or

$$\frac{A}{\cosh\alpha_2\lambda a} = -\frac{B}{\cosh\alpha_1\lambda a} = k(\lambda) \ . \qquad \text{(G3-33)}$$

Substitution into Equations G3-27, G3-30, G3-31 and G3-32 yields

$$\Phi = k(\lambda)\left[(\cosh\alpha_2\lambda a)(\cosh\alpha_1\lambda y) - (\cosh\alpha_1\lambda a)(\cosh\alpha_2\lambda y)\right]\sin\lambda x, \qquad \text{(G3-34)}$$

$$-\tau_{xy} = \lambda^2 k(\lambda)\left[(\alpha_1\cosh\alpha_2\lambda a)(\sinh\alpha_1\lambda y) - (\alpha_2\cosh\alpha_1\lambda a)(\sinh\alpha_2\lambda y)\right]\cosh\lambda x, \qquad \text{(G3-35)}$$

$$k_x P_x = \lambda^2 k(\lambda)\left[(\alpha_1{}^2 \cosh\alpha_2\lambda a)(\cosh\alpha_1\lambda y) - (\alpha_2{}^2 \cosh\alpha_1\lambda a)(\cosh\alpha_2\lambda y)\right]\sin\lambda x, \tag{G3-36}$$

$$k_y P_y = -\,{}^2 k(\lambda)\left[(\cosh\alpha_2\lambda a)(\cosh\alpha_1\lambda y) - (\cosh\alpha_1\lambda a)(\cosh\alpha_2\lambda y)\right]\sin\lambda x\ . \tag{G3-37}$$

The end load in the skin from y = 0 to y = a is given by

$$\int_o^a P_x k_x t\,dy = \lambda t k(\lambda)\left[(\alpha_1 \cosh\alpha_2\lambda a)(\sinh\alpha_1\lambda a) - (\alpha_2 \cosh\alpha_1\lambda a)(\sinh\alpha_2\lambda a)\right]\sin\lambda x, \tag{G3-38}$$

and the end load in one flange is given by

$$(A_F P_x)_{y=a} = \frac{A_F{}^2 k(\lambda)}{k_x}\left[(\alpha_1{}^2 - \alpha_2{}^2)(\cosh\alpha_1\lambda a)(\cosh\alpha_2\lambda a)\right]\sin\lambda x. \tag{G3-39}$$

If $2T_o$ is the total end load, integration with respect to λ from 0 to ∞ yields

$$\frac{2T_o}{\pi} = \int_0^\infty \lambda t k(\lambda)\left[(\alpha_1 \cosh\alpha_2\lambda a)(\sinh\alpha_1\lambda a) - (\alpha_2 \cosh\alpha_1\lambda a)(\sinh\alpha_2\lambda a) + \frac{A_F}{k_x t}(\alpha_1{}^2 - \alpha_2{}^2)(\cosh\alpha_1\lambda a)(\cosh\alpha_2\lambda a)\right]\sin\lambda x\,d\lambda\ . \tag{G3-40}$$

If T_o is constant, it may be represented by the integral

$$\frac{2T_o}{\pi}\int_o^\infty \frac{\sin\lambda x}{\lambda}\,d\lambda\ . \tag{G3-41}$$

Since the two integrals must be the same,

$$k(\lambda) = \frac{2T_o a}{\pi t x}\left[\frac{1}{\alpha_1\lambda a(\cosh\alpha_2\lambda a)(\sinh\alpha_1\lambda a) - \alpha_2\lambda a(\cosh\alpha_1\lambda a)(\sinh\alpha_2\lambda a) + m\lambda^2 a^2(\alpha_1{}^2 - \alpha_2{}^2)(\cosh\alpha_1\lambda a)(\cosh\alpha_2\lambda a)}\right] \tag{G3-42}$$

where $m = \dfrac{A_F}{a k_x t}$. Therefore

$$\Phi = \frac{2T_o a}{t} \int_o^\infty \frac{(\cosh\alpha_2\lambda a)(\cosh\alpha_1\lambda y) - (\cosh\alpha_1\lambda a)(\cosh\alpha_2\lambda y)\sin\lambda x d\lambda}{\left[\begin{array}{l}\alpha_1\lambda a(\cosh\alpha_2\lambda a)(\sinh\alpha_1\lambda a) - \alpha_2\lambda a(\cosh\alpha_1\lambda a)(\sinh\alpha_2\lambda a) \\ + m\lambda^2 a^2(\alpha_1^2 - \alpha_2^2)(\cosh\alpha_1\lambda a)(\cosh\alpha_2\lambda a)\end{array}\right]\lambda} \cdot$$

(G3-43)

Letting $\theta = \lambda a$, Equation G3-43 may be simplified in appearance becoming

$$\Phi = \frac{2T_o a}{\pi t} \int_o^\infty \left[\frac{\cosh\frac{\alpha_1\theta y}{a}}{\cosh\alpha_1\theta} - \frac{\cosh\frac{\alpha_2\theta y}{a}}{\cosh\alpha_2\theta y}\right] \cdot \left[\frac{\frac{1}{\theta^2}\sin\frac{\theta x}{a}\, d\theta}{\alpha_1\tanh\alpha_1\theta - \alpha_2\tanh\alpha_2\theta + m(\alpha_1^2 - \alpha_2^2)\theta}\right] . \quad \text{(G3-44)}$$

Evaluation of this integral was accomplished using the theory of residues. The result obtained was

$$\Phi = \frac{T_o a}{t}\left[\frac{(y^2-a^2)}{2a^2(1+m)} - 2\sum \frac{\frac{\cos\frac{\alpha_1\theta_n y}{a}}{\cos\alpha_1\theta_n} - \frac{\cos\frac{\alpha_2\theta_n y}{a}}{\cos\alpha_2\theta_n} e^{-\frac{\theta_n x}{a}}}{\theta_n^2\,\alpha_1^2\sec^2\alpha_1\theta_n - \alpha_2^2\sec^2\alpha_2\theta_n - m(\alpha_1^2-\alpha_2^2)}\right] \quad \text{(G3-45)}$$

where the coefficients θ_n are roots of the equation

$$\alpha_1\tan\alpha_1\theta - \alpha_2\tan\alpha_2\theta + m(\alpha_1^2 - \alpha_2^2)\theta = 0 . \quad \text{(G3-46)}$$

The stresses are now obtained from Equation G3-45 by differentiation. Letting $T_o = p_o a k_x t(1+m)$ where p_o is the uniform stress at $x = \infty$, the stresses are

$$\tau_{xy} = -\frac{\partial^2\Phi}{\partial x \partial y} = 2P_o k_x(1+m)\sum \frac{\left[\frac{\alpha_1\sin\frac{\alpha_1\theta_n y}{a}}{\cos\alpha_1\theta_n} - \frac{\alpha_2\sin\frac{\alpha_2\theta_n y}{a}}{\cos\alpha_2\theta_n}\right] e^{-\frac{\theta_n x}{a}}}{\alpha_1^2\sec^2\alpha_1\theta_n - \alpha_2^2\sec_2\alpha_2\theta_n + m(\alpha_1^2-\alpha_2^2)} ,$$

(G3-47)

$$P_x = \frac{1}{k_x}\frac{\partial^2\Phi}{\partial y^2} = P_o + 2P_o(1+m)\sum \frac{\left[\frac{\alpha_1^2\cos\frac{\alpha_1\theta_n y}{a}}{\cos\alpha_1\theta_n} - \frac{\alpha_2^2\cos\frac{\alpha_2\theta_n y}{a}}{\cos\alpha_2\theta_n}\right] e^{-\frac{\theta_n x}{a}}}{\alpha_1^2\sec^2\alpha_1\theta_n - \alpha_2^2\sec^2\alpha_2\theta_n + m(\alpha_1^2-\alpha_2^2)} ,$$

(G3-48)

$$P_y = \frac{1}{k_y}\frac{\partial^2\Phi}{\partial x^2} = -\frac{2P_o k_x(1+m)}{k_y}\sum \frac{\left[\frac{\cos\frac{\alpha_1\theta_n y}{a}}{\cos\alpha_1 n} - \frac{\cos\frac{\alpha_1\theta_n y}{a}}{\cos\alpha_2 n}\right] e^{-\frac{\theta n x}{a}}}{\alpha_1^2\sec^2\alpha_1\theta_n - \alpha_2^2\sec^2\alpha_2\theta_n + m(\alpha_1^2-\alpha_2^2)} .$$

(G3-49)

Numerical Example

Applying the analysis to panel C shown in Figure G2 with a 1000 compressive load acting on each of the outer flanges, for the average dimensions,

$$P_o = \frac{2000}{2(0.5557)+2(0.5632)+2(0.5618)+0.5612+2(0.099)(2.84)+(0.1014)(2.846)+(0.99)(2.845)}$$

$$= 355.4 \text{ psi}$$

$$t_x = \frac{2(0.5557)+2(0.5632)+2(0.5618)+0.5612}{2(2.84+2.84+2.845)} = 0.19701 .$$

$$k_x = 1 + \frac{t_x}{t} = 1 + \frac{0.19701}{0.1} = 2.9701 .$$

$$k_y = 1 .$$

$$\frac{1}{k_x k_y} = \frac{1}{2.9701} = 0.3366 .$$

$$\frac{\alpha_1^2}{k_x} = 1 + \mu(1 - \frac{1}{k_x k_y}) + \sqrt{\left[1 + \mu(1 - \frac{1}{k_x k_y})\right]^2 - \frac{1}{k_x k_y}}$$

$$\frac{\alpha_1^2}{k_x} = 1 + \frac{1}{3}(1 - 0.3366) + \sqrt{\left[1 + \frac{1}{3}(1 - 0.3366)\right]^2 - 0.3366}$$

$$= 2.2956.$$

$$\alpha_1 = \sqrt{2.2956(2.9701)} = 2.611$$

$$\frac{\alpha_2^2}{k_x} = 1 + \frac{1}{3}(1-0.3366) - \sqrt{\left[1 + \frac{1}{3}(1-0.3366)\right]^2 - 0.3366} = 0.1466.$$

$$\alpha_2 = \sqrt{0.1466(2.9701)} = 0.6599.$$

θ_n are given by the roots of the equation

$$2.611\tan 2.611\theta - 0.6599\tan 0.6599\theta + m(6.81816 - 0.43542)\theta = 0,$$

where

$$m = \frac{A_F}{ak_x t} = 0.2268,$$

or

$$2.611\tan 2.611\theta - 0.6599\tan 0.6599\theta + 1.4476\theta = 0. \qquad \text{(G3-50)}$$

A digital computer program written in Bama Bell for the Univac Solid State 80 computer at the University of Alabama was used to determine the roots to this equation.

It should be noted that the discontinuities existing in Equation G3-50 can be avoided by rewriting it as

$$2.611\sin 2.611\theta\cos 0.6599\theta - 0.6599\sin 0.6599\theta\cos 2.611\theta$$
$$+ 1.4465\theta\cos 2.611\theta\cos 0.6599\theta = 0. \qquad \text{(G3-51)}$$

The computer program used in solving for the roots to Equation G3-51 is as follows:

```
193     I556901000
194     I506901000
195     I202193223
```

196 0600000000

197 0800000005

198 I201100106

199 5001100400

200 3101400401

201 3102400402

202 R602401403

203 R603401404

204 R602402405

205 R603402406

206 3101406407

207 3407403407

208 3102405408

209 3406408408

210 3103400409

211 3409404409

212 3409406409

213 2407408410

214 1410409410

215 3410104411

216 9411105218

217 R400598000

218 5001410104

219 5001400500

220 1400100400

221 5001250620

222 5001251626

223	R400200000
250	7000010600
251	7000010600
598	5001104299
599	5001400300
600	1500300501
601	3106501501
602	3101501503
603	3102501503
604	R602502504
605	R603502505
606	R602503506
607	R603503507
608	3101507508
609	3508504508
610	3102506509
611	3509505509
612	3103501510
613	3510505510
614	3510507510
615	2508509511
616	1510511510
617	3510299511
618	9511105624
619	5001501300
620	7000010600
621	5001501509

```
622     I241509510
623     R400218000
624     5001501500
625     5001510299
626     7000010600
627     5001501509
628     I241509510
629     R400218000
zzz        193
```

If we write Equation G3-51 in the general form

$$C_1 \cos C_2\theta \sin C_1\theta - C_2 \cos C_1\theta \sin C_2\theta + C_3\theta \cos C_1\theta \cos C_2\theta = 0, \qquad \text{(G3-52)}$$

the data used in the computer program and their locations are as follows:

```
100     4850000000
101     C1          (in floating point)
102     C2          (in floating point)
103     C3          (in floating point)
104     5010000000
105     0000000000
106     4950000000
```

The print out format is as follows:

θ $f(\theta)$.

The magnitude of $f(\theta)$ is an indication of the accuracy of the computation; the nearer it is to zero, the more accurate is the root.

The above program does not have a stop order and will run until the desired number of roots have been found. In this example, the computation was stopped after the first 12 roots were found. They were as follows:

θ	f(θ)
0.9999756	0.40652682
2.1499756	- 0.38730410
2.3500245	- 0.59294616
3.1715868	0.00000013
4.3577845	0.00000570
5.5404765	- 0.00000300
6.6999760	0.27386818
7.1000245	0.38465892
7.9000245	- 0.01819730
9.0980275	- 0.00001230
10.295401	- 0.00002060
11.500111	0.00009496

The above roots to the transcendental equation were used in Equation G3-48 for the evaluation of the stringer stresses in the x direction. Evaluation of Equation G3-48 was carried out from x = 0 to x = 24 at increments of x = 1. A digital computer program was also written to perform these calculations. It was as follows:

```
204     I556901000
205     I506901000
206     0600000000
207     0800000005
208     I201098123
209     6700701000
210     3103111400
2111    3112400401
212     R603401401
213     3104401402
```

2141	3112105403
215	R603403403
216	4402403402
217	4401403401
218	3106111404
2191	3112404405
220	R603405405
221	3107405406
2221	3112108407
223	R603407407
224	4406407406
225	4405407405
226	3403403403
227	4099403403
228	3104403403
229	3407407407
230	4099407407
231	3107407407
232	2403407403
233	1403109403
234	R400236000
236	2402406402
237	4402403402
238	R400240000
240	Z082241001
241	5001402599
242	Z100011211

```
243     R400800000
800     Z092239499
801     Z092241599
8021    3112098415
803     R400244000
244     4415110415
245     R601415415
246     4099415415
2471    R400249000
2491    3600415417
250     1417701701
251     Z100011802
252     3700102700
253     3701101701
254     1100701700
255     R400256000
256     5001098698
257     5001111699
258     I241698700
259     1099098098
260     6700701000
261     7000024802
262     1110111111
263     6098098000
264     7000001209
265     I260000000
266     R403000000
zzz       204
```

Equation G3-48 is shown plotted in Figure G7 along with experimental data for comparison.

Stringer Sheet Solution

Consider Figure G3-2 which shows a reinforced cylindrical shell. Take axes O_x, O_y, O_z as shown in Figure G3-2, O_z being parallel to the axis of the cylinder and O any convenient point of its cross section.

Let w = displacement in direction O_z

s = distance along the circumference, measured from some fixed point on the circumference.

u,v = displacements of the point O parallel to O_x and O_y respectively.

β = angle of rotation of the cross section about O.

Refering to Figure G3-3 the displacement of the point P parallel to the tangent at P is

$$\beta h + u\cos\Phi + v\sin\Phi \quad . \tag{G3-53}$$

The shear strain is

$$\varepsilon_{sz} = \frac{\partial w}{\partial s} + \frac{\partial}{\partial z}\left(\beta h + u\cos\Phi + v\sin\Phi\right) \tag{G3-54}$$

$$= \frac{\partial w}{\partial s} + \frac{\partial}{\partial z}\left(\beta h + u\frac{dx}{ds} + v\frac{dy}{ds}\right)$$

$$= \frac{\partial w}{\partial s} + h\frac{d\beta}{dz} + \frac{du}{dz}\cdot\frac{dx}{ds} + \frac{dv}{dz}\cdot\frac{dy}{ds} = \frac{2(1+\mu)\tau_{sz}}{E}$$

Also, the longitudinal strain

$$\varepsilon_{zz} = \frac{\partial w}{\partial z} = \frac{P_z}{E} \quad , \tag{G3-55}$$

P_z being the average longitudinal stress in skin and stiffeners, as

defined in the first part of this appendix. Summing forces on an element of the shell in direction O_z,

$$\frac{\partial \tau_{zs}}{\partial z} + k_z \frac{\partial P_z}{\partial z} = 0, \tag{G3-56}$$

where

$$k_z = 1 + \frac{t_z}{t} . \tag{G3-57}$$

Substituting equations G3-54 and G3-55 into equation G3-56

$$\frac{\partial^2 w}{\partial s^2} + k^2 \frac{\partial^2 w}{\partial z^2} = - \left(\frac{dh}{ds} \cdot \frac{d\beta}{dz} + \frac{du}{dz} \cdot \frac{d^2x}{ds^2} + \frac{dv}{dz} \cdot \frac{d^2y}{ds^2} \right) \tag{G3-58}$$

where

$$k^2 = 2(1 + \mu)k_z . \tag{G3-59}$$

For a flat panel, the right hand side of equation G3-58 is zero since the substitutions

$$S = x$$

$$y = 0$$

$$h = 0$$

can be made.

Assuming the fundamental solution

$$w = A[(\cosh\lambda ks)(\cos\lambda z) - 1], \tag{G3-60}$$

the normal stress is

$$P_z = E \frac{\partial w}{\partial z} = - EA\lambda \cosh\lambda ks(\sin\lambda z) . \tag{G3-61}$$

The end load in the skin is given by

$$\int_o^a k_z t P_z ds = - \frac{k_z tEA}{k} (\sinh\lambda ka)(\sin\lambda z) \tag{G3-62}$$

Also, the strain in the flange is equal to the strain in the skin

at z = a. Therefore, the end load in one flange is

$$-A_F E A\lambda \cosh\lambda ka(\sin\lambda z) = - mak_z tEA\lambda\cosh\lambda ka(\sin\lambda z) \qquad (G3\text{-}63)$$

where $A_F = mak_z t$. (G3-64)

Integrating from 0 to ∞ with respect to λ to obtain the complete solution,

$$T_o = - \frac{k_z tE}{k} \int_o^\infty A(\sinh\lambda ka + m\lambda ka\cosh\lambda ka)\sin\lambda z d\lambda . \qquad (G3\text{-}65)$$

Putting $\lambda ka = \theta$, the equation becomes

$$T_o = \frac{k_z tE}{k^2 a} \int_o^\infty A(\theta) \left(\sinh\theta + m\cosh\theta\right) \sin\frac{\theta z}{ka}\, d\theta . \qquad (G3\text{-}66)$$

If T_o is constant, it may be expressed by the integral

$$T_o = \frac{2T_o}{\pi} \int_o^\infty \sin\frac{\theta z}{ka} \frac{d\theta}{\theta} . \qquad (G3\text{-}67)$$

Equations G3-66 and G3-67 are identical, and therefore true for all values of z if

$$A(\theta) = - \frac{2T_o k^2 a}{k_z tE\ (\sinh\theta + m\theta\cosh\theta)} . \qquad (G3\text{-}68)$$

Hence the required solution, using equation G3-53 is given by

$$w = \int_o^\infty A(\cosh\lambda ks\cos\lambda z - 1)\, d\lambda$$

$$= \frac{2T_o}{\pi k_z tE} \int_o^\infty \frac{1 - \cosh\frac{\theta s}{a}\cos\frac{\theta z}{ka}\ d\theta}{\theta(\sinh\theta + m\theta\cosh\theta)} \qquad (G3\text{-}69)$$

When evaluated using complex integration, the final result is

$$w = \frac{T_o k}{k_z tE}\left[\frac{z}{ka(1+m)} + 2\sum \frac{\cos\theta_n\ 1 - \cos\frac{\theta_n s}{a}\ e^{-\frac{\theta_n z}{ka}}}{\theta_n(1 + m\cos^2\theta_n)}\right]$$

where the θ_n's are the roots to the equation

$$\tan\theta_n + m\theta_n = 0.$$

Now the normal stress is

$$P_z = P_o\left[1 + 2(1+m)\sum \frac{\cos\theta_n \cdot \cos\frac{\theta_n s}{a}\, e^{-\frac{\theta_n x}{ka}}}{1 + m\cos^2\theta_n}\right] \qquad \text{(G3-70)}$$

Equation G3-70 has been written as a funetion of x to agree with the other solutions in this paper.

Numerical Example

Applying the stringer-sheet analysis to panel B shown in Figure G1 with a 1000 compressive load acting on each of the outer flanges, for the given dimensions

$$P_o = \frac{2000}{0.282 + 0.285 + 0.275 + 0.282 + 0.282 + 0.285 + 0.282 + 0.1(2.61)6}$$

$$= 565.13 \text{ psi}$$

$$t_x = \frac{0.282+0.285+0.275+0.282+0.282+0.285+0.282}{6(2.61)} = 0.12598.$$

$$k_x = k_z = 1 + \frac{tx}{t} = 2.2598.$$

$$A_F = 0.282.$$

$$a = 8.69.$$

$$k^2 = 2(1+\mu)k_z$$

$$= 2(1 + \tfrac{1}{3})(2.2598) = 6.026133$$

$$k = 2.455$$

$$m = \frac{A_F}{ak_z t} = \frac{0.282}{0.69(2.2598)(0.1)} = 0.1436.$$

θ_n are the roots to

$$\tan\theta_n + m\theta_n = 0 ,$$

or, rewriting

$$\sin\theta_n + 0.1436\theta_n\cos\theta_n = 0. \qquad \text{(G3-71)}$$

The computer program used in the determination of the roots to equation G3-51, with some changes, was used in the determination of the roots to the above transcendental equation. Instruction cards 200 through 214 and 602 through 616 were replaced by the following cards:

```
200     R602400401
201     R603400402
202     3161400403
203     3402403402
204     1401402410
205     R602501502
602     R602501502
603     R603501503
604     3101501504
605     3504503503
606     1502250510
607     R400617000
```

Writing equation G3-71 in the general form

$$\sin\theta_n + C_1\theta_n\cos\theta_n = 0, \qquad \text{(G3-72)}$$

the data used in the computer program and their locations are as follows:

100 4850000000

101 C_1 (in floating point)

102 5010000000

103 5010000000

104 5010000000

105 0000000000

106 4950000000

The first 12 roots of Equation G3-71 were found to be

θ	f(θ)
2.6075298	-0.00000006
5.3973575	-0.00000068
8.3402930	-0.00000053
11.365641	0.00000314
14.433643	-0.00000176
17.525235	0.00000531
12.630902	-0.00000340
23.745538	0.00000264
26.866203	-0.00000151
29.991100	0.00000269
33.119075	-0.00000353
36.249355	0.00000697

The above roots to the transcendental equation were used in equation G3-70 for the evaluation of the stringer stresses in the x direction. Evaluation of equation G3-70 was carried out from x = 0 to x = 24 at increments of x = 1. A digital computer program was written to perform these calculations. It was as follows:

193 I556901000

194	I506901000
195	I202193226
196	R400197000
197	0600000000
198	0800000005
199	I201099116
200	6700702000
2011	R603105400
202	3400400400
203	3103400401
204	1101401401
205	4400401401
206	Z082207001
207	5001401599
208	Z010011201
209	Z092207599
2101	Z105099410
211	4410104410
212	R601410410
213	4101410410
2141	3500410415
215	1415702702
216	Z100011210
217	3702102702
218	1101702702
219	3702100702
220	5001099701

```
221     I241701702
222     1101099099
223     6700702000
224     7000023210
225     I260000000
226     R403000000
zzz        193
```

Equation G3-70 is plotted in Figure G8 along with experimental data for comparison.

APPENDIX G4

THE SUBSTITUTE SINGLE STRINGER METHOD

In this appendix, the substitute-single-stringer method presented by Kuhn and Chiarito in Reference G19 will be applied to panel C.

The analysis of a multistringer panel by the substitute single stringer method requires the following steps:

1. The properties of the substitute panel are established as follows:
   A. The substitute single stringer is first located at the centroid of the internal forces in the stringers. Although the sheet is assumed to carry only shear stresses, an effective width of sheet is considered to be acting with the sheet. The distance from the outer flange to the centroid of the stringer areas is b_c.
   B. The area of the flange in the substitute panel is equal to the area of the flange in the actual panel. The area of the substitute stringer is equal to the sum of the areas of the stringers in the actual panel plus the effective area of sheet acting with them.
   C. The substitute stringer is then located according to the empirical relation

$$b_s = \left[0.65 + \frac{0.35}{n^2}\right] b_c$$

   where n is the number of stringers in the half panel.

2. The substitute panel is analyzed as follows:

   From Figure G3-1b

$$A_F\sigma_F + \tau t dx - (\sigma_F + d\sigma_F)A_F = 0$$

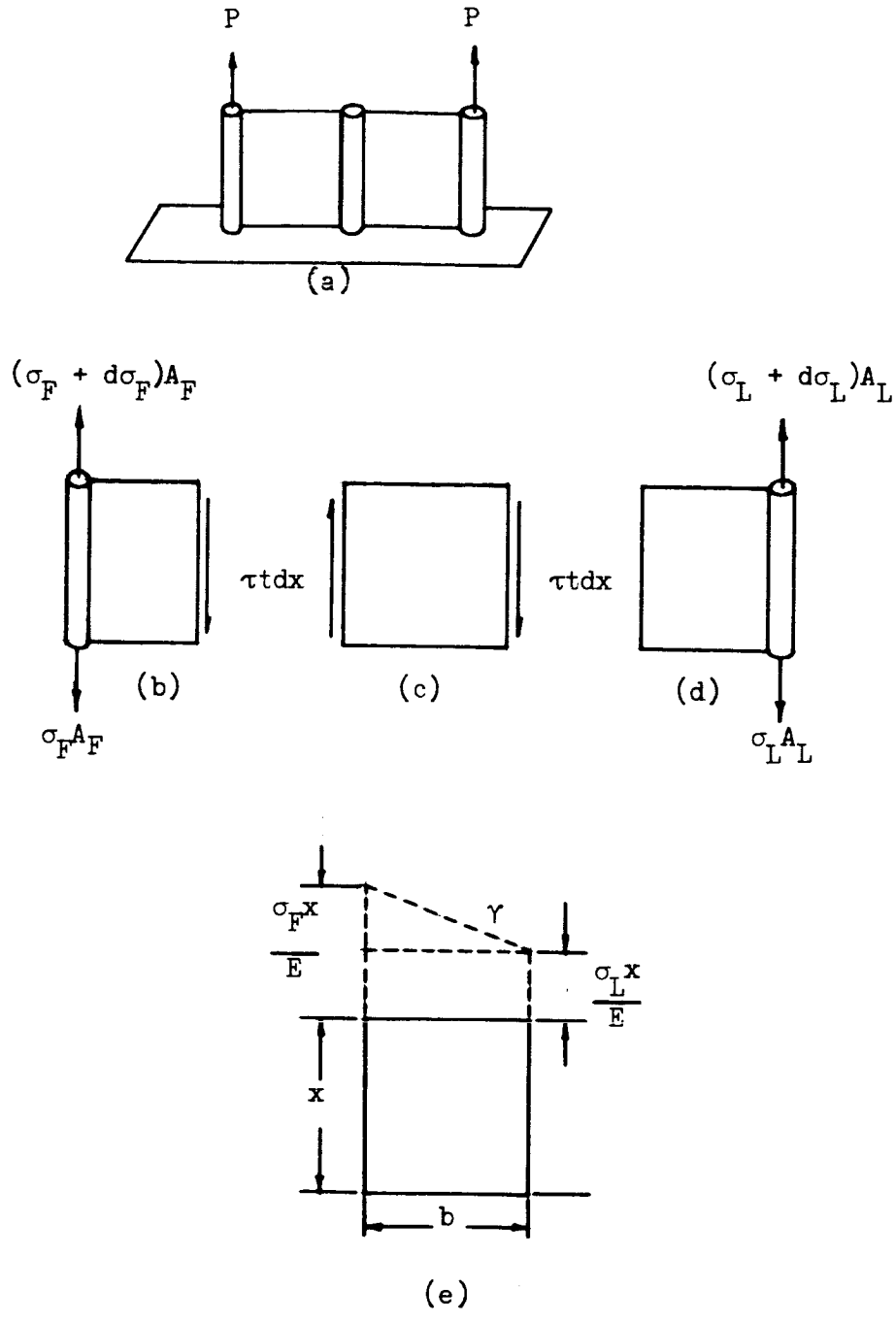

FIGURE G3-1. - THREE STRINGER PANEL WITH SYMMETRICAL AXIAL LOAD.

$$A_F d\sigma_F = \tau t dx \ .$$

Also,

$$A_L(\sigma_L + d\sigma_L) - A_L\sigma_L + \tau t dx = 0$$

$$A_L d\sigma_L = -\tau t dx$$

so

$$A_F d\sigma_F = \tau t dx = -A_L d\sigma_L \ . \qquad \text{(G4-1)}$$

From Figure G4-1e, the shear strain at station x is given by

$$\gamma = \frac{x}{bE}(\sigma_F - \sigma_L) \ .$$

The increment of shear strain is

$$d\gamma = \frac{(\sigma_F - \sigma_L)}{bE} dx \ .$$

The increment of shear stress is

$$d\tau = G d\gamma = \frac{G}{bE}(\sigma_F - \sigma_L) dx \ . \qquad \text{(G4-2)}$$

Differentiating equation G4-2,

$$\frac{d^2\tau}{dx^2} = \frac{G}{bE}(d\sigma_F - d\sigma_L) \ . \qquad \text{(G4-3)}$$

Substituting equation G4-1 into equation G4-3,

$$\frac{d^2\tau}{dx^2} = \frac{G}{bE}\left[\frac{\tau t}{A_F} + \frac{\tau t}{A_L}\right] ,$$

or

$$\frac{d^2\tau}{dx^2} - k^2\tau = 0, \qquad \text{(G4-4)}$$

where

$$k = \sqrt{\frac{Gt}{bE}\left[\frac{1}{A_F} + \frac{1}{A_L}\right]} \ . \qquad \text{(G4-5)}$$

Assuming a solution to equation G4-4 of the form

$$\tau = C_1 e^{kx} + C_2 e^{-kx}, \tag{G4-6}$$

application of the boundary condition $\tau = 0$ at $x = 0$ yields

$$0 = C_1 e^{0} + C_2 e^{-0}.$$

$$\therefore C_1 = -C_2 ,$$

so

$$\tau = C_1 (e^{kx} - e^{-kx}). \tag{G4-7}$$

Differentiating equation G4-7

$$\frac{d\tau}{dx} = C_1 k (e^{kx} + e^{-kx}) .$$

Equating equations G4-2 and G4-8,

$$C_1 = \frac{G(\sigma_F - \sigma_L)}{bEk(e^{kx} + e^{-kx})} . \tag{G4-9}$$

Application of the boundary condition $\sigma_F = P/A_F$, $\sigma_L = 0$ at $x = L$ yields

$$C_1 = \frac{G(P/A_F)}{bEk(e^{kL} + e^{-kL})} . \tag{G4-10}$$

Substituting equation G4-10 into equation G4-7

$$\tau = \frac{GP}{bEA_F k} \frac{\sinh kx}{\cosh kL} . \tag{G4-11}$$

Defining

$$A_T = A_F + A_L \tag{G4-12}$$

and substituing into equation G4-5,

$$k = \frac{GtA_T}{bEA_F A_L} . \tag{G4-13}$$

Now, from equation G4-11

$$\tau = \frac{GPk}{bEA_F k^2} \frac{\sinh kx}{\cosh kL} = \frac{GPk}{bEA_F \left(\frac{GtA_T}{bEA_F A_L}\right)} \frac{\sinh kx}{\cosh kL} ,$$

$$\tau = \frac{PkA_L}{tA_T} \frac{\sinh kx}{\cosh kL} . \qquad \text{(G4-14)}$$

Substituting equation G4-14 into equation G4-1

$$d\sigma_F = \frac{t}{A_F} \tau dx = \frac{PkA_L}{A_F A_T} \frac{\sinh kx}{\cosh kL} dx . \qquad \text{(G4-15)}$$

Integrating,

$$\sigma_F = \frac{PA_L}{A_F A_T} \frac{\cosh kx}{\cosh kL} + C_3 . \qquad \text{(G4-16)}$$

Since $\sigma_F = P/A_F$ at $x = L$,

$$\frac{P}{A_F} = \frac{PA_L}{A_F A_T} + C_3 .$$

$$\therefore C_3 = \frac{P}{A_F} \left[1 - \frac{A_L}{A_T}\right] = \frac{P}{A_F} \left[\frac{A_T - A_L}{A_T}\right] = \frac{P}{A_F} \left[\frac{A_F + A_L - A_L}{A_T}\right] = \frac{P}{A_T} .$$

(G4-17)

Now

$$\sigma_F = \frac{PA_L}{A_F A_T} \frac{\cosh kx}{\cosh kL} + \frac{P}{A_T} \left[1 + \frac{A_L}{A_F} \frac{\cosh kx}{\cosh kL}\right] \frac{P}{A_T} . \qquad \text{(G4-18)}$$

Also from equation G4-1

$$d\sigma_L = - \frac{t}{A_L} \tau dx = - \frac{Pk}{A_T} \frac{\sinh kx}{\cosh kL} dx . \qquad \text{(G4-19)}$$

Integrating,

$$\sigma_L = - \frac{P}{A_T} \frac{\cosh kx}{\cosh kL} + C_4 . \qquad \text{(G4-20)}$$

Since $\sigma_L = 0$ at $x = L$,

$$C_4 = \frac{P}{A_T} .$$

$$\therefore \sigma_L = \frac{P}{A_T}\left[1 - \frac{\cosh kx}{\cosh kL}\right]. \qquad (G4\text{-}21)$$

Equations G4-14, G4-18, and G4-21 determine the stress distribution in the substitute stringer. Taking the origin at the tip, the change in coordinates can be expressed as

$$x = L - x_1 . \qquad (G4\text{-}22)$$

Now the approximation

$$\frac{\sinh kx}{\cosh kL} = \frac{\sinh k(L-x_1)}{\cosh kL} = \frac{\sinh kL \cosh kx_1}{\cosh kL} - \frac{\cosh kL \sinh kx_1}{\cosh kL}$$

$$= \tanh kL \cosh kx_1 = \frac{1}{2}(e^{kx_1+e^{-kx_1}-e^{kx_1}+e^{-kx_1}}) = e^{-kx_1} \qquad (G4\text{-}23)$$

may be made, since $\tanh kL \to 1$ for large values of kL.

Dropping the subscript on the x and considering the tip as the origin, Equations G4-14, G4-18 and G4-21 may now be written

$$\tau = \frac{PkA_L}{tA_T} e^{-kx}, \qquad (G4\text{-}24)$$

$$\sigma_F = \frac{P}{A_T}\left[1 + \frac{A_L}{A_F} e^{-kx}\right] , \qquad (G4\text{-}25)$$

$$\sigma_L = \frac{P}{A_T}(1 - e^{-kx}) . \qquad (G4\text{-}26)$$

Numerical Example

For panel C, the location of the centroid of the internal forces is (using an effective width equal to one half the distance between stringers)

$$b_c = \frac{1}{3(2.5575)+3(0.565)+0.280}\,[(2.5575+4.265+7.11)(2.275)(0.1)$$

$$+2.84(0.564)(1)+5.69(1)+8.1075(0.280)(1)] ,$$

$$b_c = 3.740.$$

The areas of the substitute stringer and the flange are

$$A_L = 0.7917 + 0.7908 + 0.3938 = 1.9763 \text{ in}^2.$$

$$A_F = 0.565 \text{ in}^2.$$

The location of the substitute stringer is

$$b_s = (0.65 + 0.35/2^2)(3.740) = 2.75825 \text{ in.}$$

Now substituting the above into the appropriate formulas

$$k = \sqrt{\frac{(3.9)(10^6)(0.1)}{(10.5)(10^6)(2.75825)}\left[\frac{1}{0.565} + \frac{1}{1.9763}\right]} = 0.17503 .$$

$$A_T = A_F + A_L = 0.565 + 1.9763 = 2.5413 \text{ in}^2.$$

$$\tau = \frac{PkA_L}{tA_T} e^{-kx} = \frac{1000(0.17503)(1.9763)}{0.1(2.5413)} e^{-0.17503x}$$

$$= 1,361.15e^{-0.17503x}.$$

$$\sigma_F = \frac{P}{A_T}\left[1 + \frac{A_L}{A_F} e^{-kx}\right] = \frac{1000}{2.5413}\left[1 + \frac{1.9763}{0.565} e^{-0.17503x}\right]$$

$$= 393.5 + 1,376.4e^{-0.17503x}.$$

$$\sigma_L = \frac{P}{A_T}\left[1 - e^{-kx}\right] = \frac{1000}{2.5413}(1 - e^{-0.17503x})$$

$$= 393.5(1 - e^{-0.17503x}).$$

The above equations are shown plotted in Figure G11 with experimental data for comparison.

APPENDIX G5

MINIMUM ENERGY SOLUTION USING MATRIX METHODS

Dividing panel C into bays with generalized forces as shown in Figure G5-1, results in a statically indeterminate system which may be solved by matrix methods. The type of stress distribution assumed as well as the number of bays used determine the accuracy of the method. For this analysis it was assumed that the stiffeners transmit only normal stresses and the sheet material transmits only shearing stresses. It was further assumed that the panel and loading are symmetrical.

The notation used is the same as used by Bruhn [G4].

For the analysis the following matrix operations are required:

1. Evaluate $\left[a_{rn}\right] = \left[g_{ri}\right]\left[a_{ij}\right]\left[g_{jn}\right]$

2. Evaluate $\left[a_{rs}\right] = \left[g_{ri}\right]\left[a_{ij}\right]\left[g_{js}\right]$

3. Evaluate $\left[a_{rs}^{-1}\right]$ the inverse of $\left[a_{rs}\right]$

4. Evaluate $\left[G_{rm}\right] = \left[a_{rs}^{-1}\right]\left[a_{rn}\right]$

5. Evaluate $\left[G_{im}\right] = \left[g_{im}\right] + \left[g_{ir}\right]\left[G_{rm}\right]$

6. Evaluate $\left[q_{in}\right] = \left[G_{im}\right]\left[P_{mn}\right]$

7. As a check the matrix

$$\left[A_{rn}\right] = \left[g_{ri}\right]\left[a_{ij}\right]\left[G_{jn}\right]$$

may be evaluated. If all matrix operations have been exact, each element of $\left[A_{rn}\right]$ should be zero. Due to rounding errors some of the elements may not be zero, but they should be small compared with corresponding elements of $\left[a_{rn}\right]$.

A Fortran IV program was written to perform the above matrix operations and the computation for panels B and C was performed by the Univac 1107 at the University of Alabama Research Institute located in Huntsville, Alabama. Additional details are given in Appendix F.

Results of these analyses are shown compared with experimental data in Figures G12 and G13.

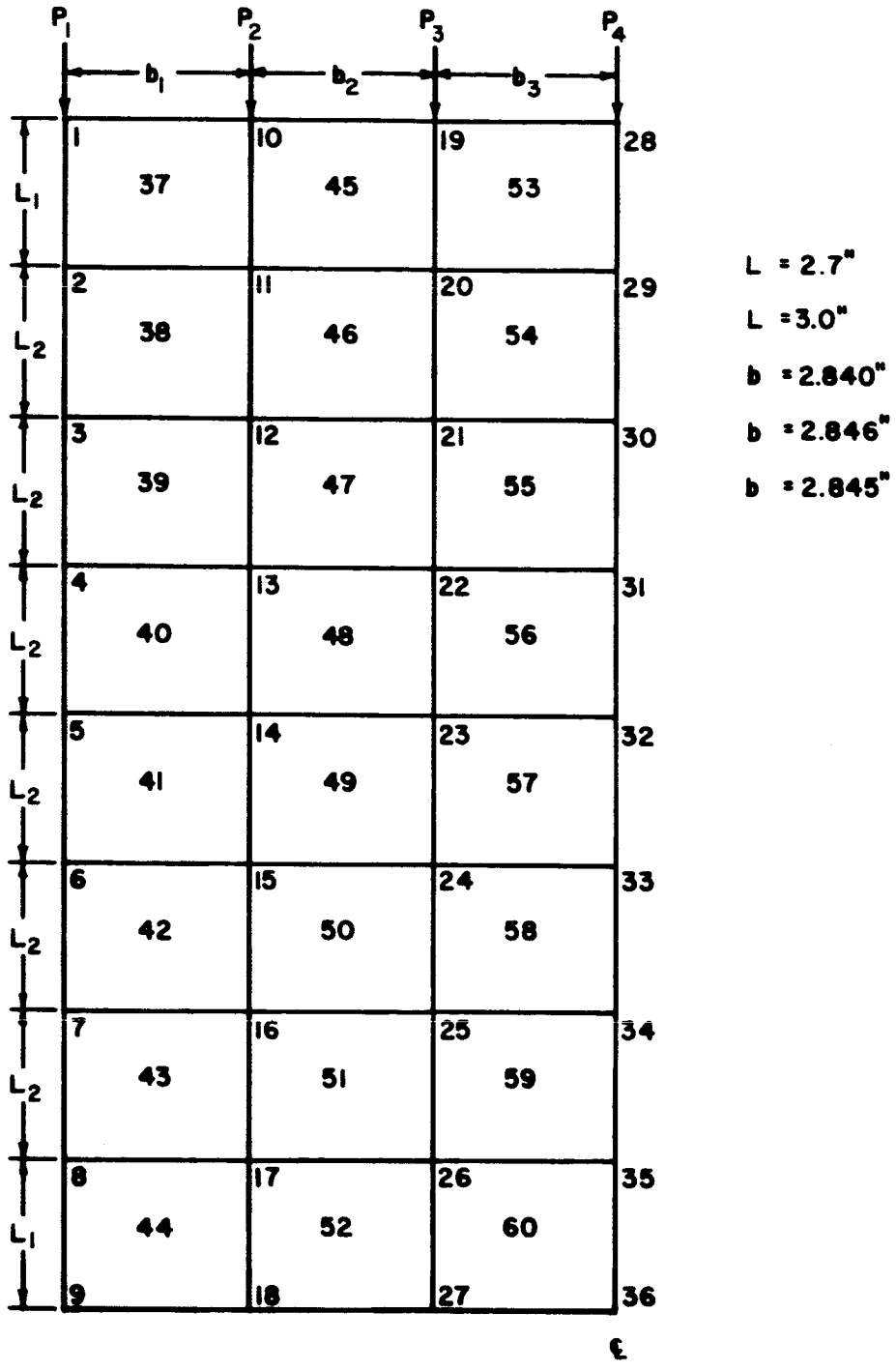

FIGURE G5-1. - GENERALIZED FORCE SYSTEM USED IN MATRIX ANALYSIS OF PANEL C. THE PANEL AND LOADING ARE ASSUMED TO BE SYMMETRICAL.

REFERENCES

G1. Akao, S.: Analysis of Shear Lag Problems by Means of Difference Equations. Technol. Rep. Osaka Univ., Vol. 9, March 1959, pp. 91-99.

G2. Anderson, R. A. and Houbolt, J. C.: Effect of Shear Lag on Bending Vibration of Box Beams. NACA TN 1583, 1948.

G3. Borsari, P. and Yu, A.: Shear Lag in a Plywood Sheet Stringer Combination Used for the Chord Member of a Box Beam. NACA TN 1443, 1948.

G4. Bruhn, Elmer F.: Analysis and Design of Flight Vehicle Structures. Tri State Offset Company, Cincinnati, Ohio, 1965.

G5. Chiarito, P. T.: Shear Lag Tests of Two Box Beams with Corrugated Covers Loaded to Failure. NACA Wartime Rep. L-482, 1944.

G6. Chiarito, P. T.: Shear Lag Tests of Two Box Beams with Flat Covers Loaded to Destruction. NACA Wartime Report L-307, 1942.

G7. Cox, H. L.: Stress Analysis of Thin Metal Construction. Journal of the Royal Aeronautical Society, Vol. 44, March, 1940, pp. 231-282.

G8. Davenport, W. W. and Kruszewski, E. T.: A Substitute-Stringer Approach for Including Shear-Lag Effects in Box Beam Vibrations. NACA TN 3158, 1954.

G9. Duncan, W. J.: Diffusion of Load in Certain Sheet-Stringer Combinations. ARC (Great Britain), R. and M. No. 1825, 1938.

G10. Fine, M.: A Comparison Between Plain and Stringer Reinforced Sheet from the Shear Lag Standpoint. ARC (Great Britain), R. and M. No. 2618, 1942.

G11. Gantmacher, F. R.: The Theory of Matrices, Vol. 1. Chelsea Publishing Company, New York, New York, 1960.

G12. Goland, M.: Shear Lag Solutions for Sheet-Stringer Panels by Means of a Hydrodynamic Analogy. Journal of the Aerospace Sciences, Vol. 27, April 1960, pp. 291-295, 303.

G13. Goodey, W. J.: Stress Diffusion Problems. Aircraft Engineering, Vol. 18, 1946, pp. 227-230, 234, 271-276, 313-316, 343-346, 385-389.

G14. Kempner, J.: Recurrence Formulas and Differential Equations for Stress Analysis of Cambered Box Beams. NACA TN 1466, 1947.

G15. Kuhn, P.: Approximate Stress Analysis of Multi-Stringer Beams with Shear Deformation of the Flanges. NACA Rep. No. 636.

G16. Kuhn, P.: Stress Analysis of Beams with Shear Deformation of the Flanges. NACA Report No. 608.

G17. Kuhn, P.: Shear Lag Stresses in Aircraft and Shell Structures. McGraw-Hill Book Company, Inc., 1956, pp. 101-154, 354-382.

G18. Kuhn, P.: A Recurrence Formula for Shear Lag Problems. NACA TN 739, 1939.

G19. Kuhn, P. and Chiarito, P.: Shear Lag in Box Beams--Methods of Analysis and Experimental Investigations. NACA TR 739, 1943.

G20. Kuhn, P. and Peterson, J.P.: Shear Lag in Axially Loaded Panels. NACA TN 1728, 1948.

G21. Lovett, B. B. C. and Rodee, W. F.: Transfer of Stress from Main Beams to Intermediate Stiffeners in Metal Sheet Covered Box Beams. Journal of the Aeronautical Sciences, Vol. 3, October 1936, pp. 426 -430.

G22. Lundquist, E. E.: Comparison of Three Methods for Calculating the Compressive Strength of Flat and Slightly Curved Sheet and Stringer Combinations. NACA TN 455.

G23. Newton, R. E.: Electrical Analogy for Shear Lag Problems. Proceedings of the Society for Experimental Stress Analysis, Vol. 2, No. 2, 1945, pp. 71-80.

G24. Peterson, J. P.: Shear Lag Tests on a Box Beam with a Highly Cambered Cover in Tension. NACA Wartime Report L-106, 1945.

G25. Reissner, E.: On the Problem of Stress Distribution in Wide Flanged Box Beams. Journal of the Aeronautical Sciences, Vol. 5, June 1938, pp. 295-299.

G26. Rey, William K.: A Study of the Stability of Reinforced Cylindrical and Conical Shells Subjected to Various Types and Combinations of Loads, Section IV--Matrix Shear Lag Analysis Utilizing a High Speed Digital Computer. Bureau of Engineering Research, University of Alabama, November 1962.

G27. Ross, R. D.: An Electrical Computer for the Solution of Shear-Lag and Bolted Joint Problems. NACA TN 1281, May 1947.

G28. White, R. J. and Antz, H. M.: The Stress Distribution in Reinforced Plates Under Concentrated Edge Loads. Journal of Aeronautical Sciences, Vol. 3, No. 6, April 1936, pp. 209-212.

G29. Winny, H. F.: The Distribution of Stress in Monocoque Wings. ARC (Great Britain), R. and M. No. 1756, 1938.

G30. Younger, J. E.: Miscellaneous Collected Airplane Structural Design Data, Formulas, and Methods. A.C.I.C. No. 644, Material Division, Army Air Corps, 1930.

APPENDIX H

LITERATURE SURVEY

The contents of this appendix were previously submitted as parts of Monthly Progress Reports Numbers 3, 6, and 7 for NASA Contract NAS8-11155.

APPENDIX H

LITERATURE SURVEY

During the performance of NASA Contract NAS8-11155, a literature survey was undertaken to identify current publications related to the contract work scope. Abstracts were prepared of some of these publications. This appendix contains a list of publications related to the project and the abstracts that were prepared.

List of Publications

1. Abraham, L. H.: Important Structural Research Problems for the Support of Future Space Missions NASA TN D-2059, August 1963.

2. Adachi, J., and Benicek, M.: Buckling of Torispherical Shells under Internal Pressure. U.S. Army Materials Research Agency, Technical Report No. 64-10, March 1964.

3. Air Force Systems Command: Fuselage Torsional Test of Aluminum Alloy Monocoque Cylinders. Aeronautical Systems Division, Wright-Patterson Air Force Base, Ohio, FTDM-2869, January 1964.

4. Akhmetzyanov, M. K.: Application of the Method of Photoelastic Coatings to the Determination of the Stresses and Deformations in Flexible Plates and Shells. NASA TT F-220, July 1964.

5. Almroth, B. O.: Buckling of Axially Compressed Sandwich Cylinders. Lockheed Missiles and Space Company, Technical Report: Solid Mechanics Department, 6-62-64-9, July 1964.

6. Ang, D. D., Folias, E. S., and Williams, M. L.: The Effect of Initial Spherical Curvature on the Stress Near a Crack Point. Aeronautical Research Laboratories, United States Air Force, ARL 62-356, August 1962.

7. Au, N. N.: Stresses and Strains in Multi-Layer Disks, Cylinders, and Spheres Under Pressure Loadings and an Arbitrary Radial Temperature Gradient. Aerospace Corporation, Report No. TDR-269(4304)-2, October 1963.

8. Au, N. N.: Stresses in Thin Vessels Under Internal Pressure. Aerospace Corporation, Report No. TDR-269(4304-5), January 1964.

9. Baltrukonis, J. H.: Influence Coefficients for Edge-Loaded Short, Thin Conical Frustums. Space Technology Laboratories, Engineering Mechanics Department, GM-TR-0165-00317, January 30, 1958.

10. Bauer, F., and Reiss, E. L.: Stresses in a Perforated Cylindrical Shell. New York University, Courant Institute of Mathematical

Sciences, IMM-NYU 320, February 1964.

11. Block, D. L.: Influence of Ring Stiffeners on Instability of Orthotropic Cylinders in Axial Compression. NASA TN D-2482, October 1964.

12. Bolotin, V. V., Boichenko, G. A., Makharov, B. P., Sudakova, N. I., and Shveiko, Y. Y.: Loss of Stability of Thin Elastic Shells Under the Effect of Impulsive Loads. Space Technology Laboratories, Inc., Translation No. 73, February 1963.

13. Bowie, O. L.: A Method of Successive Approximation Applied to a Class of Shells of Revolution with Regions of Rapidly Varying Thickness. Watertown Arsenal Laboratories, Technical Report WAL TR 893. 3/4, March 1963.

14. Card, M. F.: Bending Tests of Large-Diameter Stiffened Cylinders Susceptible to General Instability. NASA TN D-2200, April 1964.

15. Churchill, M. V.: Design Method for Double-Walled External Pressure Vessels. U. S. Naval Ordnance Laboratory, NOLTR 63-249, February 1964.

16. Clark, R. A. and Garibotti, J. F.: Longitudinal Bending of Conical Shell. Douglas Missile and Space Systems Division, Engineering Paper 1547, March 1963.

17. Czerwenka, G.: Introduction of Shearing Forces in Cylindrical or Sectionally Variable Conical Thin Shells. DVL-Report No. 274, Deutsche Versuchsanstalt für Luft-und Raumfahrt E. V., Proz-Wahn/ Rhld., 1963.

18. Darms, F. J., Molho, R., and Chester, B. E.: Improved Filament-Wound Construction for Cylindrical Pressure Vessels, Volume I. Wright-Patterson AFB, Technical Documentary Report No. ML-TDR-64-43, March 1964.

19. Darms, F. J., Molho, R., and Chester, B. E.: Improved Filament-Wound Construction for Cylindrical Pressure Vessels, Volume II. Wright-Patterson AFB, Technical Documentary Report No. ML-TDR-64-43, March 1964.

20. Dawson, V. C. D.: Elastic and Plastic Stress Equations for Hollow Cylinders and Spheres Subjected to Internal and External Pressure. U. S. Naval Ordnance Laboratory, NAVORD Report No. 6786, February 4, 1960.

21. Edenfield, C. E. and Lowry, J. K.: A Specialized Toroidal Pressure Vessel. General Dynamics/Astronautics, ERR-AN-174, July 1962.

22. Evan-Iwanowski, R. M. and Loo, T. C.: Deformations and Stability of of Spherical Shells Subjected to the Action of the Systems of Line Loads and Concentrated Loads. Syracuse University Research Institute, Technical Report No. 834-5, September 1962.

23. Evan-Iwanowski, R. M. and Loo, T. C.: Deformations and Stability of

Spherical Shells Under Action of Eccentric Concentrated Loads and Uniform Pressure. Syracuse University Research Institute, Technical Report No. 834-6, March 1963.

24. Evans, G. R. and Eisentraut, R. A.: Theory of Optimum Structures: An Annotated Bibliography. Lockheed Missiles and Space Company, Special Bibliography 5-10-62-38/SB-62-49, October 1962.

25. Friedrich, C. M.: Seal-Shell-2-A Computer Program For the Stress Analysis of a Thick Shell of Revolution With Axisymmetric Pressures, Temperatures, and Distributed Loads. AEC Research and Development Report WAPD-TM-398, December 1963.

26. Fulton, R. E., et al: Selected Bibliography of Works on the Use of Digital Computers in Structural Engineering. American Society of Civil Engineers, Committee on Electronic Computation of the Structural Division, April 1, 1963.

27. Galimov, K. Z.: On the Large Deflection of a Rectangular Cylindrical Panel. Royal Aircraft Establishment Translation U.D.C. No. 539.384: 621-434, November 1963.

28. Garnet, H., Crouzet-Pascal, J., and Nolan, F.: The Free Vibrations of Thick, Composite, Orthotropic, Circular Cylindrical Shells. Grumman Research Department, Report No. RE-165, August 1963.

29. Gerard, G. and Parirno, R.: Minimum Weight Design of Stiffened Cylinders for Launch Vehicle Applications. Allied Research Associates, Inc., Technical Report No. 235-5, March 1964.

30. Goldberg, J. E.: Analysis of Conical Shells under Unsymmetrical conditions. General Dynamics/Astronautics, ERR-AN-080, November 15, 1961.

31. Goodier, J. N., McIvor, I. K., and Lindberg, H. E.: Elastic Motion and Plastic Buckling of Cylindrical Shells Under Nearly Uniform Radial Impulse; Parts I and II. Part I--The Elastic Shell Under Nearly Uniform Radial Impulse' Part II--Buckling of a Very Thin Cylindrical Shell Due to an Impulsive Load. Poulter Labs. TR-001-63, March 1963.

32. Goodier, J. N. and Ramsey, H.: Problems of Related Elastic and Viscoelastic Buckling in One and Two Dimensions. Stanford University, Technical Report No. 133, September 1963.

33. Greenspon, J. E.: Collapse, Buckling and Post Failure of Cylindrical Shells. J. G. Engineering Research Associates, Contract No. DA 36-034-ORD-3081 RD, Technical Report No. 4, December 1963.

34. Grigolyuck, E. I.: Concerning the Strength and Stability of Cylindrical Bimetallic Shells. Inzhernoi Sbornik, 16, 119-48 (1953), Academy of Sciences, SSSR, Institute of Mechanics, April 19, 1963.

35. Gros, C. G., and Forsberg, K.: Vibrations of Thin Shells: A Partially Annotated Bibliography. Lockheed Missiles and Space Company

SB-63-43, April 1963.

36. Guz', O. M.: Axially Symmetrical Deformation of Hollow Orthotropic Shells of Rotation. Ukrainian periodical, Dopovidi AN Ukrains'koyi RSR, pp. 1044-1047, 1962.

37. Hardenbergh, D. E. and Zamrik, S. Y.: Effects of External Loadings on Large Outlets in A Cylindrical Pressure Vessel. Department of Engineering Mechanics, Pennsylvania State University, January 1964.

38. Hayashi, T., and Hirano, Y.: Buckling of Orthotropic Cylinders Under External Pressure. Transactions Japan Society for Aeronautics and Space Sciences, pp. 18-26, 1963.

39. Heise, O.: The Experimental Determination of the Buckling Loads of Longitudinally Pressed Thin-Walled Circular Cylindrical Shells. Deutsche Forschungsanstalt Fur Luft-Und Raumfahrt E. V. DFL-Bericht Nr. 214, 1963.

40. Hill, P. W.: Plastic Buckling Analysis of Rib Cored Cylindrical Sandwich Shells Subjected to Hydrostatic Pressure. Pennsylvania State University, Ordnance Research Laboratory, TM 619.3111-02, March 24, 1964.

41. Hoff, N. J.: A Non-Linear Model Study of the Thermal Buckling of Thin Elastic Shells. Stanford University Department of Aeronautics and Astronautics, SUDAER No. 173, October 1963.

42. Hoff, N. J., and Rehfield, L. W.: Buckling of Axially Compressed Circular Cylindrical Shells at Stresses Smaller Than the Classical Critical Value. Stanford University Department of Aeronautics and Astronautics, SUDAER No. 191, May 1964.

43. Hoff, N. J., and Soong, T. C.: Lower Bounds for the Buckling Pressure of Spherical Shells. Stanford University Department of Aeronautics and Astronautics, SUDAER No. 133, July 1962.

44. Holdenblat, I. I. and Nikolayenko, N. A.: Creep and Carrying Capacity of Shells. Redstone Scientific Information Center, RSIC-132, February 1964.

45. Horton, W. H., and Durham, S. C.: Repeated Buckling of Circular Cylindrical Shells and Conical Frusta by Axial Compressive Forces. Stanford University Department of Aeronautics and Astronautics, SUDAER No. 175, November 1963.

46. Hoskin, B. C.: A Note on Modifications in Redundant Structures. Department of Supply, Australian Defense Scientific Service, Aerospace Res. Laboratory Note ARL/SM 280, April 1963.

47. Huang, N. C.: Unsymmetrical Bending of Thin Shallow Spherical Shells. Harvard University, Division of Engineering and Applied Physics, Technical Report No. 15, March 1963.

48. Huang, N. C.: Unsymmetrical Buckling of Thin Shallow Spherical Shells. Harvard University, Engineering and Applied Physics, Tech. Rept. No. 15, October 1963.

49. Hubka, R. E.: Approximate Influence Coefficients of Cantilevered Stiffened Thin-Walled Conical Frustums Under End Load. Space Technology Laboratories, Inc., BSD-TDR-63-14, January 1963.

50. Jackson, L. R., McClure, G. M., and Kasuba, J. A.: Some Design Aspects of Fracture in Flat-Sheet Specimens and Cylindrical Pressure Vessels. Defense Metals Information Center, Battelle Memorial Institute, DMIC Memorandum 174, August 9, 1963.

51. Jacobson, H. R.: Obtimum Construction of Reinforced Plastic Cylinders Subjected to High External Pressure. Douglas Aircraft Company, Inc., Missile and Space Systems Division, Report SM-44057, June 6, 1963.

52. Jaworski, A., Mayers, J., and Ross, B.: Buckling Test of Thin Circular Cylindrical Shells Heated Along An Axial Strip. Department of Aeronautics and Astronautics, Stanford University, SUDAER No. 163, June 1963.

53. Jones, P. and Bhuta, G.: Stability and Response of Cylindrical Shells to Moving Loads. Aerospace Corporation Report No. TDR-169(3153-10) TN-1, March 1963.

54. Kan, S. N. and Lipovsky, D. Y.: Longitudinal-Transverse Bending of Stiffened Circular Cylindrical Shells. NASA TT F-194, April 1964.

55. Karavanov, V. F.: The Equations of Axisymmetrical Three-Layer Shells with a Light Filler. FTD-TT-62-1652, Air Force Systems Command, Wright-Patterson Air Force Base, Ohio, March 1963.

56. Kawai, T.: Influence Surfaces of Orthotropic Plate. Report of the Institute of Industrial Science, The University of Tokyo, Vol. 13, No. 6, February 1964.

57. Kempner, J.: Investigation of Plates and Shells Under External Loading and Elevated Temperatures. Polytechnic Institute of Brooklyn, PIBAL Report No. 664, April 1963.

58. Kempner, J., Vafakos, W. P., and Nissel, N.: Pressurized Ring-Reinforced Oval Cylinder-Comparison of Theory and DTMB Tests. Polytechnic Institute of Brooklyn, PIBAL Report No. 671, September 1963.

59. Koh, S. L., Thiel, C. C., and Eringen, A. C.: Computations for Stress and Stress Concentration in a Circular Cylindrical Shell With Circular Cutout. General Technology Corporation Technical Report No. 3-3, April 1963.

60. Konovalov, B. A.: The Calculation of Conical Shells By The Variational Method of V. Z. Vlasov. FTD-TT-62-1652, Air Force Systems Command, Wright-Patterson Air Force Base, Ohio, March 1963.

61. Kuenzi, E. W. and Zah, J. J.: Classical Buckling of Cylinders of Sandwich Construction in Axial Compression--Orthotropic Cores. Forest Products Laboratory, Forest Service, U. S. Department of Agriculture, FPL-018, November 1963.

62. Kumar, Sudhir.: Dynamic Behavior of Materials and Structures. Proceedings of Army Conference Held at Springfield Armory. September 1962.

63. Krenzke, M. A.: The Elastic Buckling Strength of Near-Perfect Deep Spherical Shells with Ideal Boundaries. David Taylor Model Basin, Report 1713, July 1963.

64. Lakshmikantham, C. and Gerard, G.: Elastic and Plastic Stability of Geometrically Orthotropic Spherical Shells. Allied Research Associates, Inc., Technical Report No. 235-3, January 1963.

65. Lakshmikantham, C. and Gerard, G.: Elastic Stability of Cylindrical Shells Under Axial and Lateral Loads. Allied Research Associates, Inc., Technical Report No. 235-4, February 1964.

66. Leonard, R. W.: Comments on "A Note on the Classical Buckling Load of Circular Cylindrical Shells Under Axial Compression", AIAA Journal Vol. 1, No. 9, September 1963.

67. Libove, C.: Complementary Energy Method for Structures with Finite Deformations. Syracuse University Research Institute, Report No. ME836-639, September 1963.

68. Libove, C.: A Complementary Energy Theorem for Axially Symmetric Shells with Large Deformations. Syracuse University Research Institute, Report No. ME836-6310, October 1963.

69. Lietzke, M. H., Stoughton, R. W., and Lietzke, P.: A Comparison of Several Methods For Inverting Large Symmetric Positive Definite Matrices. Oak Ridge National Laboratory, Chemistry Division, Contract No. W-7405-eng-26 ORNL-3430, May 1963.

70. Lindsey, G. H., Schapery, R. A., Williams M. L., and Zak, A. R.: The Triaxial Tension Failure of Viscoelastic Materials. Aerospace Research Laboratories, United States Air Force, ARL 63-152, September 1963.

71. Lu, Z. A., Penzien, J., and Popv, E. P.: Finite Element Solution for Thin Shells of Revolution. NASA CR-37, July 1964.

72. Lunchick, M. E.: Plastic Buckling Pressure for Spherical Shells. David Taylor Model Basin, Structural Mechanics Laboratory, R and D Report 1493, July 1963.

73. Lunsford, L. R.: Development of Shear Strength and Shear Modulus Test Specimens for Adhesives (ASTM Related Test Program). General Dynamics/Fort Worth, Structures ERR-FW-045, August 1963.

74. MacKenzie, A., and Dalrymple, E.: The Dependence of Dynamic Strength

of Cylindrical Pressure Vessels on Geometric Parameters. Picatinny Arsenal Technical Memorandum 1206, May 1963.

75. Makky, S. M.: Rupture Surfaces of Thick Spherical Shell Under Internal Pressure. Mathematics Research Laboratory, Boeing Scientific Research Laboratories, Mathematical Note No. 339, April 1964.

76. Mansfield, E. H.: On Axial Load Diffusion Into a Thin-Walled Reinforced Cylindrical Shell. Ministry of Aviation, Aeronautical Research Council(Great Britain), CP No. 644, 1963.

77. Martin, D. J., and Lauten, W. T.: Measurement of Structural Influence Coefficients, Part IV: Experimental Methods. NASA Langley Research Center 1960.

78. Matigian, M. H.: A Test To Determine The Reliability of Analytical Methods of Design of Aluminum Honeycomb Sandwich Cylinders in the Euler Buckling Range. Watertown Arsenal, Technical Report WARD-TR 766.9/1, June 1962.

79. May, J.: Fuselage Torsional Test of Aluminum Monocoque Cylinders. General Dynamics/Fort Worth, FTDM-2879, June 1961.

80. Medick, M. A.: On the Initial Response of Thin Elastic Shells to Localized Transient Forces. Research and Advanced Development Division, AVCO Corporation, TR RAD-TR-61-6, Contract AF04(647)-258, April 4, 1961.

81. Meissner, C. J.: Analysis of Complex Redundant Structures By the Flexibility Method. Republic Aviation Corporation, RAC 406-3. December 1962.

82. Mente, L. J.: On the Dynamic Response of Thin Cylindrical Shells to Impulsive Loading. The Mitre Corporation, Technical Documentary Report No. ESD-TDR-63-258, August 1963.

83. Mentel, T. J.: Comparison of Matrix Methods for Inelastic Structural Analysis. Grumman Aircraft Engineering Corporation, Report No. ADR 02-11-64, February 1964.

84. Mescall, J.: Stability of Thin Torispherical Shells Under Uniform Internal Pressure. Metals and Ceramics Research Laboratories, United States Army Materials Research Agency, Technical Report AMRA TR 63-06, June 1963.

85. Micks, W. R.: Selection of Materials in Minimum Weight Design. The Rand Corporation, P-2729, March 1963.

86. Milosavljevitch, M.: On the Stability of Rectangular Plates Reinforced by Stiffeners and Subjected to Bending and Shear. Redstone Scientific Information Center, RSIC-86, October 1963.

87. Mirsky, I.: Vibrations of Orthotropic Thick Cylindrical Shells. Rocketdyne Report R-5273, July 18, 1963.

88. Naghdi, A. K., and Eringen, A. C.: Stress Analysis of a Circular Cylindrical Shell with Circular Cutout. General Technology Corporation Technical Report No. 3-2, January 1963.

89. Navy Department: The Effects of Shell Joints and Bonding on the Stability of Acrylic Resin Cellular Shells. Navy Department Bureau of Naval Weapons, Serial No. NORD 16597-97, September 1963.

90. Norris, C. B., and Zahn, J. J.: Design Curves for the Buckling of Sandwich Cylinders of Finite Length under Uniform External Lateral Pressure. U. S. Forest Service Research Note FPL-07, May 1963.

91. Paramerter, R. R.: The Buckling of Clamped Shallow Spherical Shells Under Uniform Pressure. Graduate Aeroanutical Laboratories, California Institute of Technology, AFOSR 5362, November 1963.

92. Percy, J. H., Loden, W. A., and Navaratna, D. R.: A Study of Matrix Analysis Methods for Inelastic Structures. Air Force Systems Command, Wright-Patterson Air Force Base, Ohio, Technical Documenatry Report No. RTD-TDR-63-4032, October 1963.

93. Pestel, E.: Investigation of Plate and Shell Models by Matrices. European Office, Office of Aerospace Research, U. S. Air Force, AF-EOAR-61-46, 1963.

94. Peterson, J. P., and Dow, M. B.: Compression Tests on Circular Cylinders Stiffened Longitudinally by Closely Spaced Z-Section Stringers. NASA MEMO 2-12-59L, March 1959.

95. Pierce, C. M.: Post-Buckling Behavior of Stiffened Cylinders and Curved Panels: An Annotated Bibliography. Lockheed Missiles and Space Company Special Bibliography SB-62-37, September 1962.

96. Pogorelov, A. V.: Post-Buckling Behavior of Cylindrical Shells. NASA TT F-90, March 1964.

97. Pogorelov, A. V.: Post-Buckling Behavior of Cylindrical Shells. NASA TT F-196, June 1964.

98. Pope, G. G.: The Buckling of Plates Tapered in Thickness. Royal Aircraft Establishment (Farnborough) Report No. Structures 272, October 1961.

99. Price, H. L., and Pezdirtz, G. F.: Mechanical Properties of Echo II Laminate. NASA TN D-2367, August 1964.

100. Quinlan, P. M.: Thin Elastic Shells, Double Fourier Series for Boundary-Value Problems and Non-Linear Elasticity. Technical Report for United States Air Force EOAR Grant 62-43, September 1963.

101. Reiss, E. L.: Bifurcation Buckling of Spherical Caps. New York University, Courant Institute of Mathematical Sciences, IMM-NYU 324, April 1964.

102. Rogers, T. G., and Lee, E. H.: The Cylinder Problem in Viscoelastic Stress Analysis. Stanford University, Division of Engineering Mechanics, Technical Report No. 138, June 1963.

103. Schumacher, J. G.: Development of Design Curves for the Stability of Thin Pressurized and Unpressurized Circular Cylinders. Convair/Astronautics, Report No. AZS-27-275, May 1959.

104. Schumacher, J.: Statistical Determination of Strength Properties. Convair/Astronautics, Report AZS-27-274A, November 1958.

105. Schuman, W. J.: The Response of Cylindrical Shells to External Blast Loading. Ballistic Research Laboratories, Memorandum Report No. 1461, March 1963.

106. Seide, P.: Compressive Buckling of Longitudinally Stiffened Circular Cylinders. The Ramo-Wooldridge Corporation, Guided Missile Research Division, AM 6-11, GM-TR-33, May 31, 1956.

107. Serpico, J. C.: Elastic Stability of Orthotropic Conical and Cylindrical Shells Subjected to Axisymmetric Loading Conditions. Research and Advanced Development Division, AVCO Corporation, TR RAD-TR-61-7, Contract AR04(647)-258, April 19, 1961.

108. Sewall, J. L., Clary, R. R., and Leadbetter, S. A.: An Experimental and Analytical Vibration Study of a Ring-Stiffened Cylindrical Shell Structure with Various Support Conditions. NASA TN D-2398, August 1964.

109. Shevchenko, Y. M.: Temperature Stresses in a Thick-Walled Cylinder With Longitudinal Variation of the Modulus of Elasticity. Prikl. Mekh. 4, (4), 401-410, 1958.

110. Singer, J., Eckstein, A., Fersht-Scher, R., and Berkovits, A.: Buckling of Isotropic Orthotropic and Ring-Stiffened Conical Shells. Technion Research and Development Foundation, Israel Institute of Technology, Department of Aeronautical Engineering, TAE Report No. 30, September 1963.

111. Steele, C. R.: A Systematic Analysis For Shells of Revolution With Nonsymmetric Loads. Lockheed Missiles and Space Company, Technical Report No. 6.90.61.58, June 1962.

112. Steele, C. R.: Discontinuity Stresses in Shells of Revolution. Lockheed Missiles and Space Company, Technical Report: Math. 6-90-62-47, August 1962.

113. Stein, M.: The Influence of Prebuckling Deformations and Stresses On the Buckling of Perfect Cylinders. NASA TR R-190, February 1964.

114. Stroud, W. J.: Elastic Constants for Bending and Twisting of Corrugation-Stiffened Panels. NASA TR R-166, December 1963.

115. Stuart, F. R.: The Buckling of Thin-Walled Circular Cylindrical

Shells Under Combined Axial Compression and Bending. Thesis, California Institute of Technology, 1963.

116. Tsao, C. H.: Large Displacement Analysis of Buckling of Axially Compressed Circular Cylindrical Shells. Aerodynamics and Propulsion Research Laboratory, Aerospace Corporation, Report No. TDR 269(4230-30)-3, March 27, 1964.

117. Vinson, J. R., and Brull, M. A.: Approximate Solutions for Rectangular Orthotropic Plates. Towne School of Civil and Mechanical Engineering, Technical Report No. 1, Contract No. NONR 551(44), September 1963.

118. Vol'mir, A. S.: Survey of Investigations on the Theory of Flexible Plates and Shells, NASA TT F-180, October 1963.

119. Weigle, R. E., Sutherland, R. D.: Bending Stresses in Cylindrical Shells. Watervliet Arsenal, Research and Engineering Division, D. A. Project 501-01-033, OCMS Code 5520.11.439A, August 1963.

120. Weiss, V., Sessler, J., and Kushwant, G.: The Effect of Stress Gradient and Stress Biaxiality on the Behavior of Materials. Aeronautical Systems Division, Wright-Patterson Air Force Base, Ohio, Technical Report No. ASD-TR-61-725, May 1962.

121. Wilson, P. E., and Boresi, A. P.: Annotated Bibliography of Selected References on the Theory of Elastic Plates. Department of Theoretical and Applied Mechanics, University of Illinois, Project NR 064 413, Contract NR 1834(14), January 1960.

122. Wilson, P. E., Dharmarajan, S., and Rogers, P. W.: Linear Bending Analysis of a Pressurized Multicell Shell Structure, Engineering Department, General Dynamics/Astronautics 63-0968, September 1963.

123. Wilson, P. E. and Spier, E. E.: On Nonlinear Pressure Coupling Cylindrical Shell Analysis. General Dynamics/Astronautics, GD/A 63-0767 ERR-AN-316 Stress, November 1963.

124. Worley, W. J., and Wang, H.: Geometrical and Inertial Properties of a Class of Thin Shells of Revolution. NASA CR-89, September 1964.

125. Wu, E. E.: Application of Fracture Mechanics to Orthotropic Plates. University of Illinois, Department of Theoretical and Applied Mechanics, T AM Report No. 248, June 1963.

126. Yao, J. C.: Thermoelastic Differential Equations for Shells of Arbitrary Shape. Aerospace Corporation Report No. TDR-169(3560-30) TN-4 SSD-TDR-63-20, January 1963.

127. Yao, J. C.: Bending Due to Ring Loading of a Cylindrical Shell with an Elastic Core. Aerospace Corporation, Report No. TDR-169(3560-30) TN-5, SSD-TDR-63-123, May 20, 1963.

1. Babcock, C. D. and Sechler, E. E.: The Effect of Initial Imperfections on the Buckling Stress of Cylindrical Shells. NASA TN D-2005, July 1963.

Results of an experimental investigation carried out to determine the effect of axially symmetric initial imperfections on the buckling load of a circular cylindrical shell under axial compression are presented.

Fabrication of the shells basically consisted of plating a copper shell on an accurately machined wax mandrel and melting the mandrel out of the shell. The wax core was a two to one mixture of refined paraffin and Mobile Cerese Wax 2305. Plating was accomplished with Cupric Fluoborate, $Cu(BF_4)_2$. A photograph of the mandrel and finished wax form is included. All shells had a base diameter of 8 inches and a length of 10 inches.

Tests were conducted to determine characteristics of the plated copper. A typical stress-strain curve is presented. Young's modulus was determined as 13.0×10^6 psi. Evaluation of Poisson's ratio was not attempted. A value of 0.3 was used for Poisson's ratio.

Testing was accomplished using a controlled displacement testing machine. Loads were monitored using a cylindrical shell on which 24 foil strain gages were mounted. A photograph of the testing machine and load measuring shell is included.

After fabrication, the shells were measured for initial imperfection. This was accomplished by determining the deviation of the generators of the shell from a straight line. Measurements were made with a reluctance-type pickup.

The shells were mounted in the testing machine and secured with a thin layer of Devcon between the cylinder and the testing machine head. The buckling load of the shells was then determined. Thirty-seven shells with initial imperfections in the form of a half sine wave along the generator were tested along with three cylinders with a constant curvature imperfection along the generator.

Results of the tests are presented in tabular and graphical form. The table indicates model geometry, intended initial imperfection, buck-

ling stress, Eigen number, and the variation of load distributions near buckling. Load distribution as a function of applied load is shown graphically for two of the cylinders tested.

The analysis developed in the Appendix is used for comparison with experiments. The solution of the perturbation equations satisfies compatibility exactly and equilibrium approximately. Experimental results were well below those predicted analytically for the buckling stress (about 0.7 of the theoretical stess). Test results show reasonable scatter for tests on cylinders.

The authors are at the California Institute of Technology. 7 References.

2. Card, M. F.: Bending Tests of Large-Diameter Stiffened Cylinders Susceptible to General Instability. NASA TN D-2200, April 1964.

Seven ring-and-stringer stiffened, circular cylinders were loaded to failure in bending. Correlation between orthotropic buckling theory and experiment was found to be fairly good, discrepancies being attributed mainly to uncertainties in two of the orthotropic stiffenesses. Graphs are presented showing both calculated and test results. Calculated data is about 10 percent conservative for the group I (b/t = 125) cylinders and 20 to 30 percent conservative for the group II (b/t = 200) cylinders.

Test specimens consisted of seven 77-inch-diameter cylinders, stiffened on the outer surface with extruded Z-section stringers and on the inner surface with small, formed hat-section rings. Dimensions of the small rings and stringers as well as the overall dimensions of the cylinders are presented in figures and tables. Cylinders were constructed of 7075-T6 aluminum alloy.

The cylinders were loaded in bending through a loading frame with the use of a hydraulic jack. A photograph of the test setup is shown. Each cylinder was instrumented with resistance-type wire strain gages, to detect local buckling; to detect overall buckling of the cylinder wall; and to indicate stress distribution in the cylinder. Strains were recorded at a virtually continuous rate.

To predict general instability loads for the test cylinders, an orthotropic compressive stability equation that is a function of eight stiffnesses. Methods of evaluating these stiffnesses are presented and the

sensitivity of general instability predictions to these stiffnesses is given in the appendix. The results of this study indicated that the general instability curves could be affected considerably by the magnitudes of the circumferential bending stiffness and the shearing stiffness.

It is suggested that one cause of the discrepancy between theory and experiment might be attributed to the customary lack of agreement between small-deflection buckling theory and experiment. A correlation factor is usually applied to buckling computations to bring them into better agreement with experiment. For orthotropic cylinders there is a lack of experimental information upon which to base this emperical parameter.

The effects of asymmetry of the walls of the test cylinders was investigated and found to be negligible.

The author is at Langley Research Center. 14 References.

3. Clark, R. A. and Garibotti, J. F.: Longitudinal Bending of A Conical Shell. Douglas Missile and Space Systems Division, Engineering Paper 1547, March 1963.

Longitudinal bending of an elastic truncated conical shell under lateral or "wind" loads is considered. Corrections to the membrane solution are obtained by applying the general linear bending theory of thin elastic shells.

The basic eighth-order system of differential equations obtained by linear bending theory is reduced following the method of Chernina to a pair of coupled second-order non-homogeneous differential equations. An approximation consistent with thin shell theory is made and the pair of second-order equations are reduced to a single complex differential equation of second-order.

Approximate edge-zone solutions are given in terms of elementary functions. Explicit formulas for maximum edge-zone stresses are given. The solutions are illustrated by applying them to a shell subjected to a resultant bending moment at each end. A numerical example is solved and compares favorably with a numerical study of G. A. Thruston.

The author is at Case Institute of Technology, Cleveland, Ohio. 8 References.

. Gerard, G., and Papirno, R.: Minimum Weight Design of Stiffened Cylinders for Launch Vehicle Applications. Allied Research Associates, Inc., Technical Report No. 235-5, March 13, 1964.

The minimum weight analysis of moderate length, grid stiffened cylinders under axial compression is presented based on the use of orthotropic cylinder theory.

The comparative efficiencies of various types of stiffening systems are presented for a broad range of the governing structural loading parameter. Design data on current and projected launch vehicles indicate that all such designs fall within a very narrow range of the structural loading parameter. This observation permits a set of generalized conclusions to be drawn concerning the solution of the efficient stiffening systems and materials for launch vehicle design:

1. The N/Ed range of current and projected launch vehicles is such that elastic buckling considerations govern if reasonable compressive yield strength materials are utilized. Because elastic buckling governs the lower density alloys become desirable (except for the pressure stabilized case).
2. On the basis of compressive loading as the design criterion, there is no advantage in using high strength sheet materials for the primary launch vehicle structure (except for the pressure stabilized case) since the N/Ed range is relatively low. In fact, aluminum alloys with a compressive yield strength of 50 psi should be quite adequate.
3. In the launch vehicle N/Ed range considered, optimum grid stiffened cylinders are roughly one-quarter of the weight of unstiffened cylinders. Moreover, they are directly competitive with optimum sandwich cylinders.
4. Pressure stabilized cylinders that utilize high strength sheet materials ($E/\sigma_{ty} = 100$) are distinctly superior to other forms of construction at the lower end of the launch vehicle N/Ed range. From a materials viewpoint, the efficiency of pressure stabilized structures depends upon the tensile strength/density ratio.

The Authors are with Allied Research Associates. 10 References.

5. Goldberg, J. E.: Analysis of Conical Shells Under Unsymmetrical Conditions. General Dynamics/Astronautics, ERR-AN-080, November 15, 1961.

The differential equations for determining the stresses and displacements in this conical shells under unsymmetrical loads are presented. The equations are in a form which is especially convenient for numerical integration on a digital computer. The usual assumptions of classical shell theory are employed. Variations in thickness and mechanical properties may exist along the generatory; however, thickness and mechanical properties are assumed not to vary in the circumferential direction. Also, temperature gradients along the generator and through the thickness but having no circumferential variation are included.

The final forms of the equations are presented as an eighth order system of first order equations. They are presented in a form which makes them particularly convenient for numerical integration, and the fact that the equations do not involve derivatives of the thickness or of the wall rigidities makes them particularly convenient for non-uniform shells.

Equations for normal and shearing forces, and bending and twisting moments are also presented.

The author is at General Dynamics/Astronautics. No References.

6. Hayashi, T. and Hirano, Y.: Buckling of Orthotropic Cylinders Under External Pressure. Transactions-Japan Society for Aeronautics and Space Sciences, Vol. 6, No. 9, 1963, pp. 18-26.

This paper presents the solution for the buckling of orthotropic circular cylindrical shells under external pressure. The formulas for the buckling pressure are derived using the small deflection theory.

Some experimental studies were carried out using three circular cylindrical shells made of fiber reinforced plastics. The test results were compared with the theoretical results for the case of hydrostatic pressure. The external pressure was applied by decreasing the pressure inside the cylinders by a vacuum pump.

The cylinders were laminated using a wooden mandrel of cylindrical

form. Materials used in making the cylindrical bulkheads were glass cloths and polyester resin. The cylinders were bonded to the bulkheads using polyester resin. Wire strain gages were attached to the outside of the wall to measure the circumferential strain distribution. The dimensions and elastic properties of the cylinders are given in tabular form and the experimental setup is shown in a schematic diagram.

The measured buckling pressure is compared with the theoretical in tabular form. Agreement is good. However, the authors suggest that more tests on cylinders with higher orthotropy be performed to check the theory more extensively.

The authors are members of the Faculty of Engineering, University of Tokyo. 7 References.

7. Horton, W. H. and Durham, S. C.: Variation in Buckle Shape in Cylindrical Shells Under External Pressure and Axial Load. AIAA Journal, Vol. 2, No. 5, May 1964.

Literature on the behavior of cylindrical shells under the combined action of internal or external pressure and axial compression is reviewed.

An examination of results of other investigations led to a corollation between the buckling angle and the pressure ratio, p/σ_{cr}. The results are shown graphically. Geometric parameters for shells used by the other investigators are collected in tabular form.

It is emphasized that the shells used to obtain corollation between the buckling angle and p/σ_{cr} had a large variation in (R/t) ratios and in Modulus of Elasticity (some cylinders were made from steel and others were made from aluminum). There was no significant variation in the L/D ratio.

An elliptic curve is used to fit the data and the equation of the curve is presented.

The author is at Stanford University. 7 References.

8. Hubka, R. E.: Approximate Influence Coefficients of Cantilevered Stiffened Thin-Walled Conical Frustums Under End Load. Space Technology Laboratories, Inc., BSD-TDR-63-14, January 1963.

The problem of determing approximate influence coefficients for a cantilevered stiffened thin-walled conical frustum is considered. The large end of the frustum is considered built into a rigid wall while the small end is considered attached to a rigid movable plate. Assuming that the stiffeners are close together, the cone is treated as a uniform orthotropic material. Influence coefficients associated with both the shear and moment at the loaded (movable) end are derived using membrane theory. Example values of influence coefficients are presented for both stiffened and unstiffened cases. Results indicate that a negative coupling effect is more pronounced for a stiffened than an unstiffened cone.

The author is at Space Technology Laboratories, Inc., Redondo Beach, California. 4 References.

9. Peterson, J. P., and Dow, M. B.: Compression Tests on Circular Cylinders Stiffened Longitudinally by Closely Spaced Z-Section Stringers. NASA MEMO 2-12-59L, March 1959.

Six circular cylinders stiffened longitudinally by closely spaced Z-section stringers were loaded to failure in compression. Stiffeners were closely spaced so that local buckling of the cylinder wall did not occur prior to general or overall buckling. The results obtained are presented and compared graphically with available theoretical results for the buckling of orthotropic cylinders. Buckling loads were predicted with an error of 15 percent which was reduced to very nominal values after modification of the theories with empirical correction factors deduced from supplementary panel tests and unstiffened cylinder tests.

The main series of tests were conducted on 7075-T6 aluminum allow circular cylinders stiffened longitudinally by Z-section stringers and loaded in compression. Auxiliary test specimens, used in determination of the value for the fixity coefficient and the effectiveness factor, consisted of a series of four longitudinally stiffened flat panels and of three unstiffened circular cylinders. Dimensions of all specimens are given in tabular form.

The authors are at Langley Research Center. 7 References.

10. Pogorelov, A. V.: Post-Buckling Behavior of Cylindrical Shells.

NASA TT F-90, April 1964.

This report is a translation that is divided into two parts: axial compression and external pressure.

The problem of loss of stability of a cylindrical shell in axial compression is presented with special attention devoted to the equilibrium condition for a cylindrical shell and the upper critical load. Some experimental data are given.

A general investigation of the transcritical elastic state of a cylindrical shell in compression follows. The shape of the compressed cylindrical shell in the transcritical state of deformation is defined. The energy of elastic deformation of the shell is determined and a section is devoted to the determination of the state of equilibrium of a compressed cylindrical shell under conditions of transcritical deformation.

The lower critical load for the basic case of a cylindrical shell in compression is determined by first determining the parameters characterizing the derformation of the shell as a whole, then setting up numerical calculations to determine the lower critical load. Results of these numerical calculations are given.

The last chapter dealing with axial compression is devoted to a qualitative investigation of the transition to transcritical deformation of a cylindrical shell in compression. The shape of the shell surface under conditions of transcritical deformation is discussed as well as the equilibrium state of a shell under conditions of transcritical deformation.

The next chapter is devoted to the study of the loss of stability of a cylindrical shell acted upon by external pressure. The state of elastic equilibrium following loss of stability of primary form is discussed. The upper critical load is determined and some experimental data are presented.

An investigation of the equilibrium of the buckled shell and the determination of the lower critical load is made for the case of relatively thick shells and for the case of relatively thin shells.

The post-buckling behavior of a cylindrical shell under the combined action of an axial and a transverse load is examined by first discussing the loss of stability of the shell and then examining the elastic energy of the shell and the work done by the external load.

The author is at Izdatel'stvo Khar'lovskogo Universiteta. No References.

11. Schumacher, J.: Statistical Determination of Strength Properties. Convair Astronautics Report AZS-27-274A, November 1958.

Methods of evaluating strength properties statistically are presented for the cases when scatter of test results necessitates that design properties be defined in terms of probability levels. Selection of these levels depends on the particular design, its chances of failure, and the consequences of failure.

Two strength levels now in use are "A" and "B" values defined as follows:

"A" value-that level which would be exceeded by at least 99% of the entire population with 95% confidence.

"B" value-that level which would be exceeded by at least 90% of the entire population with 95% confidence.

The various terms used in statistical analysis are defined. These terms include normal distribution, mean value, standard deviation, sample mean, sample variance, sample standard deviation, confidence level, confidence interval, confidence limits, one- and two-sided tolerance limits.

Several example problems are given.

The first example is one in which six specimens were tested for ultimate tensile strength and the mean value of UTS and the standard deviation are calculated.

The second is an example in which a 95% confidence interval for the mean value in the first example is computed.

The third is a continuation of the first example in which an "A" value for the ultimate tension allowable is computed.

The last example is a continuation of the first example in which a "B" allowable value is determined.

Included in the appendix is a table of one sided tolerance factors for the normal distribution.

The author is at Convair Astronautics. 7 References.

12. Stachiw, J. D.: The Effects of Shell Joints and Bonding on the Stability of Acrylic Resin Cellular Shells. Pennsylvania State University, Ordinance Research Laboratory, Report No. NOrd 16597-97, September 1963.

Six acrylic resin cellular shells were tested under external hydrostatic pressure in a small pressure tank to determine the effects of joints between individual shell structure components and the effects of bonding on cellular shell stability. When the shell stiffeners were restrained from moving laterally, the location of joints and the degree of bonding did not affect the general elastic stability enough to cause failure by elastic buckling. The shells tested were 15.700" long with an I.D. of 6.625" and O.D. of 8.715". They were constructed of concentric cylinders separated by stiffeners. The following methods were used to fabricate the acrylic resin circular shells:

Model 6--smooth tube slip-fitted over an externally ribbed tube.

Model 7--internally ribbed tube slip-fitted over a smooth tube.

Model 8--stacked H-ring modules.

Model 9--stacked U-ring modules.

Model 10--annular stiffeners, inserted between concentric tubes. These annular stiffeners fitted loosely and were separated by three spacers located 120° apart.

Model 11--stacked concentric rings and spacers.

All shells failed by material yielding except the one in which the stiffeners were not restrained from moving laterally. However, the distribution of stresses and strains on the other shell surfaces was considerably influenced by the location of joints and the degree of bonding. The shell stresses are calculated by Pulos' and Mihta's formulas. Comparison between experimental and theoretical stresses is presented graphically. Curves are not plotted beyond 1000 psi of external hydrostatic pressure. SR-4 strain gages 1/4" long were mounted on the test specimens to measure experimental strains.

Four epoxy resin models of the cellular shells were pressure-tested and analyzed photoelastically to determine the effects of stress concentration at the junctures of the stiffeners and the inner and outer shell facings. It was determined that when the fillet radius at the juncture of the stiffeners and facings is small, serious stress concentrations are present at these points along the axis of the cellular shell.

The author is at Pennsylvania State University. 6 References.

13. Stein, M.: The Influence of Prebuckling Deformations and Stresses on The Buckling of Perfect Cylinders. NASA Technical Report TR R-190, February 1964.

Large deflection theory is used to compute buckling loads of simply supported perfect cylinders under combined axial compression and external pressure considering prebuckling deformations and stresses induced by the edge support.

Donnell's large deflection theory and boundary conditions for simple support are used. Prebuckling deformations are initially considered axisymmetric. The nonaxisymmetric displacements that occur at buckling are added to the prebuckling axisymmetric displacements. Continuity is expressed by the periodicity of the displacements resulting in a set of equations for displacements that have complicated variable coefficients. The equations are not solved directly rather an equivalent energy approach is introduced using a variational approach.

Due to the fact that for large curvature parameters, Z = 1000, the solution led to large determinants, results are only presented for Z = 1000. Interaction curves are presented for Z = 50, 100, 200, and 500. Stress coefficients are presented graphically for external pressure alone, hydrostatic pressure alone, and axial compression alone for a wide range of Z within previously prescribed limits.

Previously published experimental results are plotted on the interaction curves. Quantitative agreement is good but the lack of qualitative agreement is not explained.

The author is at Langley Research Center, NASA. 12 References.

14. Tennyson, R. C.: Buckling of Circular Cylindrical Shells in Axial Compression. AIAA Journal, Vol. 2, No. 7, July 1964.

Photographs of a photoelastic study of the mechanism of buckling of circular cylindrical shells under axial compression are presented. Photographs were made with a Fastax camera. The change in the isoclinic patterns with the buckled waveform are shown. The five shells tested had geometrical parameters in the ranges, 100 R/t 170, and 2 L/R 6, and were constructed of photoelastic plastic. Buckling loads were within

10% of classically predicted values.

By using plane elasticity equations with the assumption that the shear is zero along the 45° isoclinic, and equation for the isoclinics is obtained. The family of isoclinics is shown in a graph for the classical buckling mode shape. The boundary of the isoclinic region is shown and is in agreement with the photographs.

It is shown that buckling is initially localized; that buckling proceeds rapidly in the transverse direction; that initial buckling occurs with n = 10 and m = 12 for the cylinders tested in agreement with classical theory; and that the final buckled state occurs with n = 5. This behavior is explained analytically.

The author is at the University of Toronto, Toronto, Ontario, Canada.
5 References.